Understanding Heterogeneously Catalysed Transformations

Muhammad Bilal

School of Chemistry
University of Glasgow

Submitted in fulfilment of the requirements for the Degree of Doctor of Philosophy

April 2012

Abstract

Industrial reactions can either be catalysed by acidic, basic or neutral supported catalysts. The work within this thesis includes two different projects of industrial interest, both of which are catalysed by basic and acidic supported catalysts.

1) Acrylonitrile is one of the top twenty large-volume commodity chemicals in the world. Nearly every person in the modern world owns something that is made of acrylonitrile. Currently acrylonitrile is synthesised industrially by the ammoxidation of propylene. During this process acetonitrile is produced as by product and is used commercially as a solvent. However, the production of acetonitrile is far greater than demand therefore considerable interest lies in the conversion of acetonitrile to acrylonitrile. In our studies the synthesis of acrylonitrile from methanol and acetonitrile was attempted using magnesium oxide and chromium-doped magnesium oxide catalysts. The catalysts were initially prepared by impregnation methods and then subsequently characterised. It was found that an impregnation of the magnesium hydroxide by chromium salt decreased the phase transformation temperature from magnesium hydroxide to magnesium oxide and yielded larger crystallite sizes. Using the chromium-doped magnesium oxide catalyst the reaction between acetonitrile and methanol gave 100% selectivity towards acrylonitrile. It is suggested that $Cr^{VI/V}$ species play an important role in this reaction and act as a stabiliser for the acetonitrile carbanion. Further study showed that the main deactivation route was the reduction of the chromium from $Cr^{VI/V}$ to lower oxidation states and the deposition of coke. It was found that over the course of a year the Cr/MgO catalyst significantly aged. Because the extent of ageing was so significant, it was decided to cease work on this project as it was of concern that the relationship between structure and activity would be difficult to rely on.

2) Hydrogen (H_2) is one of the clean sources of energy which is currently obtained by the steam reforming of non-renewable fossil-fuel resources. However the rapid depletion of fossil-fuel resources has spurred further research into alternative and renewable H_2 sources. Among the many different renewable sources available for H_2 production, the steam reforming of bioethanol has attracted significant interest in recent years. However, crude bioethanol contains organic impurities which may deactivate the catalyst more rapidly than the pure ethanol. Therefore in the current project we have examined the tolerance of pure Al_2O_3 and Al_2O_3 supported noble metal (Rh, Ru and Pt) catalysts to the different impurities present in crude bioethanol. The direct use of crude bioethanol in the steam reforming

reaction could result in a huge saving in capital expenditure for an industrial plant, as huge capital costs are associated with the distillation of the crude bioethanol.

In the initial stage of the project, the Al_2O_3 and the noble metal impregnated Al_2O_3 catalysts were tested over a range of temperatures, under 20 barg pressures and a 5:1 steam to ethanol ratio. This was to determine the optimum temperature of reaction. A temperature of 500^oC was found to be the optimum reaction temperature due to “hard” coke formation at higher temperatures over the Ru and Rh catalyst.

The effect of the different impurities was examined by systematically adding 1mol.% of each impurity separately with respect to ethanol content in the water/ethanol mixture. The different noble metal catalysts showed similar tolerances towards the impurities. The addition of C_3 alcohols significantly decreased the conversion of ethanol and increased the rate of catalyst deactivation. This deactivation of the catalyst in the presence of C_3 alcohols was attributed to high olefin formation and incomplete decomposition of the C_3 alcohols which deposited over the catalysts as coke. Separate propanal, propylamine and acetone addition to the water/ethanol mixture significantly increased the ethanol conversion and the activity of all the noble metal catalysts tested. It was found that the presence of these impurities in the ethanol significantly decreased the C_2H_4 in effluent mixture as these impurities blocked the acidic sites of the catalysts. The compound C_2H_4 was found to be the main route towards coke formation.

Dedication

My parents

&

Late sister Razia Azim

Acknowledgements

I am eager to express my sincere gratitude to my supervisor, Prof. David Jackson, for his selfless input, valuable recommendations and smiling face which made my PhD and stay in Glasgow possible and comfortable. I also appreciate the valuable advice of my second supervisor, Dr. Justin Hargreaves, who helped, explain to me many different aspects of my projects.

I also wish to say a huge thank you to Ron Spence for all his help in solving different problems related to the glass line, rig and GC and ordering different chemicals for me. I would also like to show my appreciation to Andy Monaghan for all his help with everything and anything during my PhD. I would also like to thank him for all the conversations and encouragement he gave me when I was sad. I also extend my thanks to Jim Gallagher for his help with the SEM images.

Every member of my lab group, past and present, has greatly helped me throughout my PhD. In the early stages, Fiona greatly assisted me in operating the different instruments and plotting the data and Lynsey and Claire gave invaluable guidance about the glass line. I have no words to express my gratitude to Ailsa, Kathryn, Alex and Stuart for the proof reading of my thesis. I also express huge thanks to Javed, whose company greatly helped me to complete the PhD work on time. I would also like to extend my thanks to the other members of the Catalysis group; Anne-Marie, Liam, Dr. Majid and Abdurrahman who helped me at many points throughout my project.

I would like to acknowledge, Kohat University of Science and Technology (KUST), Pakistan for giving me this opportunities and financial support.

Last but not least, my biggest thanks go to my parents, sisters and brothers for their endless patience and enthusiastic moral support at all times. Without my father’s continual encouragement, my mother’s love and prayers and especially not forgetting the enthusiastic desires of my late sister Razia for my PhD, I would never have got to where I am today.

Declaration

The work contained in this thesis, submitted for the degree of Doctor of Philosophy, is my own work, except where due reference is made to other authors. No material within this thesis has been previously submitted for a degree at this or any other university.

_____

Muhammad Bilal

Table of contents

General introduction

Catalysts are materials that enhance the rate (and potentially the selectivity) of the thermodynamically favourable chemical reaction and in the process are cyclically regenerated [1-2]. They have been used on a small scale for centuries in inorganic form to make soap, and in the form of enzymes to prepare wine, cheese and other foods, although without knowledge or understanding of their mechanism [3]. The word “catalysis” was first used by Jackob Berzelius in 1836 and is the combination of two Greek words *kata* and *lysis* meaning down and breaking respectively.

Reactions can be catalysed by either heterogeneous or homogenous catalysts. A catalyst which exists in a different phase from the reactants is called a heterogeneous catalyst, whereas when both the reactants and catalyst are in the same phase they are known as homogenous catalysts [2].

In heterogeneous catalysis, the reactants must first become adsorbed onto the surface of a solid catalyst, undergo transformation to adsorbed product, and then desorbs from the catalyst surface. Once the products desorb from the catalyst surface the catalyst momentarily returns to its original status until additional reactants adsorb. The interaction between catalyst and reactants provide a chemical shortcut to the product, therefore speeding up the reaction at much milder conditions than if no surface interactions occur [1].

In heterogeneous catalysis the majority of industrial reactions take place on the surfaces of catalysts. The surface area of the active species can be increased by using supports or carriers. Catalyst supports are generally porous materials, where the active metal species are highly dispersed. Supports or carriers are usually inorganic materials but do not involve any heavy metals. Supports may be acidic or basic depending upon their chemical compositions [4, 5].

The work within this thesis has been divided into two sections which are catalysed by basic and acidic supported catalysts respectively.

- A novel route to acrylonitrile
- The effect of impurities on the steam reforming of bioethanol

A Novel Route to Acrylonitrile

1. Introduction

Acrylonitrile is a colourless to pale yellow chemical, composed of a vinyl group linked to a nitrile group [6]. Due to the presence of a carbon-carbon double bond and a carbon-nitrogen triple bond in the same molecule, acrylonitrile is a very reactive molecule. As it is not known to occur naturally, it must be produced synthetically [6-8].

$$CH_2=CHCN$$

Acrylonitrile is one of the top twenty large-volume commodity chemicals in the world. Nearly every person in the modern world owns something that is made of acrylonitrile, whether it is a telephone, computer housing, clothes or a small appliance. The world production capacity of acrylonitrile was 6.14 million tons in 2005, 7 million tons in 2006 whilst in 2010 it was only 6.2 million tons per annum. North America is the largest acrylonitrile exporter while Asia is the largest importer [7, 8].

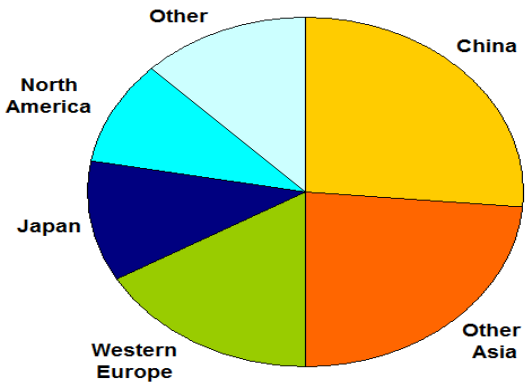

Figure 1.1-1 World consumption of acrylonitrile in 2011 [8]

1.1 Industrial importance of acrylonitrile

Acrylonitrile is a very important chemical for the polymer industries. It is used as a monomer and comonomer in large synthetic fibres, plastics and elastomers. Acrylic fibres production is the main market for acrylonitrile, as acrylic fibres contain 85% acrylonitrile. Acrylonitrile also plays an important role in the global polymer market because it used in

acrylonitrile-butadiene-styrene resins, adiponitrile, nitrile rubbers, elastomers and styrene acrylonitrile resins (SAN). Acrylonitrile-butadiene-styrene resins contain 25% acrylonitrile whilst styrene acrylonitrile resins (SAN) contain 25-30% acrylonitrile. However, the main use of acrylonitrile, which brings acrylonitrile to third largest position in terms of usage, is in the manufacture of adiponitrile, which is used exclusively for the manufacture of nylon-6, 6 [6, 8].

1.2 Synthesis of acrylonitrile

1.2.1 Current industrial process

Prior to 1960, acrylonitrile was commercially produced either from ethylene oxide and hydrogen cyanide or acetylene and hydrogen cyanide. In 1959 Standard Oil (later Sohio and now part of BP) developed a heterogeneous vapour-phase catalytic process for the synthesis of acrylonitrile by selective oxidation of ammonia and propylene. The process uses a catalyst based on bismuth, tin and antimony salts of molybdic and phosphomolybdic acids and bismuth phosphor-tungstanate. This process is also commonly known as propylene ammoxidation. Fluid bed reactors were used by Sohio for the synthesis of acrylonitrile. [6, 7, 8, 9]

$$H_2C{=}CHCH_3 + NH_3 + 1.5O_2 \rightarrow CH_2{=}CHCN + 3H_2O \qquad (1.1)$$

$$\Delta H^o = -515 \text{ kJ mol}^{-1}$$

Different catalysts were used to increase the selectivity towards acrylonitrile and during the last 50 years the process selectivity has increased from 50 to over 80%. About 90% of the worldwide production of acrylonitrile is made using the Sohio ammoxidation process. The most useful by-product of the process is HCN, which is produced at the rate of around 0.1kg per kg of acrylonitrile production, and is primarily used in the manufacture of methyl methacrylate. Another useful by-product is acetonitrile, which is produced at the rate of 0.03 kg per kg of acrylonitrile and is used as a solvent in industry [7].

1.2.2 Other routes for acrylonitrile

As acetonitrile production became greater than demand, chemists took an interest in the usefulness of the by-product in the production of acrylonitrile. Different raw materials such as CH_4, H_2CO and CH_3OH were used to convert acetonitrile into acrylonitrile over a range of catalysts, which have included magnesium oxide [10, 11].

1.3 MgO as a base catalyst

Base catalysis was first reported by Pines *et al.* [12] in 1955. They showed that sodium metal dispersed over alumina acts as an effective catalyst for the double bond migration of alkenes.

Several reactions including; addition, alkylation, cyclisation, and isomerisation are carried out industrially using liquid base catalysts. However, very few solid base catalysts are reported in the literature. The replacement of basic catalytic liquids with basic catalytic solids would have the advantage of decreasing corrosion and environmental problems, whilst also allowing easier separation and recovery of the catalysts.

In the 1970s scientists began studying solid base catalysts for various reactions. Numerous metal oxides such as alkaline earth metal oxides, ZnO and ThO_2 were found to act as Brönsted base catalysts. The metal (Mg, Zn, etc) increased the electron density over the oxygen which could then abstract H^+ from strongly acidic molecules. Following this finding, numerous solid base catalysts have been identified [13].

In 1999 Tanabe *et al.* [14] reviewed all the industrial processes at that time and found that among the 127 industrial processes, 10 processes used solid base catalysts, 14 processes used acid-base bifunctional catalysts and the remaining processes used acid catalysts. Most industrial processes, which use base catalysts, were developed within the last 20 years [14].

Among base catalysts, magnesium oxide has been widely used as a catalyst and a support for a variety of reactions since 1970. Its catalytic abilities lie essentially in its basic surface character [14]. There is extensive electron transfer from the magnesium to the oxygen upon the formation of magnesium oxide. The electron-rich oxygen anions on the magnesium oxide surface act as strong basic electron-donating sites, whilst the electron deficient magnesium cations act as weak acidic electron-accepting sites. Three different coordination sites have been found on the magnesium oxide surface, as shown in Figure 1.3-1. According to Supanee [15], these different unsaturated sites are produced using different calcination temperatures. They elucidated that sites of lower coordination have a stronger basicity and are mostly present at the corner of lattices and are thus capable of reacting with weaker acids.

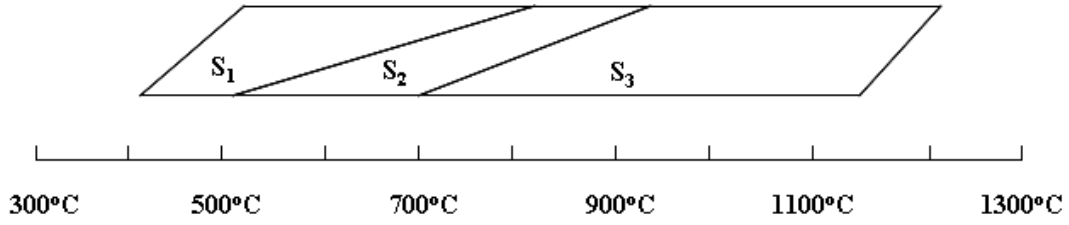

Figure 1.3-1 Different active sites at different calcination temperatures [15]

Figure 1.3-1 shows that the nature of the basic sites changes with the pre-treatment temperature, and the nature of the basic site reactions varies with the type of reaction.

There are a variety of precursors used for the preparation of magnesium oxide which include magnesium hydroxide, magnesium nitrate, magnesium sulphate, magnesium carbonate and rehydration of magnesium oxide. Aramendia *et al.* [16] examined the effect of different precursors and reported that the hydration of magnesium oxide followed by dehydration gave magnesium oxide with excellent chemical texture properties that make it highly suitable for use as a catalyst and catalyst support.

Magnesium oxide can be doped with different chemicals to increase its basicity, activity and selectivity for different types of reactions. Kanno *et al.* [17] studied the effect of the addition of the alkali metals on magnesium oxide and reported that the basicity of magnesium oxide increased with the addition of alkali metals. Among the alkali metals, lithium had the greatest effect due to its small size which allowed it to be incorporated into the magnesium oxide lattice whilst the effect of caesium is almost zero due to its large size.

The literature shows that alkali metal doping increases the partial oxidation property of magnesium oxide, whilst keeping the activity of total oxidation low [18]. Matsuda *et al.* [19] studied the doping of magnesium oxide with different precursors and found that the doping of magnesium oxide with sodium increased the basic strength of magnesium oxide and decreased the surface area, especially when sodium nitrate was the dopant. They attributed this basicity increase to the perturbation of the charge distribution over the magnesium oxide upon doping with the alkali metal ions [19].

Very little literature has been published with regard to the doping of magnesium oxide with transition metals. However, the presence of transition metals in different atmospheres is known to have a strong effect on the growth of magnesium oxide. Guilliatt [20] described

that in an oxygen atmosphere Mn metal doping increased the crystal size of magnesium oxide.

1.4 Synthesis of acrylonitrile over MgO

As discussed before, acrylonitrile was studied over range of catalysts. However, Ueda and co-workers [21, 22] appear to be the first group to work on the synthesis of acrylonitrile from methanol and acetonitrile over magnesium oxide catalyst. They synthesised acrylonitrile from methanol and acetonitrile using magnesium oxide as a base catalyst. However, the conversion and selectivity were not high as more propionitrile than acrylonitrile was produced. They continued this research and by using a chromium-doped magnesium oxide catalyst obtained 90% selectivity towards acrylonitrile, although conversion was still low.

$$CH_3CN + CH_3OH \rightarrow CH_2{=}CHCN + H_2 + H_2O \quad (1.2)$$

The coupling of acetonitrile and methane gave a high conversion of acetonitrile but the selectivity towards acrylonitrile was low [10].

In 2003 Jackson *et al*. [11] studied the formation of acrylonitrile from acetonitrile and methanol over chromium and manganese-doped magnesium oxide and explained the mechanism of the overall reaction. They found that the reaction proceeded in four steps *i.e.*

(i) the dehydrogenation of methanol to form formaldehyde

$$CH_3OH \rightarrow CH_2O + H_2 \quad (1.3)$$

(ii) the deprotonation of acetonitrile to form an active carbanion species.

$$CH_3CN \rightarrow {}^{-}CH_2CN + H^{+} \quad (1.4)$$

(iii) the cross coupling of formaldehyde and the carbanion.

$$CH_2O + {}^{-}CH_2CN + H^{+} \rightarrow HOCH_2CH_2CN \quad (1.5)$$

(iv) dehydration to form acrylonitrile.

$$HOCH_2CH_2CN \rightarrow CH_2{=}CHCN + H_2O \quad (1.6)$$

They also found that there were decomposition reactions of methanol and the hydrogenation reaction of acrylonitrile to give propionitrile (PPN).

$$CH_2{=}CHCN + H_2 \rightarrow CH_3CH_2CN \quad (1.7)$$

They revealed that the reaction is base catalysed and the calcination of magnesium oxide in air catalyzed the methanol to formaldehyde reaction better than simple heating in inert gases.

The effect of impregnation of magnesium oxide with alkali metals was investigated for the synthesis of acrylonitrile from acetonitrile and methanol [23]. Alkali metals with larger cationic radii than that of Mg were found to show high catalytic activity toward acrylonitrile synthesis. This shows that alkali metal doping facilitated the formation of the acetonitrile carbanion, a reaction intermediate for acrylonitrile synthesis, and also restrained the complete oxidation of the anionic intermediate [23].

Xie *et al.* [24] used temperature programmed desorption to study chromium-doped magnesium oxide catalysts that had been used in the formation of acrylonitrile from methanol and acetonitrile. They concluded that the dissociation temperatures of methanol and acetonitrile over chromium-doped magnesium oxide were lower than on the pure magnesium oxide. They also determined that the dissociation temperature of methanol over the calcined chromium-doped magnesium oxide catalyst was also lower than on the catalyst reduced by hydrogen before the reaction.

To best of our knowledge, there is very little literature which investigates, in detail, the relationship between the formation of acrylonitrile from methanol and acetonitrile and the catalyst behaviour. Furthermore, there is no evidence of a detailed study of post reaction catalyst characterisation to determine the cause of catalyst deactivation during reaction.

1.5 Project aim

The aim of this project was therefore to study;

- Catalyst preparation; the effect of different metal loadings.
- Pre and post reaction characterisation of the catalysts using different techniques such as TGA/DSC connected to a mass spectrometer, BET, powder XRD and TPO.
- The synthesis of acrylonitrile from acetonitrile and methanol using magnesium oxide and chromium-doped magnesium oxide catalysts to obtain maximum yields and high selectivity toward acrylonitrile.

2. Experimental

2.1 Catalyst characterisation

2.1.1 BET analysis

BET analysis of pre and post-reaction catalysts was measured using a Micromeritics Gemini III 2375 Surface Area Analyser. Prior to analysis between 0.04-0.05g of catalyst was placed in a vial and purged under a flow of N_2 (30ml min^{-1}) overnight at 110^oC to remove moisture and any physisorbed gases from the catalyst sample. Total surface area was calculated using Brunauer-Emmett-Teller (BET) equation (2.1) [25].

$$\frac{P}{V(P_o-P)} = \frac{1}{V_mC} + \frac{(C-1)P}{V_mCP_o} \quad (2.1)$$

Where P = Equilibrium pressure of adsorbate gases

P_o = Saturated pressure of adsorbate gases

V = Volume of adsorbed gas

V_m= Volume of monolayer adsorbed gas

C = BET Constant

The surface area can be calculated using the following formula

$$S_{BET} = V_m N\sigma/M_v \quad (2.2)$$

Where M_v is the molar volume of adsorbed gas (0.0224 m^3)

N = Avogadro's constant

σ = Adsorption cross-sectional area of the adsorbed gas/molecule which is N_2 ($16.2x10^{-20}$ m^2) in our case.

The specific surface area per unit weight of catalyst of the sample can be measured by the following formula.

$$\text{Specific surface area} = S_{BET}\ \text{total}/m \quad (2.3)$$

Where m is the mass of catalyst in gram

2.1.2 Thermo-gravimetric analysis

Thermo-Gravimetric Analysis (TGA) was carried out on catalyst samples using a combined TGA/DSC Q600 thermal analyser attached to an ESS Mass Spectrometer for evolved gas analysis. For each sample the temperature profile and gases used are reported in Table 2.1-1. The gases were used at a flow rate of 100 ml min^{-1}. For Mass Spectrometric analysis, mass fragments with m/z values of 2, 14, 16, 17, 18, 28, 30, 32, 40, 41, 44 and 53 (amu) were followed. The typical sample loading was 10-15mg.

Serial. No	Catalyst condition	Atmosphere	Temperature range (^oC)	Ramp
1	Pre-reaction	Argon	30 to 800	$10^oC\ min^{-1}$
2	Post-reaction	2% O_2/Ar	30 to 800	$10^oC\ min^{-1}$

Table 2.1-1 Treatment for TGA/DSC characterisation

2.1.3 Powder X-ray diffraction (XRD)

To obtain information concerning the phase composition and the distribution of the crystallite size of the catalyst before and after reaction, X-ray diffraction patterns were obtained using a Siemens (D 5000) X-ray Diffractometer (40 kV, 40 mA, monochromatic) using a CuK alpha source (1.5418 Å). The scanning range used for the acrylonitrile project was $5^o \leq 2\theta \geq 85^o$ with a scanning rate of 2 seconds per step and a step size of 0.02°.

2.1.3.1 Powder hot stage X-ray diffraction (XRD)

Powder hot stage XRD analysis was also carried out on the Siemens D5000 X-ray Diffractometer using an Anton-Paar XRK reaction cell. The scanning procedure was identical to that for the standard analysis, however the sample was heated *in-situ* in an argon atmosphere with a heating rate of $12^oC\ min^{-1}$. Scans were taken at 30^oC, 100^oC and at 100^oC increments thereafter to 600^oC. At each 100^oC increment the sample was held for 15 minutes before the scan was taken.

2.1.3.2 Scherrer equation

The approximate average crystallite size from the powder XRD pattern was calculated using the Scherrer equation:

$$d = \frac{K\lambda}{B\cos\theta} \qquad (2.4)$$

Where d = Average crystallite size (Å)

K = Scherrer constant (0.87-1.0, normally taken to be 1.0)

λ = wavelength of X-ray source (1.541 Å)

θ = 2 theta angle of peak

B = full peak width at half maximum (FWHM)

This is only an approximate method because the results can be influenced by various factors such as lattice distortion as well as instrumental parameters.

2.1.4 UV-visible spectroscopy

UV-visible analysis was carried out on a solid-state Varian Cary 500 spectrophotometer on fresh and used catalysts. The instrument was equipped with a reflectance accessory (Praying Mantis; Harrick) and a temperature controlled reaction chamber connected to a gas dosing system. Uncalcined catalysts were heated from 30^{o}C to 600^{o}C in 2% O_2/Ar, Ar and 2% H_2/N_2 atmosphere using a heating ramp of around 12^{o}C min^{-1}. Scans were taken at 30^{o}C, 100^{o}C and then at 100^{o}C increments thereafter to 600^{o}C. At each stage the sample was held at the desired temperature for 15 minutes before the scan was taken. Post reaction catalysts were inspected at room temperature only. The baseline was taken using magnesium oxide as the reference. The sample was ground into a fine powder (< 250 μm) before being added to the sample holder. The range of wavelengths scanned was from 800 nm to 200 nm.

2.1.5 Catalyst preparation

Pure magnesium oxide and chromium-doped magnesium oxide catalysts were prepared by an impregnation method using chromium nitrate nonahydrate. Sufficient metal nitrate solution was used to produce a metal loading both by 4% weight and 4% molar samples. The metal precursor and their pH values are listed in Table 2.1-2

The catalyst precursor was dissolved in the desired amount of deionised water. The support was mixed with deionized water separately and the pH was checked. Both precursor and support were mixed at room temperature and the mixture stirred using a

magnetic stirrer. The pH was measured and was found to range from 9 to 10. Excess water was removed by rotary evaporator (Buchi Rota vapor R-114) at 80^{o}C. The catalysts were then transferred to an oven and dried overnight at 110^{o}C. All catalysts were crushed and sieved to between 425 and 250 μm prior to testing.

Catalyst/Support	Precursor	Precursor solution (pH)
MgO	-	11
Cr/MgO	$Cr(NO_3)_3.9H_2O$	1.2

Table 2.1-2 pH of catalyst precursors

2.2 Catalyst testing

2.2.1 Glass microreactor

Catalytic tests were carried out in a silica glass microreactor with an online Varian 3300 Gas Chromatograph. The glass reactor consisted of two bubblers, a mixing chamber and a glass reaction tube, separated from each other by vacuum taps, as shown in Figure 2.2-2. The prepared catalyst was placed in a glass reaction tube, as shown in Figure 2.2-1, which was then connected to the microreactor and sealed with black wax.

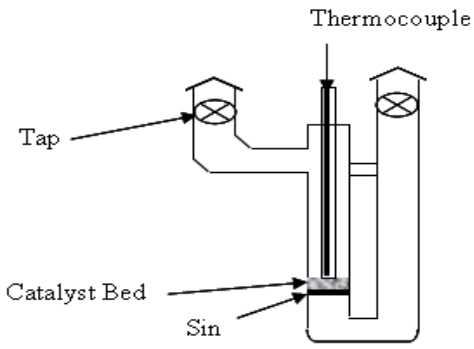

Figure 2.2-1 Glass microreactor tube

The argon gas could be fed to the bubblers and the flow of gas to each bubbler was controlled by pressure rotameter. The gas carried the vapours of the reactants from the bubbler to the mixing chamber, where both reactants' vapours mixed prior to entering the reaction tube. The glass tube was placed in a tubular furnace and the temperature of the furnace was regulated by West 4400 temperature controller. A trap positioned down-stream from the reactor was used to trap gaseous product by freezing. The glass microreactor was connected to stainless steel tubing and GC valves which were heated to 100^{o}C to prevent the condensation of reactants or products.

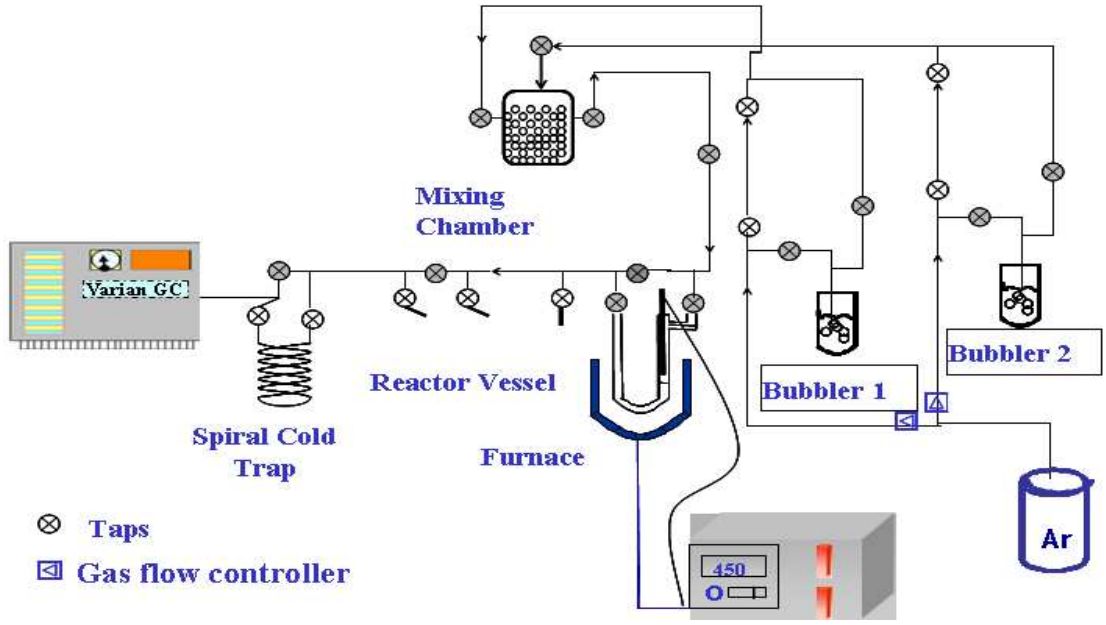

Figure 2.2-2 Glass Microreactor

2.2.2 Reaction procedure

Catalyst, typically 0.25 g with a particle size of between 250-425 μm, was placed in the glass reactor tube. The thermocouple holder was inserted into the glass tube and sealed to the glass microreactor with black wax. Argon carrier gas was passed continuously at a flow rate of 60 ml min^{-1} through the microreactor and a leak test was carried out to ensure no gas leaks were detected from the seals on the reactor or taps. The thermocouple was then placed in the thermocouple holder and the furnace was placed around the reactor tube, as shown in Figure 2.2-2. Prior to reaction the catalyst was calcined *in-situ* at 600^{o}C for 2 hours in argon at a flow rate of 60 ml min^{-1}. The temperature controller was set to a heating rate of 5^{o}C min^{-1}. The temperature was then reduced to the reaction temperature. The bubblers were filled to 2/3 capacity with methanol and acetonitrile respectively and placed in water baths to control the temperature of the reactant within the bubbler. In order to obtain reference peaks, the quartz glass reactor tube was bypassed and the flow left for a period to stabilise vapour concentration of both reactants in the carrier flow and then three reference samples were analysed by GC.

2.2.3 GC analysis

Products and reactants from the glass microreactor were analysed by online GC (Varian 3300) which was connected to a Hewlett Packard integrator. The GC was fitted with 30 m long and 0.25 mm internal diameter DB Wax column and TCD detector. The sample loop

volume was 50 μl. Prior to analysis the GC was calibrated for acetonitrile, acrylonitrile, methanol, propionitrile and hydrogen. The following temperature conditions were used.

Column temperature: 50^{o}C

Detector Temperature: 250^{o}C

Temperature of injection: 100^{o}C

Carrier gas: Argon

2.2.3.1 Calibration of reactants and products

Calibrations were carried out by varying the temperature of the reactants in the bubblers which in turn produced different vapours pressures for each of the reactants. Each reactant and product was bubbled with an argon flow (carrier gas) and analysed by GC. The temperature of the bubbler was altered by changing the temperature of the slurry bath and this in turn altered the vapour pressure of the gas in the carrier flow.

To calculate the vapour pressure in the glass line at different temperatures, the vapour pressure of each reactant and product at different temperatures was measured using an Edward Barocel pressure sensor, and using this data it was possible to calculate the pressure at which the GC reading was taken using the Clausius Clapeyron equation.

$$\text{Ln}\,(P_2/P_1) = \Delta Hv/R\,[(1/T_1)-(1/T_2)] \qquad (2.5)$$

Where T_1 and P_1 = a corresponding temperature and vapour pressure

T_2 and P_2 = the corresponding temperature and vapour pressure at another point

ΔHv = the molar enthalpy of vaporisation

R = gas constant

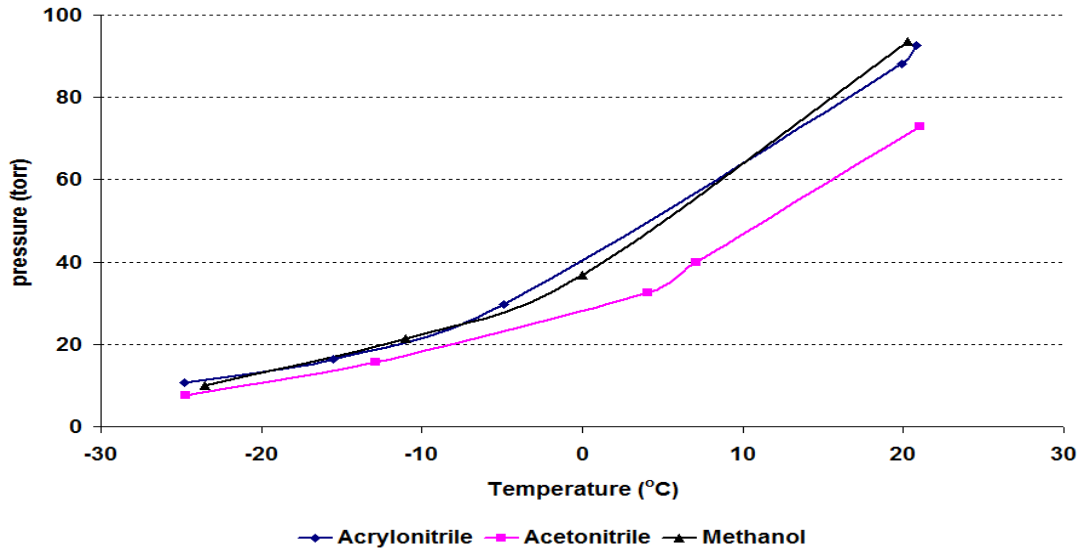

Figure 2.2-3 Calibration for Pressure versus Temperature

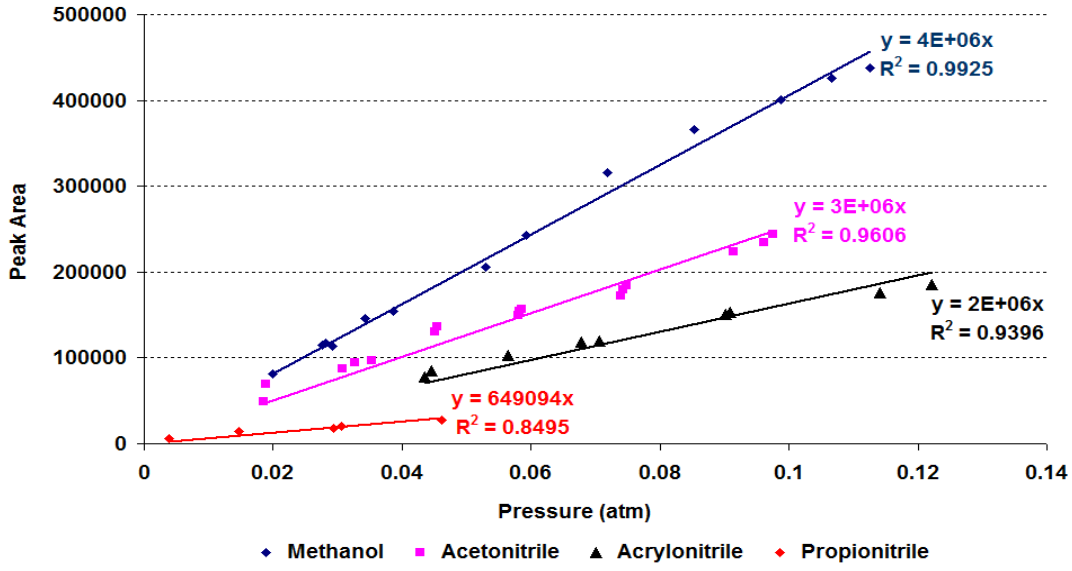

Figure 2.2-4 Gases Calibration

After determination of the vapour pressure from Clausius Clapeyron equation, the number of moles of the reactants and products was calculated using the ideal gas equation.

$$PV = nRT \qquad (2.6)$$

Where P = pressure of gas calculated from peak area, V = volume of sample (sample loop) 50 µl, R = gas constant (0.0821 L atm K^{-1} mol^{-1}) and T = temperature of laboratory.

The number of moles of hydrogen was calculated by one point formula.

2.2.4 Calculations

2.2.4.1 Conversion

Conversion was calculated as follows:

% Conversion

= [(mmoles of X in – mmoles of X out)/ mmoles of X in]*100

Where X represents either methanol or acetonitrile

2.2.4.2 Yields of products

The product yields were calculated in the following way:

% Yield for acrylonitrile

= (mmoles of acrylonitrile out / mmoles of acetonitrile in)*100

% Yield for H_2

= (mmoles of H_2 out / mmoles of methanol in)*100

2.2.4.3 Selectivity of acrylonitrile

The selectivity of acrylonitrile was calculated in the following way:

% Selectivity of acrylonitrile

= (mmoles of acrylonitrile out / mmole of acetonitrile in – mmoles of acetonitrile out)*100

3. Results and discussion

3.1 Catalyst characterisation

3.1.1 MgO

Magnesium oxide and chromium-doped magnesium oxide catalysts were characterised using techniques such as TGA/DSC connected to a mass spectrometer, powder XRD and BET to observe any changes taking place in the catalyst with temperature.

3.1.1.1 TGA/DSC

The weight and derivative weight loss profiles for the magnesium hydroxide are shown in Figure 3.1-2. The TGA profile displays distinct weight losses in different temperature regions. It shows a major weight loss (31%) occurred between 280-398^{o}C. Theoretical calculations for the dehydration of magnesium hydroxide to magnesium oxide gave a similar weight loss (30.87%).

$$Mg(OH)_2 \rightarrow MgO + H_2O \quad \text{(weight loss = (30.87\%)} \qquad (3.1)$$

This result suggests that the weight loss between 280^{o}C and 398^{o}C represents the conversion of magnesium hydroxide to magnesium oxide. This is supported by the mass spectra (Figure 3.1-3), which show that this weight loss is due to the desorption of water from the catalyst. The DSC profile (not shown) gave a sharp endothermic peak in this temperature region, indicating that the dehydration of the sample is an endothermic process, as expected from the decomposition of magnesium hydroxide. Near to 600^{o}C an additional smaller weight loss occurred. However, mass spectrometry results were unable to match this weight loss to a specific m/z value. The current study is in close agreement to the previous literature [26] which showed that during calcination of magnesium hydroxide to magnesium oxide, the first loss was physisorbed water below 150^{o}C and with further heating to 300^{o}C the phase transformation of magnesium hydroxide to magnesium oxide and the structural change from hexagonal to cubic structure occurred. It also explained that further heating produced cracking of magnesium oxide crystals into smaller fragments, gradual desorption of the remaining water and sintering of the magnesium oxide crystals.

$$Mg(OH)_2\,(xH_2O)_{ads} \xrightarrow[(\sim 6\%)]{50^oC\text{-}150^oC} Mg(OH)_2 + xH_2O \xrightarrow[93.9\%]{250^oC\text{-}350^oC} MgO + H_2O \qquad (3.2)$$

Figure 3.1-1 MgO formation from $Mg(OH)_2$

In the current study, the main weight loss took place ~ 30°C higher than the previous report [26]. This can be attributed to a different preparation method, calcination temperature, ramp rate, atmosphere under which the calcination occurred and the precursor used.

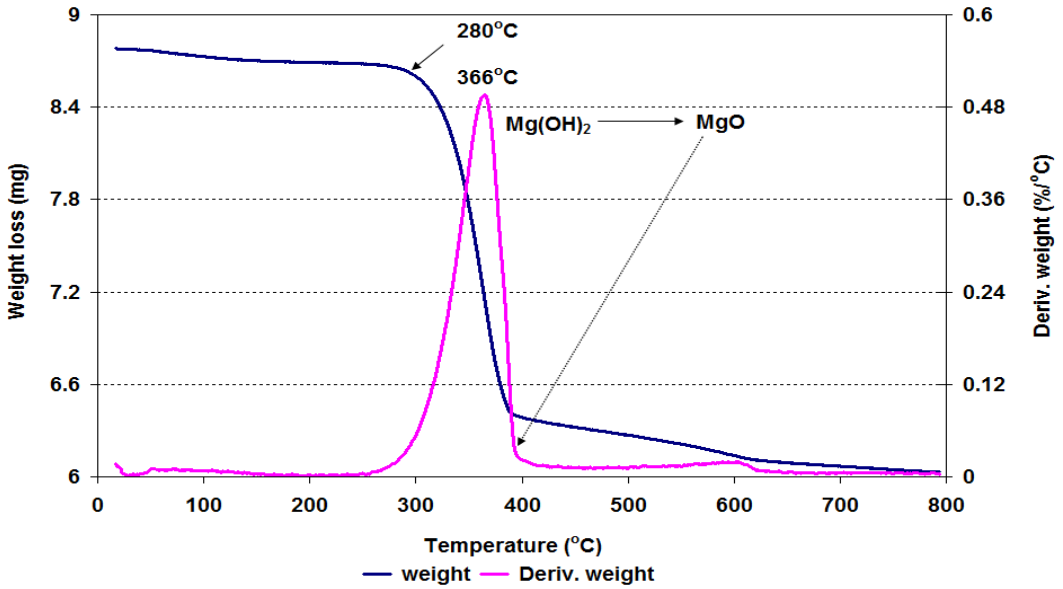

Figure 3.1-2 TGA and derivative weight of MgO in an argon atmosphere

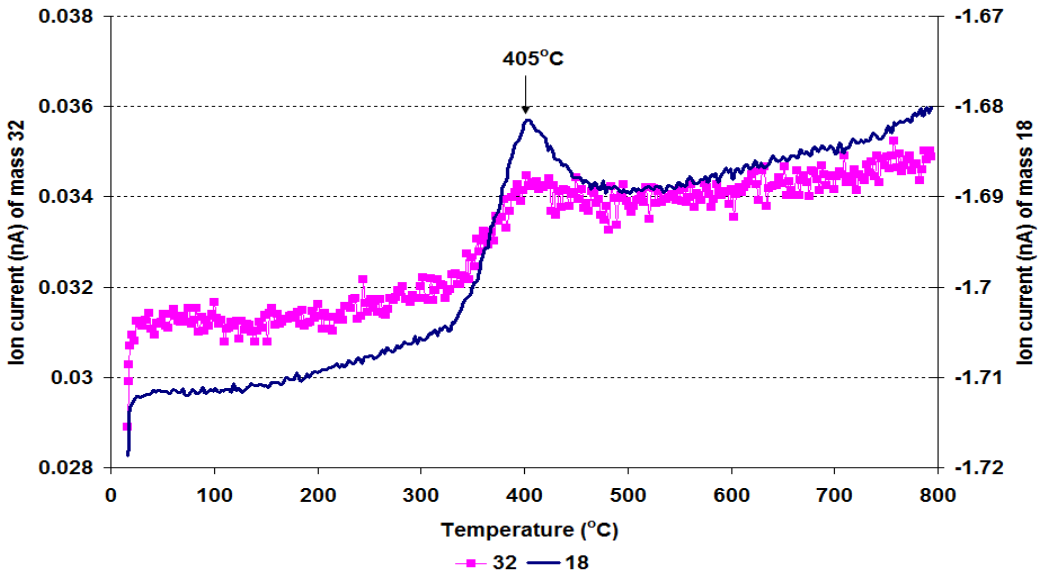

Figure 3.1-3 MS data of O_2 (m/z= 32) and H_2O (m/z=18) for MgO in an argon atmosphere

3.1.1.2 Hot stage powder X-ray diffraction (PXRD)

To investigate the changes in structure and morphology at different temperatures, pure magnesium hydroxide was characterised by hot stage powder X- ray diffraction at different temperatures, as described in section 2.1.3. Figure 3.1-4 shows the hot stage powder XRD patterns for magnesium hydroxide and the products of its calcination at various temperatures up to 600^{o}C in an argon atmosphere. The average crystallite size of the catalyst was determined at different temperatures using the Scherrer equation, as explained in section 2.1.3, where the average particle size at a given temperature is calculated by the full width half maximum at the most intense peak, as shown in Table 3.1-1. Figure 3.1-4 shows that the patterns of the catalyst calcined up to 600^{o}C has two phases; brucite ($Mg(OH)_2$) and periclase (MgO). The powder XRD patterns at temperatures up to 300^{o}C were similar and can be identified as brucite. However, the average crystallite size slightly changed with an increase in the calcination temperature up to 300^{o}C. Further increase in the calcination temperature changed the patterns of the peaks and new peaks appeared which had smaller crystal sizes and could be identified as periclase. This suggests that the transformation of brucite to periclase produced small size crystallites [27]. This phase transformation was also confirmed by the TGA profile, shown in Figure 3.1-2. After the phase transformation, further increases in the calcination temperature gave a similar crystallite size up to 600^{o}C. With the decrease in temperature after calcination at 600^{o}C, the pattern of periclase was not changed. This suggests that after calcination of the catalyst at 600^{o}C, a decrease in temperature does not change the phase of periclase back to brucite.

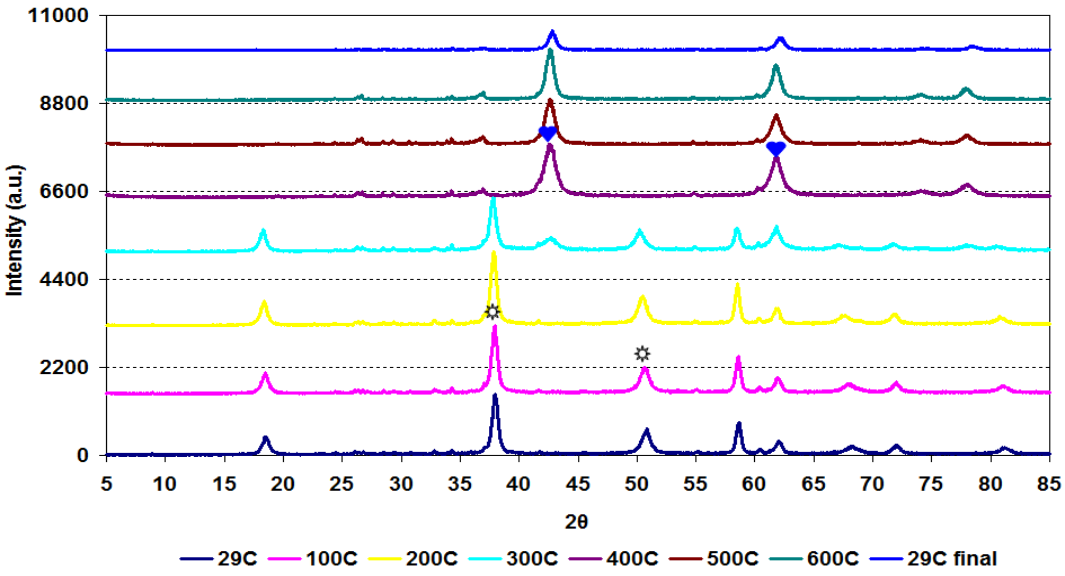

Figure 3.1-4 Hot-stage powder XRD patterns of MgO in an argon atmosphere (The phases denoted are (☼) magnesium hydroxide and (♥) magnesium oxide. The powder XRD patterns are offset for clarity).

Temperature (^oC)	29	100	200	300	400	500	600	29 final
Average crystallite size (Å)	170 (±7)	128 (±0.6)	150 (±2)	152 (±4)	84 (±5)	91 (±5)	93 (±6)	138 (±8)
Phase	Brucite				Periclase			

Table 3.1-1 Average crystallite size of the sample in-situ calcined at different temperatures

3.1.1.3 BET analysis

In order to observe any changes in the BET surface area following calcination, the brucite sample was analysed at room temperature and then after calcination at 600^{o}C. Before calcination the sample was hydrated then dehydrated by rotary evaporator at 80^{o}C. Table 3.1-2 shows that the calcination of the sample at 600^{o}C results in an increase in the BET surface area and average pore diameter. A previous investigation [26] showed that the BET surface area of magnesium oxide is strongly dependent upon on the nature of the precursor and method of preparation. Ding *et al.* [26] prepared magnesium oxide from different precursors and solvents, compared their BET surface areas and found that the magnesium oxide prepared by the hydrothermal method gave a high BET surface area whilst the magnesium oxide prepared from magnesium sulphate decomposition gave a smaller BET surface area. It has been reported in the literature that, during the thermal dehydroxylation process, water molecules are formed and lost between the two adjacent layers of hydroxyl ions, leaving a periclase structure with many defects and irregular inter-crystallite channels (cracks) and the specific surface area is therefore greatly increased. However, the size and the dimensions of the pores, in which capillary condensation occurred, remained constant [26, 28]. In contrast to the previous investigations, the current results show that calcination of the catalyst at 600^{o}C significantly increased the average pore diameter while the BET surface area slightly increased. This indicates that thermal dehydration of brucite caused restructuring of the crystallite framework and produced defects (cracks) in the crystallite which increased the pore volume and the average pore diameter. However, during restructuring some small pores may have disappeared and so the BET surface area is not significantly increased.

Serial No	Conditions	BET Surface area (m^2/g)	Pore volume (cm^3/g)	Average pore diameter (Å)
1	Uncalcined	113	0.20 (± 0.35)	71 (± 6.56)
2	Calcined at 600^{o}C	120	0.52 (± 1.51)	167 (± 7.42)

Table 3.1-2 BET analysis of MgO at different temperatures

3.1.2 4wt.% Cr/MgO

3.1.2.1 TGA/DSC

The decomposition of chromium nitrate nonahydrate was followed by TGA/DSC with the gases evolved being identified by mass spectrometry to determine at what temperature pure chromium nitrate would form chromium oxide. The TGA results in Figure 3.1-5 show that the major weight loss (89.28% of total weight loss) took place below 200^{o}C. This result was in close agreement to that obtained by Malecki *et al.* [29] from chromium nitrate nonahydrate (CNN) thermal decomposition in a helium atmosphere. The derivative weight profile (Figure 3.1-5) shows that the weight loss took place in three steps at temperatures of 89^{o}C, 114^{o}C and 139^{o}C which correspond to the evolution of water and nitrogen monoxide seen in the mass spectrometry data (Figure 3.1-6). In agreement with the theoretical calculations Gubrynowicz *et al.* [30] showed that 82.1% weight loss of CNN gave Cr_2O_3. In the current TGA results chromium nitrate nonahydrate also gave 82% weight loss up to 700^{o}C. From a previous report [30] and current results it is proposed that chromium nitrate nonahydrate decomposed and formed Cr_2O_3. In the 76^{o}C to 200^{o}C temperature region, a small broad band of CO_2 appeared (not shown) which was observed at trace levels and this may be due to desorption of adsorbed atmospheric CO_2 by chromium nitrate nonahydrate. There was also a small weight loss that took place between 400^{o}C and 460^{o}C which corresponded to 5.6% of the total weight loss. From mass spectrometry results no m/z value matched with this weight loss, however, Labus *et al.* [31] reported that this weight loss would be due to evolution of oxygen produced from the decomposition and reconstruction of Cr_xO_y to Cr_2O_3.

$$Cr_xO_y \rightarrow Cr_2O_3 + O_2 \qquad (3.3)$$

The sample had lost 82.1% of its weight by 500^{o}C with little changes subsequently up to 700^{o}C. The heat flow profile showed that the first weight loss was an endothermic process whilst the second one was an exothermic process. According to Labus *et al.* [31] the exothermic event in the later stage may be due to reconstruction of the Cr_xO_y structure.

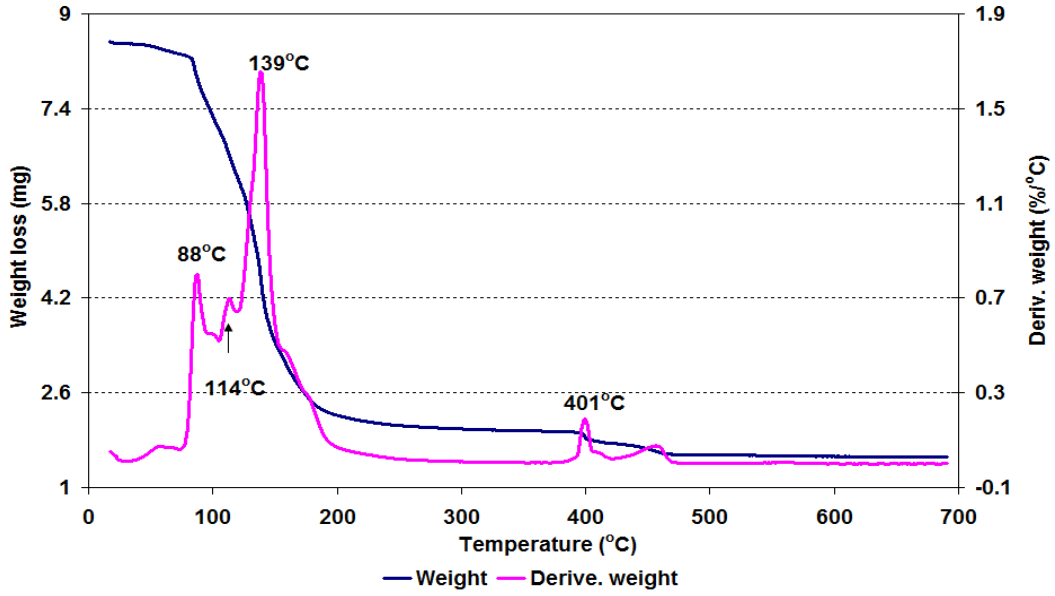

Figure 3.1-5 TGA and derivative weight of $Cr(NO_3)_3.9H_2O$ in an argon atmosphere

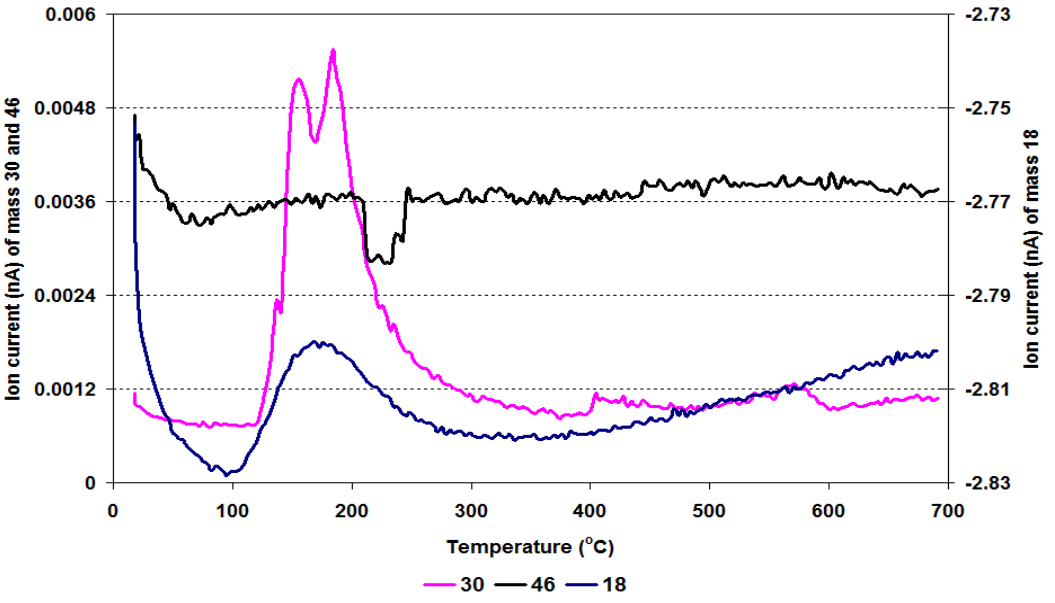

Figure 3.1-6 MS data of NO_2 (m/z= 46), NO (m/z= 30) and H_2O (m/z=18) for $Cr(NO_3)_3.9H_2O$ in an argon atmosphere

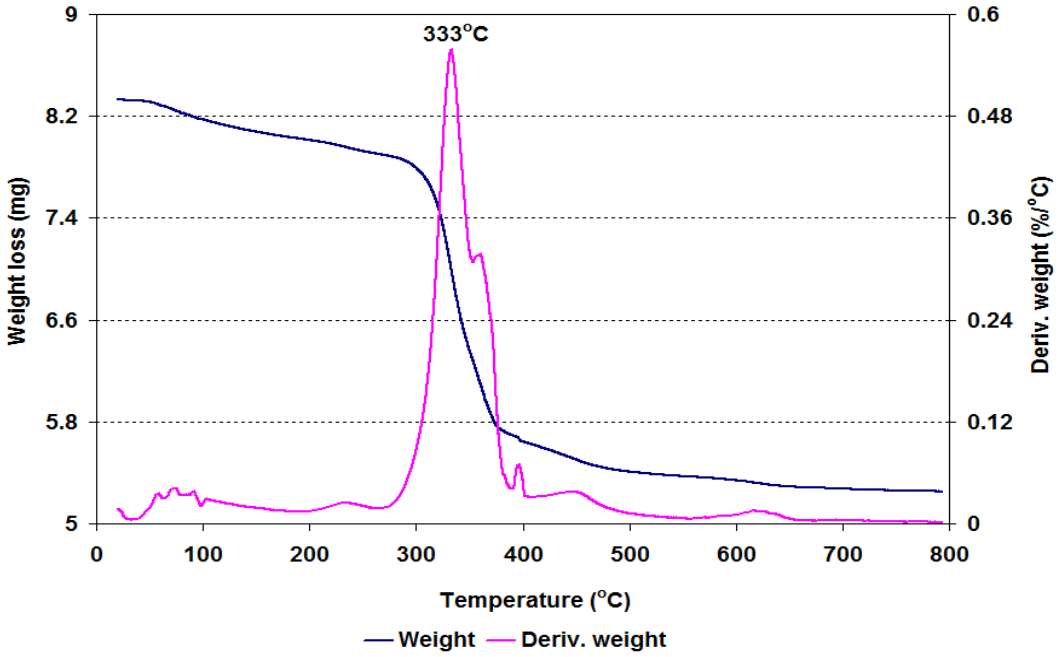

Figure 3.1-7 TGA and derivative weight of 4wt.% Cr/MgO in an argon atmosphere

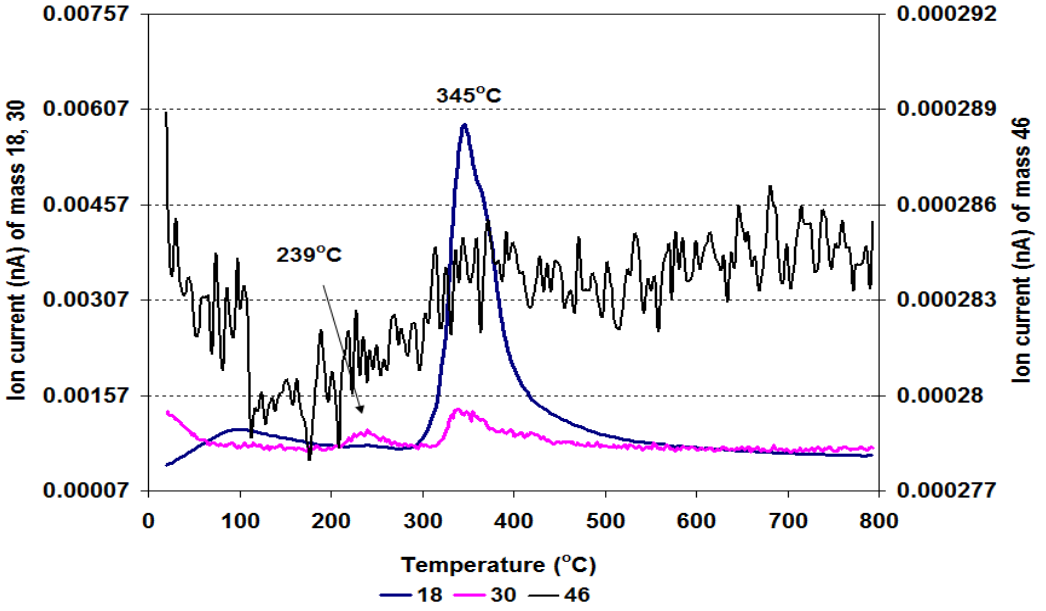

Figure 3.1-8 MS data of NO_2 (m/z= 46), NO (m/z= 30) and H_2O (m/z=18) for 4wt.% Cr/MgO in an argon atmosphere

After investigation of both the pure precursor and support, chromium nitrate nonahydrate was impregnated onto the magnesium hydroxide support in order to study the effect of chromium salt on the structure of magnesium hydroxide. The catalyst was studied by TGA/DSC connected to a mass spectrometer and raised to a temperature of 800°C. Due to the hydroxylated surface of the magnesium hydroxide, chromium nitrate is expected to interact with the hydroxyl groups during the decomposition process. The interaction

between precursor and support affects the decomposition temperature and bond strength of support. The TGA profile in Figure 3.1-7 of the chromium salt doped magnesium hydroxide sample showed a 36% weight loss up to 800^{o}C in an argon atmosphere. The derivative weight profile shows that this weight loss occurred stepwise at different temperatures. However, the major weight loss took place in the temperature region from 275^{o}C to 390^{o}C and corresponded to water and nitrogen monoxide evolution (in the mass spectrometry results in Figure 3.1-8). From the TGA profile of the chromium salt doped magnesium hydroxide catalyst it can be observed that the addition of chromium nitrate nonahydrate to brucite ($Mg(OH)_2$) decreased the dehydration temperature of the brucite by 33^{o}C, which is also supported by hot stage powder XRD results. This decrease in the dehydration temperature in brucite by the addition of the chromium salt could be due to the incorporation of Cr into the structure of the brucite which weakens the bond strength of brucite and subsequently brucite is easily transformed to periclase at a lower temperature. Ueda *et al.* [32] showed that the Cr^{3+} ion has a similar ionic radius as Mg^{2+} ion which can be incorporated in the lattice of brucite, causing a shift of electrons to the oxygen and possibly resulting in the expansion of the Mg-OH bond. So, it is suggested that due to this expansion the breakage of the Mg-OH bond can occur more readily. The derivative weight profile illustrates that there is also a small weight loss (2.5% of total weight loss) around 625^{o}C. However, no peak was found in the mass spectrometry results corresponding to this weight loss.

Initially the pH of the support solution was 11, and when chromium nitrate solution was added it reduced to 10. A previous investigation [33] showed that at pH 10, chromium exists in mono and dichromate forms. So, it is expected that before the dehydration of brucite, the chromium salt and some corresponding decomposition products are present on the brucite surface in mono and dichromate forms. When the temperature was increased above 300^{o}C, they reacted with the OH groups of brucite to form esters. The formation of esters between chromium and other supports such as TiO_2, SiO_2, Al_2O_3 and ZrO_2 has been reported previously [34, 35]. Magnesium hydroxide is more basic than the supports previously mentioned, so it could easily form the ester with the chromate by the reaction shown in Figure 3.1-9.

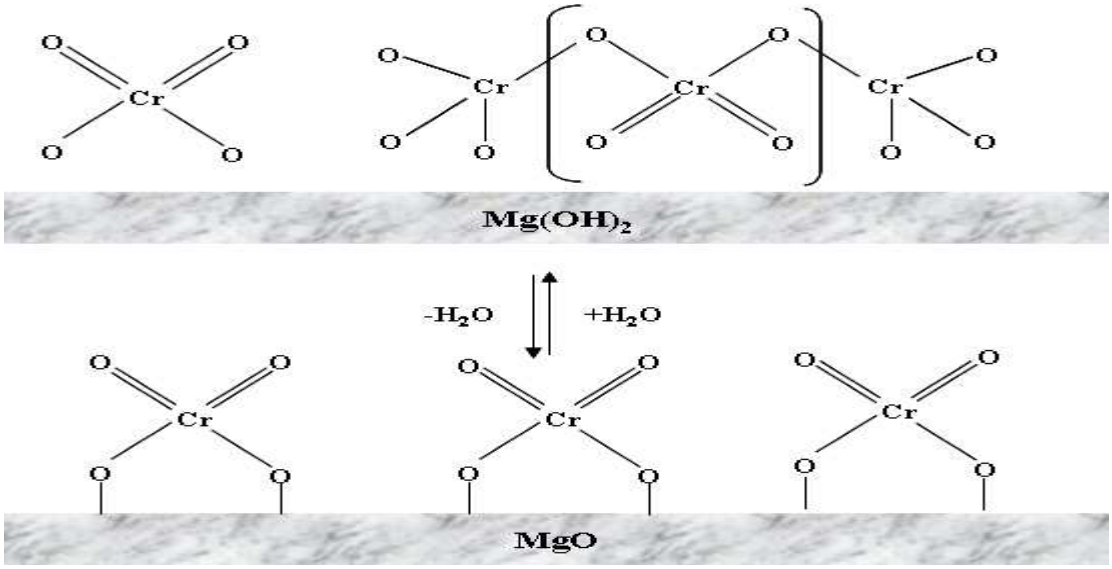

Figure 3.1-9 Ester formation between chromate and brucite

From the above discussion, it can be deduced that the impregnation of chromium salts onto magnesium hydroxide effects the lattice of the magnesium oxide crystals: decreasing the Mg-OH bond strength by distortion and hence, at lower temperatures, the conversion of magnesium hydroxide to magnesium oxide occurs.

3.1.2.2 Powder XRD

Figure 3.1-10 shows the powder XRD pattern of the chromium-doped magnesium hydroxide at room temperature. The peaks at 2θ 37.8^{o} and 50^{o} are matched with the magnesium hydroxide pattern in the ICDD (International Centre Diffraction Database). The hot stage powder XRD patterns illustrate that doping of magnesium hydroxide with chromium nitrate nonahydrate catalysed the decomposition of brucite to periclase and reduced the phase transformation temperature from 400^{o}C to 300^{o}C, as shown in Figure 3.1-11. This result is also in keeping with the TGA analysis. However, in powder XRD the phase transformation occurred at a lower temperature compared to TGA analysis. This can be explained in that prior to scanning when using hot stage powder XRD, the sample was held for 15 minutes after each 100^{o}C increment in temperature, whereas in the TGA the temperature was progressively increased at 10^{o}C min^{-1}. The average crystallite size from Table 3.1-3 indicates that doping of magnesium hydroxide with a chromium salt increased the crystallite size. This is an agreement with the results reported by Gilliant [20], who mentioned that doping of magnesium oxide with Mn increased the aggregation and increased the crystallite size.

The low metal loading and close resemblance between most of the powder XRD peaks of both the chromate and the magnesium oxide phases makes differentiating between them difficult. In the literature [31, 36] it was explained that up to 310^{o}C chromium was present in the form of an amorphous oxide mixture. However, with an increase of the calcination temperature, these amorphous oxide mixtures changed to the crystalline phases Cr_2O_5, CrO_3 and Cr_2O_3.

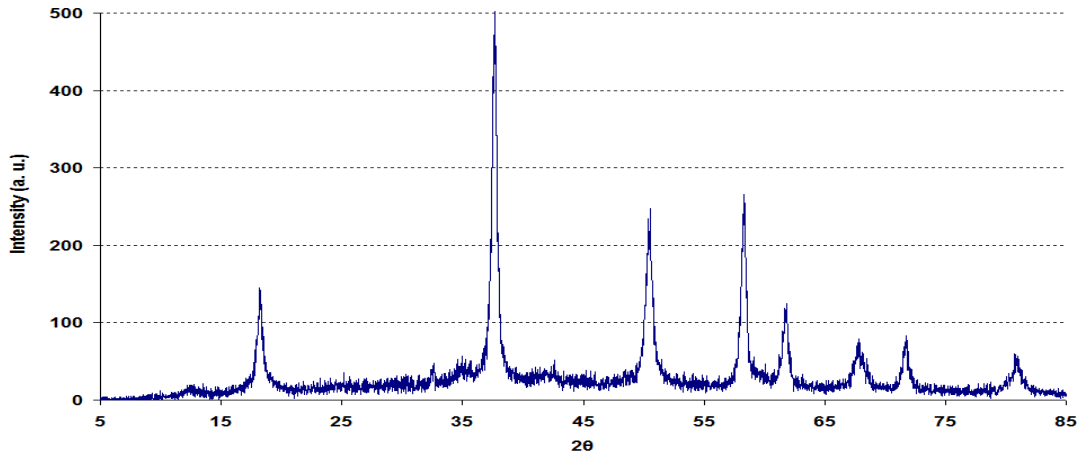

Figure 3.1-10 Powder XRD pattern of 4wt.% Cr/MgO catalyst at room temperature

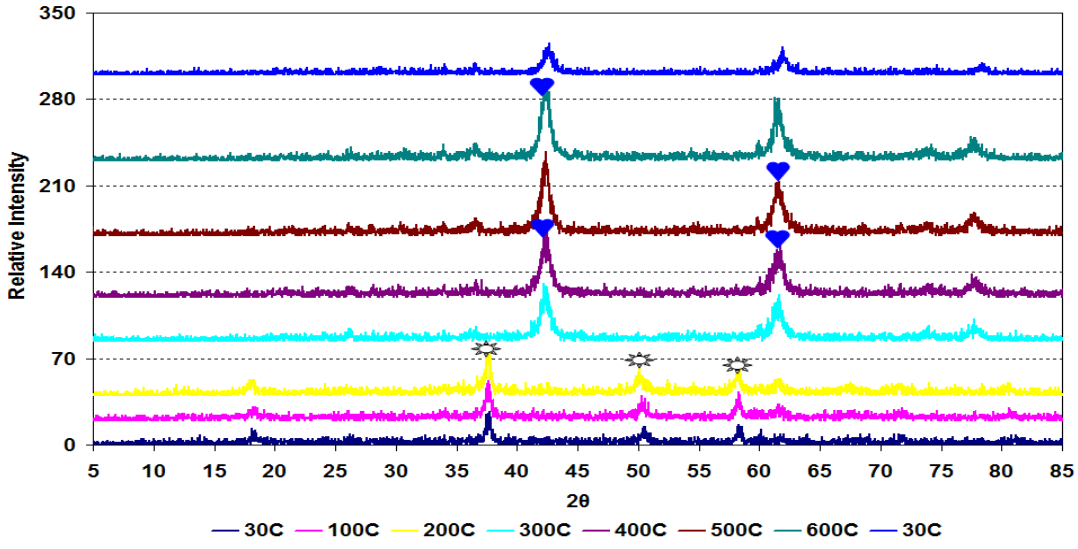

Figure 3.1-11 Hot-stage powder XRD patterns of 4wt.% Cr/MgO in an argon atmosphere. Phase denoted are (☼) magnesium hydroxide and (♥) magnesium oxide. The powder XRD patterns are offset for clarity.

Temperature (^{o}C)	29	100	200	300	400	500	600	29 final
Average crystallite size (Å)	254 (±7)	257 (±8)	213 (±5)	129 (±2)	117 (±5)	129 (±5)	103 (±4)	144 (±9)
Phase	Brucite			Periclase				

Table 3.1-3 Average crystallite size of the in-situ calcined 4wt.% Cr/MgO at different temperatures

3.1.2.3 BET analysis

The BET surface areas of the 4wt.% chromium-doped magnesium hydroxide sample after calcination at 100, 200, 300, 400, 500 and 600^{o}C for two hours were determined and the data obtained is tabulated in Table 3.1-4. It can be seen that the BET surface area of the chromium-doped magnesium hydroxide significantly decreased compared to the pure magnesium hydroxide by addition of the chromium salt to the magnesium hydroxide. This decrease in the BET surface area could be due to agglomeration and sintering in the particles by the addition of the chromium salt to the surface of the magnesium hydroxide, which is supported by the increase in crystallite size, as shown in Table 3.1-3. This result is in close agreement with the previous studies [19, 37, 38]. Matsudo *et al.* [19] mentioned that BET surface area of magnesium oxide decreased due to sintering caused by doping of magnesium oxide with sodium. The effect of temperature on the catalyst BET surface area can be divided into two portions corresponding to the two phases of the catalyst; brucite and periclase. With brucite, an increase in the calcination temperature from 100^{o}C to 200^{o}C had no significant effect on the BET surface area, whilst the average pore diameter and pore volume significantly increased. This change in average pore diameter and pore volume can be explained by the agglomeration and formation of cracks in the catalyst. Similarly, after completing the phase transformation from brucite to periclase the BET surface area and pore volume were significantly increased due to restructuring of the catalyst during the phase transformation. Further increase in the calcination temperature brought about little change in the BET surface area, whilst the pore volume slightly increased with an increase in the calcination temperature, due to an increase in the number of defects in the crystallites and the evolution of the remaining water present in catalyst framework.

Temperature (^{o}C)	BET Surface area (m^2/g)	Pore volume (cm^3/g)	Average pore diameter (Å)	Phase
100	33	0.08 (± 3.37)	162 (± 4.11)	Brucite
200	26	0.29 (± 0.94)	437 (± 5.73)	
300	81	0.49 (± 1.14)	238 (± 6.06)	Periclase
400	85	0.57 (± 1.24)	264 (± 6.60)	
500	87	0.69 (± 1.32)	309 (± 4.81)	
600	74	0.60 (± 0.48)	320 (± 6.38)	

Table 3.1-4 BET analysis of the 4wt.% Cr/MgO after calcination at different temperatures

3.1.2.4 UV-visible analysis

To investigate the change in the oxidation state of chromium at different temperatures and atmospheres, 4wt.% chromium-doped magnesium hydroxide was characterised using a UV-visible NIR spectrophotometer, as discussed in section 2.1.4. Figure.3.1-12 illustrates the UV-visible spectra of chromium-doped magnesium hydroxide taken at room temperature and after heat treatment at 600^{o}C in argon, oxygen and hydrogen atmospheres. The figure shows that at room temperature no change in the band positions were observed both in hydrogen and oxygen atmospheres, suggesting that at room temperature, atmosphere has no effect on the oxidation state of the chromium. The two bands (430 nm and 600 nm) at room temperature in UV-visible spectra matched with Cr^{III} in the literature [39]. However, the bands in the current results are slightly distorted and asymmetric due to interactions with the support.

When a sample was heated above 300^{o}C, changes in the oxidation state of chromium was initiated and were visible in the UV-visible (not shown here). The spectra obtained at 600^{o}C in different atmospheres are shown in Figure 1.3-12. The figure shows that the changes in the oxidation state of chromium are different in hydrogen and oxygen atmospheres. It shows that heating of the sample to 600^{o}C in an oxygen and argon atmosphere gives a band at 370 nm with a small shoulder at 440 nm. Donatti *et al.* [40] reported that these bands would be due to the $Cr^{V/VI}$. Similarly Rahman *et al.* [41] mentioned that increasing the heat treatment of the catalyst promotes the oxidation of chromium from III to VI. In contrast to the oxygen atmosphere, the UV-visible spectrum of the catalyst at 600^{o}C in a hydrogen environment shows that the band at 430 nm decreased whilst the 600 nm band was almost flat. These results suggest that in a hydrogen atmosphere the oxidation state of chromium is partially reduced. The exact oxidation state of chromium was not determined. However, a previous report [42] showed that reduction of chromium (Cr^{VI}) on alumina produced Cr^{II}.

These results indicate that at room temperature 4wt.% chromium-doped magnesium hydroxide catalyst has Cr^{III}, whilst at above 300^{o}C, oxidation of chromium changed to VI/V and II/III in oxygen and hydrogen atmosphere respectively.

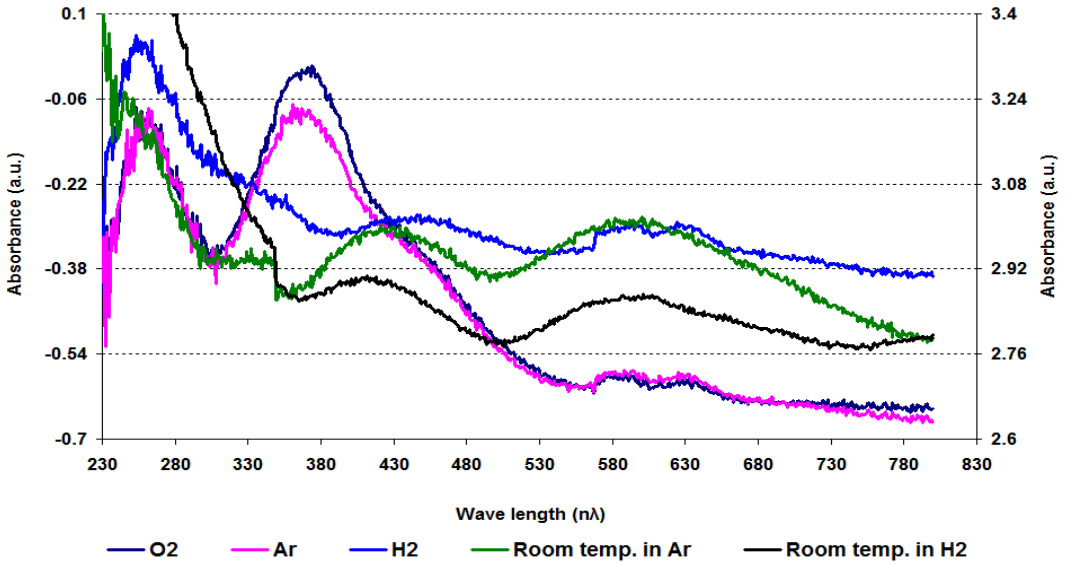

Figure 3.1-12 UV-visible spectra of 4wt.% CrMgO at different temperatures and atmospheres

3.1.3 4mol.% Cr/MgO

3.1.3.1 TGA/DSC

The TGA profile in Figure 3.1-13 illustrates that the total weight loss up to 800^{o}C of the 4mol.% chromium-doped magnesium hydroxide catalyst is 38.5% as expected from decomposition because it contains 1.2% more chromium metal than the 4wt.% chromium-doped magnesium hydroxide catalyst. Like the 4wt.% chromium-doped magnesium hydroxide catalyst, the major weight loss took place between 275^{o}C to 390^{o}C in the form of two peaks at 336^{o}C and 367^{o}C. The small change to the high temperature shoulder suggests that the rate of nitrate decomposition changed. In the heat flow profile (not shown), the major weight loss between 275^{o}C to 390^{o}C corresponds to an endothermic peak matching to the evolution of nitrogen monoxide and water as expected, as seen in Figure 3.1-14 but no prominent peak for nitrogen dioxide was observed. The derivative weight profile shows a small weight loss between 400^{o}C and 500^{o}C. This weight loss may be due to evolution of oxygen, produced from the transformation of Cr_xO_y to Cr_2O_3, as discussed before. These results indicate that an increase in chromium loading does not have a significant effect on the dehydration temperature of brucite to periclase and the catalyst follows a similar pattern as was observed in the 4wt.% chromium-doped magnesium oxide catalyst.

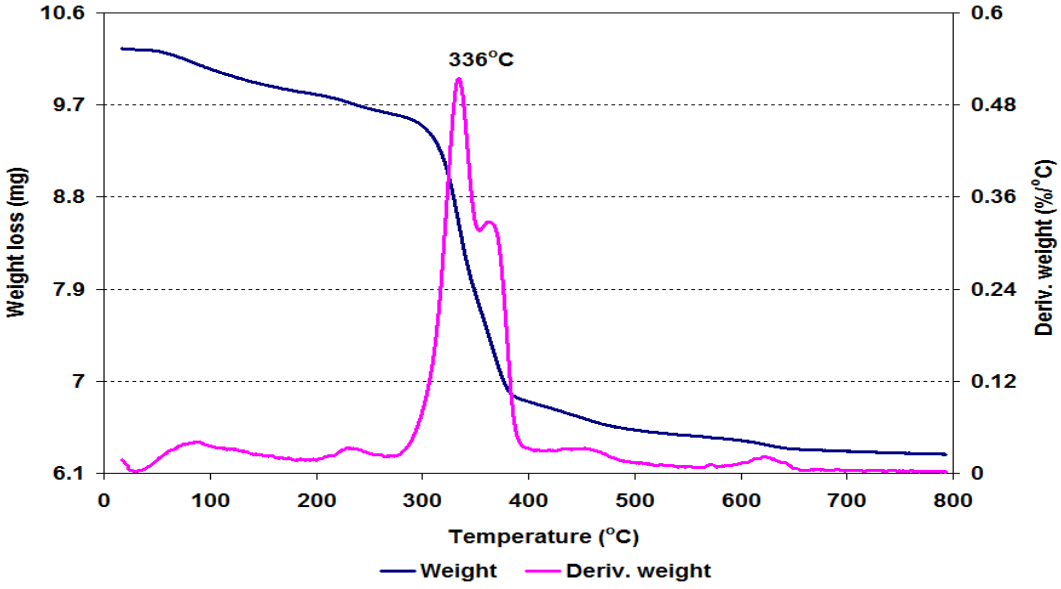

Figure 3.1-13 TGA and derivative weight of 4mol.% Cr/MgO in an argon atmosphere

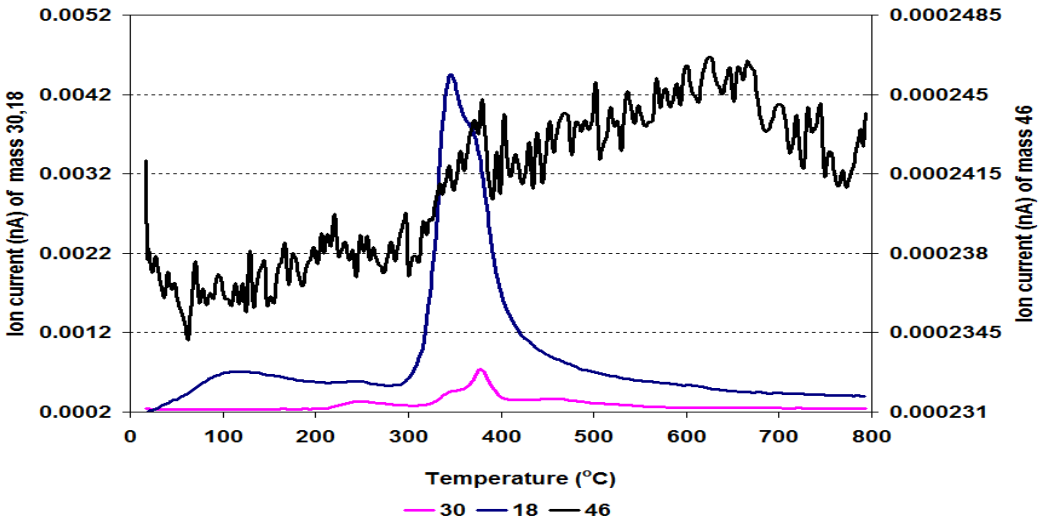

Figure 3.1-14 MS data of NO_2 (m/z= 46), NO (m/z= 30) and H_2O (m/z=18) for 4mol.% Cr/MgO in an argon atmosphere

3.1.3.2 BET

The BET surface areas of 4mol.% chromium-doped magnesium hydroxide samples and the catalyst after calcination at 100, 200, 300, 400, 500 and 600°C for two hours were determined and the data is tabulated in Table 3.1-5. Similar to the 4wt.% Cr/MgO catalyst, the 4mol.% chromium metal loading significantly decreased the BET surface area compared to pure magnesium hydroxide. The changes to the BET surface area, average pore diameter and pore volume follow similar patterns to that seen with the 4wt.% Cr/MgO catalyst. In the brucite form, the BET surface area, average pore diameter and pore volume

were small, whereas for periclase they were significantly increased. These increases can be explained due to restructuring and the formation of defects by phase transformation, as discussed in section 3.1.1.3. After phase transformation, a further increase in the calcination temperature steadily increased the BET surface area except at 600^{o}C where it slightly decreased. The decrease in BET surface area at 600^{o}C may be due to sintering of the catalyst.

Temperature (^{o}C)	BET Surface area (m^2/g)	Pore volume (cm^3/g)	Average pore diameter (Å)	Phase
100	31	0.12 (± 3.33)	149 (± 2.39)	Brucite
200	24	0.12 (± 0.0)	194 (± 3.36)	
300	79	0.54 (± 2.12)	260 (± 7.20)	Periclase
400	86	0.54 (± 0.91)	247 (± 4.73)	
500	89	0.58 (± 1.08)	257 (± 3.77)	
600	76	0.45 (± 3.26)	228 (± 4.38)	

Table 3.1-5 BET analysis of 4mol.% Cr/MgO after calcinations at different temperatures

3.2 Catalyst testing

The synthesis of acrylonitrile from methanol and acetonitrile was performed over the magnesium oxide and the chromium-doped magnesium oxide catalysts to investigate any trends and differences as discussed in section 2.2. Before the reaction each catalyst was pre-treated, as shown in Table 3.2-1

$$CH_3CN + CH_3OH \rightarrow CH_2{=}CHCN + H_2 + H_2O \quad (3.4)$$

Temperature (^{o}C)	Ramp (^{o}C/min)	Hold time (hrs)	Atmosphere
600	5	2	Argon

Table 3.2-1 Pre reaction treatment of the catalyst

3.2.1 MgO

The magnesium oxide catalyst was investigated at different temperatures to determine if it showed activity towards the formation of acrylonitrile from methanol and acetonitrile. Figure 3.2-1 shows the conversion of methanol and acetonitrile over the pure magnesium oxide catalyst. It also illustrates the yield of hydrogen at the different temperatures. The

figure shows that the conversion of acetonitrile over the pure magnesium oxide catalyst was low up to 420^{o}C and then slightly increased. This indicates that the pure magnesium oxide catalyst is not active towards acetonitrile conversion and no acrylonitrile was detected up to 550^{o}C. These results suggest that both strong acidic and basic sites over the catalyst are necessary for the synthesis of acrylonitrile. Pure magnesium oxide catalyst does not have the strong acidic sites to stabilise the carbanion formed from acetonitrile, therefore no acrylonitrile was detected over the pure magnesium oxide [43].

The conversion of methanol was low at 300^{o}C but increased with increasing reaction temperature and reached 100% at 550^{o}C. With the increase in the methanol conversion the formation of hydrogen also increased. It is inferred that the methanol oxidized to form formaldehyde and hydrogen.

$$CH_3OH \rightarrow HCHO + H_2 \qquad (3.5)$$

It may be also possible that methanol underwent decomposition and formed H_2 and CO. However, no CO was observed and the yield of H_2 was very small which suggests that no methanol decomposition took place.

$$CH_3OH \rightarrow CO + 2H_2 \qquad (3.6)$$

So, it is believed that with an increase in the reaction temperature, methanol deposition took place on catalyst surface in the form of coke, which will be discussed in detail in section 3.2.3.2.

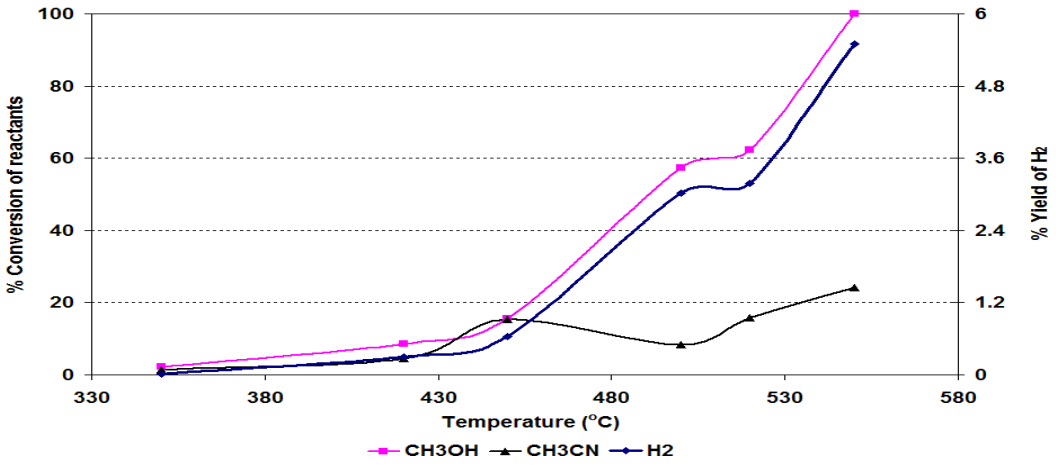

Figure 3.2-1 % Conversions of reactants and % yield of products at different temperatures in an argon atmosphere over pure MgO catalyst

3.2.2 4wt.% Cr/MgO

Synthesis of acrylonitrile from methanol and acetonitrile was carried out over the 4wt.% chromium-doped magnesium oxide catalyst at different temperatures to investigate the activity and selectivity of the catalyst towards acrylonitrile formation. The conversion of the reactants and the yields of products were calculated as discussed in section 2.2.4. The data obtained is plotted in Figure 3.2-2. The figure shows that at 410^{o}C there was high activity and selectivity towards acrylonitrile. A further increase in the reaction temperature decreased both the acetonitrile conversion and acrylonitrile yield with the yield of acrylonitrile at almost zero by 550^{o}C. This suggests that the active sites on the 4wt.% chromium-doped magnesium oxide catalyst for acetonitrile conversion were present between 410 and 450^{o}C but deactivated at higher temperatures, which also supported by Hur *et al.* [23].

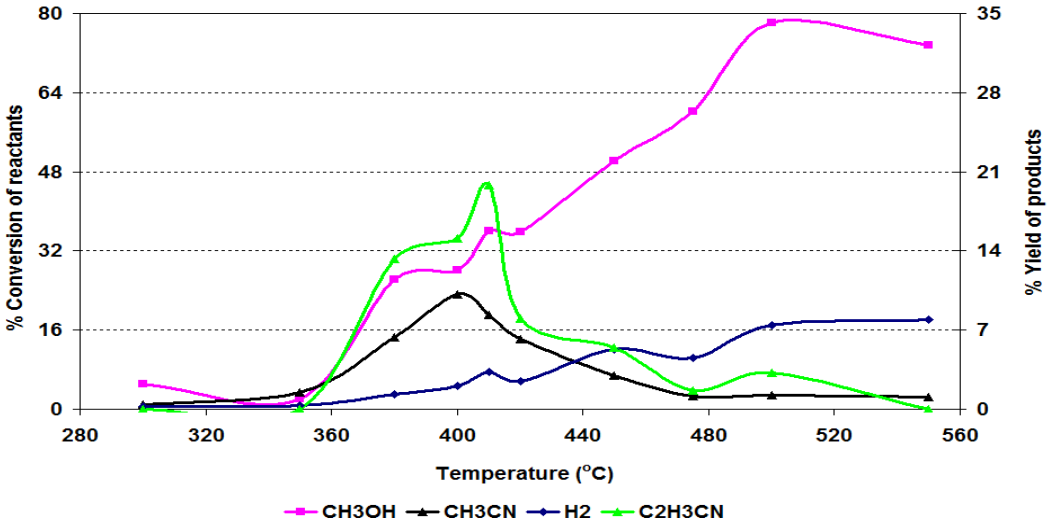

Figure 3.2-2 % Conversions of reactants and % yield of products at different temperatures in an argon atmosphere over the 4wt.% Cr/MgO catalyst

Similarly, methanol conversion increased up to 500^{o}C and then started to decrease as the temperature was further increased. This reveals that at high temperatures the active sites for methanol dehydrogenation becomes deactivated, which is in close agreement with the literature [44]. Figure 3.2-2 indicates that two types of reactions took place over the catalyst at different temperatures. At low temperature (< 450^{o}C) the main reaction is the formation of acrylonitrile from methanol and acetonitrile, while at high temperature, due to formation of coke on the surface of the catalyst the active sites for acrylonitrile were deactivated.

$$CH_3OH + CH_3CN \rightarrow C_2H_3CN + H_2O + H_2 \quad \text{(low temperature)} \qquad (3.7)$$

$$CH_3OH + CH_3CN \rightarrow \text{Coke} + H_2 \quad \text{(high temperature)} \qquad (3.8)$$

These results show that addition of a chromium salt has a synergetic effect on the magnesium hydroxide and the modification of the catalyst has enhanced the proton abstraction property of the catalyst to facilitate forming acrylonitrile from methanol and acetonitrile. This may be explained as the chromium is more acidic than the magnesium, and therefore the carbanion formed by deprotonation of acetonitrile at the basic sites on the oxide catalyst would be more stable over the chromium than the magnesium. Ultimately, cleavage of the C-H bond of the methyl groups would be more feasible on the chromium-doped magnesium oxide catalyst. Xie *et al.* [24] reported that bifunctional properties of chromium-doped magnesium oxide decreased the dissociation temperature for acetonitrile and methanol.

The 4wt.% chromium-doped magnesium oxide catalyst gave 100% selectivity towards acrylonitrile with respect to acetonitrile and no propionitrile was produced. The 100% selectivity towards acrylonitrile could be explained in two ways. Firstly, the chromium present on the magnesium oxide surface when calcined at 600^{o}C is oxidised from the III to VI/V oxidation state. The $Cr^{VI/V}$ present on the surface of magnesium oxide may enhance the dehydration of the reaction intermediate. These enhanced properties of chromium on different supports such as alumina, silica and zirconia, are different as explained by Weckhuysen *et al.* [35] in their review. Therefore, enhancement of selectivity to acrylonitrile could be due to chromium doping on magnesium oxide where chromium is present in its VI/V oxidation state.

The second reason for the enhancement of the acrylonitrile formation could be due to the use of a 1:1 ratio of methanol and acetonitrile, in contrast to previous studies which have used 10:1 ratio of methanol to acetonitrile. The use of more acetonitrile could suppress the complete oxidation of methanol to CO_x and H_2 and increase the methanol dehydrogenation rate [45].

3.2.3 4mol.% Cr/MgO

The conversion of methanol and acetonitrile and the yield of products over the 4mol.% chromium-doped magnesium oxide catalyst at different temperatures are shown in Figure 3.2-3. The figure illustrates that over the 4mol.% chromium-doped magnesium oxide catalyst the formation of acrylonitrile at different temperatures varies, as was also observed

with 4wt.% chromium-doped magnesium oxide. At first it increased from 350°C to 420°C and then remained stable up until 450°C. Further increase in temperature to above 450°C, decreased the formation of acrylonitrile to almost zero by 500°C. This data shows that chromium loading plays an important role in the activity and selectivity towards the formation of acrylonitrile. An increase in chromium loading above 4wt.% decreases the yield of acrylonitrile, as clearly seen in Figures 3.2-2 and 3.2-3. Kurokawa [46] claimed that the conversion of acetonitrile decreased above 3wt.% chromium loading whereas the selectivity toward acrylonitrile remained similar. Contrastingly, the present investigation shows the increase in chromium loading increased the conversion of acetonitrile and methanol. However, deactivation of methanol and acrylonitrile occurred at a relatively low temperature *i.e.* 500°C and no acrylonitrile was produced at ≥ 500°C. Also, the temperature for the maximum yield of acrylonitrile was shifted from 410°C to 420°C. The quick deactivation suggests that increased chromium loading on the magnesium oxide increased the coke formation and blocked the sites for methanol conversion and significantly decreased the yield of acrylonitrile. From these results, it is recognised that the temperature at which the maximum yield of acrylonitrile was obtained also varies with the loading of chromium, as illustrated by Figures 3.2-2 and 3.2-3.

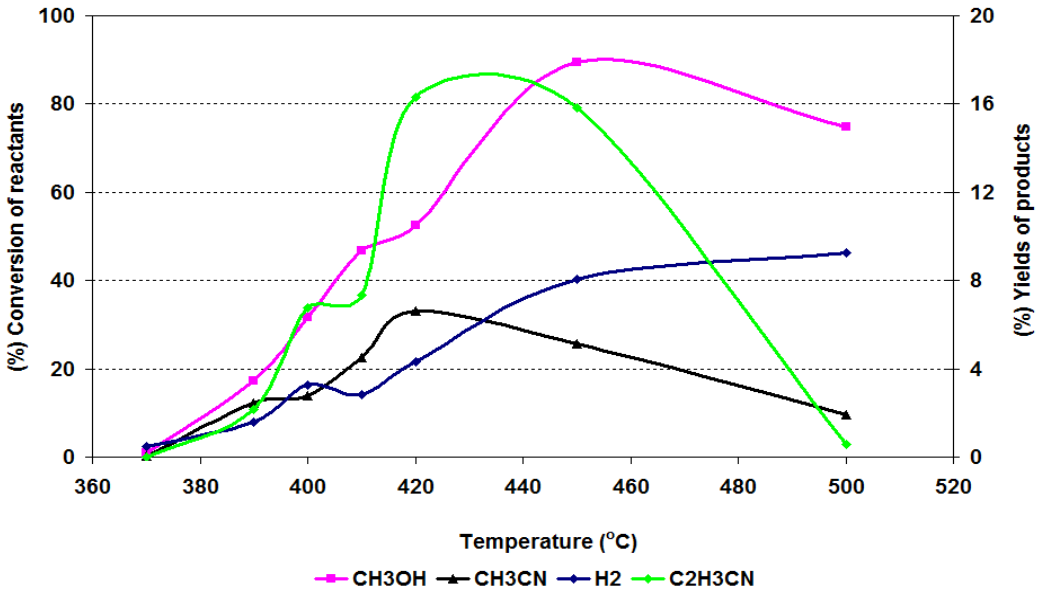

Figure 3.2-3 % Conversions of reactants and % yield of products at different temperatures in an argon atmosphere over the 4mol.% Cr/MgO catalyst

3.2.3.1 Lifetime of catalyst at different temperatures

To determine the lifetime of the catalyst at different temperatures the reaction was conducted over the 4mol.% chromium-doped magnesium oxide catalyst and the data

obtained are shown in Figures 3.2-4 to 3.2-6. Figure 3.2-4 shows that the reaction at 410^{o}C gives a low yield for acrylonitrile. However, catalyst deactivation for acrylonitrile formation took place throughout the 42 hrs TOS. It shows that at low temperatures, the catalyst was active for a longer time compared to the reaction run at high temperature. The catalyst deactivation may be due to a decrease in the dehydrogenation of methanol due to formation of coke on the catalyst surface, as supported by Figure 3.2-4. Figure 3.2-5 illustrates that the reaction at 420^{o}C gave the highest yield of acrylonitrile, which was almost double *i.e.* 14.75% that obtained through reaction at 410^{o}C. The increase in acrylonitrile yield may be due to an increase in both the conversion of acetonitrile and methanol. However, catalyst deactivation occurred faster than was observed at 410^{o}C. The reaction at 450^{o}C gave a similar yield of acrylonitrile as was observed at 420^{o}C. The conversion of methanol and acetonitrile increased with an increase of the reaction temperature. However, deactivation of the catalyst at 450^{o}C happened more rapidly than when compared to the catalyst at 420^{o}C. From the deactivation profile, it can be elucidated that the rate of deactivation increased with an increase in the reaction temperature from 420 to 450^{o}C. This suggests that the active sites for acrylonitrile formation, which are present at 420^{o}C, were deactivated by 450^{o}C due to an increase in the rate of coke formation. This increase in deactivation inferred that temperature plays an important role in coke formation over the 4mol.% chromium-doped magnesium oxide catalyst. The rate of formation of hydrogen increased with an increase in methanol conversion, which revealed that it was formed from the oxidation of methanol.

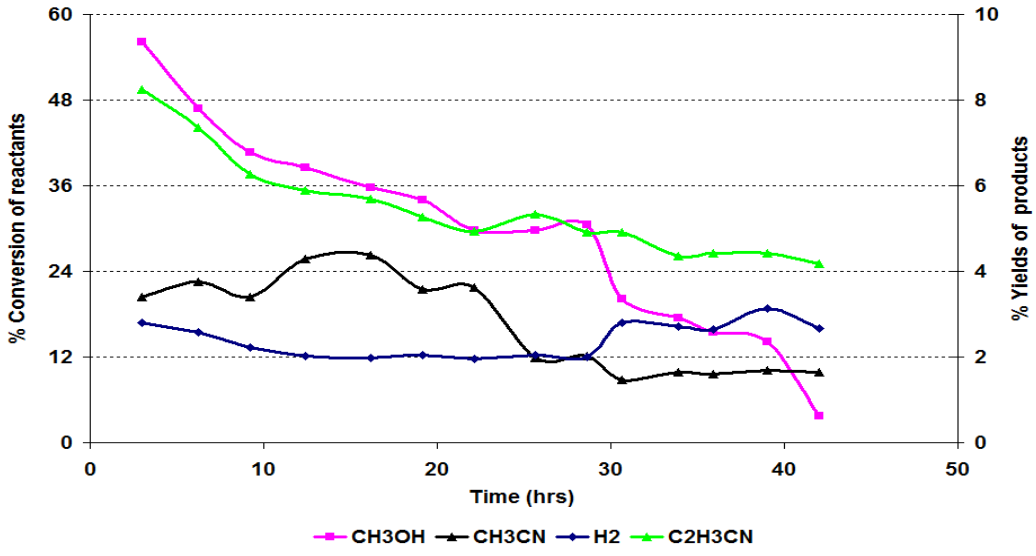

Figure 3.2-4 % Conversions of reactants and the % yield of products as function of TOS at 410^{o}C in an argon atmosphere

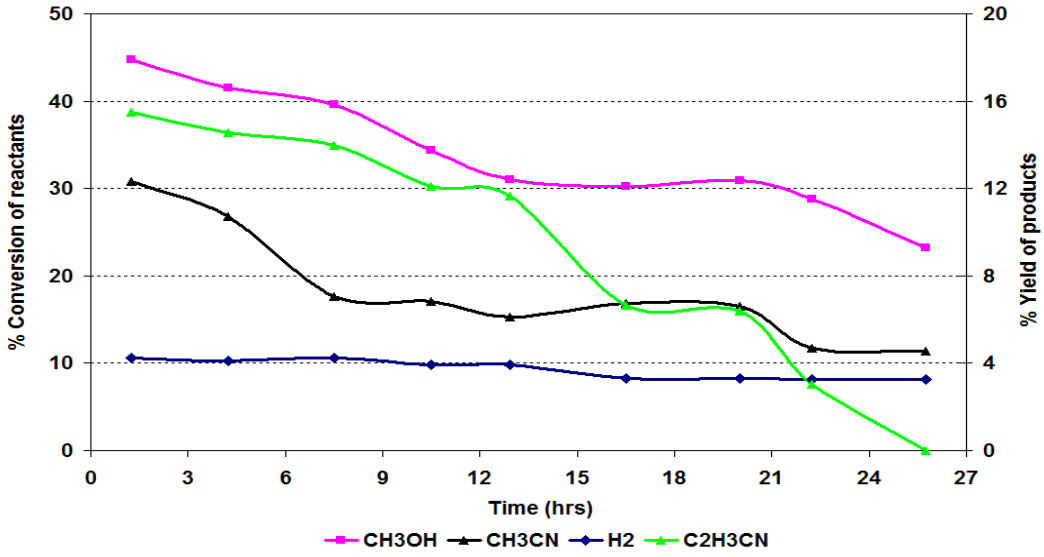

Figure 3.2-5 % Conversions of reactants and % yield of products as function of TOS at 420°C in an argon atmosphere

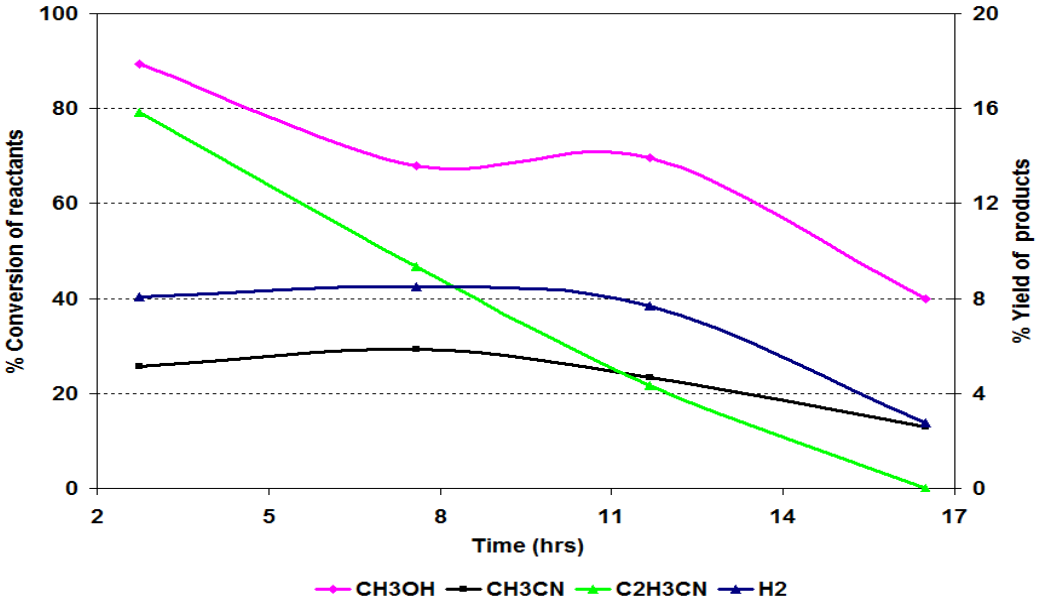

Figure 3.2-6 % Conversions of reactants and % yield of products as function of TOS at 450°C in an argon atmosphere

3.2.3.2 Deactivation

The catalyst lost about 100% of its initial activity towards acrylonitrile at different rates depending upon the reaction temperature, as shown in section 3.2.3.1. Post reaction characterisation of the deactivated catalysts was performed using techniques such as powder XRD, TPO, UV-visible spectroscopy and BET analysis to determine the cause of the catalyst deactivation. By comparing the BET surface areas, the average pore diameters and the average crystallite sizes of the catalyst particles before and after the reaction, it is

possible to determine whether deactivation of the catalyst was due to the sintering of crystals, coke formation or another reason. In Figure 3.2-7, the powder XRD patterns at 600°C and after the reaction performed at 410°C are compared. The average crystallite size of each sample was calculated using the Scherrer equation and the BET surface area was run using liquid nitrogen adsorption isotherm, as discussed in section 2.1. Table 3.2-2 shows that the crystallite size slightly increased while the BET surface area of the 4mol.% chromium-doped magnesium oxide decreased after the reaction conducted at 410°C. However, the average pore diameter and pore volume increased [47]. This data suggests that only very slight sintering of catalyst took place during the reaction. The sintering of the catalyst increased the average pore diameter whilst decreasing the BET surface area.

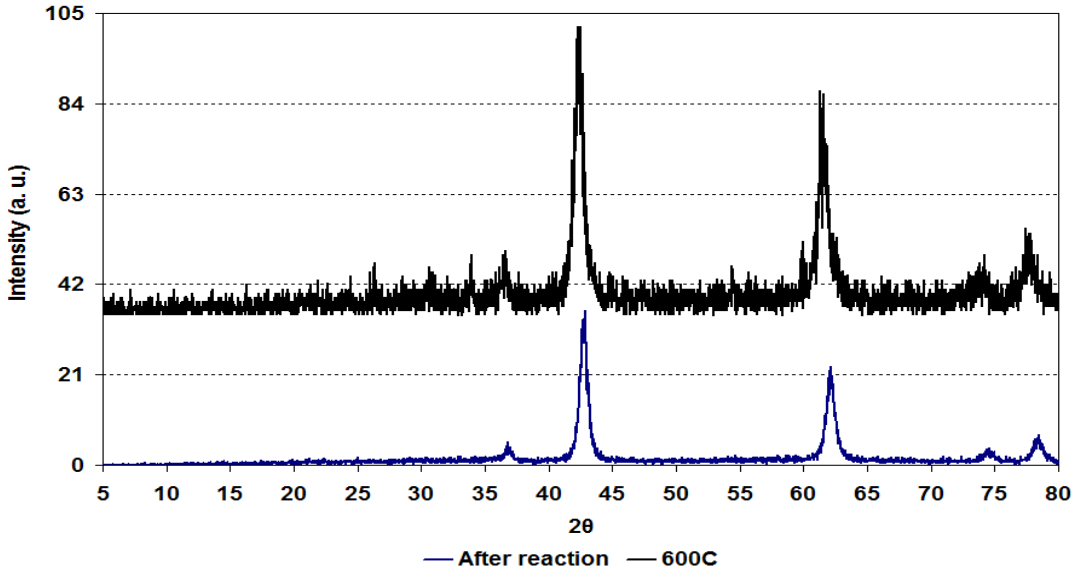

Figure 3.2-7 Powder XRD patterns of 4mol.% Cr/MgO catalyst before and after reaction

Catalyst	BET Surface area (m^2/g)	Pore volume (cm^3/g)	Average pore diameter (Å)	Average crystallite size (Å)
Before reaction	76	0.45 (± 3.26)	228 (± 4.38)	131 (± 4)
After reaction	66	0.50 (± 1.14)	298 (± 2.37)	139 (± 5)

Table 3.2-2 BET surface area and average crystallite size of 4mol.% Cr/MgO catalyst before and after reaction

3.2.3.3 Temperature programmed oxidation (TPO)

To check if any carbonaceous materials were deposited over the catalyst during the reaction, a TPO was carried in 2% O_2/Ar from room temperature to 800°C. The TPO profile shown in Figure 3.2-8 shows a 13% weight loss occurring up to 800°C for the post-

reaction 4mol.% chromium-doped magnesium oxide catalyst. From the weight loss profile, it is clear that the main weight loss occurred between 390^{o}C to 590^{o}C. From the mass spectrometry results shown in Figure 3.2-9, this weight loss corresponds to the evolution of CO_2 and CO. The coke laydown increased with an increase in the reaction temperature. Therefore, it is suggested that one of the catalyst deactivation routes could be due to the deposition of coke on the catalyst surface, which blocked the active sites for the reaction. Mass fragments with m/z values of H_2 (2), water (18), acrylonitrile (53) and acetonitrile (41) were also checked for with mass spectrometry but no prominent peaks were observed for these masses. This suggests that in the TPO amorphous type coke was oxidized to form CO (28) and CO_2 (44). However, when one of samples was analysed by in-situ TPO (not shown here), it gave trace amounts of m/z = acrylonitrile (53), methoxy (31) and formaldehyde (29) as well as CO (28) and CO_2 (44). These results indicate that the methanol first dehydrogenates to form formaldehyde and then the formaldehyde reacts with acetonitrile to produce acrylonitrile, as reported in the literature [11].

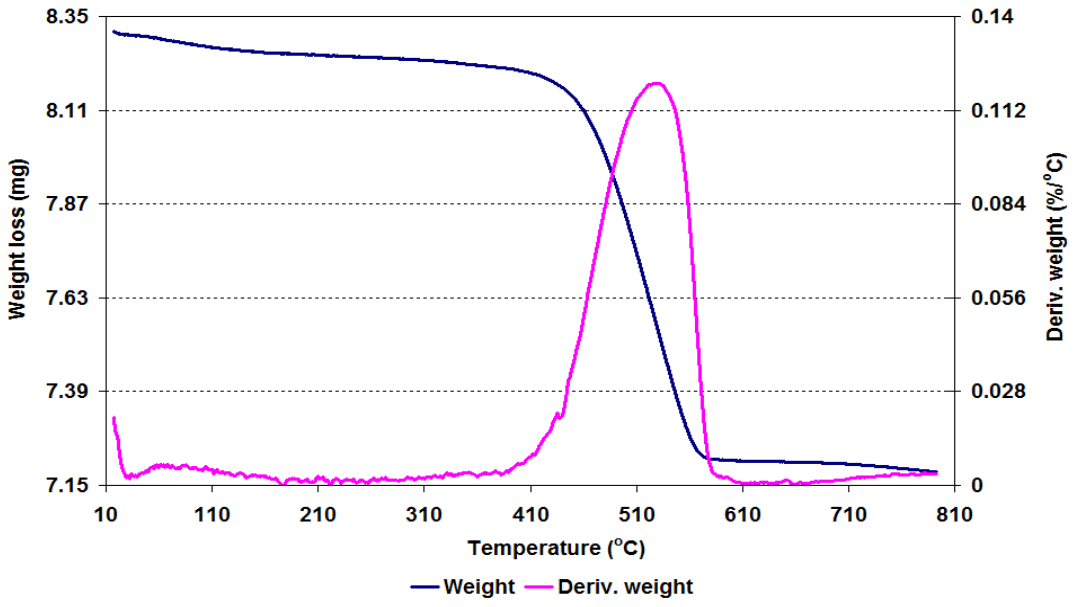

Figure 3.2-8 Post reaction TPO for the 4mol.% Cr/MgO catalyst that was run at a different temperatures

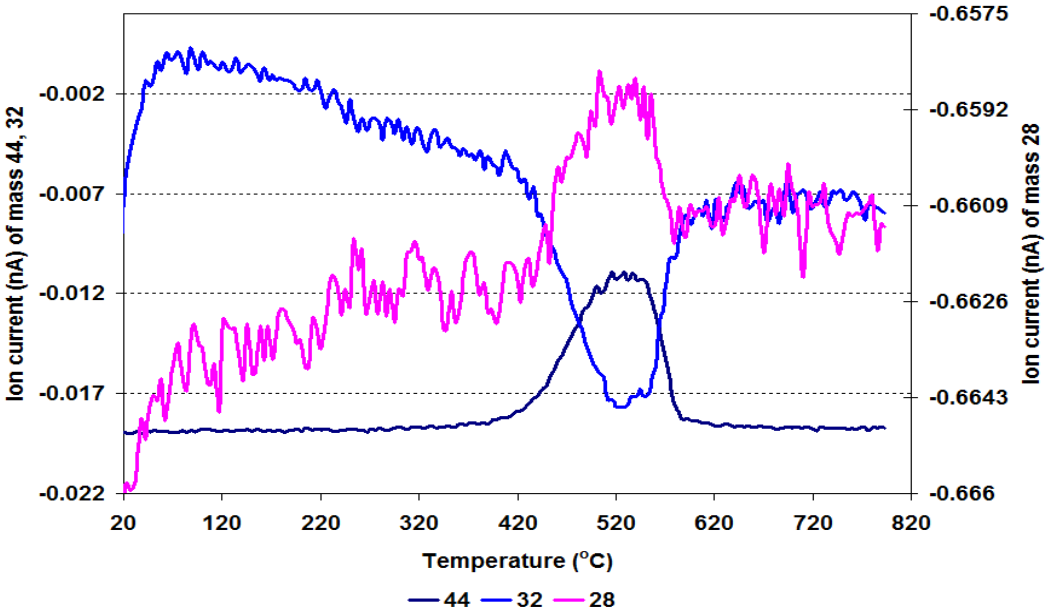

Figure 3.2-9 MS data of CO_2 (m/z=44), O_2 (m/z=32) and CO (m/z=28) for the 4mol.% Cr/MgO catalyst that was run at different temperatures

Figure 3.2-10 shows the UV-visible spectra of 4mol.% chromium-doped magnesium oxide catalyst calcined in-situ in an argon atmosphere at 600^{o}C and for post reaction 4mol.% chromium-doped magnesium oxide catalysts. The spectra of the post reaction catalysts show that the oxidation state of chromium changed after the reaction. The change in the oxidation state is clearer from the UV-visible spectra of both the reaction samples run at 410^{o}C and 450^{o}C, which show that during the reaction $Cr^{VI/V}$ present on the catalyst surface was reduced to a lower oxidation state chromium [40]. The change in the oxidation state of chromium has a significant influence on the yields of acrylonitrile [48].

In summary, from the BET, UV-visible spectroscopy, TPO and powder XRD analysis of the post reaction samples run at different temperatures, it was seen that deactivation of the catalysts towards acrylonitrile not only took place due to the deposition of coke on the catalyst surface but by a combined effect with a change in oxidation state of chromium, particle sintering and coke formation on the surface of the catalyst. Most importantly is the oxidation state of chromium VI/V, which decreased to a lower oxidation state chromium. This decrease possibly occurred due to the hydrogen produced during the formation of carbanions from the acetonitrile and from the dehydrogenation of methanol to formaldehyde.

$$CH_3CN \rightarrow {}^{-}CH_2CN + H^{+} \quad (3.9)$$

$$CH_3OH \rightarrow CH_2O + H_2 \quad (3.10)$$

This is supported by the regeneration of the catalyst at the reaction temperature, which gave acrylonitrile at 410^{o}C, despite oxidation of the coke to carbon dioxide occurring at a relatively high temperature.

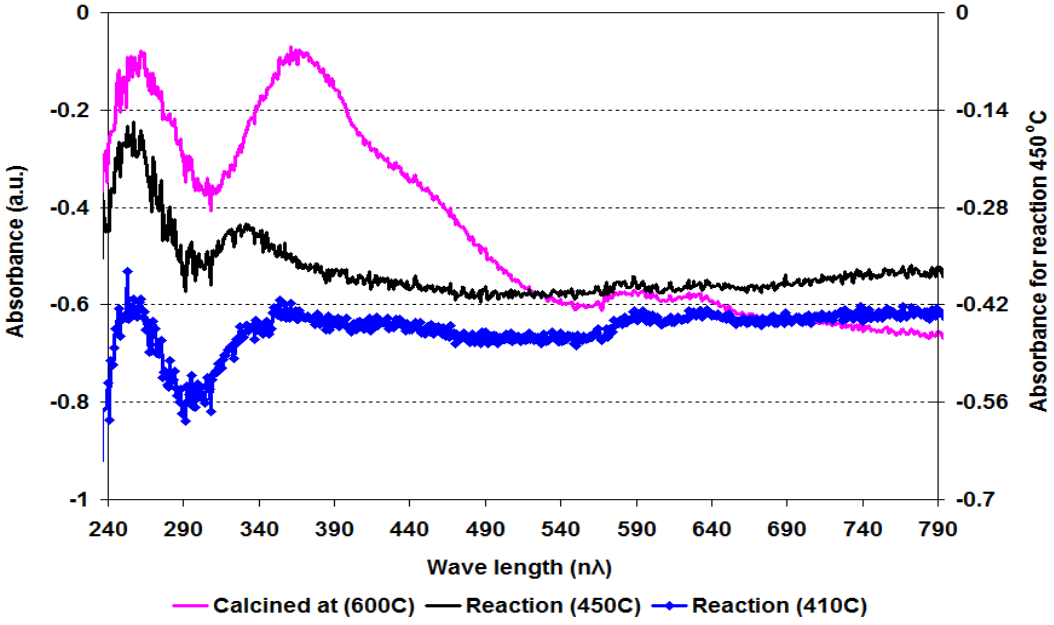

Figure 3.2-10 UV-visible spectra of 4mol.% Cr/MgO before and after reaction

3.2.3.4 Regeneration of the catalyst

The TPO results show that the removal of coke from the catalyst took place between 390^{o}C to 590^{o}C. To determine whether regeneration of the catalyst took place only above 500^{o}C or if it also occurred at lower temperature, the 4mol.% chromium-doped magnesium oxide catalyst was regenerated in-situ at 410^{o}C (reaction temperature) in a 2% O_2/Ar atmosphere for 16 hours and then run the reaction at 410^{o}C, as shown in Figures 3.2-11 and 3.2-12. These figures illustrate that the activity of the catalyst was similar to the activity shown by the pre-treatment calcined sample. However, the deactivation of regenerated catalyst occurred faster when compared to the pre-treatment calcined catalyst. When the catalyst was regenerated at a higher temperature (600^{o}C), it was active for synthesis of acrylonitrile for a longer time. This suggests that at higher temperatures both the removal of the coke deposits as well as chromium oxidation to $Cr^{VI/V}$ occurred, which increased the activity of the catalyst towards acrylonitrile for a longer time. However, at lower temperature regeneration, only the oxidation of chromium would occur. Similarly, the regeneration of the catalyst at higher temperatures also enhanced the conversions of methanol and

acetonitrile, as shown in Figure 3.2-13. In short, the deactivation of the catalyst was not permanent and it was regenerated at both low and high temperatures.

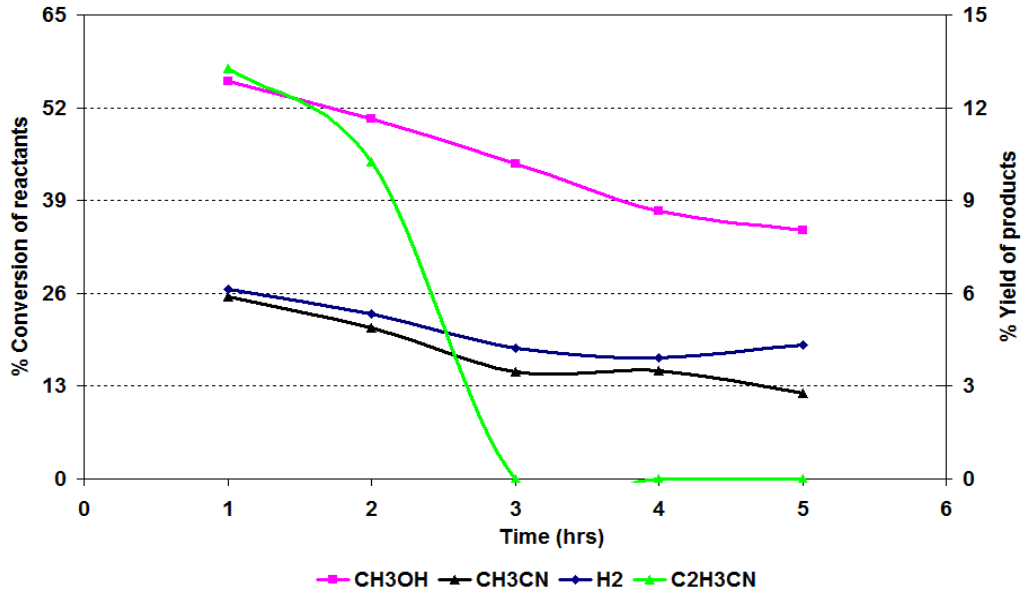

Figure 3.2-11 First regeneration of the 4mol.% Cr/MgO catalyst at 410°C in 2% O_2/Ar atmosphere

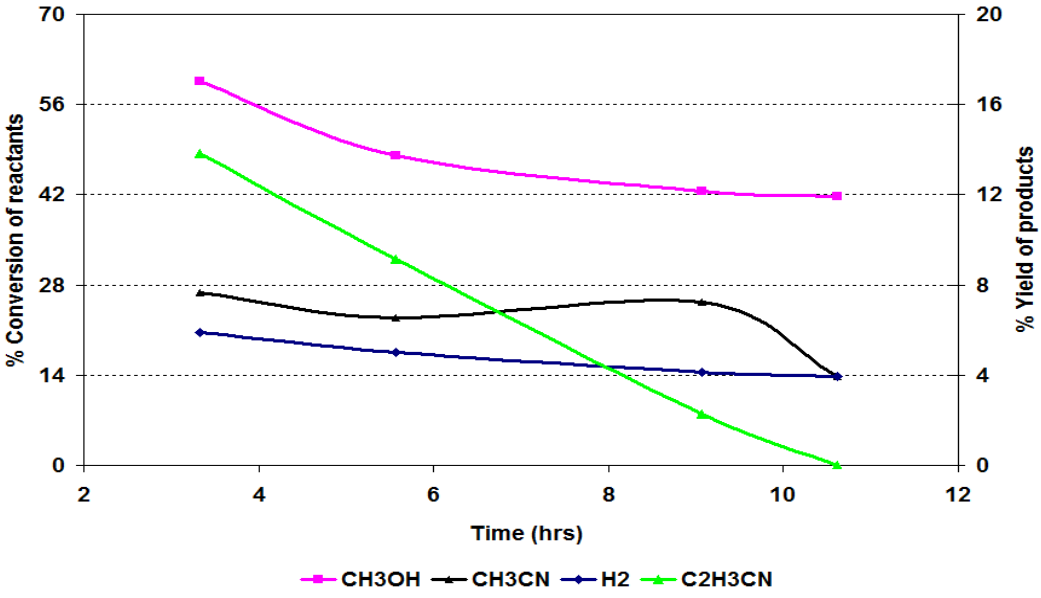

Figure 3.2-12 Second regeneration of the 4mol.% Cr/MgO catalyst at 410°C in 2% O_2/Ar atmosphere

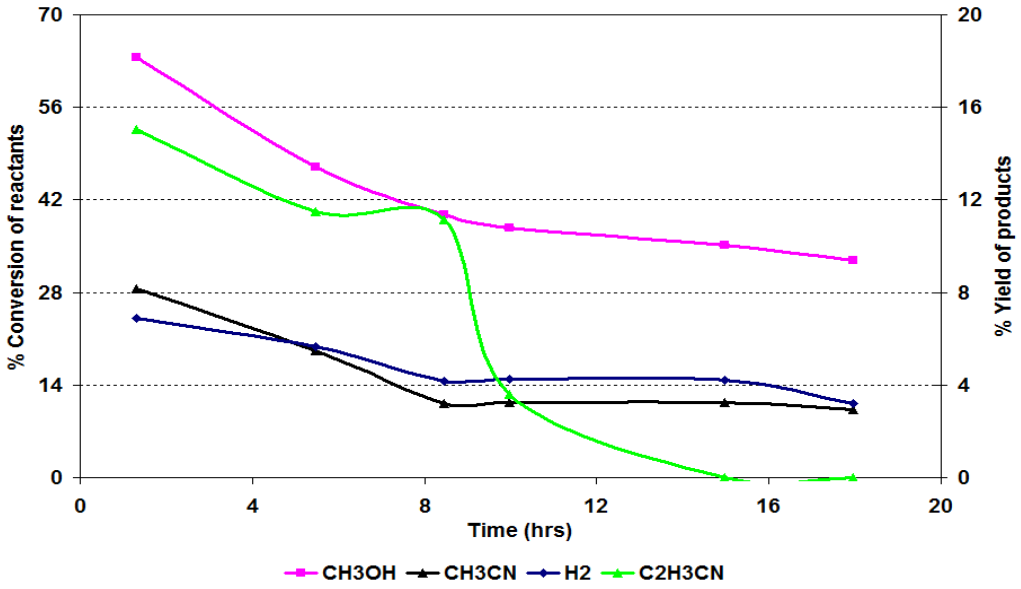

Figure 3.2-13 First regeneration of the 4mol.% Cr/MgO catalyst at 600°C in 2% O_2/Ar atmosphere

3.3 Catalyst ageing

After approximately one year the reaction was repeated over both the 4wt.% and 4mol.% Cr/MgO catalysts and neither produced acrylonitrile, although the same pre-treatment reaction conditions were used. Then pre-reduction and pre-calcination of the catalyst was tried in 2% H_2/N_2 and 2% O_2/Ar atmospheres respectively and still no acrylonitrile was produced. The catalysts were again analysed by powder XRD and UV-visible to check for any changes in the catalyst morphology but no significant changes were observed.

These results suggest that initially the chromium is present on the surface of the MgO crystallite but with time moves into the bulk. The effective concentration of chromium on the surface then becomes considerably reduced and the activity mirrors that of pure MgO. It was decided not to investigate this ageing effect and therefore cease work on this project.

4. Conclusions

The aim of this project was to study the synthesis of acrylonitrile from methanol and acetonitrile over the Cr/MgO catalyst. Initially the catalyst was prepared by an impregnation method and characterised using different techniques. From the TGA/DSC and powder XRD analysis it was established that the impregnation of pure magnesium hydroxide with chromium salt decreased the dehydration temperature of the magnesium hydroxide to magnesium oxide and gave a large crystallite size due to sintering of the catalyst. The BET surface area analysis showed that the doping of chromium salt on magnesium hydroxide significantly decreased the BET surface area and increased the average pore diameter, inferring that sintering of the magnesium hydroxide took place. Calcination of the catalyst at different temperatures indicated that after the phase transformation from brucite to periclase, the BET surface area and the average pore diameter were significantly increased due to restructuring of the crystal framework and formation of many defects in the catalyst structure.

The synthesis of acrylonitrile from methanol and acetonitrile showed that Cr/MgO gave 100% selectivity towards acrylonitrile and no propionitrile was observed. It was found that $Cr^{VI/V}$ played an important role in the formation of acrylonitrile from methanol and acetonitrile reaction and acts as good stabiliser for the acetonitrile carbanion. An increase in the reaction temperature increased the formation of acrylonitrile. However, with an increase in the reaction temperature, there was also an increase in the deactivation of the catalyst.

Post reaction characterisation of the catalyst indicates that deactivation of the catalyst for the acrylonitrile formation occurred due to the reduction of the chromium from a VI/V oxidation state to a lower oxidation state and deposition of coke on the catalyst surface. The deposition of coke played an important role in the deactivation of methanol and acetonitrile conversion over the Cr/MgO catalyst. However, the deactivation of the catalyst was not permanent and the catalysts can be regenerated by TPO.

5. References

[1] C.H. Bartholomew, R.J. Farrauto, Fundamentals of Industrial Catalytic Processes, 2nd ed., John Wiley and Sons, New Jersey, 2006.
[2] J.F.L. Page, Applied Heterogeneous Catalysis: Design, Manufacture and Use of the Solid Catalysts CRC Press, Paris, 1986.
[3] J.R. Anderson, M. Boudart, Catalysis: Science and Technology, in, Springer, New York, 1981, pp. 309.
[4] J.A. Anderson, M.F. Garcia, Supported Metals in Catalysis in: G.J. Hutchings (Ed.) Catalytic Science Series Imperial College Press, London, 2005, pp. 368.
[5] A. Takashi, Inorganic Solid Supported Reagents as Acids and Bases, in: H. Hideshi, M. Makoto, O. Yoshio (Eds.) Studies in Surface Science and Catalysis, Elsevier, 1994, pp. 9-20.
[6] J.F. Brazdil, Acrylonitrile, in: J.I. Kroschwitz, M. Howe-Grant (Eds.) Encyclopedia of Chemical Technology, John Wily and Sons New York, 1991, pp. 352-369.
[7] S.D. Jackson, S.J.J. Hargreaves, Metal Oxide Catalysis, Wiley-VCH, 2009.
[8] http://www.sriconsulting.com/CEH/Public/Reports/607.5000/ accessed on 10/01/2012.
[9] K. Weissermel, H.-J. Arpe, Industrial Organic Chemistry, 4th ed., VCH New York, 2003.
[10] C.L. Bothe-Almquist, R.P. Ettireddy, A. Bobst, P.G. Smirniotis, Journal of Catalysis, 192 (2000) 174-184.
[11] S.D. Jackson, G.J. Kelly, C.A. Hamilton, L. Davies, Reaction Kinetics and Catalysis Letters, 79 (2003) 213-218.
[12] H. Pines, H.E. Eschinazi, Journal of the American Chemical Society, 77 (1955) 6314-6321.
[13] H. Hattori, Journal of the Japan Petroleum Institute, 47 (2004) 67-81.
[14] K. Tanabe, W.F. Hölderich, Applied Catalysis A: General, 181 (1999) 399-434.
[15] C. Supanee, B.V.O. Grady, F.P. Larkins, Silpakorn University International Journal, 3 (2003) 154-167.
[16] M.A. Aramendıa, J.A. Benıtez, V. Borau, C. Jimenez, J.M. Marinas, F. Urbano, Langmuir, 15 (1999) 1192-1197.
[17] T. Kanno, M. Kobayashi, Bulletin of the Chemical Society of Japan, 66 (1993) 3806-3807
[18] Y. Li, D. Nakashima, Y. Ichihashi, S. Nishiyama, S. Tsuruya, Industrial & Engineering Chemistry Research, 43 (2004) 6021-6026.
[19] T. Matsuda, Z. Minami, Y. Shibata, S. Nagano, H. Miura, K. Sugiyama, Journal of the Chemical Society, Faraday Transactions 1: Physical Chemistry in Condensed Phases, 82 (1986) 1357-1366.
[20] I.F. Guilliatt, N.H. Brett, Journal of the Chemical Society, Faraday Transactions 1: Physical Chemistry in Condensed Phases, 68 (1972) 429-433.
[21] W. Ueda, T. Kuwabara, H. Kurokawa, Y. Morikawa, Chemistry Letters, (1990) 265-266.
[22] W. Ueda, T. Yokoyama, Y. Moro-Oka, T. Ikawa, Industrial & Engineering Chemistry Product Research and Development, 24 (1985) 340-342.
[23] J.M. Hur, B.-Y. Coh, H.-I. Lee, Catalysis Today, 63 (2000) 189-195.
[24] Y.L. Xie, M.F. Luo, J.J. Zhao, Reaction Kinetics and Catalysis Letters, 89 (2006) 29-36.
[25] S.J. Gregg, K.S.W. Sing, Adsorption Surface Area and Porosity, 2nd ed., Acadamic Press, London, 1982.
[26] Y. Ding, G. Zhang, H. Wu, B. Hai, L. Wang, Y. Qian, Chemistry of Materials, 13 (2001) 435-440.

[27] T. Yoshida, T. Tanaka, H. Yoshida, T. Funabiki, S. Yoshida, T. Murata, The Journal of Physical Chemistry, 99 (1995) 10890-10896.
[28] A.V. Kiselev, I.E. Neimark, D.P. Poshkus, M.A. Piontkovskaya, Russian Chemical Bulletin, 8 (1959) 213-217.
[29] A. Malecki, B. Malecka, R. Gajerski, S. Labus, Journal of Thermal Analysis and Calorimetry, 72 (2003) 135-144.
[30] L. Gubrynowicz, T. Strömich, Thermochimica Acta, 115 (1987) 137-151.
[31] S. Labus, A. Malecki, R. Gajerski, Journal of Thermal Analysis and Calorimetry, 74 (2003) 13-20.
[32] W. Ueda, T. Yokoyama, Y. Moro-oka, T. Ikawa, The Chemical Society of Japan, 14 (1985) 1059-1062.
[33] D.H. Cho, S.D. Yim, G.H. Cha, J.S. Lee, Y.G. Kim, J.S. Chung, I.S. Nam, Journal of Physical Chemistry A, 102 (1998) 7913-7918.
[34] D.S. Kim, J.-M. Tatibouet, I.E. Wachs, Journal of Catalysis, 136 (1992) 209-221.
[35] B.M. Weckhuysen, I.E. Wachs, R.A. Schoonheydt, Chemical Reviews, 96 (1996) 3327-3349.
[36] S.A. El-Molla, Applied Catalysis A: General, 280 (2005) 189-197.
[37] J. Green, Journal of Materials Science, 18 (1983) 637-651.
[38] A.M. Ghozza, Materials Letters, 57 (2003) 2120-2129.
[39] M.D. Lanagan, D.C. Ibana, Minerals Engineering, 16 (2003) 237-245.
[40] D.A. Donatti, A.I.R. Ruiz, F.G. De Moraes, D.R. Vollet, Journal of Sol-Gel Science and Technology, 28 (2003) 31-35.
[41] S.R. Ramanan, D. Ganguli, Journal of Non-Crystalline Solids, 212 (1997) 299-302.
[42] B.M. Weckhuysen, R.A. Schoonheydt, J.-M. Jehng, I.E. Wachs, S.J. Cho, R. Ryoo, S. Kijlstra, E. Poels, Journal of the Chemical Society, Faraday Transactions, 91 (1995) 3245-3253.
[43] H. Kurokawa, T. Kato, T. Kuwabara, W. Ueda, Y. Morikawa, Y. Morooka, T. Ikawa, Journal of Catalysis, 126 (1990) 208-218.
[44] G.M. Parker, A New Route to Polyhydric Alcohols, in: PhD thesis School of Chemistry University of Glasgow, Glasgow, 2008, pp. 134.
[45] T. Sooknoi, J. Dwyer, Journal of Molecular Catalysis A: Chemical, 211 (2004) 155-164.
[46] H. Kurokawa, T. Kato, W. Ueda, Y. Morikawa, Y. Moro-oka, T. Ikawa, Journal of Catalysis, 126 (1990) 199-207.
[47] U.C. Oh, Y.S. Chung, D.Y. Kim, Journal of the American Ceramic Society, 71 (1988) 854-857.
[48] B.M. Weckhuysen, R.A. Schoonheydt, Catalysis Today, 51 (1999) 223-232.

Steam Reforming of Ethanol

6. Introduction

6.1 Clean source of energy

The energy obtained from the combustion of fuels has brought about many technological advancements as well as instigating social-economic growth which otherwise would not have been possible [1, 2]. However, the development of technology and science has also resulted in an increased demand for energy, especially in the last few decades. According to a BP report in 2011 the price for crude oil has continuously increased in the last 11 years [3].

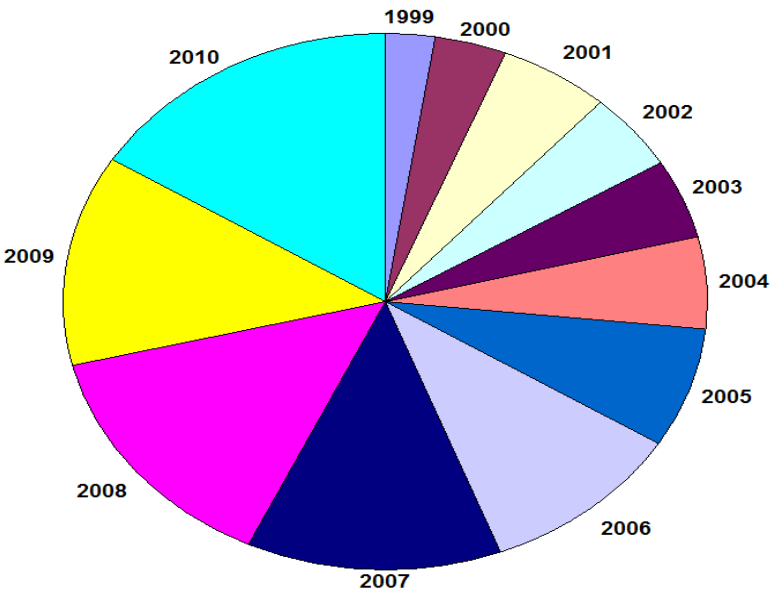

Figure 6.1-1 Crude oil price ($/barrel) in Dubai from 1999 to 2010 [3]

At present, approximately 80% of the world's energy production is derived directly or indirectly from non-renewable sources such as fossil fuels [4-6]. The increasing energy demand and depletion of petroleum reserves may result in energy shortages in the future. It is estimated that if the world's energy consumption continues to increase at the current rate, the world's proven reserves of conventional and non conventional oil would run out in 51 years [7]. Thus the petroleum and petrochemical industries are coming under increasing pressure to compete effectively with global competitors utilising more advantaged hydrocarbons feedstocks [8].

In addition to dwindling supplies, the other challenge for the use of fossil fuels is the environmental problems which are caused by their large scale use. Burning of fossil fuels produces pollutant gases such as CO_2, NO_x and SO_x, and can cause acid rain as well as contribute to global warming and health problems in the modern world [9-12].

Several technologies have been developed and touted *i.e.* wind, solar, photovoltaic and others as potential solutions for both problems [13, 14]. Among the most promising near term technologies are those based on fuel cells. The use of fuel cells for electric power generation in automobiles has immense potential. They exhibit high efficiency, are environmentally friendly and have operational benefits when compared to conventional technologies [15, 16].

Fuel cells are electrochemical devices that convert the chemical energy of a chemical reaction directly into electrical energy and heat. Electrochemical reactions are the most efficient means ($\geq$ 85%) to convert chemical energy to electrical energy. They exhibit approximately two to three times greater energy efficiency than an internal combustion engine in converting fuel to electricity and evolve only H_2O as a by-product [13, 17].

Many types of fuel cells are in existence and are classified according to the electrolyte they employ and their operational temperature. However, all fuel cells work on the same basic principle [18]. Unlike a conventional battery, in fuel cells the fuels are supplied to the device from external sources. Therefore, the device can be operated until the fuel supply is exhausted. As shown in Figure 6.1-2, on one side of the fuel cell H_2 is passed over the anode where it splits into positively charged protons and negatively charged electrons whilst oxygen from the air is provided to the cathode. The positively charged protons pass through the polymer electrolyte membrane (PEM) to the cathode, whereas the negatively charged electrons pass along the external circuit to the cathode, producing DC current. At the cathode the electrons, protons and oxygen molecules combine to form water, which is the only by-product discharged out of the cells [13, 19].

$$\text{Anode:} \quad H_2 \rightarrow 2H^+ + 2e \tag{6.1}$$

$$\text{Cathode:} \quad 0.5O_2 + 2e + 2H^+ \rightarrow H_2O \tag{6.2}$$

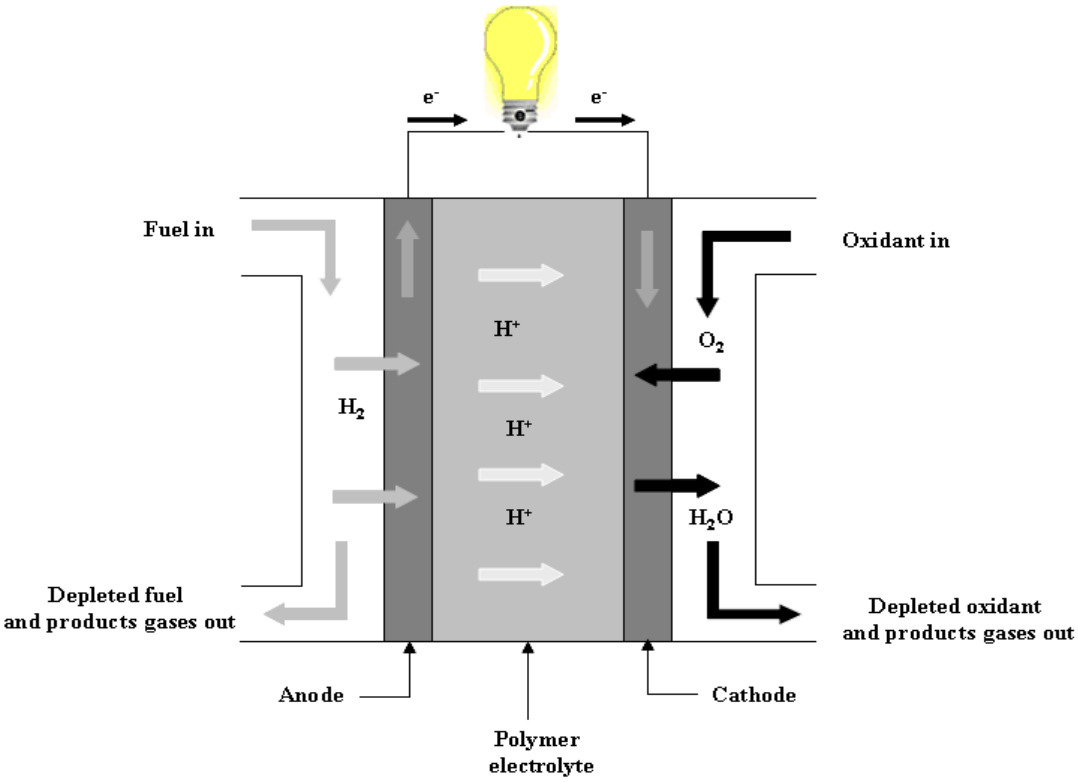

Figure 6.1-2 Polymer electrolyte membrane fuel cell

Fuel cell technology has several advantages over conventional energy sources [20];

- Fuel cells produce no or very low levels of pollutant gases.
- Fuel cells produce power at higher efficiencies than conventional power systems such as internal combustion engines.
- Fuel cells have few moving parts and thus require minimal maintenance, reducing the life cycle cost of energy production.

6.2 Fuels for fuel cell

Hydrogen is the most common fuel for fuel cells. Natural gas, methanol, gases obtained from the fossils fuels such as methane, refinery gases and kerosene are the other common fuels for the fuel cells [21, 22]. Each fuel cell has their own specific electrolyte and catalysts and use different gases as fuels [23]. The type of fuel has a great impact on the fuel cell operating temperature and on the other components used in the fuel cell system [22]. Among the different fuel cells, polymer electrolyte membrane (PEM) fuel cells have been extensively studied recently due to their wide applicability and low operating

temperature [24]. Furthermore, in a PEM fuel cell, hydrogen is used as fuel and gives only water as a by-product [19].

6.3 Production of hydrogen

Hydrogen is abundantly available in the universe and possesses the highest energy content per unit of weight (120.7 kJ/g), compared to any of the known fuels [4, 25, 26]. At present the total annual worldwide hydrogen utilisation is in the range of 400-500 billion Nm^3, which equates to approximately 3% of the total world energy consumption. It is a valuable feedstock for many industries, including petrochemical, hydro-treating/hydrocracking and fuel cells. More recently hydrogen has been cited as a clean fuel for the future, since its combustion produces only water as a by-product [27].

Although hydrogen is present in abundance in the universe, it does not exist freely on Earth. It is always present in bound form *i.e.* combined with oxygen in water or with carbon in fossil hydrocarbons. To obtain pure hydrogen requires its removal from different sources, for example coal, natural gas or liquefied petroleum [27]. Several different technologies exist for the production of hydrogen such as electrolysis, thermal decomposition and fossil fuel reforming. Today most of the hydrogen produced comes from fossil fuel sources, with about 50% of the hydrogen produced via thermo catalytic and gasification processes [28].

Of all the commercial technologies, steam reforming of hydrocarbons has emerged as the most prominent process for the production of hydrogen. Over the last two decades, research has focused on the steam reforming of various hydrocarbons such as methane, ethane and propane, as well as oxygenated compounds such as methanol and ethanol. Industrial and academic research has focused on the optimisation of the catalysts used to increase selectivity towards H_2 whilst minimizing CO production. Elimination of CO is vital for applications such as hydrogen fuel cells (CO acts as a poison to the platinum electrocatalyst in PEM fuel cell) [4, 29, 30].

Among the various oxygenated compounds which can be converted to hydrogen, alcohols are very propitious candidates because they are easily decomposed in the presence of steam and generate a H_2 rich mixture, suitable for use in fuel cells [31]. Substantial industrial and academic research on methanol steam reforming for H_2 production has been

undertaken. However, the main drawbacks of methanol reforming are its high toxicity and its production from non-renewable sources [32].

Due to many advantages, the steam reforming of bioethanol has attracted significant interest in the last few years. Most importantly for the steam reforming of bioethanol is that the feedstock is renewable and environmentally benign. Bioethanol can be produced from domestically abundant biomass such as agriculture and forestry residues, waste papers and other sizeable portions of municipal solid wastes. Secondly, a higher hydrogen yield can be obtained from the steam reforming when ethanol is used as reactant compared to methanol and methane. Moreover ethanol has no negative effect on the human body during handling. Finally, bioethanol has no heteroatom and metal so its use in steam reforming as the reactant does not result in emissions of NO_x, SO_x and other toxics gases [15, 33-36]. Steam reforming of bioethanol produces 8-10 times more energy than that consumed during processing [37]. In addition, the activation energy for the scission of C-C bond in oxygenated compounds is less than for alkanes [38].

Hydrogen can be produced from ethanol in different ways such as:

Partial oxidation

$$C_2H_5OH + 1.5O_2 \rightarrow 3H_2 + 2CO_2 \quad (6.3)$$

Oxidative steam reforming

$$C_2H_5OH + 2H_2O + 0.5O_2 \rightarrow 2CO_2 + 5H_2 \quad (6.4)$$

Steam reforming

$$C_2H_5OH + 3H_2O \rightarrow 2CO_2 + 6H_2 \quad (6.5)$$

Equation 6.5 indicates that steam reforming of bioethanol gives the maximum moles of H_2 per mole of ethanol reaction [6, 39, 40].

6.4 Mechanism of the steam reforming of ethanol

Thermodynamic calculations and studies of the mechanism of the ethanol steam reforming have revealed that it is an endothermic reaction and produces H_2 and CO_2 (as shown in Equation 6.6) [41].

However, the reaction can proceed through several pathways which depend upon the catalyst, the support employed and other variables such as temperature, pressure, GHSV, water/ethanol ratio and the metal precursor used. The product distributions are governed by a very complex reaction network which involves the following possible reactions:

Steam reforming [42]

$$C_2H_5OH + 3H_2O \rightarrow 2CO_2 + 6H_2 \quad \Delta H = 174 \text{ kJ mol}^{-1} \quad (6.6)$$

Partial steam reforming (formation of syngas) [42]

$$C_2H_5OH + H_2O \rightarrow 2CO + 4H_2 \quad \Delta H = 256 \text{ kJ mol}^{-1} \quad (6.7)$$

Ethanol cracking followed by steam reforming [26]

$$C_2H_5OH \rightarrow CO + H_2 + CH_4 \quad \Delta H = 50 \text{ kJ mol}^{-1} \quad (6.8)$$

$$CH_4 + 2H_2O \rightarrow 4H_2 + CO_2 \quad \Delta H = 165 \text{ kJ mol}^{-1} \quad (6.9)$$

Ethanol dehydrogenation followed by decarbonylation or steam reforming [43]

$$C_2H_5OH \rightarrow C_2H_4O + H_2 \quad \Delta H = 69 \text{ kJ mol}^{-1} \quad (6.10)$$

$$C_2H_4O \rightarrow CH_4 + CO \quad \Delta H = -19 \text{ kJ mol}^{-1} \quad (6.11)$$

$$C_2H_4O + H_2O \rightarrow 3H_2 + 2CO \quad \Delta H = 187 \text{ kJ mol}^{-1} \quad (6.12)$$

Acetaldehyde condensation to crotonaldehyde [44]

$$2C_2H_4O \rightarrow CH_3CH{=}CHCHO + H_2O \quad \Delta H = -10 \text{ kJ mol}^{-1} \quad (6.13)$$

Ethanol dehydration to ethylene and water followed by polymerisation of ethylene to form coke or cracking of ethylene to CH_4

$$C_2H_5OH \rightarrow C_2H_4 + H_2O \quad \Delta H = 45 \text{ kJ mol}^{-1} \quad (6.14)$$

$$nC_2H_4 \rightarrow \text{coke} + yH_2 \quad (6.15)$$

$$C_2H_4 + 2H_2 \rightarrow 2CH_4 \quad \Delta H = -127 \text{ kJ mol}^{-1} \quad (6.16)$$

Water gas shift reaction of CO [45]

$$CO + H_2O \rightarrow CO_2 + H_2 \quad \Delta H = -41 \text{ kJ mol}^{-1} \quad (6.17)$$

Ethanol conversion to acetone followed by steam reforming [43, 46]

$$2C_2H_5OH \rightarrow (CH_3)_2CO + CO + 3H_2 \quad \Delta H = 24 \text{ kJ mol}^{-1} \quad (6.18)$$

$$(CH_3)_2CO + 2H_2O \rightarrow 5H_2 + 3CO \quad \Delta H = 369 \text{ kJ mol}^{-1} \quad (6.19)$$

Condensation of ethanol to diethylether [47]

$$2C_2H_5OH \rightarrow (C_2H_5)_2O + H_2O \quad \Delta H = -24 \text{ kJ mol}^{-1} \quad (6.20)$$

Oxidation of ethanol to acetic acid

$$C_2H_5OH + H_2O \rightarrow CH_3COOH + 2H_2 \quad \Delta H = 44.4 \text{ kJ mol}^{-1} \quad (6.21)$$

Methanation [6]

$$CO_2 + 4H_2 \rightarrow CH_4 + 2H_2O \quad \Delta H = -165 \text{ kJ mol}^{-1} \quad (6.22)$$

$$CO + 3H_2 \rightarrow CH_4 + H_2O \quad \Delta H = -206 \text{ kJ mol}^{-1} \quad (6.23)$$

Methyl coupling to form ethane [43]

$$2CH_3 \rightarrow C_2H_6 \quad \Delta H = -0.159 \text{ kJ mol}^{-1} \quad (6.24)$$

Coke formation through different routes [6]

$$C_2H_4 \rightarrow \text{coke} \quad (6.25)$$

$$CH_4 \leftrightarrow C + 2H_2 \quad \Delta H = 75 \text{ kJ mol}^{-1} \quad (6.26)$$

$$2CO \leftrightarrow CO_2 + C \quad \Delta H = -172 \text{ kJ mol}^{-1} \quad (6.27)$$

The ideal reaction which gives the highest yield of H_2 is 6.6 whilst in other reactions the yield of H_2 is lowered.

6.5 Effect of temperature on the steam reforming of ethanol

Steam reforming of ethanol is an endothermic reaction ($\Delta H = + 174 \text{ kJ mol}^{-1}$) and therefore temperature has a significant effect [10, 31]. The distribution of products significantly varies with temperature. At low temperatures (< 450^{o}C), mostly C_2 and higher carbon containing products, such as acetaldehyde and ethylene are produced which polymerise and deactivate the catalyst. Whilst at high temperatures (> 550^{o}C), mostly H_2 and C_1 products such as CO, CO_2 are formed. The yield of CO formed at higher temperatures poses problems as its presence results in the deactivation of downstream fuel cells. However, high temperature steam reforming is ideal for the production of syngas which is used in Fischer-Tropsch synthesis. Roh *et al.* [10] and Wang *et al.* [48] investigated the steam reforming reaction over Rh/Al_2O_3 and Co/CeO_2 catalysts, respectively, at different temperatures and reported that ethanol conversion was low and deactivation apparent at temperatures up to 450^{o}C. Performing the reaction at higher temperatures resulted in 100% conversion and no deactivation. Liguras *et al.* [49] studied the steam reforming of ethanol

on supported metal catalysts in the temperature range of 600°C-800°C and found that with increasing temperature, ethanol conversion significantly increased. In addition high selectivity towards CO, CO_2 and H_2 was obtained [49]. The steam reforming of ethanol has been found to pass through two separate pathways; dehydration of ethanol to ethylene or dehydrogenation of ethanol to acetaldehyde [48]. At low temperatures (below 450°C) mostly C_2 products were observed due to insufficient temperature to decompose acetaldehyde completely. However, at high temperatures these products decomposed to other C_1 products or were deposited on the catalyst to form coke. The overall scheme is represented in Figure 6.5-1 [48].

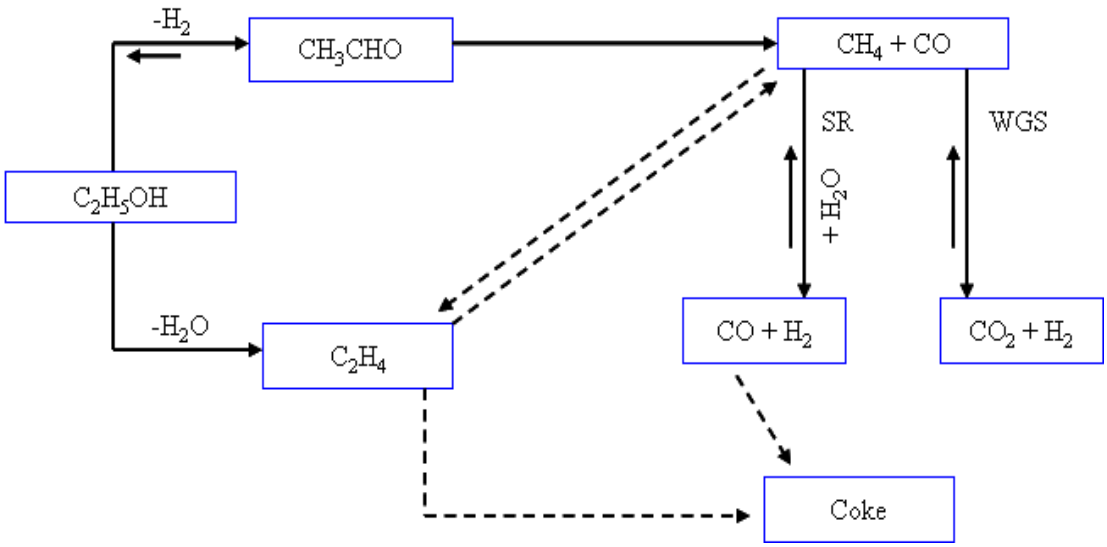

Figure 6.5-1 Sketch map for steam reforming of ethanol [48]

Acetaldehyde and ethylene cracking to CO_2 and CH_4 are exothermic reactions and are favourable at low temperature [50]. Bion [50] mentioned that the production of CH_4 significantly decreased the yield of H_2 and if CH_4 is not formed during steam reforming then the equilibrium would significantly change. Other research groups [49, 51] have also observed that increasing the reaction temperature from 500°C to 800°C significantly decreased the CH_4 yield, which in turn resulted in increased H_2 production. Thermodynamic calculations for the steam reforming of ethanol show that above 500°C the rate of CO formation via the reverse water gas shift reaction significantly increased. Fishtik *et al.* [42] and Lima *et al.* [52] further explained that all other reactions favour an increase in the yield of H_2 at higher temperature, except the reverse water gas shift which has a negative effect on H_2 yield. Rabenstein *et al.* [53] did thermodynamic calculations for steam reforming of ethanol at different temperatures and different water to ethanol ratios and concluded that more than 4mole H_2/ mole ethanol can be obtained by using a water to

ethanol ratio above 4 in the reaction temperature range between 550^{o}C and 650^{o}C. Using these conditions CO formation can be minimised to 0.1 mole fraction in effluent gas mixture [53].

6.6 Catalytic system for the steam reforming of ethanol

The synthesis of effective catalysts for the steam reforming of ethanol with the criteria of ; efficiency at low temperature, selective to H_2 formation (whilst minimising CO production) and high stability represents a major challenge for catalytic chemists. As most steam reforming reactions are performed at high temperature, catalysts which exhibit high thermal stability are necessary. In the last two decades the steam reforming of ethanol has been investigated by countless research groups with significant research still being conducted into new catalyst formulations [54, 55]. Elements or their compounds that have been investigated for active phases or supports for potential catalysts are shown in Figure 6.6-1 and are marked with a circle [41].

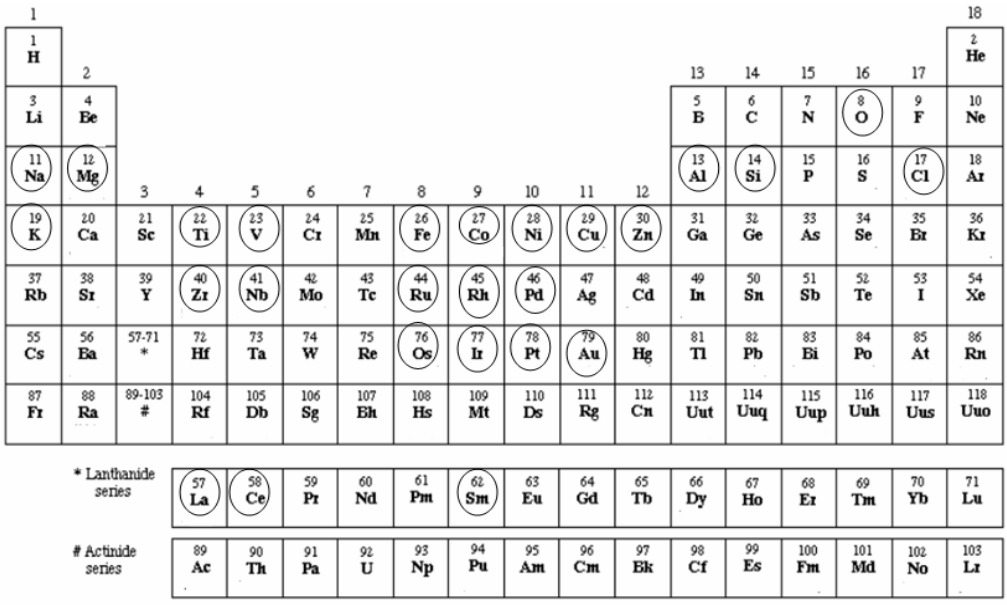

Figure 6.6-1 Element or their compounds that were tried as catalysts in the ethanol steam reforming [41]

Steam reforming of ethanol and the water gas shift (WGS) reaction take place simultaneously with the water gas shift reaction being reversible [12]. On the other hand, the complete conversion of ethanol is necessary for industrial application. The catalyst therefore plays an important role in pushing the reaction towards thermodynamic equilibrium and obtaining the complete ethanol conversion.

Different single and bimetallic noble and non-metal catalysts have been tested by several research groups for ethanol steam reforming in attempts to obtain maximum H_2 yield [56-58]. However, based on the results cited in the literature, no catalysts have been developed which exhibit both excellent performance and low cost.

6.6.1 Noble metal catalysts

Noble metals such as Ru, Rh, Pt, Pd, Ir and Au have been extensively studied in the steam reforming of ethanol, methanol and other hydrocarbons. They are well known for their high activity and low coke formation in the steam reforming of ethanol. Liguras *et al.* [49] studied the steam reforming of ethanol on Ru, Rh, Pt and Pd catalyst using different supports, such as MgO, Al_2O_3 and TiO_2, and found that for low loading catalysts, Rh was the most active and selective towards H_2 formation. However, at higher metal loading Ru exhibited good activity. The effect of metal loading on the catalytic performance of Rh/Al_2O_3 for ethanol steam reforming was investigated by Cavallaro *et al.* [59] and their results suggested that high Rh loading significantly decreased coke formation at high temperature. The activity of Rh metal in ethanol steam reforming is due to the high C-C bond cleavage propensity, which completely decomposes intermediate products such as acetaldehyde or ethylene. One of the main issues in steam reforming is the deactivation of the catalyst by coke. Rhodium has been found to have the ability to remove coke by forming C_1 chemicals. Idriss [12] proposed that the steam reforming of ethanol over Rh takes place not through the acetaldehyde route but through an oxymetallocycle intermediate which then ruptures and releases H_2 and CO_2 as shown in Figure 6.6-2.

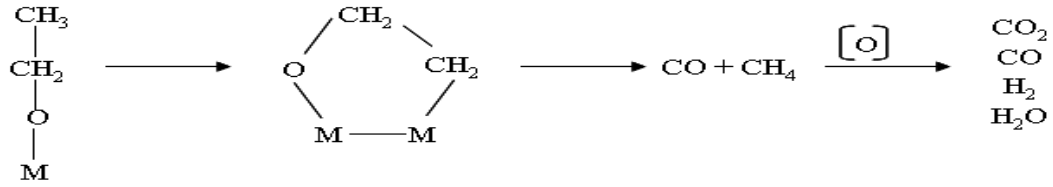

Figure 6.6-2 Steam reforming of ethanol through oxymetallocycle pathway

The metal precursor and preparation method of the catalysts play an important role in the steam reforming of ethanol. Aupretre *et al.* [60] found that Rh metal obtained from a nitrate precursor (700^{o}C calcination temperature) gave a high H_2 yield compared to a chloride precursor (500^{o}C calcination temperature). At high metal loading, the high activity and selectivity of Ru catalysts was comparable to that of Rh. Above 700^{o}C, at high water to ethanol ratios and low residence time, Ru gave a high H_2 yield [49, 61]. In

addition, the deposition of carbon was negligible at that temperature over the Ru catalyst. At low temperature (400^{o}C) Ru catalysts gave full conversion of ethanol. However, ethylene was produced at high yield [62]. The high activity of Ru catalysts are not only limited to ethanol steam reforming but also in the steam reforming of bio-oil and acetic acid. In addition, little to no coke was formed over the catalyst [16, 63]. The deposition of coke has been studied previously on Pd, Ag and Ru supported on CeO_2/YSZ during the steam reforming of ethanol. Less carbon formation on the Ru based catalyst was observed [64]. However, Ru based catalysts have been found to catalyse the dehydration of ethanol to ethylene, which is detrimental to catalyst performance [65].

It was found that Pt based catalysts showed the lowest activity compared to other noble metals in the steam reforming of ethanol. However, at high temperatures (above 500^{o}C) by combining noble metals supported on ceria/zirconia catalyst with alumina support the reactivity was changed to Pt ~ Rh > Pd [66]. Pt/CeO_2 catalyst was investigated by Jacobs *et al.* [67] for steam reforming of ethanol and found that the choice of support was crucial. They suggested that Pt metal catalyses the hydrogenolysis of surface species to CH_4 [67]. During steam reforming of ethanol, CO is produced, which is a poison for a proton fuel cell. In comparison to other noble metals, Pt has a higher WGS activity and also has good thermal stability. Therefore, CO production is significantly decreased when using Pt based catalysts in ethanol steam reforming [46]. Nickel catalysts have also been explored for steam reforming of ethanol and were found to have a propensity to form coke on the catalyst surface. Promotion of the nickel catalyst with Pt has been shown to significantly inhibit coke formation and consequently extend the life of the catalyst [35].

Pd and Ir metals on various supports were also tested for the steam reforming of ethanol by several research groups. Goula *et al.* [31] found that formation of CO and CH_4 took place on Pd at low temperatures (300^{o}C to 350^{o}C) which corresponded with ethanol decomposition. Other research group studied Pd/ZnO using steam : ethanol ratio of 13 and reported that this catalyst showed good activity at medium temperatures although a significant amount of acetaldehyde was produced which is an undesired product [68]. Zhang *et al.* [69] reported that Ir/CeO_2 shows good activity for ethanol steam reforming (ESR) and that the catalyst remained stable for over 60 hrs. It appears that the combination of Ir metal and ceria support inhibits the formation of coke at low temperature. However, the catalyst also produced significant amounts of acetaldehyde and acetone.

6.6.2 Non-Noble metal catalysts

Besides noble metals, non-noble metals catalysts have also been examined for the steam reforming of ethanol reaction. Nickel is widely used in steam reforming due to its low cost and high performances towards C-C rupture. Various formulations have been investigated, including nickel supported on Al_2O_3, MgO, La_2O_3, and SiO_2 and with different promoters such as K, Na, Cu and Zn [50, 70]. It has been found that the nickel component is active for C-C scission, whilst the additives play a role in the oxidation of the surface species to form CO_2 and H_2 [71]. Fatsikostas *et al.* [45] investigated ethanol steam reforming on nickel supported on Al_2O_3, La_2O_3 and La_2O_3-Al_2O_3 and found that Al_2O_3 promoted dehydration and produced C_2H_4, whereas La_2O_3 promoted dehydrogenation and cracking of ethanol. The impregnation of the Al_2O_3 support with La_2O_3 reduced carbon deposition, which was attributed to the formation of lanthanum oxycarbonate species. Fatsikostas *et al.* [45] also reported that nickel promotes reforming of ethanol and the water gas shift reaction as well as methanation. Epron and Comas [72] reported that nickel has limited ability for the water gas shift reaction and a promoter like Cu or Fe is necessary to enhance the water gas shift reaction and increase the H_2 yield [50, 72].

The main issue with nickel catalysts is deactivation due to sintering of the metal particles at high temperature, as well as coke deposition. Attempts to enhance the stability of the catalyst have revealed that a basic support decreases the deposition of coke. Basic supports favour ethanol dehydrogenation instead of dehydration, which is the main route to the formation of coke. Different dopants such as alkali metals have been shown to improve the stability of the Ni/MgO catalyst by retarding the sintering of the nickel particles [11, 73].

Copper and cobalt based catalysts have also been studied. It has been shown that choice of support is crucial in Co catalysts. Haga *et al.* [74] carried out the steam reforming of ethanol over Co supported Al_2O_3, SiO_2, MgO, ZrO_2 and carbon, and reported that Co/Al_2O_3 gave high selectivity to H_2 (67% at 400^oC) by suppressing the methanation of CO and decomposition of ethanol. Cavallaro *et al.* [75] showed that Co/MgO was more resistant to coke compared to Co/Al_2O_3 and had comparable performance to that of Rh/Al_2O_3. Recently Uraski *et al.* [76] reported that $SrTiO_3$ and $LaAlO_3$ supported Co catalysts exhibited higher catalytic activities and higher stability compared to Al_2O_3 and MgO supported Co catalysts. It was found that less coke formation took place, which was attributed to the lattice oxygen in the perovskite-type supports which played a role in oxidation of the coke precursor.

Copper based catalysts have been used for the steam reforming of methanol. They also exhibit high activity for the water gas shift reaction. It has been shown that copper catalysts are also active for ethanol steam reforming, giving high yields of CO, CO_2 and H_2 as the main products at low temperature (above 360^oC). Nishiguchi [25] studied a Cu/CeO_2 catalyst for the steam reforming of ethanol and found that the main reaction products below 300^oC, were H_2 and acetaldehyde, whilst at 380^oC the formation of acetone and H_2 proceeded. In other studies, Ni, Co and Mn modified Cu/Zn catalysts operated at below 480^oC revealed significantly decreased methane formation and an increased H_2 yield and selectivity [77]. The main cause of deactivation in copper based catalysts is aggregation of copper particles (sintering) at higher temperatures [26].

6.6.3 Combined metal based catalysts

Steam reforming of ethanol is a very complex reaction with a broad range of secondary reactions, as discussed in section 6.4. In addition, deactivation of the catalyst via coke formation and sintering is a problem [7, 34]. No single metal has been found to be a solution to these challenges. To minimise these problems various research groups have taken a bimetallic approach for the steam reforming of ethanol [56, 78-81]. Using bimetallic catalysts, the performance of the ESR and life time of the catalyst significantly increased [82]. When platinum is combined with rhenium, the performance of the catalyst dramatically changes due to the stabilising effect of rhenium to coking/sintering effects [83]. Zhang *et al.* [84] investigated the influence of a second metal on a SiO_2-Al_2O_3 supported Ni catalyst by adding La, Co, Cu, Zr and Y, and found that the addition of La inhibits the growth of nickel particles and the catalyst remains stable. Modification of the support has also been observed to have an effect. Domok *et al.* [85] examined the effect of ZrO_2 addition to Pt/Al_2O_3 and found that the decay in H_2 and CO_2 production decreased dramatically, which was postulated to be due to poisoning effects of acetate species deposited on the catalyst surface [85].

6.7 Support

The number of active sites of a catalyst usually depends upon its surface area. The surface area of the active component can be increased by the preparation of small metal particles. However, at high temperatures small particles are not stable and sintering or occasionally degradation of the active metal particles takes place. For high stability and dispersion, different supports are used. The support or carrier usually has high surface area, high

mechanical strength, stability, low cost and has low pressure drop characteristics. They are usually inert, although in some cases can have a promotional effect on the catalysis [86, 87]. Different oxides which are used as supports include carbon, Al_2O_3, MgO, SiO_2, TiO_2, ZrO_2 and La_2O_3.

6.7.1 Steam reforming of ethanol supports

Steam reaction of ethanol is usually performed at high temperature and high partial pressure of steam. Therefore, the use of a support which is mechanically stable is required. It must also be suitable for the dispersion of metal and exhibit no activity in catalysing side reactions. α-Al_2O_3 shows good properties in this regard as it is stable at high temperature. Silica is used as support, however it is volatile at high temperature and is slowly removed from the catalyst. Magnesium oxide can be used as a support in ESR because it is stable at high temperature. However, at low temperature it can be hydrated. This could lead to damage to the catalyst and even the reactor during starting or shutdown as the hydrated magnesia has almost twice the molar volume of the dry magnesia [88].

6.7.2 Acidic supports

The support may be acidic, neutral or basic depending upon the chemical structure. Alumina is a common example of an acidic material, which is widely used in industry and in academia as a support because it is inexpensive, structurally stable and has a wide range of pore distribution and surface areas. Alumina exists in different crystalline phases such as gamma, delta, theta, eta, kappa, alpha and omega which can be produced by different heat treatment preparation methods. All phases of alumina are eventually converted to the alpha form above 1000^{o}C. The different phase changes of alumina are shown in Figure 6.7-1 [13, 87, 89].

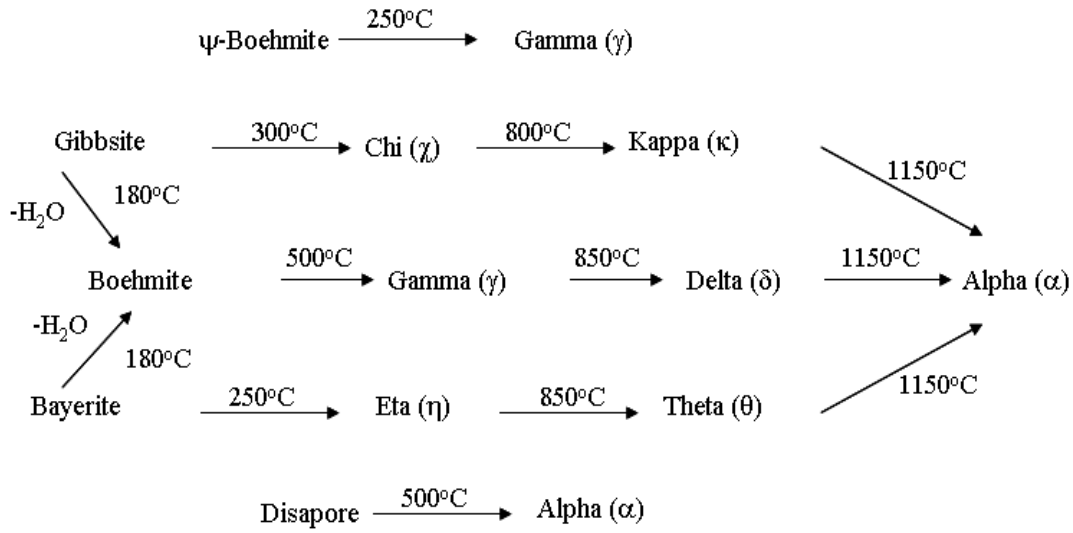

Figure 6.7-1 Relationship between the "various alumina" [90]

For ethanol steam reforming, Al_2O_3 supported noble and non-noble metals catalysts are widely used. Vizcaıno *et al.* [80] investigated Ni/Al_2O_3 and found that it showed good stability for the steam reforming reaction. However, a significant amount of coke was produced through the dehydration of ethanol over the Al_2O_3 supported catalyst. They further examined the addition of Mg metal to the aforementioned catalyst and found that the deposition of coke decreased due to blocking of the acidic sites by Mg. Rasko *et al.* [44] presented the mechanism of the ethanol steam reforming reaction on Pt/Al_2O_3 and Pt/TiO_2 catalysts and showed that the presence of water increased the stability of surface ethoxides which are the first step in the ethanol steam reforming reaction. The high activity of alumina supports was also reported by Luengo [91] and Aupretre [73] using different phases of alumina. They found that Al_2O_3 showed good activity and selectivity to H_2 when Rh and Ni were the active phase [73, 91].

6.7.3 Basic supports

Various research groups have reported on the effects of using a basic support [11, 92, 93]. Due to the absence of active acidic sites no C_2H_4 is produced over basic supports (shown to be main source of coke formation). Frusteri *et al.* [11] reported that among MgO supported Ni, Rh, Pd and Co catalysts, Rh gave high activity and stability. However, low H_2 formation was observed. To examine the support contribution, Llorca *et al.* [93] performed the ethanol steam reforming reaction over different supports and found that ZnO, which is basic in nature gave 100% conversion of ethanol at 450°C and 5.1 moles of H_2 per mole of ethanol reacted.

6.7.4 Redox supports

Several approaches have been taken to avoid coke formation during steam reforming [94]. Reducible oxide or oxygen conducting supports, which have oxygen ion properties to reduce the carbon deposition, have been used. The oxygen present in the lattice reacts with coke to form CO_x. Ceria (CeO_2) is well documented for its oxygen release and storage properties. Laosiripojana [95] investigated the steam reforming of ethanol on CeO_2 and found that it showed good reforming reactivity and high resistance towards coke deposition compared to a Ni/Al_2O_3 catalyst. Frusteri [96] studied the steam reforming reaction on ceria supported nickel and found that it gave above 98% H_2 selectivity at 650^oC whilst in autothermal reforming ceria acts as oxygen storage and enhances the gasification of the deposited coke residue.

6.8 Deactivation

Catalyst deactivation is the loss of the catalyst activity or selectivity during reaction time. Catalysts have a limited lifetime and depending upon the catalyst, some lose their activity after a few minutes, whilst others remain active for more than ten years, but ultimately they all succumb [83]. To maintain catalyst activity and avoid deactivation is of major economical importance for industry in reducing capital costs. James [83] wrote very beautiful words “Catalyst and process designers can do much to prolong lifetime of catalyst, but as one illness is cured the victim falls prey to another”. Therefore, in summary the deactivation of a catalyst is usual in any chemical process but can only be minimised to prolong the lifetime of the catalyst. The different causes of deactivation are summarised in Figure 6.8-1 [83, 97].

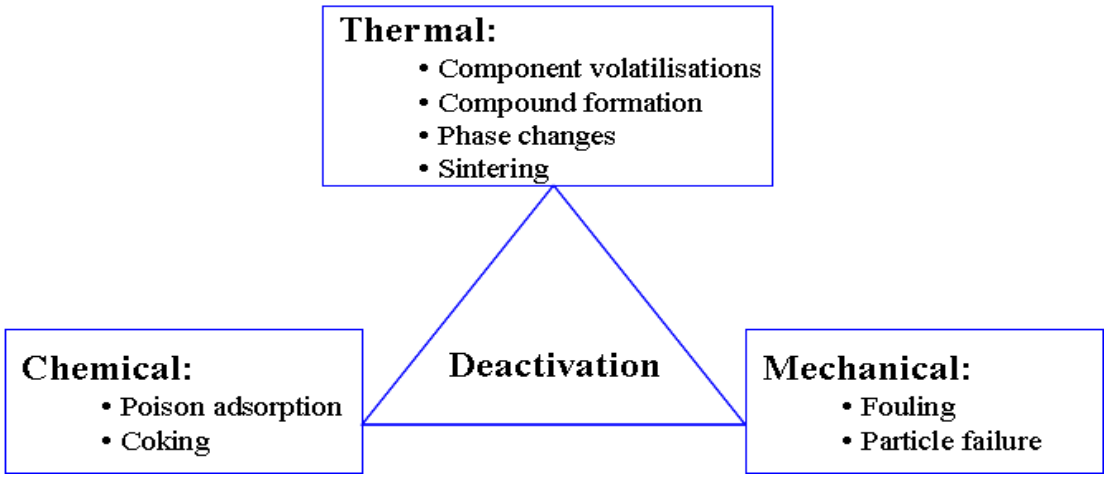

Figure 6.8-1 Different causes of deactivation

Mechanical and thermal deactivation is significant in steam reforming reaction catalysts due to the high temperature employed and the steam present. In thermal deactivation, highly volatile components gradually leave the catalyst and eventually deactivate the catalyst. This phenomenon is more common in alkali metals catalysts [83]. The active metal interacts with reactant species and forms volatile compounds which vaporise from the catalyst surface. This type of deactivation was found in nickel catalysts during the methanation reaction. When the temperature drops below 150^{o}C, nickel reacts with CO and forms nickel tetracarbonyl, which is volatile and removes Ni from the catalyst surface [98]. However, catalyst deactivation through direct vaporisation of active metal species from the catalyst surface is an insignificant route of catalyst deactivation [86]. Phase transformations of metal or the support from active phase to inactive phase are also responsible for decreased catalytic activity. For example, conversion of γ-Al_2O_3 to α-Al_2O_3 during steam reforming at high temperature results in significantly decreased surface area and active sites. Another cause of deactivation is the loss of active metal area via interaction with the support *i.e.* such as in nickel/alumina catalyst converted to a nickel aluminate [87].

Among different thermal phenomena, sintering is one of the main causes of catalyst deactivation during steam reforming. Sintering of supported metals is the complex physical and chemical phenomenon which involves diffusion of metal particles across the support surfaces. Sintering is significantly influenced by temperature, time, support and promoter [99]. Devianto [34] investigated the effect of aluminium addition to a Ni/MgO catalyst during ethanol steam reforming and found that aluminium addition significantly decreased the sintering of Ni and the catalyst showed activity up to 2000 hours without any significant change in its performance [34]. Sintering is more commonly observed in metal catalysts with a low Tammann temperature. Noble metals are more resistant to sintering compared to nickel due to their high Tammann temperatures [13]. Trimm [100] mentioned that performing steam reforming on Ni catalysts above 590^{o}C is greatly influenced by the sintering of the metals particles due to the Tammann temperature.

Feedstocks for steam reforming contain different types of impurities because they are obtained from natural sources. Poisoning is the strong chemisorption of a chemical species on to the active sites which may be reversible or irreversible and regenerable or not depending upon the type of poison and catalyst [13]. In group VIII, nickel is more sensitive to sulphur compared to other elements of that group. Rostrup-Nielsen [101] studied the effect of sulphur on a nickel catalyst during catalytic partial oxidation (CPO) of CH_4 and

revealed that CPO is less sensitive to sulphur than the steam reforming reaction. Sulphur impurities in natural gas poison the anode capability of proton exchange membrane fuel cells (PEMFC). Screening different catalysts for the removal of sulphur compounds from diesel and gasoline has shown a Ni/NiO catalyst to perform well (decrease of sulphur compounds like 4,6-dimethyl-dibenzothiophene to below 1ppm) [102]. During the high temperature water gas shift reaction over iron catalysts, sulphur reacts with iron to form iron sulphide and deactivates the catalyst [88, 90].

$$Fe_3O_4 + 3H_2S + H_2 \rightarrow 3FeS + 4H_2O \quad (6.28)$$

Fouling, the deposition of species on the catalyst surface, results in loss of activity due to blockage of sites and pores [84, 97]. Fouling is one of the main sources of catalyst deactivation in the steam reforming reaction. An important example of fouling is the deposition of coke in porous catalysts. Coke may strongly chemisorb on to the catalyst surface as a monolayer or physically adsorb in multilayers and blocks the access of reactant species to active sites on the metal surface. It can totally encapsulate metal particles or plug micro and mesopores so that access of reactants to crystallites inside the pores is restricted. The growth of coke inside the pores can cause stress and eventually fracture the support materials and disintegrate the catalyst pellet [84].

The deactivation of catalysts by coke in steam reforming is a major problem for industry. During the reforming reaction 1/200000 kg of hydrocarbons feed converts to coke which deposits on the catalyst surface and ultimately deactivates the catalyst [103]. Disproportionation of CO and CH_4 usually produces carbon whilst condensation or decomposition of hydrocarbons causes coke deposition on the catalyst [104]. Coke can be formed by different routes depending upon the temperature, pressure and feedstock. Besides reactions 6.25 to 6.27, reaction 6.29 may also contribute to coke formation.

$$C_nH_{2n+2} \rightarrow nC + (n+1)H_2 \quad (6.29)$$

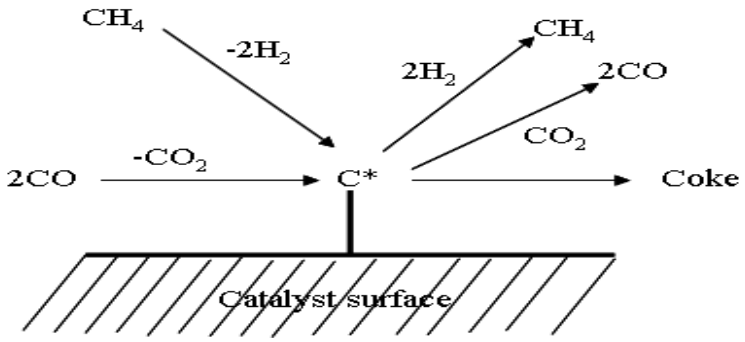

Figure 6.8-2 Formation of coke during steam reforming of CH_4

The carbon formed from reaction 6.26 to 6.27 is reversible or irreversible depending upon the conditions. CO dissociation on metal to form carbon can reverse to form CO or react and polymerise with other carbon, forming encapsulated carbon as illustrated by Figure 6.8-2. If the catalyst is nickel it may react with nickel metal and form tri-nickelcarbide (Ni_3C) [105]. The fundamental principle for deactivation over metals is that it is significantly rate dependent on the difference in rate of formation and gasification of carbon or coke precursors. If the rate of gasification is equal to or greater than that of formation, carbon or coke does not form over the catalyst [106]. The order of propensity of different hydrocarbons for coke formation is aromatic > olefinic > parafinic. Over steam reforming catalysts, dehydrogenation and dehydration are the primary routes for coke formation. Coke formation either takes place by polymerisation of alkenes or cyclization of alkenes by Diels-Alder reaction to aromatic compounds which condense as coke on the catalyst surface and form polyaromatic coke [103]. Bartholomew [106] proposed the following mechanism for coke formation.

Step 1: Reaction of olefin with Brönsted acid to form secondary carbenium ion:

$$H_2C{=}CHCH_3 + HX \quad \leftrightarrow \quad CH_3\text{-}^{+}CHCH_3 + X^{-} \qquad (6.30)$$

Step 2: Condensation of carbenium ion with other olefins to form branched chain carbenium ion

$$CH_3\text{-}^{+}CHCH_3 + H_2C{=}CHCH_3 \quad \leftrightarrow \quad \begin{matrix} H_3C\text{-}CHCH_3 \\ \quad\quad | \\ \quad CH_2\text{-}^{+}CHCH_3 \end{matrix} \qquad (6.31)$$

Step 3: Reaction of carbenium ion with base to form olefin

$$\begin{matrix} H_3C\text{-}CH\text{-}CH_2\text{-}^{+}CHCH_3 \\ \quad\quad | \\ \quad\quad CH_3 \end{matrix} + X^{-} \quad \leftrightarrow \quad \begin{matrix} H_3C\text{-}CH\text{-}CH_2\text{-}CH{=}CH_2 \\ \quad\quad | \\ \quad\quad CH_3 \end{matrix} + HX \qquad (6.32)$$

Step 4: Formation of aromatic compounds from olefins through Diels-Alder reaction.

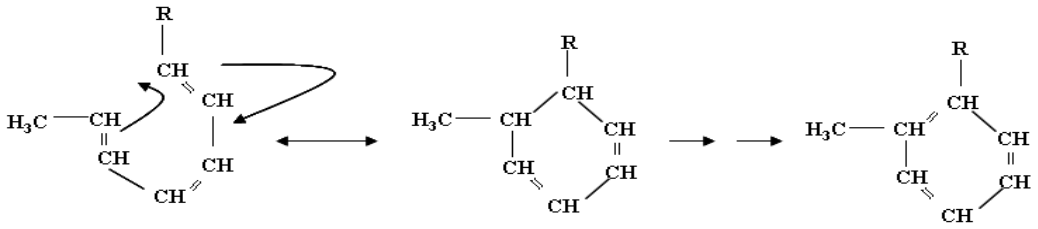

(6.33)

In steam reforming of ethanol, ethylene is the main source of coke formation although CH_4 and CO contribute to a small extent [7, 97]. Coke formation involves dehydrogenation, polymerisation and aromatization of the feed species. The hydrogen to carbon atomic ratio correlates to the nature of coke which can change with temperature and residence time. After an indefinite residence time graphitic type carbon forms. Coke having a high hydrogen to carbon ratio is called “soft coke” and is usually present on metal surfaces over bifunctional catalysts. Coke which has a low H/C ratio is called “hard coke” and is present on the support in catalytic reforming catalysts [103, 106-108]. Somorjai [109] investigated coke formation from C_2H_4 over a Pt catalyst and found that when the ratio of H/C decreases to 0.2, 75% of the coke becomes graphitic and irreversible. Guisnet *et al.* [110] explained that the formation of coke on acidic and bifunctional catalysts significantly depends upon reaction temperature. At low temperature (< 200^{o}C) carbonaceous deposits mainly form from the condensation and rearrangement of reactants on the catalyst surface which are generally non aromatic and their composition mainly depends upon the reactants. At high temperature (> 350^{o}C), carbon deposit composition is independent of reactants and mainly contains polyaromatics. Hence at high temperature, coke formation involves not only condensation and rearrangement steps but also passes through different dehydrogenation processes [110]. Coke formation over Co/CeO_2 was demonstrated from the steam reforming of ethanol and was found that at low temperature ($\leq$ 450^{o}C) mostly dehydrogenation and dehydration of ethanol occurred whilst at high temperature ($\geq$ 500^{o}C) disproportionation of CO and cracking of CH_4 took place. In the later stage, encapsulation of catalyst took place which led to severe deactivation of the catalyst [48].

Deposition of coke during the steam reforming reaction is influenced by the steam to carbon ratio because the presence of steam removes coke from the catalyst surface. Thermodynamic calculations performed by Alberton *et al.* [7] revealed that a steam to ethanol ratio above 2 would produce no carbonaceous deposit on the catalyst surface above 300^{o}C. However, experimentally a carbonaceous deposit was observed on the catalyst surface. Alberton *et al.* [7] demonstrated that deposition on catalyst is controlled by kinetics and not by thermodynamics. Cavallaro [59] calculated that a slight excess of water

(S/C = 4.2) is able to guarantee the inhibition of coke formation on Rh/Al_2O_3 catalyst even after several hours. During steam reforming of ethanol, coke formation not only takes place on acidic supports but has also been observed on basic supported nickel catalysts. However, the relative amount of coke was significantly decreased due to no C_2H_4 production over basic supports [111]. Ramos *et al.* [64] compared Ru, Pd and Ag catalysts on CeO_2 support for H_2 production from steam reforming of ethanol and found that compared to other catalysts, less coke was produced over the Ru based catalyst.

A series of supported Rh catalysts were studied by Mizuno *et al.* [112] for steam reforming of IPA and it was found that ceria supported rhodium produced the least coke compared to other supports. This was due to the redox properties of ceria which oxidised the carbonaceous material deposited on the catalyst surface.

Recently, the partial oxidation steam reforming of ethanol was attempted which drastically decreased the amount of the coke deposited on the catalyst surface. However, sintering was promoted due to hot spot phenomena [113].

6.9 Effect of impurities present in bioethanol

Similar to the effect of inorganic impurities in feed stocks such as sulphur, halogens and arsenic, the presence of different organic impurities in bioethanol such as amines, acetic acid and higher alcohols significantly impacts on the catalytic activity of steam reforming catalysts. Significant research is being undertaken into the steam reforming of ethanol for H_2 production. However, most of the researchers used pure ethanol and water mixtures and there are only limited studies performed on crude bioethanol or representative bioethanol samples. Direct use of crude bioethanol for steam reforming is cost effective because it will decrease the capital cost of the bioethanol distillation process [72, 114]. Ladish *et al.* [115] reported that 70-85% of energy in bioethanol preparation is consumed in distillation. However, the use of crude bioethanol is different from pure ethanol because the impurities present in crude bioethanol influence the H_2 yield as well as affecting catalyst activity and stability.

Two types of bioethanol of exist, 1^{st} generation bioethanol and 2^{nd} generation bioethanol and differ depending upon their origin. First generation bioethanol is produced from fermentation of sugar cane, corn and sugar beets whilst 2^{nd} generation is obtained from

wood, household waste and wheat straw [62]. The different impurities present in both types of bioethanol are tabulated in Table 6.9-1 [50].

Impurity	Rectified alcohol (g m^{-3})	Raw alcohol (g m^{-3})
Alcohol	96.3	92.9
Acetic acid	0.8	0.4
Esters	< 1	123
Aldehydes	< 1	108
Methanol	42.5	94
Butan-2-ol	0.5	<10
Propan-1-ol	0.5	581
2-Propen-1-ol	n.d	<10
Butan-1-ol	< 0.5	<10
2-Methyl-butan-1-ol	n.d	273
Total higher alcohols	n.d	582
Total sulphur	< 0.5	855
Volatile nitrogenated bases	< 1.0	1746

Table 6.9-1 Composition of rectified and crude alcohol [116], Where n.d refers to not detected.

As discussed previously, only very few studies have used crude bioethanol for steam reforming. Direct crude bioethanol obtained by fermentation of high starch feed wheat straw was first used by Akande *et al.* [117] for steam reforming over nickel catalysts prepared by different methods. They found that the nickel catalyst prepared by precipitation gave high ethanol conversion (85 mol%) due to its smaller crystallite size and high reducibility. They also demonstrated that coking was observed at the onset of the reaction but stabilised after 180 min TOS. Vargas *et al.* [118] compared the steam reforming of ethanol obtained from the fermentation of molasses of sugar cane with 1 : 5.95 pure ethanol water mixture and found slightly higher H_2 production from bioethanol due to the presence of different higher alcohols impurities. However, catalytic activity was similar in both systems. Recently Epron *et al.* [50] studied the effect of various impurities on the steam reforming of bioethanol by using model raw bioethanol feeds. They prepared model raw bioethanol by addition of 1 mol% of each impurity in pure ethanol individually. They found that addition of a diethylamine impurity to ethanol favoured the ethanol conversion and slightly increased the H_2 yield. The promoting influence of diethylamine was explained by the competition of the basic molecule with alcohol molecules for the

acidic sites present on the catalyst surface [116]. On the other hand, acetic acid decreased the conversion of ethanol and H_2 yield compared to the pure ethanol system. This was explained by its acidic character which may increase the acidity of the support, thereby favouring the dehydration route and leading to coke formation on the catalyst. Epron [119] also studied the effect of different organic functional groups and found that esters, acids and higher alcohols strongly deactivate the catalyst whilst the addition of butanal, methanol and diethylamine had no negative effect on the catalyst [119]. Devianto *et al.* [120] studied the steam reforming of ethanol over Ni/MgO catalyst and examined the influence of different impurities. They demonstrated that acetic acid and higher alcohols have an adverse effect on the steam reforming of ethanol. They explained that acetic acid increased the acidity of the catalyst which in turn led to more coke formation, whilst deactivation of the catalyst by alcohols was due to their incomplete decomposition on the catalyst surface (site blocking) [120]. To investigate the decomposition of different alcohols for H_2 production, Mostafa *et al.* [121] examined C_1 to C_4 alcohols over Pt/ZrO_2 and in the temperature range from 150 to 200^{o}C. The authors observed the following order of decomposition of different alcohols and H_2 production ethanol ≥ methanol > butanol ≥ propanol [121]. Epron and her group [55] also studied the effect of modified catalysts for model bioethanol and concluded that addition of nickel and yttrium significantly increased the stability of Rh/Al_2O_3 catalyst for raw bioethanol steam reforming reaction.

Hence it is clear that impurities in bioethanol may have a significant effect on the ethanol steam reforming reaction.

6.10 Project aim

As discussed previously, direct use of crude bioethanol will reduce the capital cost of a commercial plant. However, the main challenge in the use of crude bioethanol is the presence of different impurities which significantly influence the catalyst activity, stability and product distribution. The small quantities of these impurities in bioethanol either promote or deactivate the catalyst for ethanol steam reforming reaction, as discussed in section 6.9.

The aim of this project therefore, was;

- To investigate an Al_2O_3 support and Al_2O_3 supported noble metal (Ru, Rh and Pt) catalysts for the steam reforming of ethanol. Temperature was to be varied to investigate ideal process conditions for maximum H_2 yield.
- To investigate the tolerance of Al_2O_3 support and Al_2O_3 supported noble metal catalysts for different impurities present in bioethanol using model bioethanol containing 1mol.% C_3 impurities such as 1-propanol, 2-propanol (IPA), propanal, acetone and propylamine.
- Post reaction characterisation of spent catalysts using different techniques to investigate the cause of catalyst deactivation during steam reforming of ethanol.

7. Experimental

7.1 Catalyst characterisation

7.1.1 Temperature programmed oxidation (TPO)

TPO was carried out on post reaction samples using a combined TGA/DSC SDT Q600 thermal Analyser connected to an ESS Mass Spectrometer for evolved gas analysis. Each sample was heated from room temperature (28^{o}C) to 1000^{o}C using a heating ramp of 5^{o}C min^{-1} in a 2% O_2/Argon gas flow (100 ml min^{-1}). For mass spectrometric analysis, mass fragments with m/z values of 2, 12, 15, 16, 17, 18, 25, 26, 28, 29, 30, 32, 41, 44, 45, 46, 58, 59, 60 and 78 (amu) were followed.

7.1.2 Raman spectroscopy

Raman spectroscopy is a spectroscopic technique similar to Infrared spectroscopy. However, in this technique, the vibrational motion must change the polarisability of the molecule if the molecule is to be Raman active. Raman spectroscopy is commonly used in chemistry and other fields of science.

Raman spectra of post reaction catalysts were obtained with a Horiba Jobin Yvon LabRAM High Resolution spectrometer. A 532.17 nm line of a coherent Kimmon IK series He-Cd laser was used as the excitation source for the laser. Laser light was focused for 10 seconds using a 50x objective lens and grating of 600. This was repeated for 4 points to improve the resolution of the peak. The scattered light was collected in a backscattering configuration and was detected using a nitrogen cooled charge-coupled detector. A scanning range of between 100 and 4100 cm^{-1} was applied.

7.1.3 Scanning electron microscopy

Scanning electron microscopy is a technique that is used to study the surface morphology or physical nature of solids.

Post reaction catalysts were mounted on aluminium pin stubs with carbon taps as support. Due to charging, the catalysts were coated with gold palladium (60/40) sputter for 2 minutes with 2 kV and 25 μA in an argon atmosphere. Viewing of the catalyst was performed by mounting the sample to in a Philips XL30 Environmental SEM and

irradiating the specimen with a beam of electrons, this was followed by changing magnification and focusing for increasing resolution of the catalyst surface.

7.1.4 Powder X-ray diffraction (XRD)

To obtain information concerning the phase composition of the catalyst and nature of coke after exposure to the steam reforming reaction, X-ray diffraction patterns of the post reaction samples were obtained using a Siemens D 5000 X-ray Diffractometer (40 kV, 40 mA, monochromatic) using a CuK alpha source (1.5418 Å). The scanning range used for samples in the steam reforming of ethanol project was $5^o \leq 2\theta \leq 85^o$ with a step size of 0.02^o and dwell time of 10 seconds per step.

7.2 Steam reforming of ethanol

The catalysts used in the steam reforming of ethanol project were Al_2O_3 supported precious metal catalysts. Lower loaded (0.2%) Rh, Ru and Pt supported Al_2O_3 catalysts were prepared via a wet impregnation method by E.M. Opara [122]. The precursors used in these catalysts are given in Table 7.2-1.

Catalyst	Precursor
Pt	H_2PtCl_6
Rh	$Rh(NO_3)_2$
Ru	$Ru(NO)(NO_3)_3$

Table 7.2-1 Catalysts used in ethanol steam reforming project

All the calcined catalysts were characterised by BET and powder XRD. The catalysts were then crushed and particle sizes 425-600 μm were collected by sieving. 0.5g of catalyst was loaded into the glass microreactor as discussed in section 2.2.1 and reduced using the condition shown in Table 7.2-2. The reduced catalysts were characterised prior to reaction using powder XRD and BET analyses.

Reduction Temperature (^{o}C)	Ramp (^{o}C/min)	Hold time (hrs)	Atmosphere
600	10	2	Hydrogen

Table 7.2-2 Pre-treatment of catalyst for steam reforming of ethanol reaction

7.2.1 High pressure reactor

The steam reforming of ethanol reaction was performed in a high pressure, fixed bed reactor using a 3/16 inch internal diameter and 18.5 inch long glass-lined stainless steel reactor tube. A diagram of the apparatus is shown in Figure 7.2-1.The catalyst bed within the reactor was carefully positioned so it was in line with the external thermocouple. Either side of the catalyst bed in the reactor tube was packed fused alumina. The thermocouple and the heater were linked via a West 4400 temperature controller, allowing temperature programmes to be set and executed. The total pressure in the apparatus was controlled by a Tescom variable pressure valve and the system was operational up to a maximum of 20 barg. The flow rates of the gases entering the reactor were controlled using Brooks 5855 mass flow controllers that allowed flows of between 5 and 250 ml min^{-1}.The carrier gas (argon) was supplied from an external cylinder and the water/ethanol solution, which was introduced via a Gilson pump were mixed in the vaporiser, at a temperature of 500^{o}C. The water/ethanol solution was pumped through the Gilson pump at a rate of 0.4120 ml min^{-1}. The argon flow rate was kept constant at 10 ml min^{-1} in order to obtain steady steam production.

The lines between the vaporiser and the reactor tube were heated to 250^{o}C to avoid condensation. The gas flow could be directed through the reactor tube or through a by pass, as shown by arrows A and B respectively, using three-way taps 2 and 3 in Figure 7.2-1. Eluents from the reactor tube in gaseous form entered the knockout pot where high boiling point products were collected and analysed by an offline GC-2000 Series. The temperature of the knockout pot (chiller) was kept at 0^{o}C. The gaseous products remaining were analysed using an on-line GC (Varian 3400).

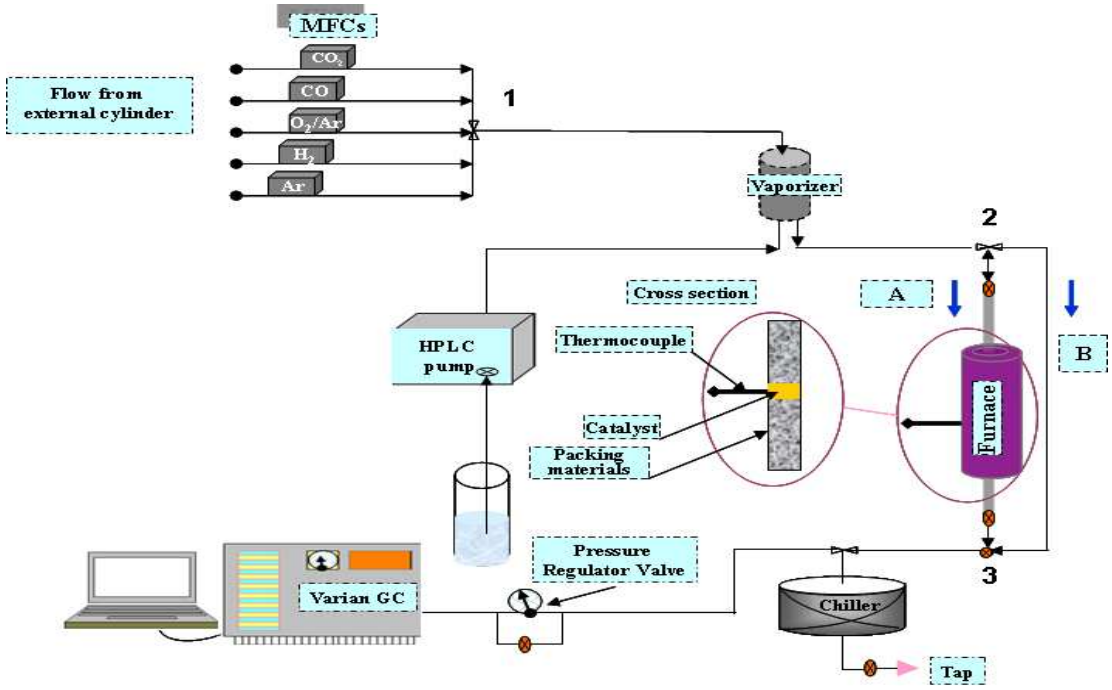

Figure 7.2-1 High pressure steam reforming of ethanol reactor

7.2.1.1 Mass flow controllers (MFCs)

The MFCs, which controlled the flow of gases to the reactor, were calibrated using a digital flow meter connected to the vent of the high-pressure reactor. For each gas, the MFC was fixed at a particular flow rate and allowed to stabilise before a reading was taken. The MFC set points and actual readings from the digital flow meter are plotted in Figure 7.2-2. The actual flow rate calculated from Graph 7.2-2 was used to determine the MFCs set point for the reaction.

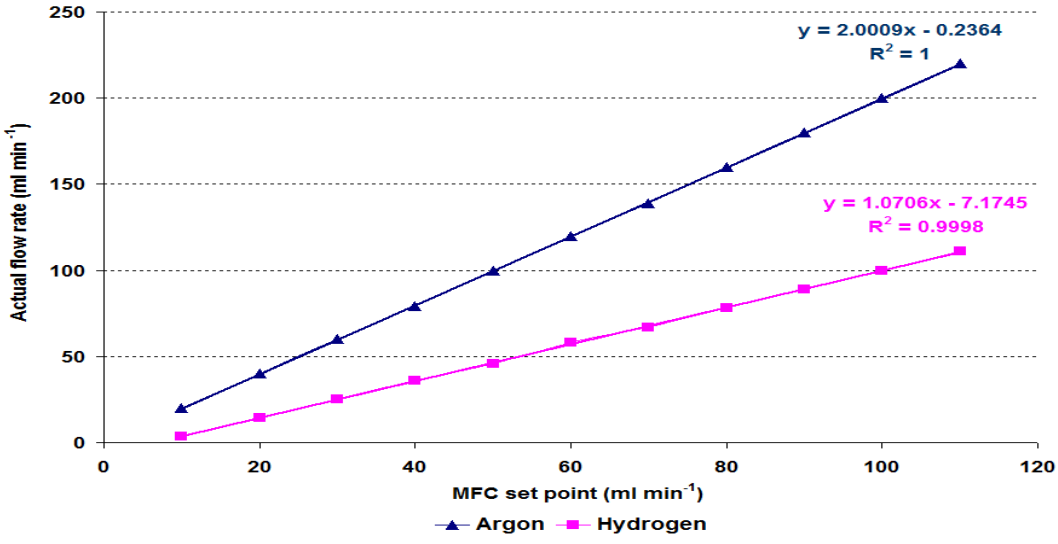

Figure 7.2-2 Mass flow controller calibration

7.2.2 Reaction procedure

The 3/16 inch diameter reactor tube was filled with fused alumina (boiling chips) to just lower than the point at which the thermocouple contacts the tube. The catalyst (0.25 g) was loaded and the remainder of the tube packed with boiling chips to ensure that the thermocouple was in contact with the section of tube where the catalyst was situated. Prior to the reaction, a leak test was carried out using an inert gas feed and the catalyst was reduced *in-situ* at 600^{o}C for 2 hours using hydrogen gas with a flow rate of 50 ml min^{-1}. The temperature was set to the desired reaction temperature and the pressure in the reactor was increased to 20 barg using argon gas. The water and ethanol mixture was mixed in order to obtain a steam to ethanol ratio of 5:1 in the gas phase. The flow rate of steam and ethanol solution was set at 416.6 ml min^{-1}, which was generated by pumping through a Gilson pump at a rate of 0.412 ml min^{-1}. The argon gas flow rate was set to 10 ml min^{-1} to obtain ~ 50000 h^{-1} GHSV. The carrier gas and water/ethanol mixture were mixed in the vaporiser. Once all the reaction parameters had been fixed, the analysis was begun by allowing the flow of reactants through path A as shown in Figure 7.2-1. A liquid sample was taken at 30 minute intervals for the initial 3 hrs with subsequent hourly samples for the remainder of the reaction. Following the initial sample on each day the pressure in the reactor dropped by ~ 2 bar. The required pressure was regained by doubling the feed of liquid solution and carrier gas.

7.2.3 Gas phase GC analysis

Gaseous products leaving the knockout out pot (0^{o}C) were analysed using online Varian Gas Chromatography 3400, fitted with a 30 m carboxen^{Tm}1010 plot column and TCD detector. The carboxen^{Tm}1010 plot column was used for the separation of H_2, CO, CO_2, CH_4, C_2H_4 and C_2H_6 where the sample loop volume in this GC was 250 µl. An initial sample was taken 10 minute after the start of the reaction and then at 30 minutes intervals for the duration of the reaction. This time allowed for complete elution of all the products plus 2 minutes for GC equilibrium. The computer software used for this analysis was Star Chromatography workstation version 5.5.1.

7.2.3.1 Column conditions

Injector temperature: 150^{o}C
Carrier gas: Argon
Detector temperature: 240^{o}C

The column heating profile is shown below;

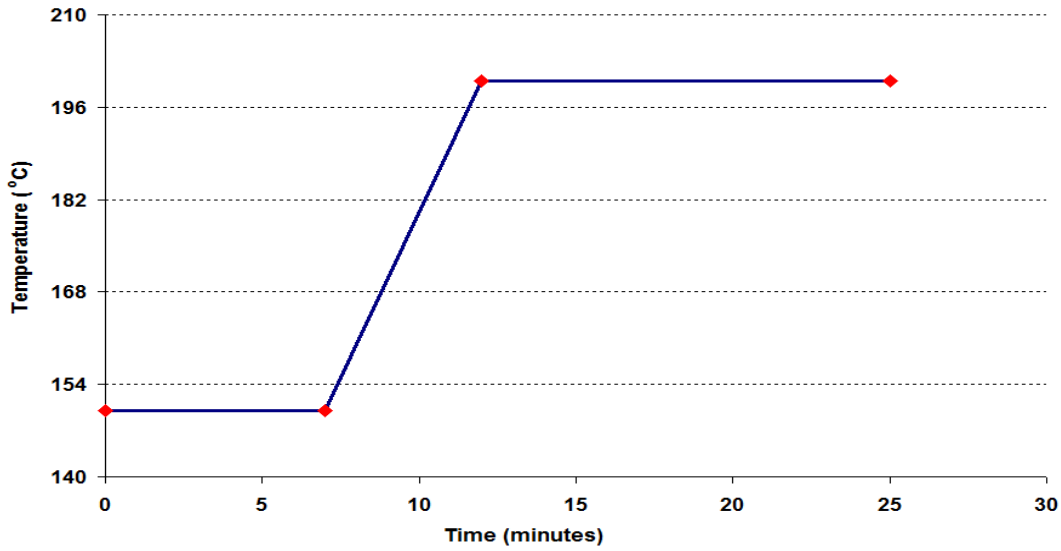

Figure 7.2-3 Temperature ramping profile for Varian Gas Chromatography 3400

7.2.3.2 Calibration of gases products

Prior to the reaction, calibration of H_2, CO, CO_2, CH_4, C_2H_4 and C_2H_6 was carried out by connecting the appropriate gas cylinder to the reactor MFC. Different concentrations were passed through the GC by varying the flow rate of the gas and the inert carrier gas (argon), whilst ensuring the total flow rate of the gas mixture was kept constant. This was monitored by digital flow meter on the vent of the reactor. The number of moles of gas being injected into the GC was calculated using the following relationship.

$$\text{Number of moles} = (PV/RT)^* \text{ \% of gas in mixture}$$

Where P = pressure (1atm), V = volume of sample loop (250 µl), R = gas constant (0.0821 L atm K^{-1} mol^{-1}), T = temperature of laboratory

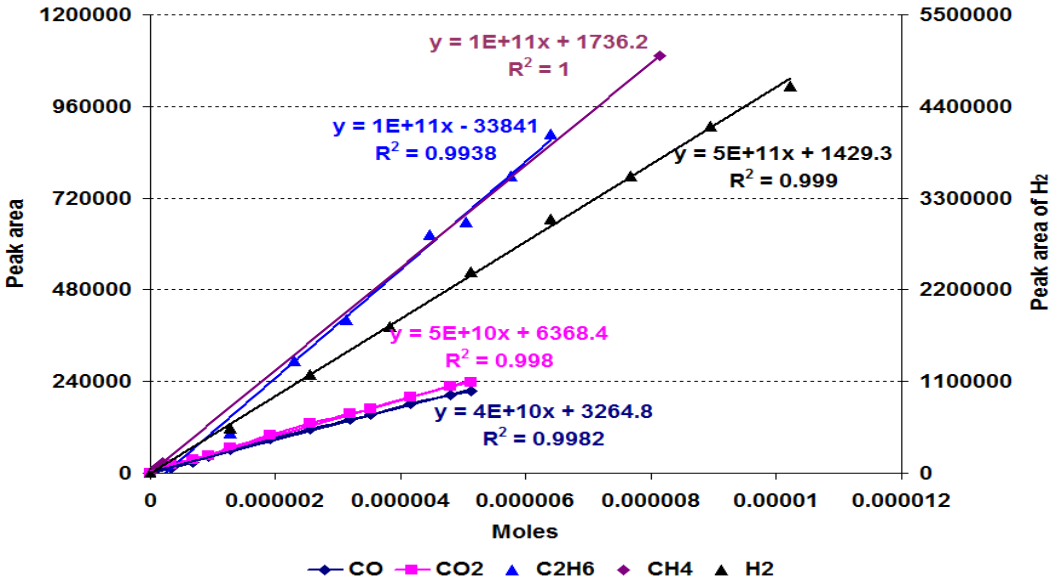

Figure 7.2-4 GC calibration for gaseous products

7.2.4 Liquid phase GC analysis

High boiling point products were liquefied in the knockout pot and collected for analysis. These products were analysed by an offline Trace Gas Chromatography 2000 Series Gas using a 30 m Zebron Wax plus column and FID detector. The Zebron Wax plus column was used to separate a large range of compounds such as diethyl ether, ethanol, acetaldehyde, acetone, ethyl acetate, 1,1-diethoxyethane, methanol, acetic acid, IPA and 1-Propanol.

7.2.4.1 Column conditions

Injector temperature: 140^{o}C

Carrier gas: Helium

Detector temperature: 280^{o}C

The column heating profile is shown below;

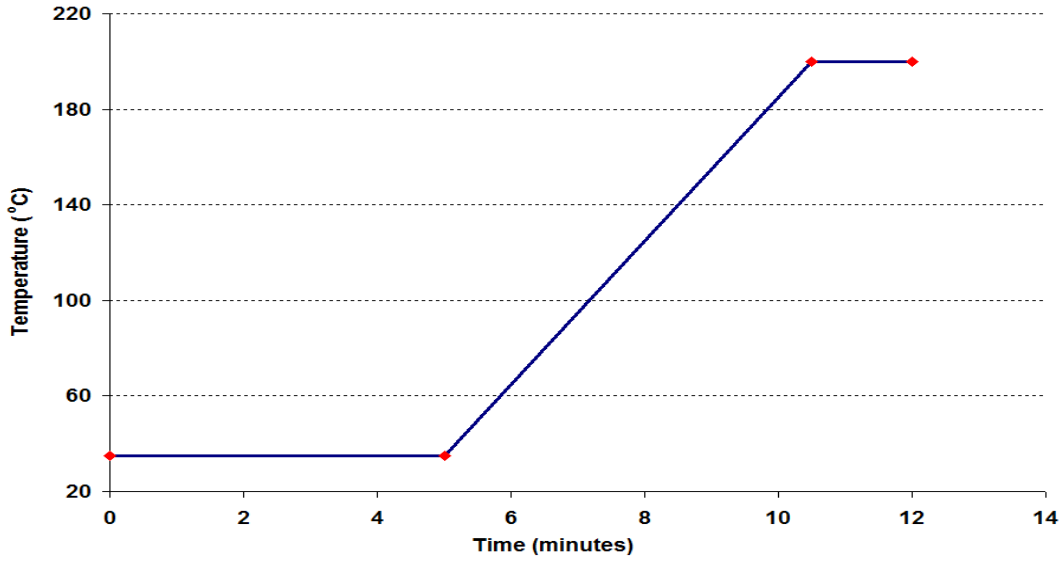

Figure 7.2-5 Temperature ramping profile for Gas Chromatography 2000 Series

7.2.4.2 Calibration of liquid reactants and products

Prior to the reactions, all possible products and reactants were prepared in varying concentrations using deionized water as the solvent. The relationship between the varying concentrations and the corresponding peak areas obtained from GC were identified by plotting the concentration against the GC response. The resulting slopes from graphs were used to calculate the unknown concentration of reactants and products.

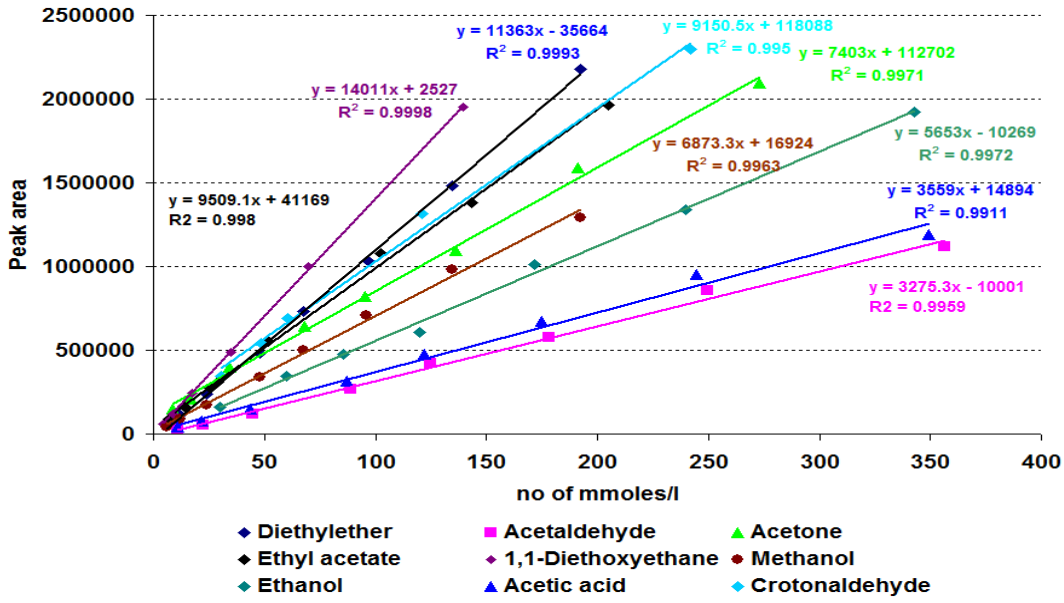

Figure 7.2-6 GC calibration for liquid products

7.2.5 Calculations

The calculations used for the ethanol steam reforming results are summarised here.

7.2.5.1 Conversion

Ethanol conversion was calculated as follow;

% Conversion

= [mmoles of ethanol in – mmoles of ethanol out]/ [mmoles of ethanol in]*100

7.2.5.2 Rate of formation of products

Similarly the rates of formation of liquid products were calculated using the following formula.

Rate = [mmoles of product X out]/ [gram of catalyst*s]

Rate of formation of gaseous products were calculated using the following formula.

Rate = [mmoles of product X out]/ [gram of catalyst*residence time]

7.2.5.3 Yields of products

The yields for products were calculated as follows;

%Yield for liquid products =

[mmoles of product X out]/ [mmoles of ethanol in]*100

%Yield for H_2

[mmoles of H_2 produced per unit time]/ [3*(mmoles of ethanol in per unit time)]*100

%Yield for CH_4, CO_2 and CO

[mmoles of X produced per unit time]/ [2* (mmoles of ethanol in per unit time)]*100

Where X represent CH_4, CO_2 and CO

%Yield for C_2H_4, and C_2H_6

[mmoles of X produced per unit time]/ [mmoles of ethanol in per unit time]*100

Where X represent C_2H_4, and C_2H_6

7.2.6 Steam reforming of ethanol reactions

The reactions performed in the steam reforming of ethanol reactor are summarised in Table 7.2-3 and 7.2.4

Catalyst	Temperature (^oC)		
	500	550	600
Al_2O_3	√	-	√
Ru/Al_2O_3	√	√	√
Rh/Al_2O_3	√	√	√
Pt/Al_2O_3	√	√	√

Table 7.2-3 Steam reforming of ethanol reaction at different temperatures

The amount of each impurity added to water/ethanol mixture was 1mol.% with respect to ethanol.

Catalyst	Impurity				
	1-Propanol	IPA	Acetone	Propanal	Propylamine
Al_2O_3	√	-	-	-	√
Ru/Al_2O_3	√	√	√	√	√
Rh/Al_2O_3	√	√	√	√	√
Pt/Al_2O_3	√	√	√	√	√

Table 7.2-4 Steam reforming of ethanol reaction using different impurities

7.3 Materials

The following materials were used as reactants and for GC calibrations with no further purification.

Chemicals/gases	Suppliers	Purity (%)
Methanol	Fisher Scientific	99.99
Ethanol	AnalaR Normapur	99.99
Diethylether	Fisher Scientific	99.88
Acetaldehyde	Aldrich	99.00
Acetone	Fisher Scientific	99.99
Ethyl acetate	Aldrich	99.80
1,1-Diethoxyethane	Acros Organic	99.99
Acetic acid	AnalaR Normapur	99.99
Isopropyl alcohol	Sigma Aldrich	99.50
1-Propanol	Alfs Aesar	99.00
Propylamine	Aldrich	99.00
Propanal	Sigma Aldrich	97.00
H_2	BOC	99.98
CO/CO_2	BOC	99.00
C_2H_6	BOC	99.00
C_2H_4	Scientific and Technical gases Ltd	-
Ar	BOC	100.00
2% O_2/Ar	BOC	99.96

Table 7.3-1 Materials used

8. Results

All catalysts used for the steam reforming of ethanol were previously characterised by Opera and reduced according to the procedure laid out in section 7.2. The catalysts were characterised by powder XRD and BET, to investigate if any variation in the crystallinity and surface area of catalysts took place after reduction at 600^{o}C. The analysis was also used for comparison with post reaction catalysts to determine if any change in catalyst phase and surface area occurred after exposure to the ethanol steam reforming reaction.

8.1 Catalyst characterisation

8.1.1 Powder XRD

All samples were studied by powder XRD to examine the degree of crystallinity and phase in the calcined and reduced catalysts. Alumina has more than a dozen well documented and characterised amorphous and crystalline structures as discussed in section 6.7 [123]. Thus, to determine which phase of alumina is present in the catalysts, samples were run on powder X-Ray diffraction.

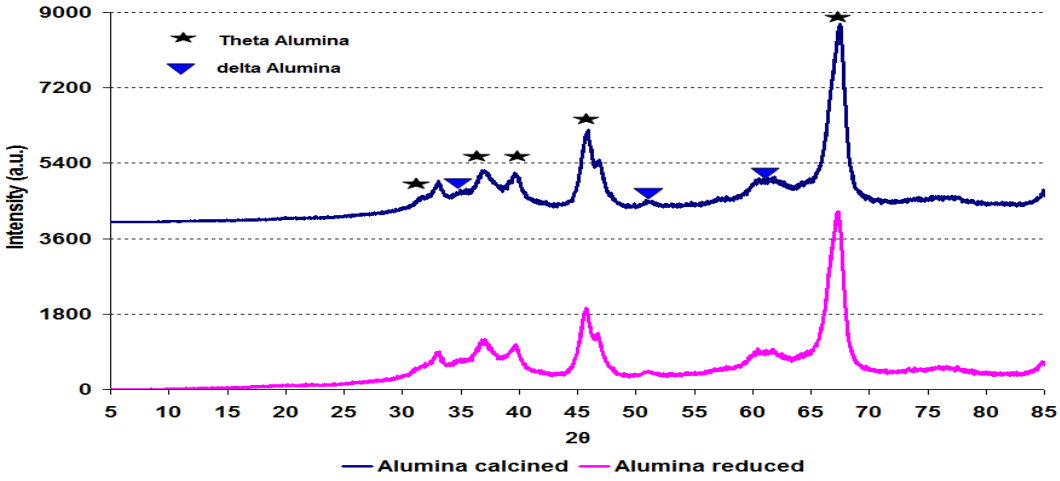

Figure 8.1-1 Powder XRD patterns for pure Al_2O_3 catalyst

Figure 8.1-1 shows that the powder XRD patterns for both the calcined and reduced alumina samples give similar peaks at different 2θ positions. This suggests that there is no variation in the phase of alumina due to the heat treatment received during the reduction process. In addition the calcined sample had very similar crystallite sizes (130 Å) when compared to the reduced sample (126 Å), suggesting that no significant change in crystallinity occurred during reduction. The powder XRD patterns matched well with the

fingerprint pattern of the theta alumina and delta alumina reported in the literature and also with the ICDD database. These phases of alumina were expected from the thermal treatment during alumina preparation [123, 124].

The structure of the rhodium, platinum and ruthenium doped alumina supports were characterised by powder XRD using the method described in section 7.1.4. Scans were carried out at room temperature for both the calcined and the reduced samples for each catalyst. The results obtained showed similar patterns for all the catalysts to those seen in the alumina support powder XRD patterns. These results suggest that metal doping results in no significant change in the alumina structure.

8.1.2 BET analysis

BET surface area analysis was carried out on both the calcined and the reduced catalysts to inspect for changes in the surface area and average pore diameter with changes to the pre-treatment atmosphere. In addition both forms of pure alumina were examined by BET for comparison with the spent catalysts. The detailed procedure was discussed in section 2.1 and results obtained are tabulated below in Table 8.1-1

Catalyst	Thermal treatment (^oC)	BET Surface area (m^2/g)	Average pore diameter (Å)
Al_2O_3	Calcined (450)	99	175 (± 9.61)
	Reduced (600)	101	180 (± 8.60)
Ru/Al_2O_3	Calcined (450)	107	168 (± 4.03)
	Reduced (600)	100	172 (± 3.57)
Rh/Al_2O_3	Calcined (450)	106	170 (± 1.79)
	Reduced (600)	101	174 (± 0.98)
Pt/Al_2O_3	Calcined (450)	107	162 (± 1.35)
	Reduced (600)	100	180 (± 8.41)

Table 8.1-1 BET analysis of pure and noble metal supported alumina

Table 8.1-1 shows, upon the addition of the metal to the alumina support in calcined form a small increase occurred in the surface area whilst no significant change in average pore diameter was observed. On the contrary, in the reduced form, the surface area of metal doped catalyst was similar to the pure alumina whilst the average pore diameter, especially in Ru and Rh catalysts, slightly decreased.

8.2 Effect of temperature

Although the main aim of this project was to examine the tolerance of different catalysts to the different impurities present in crude ethanol during a steam reforming reaction, the influence of temperature on catalyst activity and selectivity was also studied. The yields of different products produced during steam reforming of ethanol were determined. Three reaction temperatures of 500^{o}C, 550^{o}C and 600^{o}C were employed with each catalyst to examine the effect of temperature on the reaction. Reactions were also carried out over pure alumina for comparison to identify any possible role of the alumina in the reaction.

8.2.1 Al_2O_3

The Al_2O_3 was investigated for steam reforming of ethanol at different temperatures to show if it had a role in the steam reforming reaction of ethanol. In order to assess the alumina support, two reactions were performed at varying temperatures.

8.2.1.1 Reaction at 500^{o}C

Initially the reaction was carried out at 500^{o}C, following the procedure discussed in section 7.2.2. The activity of the catalyst towards ethanol; the conversion of ethanol, the yield and the rate of formation of products were calculated as discussed in section 7.2.5. The results obtained are plotted against time on stream, shown in Figures 8.2-1 to 5.

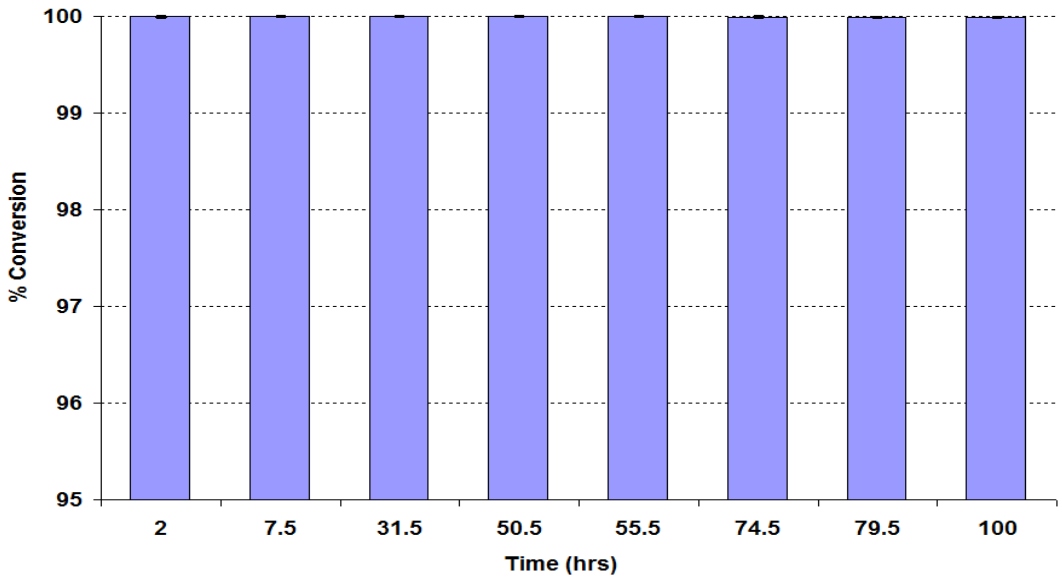

Figure 8.2-1 % Conversion of ethanol over Al_2O_3 catalyst at 500^{o}C

The experimental data in Figure 8.2-1 show that the conversion of ethanol was 99.9% at 500^{o}C and Al_2O_3 was active for 55.5 hours time on stream (TOS). The above figure also illustrates that insignificant deactivation of the catalyst started after 55.5 hours, although it was still active, with a very small deactivation observed up to 100 hours TOS.

Different liquid and gaseous products were formed throughout the reaction at different rates. The products were analysed at different intervals by GC and plotted against time on stream and are shown in Figures 8.2-2 to Figure 8.2-3.

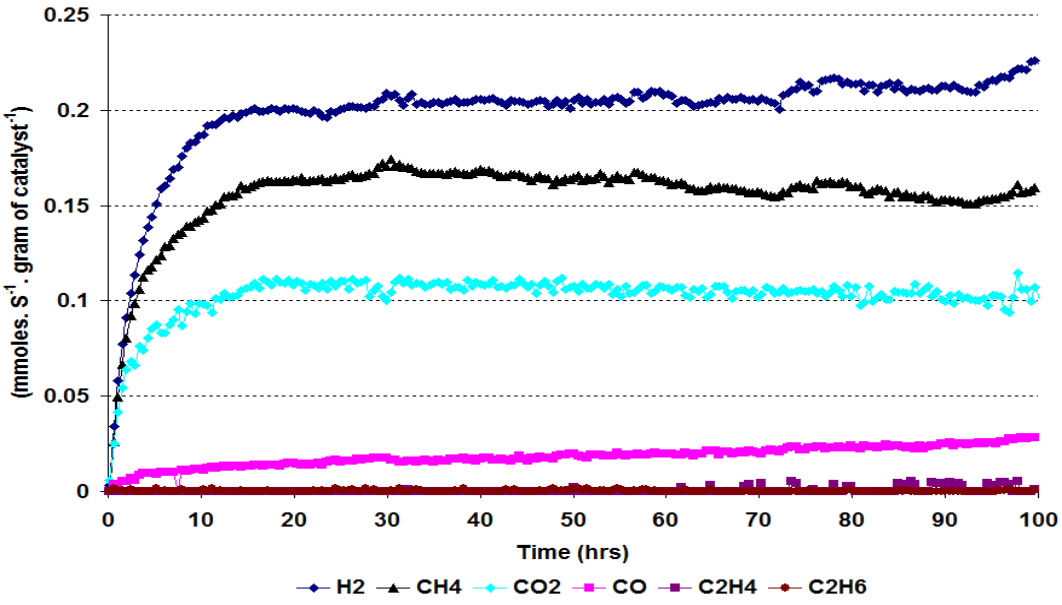

Figure 8.2-2 Rate of formation of gaseous products over Al_2O_3 catalyst at 500^{o}C

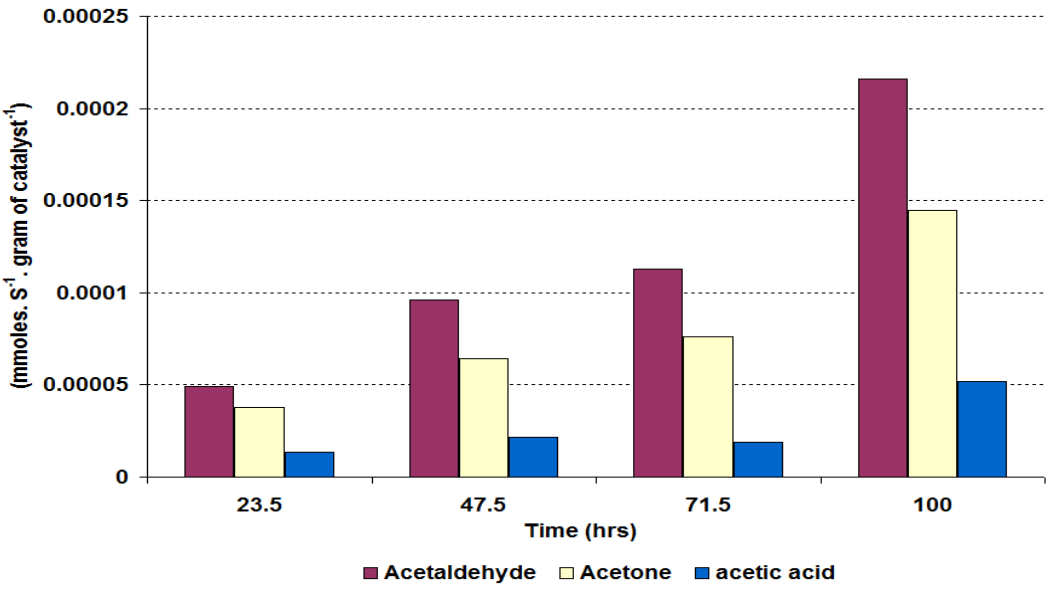

Figure 8.2-3 Rate of formation of liquid products over Al_2O_3 catalyst at 500^{o}C

Figure 8.2-2 to Figure 8.2-3 illustrates the distribution of the gaseous and liquid products of the reaction at 500^{o}C. H_2, CH_4 and CO_2 were the major gaseous products and achieved steady state conditions after 12 hours time on stream (TOS), with no deactivation noticeable up to 100 hours. Minor gaseous products formed were CO, C_2H_4, and C_2H_6. It is noticeable that the trace rate of formation of CO steadily increased with time but did not reach steady state condition within the 100 hours TOS.

Figure 8.2-3 compares the rate of formation of liquid products produced at a reaction temperature of 500^{o}C. As the figure illustrates, only acetone, acetaldehyde and acetic acid were formed during the reaction at 500^{o}C. The rate of formation of these products increased with time, however, by 100 hours time on stream no liquid product achieved steady state. Trace levels of methanol were also detected by GC.

Yields of both liquid and gaseous products were calculated for reaction at 500^{o}C, as described in section 7.2-5. The results obtained are plotted as a function of time on stream, as presented in Figures 8.2-4 to 5.

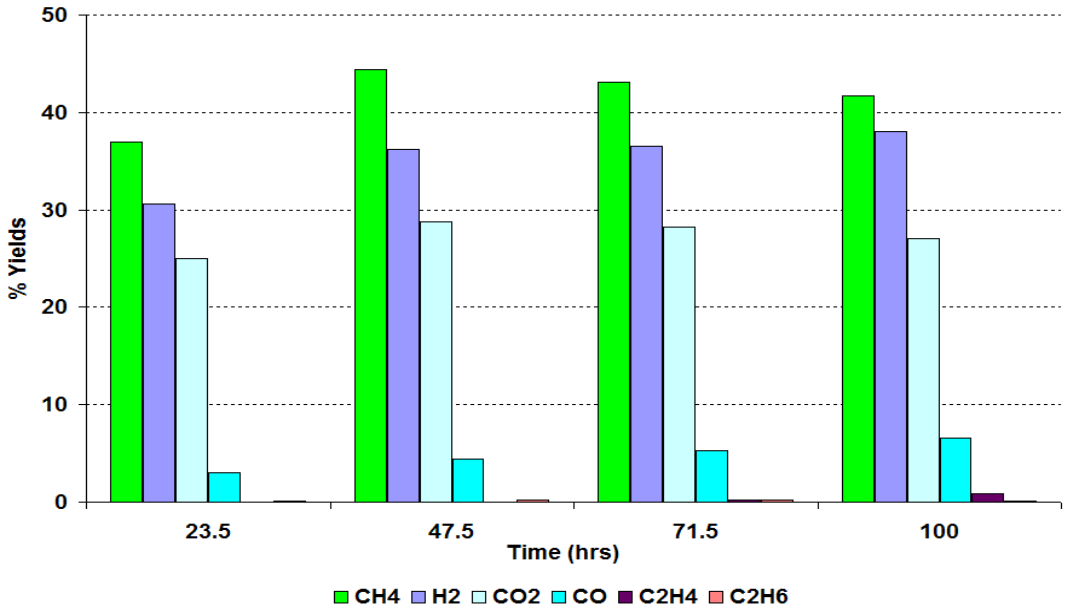

Figure 8.2-4 % Yield of gaseous products over Al_2O_3 catalyst at 500^{o}C

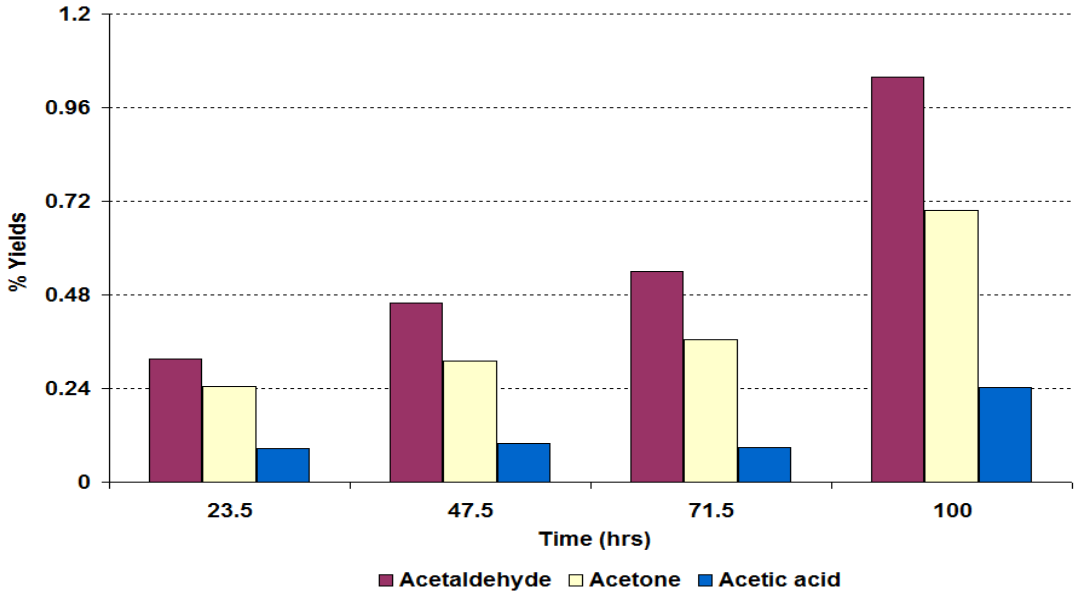

Figure 8.2-5 % Yield of liquid products over Al_2O_3 catalyst at 500°C

CH_4, H_2 and CO_2 were the major gaseous products at 500°C. The yields of liquid products at 500°C were small, the maximum yield for acetaldehyde was 1%, and was less than 1% for acetone and other liquid products.

8.2.1.2 Post reaction characterisation

Post reaction catalyst characterisation was carried out using TPO, powder XRD, Raman spectroscopy, SEM and BET to examine any changes taking place in the morphology and phase of the catalyst after 100 hours on stream.

8.2.1.2.1 TPO

A TPO was carried out on the spent Al_2O_3 to check for any coke lay down that may have occurred on the catalyst. This was done using TGA/DSC connected to a mass spectrometer as discussed in section 7.1-1.

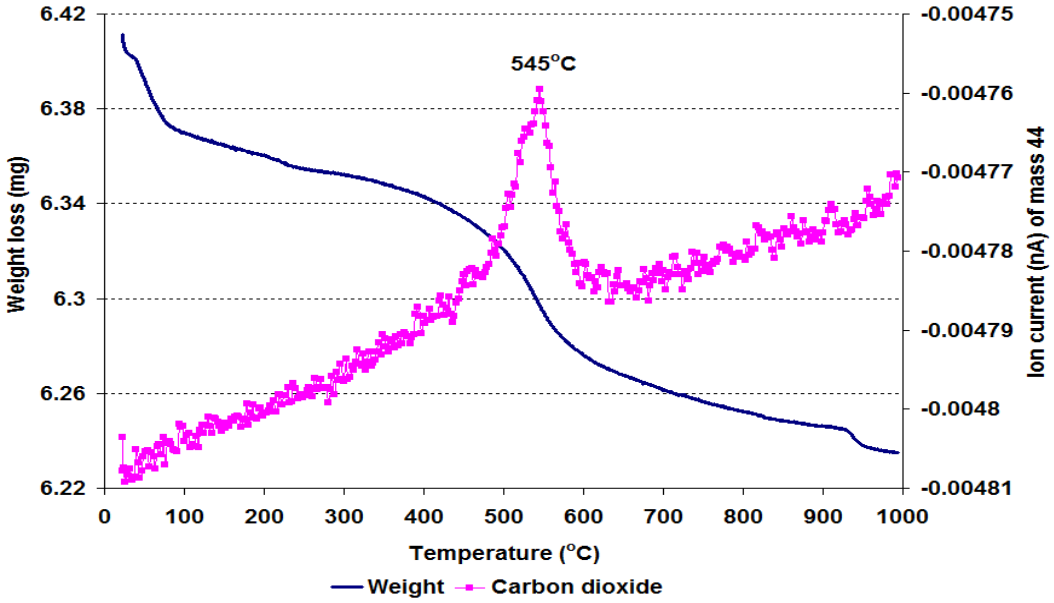

Figure 8.2-6 Post reaction TPO and m/z= 44 (CO_2) for Al_2O_3 catalyst at 500°C

From Figure 8.2-6 it is obvious that a small weight loss takes place during the TPO *i.e.* only a 2.75% weight loss occurred by 1000°C. This weight loss was equal to 27.5 mg g^{-1} of sample. From the mass fragments, the weight loss below 100°C corresponded to physisorbed water. The major weight loss occurring from 400°C to 650°C matches mass CO_2 and trace amounts of ethanol fragments (m/z 45) as shown in Figure 8.2-6.

8.2.1.2.2 Powder XRD

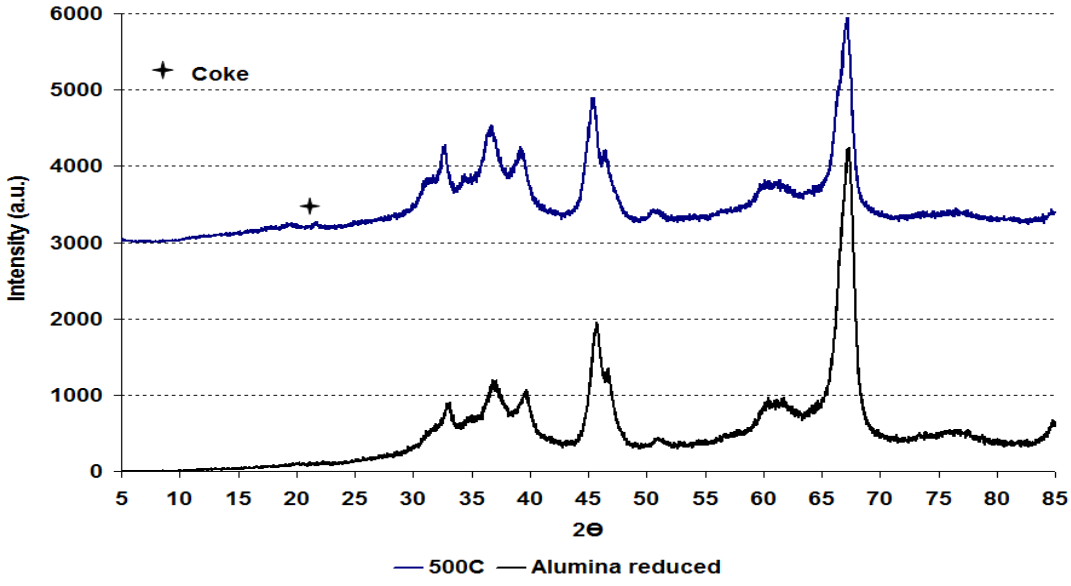

Figure 8.2-7 Powder XRD patterns of reduced and post reaction Al_2O_3 catalyst at 500°C

The post reaction catalyst was run at room temperature on powder XRD and data obtained was plotted and shown in Figure 8.2-7. The peaks for the Al_2O_3 particles before and after the reaction were compared. Comparison showed that after reaction at 500^oC, the Al_2O_3 gave a comparatively similar pattern and crystallite size to the Al_2O_3 in reduced form. Hence no distinguishable changes in the phase of alumina support occurred during the reaction. There also appeared to be a small peak at 2θ position of 26^o that could be assigned to coke. Similar results were obtained for the 600^{o}C reaction sample although the peak for coke was comparatively more intense than in the 500^{o}C reaction sample.

8.2.1.2.3 Raman analysis

The graph shown in Figure 8.2-8 represents the Raman spectra of the post reaction catalyst from the reaction at 500^{o}C. It illustrates the three different coloured particles *i.e.* black, gray and white seen in the sample. These are expected to originate from the upper, middle and lower portion of the catalyst bed. However, they were collected randomly from the post reaction sample. The white particles gave a peak at wavenumber 1621 cm^{-1} which is a characteristic band of graphitic carbon (G band) and according to the literature, is produced due to an E_{2g} mode vibration of graphitic carbon. On the other hand, the gray and black particles both gave peaks at wavenumber 1599 cm^{-1} and 1328 cm^{-1} which correspond to G and D bands. The D band in the Raman spectrum of graphitic carbon gives an indication of disorder in the graphitic structure [125]. The intensity of both of these peaks decreased when going from the gray to the black particle.

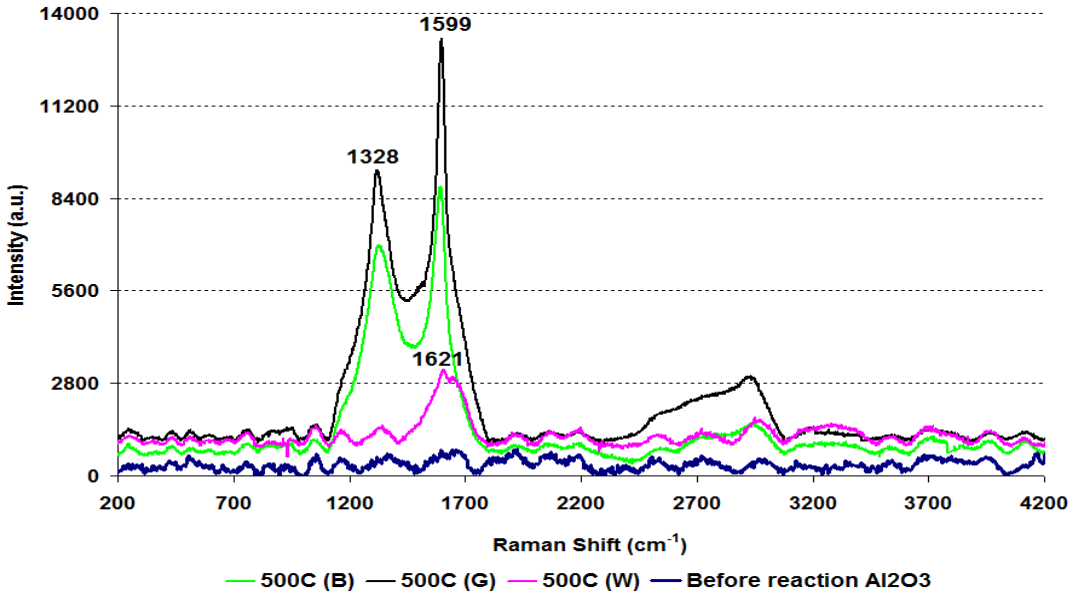

Figure 8.2-8 Post reaction Raman spectra for Al_2O_3 catalyst at 500^{o}C

8.2.1.2.4 SEM

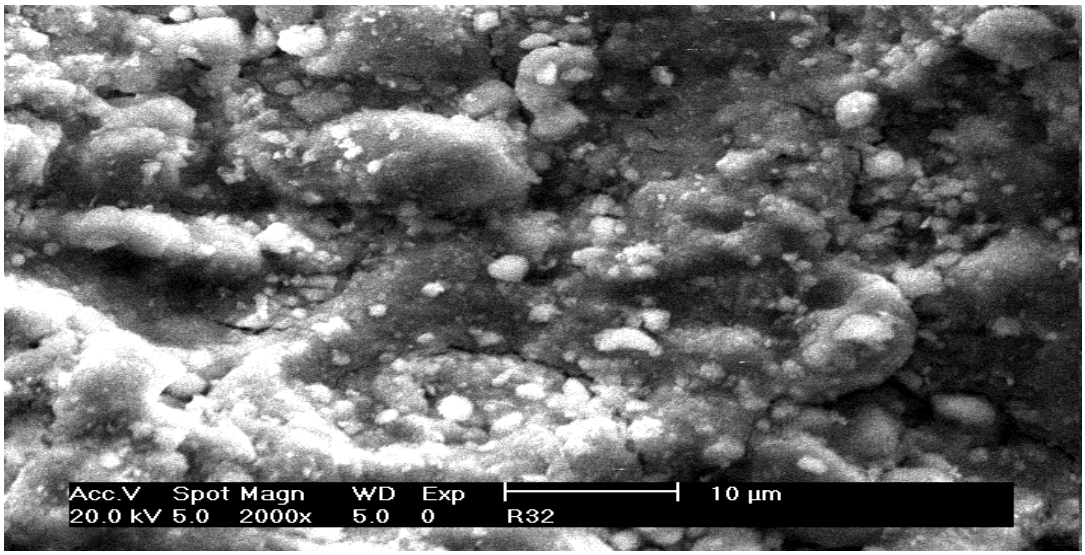

Figure 8.2-9 Post reaction SEM image of Al_2O_3 catalyst at 500°C

SEM image of post reaction Al_2O_3 shows similar structures to the reduced form.

8.2.1.2.5 BET analysis

Catalyst	Conditions	BET Surface area (m^2/g)	Pore volume (cm^3/g)	Average pore diameter (Å)
Al_2O_3	Reduced (600°C)	101	0.45 (± 0.31)	180 (± 8.60)
	500°C	80	0.40 (± 0.45)	202 (± 3.97)

Table 8.2-1 BET analysis of post reaction Al_2O_3 catalyst at 500°C

BET analysis shows that both the surface area and the pore volume of the Al_2O_3 catalyst decreased after the catalyst was exposed to the steam reforming reaction at 500°C whilst the average pore diameter increased.

8.2.1.3 Reaction at 600°C

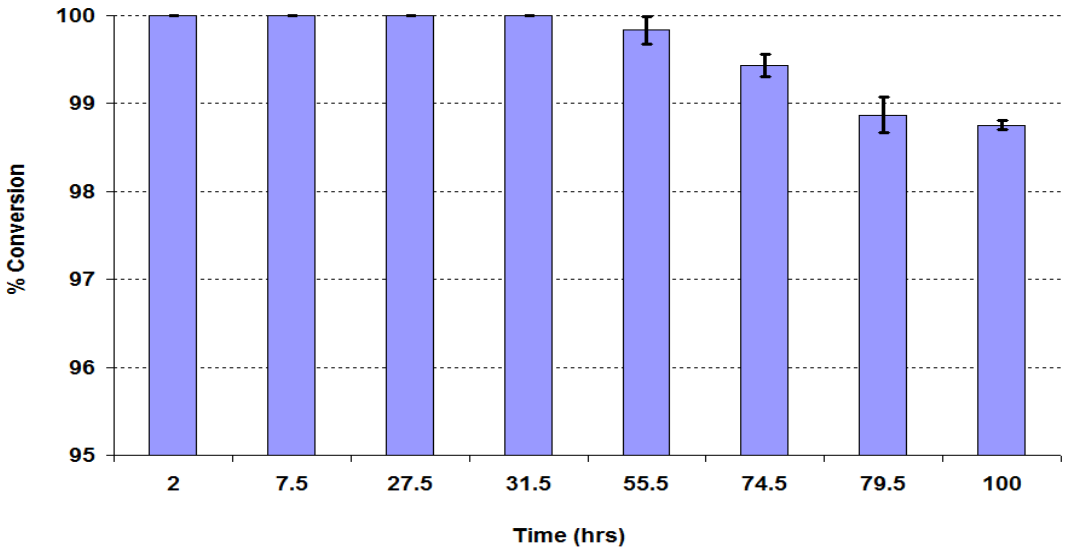

Figure 8.2-10 % Conversion of ethanol over Al_2O_3 catalyst at 600°C

When the steam reforming of ethanol reaction was run at 600°C with the Al_2O_3, initially the conversion of ethanol was similar to that of the reaction at 500°C, as shown in the Figure 8.2-10. Also, the deactivation of catalyst started at the same interval time on stream. However, comparatively severe deactivation was observed to that of 500°C and the conversion of ethanol decreased to 98.7% after 100 hours time on stream.

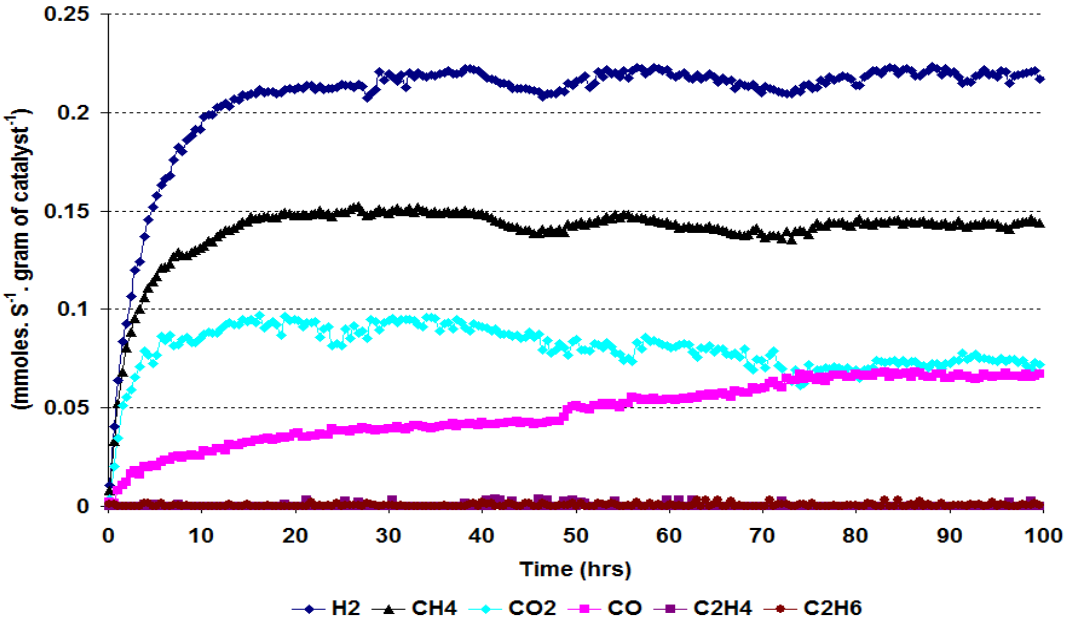

Figure 8.2-11 Rate of formation of gaseous products over Al_2O_3 catalyst at 600°C

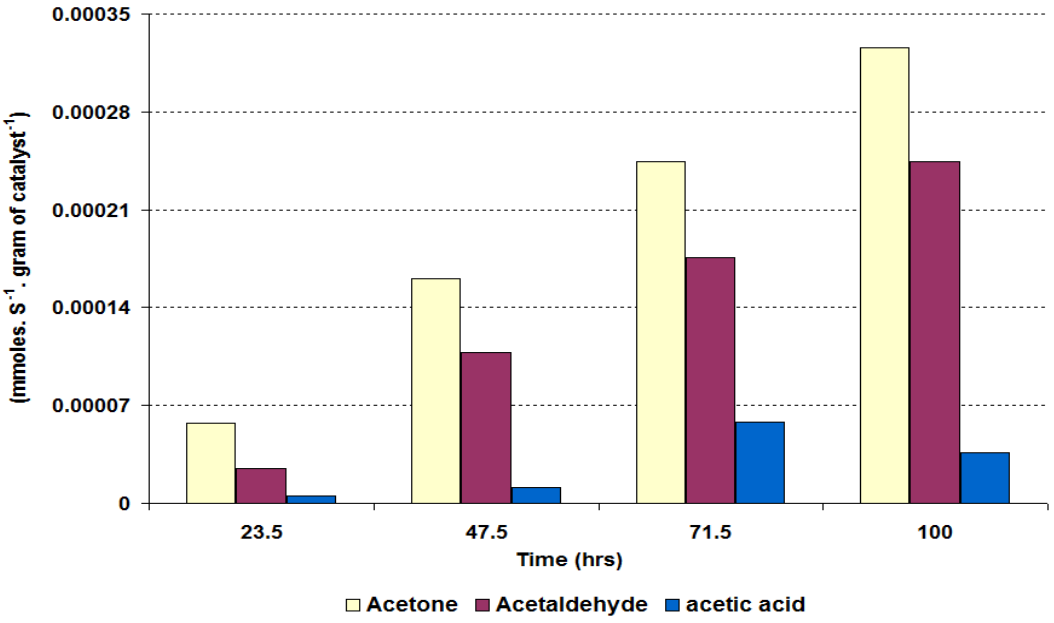

Figure 8.2-12 Rate of formation of liquid products over Al_2O_3 catalyst at 600°C

Figure 8.2-11 and 12 illustrate the distribution of the gaseous and liquid products of the reaction at 600°C. Similar to 500°C, the major gaseous products were H_2, CH_4 and CO_2. After 16 hours time on stream CH_4 and H_2 obtained steady state condition that was continuous until the end of the reaction, and no deactivation in the rate of either product was observed. However, the rate of CO_2 initially increased up to 16 hours TOS, stabilised for some time and then started to decrease gradually. The rate of CO product increased progressively through the 100 hours TOS. After 74 hours both CO_2 and CO had obtained similar reaction rates and had become stable. Also produced were trace amounts of C_2H_4 and C_2H_6.

Liquid products produced at 600°C are shown in Figure 8.2-12. At 600°C the liquid products follow the same pattern as was observed at 500°C. The rate of both the acetone and the acetaldehyde increased with time on stream, whereas the rate of acetic acid production initially increased up to 72 hours and then decreased. From the graph it is shown that neither liquid product achieved steady state condition throughout the 600°C reaction. Also produced were trace amounts of diethyl ether and methanol.

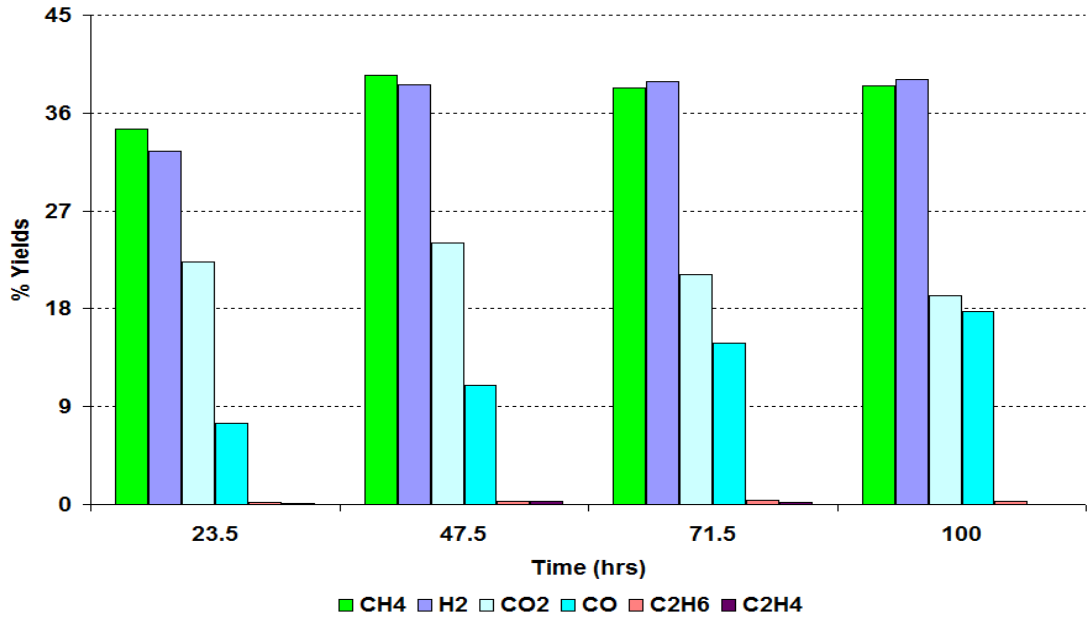

Figure 8.2-13 % Yields of gaseous products over Al_2O_3 catalyst at 600°C

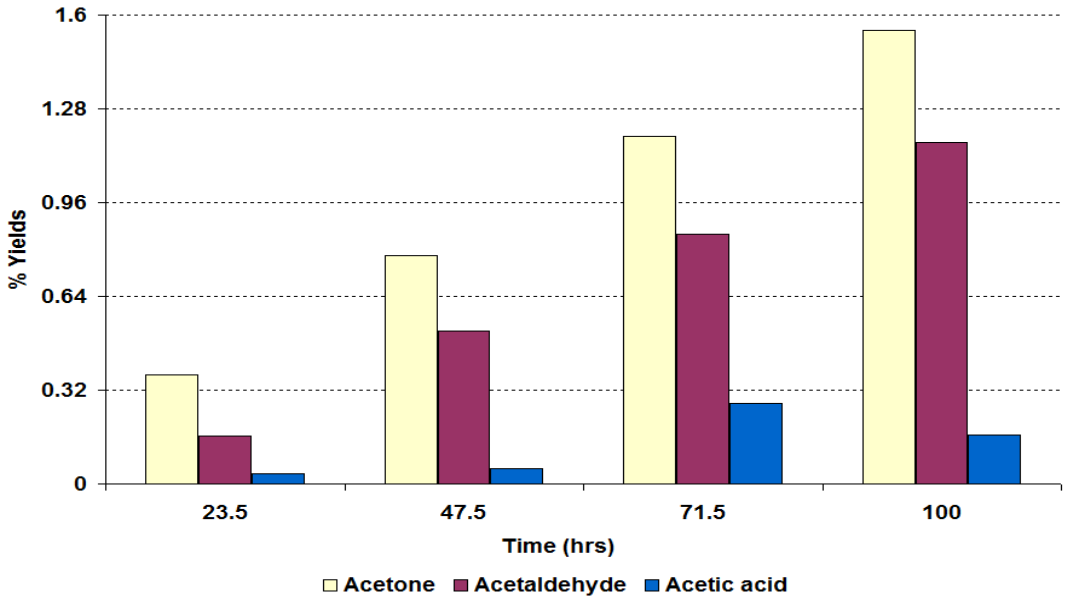

Figure 8.2-14 % Yields of liquid products over Al_2O_3 catalyst at 600°C

CH_4 and H_2 were produced with high yields but showed a slight increase after 24 hours TOS. The yield of CO_2 gradually decreased whilst that of CO increased and both obtained a similar yield at 100 hours TOS.

Similar to the reaction run at 500°C, the yields of the liquid products were much lower with a maximum value of ~ 1.5% for acetone and with < 1.2% for the other liquid products.

8.2.1.4 Post reaction characterisation

8.2.1.4.1 TPO

A TPO was carried out for the Al_2O_3 catalyst from the steam reforming reaction at 600°C. The TGA profile, along with mass fragments, is plotted against temperature and shown in Figures 8.2-15 and 8.2-16.

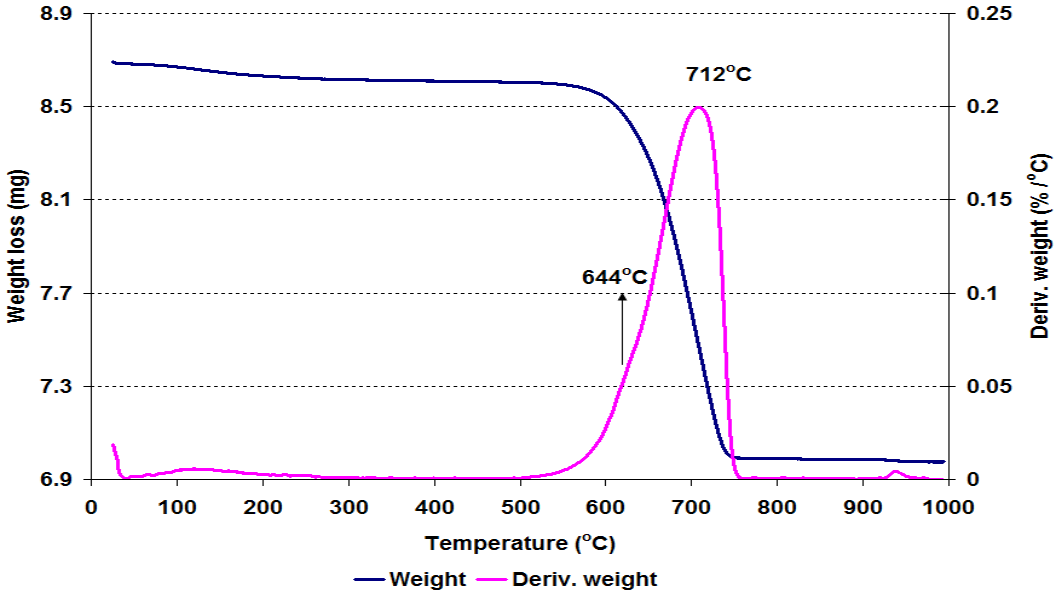

Figure 8.2-15 Post reaction TPO for Al_2O_3 catalyst at 600°C

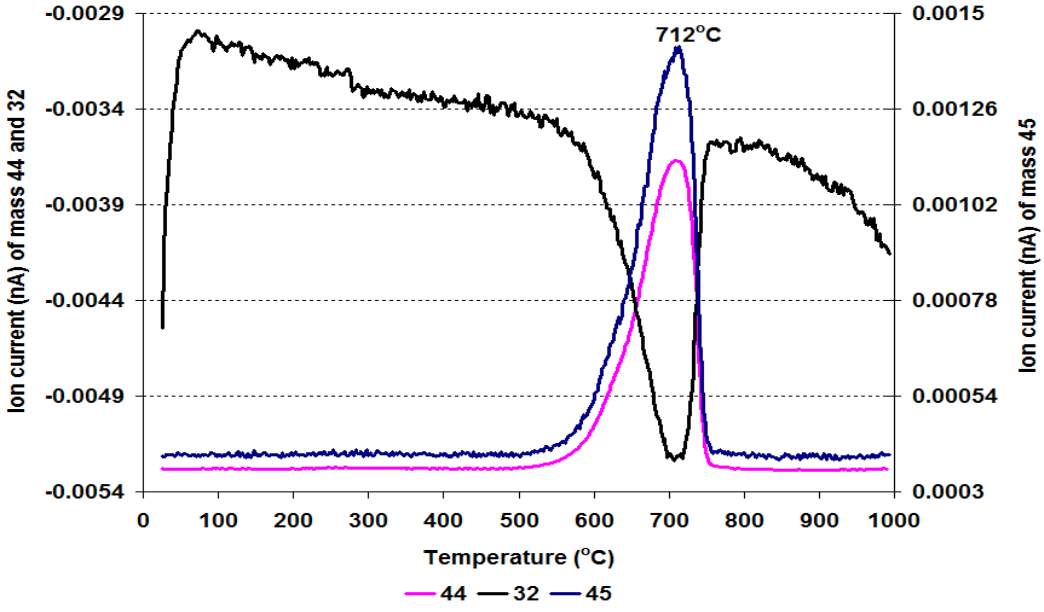

Figure 8.2-16 MS data of CO_2 (m/z=44), O_2 (m/z=32) and C_2H_5OH fragment (m/z=45) for Al_2O_3 catalyst at 600°C

Figure 8.2-15 demonstrates the presence of two weight loss events taking place up to 1000^{o}C. The initial, very small weight loss occurred below 200^{o}C and corresponds to desorption of water in the mass spectrometry results. The second, and major weight loss occurred between 550^{o}C and 760^{o}C. The heat flow profile (not shown here), described that both weight loss events were exothermic processes. The second weight loss was the result of the evolution of CO_2 and principal mass fragments of ethanol as distinguishable from the mass spectrometry data. The total weight loss up to 1000^{o}C was 198 mg g^{-1} of catalyst sample.

8.2.1.4.2 Raman analysis

Figure 8.2-17 shows the Raman spectrum for the spent Al_2O_3 catalyst at 600^{o}C. Two bands at 1345 cm^{-1} and 1595 cm^{-1} were observed. As mentioned for the previous sample, these peaks correspond to D and G bands, which are characteristic bands for graphitic carbon. The graphitic carbon was also confirmed by overtone of the D band between 2680 cm^{-1} to 2700 cm^{-1} as indicated by the small band in Figure 8.2-17.

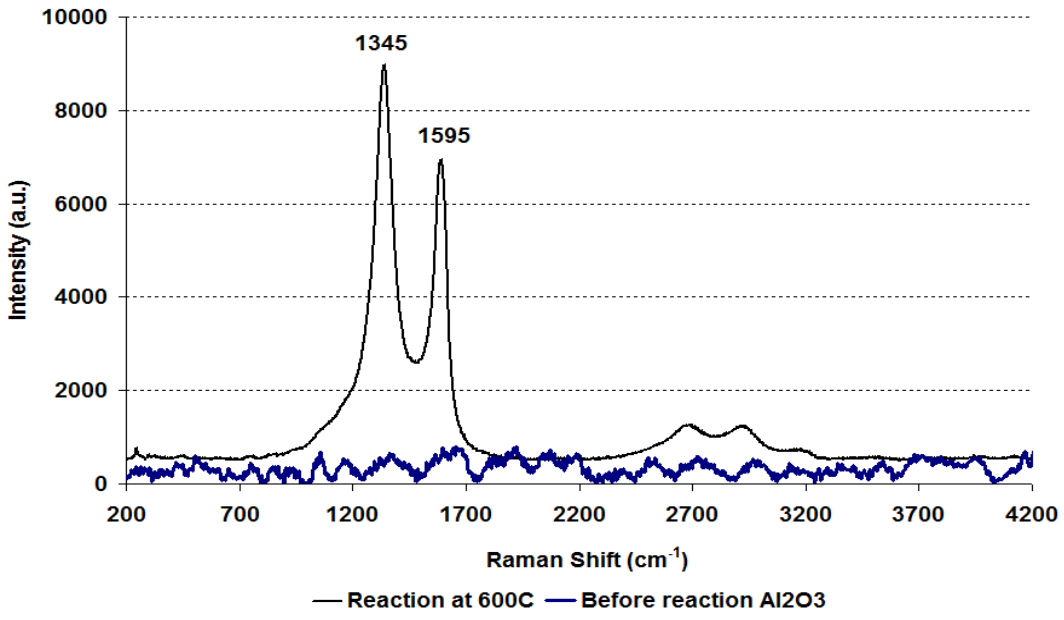

Figure 8.2-17 Post reaction Raman spectrum for Al_2O_3 catalyst at 600^{o}C

8.2.1.4.3 SEM

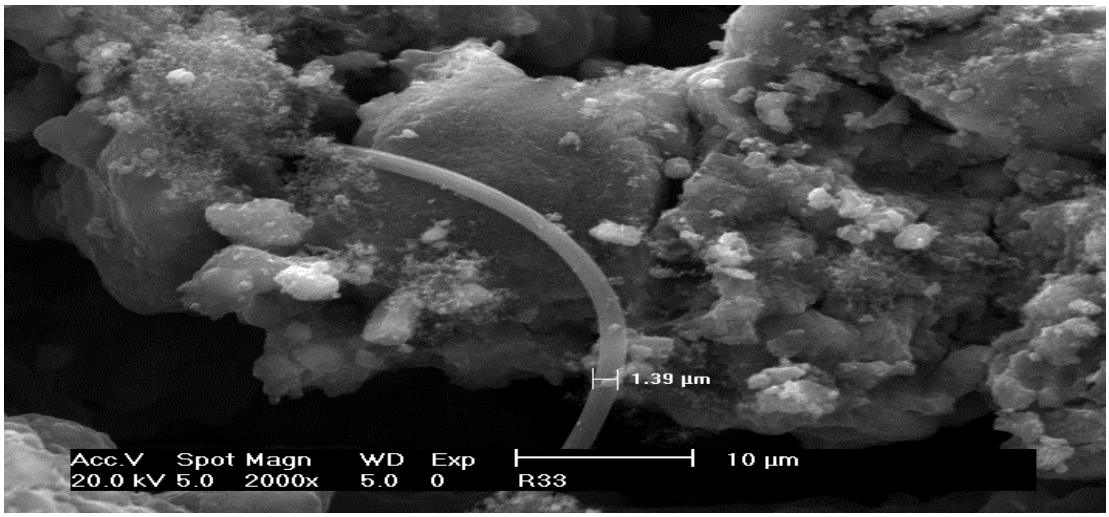

Figure 8.2-18 Post reaction SEM image of Al_2O_3 catalyst at 600^{o}C

Figure 2.3-18 illustrates the formation of filamentous carbon over Al_2O_3 catalyst during steam reforming of ethanol at 600^{o}C. The SEM image shows a bundle of small filamentous fibre deposits on different sites of the particle surface. Interestingly, there is also a nanotube type carbon present which is originating from the bundle of small filamentous fibre.

8.2.1.4.4 BET analysis

Catalyst	Conditions	BET Surface area (m^2/g)	Pore volume (cm^3/g)	Average pore diameter (Å)
Al_2O_3	Reduced (600^{o}C)	101	0.45 (± 0.31)	180 (± 8.60)
	600^{o}C	65	0.24 (± 0.05)	148 (± 4.84)

Table 8.2-2 BET analysis of post reaction Al_2O_3 catalyst at 600^{o}C

The BET surface area, pore volume and average pore diameter of the spent Al_2O_3 catalyst of the 600^{o}C are significantly decreased. The decrease in surface area and pore volume show that blocking of the pores with coke takes place and this is also evident from the SEM image.

8.2.2 Ru/Al_2O_3

After investigating the temperature effect on Al_2O_3 support in the steam reforming of ethanol reaction, the Ru/Al_2O_3 catalyst was examined at three different temperatures to examine the temperature effect on conversion and product distribution obtained during the steam reforming reaction.

8.2.2.1 Reaction at 500°C

The reaction was carried out over Ru/Al_2O_3 catalyst at 500°C following the procedure as discussed in section 7.2.2.

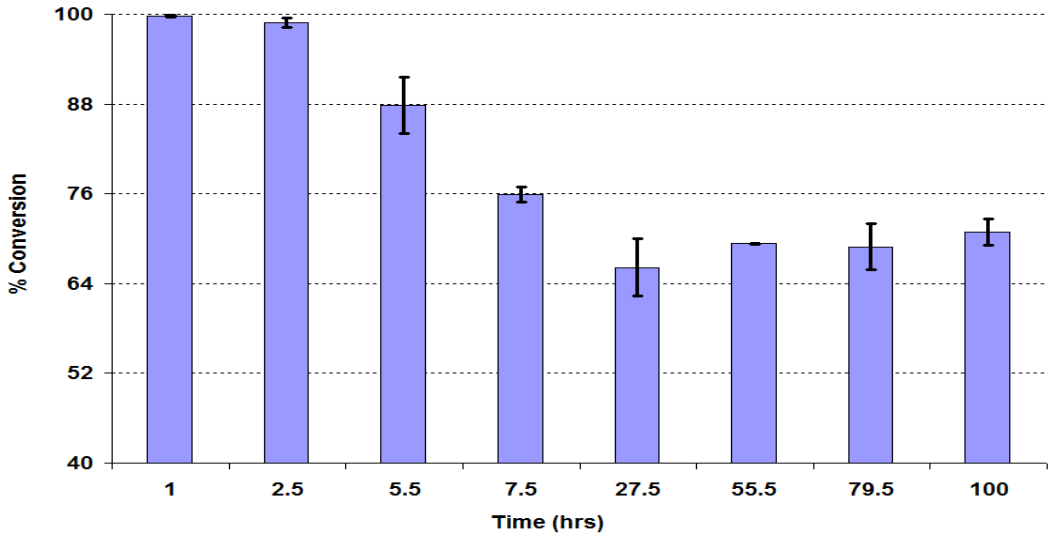

Figure 8.2-19 % Conversion of ethanol over Ru/Al_2O_3 catalyst at 500°C

Figure 8.2-19 shows that the conversion of ethanol at 500°C over the Ru/Al_2O_3 catalyst in the initial 2.5 hours was almost 99%. However, after 2 hours TOS deactivation of the catalyst took place and the conversion of ethanol decreased to 66%. After the initial deactivation, the rate stabilised and gave a steady conversion through to the end of the reaction.

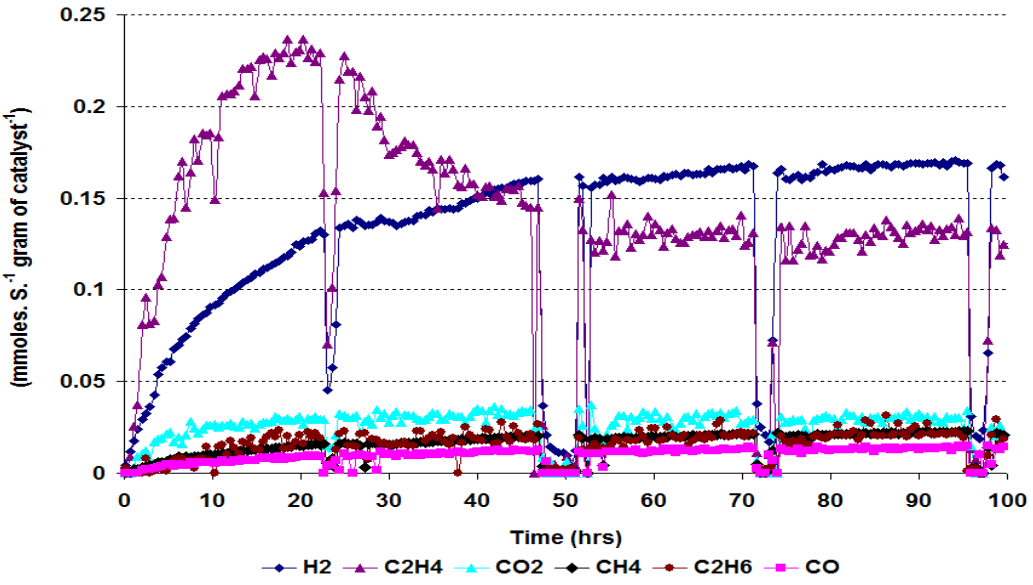

Figure 8.2-20 Rate of formation of gaseous products over Ru/Al_2O_3 catalyst at 500°C

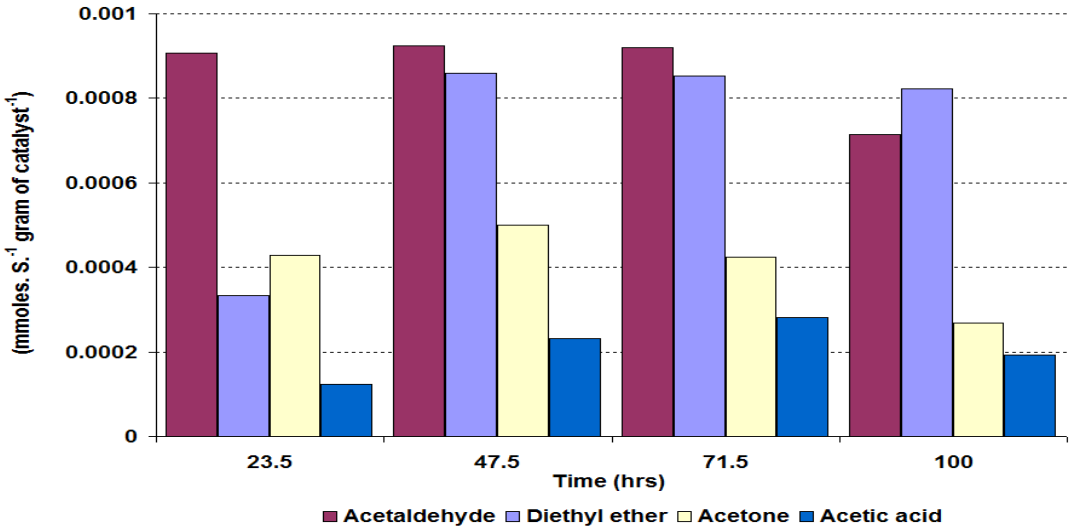

Figure 8.2-21 Rate of formation of liquid products over Ru/Al_2O_3 catalyst at 500°C

Figure 8.2-20 and 21 illustrate the rate of formation of gaseous and liquid products respectively over the Ru/Al_2O_3 catalyst at 500°C. C_2H_4 and H_2 were the major gaseous products, whilst minor amounts of CH_4, CO, C_2H_6 and CO_2 were also produced. The rate of formation of C_2H_4 rapidly increased in the initial 24 hours and then slowly decreased to a steady state condition after 48 hours. The rate of formation of H_2 steadily increased with time and achieved steady state values after 48 hours. Furthermore, it should be pointed out that due to the pressure drop after the initial liquid sample of each day the flow of gas to on-line GC was stopped which is clear from the drop in gaseous product distributions in Figure 8.2-20. However, it was resumed as discussed in section 7.2.2.

Acetaldehyde, diethyl ether, acetone and acetic acid were the major liquid products.

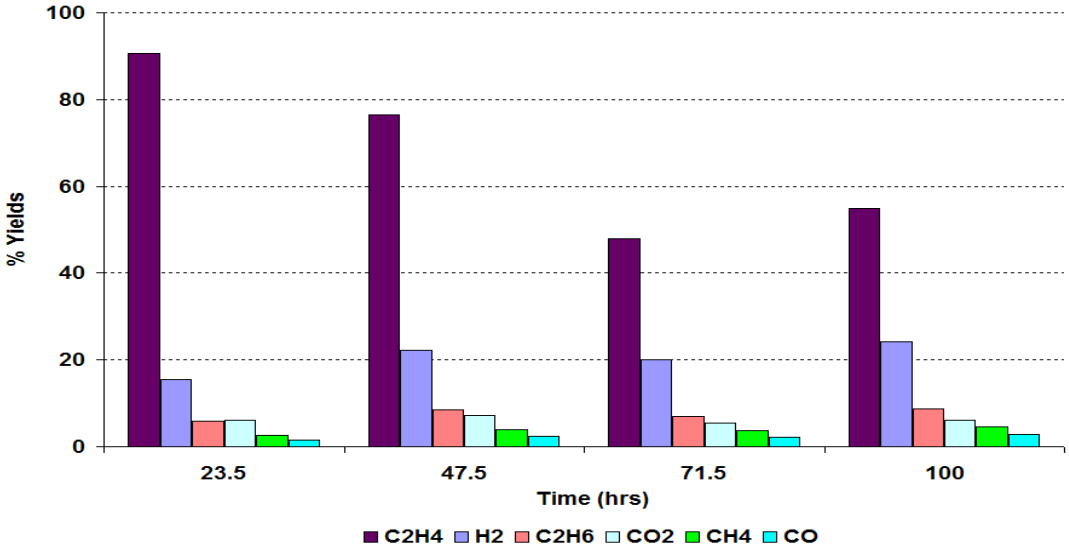

Figure 8.2-22 % Yield of gaseous products over Ru/Al_2O_3 catalyst at 500°C

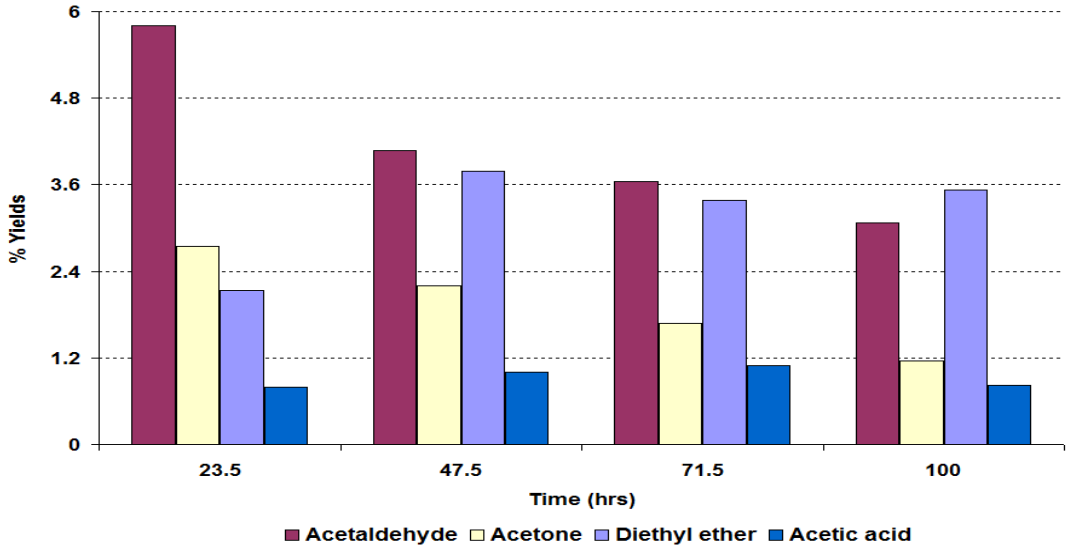

Figure 8.2-23 % Yield of liquid products over Ru/Al_2O_3 catalyst at 500°C

C_2H_4 gave a maximum yield of 90% however, with passage of time it decreased and reached 55% by the end of the reaction. H_2 was the other major gaseous product which had a 16% yield initially and after an initial slight increase, it stabilised throughout the reaction. Among the liquid products, acetaldehyde was the major product, giving above 5% yield at the start which decreased over reaction time. 1,1-Diethoxyethane, ethyl acetate, crotonaldehyde and methanol were also produced during the reaction in trace amounts.

8.2.2.2 Post reaction characterisation

To study the chemistry of the carbonaceous deposit on the Ru/Al_2O_3 catalyst, the used catalyst was characterised using different techniques as discussed in section 7.1.

8.2.2.2.1 TPO

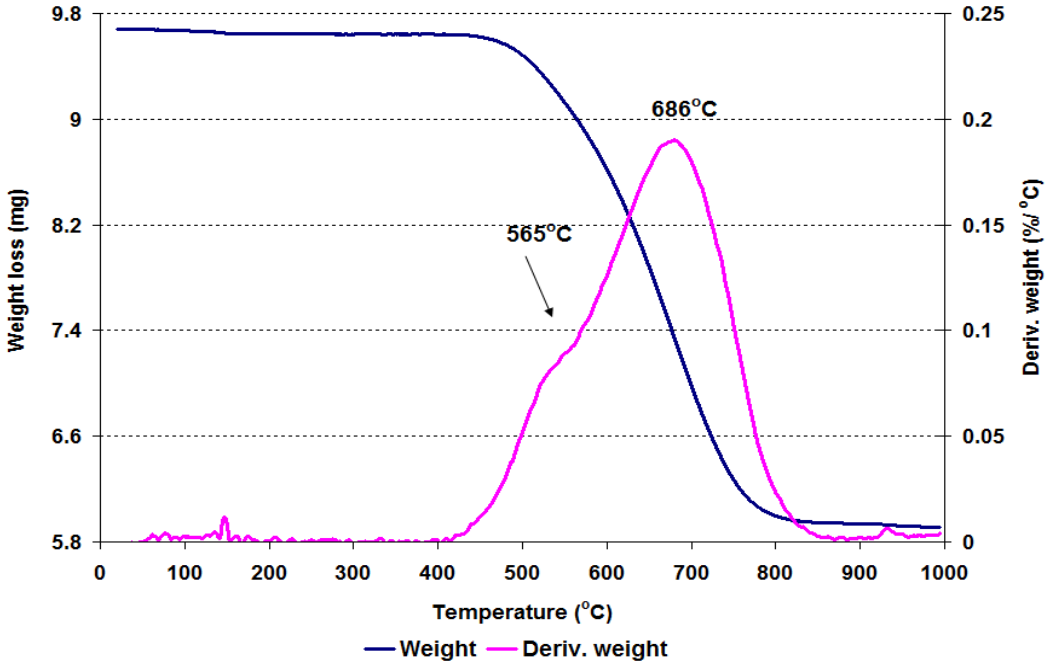

Figure 8.2-24 Post reaction TPO for Ru/Al_2O_3 catalyst at 500°C

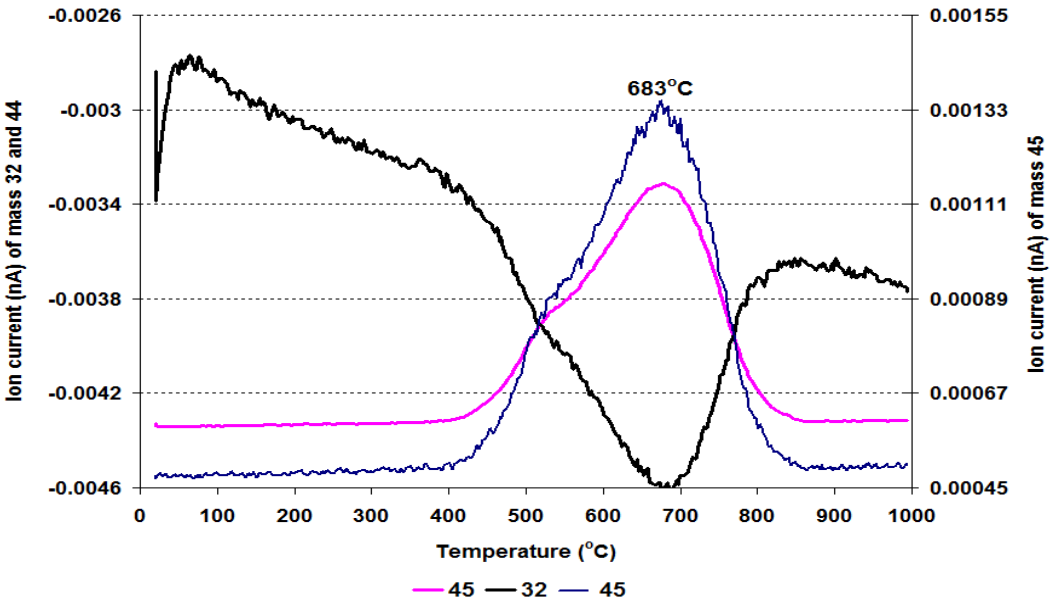

Figure 8.2-25 MS data of CO_2 (m/z=44), O_2 (m/z=32) and C_2H_5OH fragment (m/z=45) for Ru/Al_2O_3 catalyst at 500°C

The TPO results show that 389.45 mg g^{-1} of catalyst weight loss occurred between 23 and 1000^{o}C. The derivative weight profile illustrates that the main weight loss occurred at 686^{o}C, while there was also a small shoulder to the main weight loss events at around 565^{o}C. The weight losses matched with CO_2 and C_2H_5OH fragment (m/z 45) evolution on the mass spectra. In addition to these masses, fragments with m/z values of 2, 18, 26, 27, 28, 29, 31, 58, 59, 60 and 78 were monitored, however a trace amount of water was detected at 637^{o}C whilst no prominent peaks were observed for other masses.

8.2.2.2.2 Powder XRD

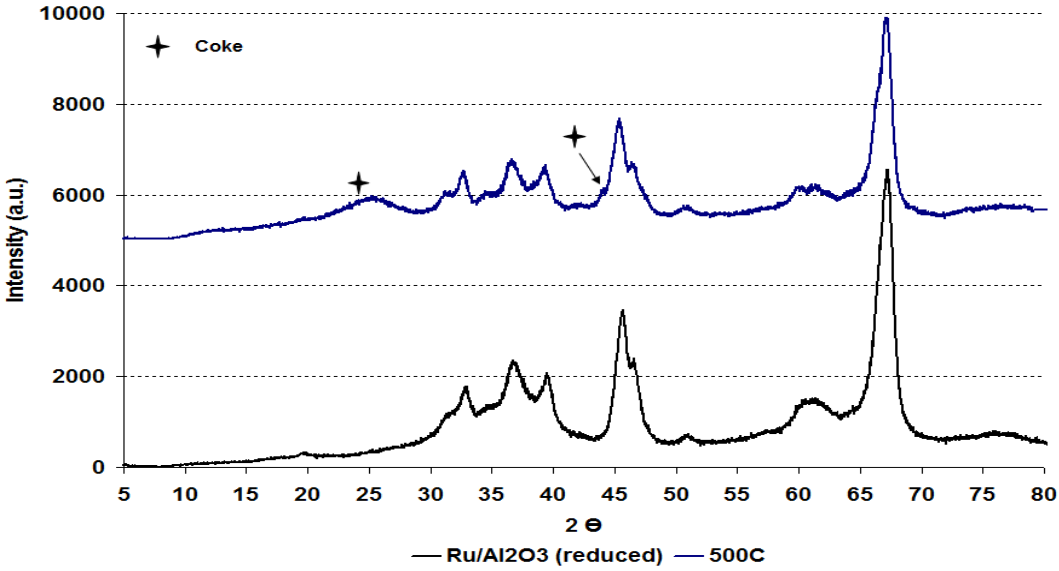

Figure 8.2-26 Powder XRD patterns of reduced and post reaction Ru/Al_2O_3 catalyst at 500^{o}C

The powder XRD patterns in Figure 8.2-26 illustrates that degree of crystallinity (123 Å) of spent Ru/Al_2O_3 catalyst is similar to the reduced form. The broad peak at a 2θ position of 26^{o} invoked the possible presence of coke on the catalyst. Similar results were obtained for Ru/Al_2O_3 catalyst at 550^{o}C and 600^{o}C.

8.2.2.2.3 Raman analysis

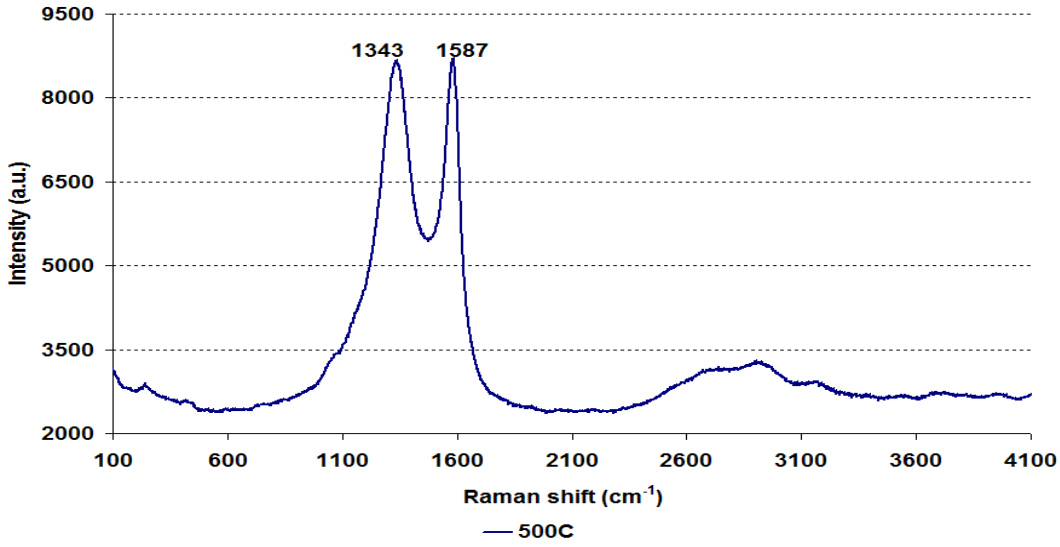

Figure 8.2-27 Post reaction Raman spectrum for Ru/Al_2O_3 catalyst at 500°C

The post reaction Raman spectrum as shown in Figure 8.2-27 shows two bands at wavenumber 1343 cm^{-1} and 1587 cm^{-1}, which are the characteristic bands of graphitic carbon.

8.2.2.2.4 SEM

The SEM image of post reaction Ru/Al_2O_3 from the 500°C reaction shows that no filamentous carbon is formed. However, the morphology of particles appears to change and a cavity produced as shown in Figure 8.2-28.

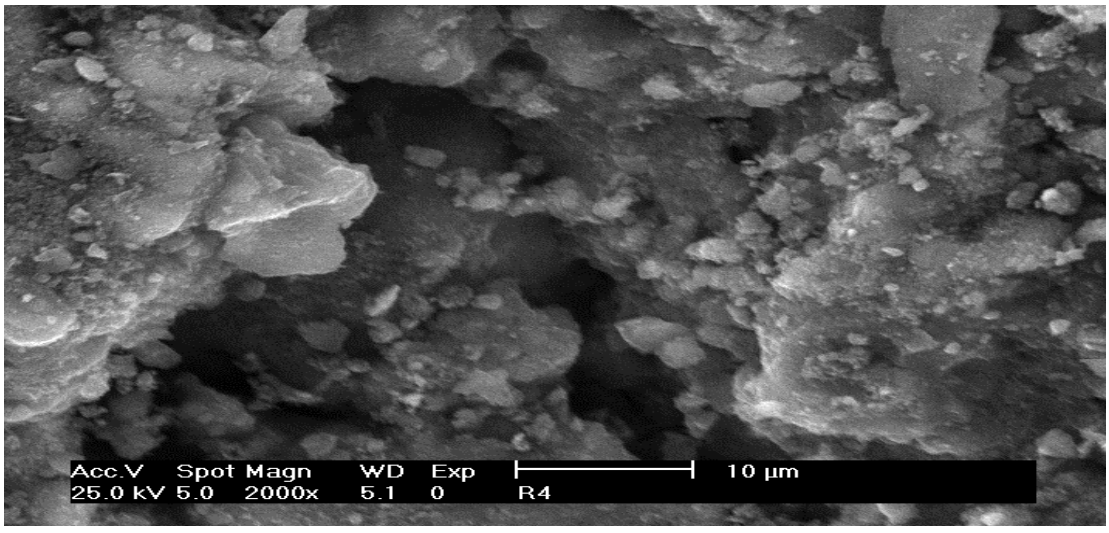

Figure 8.2-28 Post reaction SEM image of Ru/Al_2O_3 catalyst at 500°C

8.2.2.2.5 BET analysis

Catalyst	Conditions	BET Surface area (m^2/g)	Pore volume (cm^3/g)	Average pore diameter (Å)
Ru/Al_2O_3	Reduced (600°C)	100	0.43 (± 0.16)	172 (± 3.57)
	500°C	32	0.07 (± 2.17)	78 (± 6.57)

Table 8.2-3 BET analysis of post reaction Ru/Al_2O_3 catalyst at 500°C

BET analysis showed that the BET surface area, the average pore diameter and the pore volume decreased compared to the fresh catalyst in reduced form.

8.2.2.3 Reaction at 550°C

After investigating the reaction at 500°C over Ru/Al_2O_3 catalyst, a reaction was conducted at 550°C to compare the temperature effect.

The Ru/Al_2O_3 catalyst gave a maximum 99% ethanol conversion at 550°C in the initial 2 hours time on stream. However, the conversion of ethanol started to decrease after 2 hours time on stream and continued to decrease further up to 28.5 hours. The figure shows that the conversion of ethanol gave a similar profile to that seen at 500°C on Ru/Al_2O_3 catalyst.

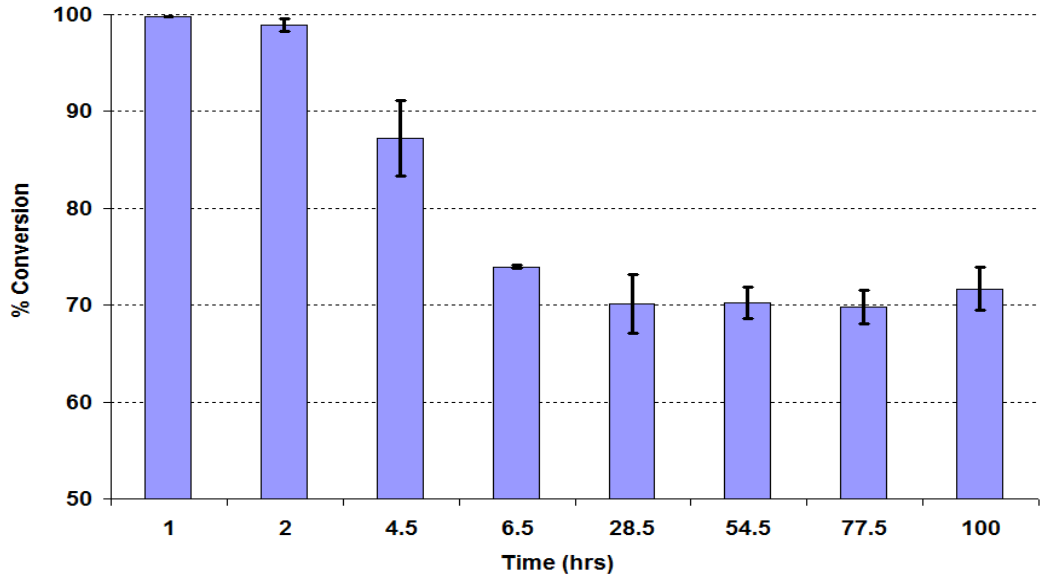

Figure 8.2-29 % Conversion of ethanol over Ru/Al_2O_3 catalyst at 550°C

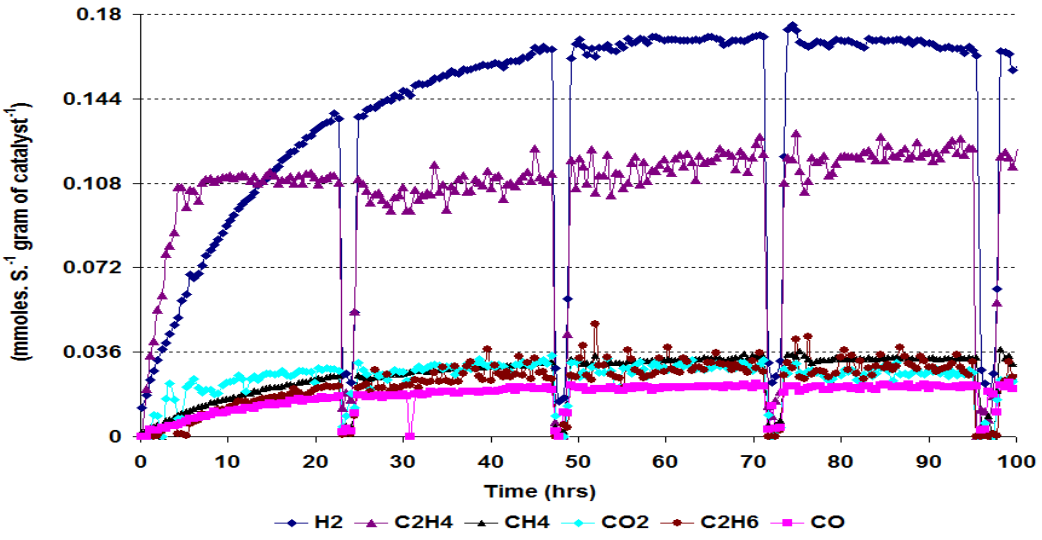

Figure 8.2-30 Rate of formation of gaseous products over Ru/Al_2O_3 catalyst at 550°C

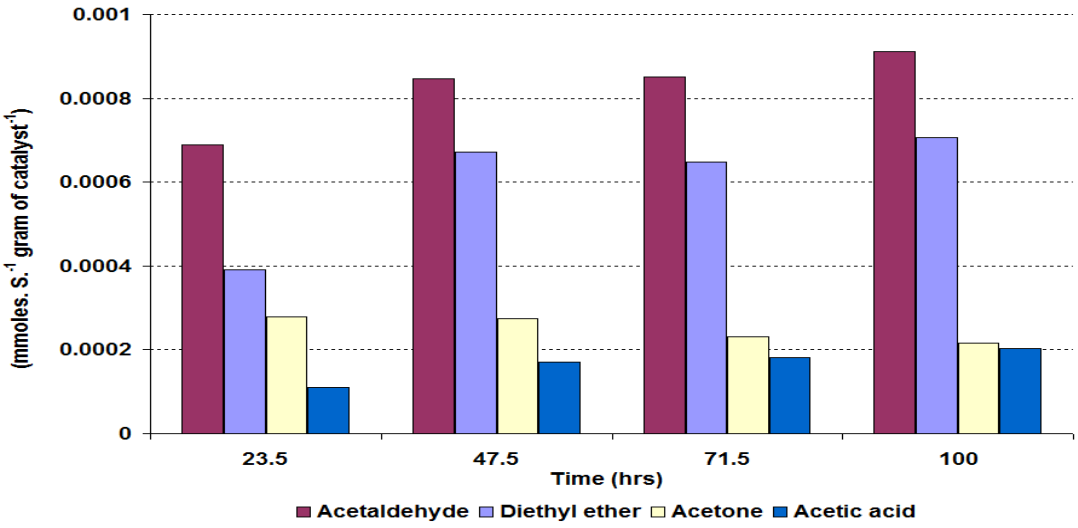

Figure 8.2-31 Rate of formation of liquid products over Ru/Al_2O_3 catalyst at 550°C

In the reaction run at 550°C the rate of formation of C_2H_4 increased for the initial 4 hours then stabilized for 48 hours and slowly increased until 60 hours TOS. After 60 hours the rate achieved steady state condition which continued until the end of the reaction. This is similar to the reaction at 500°C. H_2 gave the maximum rate of all the gaseous products at this temperature. Other gaseous products were CO_2, CH_4, C_2H_6 and CO. Like the 500°C reaction, CO has the lowest rate with respect to the other gaseous products. For the liquid products, acetaldehyde and diethyl ether were produced at higher rates which steadily increased over time. Acetone and acetic acid were the other liquid products produced during the reaction, however, the rate of formation of acetone production decreased over time whilst the rate of formation of acetic acid gradually increased.

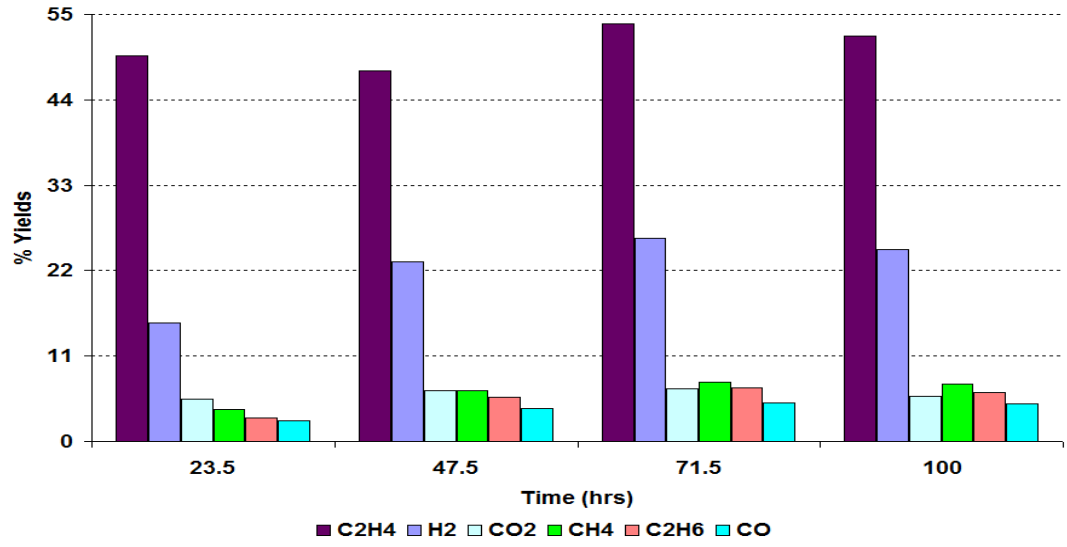

Figure 8.2-32 % Yield of gaseous products over Ru/Al_2O_3 catalyst at 550°C

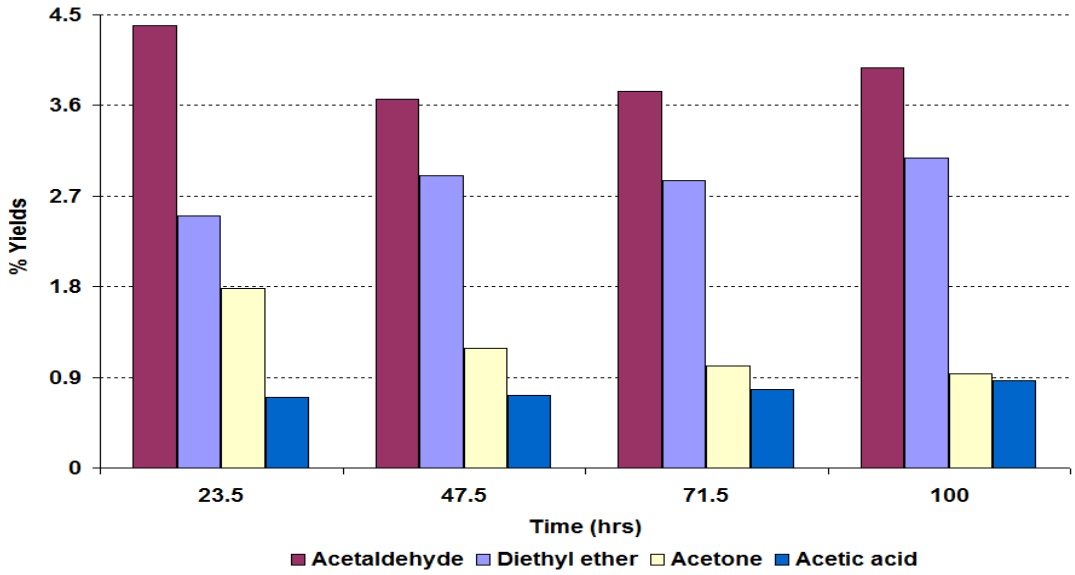

Figure 8.2-33 % Yield of liquid products over Ru/Al_2O_3 catalyst at 550°C

Figure 8.2-32 shows that the main gaseous product produced at 550°C is C_2H_4, which gave a maximum yield of 54%. The second was H_2, which was generated with a maximum yield of 26%. Also produced were C_2H_6, CO_2, CH_4 and CO, in gaseous form and gave less than 10% yield individually.

Similar liquid products were produced as for the reaction at 500°C. However the yields for the 550°C were less than 5%.

8.2.2.4 Post reaction characterisation

Post reaction Ru/Al_2O_3 catalyst was characterised using different techniques as discussed in section 7.1.

8.2.2.4.1 TPO

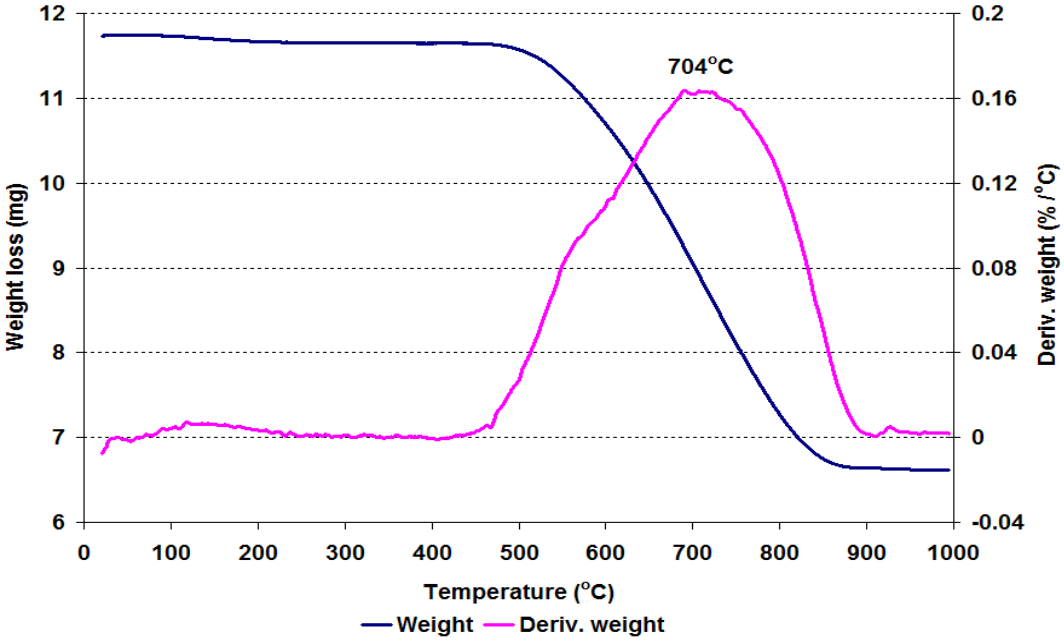

Figure 8.2-34 Post reaction TPO for Ru/Al_2O_3 catalyst at 550°C

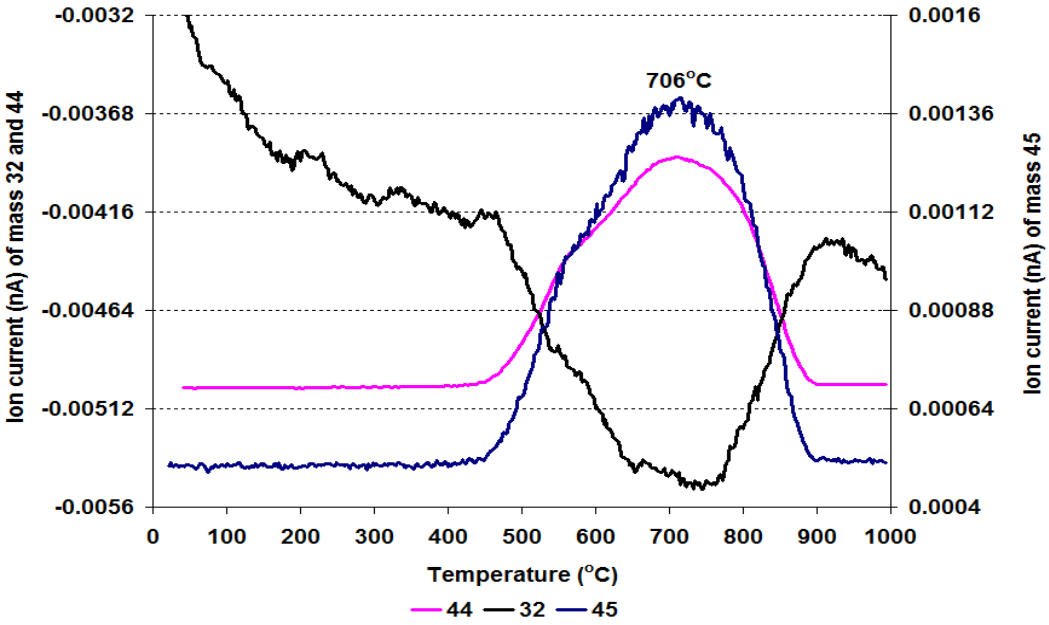

Figure 8.2-35 MS data of CO_2 (m/z=44), O_2 (m/z=32) and C_2H_5OH fragment (m/z=45) for Ru/Al_2O_3 catalyst at 550°C

TGA was run for the post reaction Ru/Al_2O_3 catalyst as shown in Figure 8.2-34. The TGA results illustrate that a weight loss takes place upon exposing the sample to an oxygen atmosphere. A total of 436 mg g^{-1} of weight loss of catalyst took place up to 1000^oC. The major weight loss events corresponded to CO_2 and C_2H_5OH fragment and small amounts of H_2O evolution in the mass spectrometry profiles. The weight loss occurred over a wide temperature range of between 460^oC and 900^oC. There was also a small broad weight loss event that occurred in a lower temperature region *i.e.* below 300^oC, which, matched with the evolution of physisorbed water.

8.2.2.4.2 Raman analysis

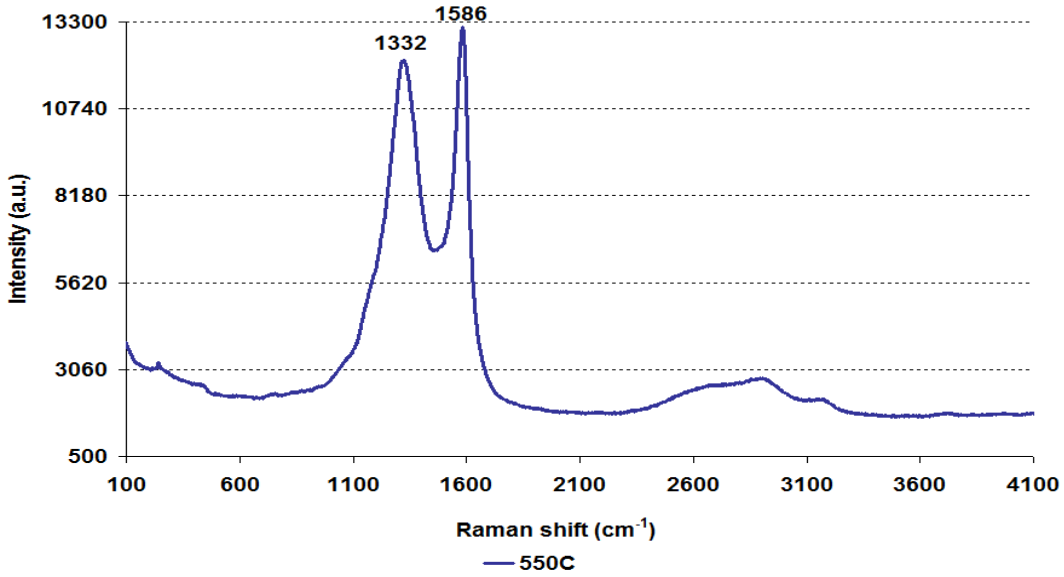

Figure 8.2-36 Post reaction Raman spectrum for Ru/Al_2O_3 catalyst at 550^oC

The Raman results for the post reaction catalyst show similar results to those obtained for the catalyst run at 500^oC. However, the lower frequency band has shifted to a small extent downwards in this sample. Also the intensity of G band slightly increased compared to D band.

8.2.2.4.3 SEM

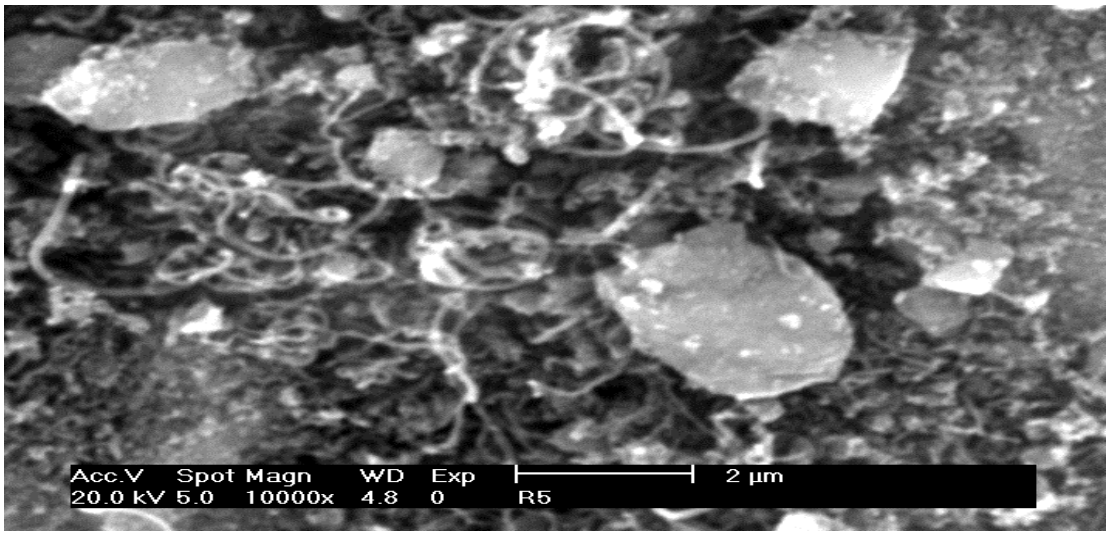

Figure 8.2-37 Post reaction SEM image of Ru/Al_2O_3 catalyst at 550°C

The SEM image shown in Figure 8.2-37 of the post reaction catalyst illustrates that a network of filamentous carbon is present on the catalyst. The low resolution SEM image (not shown) revealed that carbon deposition was only seen on the particle corners or in the regions where particles had disintegrated into small particles.

8.2.2.4.4 BET analysis

Catalyst	Conditions	BET Surface area (m^2/g)	Pore volume (cm^3/g)	Average pore diameter (Å)
Ru/Al_2O_3	Reduced (600°C)	100	0.43 (± 0.16)	172 (± 3.57)
	550°C	12	0.03 (± 5.43)	82 (± 7.58)

Table 8.2-4 BET analysis of post reaction Ru/Al_2O_3 catalyst at 550°C

BET analysis illustrated that there was a significant change in the surface area, the pore volume and the average pore diameter taking place after exposing the catalyst to the steam reforming reaction at 550°C.

8.2.2.5 Reaction at 600°C

To further assess the effect of temperature the experiment was repeated with Ru/Al_2O_3 at 600°C

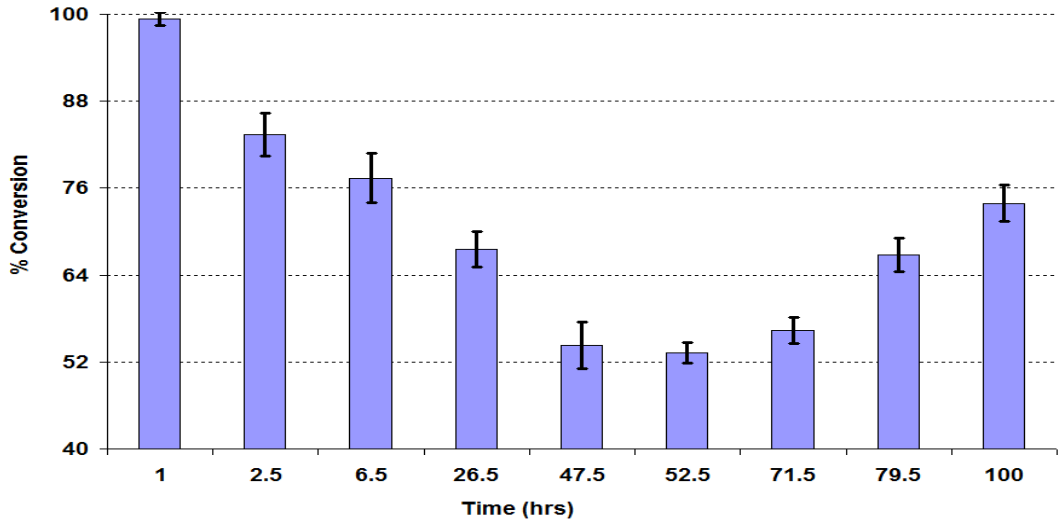

Figure 8.2-38 % Conversion of ethanol over Ru/Al_2O_3 catalyst at 600°C

The conversion of ethanol over the Ru/Al_2O_3 catalyst at 600°C is shown in the Figure 8.2-38. The figure reveals that, as with the reactions at 500°C and 550°C the conversion of ethanol was 99% in the initial 1 hour. However after 1 hour TOS it progressively decreased with time and reduced to 53% after 52 hours time on stream. Interestingly, after the initial decrease the conversion of ethanol again started to increase which continued till to the end of the reaction.

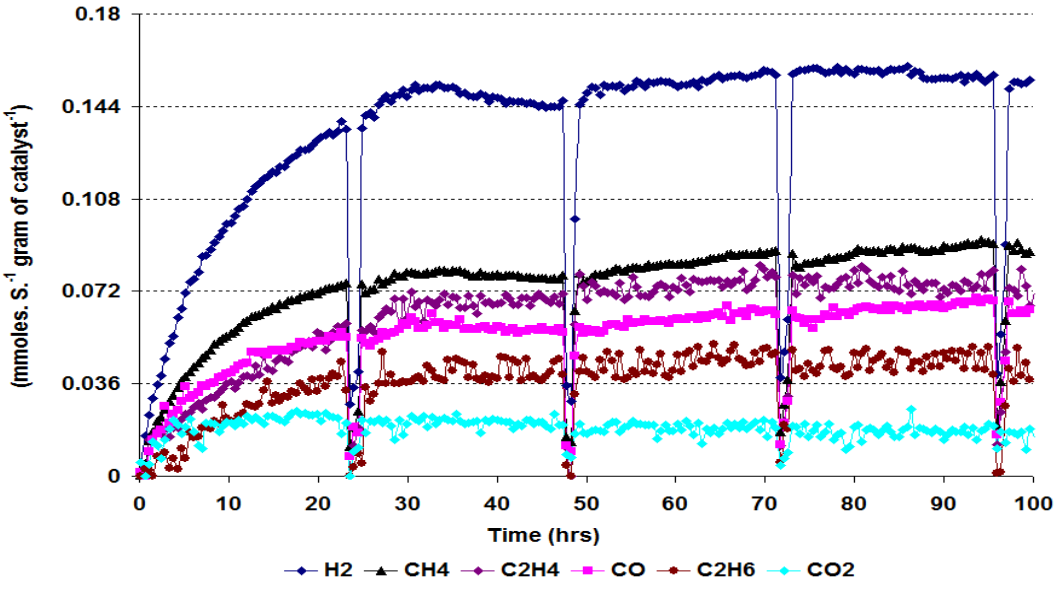

Figure 8.2-39 Rate of formation of gaseous products over Ru/Al_2O_3 catalyst at 600°C

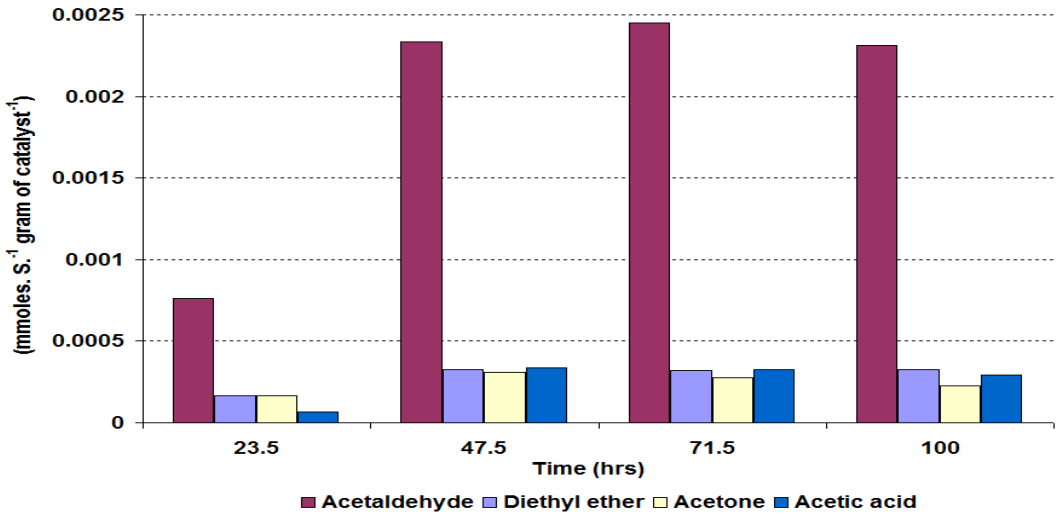

Figure 8.2-40 Rate of formation of liquid products over Ru/Al_2O_3 catalyst at 600°C

The increase of temperature from 550°C to 600°C significantly changed the rate of formation of the gaseous and liquid products as shown in Figures 8.2-39 and 8.2-40. Figure 8.2-39 illustrates that H_2 gave the maximum rate which, achieved steady state values after 30 hours and stabilised till the end of reaction. CH_4 and CO were the other major gaseous products whose rates significantly increased with the increase in temperature, and followed the same reaction patterns as hydrogen, except at the last stage where the rate of formation of these products increased rather than decreased. On the other hand, with the increase in temperature from 550°C to 600°C, the rate of C_2H_4 and CO_2 production significantly decreased.

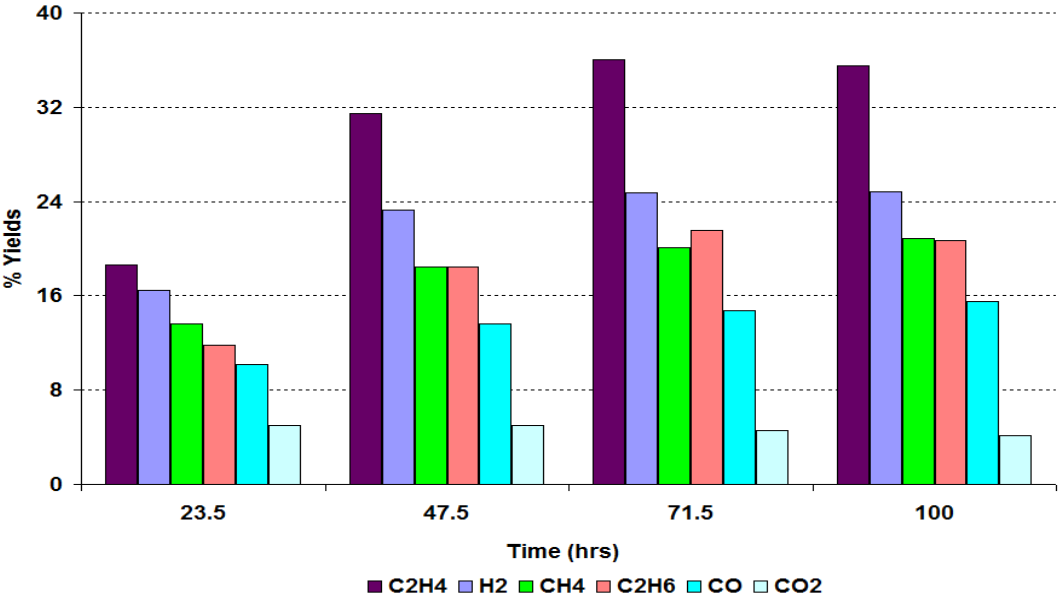

Figure 8.2-41 % Yield of gaseous products over Ru/Al_2O_3 catalyst at 600°C

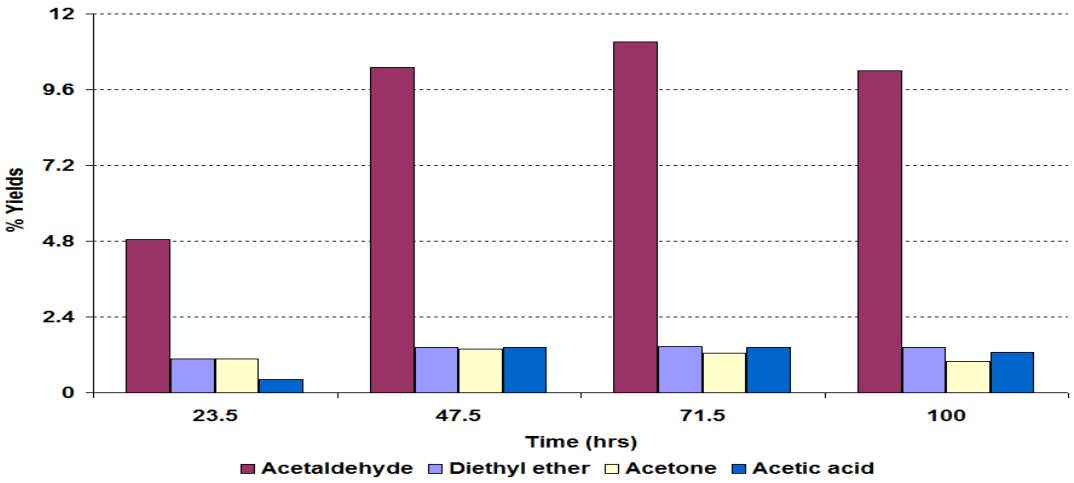

Figure 8.2-42 % Yield of liquid products over Ru/Al_2O_3 catalyst at 600°C

Figure 8.2-41 illustrates that C_2H_4 gave the maximum yield of 36%. The yield of H_2, CO, C_2H_6 and CH_4 increased while the yields of CO_2 remained roughly similar to that observed at 550°C.

Figure 8.2-42 shows that for the liquid products, acetaldehyde gave the highest yield whilst the yields of the other liquid products were less than 2%.

8.2.2.6 Post reaction characterisation

Post reaction catalyst characterisation was undertaken using different techniques to determine the cause of deactivation of catalyst.

8.2.2.6.1 TPO

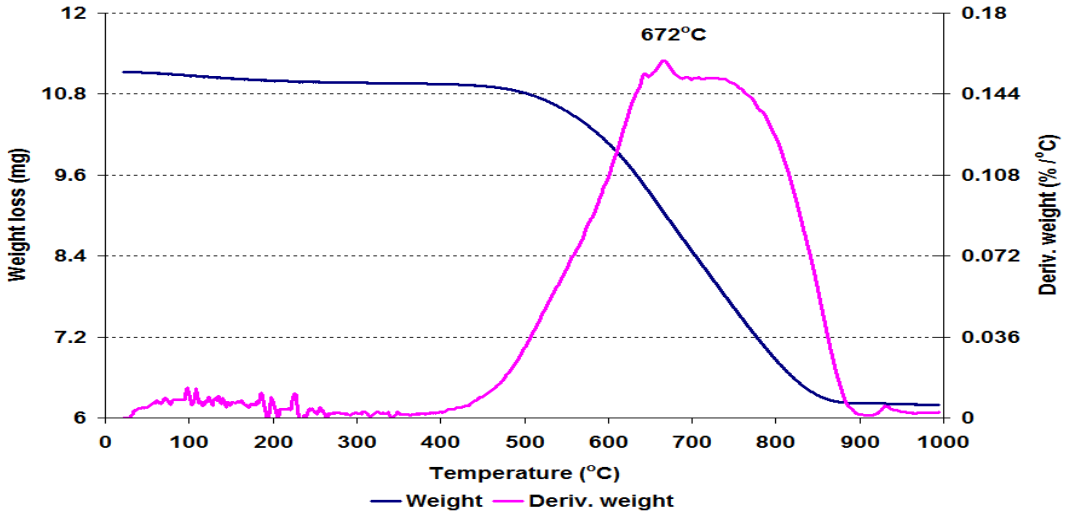

Figure 8.2-43 Post reaction TPO for Ru/Al_2O_3 catalyst at 600°C

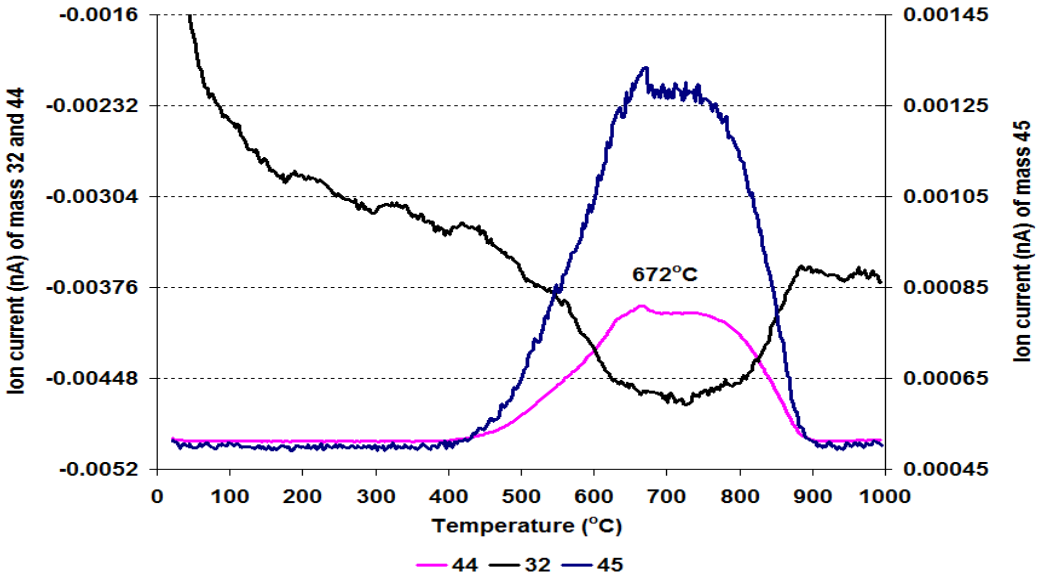

Figure 8.2-44 MS data of CO_2 (m/z=44), O_2 (m/z=32) and C_2H_5OH fragment (m/z=45) for Ru/Al_2O_3 catalyst at 600°C

The TPO and the associated mass fragment peaks obtained for the post reaction catalyst are shown in Figures 8.2-43-44. The total weight loss of catalyst was found to be 444 mg g^{-1} of catalyst. The TGA profile shows that the main weight loss occurred in a broad temperature region between 400°C and 900°C. The associated heat flow diagram, which is not shown here, illustrated that the weight loss events were exothermic. The main weight loss corresponded to CO_2 and ethanol fragment evolution in the mass profile.

8.2.2.6.2 Raman analysis

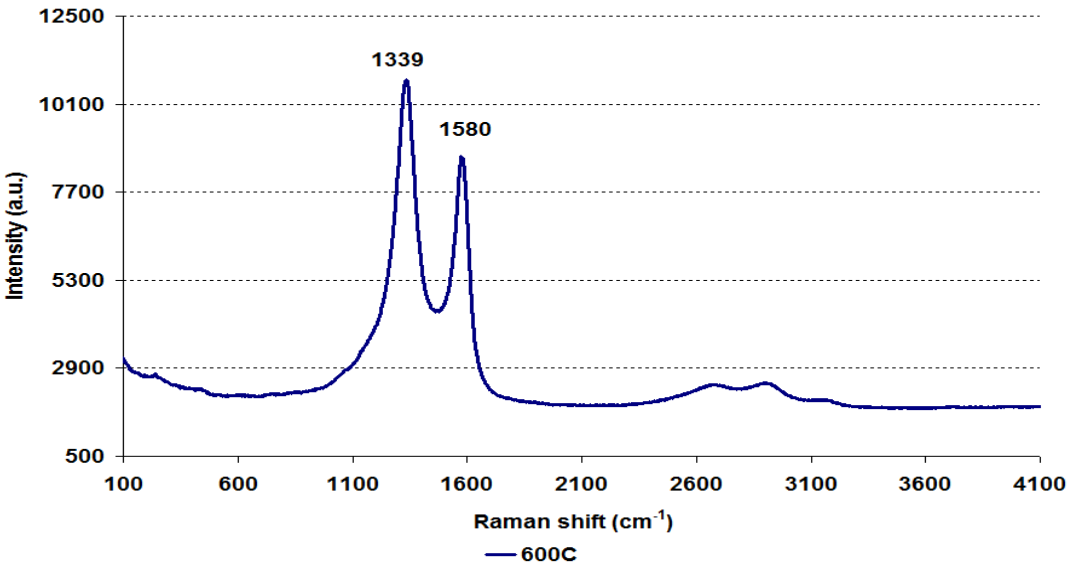

Figure 8.2-45 Post reaction Raman spectrum for Ru/Al_2O_3 catalyst at 600°C

The Raman spectrum for the post reaction catalyst shows similar peaks to those observed for the previous catalyst run at 500^{o}C and 550^{o}C. However, the intensity of the lower wave number peak has increased compared to the higher wave number peak suggesting that the disorder in the graphitic carbon deposits had increased with an increase in temperature.

8.2.2.6.3 SEM

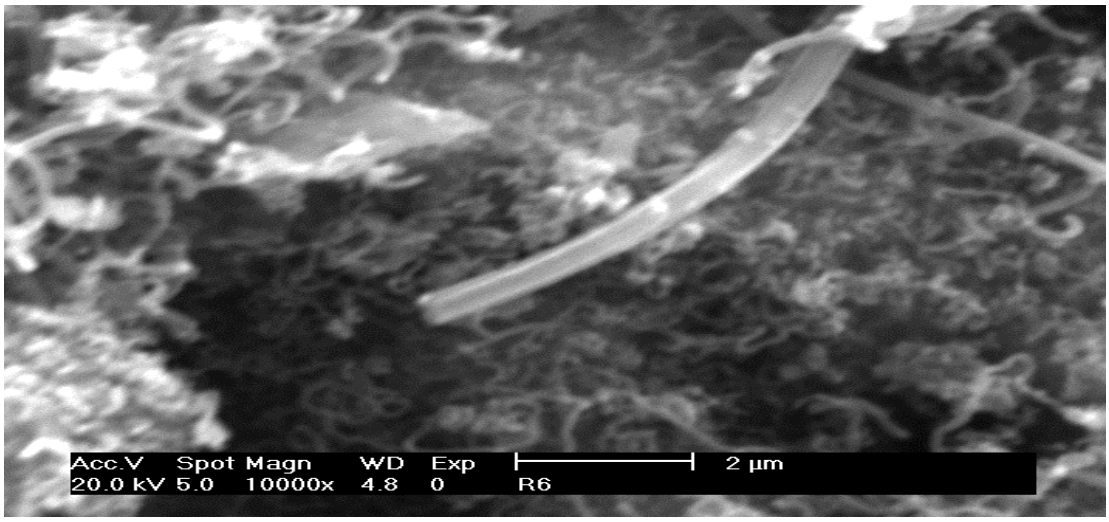

Figure 8.2-46 Post reaction SEM image of Ru/Al_2O_3 catalyst at 600^{o}C

The SEM image for the spent Ru/Al_2O_3 catalyst at 600^{o}C shows similar filamentous carbon to that observed in the previous samples. However, at this temperature there is also a new rod type carbon nanotube observed which was not seen in the previous samples.

8.2.2.6.4 BET analysis

Catalyst	Conditions	BET Surface area (m^2/g)	Pore volume (cm^3/g)	Average pore diameter (Å)
Ru/Al_2O_3	Reduced (600^{o}C)	100	0.43 (± 0.16)	172 (± 3.57)
	600^{o}C	23	0.01 (± 5.89)	37 (± 6.08)

Table 8.2-5 BET analysis of post reaction Ru/Al_2O_3 catalyst at 600^{o}C

Table 8.2-5 demonstrates that the BET surface area decreased after exposure of the catalyst to steam reforming reaction at 600^{o}C. The average pore diameter and the pore volume also significantly decreased upon exposure to steam reforming reaction at 600^{o}C.

8.2.3 Pt/Al_2O_3

After performing the reactions with a Ru/Al_2O_3 catalyst at three different temperatures *i.e.* 500°C, 550°C and 600°C, a second catalyst, Pt/Al_2O_3, was tested at the same temperatures using the procedure discussed in section 7.2.2.

8.2.3.1 Reaction at 500°C

The initial reaction was run at 500°C and the results obtained were plotted as a function of time.

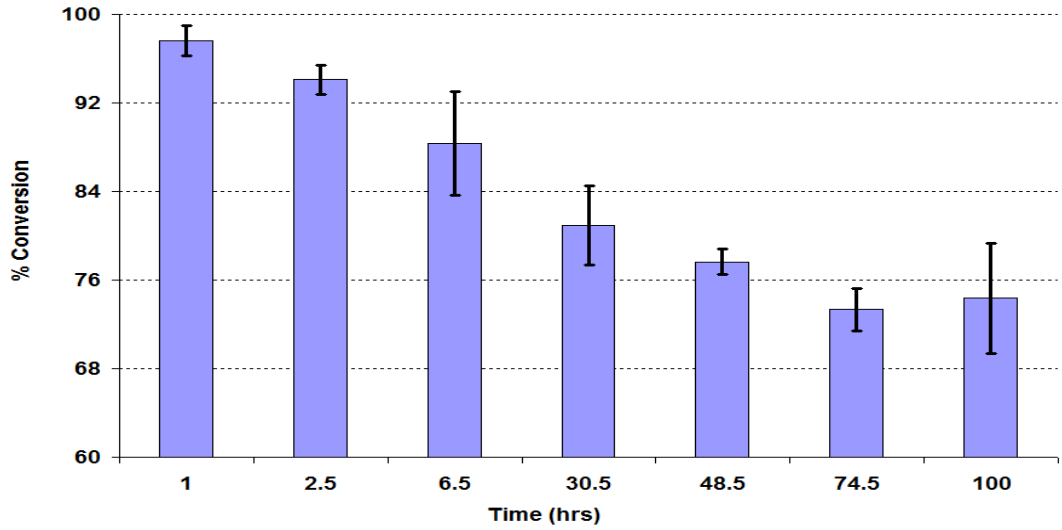

Figure 8.2-47 % Conversion of ethanol over Pt/Al_2O_3 catalyst at 500°C

The conversion of ethanol over the Pt/Al_2O_3 catalyst at 500°C is shown in Figure 8.2-47. The figure indicates that initially the conversion of ethanol was 97% which gradually decreased throughout the reaction and after 100 hours has reduced to 74%. Also, after 74.5 hours TOS the conversion of ethanol has obtained steady state condition.

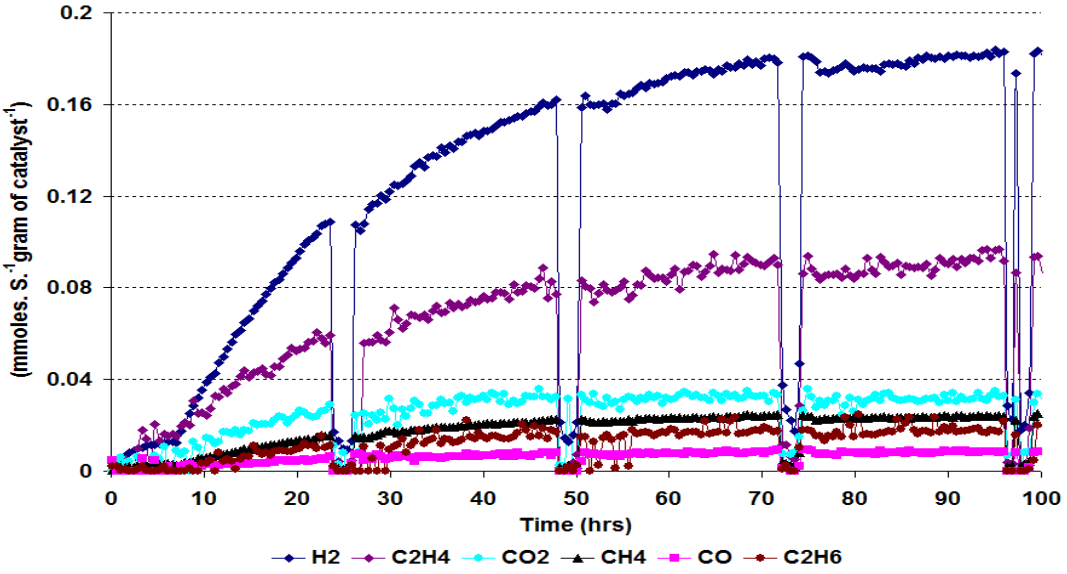

Figure 8.2-48 Rate of formation of gaseous products over Pt/Al_2O_3 catalyst at 500°C

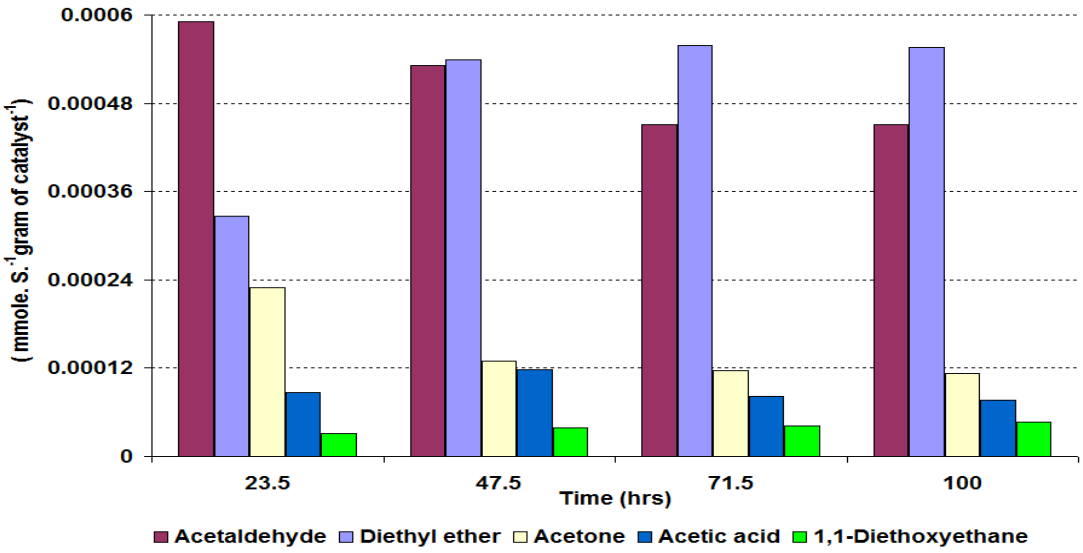

Figure 8.2-49 Rate of formation of liquid products over Pt/Al_2O_3 catalyst at 500°C

Figures 8.2-48 and 49 show the rates of formation for the gaseous and liquid products respectively. Figure 8.2-48 shows that H_2 and C_2H_4 gave the highest rates, which increased gradually over time and obtained steady state condition after 72 hours. On the other hand the minor gaseous products stabilised much faster. Amongst the gaseous products, CO gave the lowest rate of formation.

Acetaldehyde and diethyl ether were the liquid products that gave the maximum rate of formation. However, the rate of acetaldehyde decreased while the rate of diethyl ether increased. The rate of formation of all other liquid products decreased over time.

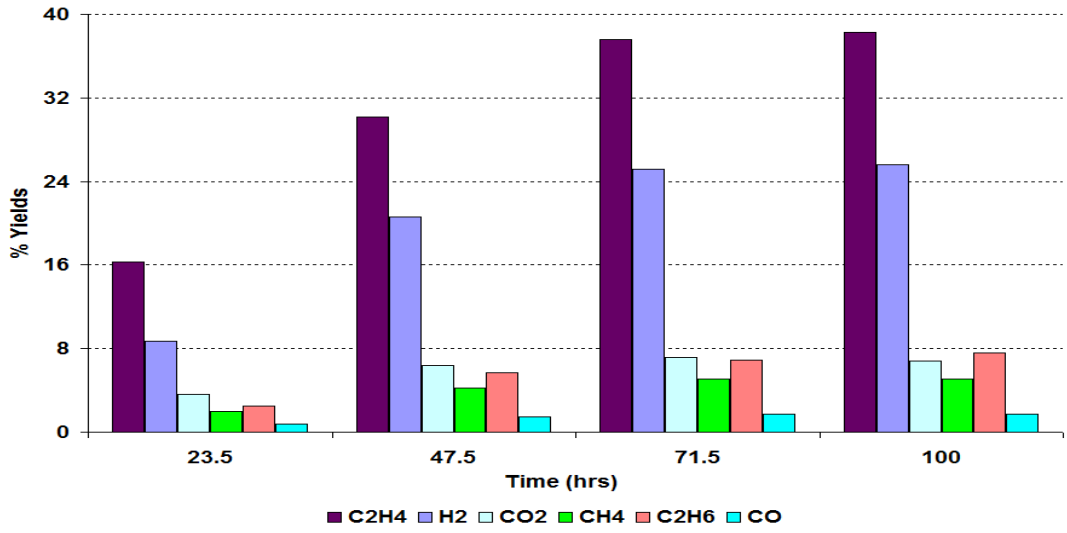

Figure 8.2-50 % Yield of gaseous products over Pt/Al_2O_3 catalyst at 500°C

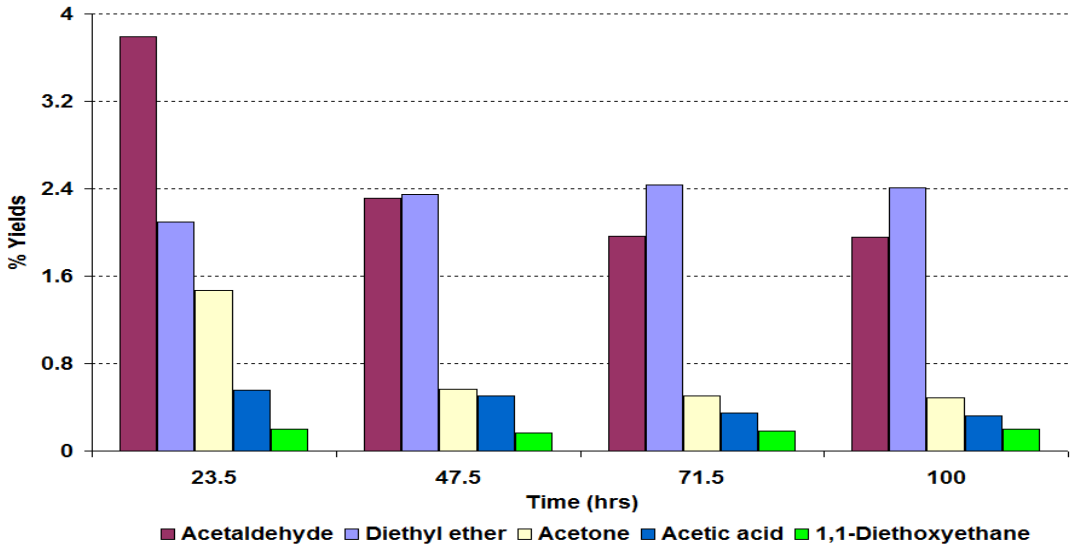

Figure 8.2-51 % Yield of liquid products over Pt/Al_2O_3 catalyst at 500°C

Out of the gaseous products, C_2H_4 gave the highest yield at ~ 38%. H_2 was the second largest gaseous product, whose rate increased over time and obtained a maximum yield of 25%. CO_2, CH_4, C_2H_6 and CO were the minor gaseous products and none of these products produced a yield of more than 8%.

Figure 8.2-51 shows the yields of the liquid products. It illustrates that acetaldehyde gave the highest yield of ~ 4%, however, with the passage of time it decreased. Diethyl ether was the other major liquid product which increased with time and acquired steady state condition after 48 hours. The other liquid products which were produced in trace amounts are not shown in the Figure 8.2-51.

8.2.3.2 Post reaction characterisation

Post reaction catalyst was characterised to determine the mechanism of catalyst deactivation.

8.2.3.2.1 TPO

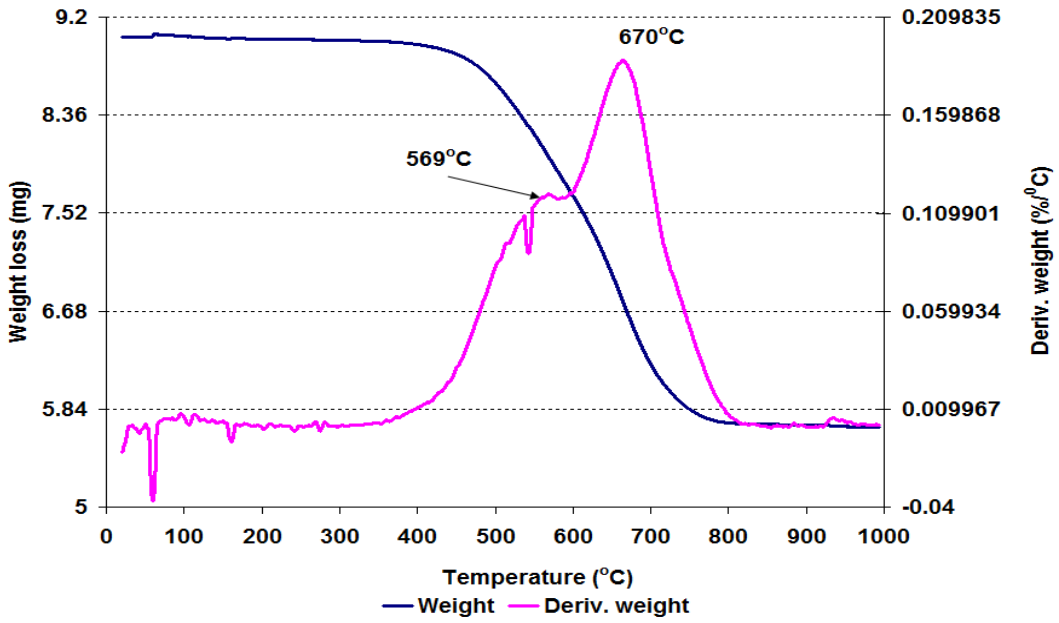

Figure 8.2-52 Post reaction TPO for Pt/Al_2O_3 catalyst at 500°C

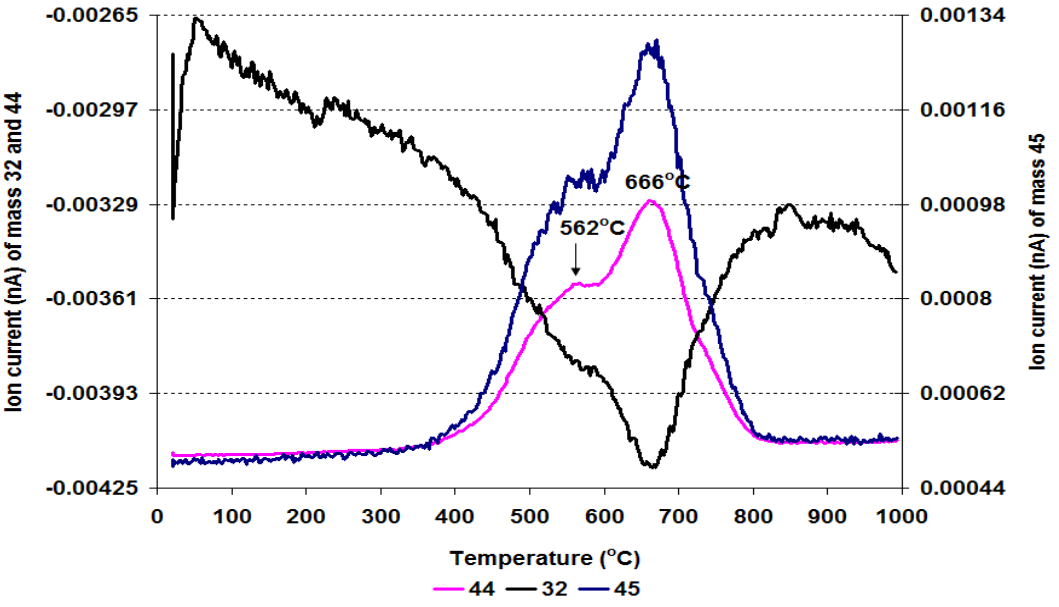

Figure 8.2-53 MS data of CO_2 (m/z=44), O_2 (m/z=32) and C_2H_5OH fragment (m/z=45) for Pt/Al_2O_3 catalyst at 500°C

Figure 8.2-52 shows the TGA profile for post reaction Pt/Al_2O_3 catalyst in 2% O_2/Ar atmosphere at 500^oC. From the figure, it is apparent that a total of 370.2 mg g^{-1} of sample weight loss took place up to 1000^oC. The main weight loss event occurred in two steps in the 357^oC to 820^oC temperature region, which equated to the evolution of CO_2, H_2O and m/z 45 of ethanol fragment and the consumption of O_2 in the mass profiles. In addition, mass fragments with m/z values of 2, 26, 27, 28, 29, 31, 58, 59, 60 and 78 were monitored, however only a small amount of mass 2 and 18 were observed which is not shown in the above figure.

8.2.3.2.2 Powder XRD

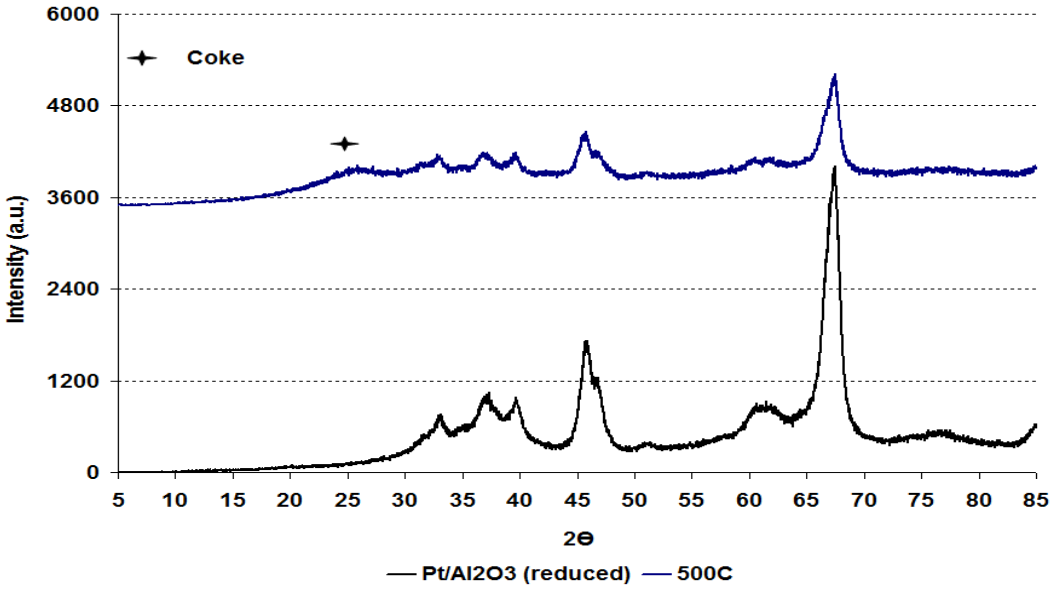

Figure 8.2-54 Powder XRD patterns of reduced and post reaction Pt/Al_2O_3 catalyst at 500^oC

Powder XRD patterns were acquired for the spent catalyst of Pt/Al_2O_3 at 500^oC and then plotted together with the pre-reaction catalyst in its reduced form. The post reaction sample had similar patterns to the reduced sample although the peak intensity slightly decreased. As expected, a broad peak was observed for coke deposited during the reaction at 26^o 2θ position. Also, similar results were obtained for Pt/Al_2O_3 catalyst at 550^oC and 600^oC.

8.2.3.2.3 Raman analysis

The Raman analysis of spent Pt/Al_2O_3 catalyst after the 500°C reaction illustrated similar results to those observed for the Ru/Al_2O_3 catalyst. However, the lower frequency band appears to have shifted further downwards to1332 cm^{-1}

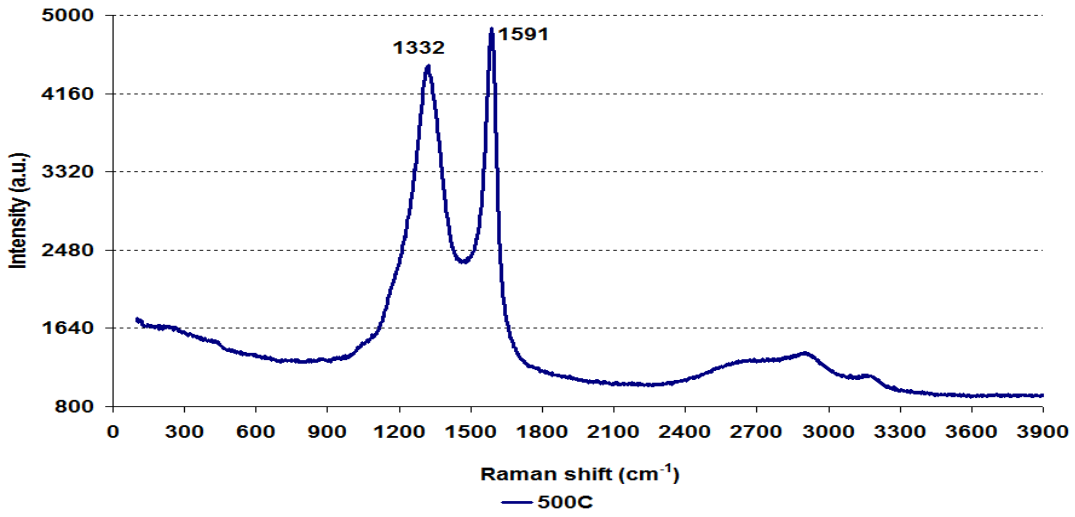

Figure 8.2-55 Post reaction Raman spectrum for Pt/Al_2O_3 catalyst at 500°C

8.2.3.2.4 SEM

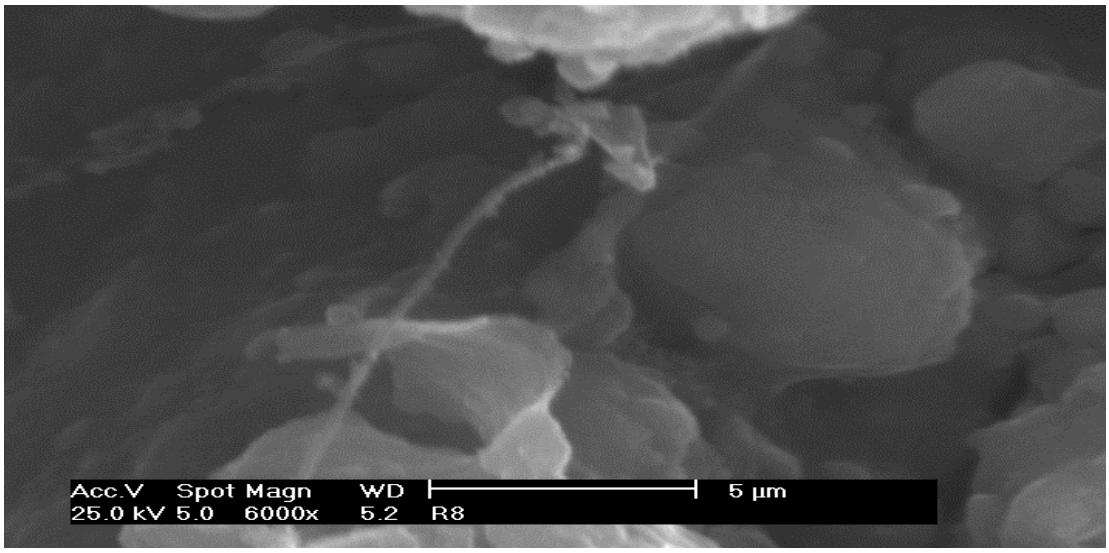

Figure 8.2-56 Post reaction SEM image of Pt/Al_2O_3 catalyst at 500°C

The SEM image shown in Figure 8.2-56 shows the spent Pt/Al_2O_3 catalyst. The image clearly indicates that filamentous type coke is present on the catalyst surface.

8.2.3.2.5 BET analysis

Catalyst	Conditions	BET Surface area (m^2/g)	Pore volume (cm^3/g)	Average pore diameter (Å)
Pt/Al_2O_3	Reduced (600°C)	100	0.46 (± 0.62)	180 (± 4.48)
	500°C	41	0.09 (± 0.81)	80 (± 3.97)

Table 8.2-6 BET analysis of post reaction Pt/Al_2O_3 catalyst at 500°C

Table 8.2-6 indicates that a significant change in the surface area, the pore volume and the average pore diameter of catalyst occurred during the reaction.

8.2.3.3 Reaction at 550°C

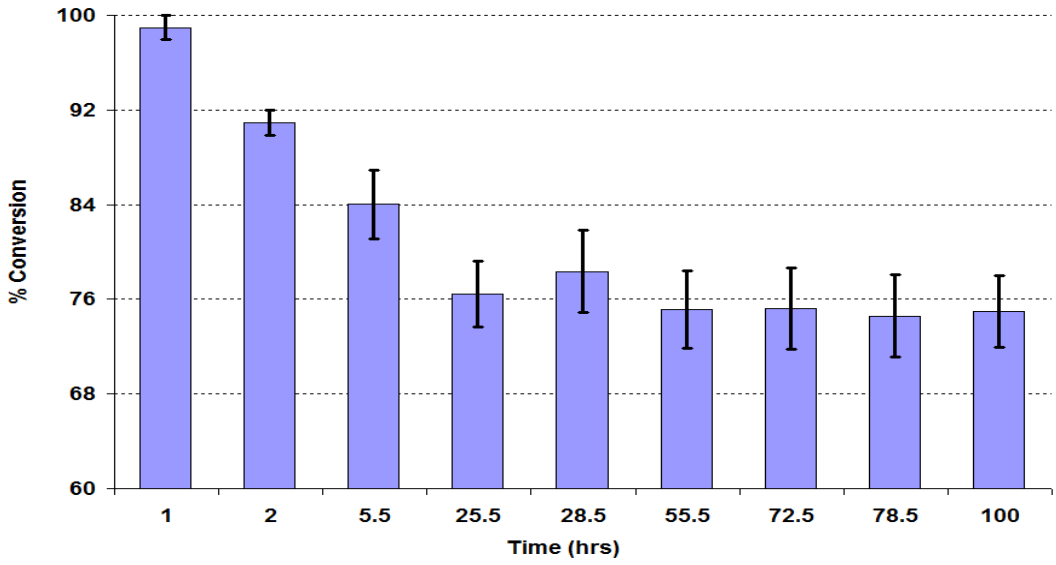

Figure 8.2-57 % Conversion of ethanol over Pt/Al_2O_3 catalyst at 550°C

The steam reforming of ethanol reaction was run at 550°C over Pt/Al_2O_3. Initially, the conversion of ethanol was high but after 5.5 hours TOS a swift deactivation of the catalyst was observed and the conversion of ethanol decreased from 98% to 76%. However, after the initial deactivation, it stabilised and gave steady conversion through to the end of the reaction.

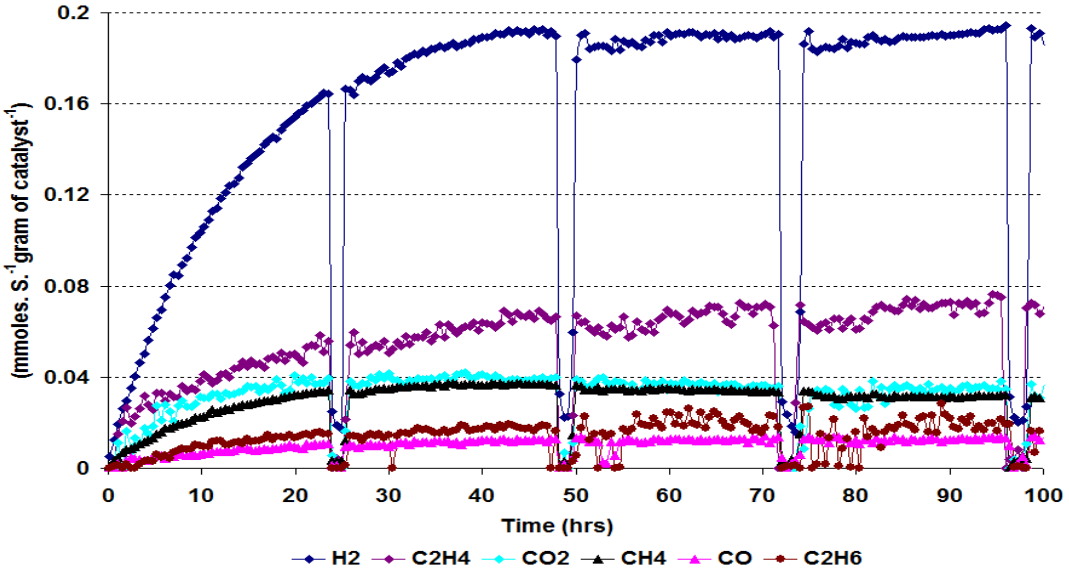

Figure 8.2-58 Rate of formation of gaseous products over Pt/Al_2O_3 catalyst at 550°C

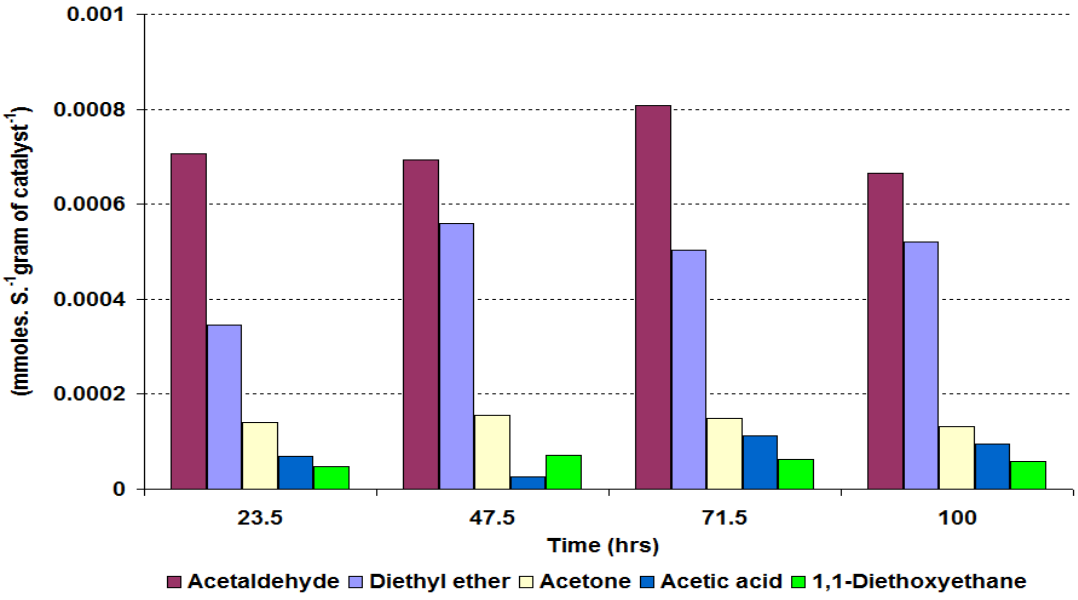

Figure 8.2-59 Rate of formation of liquid products over Pt/Al_2O_3 catalyst at 550°C

The results obtained for the rate of formation of the gaseous and liquid products at 550°C are plotted and shown in Figures 8.2-58 to 59. The gaseous products illustrate that the rate of H_2, after an initial increase, stabilised, whilst the C_2H_4 production increased throughout the reaction. The rate of formation of CO_2 and CH_4 also increased.

In the liquid products acetaldehyde and diethyl ether have higher rates of production. The rates of formation of all liquid products except 1,1-diethoxyethane fluctuated and no product achieved steady state condition over the duration of the reaction.

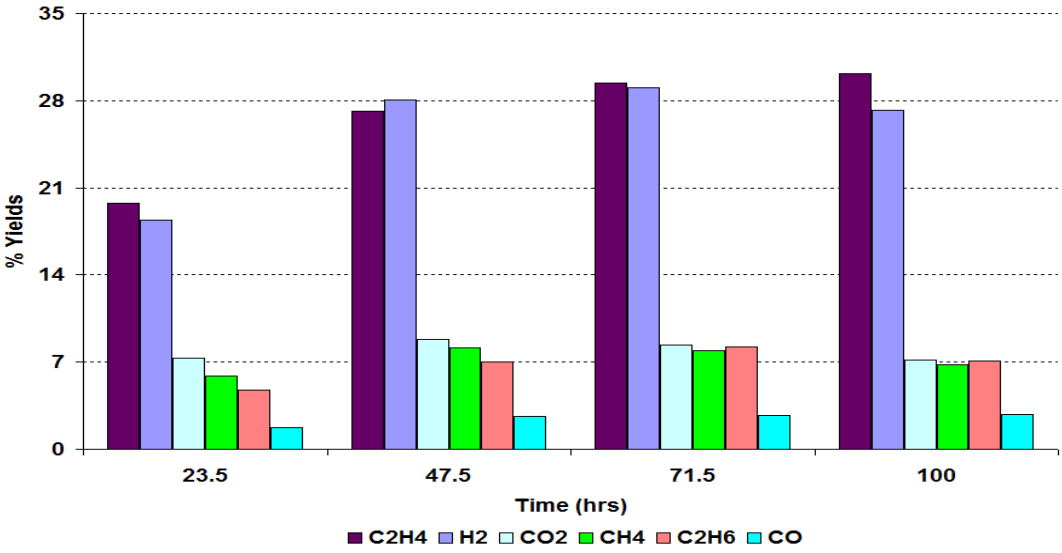

Figure 8.2-60 % Yield of gaseous products over Pt/Al_2O_3 catalyst at 550°C

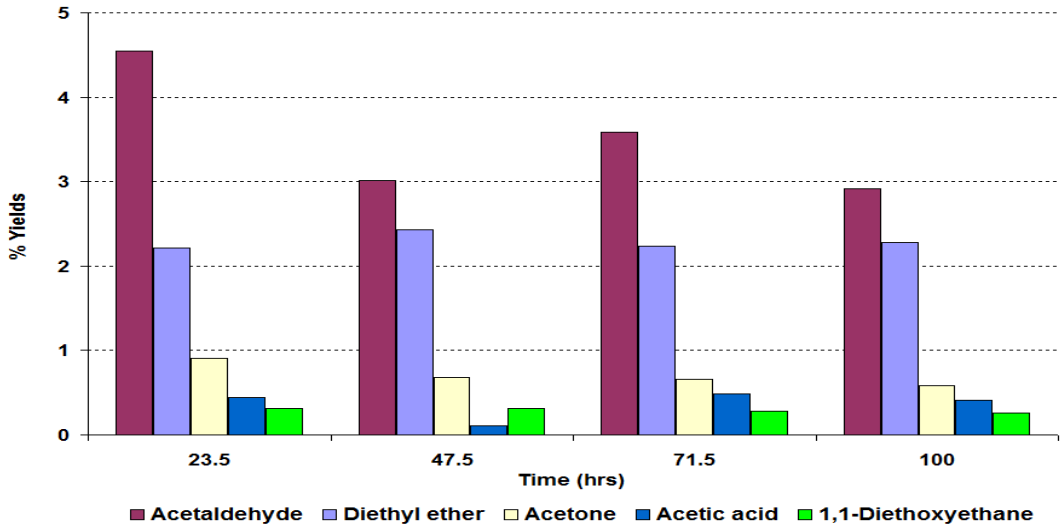

Figure 8.2-61 % Yield of liquid products over Pt/Al_2O_3 catalyst at 550°C

Figure 8.2-60 indicates that yields of C_2H_4 and H_2 are in competition with each other. The yield of H_2 slightly fluctuated while the yield of C_2H_4 progressively increased. CO_2, CH_4, C_2H_6 and CO were the other gaseous products produced during the reaction, although none of these products achieved more than a 7.5% yield.

Figure 8.2-61 shows that a series of liquid products were produced during the reaction. Of the liquid products, acetaldehyde gave the maximum yield (< 5%). Although small amounts of methanol, ethyl acetate and crotonaldehyde were produced during the reaction, these products are not shown in the figure due to their low yield.

8.2.3.4 Post reaction characterisation

8.2.3.4.1 TPO

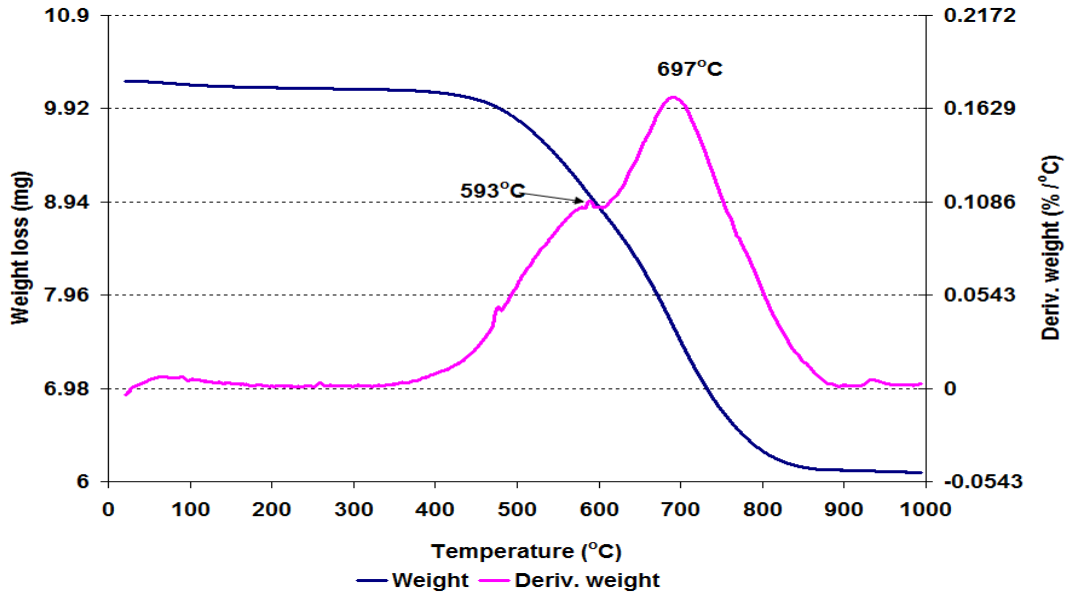

Figure 8.2-62 Post reaction TPO for Pt/Al_2O_3 catalyst at 550°C

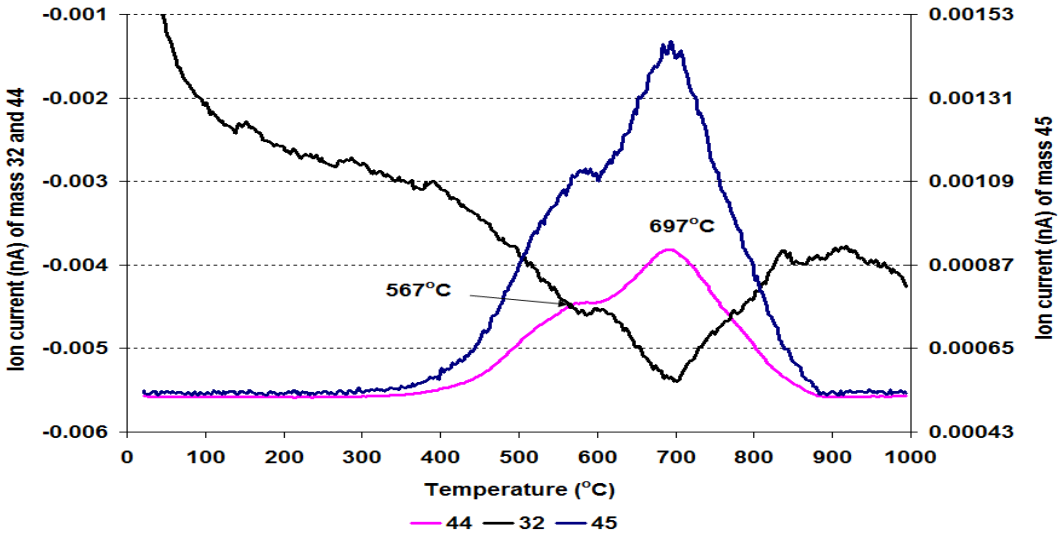

Figure 8.2-63 MS data of CO_2 (m/z=44), O_2 (m/z=32) and C_2H_5OH fragment (m/z=45) for Pt/Al_2O_3 catalyst at 550°C

Figure 8.2-62 shows the TGA results for the Pt/Al_2O_3 catalyst at 550°C. It illustrates that a major change in weight occurred between 360°C to 895°C which was equal to 402.7 mg g^{-1} of catalyst. This weight loss event took place in two steps which, merged with one another. The weight loss can be attributed to the evolution of CO_2, ethanol fragment and trace amount of H_2O.

8.2.3.4.2 Raman analysis

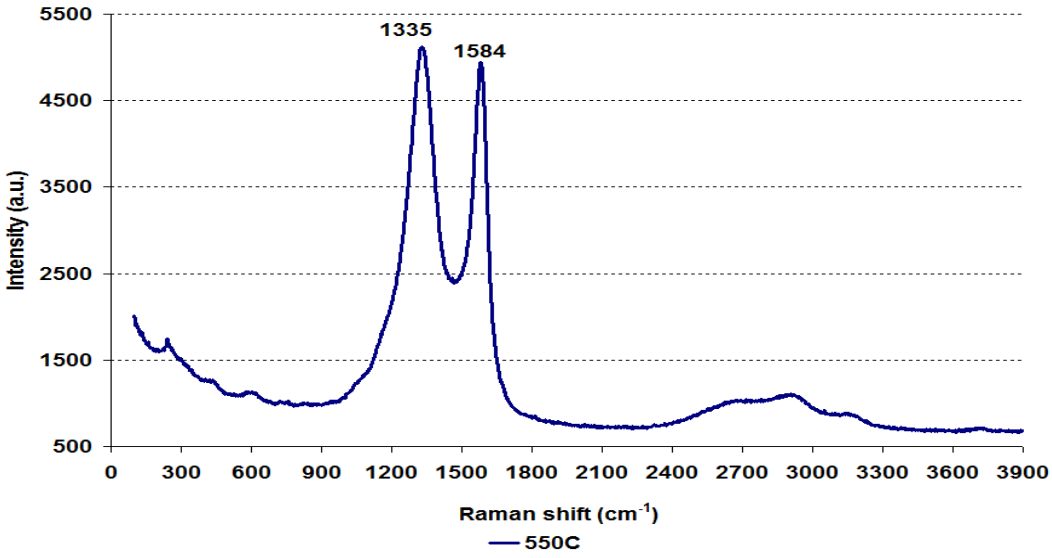

Figure 8.2-64 Post reaction Raman spectrum for Pt/Al_2O_3 catalyst at 550°C

Figure 8.2-64 illustrates the Raman data for Pt/Al_2O_3 at 550°C which gave a similar result to that was observed for the 500°C sample.

8.2.3.4.3 SEM

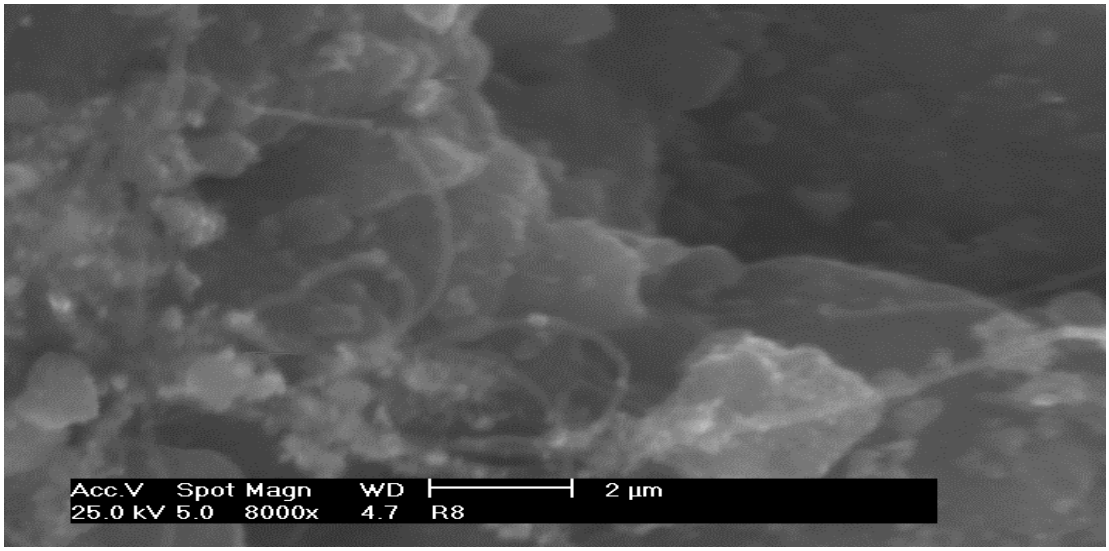

Figure 8.2-65 Post reaction SEM image of Pt/Al_2O_3 catalyst at 550°C

The SEM image shows that like the sample at 500°C filamentous type carbon on the Pt/Al_2O_3 sample was produced at 550°C.

8.2.3.4.4 BET analysis

Catalyst	Conditions	BET Surface area (m^2/g)	Pore volume (cm^3/g)	Average pore diameter (Å)
Pt/Al_2O_3	Reduced (600°C)	100	0.46 (± 0.62)	180 (± 4.48)
	550°C	27	0.05 (± 3.00)	67 (± 8.07)

Table 8.2-7 BET analysis of post reaction Pt/Al_2O_3 catalyst at 550°C

Table 8.2-7 shows that the BET surface area and the pore volume of Pt/Al_2O_3 catalyst significantly decreased compared to the fresh catalyst in the reduced form.

8.2.3.5 Reaction at 600°C

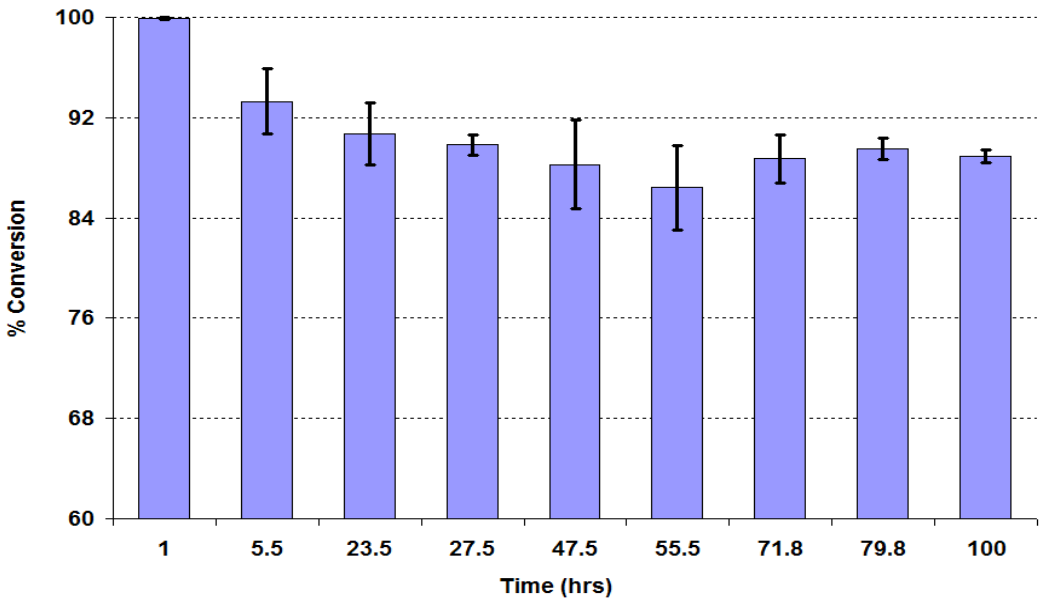

Figure 8.2-66 % Conversion of ethanol over Pt/Al_2O_3 catalyst at 600°C

The conversion of ethanol over Pt/Al_2O_3 at 600°C is shown in Figure 8.2-66. The figure illustrates that after the initial slight decrease at 5.5 hours the conversion of ethanol almost stabilised and no remarkable decrease in the conversion of ethanol was observed.

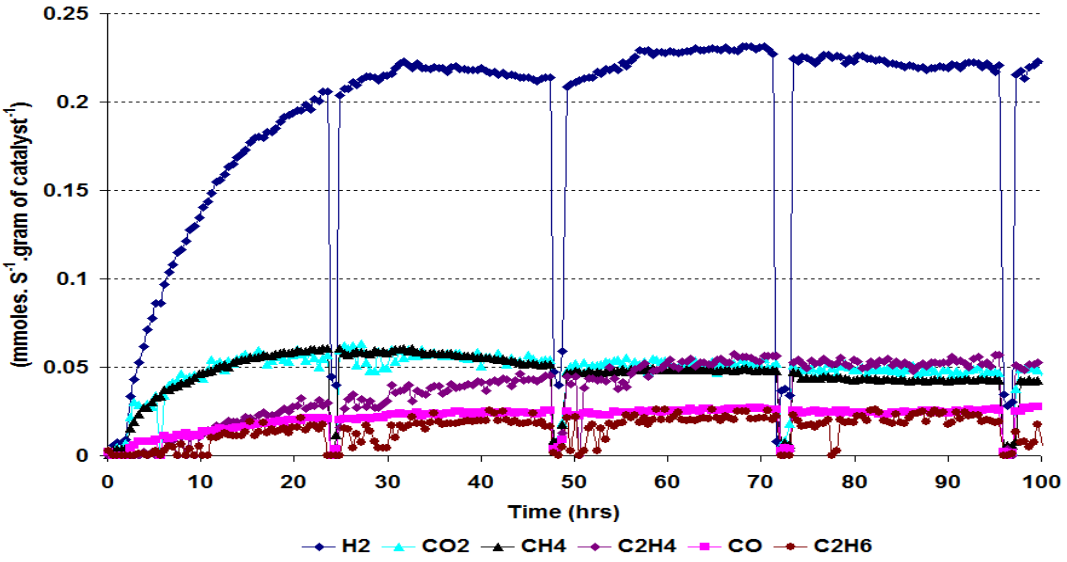

Figure 8.2-67 Rate of formation of gaseous products over Pt/Al_2O_3 catalyst at 600°C

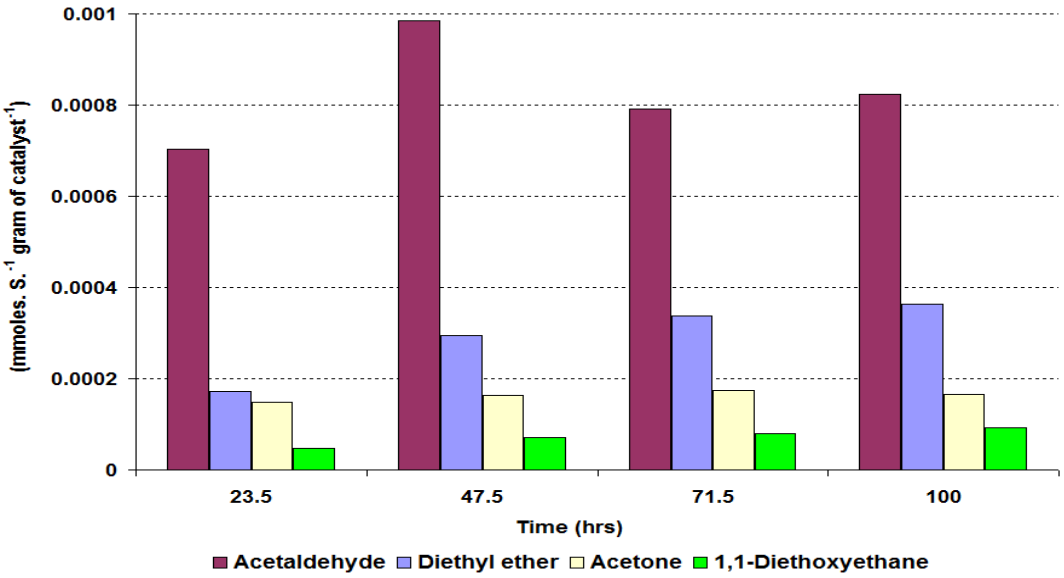

Figure 8.2-68 Rate of formation of liquid products over Pt/Al_2O_3 catalyst at 600°C

The rates of formation of the gaseous and liquid products were plotted against time on stream and are shown in Figures 8.2-67 and 8.2-68 respectively. Of the gaseous products, H_2 gave the maximum rate which stabilised after 30 hours. However, due to a change in feed flow following the overnight sample its rate was slightly disturbed. The rate of C_2H_4 formation significantly decreased whereas the rate of formation of CO_2 and CH_4 increased steadily up to 30 hours and thereafter started to decrease. In addition, small amounts of CO and C_2H_6 were also formed. In the liquid products, acetaldehyde gave a higher rate of formation than diethyl ether, acetone and 1,1-diethoxyethane, whose rates were lower but increased with the passage of time.

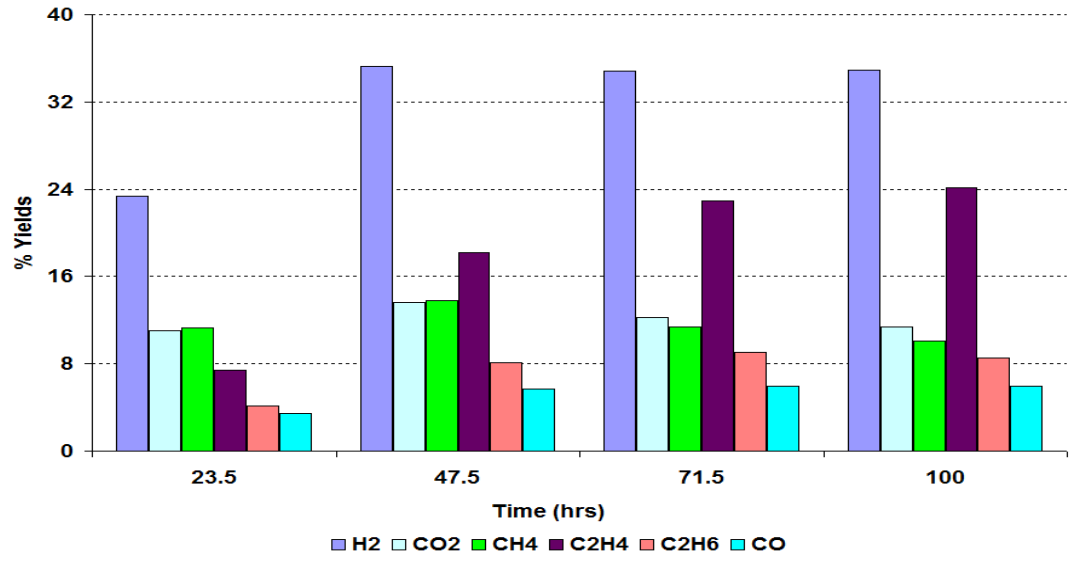

Figure 8.2-69 % Yield of gaseous products over Pt/Al_2O_3 catalyst at 600°C

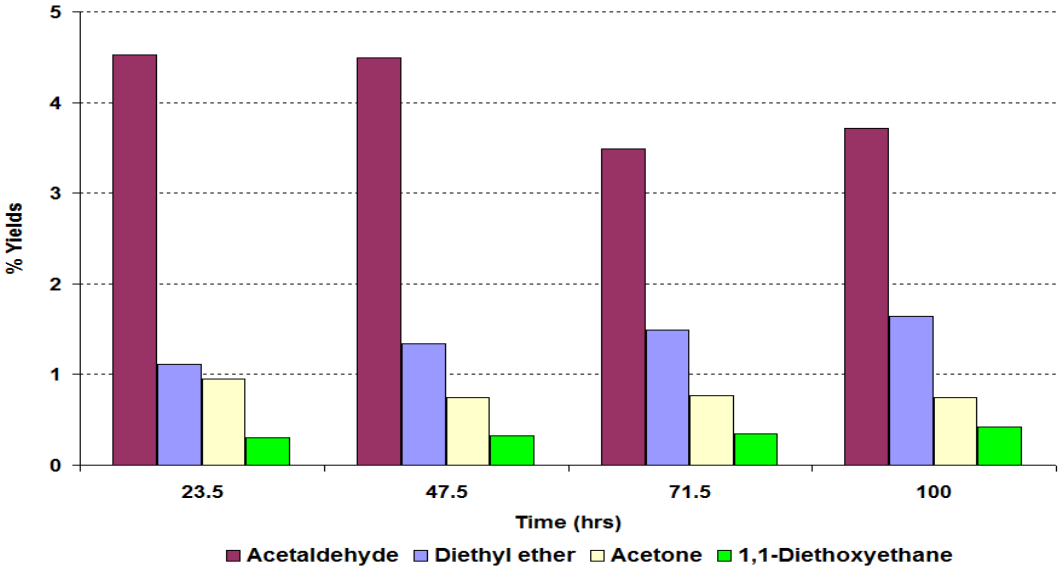

Figure 8.2-70 % Yield of liquid products over Pt/Al_2O_3 catalyst at 600°C

Of the gaseous products H_2 gave the highest yield at ~ 35%. C_2H_4 initially gave a lower yield but increased with time. All other gaseous products gave a yield of less than 14% which varied throughout the reaction.

All liquids produced gave low yields. Amongst these products, acetaldehyde gave the highest value which was < 5%. The yields of the other liquid products were less than 2%. In addition to the products already mentioned, also produced were trace amounts of methanol and crotonaldehyde.

8.2.3.6 Post Reaction Characterisation

The spent catalyst was characterised using a variety of different techniques to determine the chemistry of coke deposited on the catalyst, and the phase of catalyst.

8.2.3.6.1 TPO

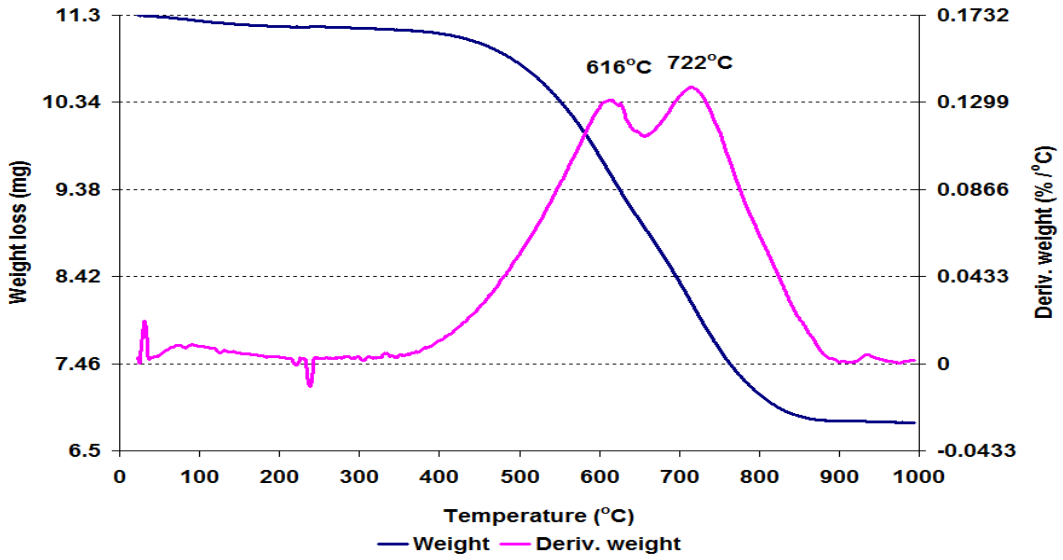

Figure 8.2-71 Post reaction TPO for Pt/Al_2O_3 catalyst at 600°C

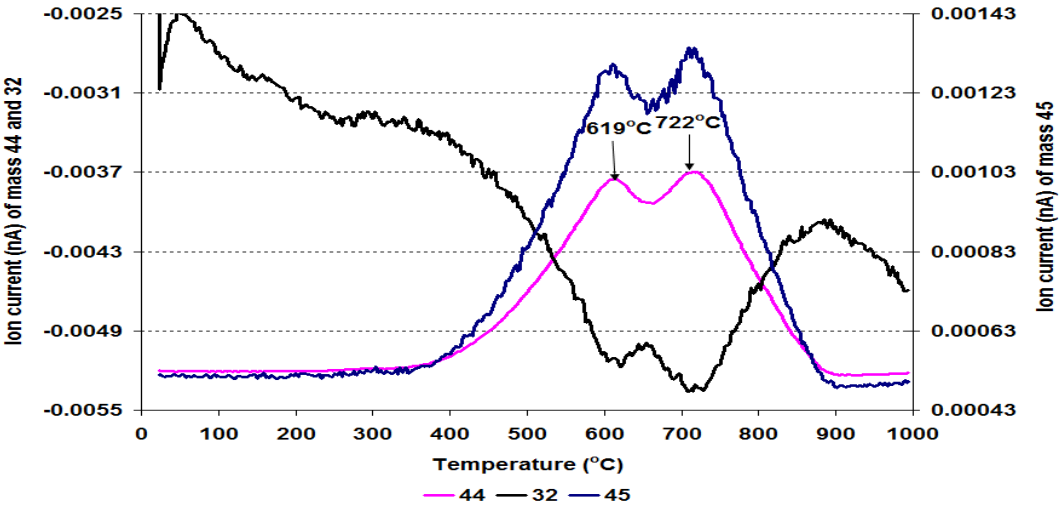

Figure 8.2-72 MS data of CO_2 (m/z=44), O_2 (m/z=32) and C_2H_5OH fragment (m/z=45) for Pt/Al_2O_3 catalyst at 600°C

The TGA profile and the associated mass spectrometry results in an oxygen atmosphere for the Pt/Al_2O_3 were acquired and are shown in Figures 8.2-71 and 8.2-72 respectively. Two main weight loss events were observed in the derivative weight loss plot. Both events were

the result of CO_2 and ethanol fragments desorption and the consumption of oxygen. The derivative weight profile also showed a small weight loss event below 100^{o}C which corresponded to removal of physisorbed H_2O.

8.2.3.6.2 Raman analysis

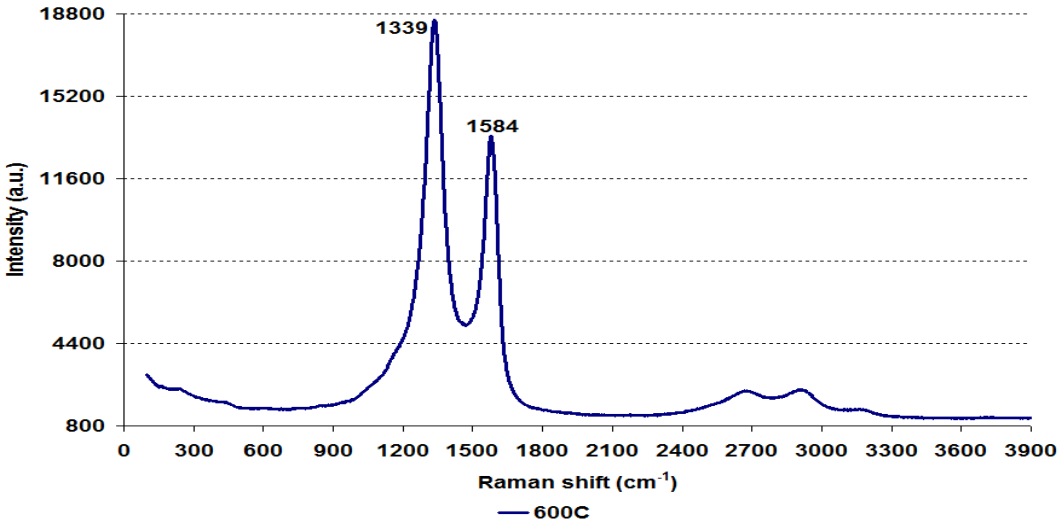

Figure 8.2-73 Post reaction Raman spectrum for Pt/Al_2O_3 catalyst at 600^{o}C

The Raman results for Pt/Al_2O_3 at 600^{o}C shows the same bands were observed to that of Pt/Al_2O_3 catalyst at 550^{o}C. However, the bands intensities significantly increased especially the lower wavenumber band.

8.2.3.6.3 SEM

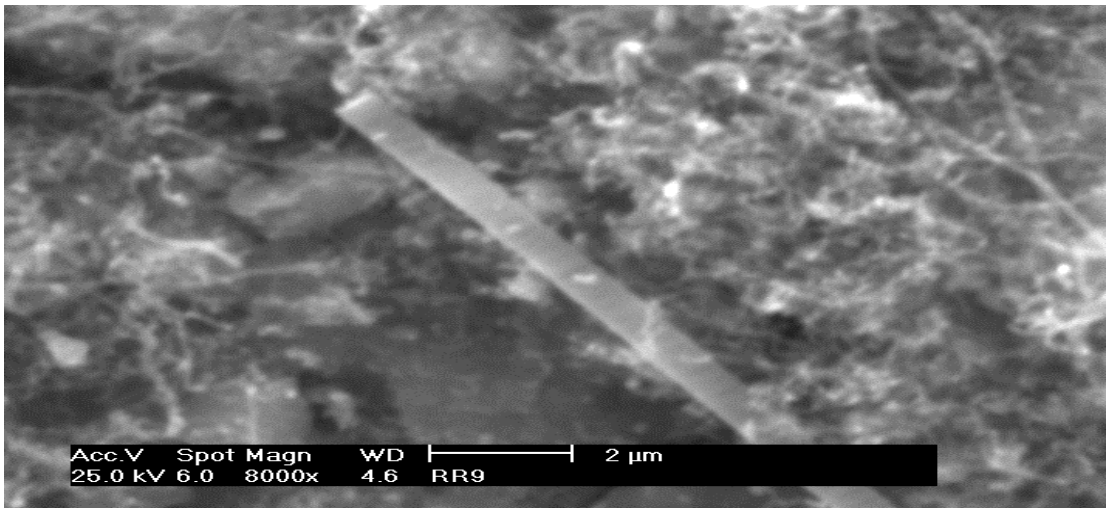

Figure 8.2-74 Post reaction SEM image of Pt/Al_2O_3 catalyst at 600^{o}C

The SEM image shown in Figure 8.2-74 illustrates that a bundle of filamentous carbon was present on the catalyst surface. In addition, there also appeared to be a rod like carbon.

8.2.3.6.4 BET analysis

Catalyst	Conditions	BET Surface area (m^2/g)	Pore volume (cm^3/g)	Average pore diameter (Å)
Pt/Al_2O_3	Reduced (600°C)	100	0.46 (± 0.62)	180 (± 4.48)
	600°C	71	0.05 (± 4.07)	37 (± 8.39)

Table 8.2-8 BET analysis of post reaction Pt/Al_2O_3 catalyst at 600°C

Unexpectedly the BET surface area of the sample after reaction at 600°C was slightly increased compared to the reaction samples run at 500°C and 550°C, although the average pore diameter decreased.

8.2.4 Rh/Al_2O_3

To examine the effect of temperature on the Rh/Al_2O_3 catalyst, reactions were conducted at different temperatures and the preliminarily results obtained were plotted against time on stream and are presented below.

8.2.4.1 Reaction at 500°C

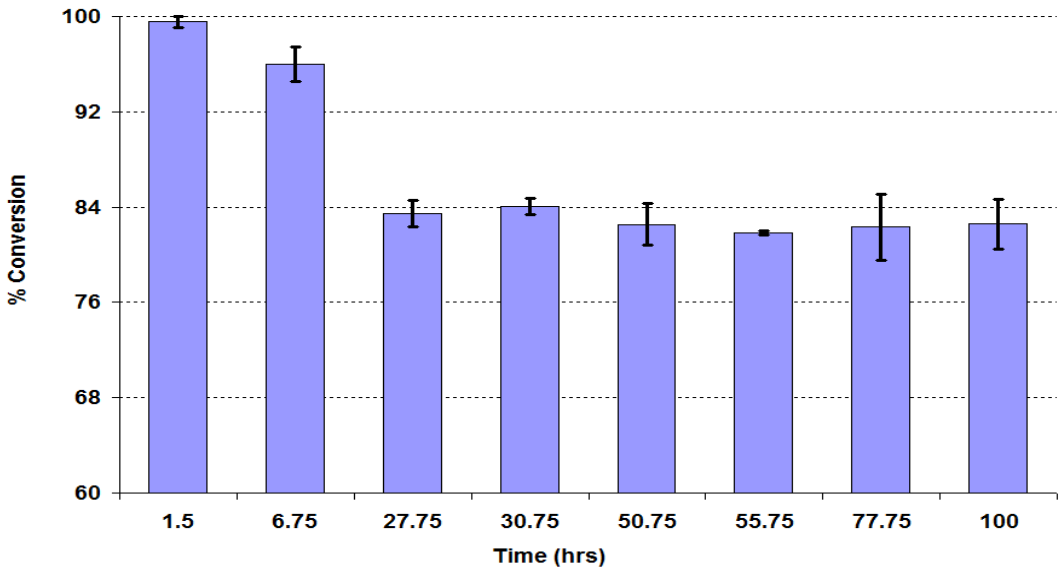

Figure 8.2-75 % Conversion of ethanol over Rh/Al_2O_3 catalyst at 500°C

Figure 8.2-75 shows the conversion of ethanol over Rh/Al_2O_3 at 500°C. These results show that the conversion of ethanol gave above 90% conversion in the initial 7 hours. However after 7 hours time on stream the conversion decreased to 83% and then stabilised for the rest of the reaction.

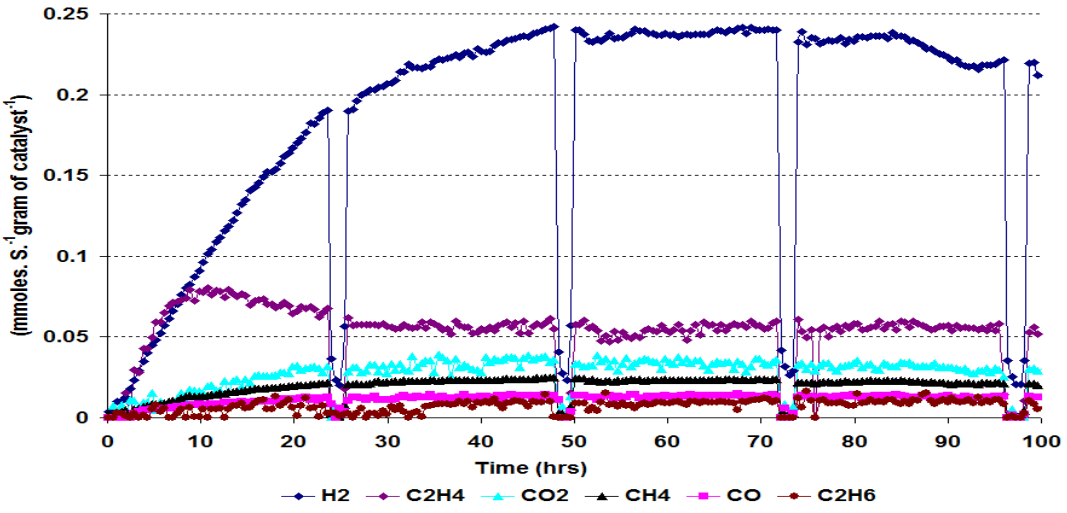

Figure 8.2-76 Rate of formation of gaseous products over Rh/Al_2O_3 at 500°C

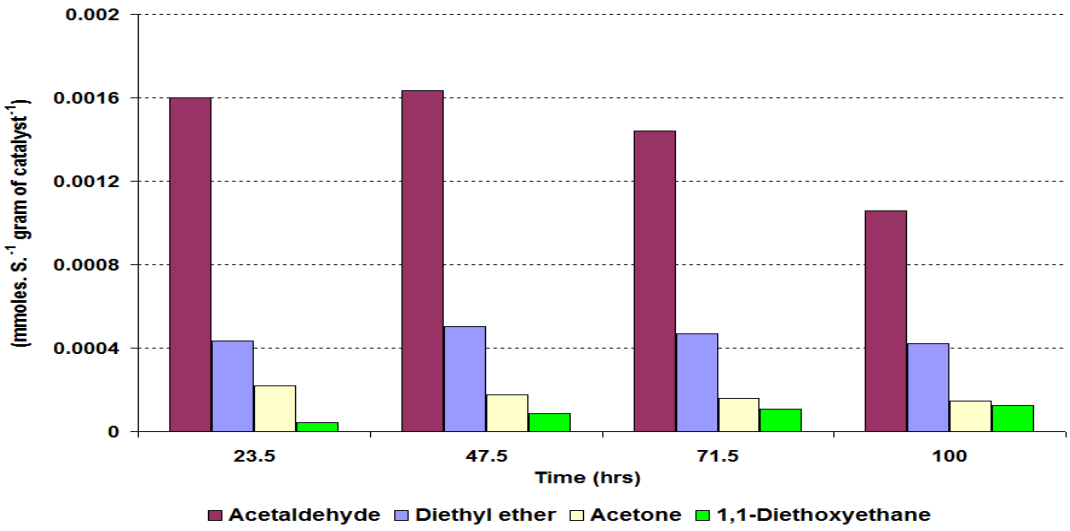

Figure 8.2-77 Rate of formation of liquid products over Rh/Al_2O_3 at 500°C

The rates of formation of the gaseous and liquid products are shown in Figures 8.2-76 and 2.3-77 respectively. It can be seen from the Figure 8.2-76 that H_2 gave a rate almost five times higher than the other gaseous products after stabilisation. However, its rate was not stable and after 85 hours time on stream it started to decrease. C_2H_4 gave interesting results; in the initial 24 hours its rate slightly increased whilst after 24 hours the rate

progressively decreased and then stabilised for the rest of the reaction. Of all the gaseous products C_2H_6 gave the lowest rate of formation.

In the liquid products, acetaldehyde was produced at a higher rate which steadily decreased with time. Figure 8.2-77 also indicates that the rate of diethyl ether formation remained almost stable throughout the reaction, while the rate of formation of acetone progressively decreased.

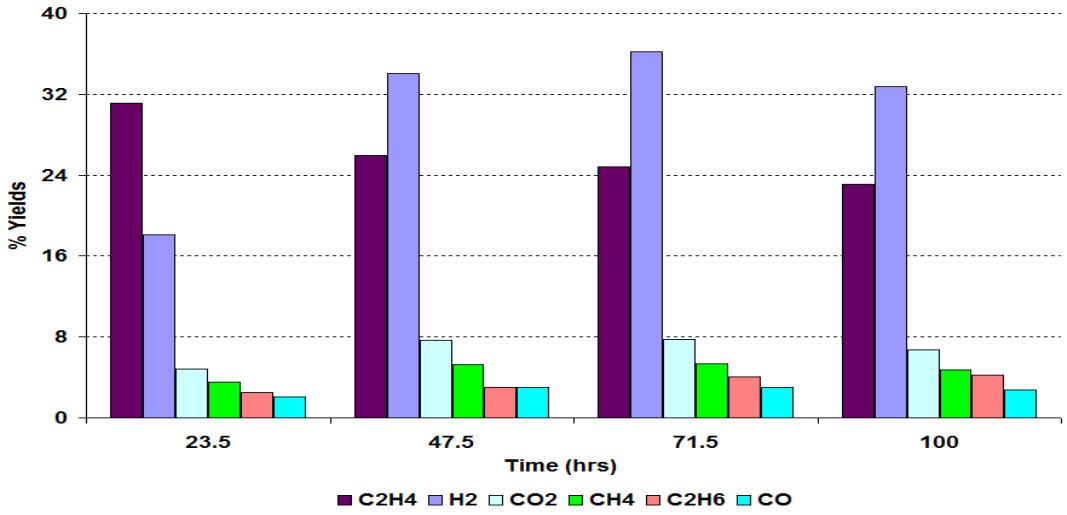

Figure 8.2-78 % Yield of gaseous products over Rh/Al_2O_3 at 500°C

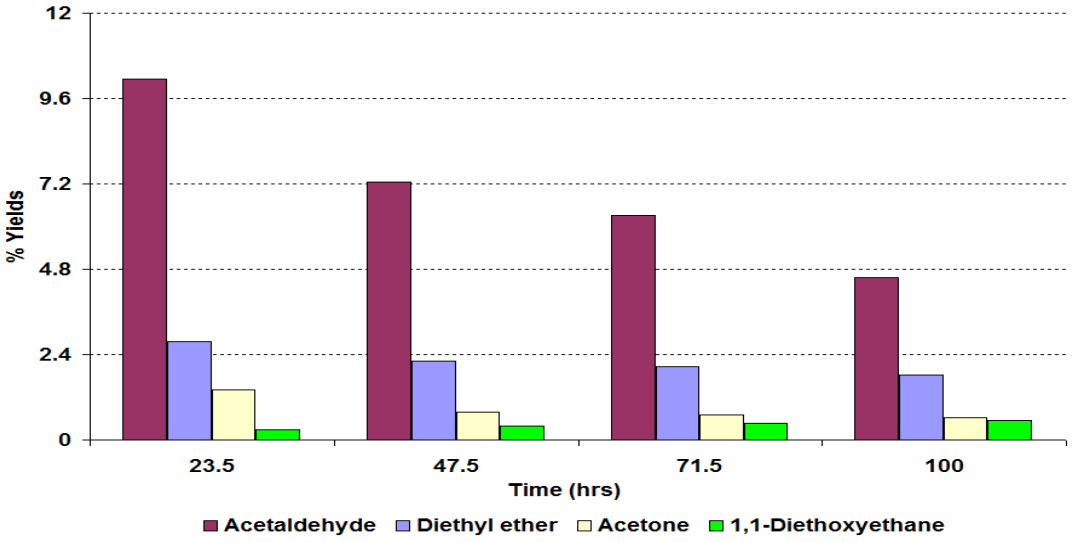

Figure 8.2-79 % Yield of liquid products over Rh/Al_2O_3 at 500°C

The initial yield of C_2H_4 was highest in all the gaseous products as seen in Figure 8.2-78. However, after 24 hours H_2 yields exceeded those of C_2H_4 and this scenario continued for the rest of the reaction. In the liquid products, acetaldehyde, diethyl ether, acetone and 1,1-

diethoxyethane gave measurable amount of yields. Also produced were ethyl acetate, methanol and crotonaldehyde.

8.2.4.2 Post reaction characterisation

After the reaction, the spent catalyst was characterised using various techniques to determine the nature of the carbonaceous deposits as discussed in section 7.1.

8.2.4.2.1 TPO

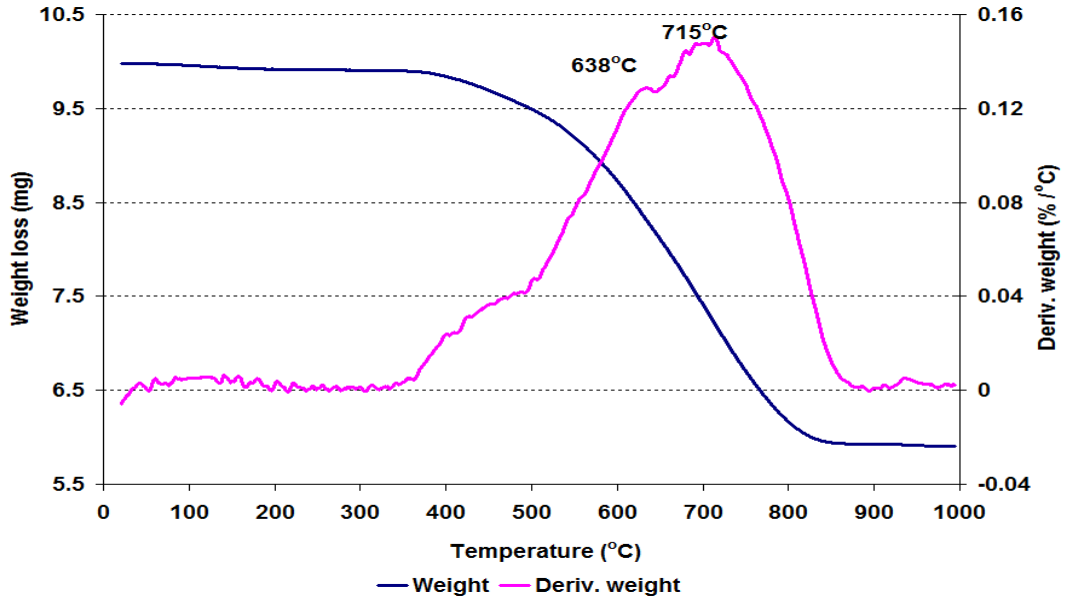

Figure 8.2-80 Post reaction TPO for Rh/Al_2O_3 at 500°C

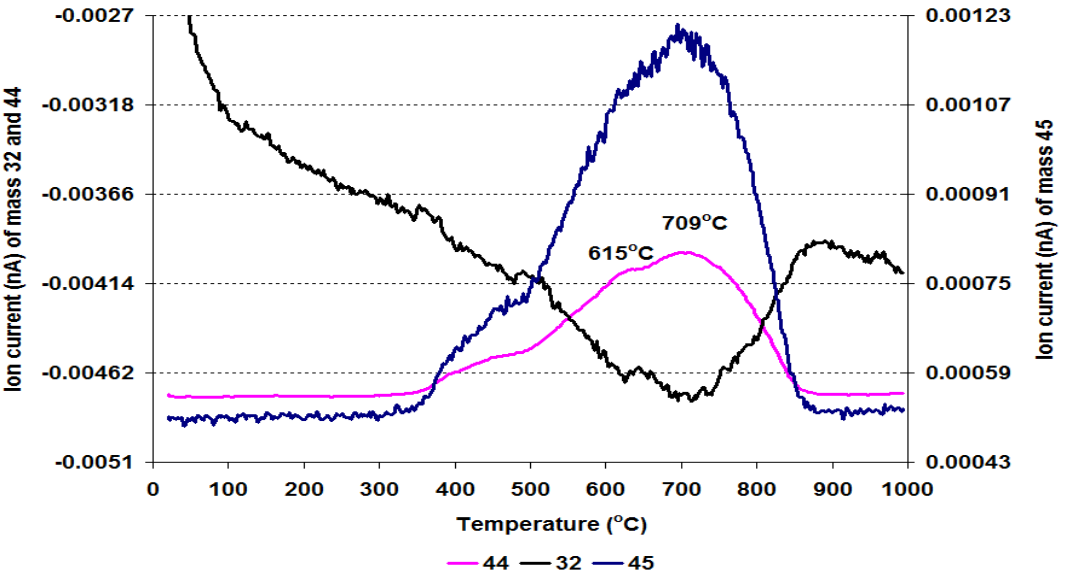

Figure 8.2-81 MS data of CO_2 (m/z=44), O_2 (m/z=32) and C_2H_5OH fragment (m/z=45) for Rh/Al_2O_3 at 500°C

The TGA profile for the spent Rh/Al_2O_3 sample run at 500^oC showed fascinating results. This illustrated that a total of 408 mg g^{-1} catalyst weight loss occurred during the temperature ramp up to 1000^oC. The weight loss events took place within a broad temperature region. The main weight loss gave a single broad peak, with a small shoulder preceding the main peak, suggesting that different types of carbonaceous materials were deposited on the catalyst surface which, was also supported by the evolution of CO_2 as identified from the mass spectrometry profile.

8.2.4.2.2 Powder XRD

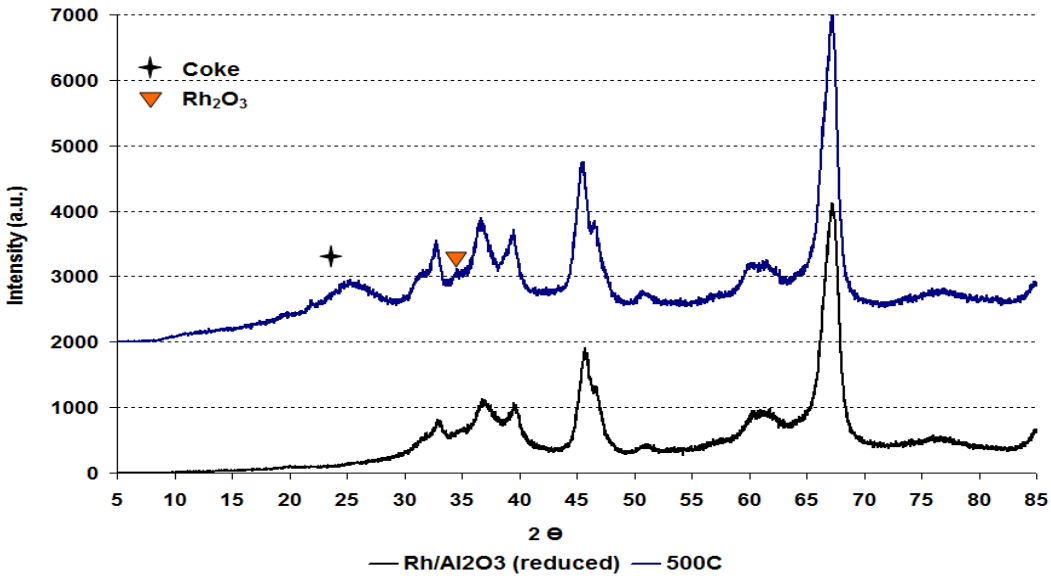

Figure 8.2-82 Powder XRD patterns of reduced and post reaction Rh/Al_2O_3 at 500^oC

The graph in Figure 8.2-82 shows that the powder XRD patterns for the fresh and spent catalysts are virtually identical to one another except for the broad peak attributed to coke at 26^o and a small peak at 35^o 2θ position which corresponded to Rh_2O_3.

8.2.4.2.3 Raman analysis

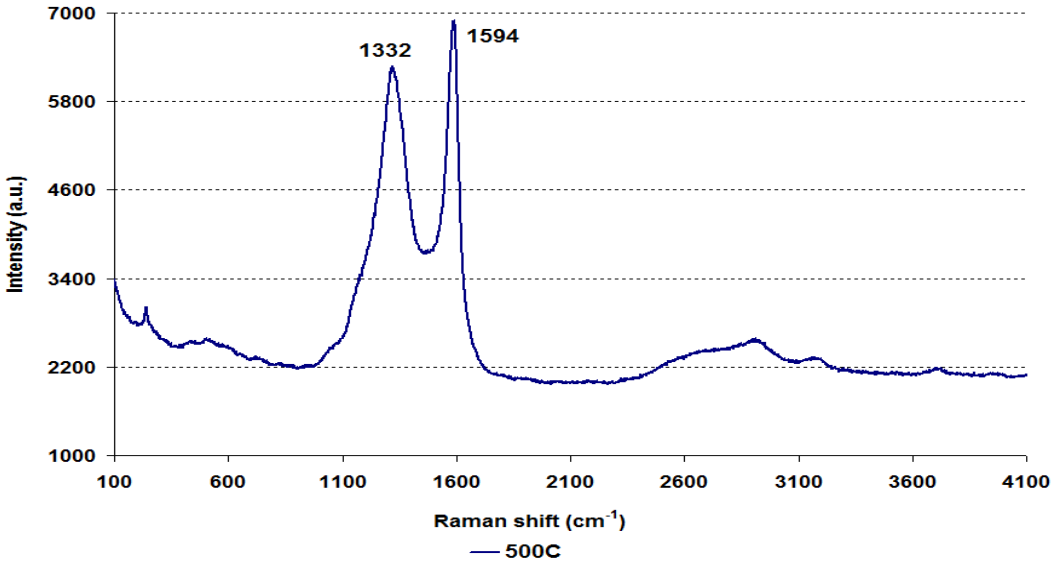

Figure 8.2-83 Post reaction Raman spectrum for Rh/Al_2O_3 at 500°C

The Raman spectrum for the spent Rh/Al_2O_3 catalyst shown in Figure 8.2-83 gives characteristic bands for graphitic carbon as observed in the Pt/Al_2O_3 catalyst.

8.2.4.2.4 SEM

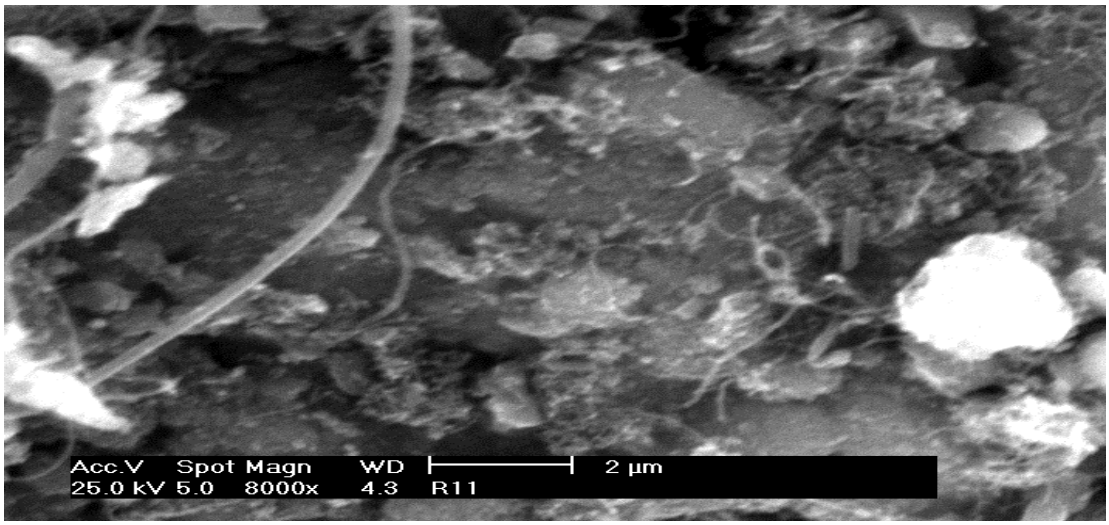

Figure 8.2-84 Post reaction SEM image of Rh/Al_2O_3 at 500°C

Two types of filamentous carbon were present on the catalyst surface as seen in the SEM image in Figure 2.3-84. The small diameter filamentous carbon is scattered across the sample surface. Also, some larger diameter filamentous carbon on the catalyst surface is observed.

8.2.4.2.5 BET analysis

Catalyst	Conditions	BET Surface area (m^2/g)	Pore volume (cm^3/g)	Average pore diameter (Å)
Rh/Al_2O_3	Reduced (600°C)	101	0.46 (± 0.31)	174 (± 0.98)
	500°C	47	0.04 (± 3.28)	42 (± 5.57)

Table 8.2-9 BET analysis of post reaction Rh/Al_2O_3 catalyst at 500°C

As observed with the previous catalysts, a significant change occurred in the BET surface area, the average pore diameter, and the pore volume of spent Rh/Al_2O_3 catalyst as shown in Table 8.2-9.

8.2.4.3 Reaction at 550°C

After performing the reaction at 500°C, the next reaction was conducted at 550°C, to examine the effect of temperature on the distribution and yields of the different products during the steam reforming reaction of ethanol over Rh/Al_2O_3.

The graph shown below in Figure 8.2-85 presents the conversion of ethanol over Rh/Al_2O_3 at 550°C. It demonstrates that for ethanol the conversion followed similar patterns to those seen at 500°C. However, the conversion started to decrease after 1 hour TOS and slightly fluctuated with reaction time.

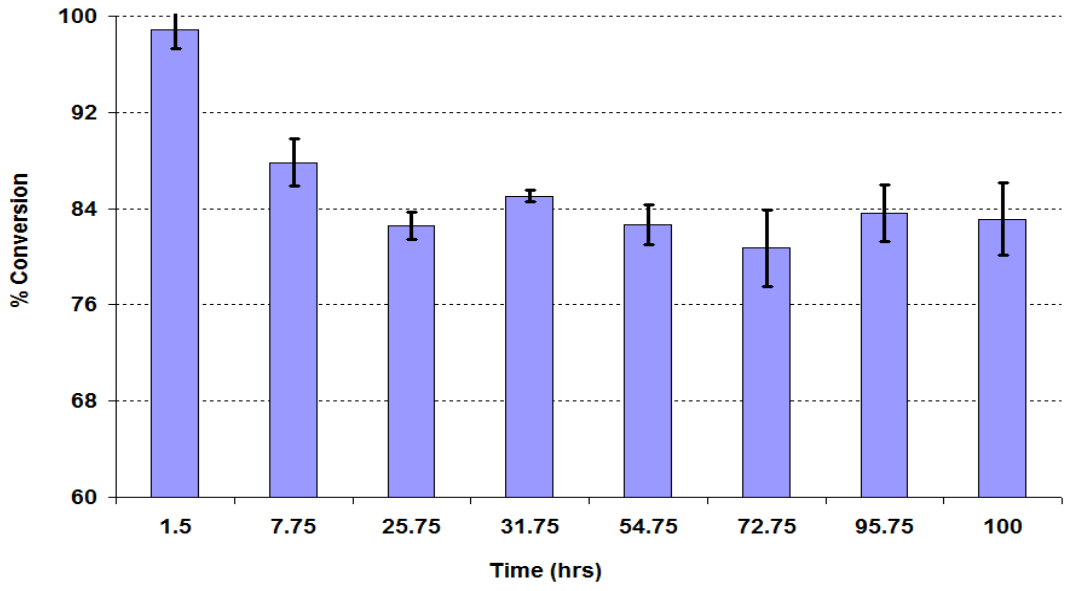

Figure 8.2-85 % Conversion of ethanol over Rh/Al_2O_3 catalyst at 550°C

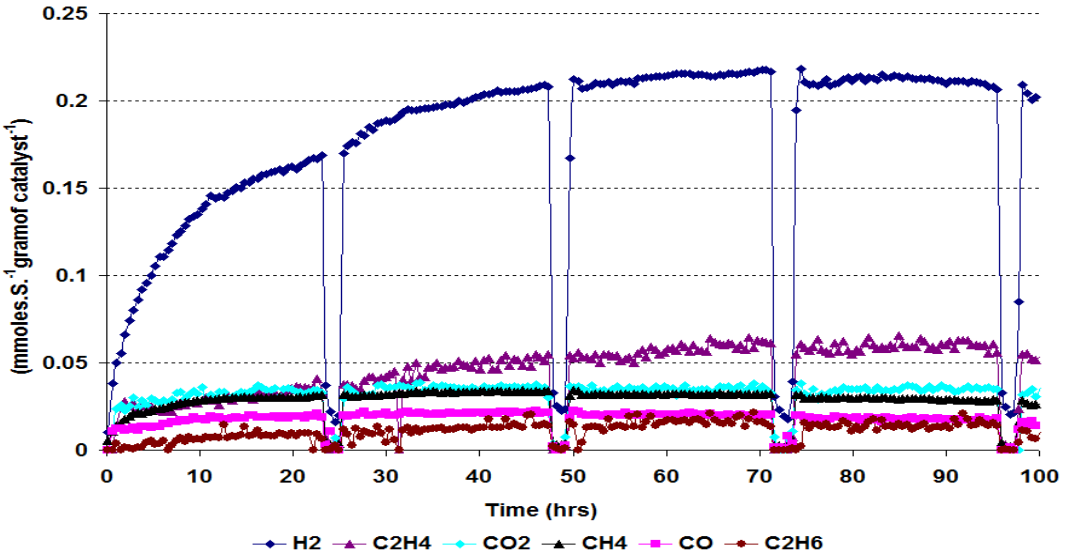

Figure 8.2-86 Rate of formation of gaseous products over Rh/Al_2O_3 at 550°C

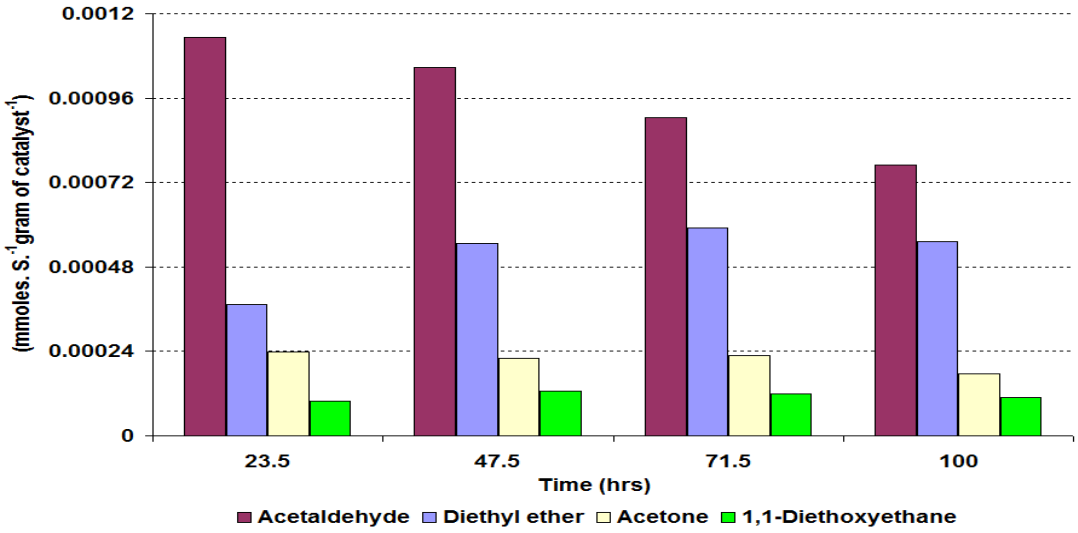

Figure 8.2-87 Rate of formation of liquid products over Rh/Al_2O_3 at 550°C

From the data in Figure 8.2-86 it is clear that H_2 was produced at a rate 4.4 times higher than the other gaseous products, and the value steadily rose and gave the highest rate after 60 hours. However, the rate started to decrease after 60 hours up to the end of the reaction. The rate of formation of the other gaseous products after the initial increase progressively decreased throughout the reaction except for C_2H_4 which increased.

With the liquid products, acetaldehyde gave the highest rate of formation which steadily decreased over time. In comparison, the rate of formation of diethyl ether increased. Also small amounts of acetone and 1,1-diethoxyethane were detected by GC.

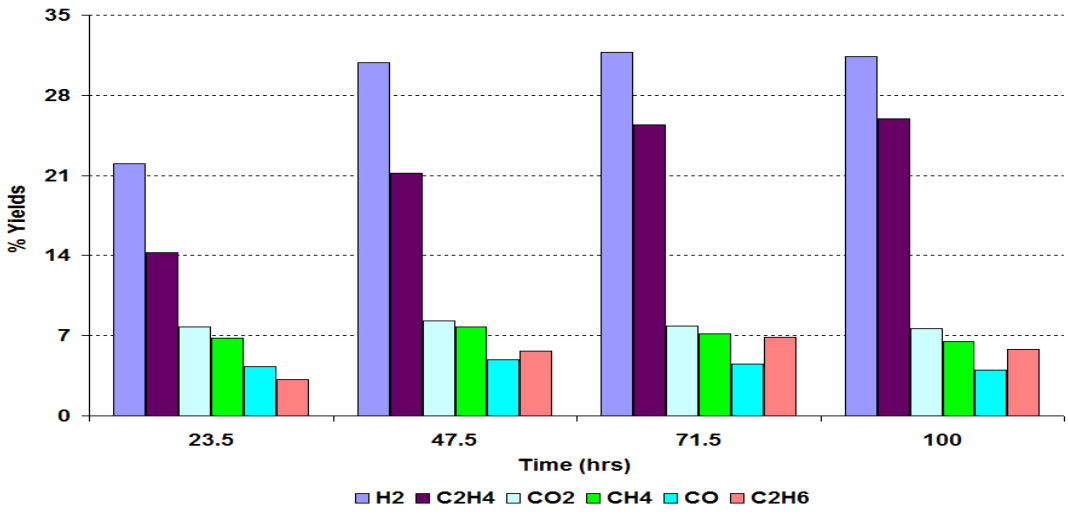

Figure 8.2-88 % Yield of gaseous products over Rh/Al_2O_3 at 550^oC

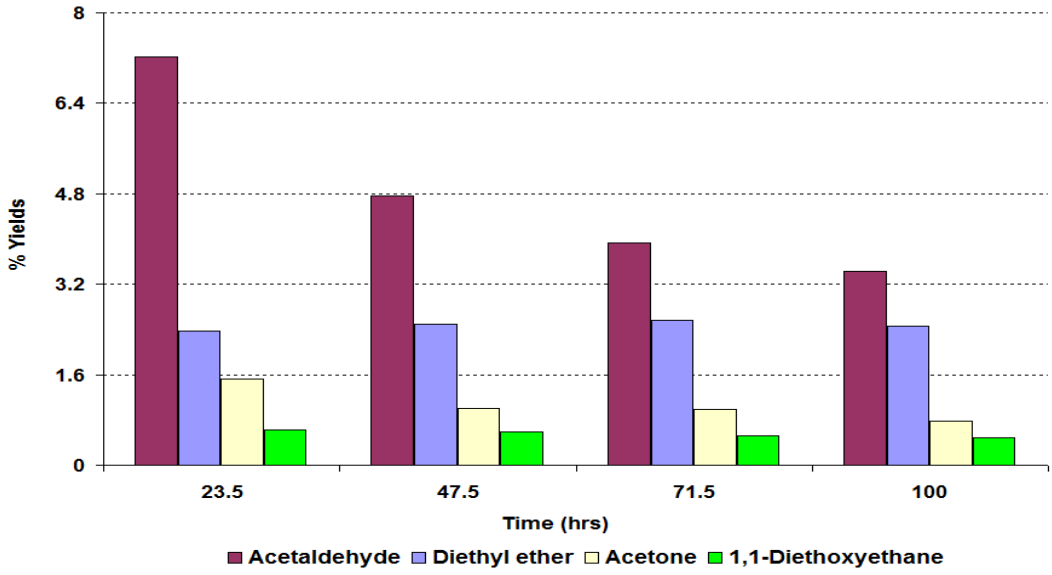

Figure 8.2-89 % Yield of liquid products over Rh/Al_2O_3 at 550^oC

Figure 8.2-88 illustrates that for gaseous products H_2 and C_2H_4 gave the highest yields whilst CH_4, CO_2, CO and C_2H_6 were produced in minor amounts. The yield of H_2 steadily increased and gave a maximum value of 32%. Whereas the yield of C_2H_4 increased till the end of the reaction and gave a maximum value of 26%.

With the liquid products, significant amounts of acetaldehyde, diethyl ether, acetone and 1,1-diethoxyethane were produced, which follows the same path to that seen in the reaction at 500^oC on Rh/Al_2O_3 catalyst. Trace levels of ethyl acetate, methanol and crotonaldehyde were also produced.

8.2.4.4 Post reaction characterisation

8.2.4.4.1 TPO

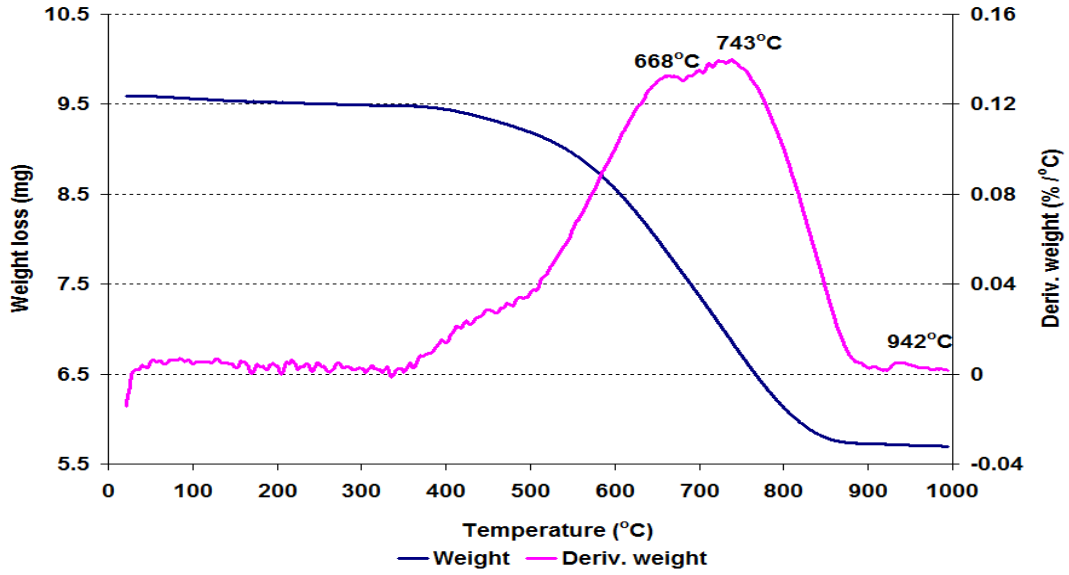

Figure 8.2-90 Post reaction TPO for Rh/Al_2O_3 at 550°C

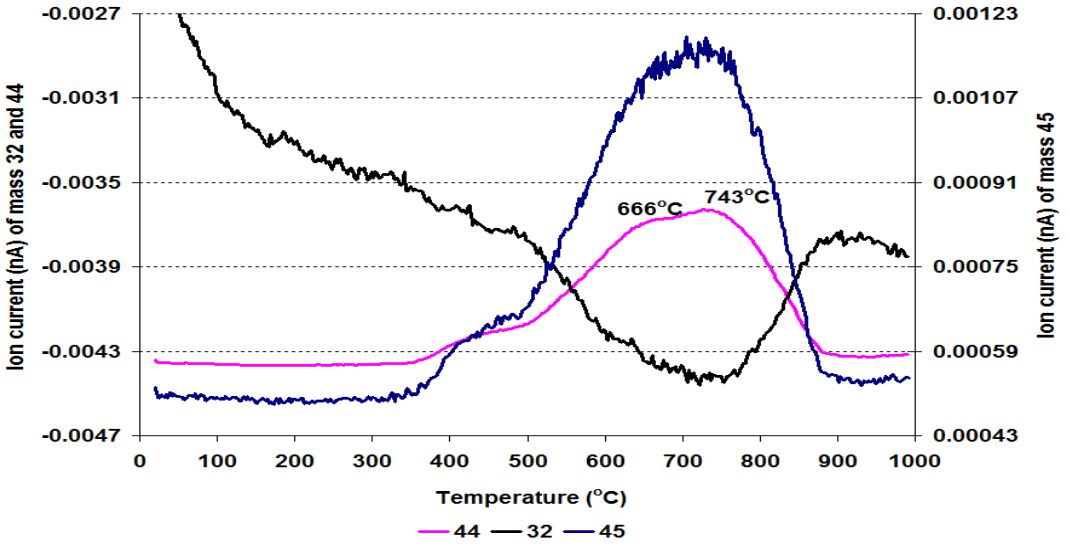

Figure 8.2-91 MS data of CO_2 (m/z=44), O_2 (m/z=32) and C_2H_5OH fragment (m/z=45) for Rh/Al_2O_3 at 550°C

The TPO results shown in Figure 8.2-90 indicates that a total of 405.9 mg g^{-1} catalyst weight loss occurred in the temperature range between 23°C and 1000°C. The derivative weight profile showed a broad peak from 355°C to 926°C which corresponds to CO_2 and ethanol fragment (m/z = 45) in the mass profile in Figure 8.2-91.

8.2.4.4.2 Raman analysis

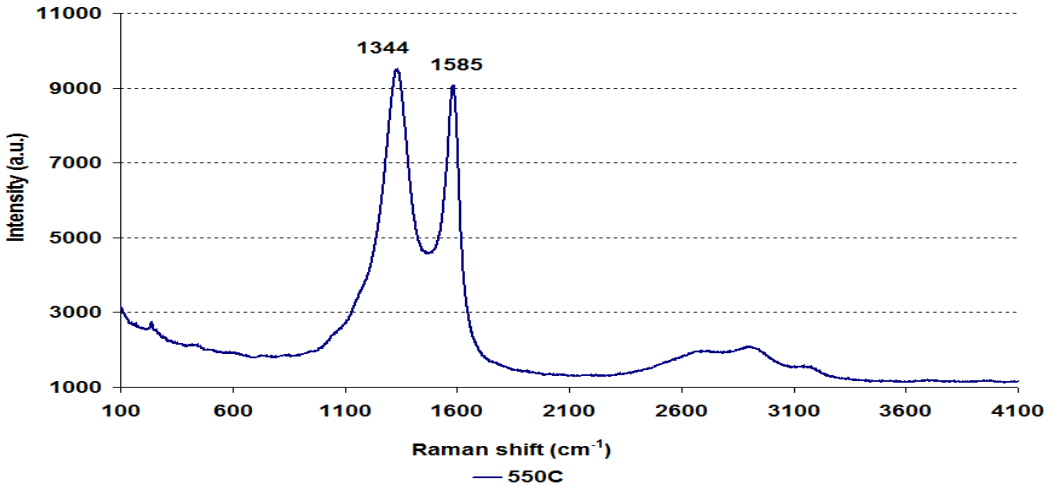

Figure 8.2-92 Post reaction Raman spectrum for Rh/Al_2O_3 at 550°C

The Raman data for the Rh/Al_2O_3 catalyst at 550°C gave bands at wave numbers 1344 and 1585 cm^{-1} which are characteristic bands for disordered graphitic carbon.

8.2.4.4.3 SEM

The SEM image of the spent Rh/Al_2O_3 catalyst showed surprising results. There were two types of filamentous carbon present. A long small diameter filamentous carbon and a second interesting large diameter coil type carbon which was first observed in this sample. For further clarification other particles of the sample were scanned and similar results were observed.

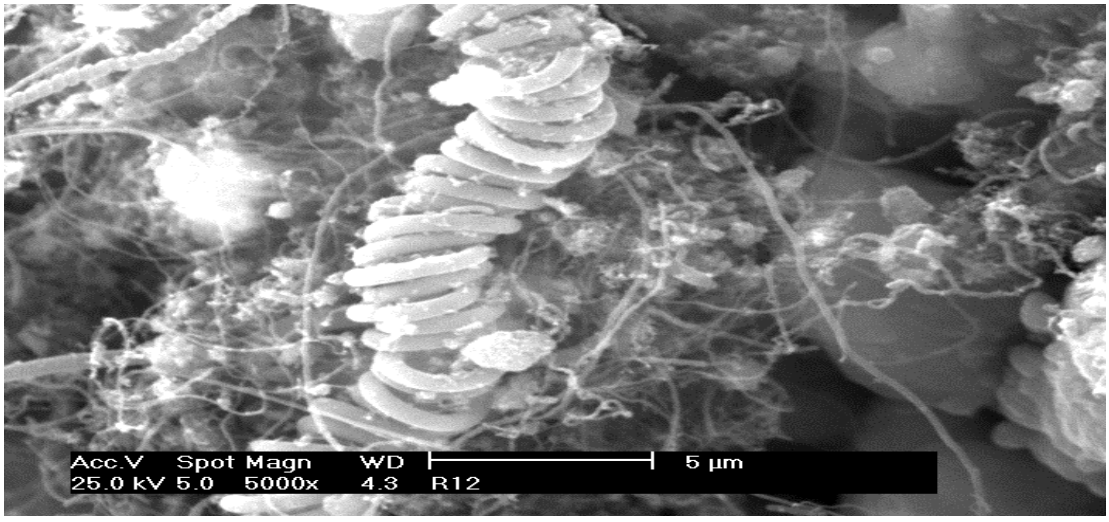

Figure 8.2-93 Post reaction SEM image of Rh/Al_2O_3 at 550°C

8.2.4.4.4 BET analysis

Catalyst	Conditions	BET Surface area (m^2/g)	Pore volume (cm^3/g)	Average pore diameter (Å)
Rh/Al_2O_3	Reduced (600°C)	101	0.46 (± 0.31)	174 (± 0.98)
	550°C	50	0.04 (± 3.53)	40 (± 3.93)

Table 8.2-10 BET analysis of post reaction Rh/Al_2O_3 catalyst at 550°C

The BET data illustrated that the average pore diameter and the pore volume for the post reaction catalyst were similar to that seen for the reaction at 500°C, except that the BET surface area was slightly greater in the 550°C sample.

8.2.4.5 Reaction at 600°C

Finally the reaction was carried out at 600°C to further investigate the effect of temperature.

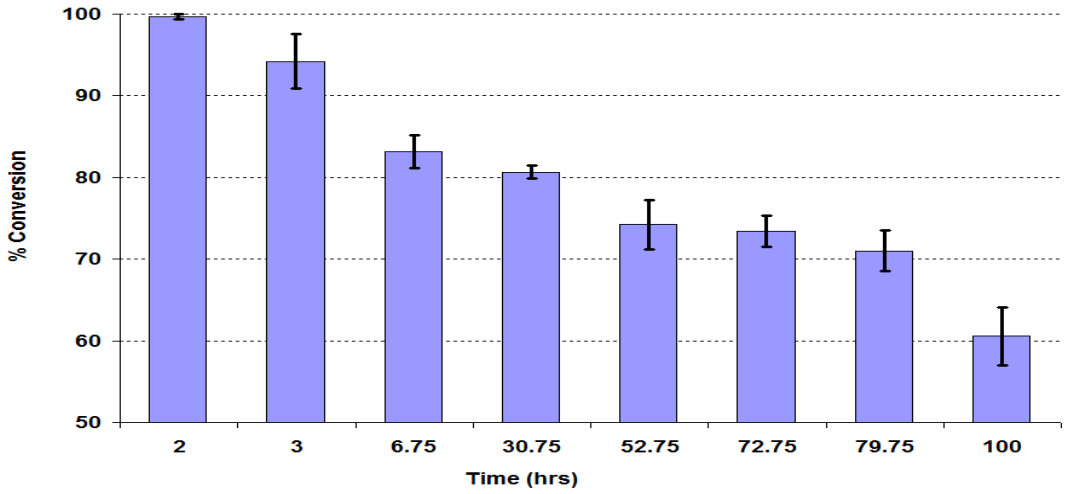

Figure 8.2-94 % Conversion of ethanol over Rh/Al_2O_3 catalyst at 600°C

The conversion of ethanol over Rh/Al_2O_3 at 600°C as shown in Figure 8.2-94 gave fascinating results. The figure reveals that initially the conversion of ethanol was almost 100% which gradually decreased with the reaction time and after 100 hours time on stream it reduced to 60%. However, throughout the reaction the conversion of ethanol did not stabilise.

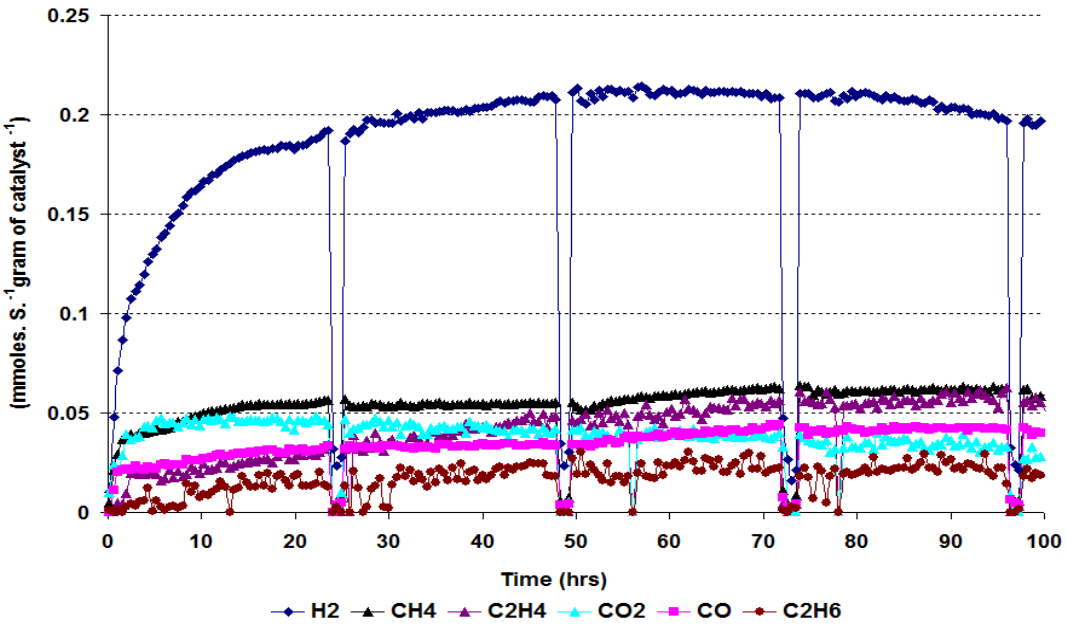

Figure 8.2-95 Rate of formation of gaseous products over Rh/Al_2O_3 at 600°C

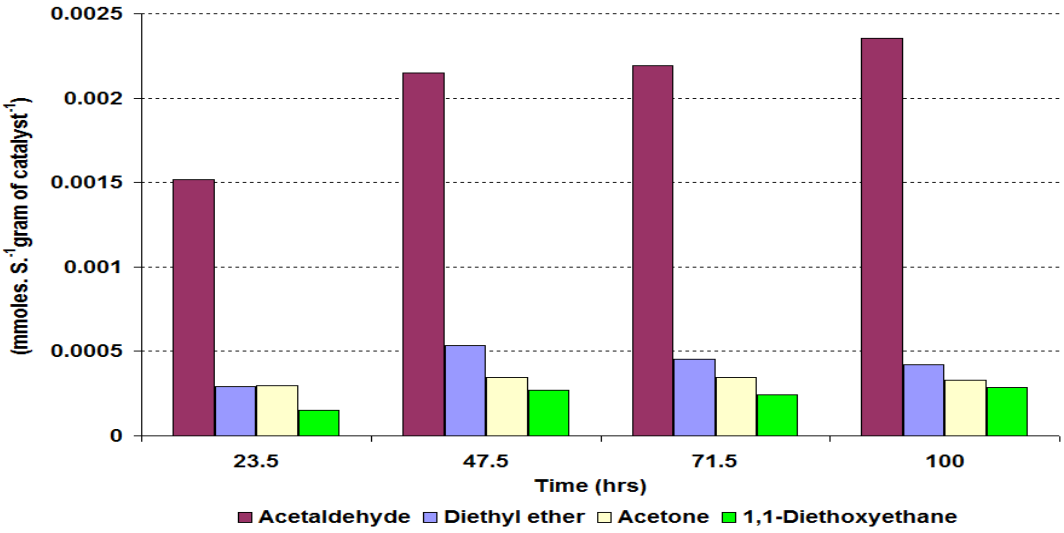

Figure 8.2-96 Rate of formation of liquid products over Rh/Al_2O_3 at 600°C

The rate of formation of H_2 followed a similar pattern to that observed for the reaction at 550°C. Interestingly, CH_4 was produced in higher rates at 600°C and achieved steady state conditions after 12 hours TOS. The rate of formation of CO and CO_2 mirror image during the course of the reaction *i.e.* initially CO_2 has a higher rate while CO has a lower rate. However, with the passage of time the rate of formation of CO increased while that of CO_2 decreased. C_2H_4 was also produced at a minor rate which steadily increased with time.

The rate of formation of the liquid products is shown in Figure 8.2-96. Like reaction at 550^{o}C, acetaldehyde gave an initial greater rate of formation which continuously increased, whilst trace amounts of diethyl ether, acetone and 1,1-diethoxyethane were detected by GC.

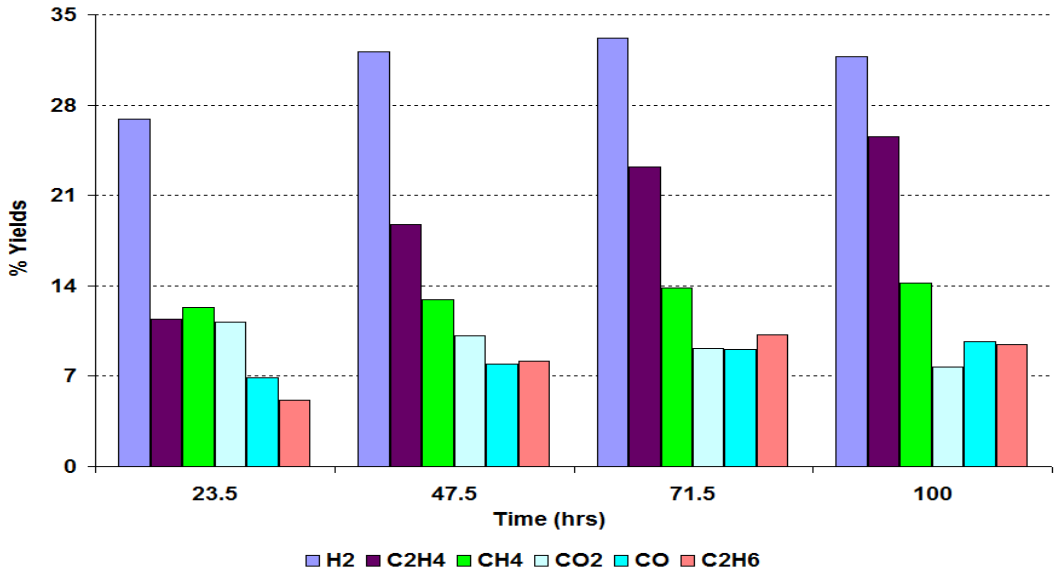

Figure 8.2-97 % Yield of gaseous products over Rh/Al_2O_3 at 600^{o}C

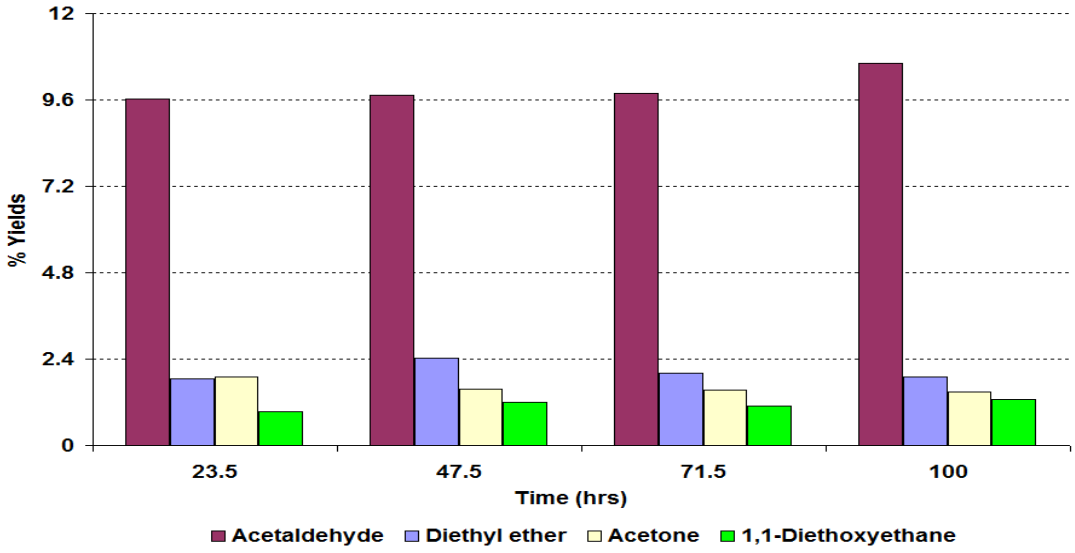

Figure 8.2-98 % Yield of liquid products over Rh/Al_2O_3 at 600^{o}C

Of the gaseous products H_2 gave the highest yield, which slightly varied throughout the reaction. Also the yields of the other gaseous products increased and fluctuated with reaction time. However, the yield of C_2H_4 increased continuously and gave the maximum yield of ~ 25%.

In the liquid products, acetaldehyde gave the highest yield which increased with time as compared to previous reaction whilst other liquid products gave yields of less than 3%.

8.2.4.6 Post reaction characterisation

The post reaction catalyst was characterised by various different techniques as discussed in section 7.1.

8.2.4.6.1 TPO

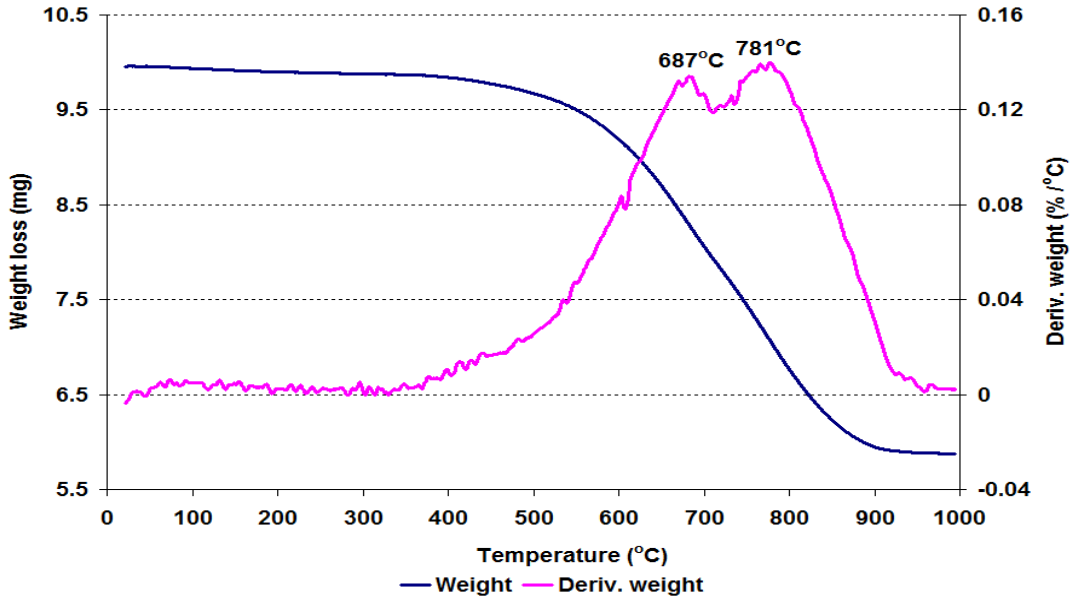

Figure 8.2-99 Post reaction TPO for Rh/Al_2O_3 at 600°C

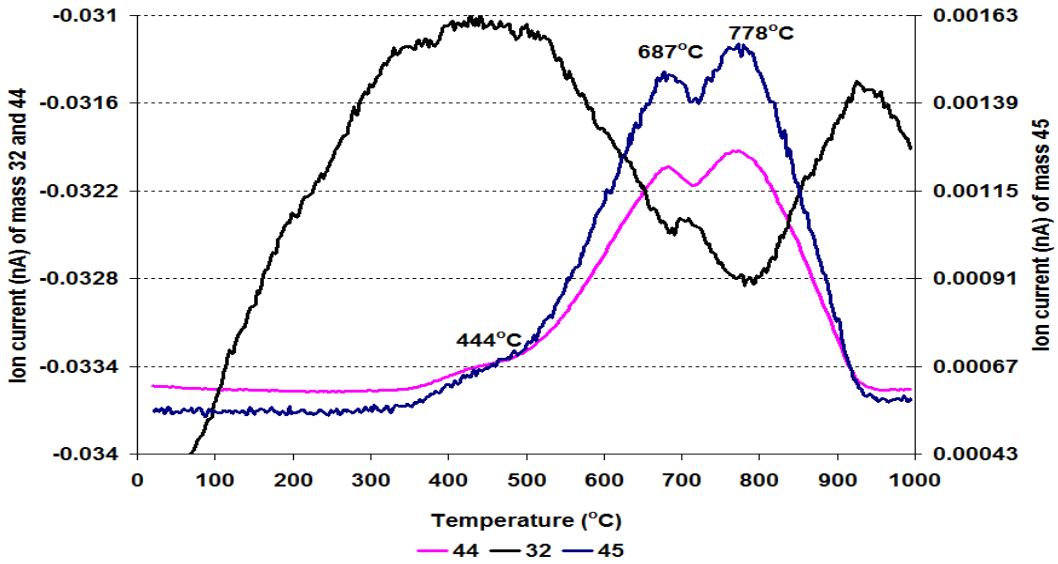

Figure 8.2-100 MS data of CO_2 (m/z=44), O_2 (m/z=32) and C_2H_5OH fragment (m/z=45) for Rh/Al_2O_3 at 600°C

The TGA profile shown in Figure 8.2-99 illustrates that 410 mg g^{-1} of weight loss occurred in the temperature region up to 1000°C. The main weight loss took place from 335°C to 962°C, and the two peaks at 687°C and 781°C suggest different types of carbonaceous materials deposited on the catalyst. These peaks matched with CO_2 and C_2H_5OH fragment desorption in the mass profile. Mass results also showed that there was a broad peak attributed to HCHO and methoxy which is not shown in Figure 8.2-100.

8.2.4.6.2 Raman analysis

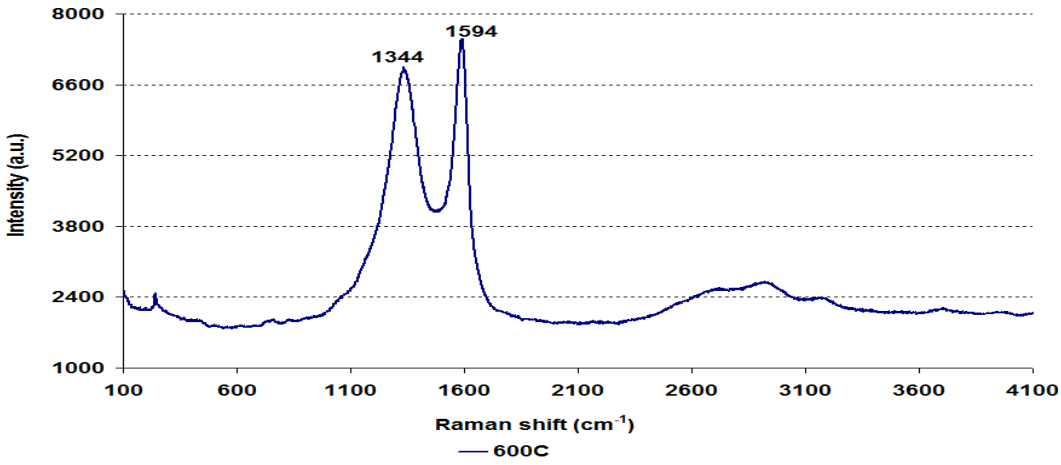

Figure 8.2-101 Post reaction Raman spectrum for Rh/Al_2O_3 at 600°C

The Raman analysis shows similar bands to those observed for previous spent samples. However, the higher wave number peak shifted slightly upwards. The intensity of the bands decreased with respect to the preceding catalyst seen in Figure 8.2-101.

8.2.4.6.3 SEM

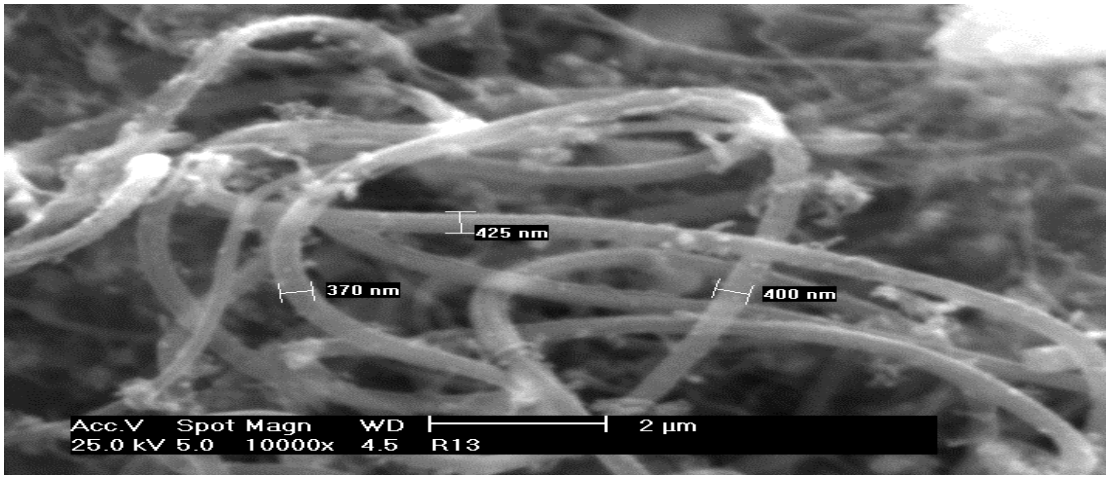

Figure 8.2-102 Post reaction SEM image of Rh/Al_2O_3 at 600°C

The SEM image of the used catalyst, shown above, has a surprising, large diameter filamentous coke scattered on the catalyst surface. Although not shown here, small filamentous coke was also present. Both types of coke were mainly present in the cavity or on the corners of the particles.

8.2.4.6.4 BET analysis

Catalyst	Conditions	BET Surface area (m^2/g)	Pore volume (cm^3/g)	Average pore diameter (Å)
Rh/Al_2O_3	Reduced (600^oC)	101	0.46 (± 0.31)	174 (± 0.98)
	600^oC	45	0.03 (± 1.41)	35 (± 4.76)

Table 8.2-11 BET analysis of post reaction Rh/Al_2O_3 catalyst at 600^oC

The spent catalyst was analysed by the BET analyser and the result obtained were tabulated and shown in Table 8.2-11. The table illustrates that a substantial change was observed for the BET surface area, the average pore diameter and the pore volume compared to the fresh sample in reduced form.

8.3 Effect of impurities

Following investigation into the influence of temperature on precious metal (Ru, Pt and Rh) supported Al_2O_3 catalysts we turned to the main aim of the project *i.e.* the effect of different impurities present in crude ethanol on the steam reforming reaction. Five different functional group representatives with basic C_3 structure, which included: 1-propanol, 2-propanol (IPA), propanal, propylamine and acetone, were added individually to the water/ethanol mixture, in 1% molar ratio with respect to ethanol content. The influences of these five types of impurities were investigated individually by performing the reactions at 500^{o}C over four different types of catalysts using the procedure as discussed in section 7.2.2.

8.3.1 Al_2O_3

The two reactions were carried out over Al_2O_3 to investigating whether the impurities have any effect on the support or not. The results obtained were plotted as a function of time on stream, and are shown below. Post reaction characterisation was carried out to examine the cause of deactivation of the support.

8.3.1.1 1-Propanol impurity

1-Propanol is present in raw ethanol in quantities in the range of 0.072 vol.%. Initially the reaction was carried out to identify any influence of 1-propanol on the steam reforming of ethanol reaction on the alumina.

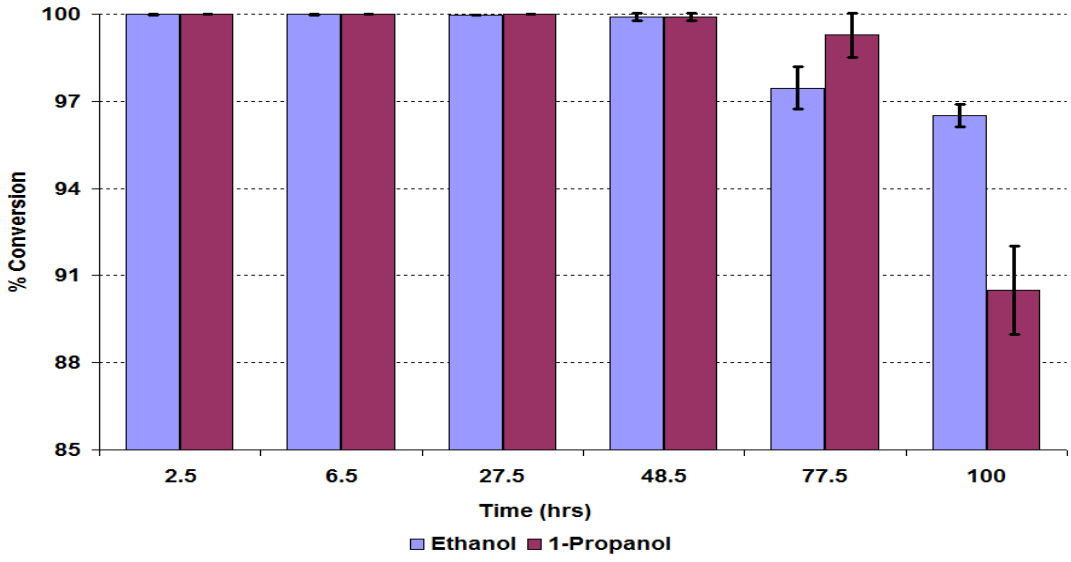

Figure 8.3-1 % Conversion of ethanol and 1-Propnaol over the Al_2O_3 catalyst during the 1-propanol impurity reaction

Figure 8.3-1 illustrates that the conversion of ethanol slightly decreased after the addition of the 1-propanol impurity to the water/ethanol mixture. Figure 8.3-1 shows that after 48 hours time on stream an apparent decrease in the conversion of ethanol was observed, which dropped conversion to 96% by the end of the reaction. On the other hand, the 1-propanol impurity gave a high conversion and followed similar patterns to those of the pure ethanol although the conversion in the 1-propanol impurity was lower than pure ethanol by the end of the reaction.

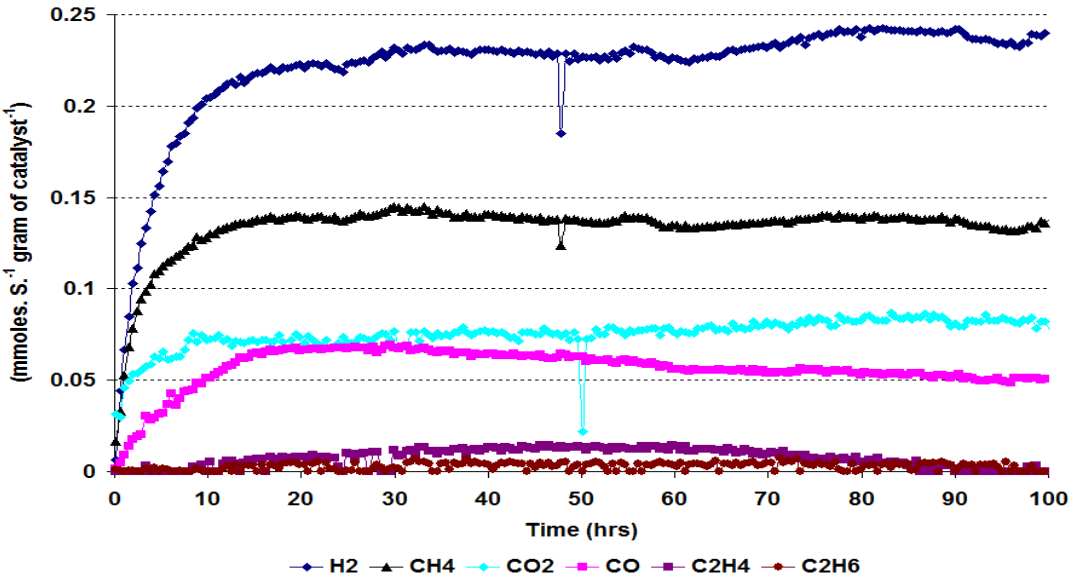

Figure 8.3-2 Rate of formation of gaseous products over Al_2O_3 catalyst during the 1-propanol impurity reaction

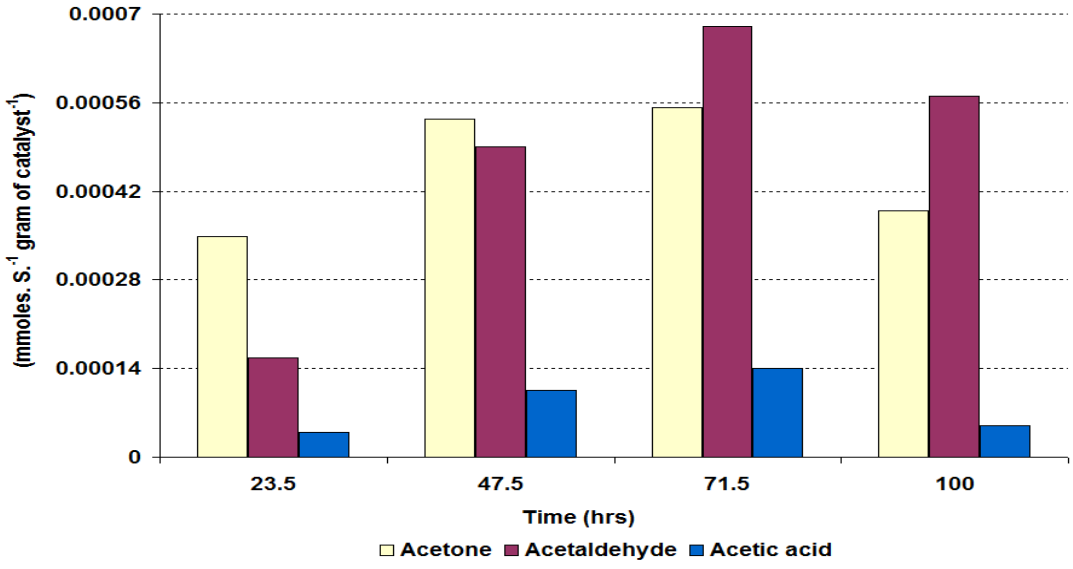

Figure 8.3-3 Rate of formation of liquid products over Al_2O_3 catalyst during the 1-propanol impurity reaction

The product distributions of all the gaseous products were similar (Figure 8.3-2) to those observed for the pure ethanol reaction at 500°C. However, the rate of formation of H_2 was increased whilst the rate of formation of CH_4 decreased. Similarly, the rate of formation of CO and CO_2 were slightly increased and decreased respectively in the 1-propanol impurity reaction. The rate of formation of C_2H_4 significantly increased compared to the pure ethanol reaction.

The rate of formation of the liquid products shown in Figure 8.3-3 illustrates some interesting results. The initial rate of formation of acetone exceeded that of acetaldehyde although after 72 hours the acetaldehyde formation overtook that of all the liquid products. Also a small amount of acetic acid was produced.

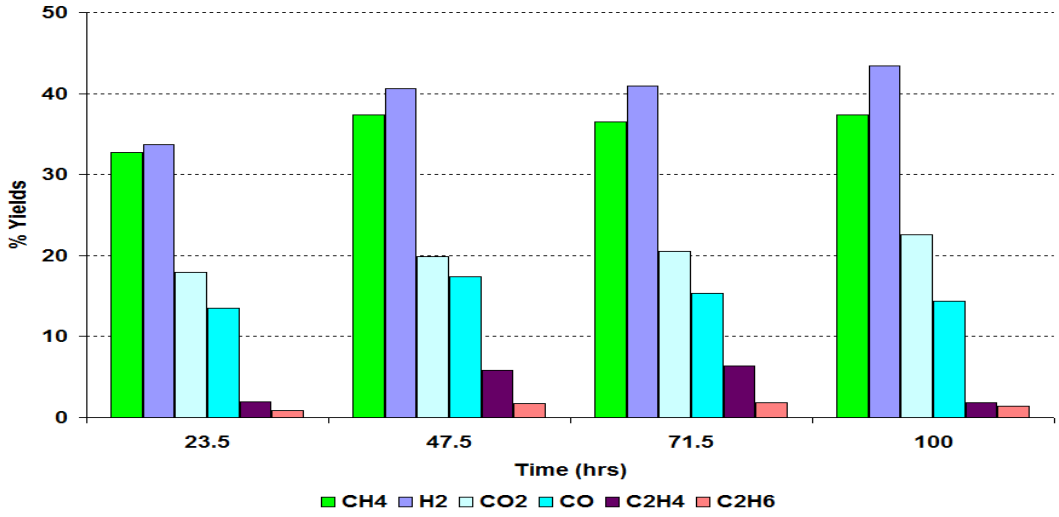

Figure 8.3-4 % Yield of gaseous products over Al_2O_3 catalyst during the 1-propanol impurity reaction

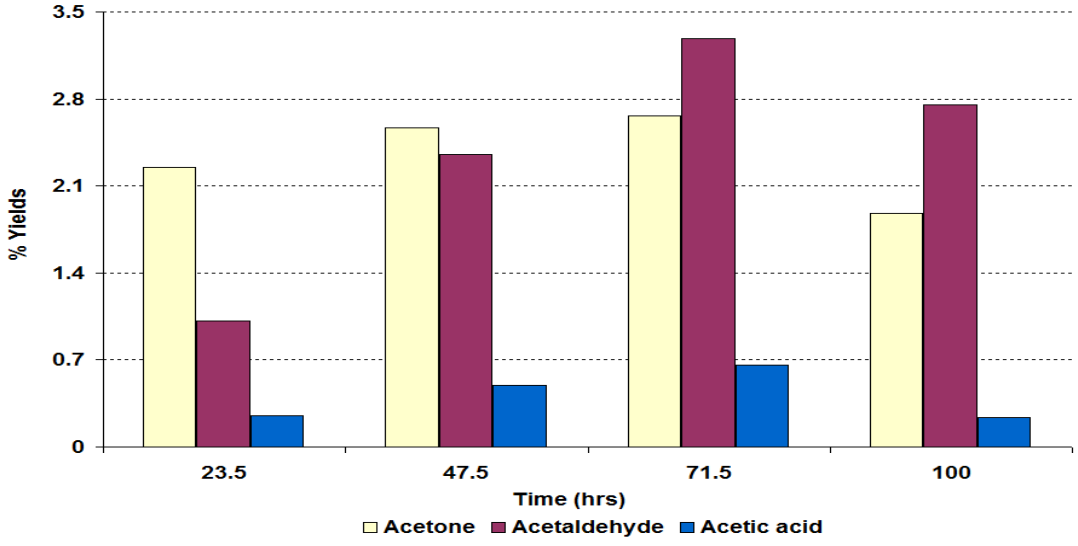

Figure 8.3-5 % Yield of liquid products over Al_2O_3 catalyst during the 1-propanol impurity reaction

The yields of the gaseous products presented in Figure 8.3-4 show similar patterns to those observed for the pure ethanol reaction at 500°C. The yields of H_2, CO and C_2H_4 were slightly increased, and the yields of CO_2 and CH_4 were decreased with respect to the gaseous products in the pure ethanol reaction as shown in Figure 8.3-4.

Figure 8.3-5 illustrates that in the 1-propanol impurity reaction, the yields of the liquid products significantly increased compared to the pure ethanol reaction. Among the various liquid products acetaldehyde gave the highest yield (~ 3%). Also observed were trace amounts of methanol in the 1-propanol impurity reaction.

8.3.1.2 Post reaction characterisation

The post reaction characterisation was performed on the spent catalyst to determine the cause of deactivation of the catalyst.

8.3.1.2.1 TPO

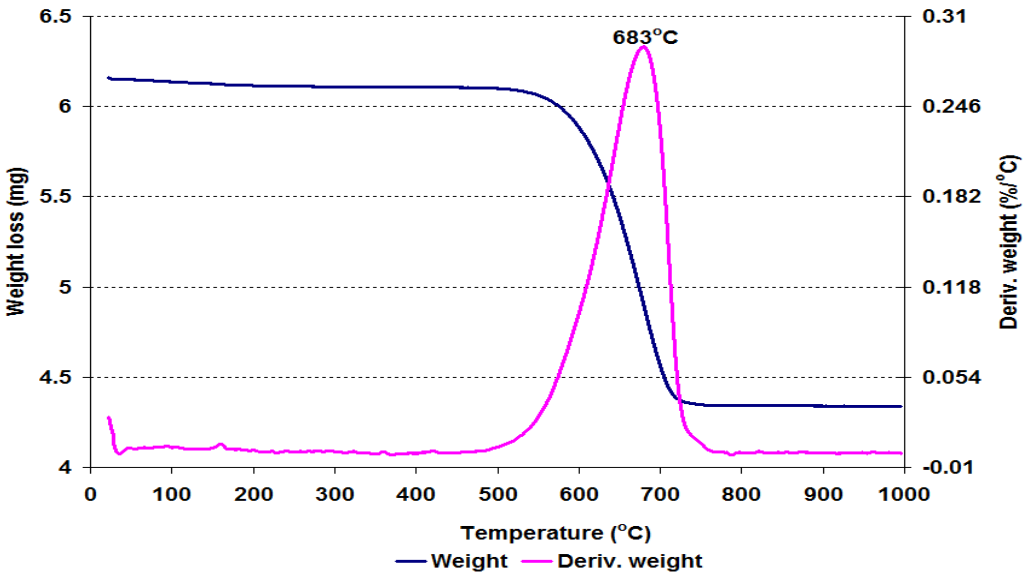

Figure 8.3-6 Post reaction TPO over Al_2O_3 catalyst following the 1-propanol impurity reaction

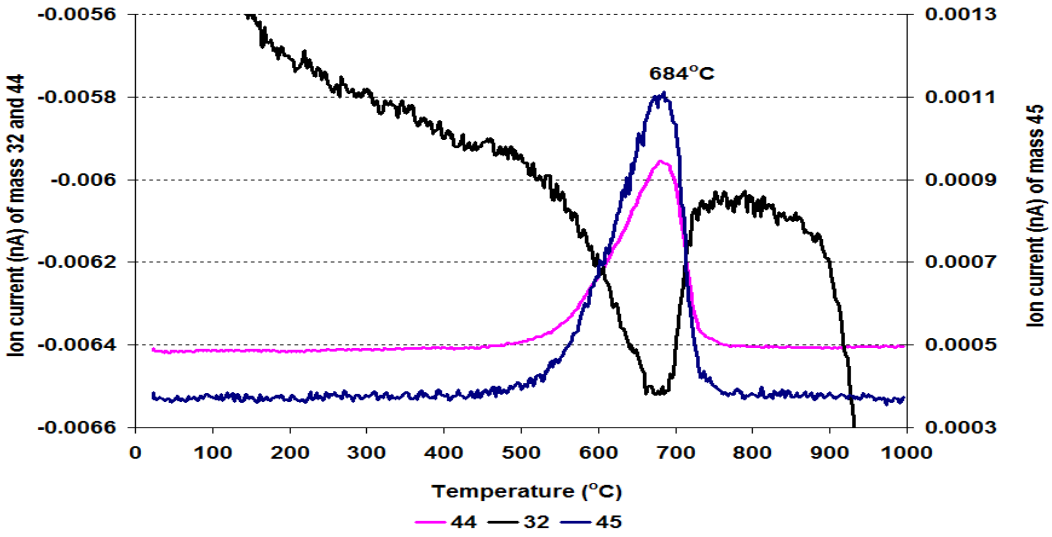

Figure 8.3-7 MS data of CO_2 (m/z=44), O_2 (m/z=32) and C_2H_5OH fragment (m/z=45) for Al_2O_3 catalyst following the 1-propanol impurity reaction

The spent catalyst was run on a TGA/DSC connected to a mass spectrometer in an oxygen atmosphere and the results obtained were plotted versus temperature and are shown in Figures 8.3-6 to 8.3-7. The TGA results indicate that 296.0 mg g^{-1} of material was carbonaceous materials that had been deposited on the surface of the catalyst. The main weight loss events occurred in the 500°C to 800°C region, which coincides with the evolution of CO_2 and principal mass fragment of C_2H_5OH in the mass spectrometry data (Figure 8.3-7).

8.3.1.2.2 Raman analysis

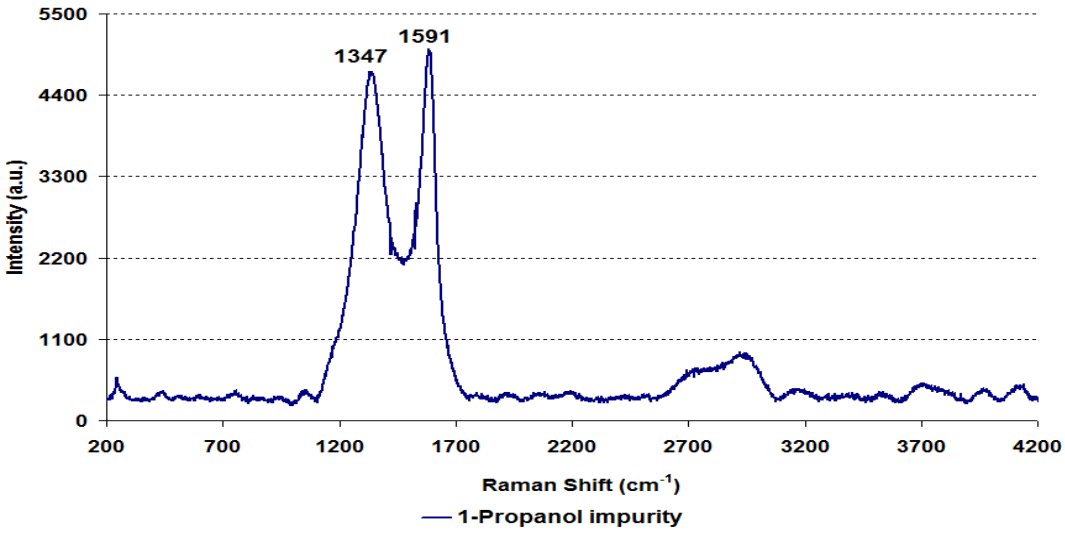

Figure 8.3-8 Post reaction Raman spectrum for Al_2O_3 catalyst following the 1-propanol impurity reaction

Figure 8.3-8 illustrates the Raman spectrum of spent catalyst from the 1-propanol impurity reaction on alumina catalyst. In contrast to the pure ethanol reaction in the post reaction 1-propanol impurity catalyst all the particles gave one pattern with the characteristic bands of graphitic carbon.

8.3.1.2.3 BET analysis

Catalyst	Conditions	BET Surface area (m^2/g)	Pore volume (cm^3/g)	Average pore diameter (Å)
Al_2O_3	Pure ethanol (500°C)	80	0.40 (± 0.45)	202 (± 3.97)
	1-Propanol impurity	54	0.14 (± 4.72)	107 (± 5.83)

Table 8.3-1 BET analysis of post reaction Al_2O_3 catalyst following the 1-propanol impurity reaction

Table 8.3-1 shows that there is a large decrease in the BET surface area, the average pore diameter and the pore volume observed in 1-propanol impurity reaction compared to pure ethanol reaction catalyst.

8.3.1.3 Propylamine impurity

Nitrogenated bases are present in raw ethanol in quantities in the range of 1.2 vol.%. A reaction to investigate the influence of nitrogen representative group on an ethanol steam reforming reaction over an Al_2O_3 was carried out by adding 1molar % propylamine with respect to ethanol in the water/ethanol mixture.

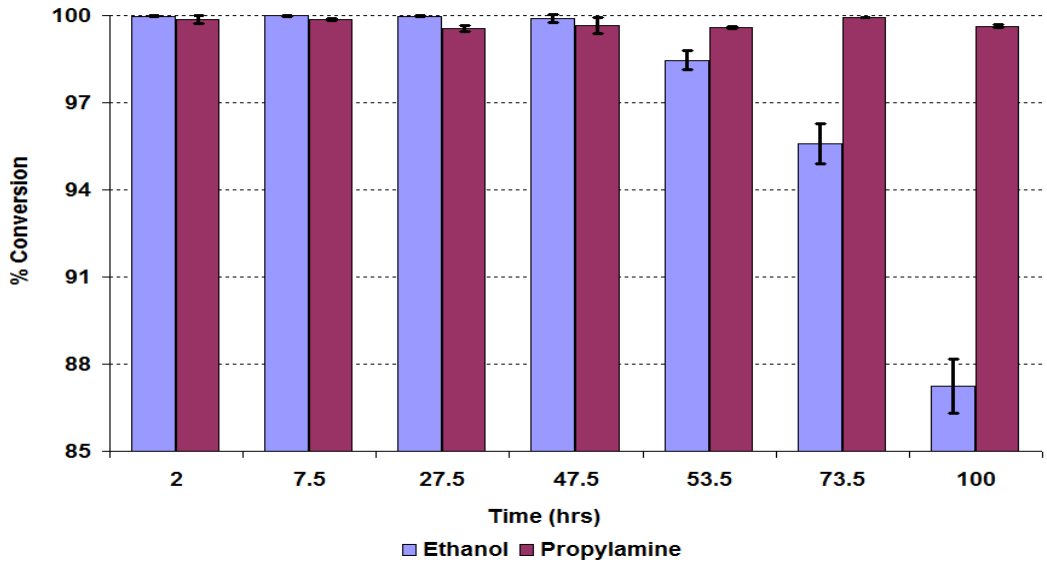

Figure 8.3-9 % Conversion of ethanol and propylamine over the Al_2O_3 catalyst during the propylamine impurity reaction

The propylamine impurity reaction has a similar influence on the conversion of ethanol in the initial 48 hours as that observed with the 1-propanol impurity reaction. However after 47.5 hours time on stream a significant deactivation of the catalyst took place. The conversion of ethanol decreased and gave 87% conversion at the end of reaction. The propylamine present in the reactants gave 99.7 % conversion and up to the end of the reaction no significant change in its conversion was observed.

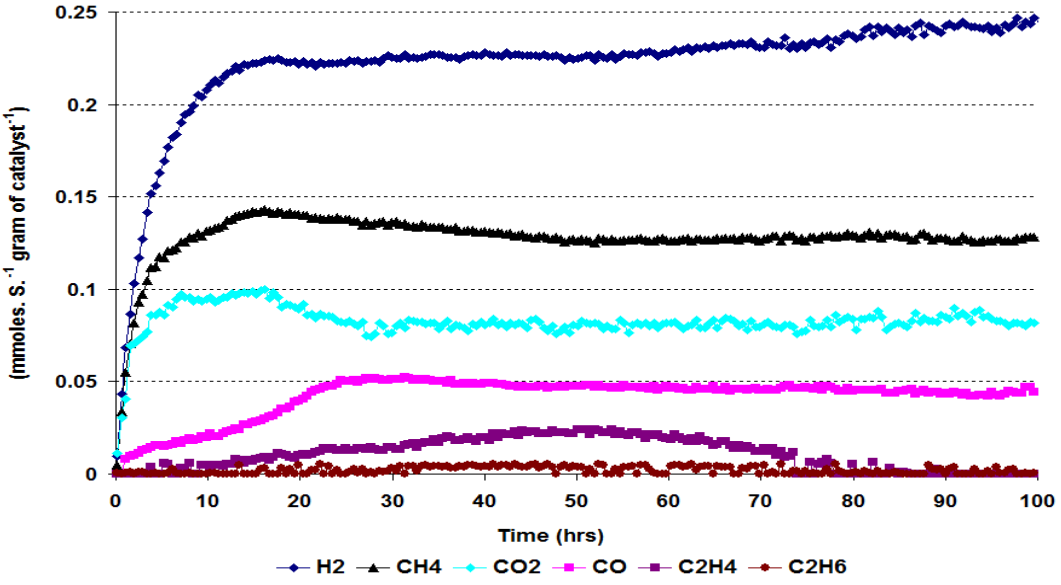

Figure 8.3-10 Rate of formation of gaseous products over Al_2O_3 catalyst during the propylamine impurity reaction

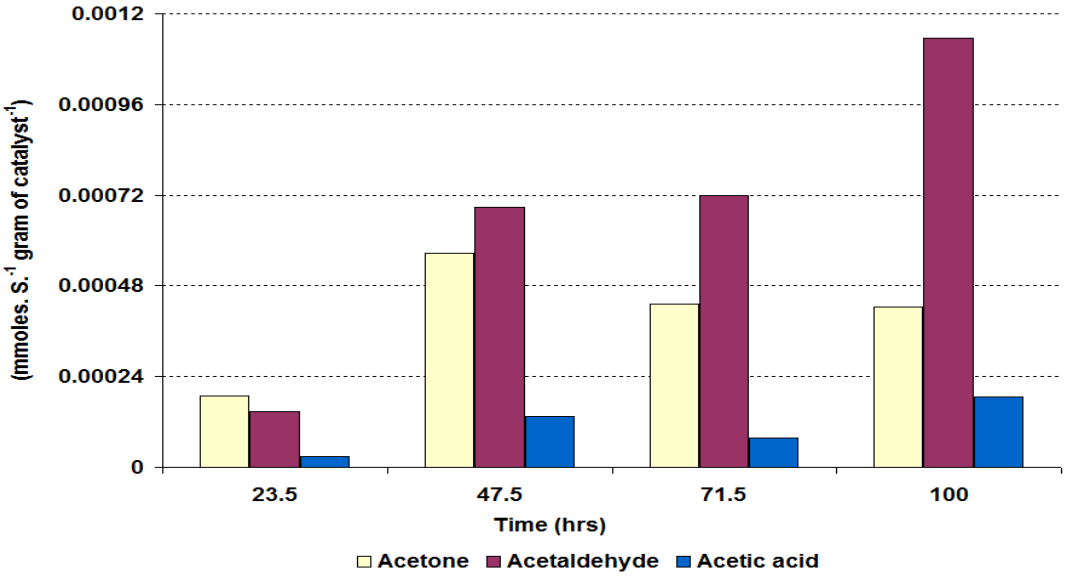

Figure 8.3-11 Rate of formation of liquid products over Al_2O_3 catalyst during the propylamine impurity reaction

The reaction profile of the gaseous products gave the same main products as those observed in the 1-propanol impurity reaction over the Al_2O_3 catalyst although the rates observed slightly were different (Figure 8.3-10). In the initial 24 hours the rates of formation of the main gaseous products varied considerably. However following the initial non steady state, the rates achieved steady state condition except for H_2 which steadily increased until the end of the reaction. Small amounts of C_2H_4 and C_2H_6 were produced which disappeared after 80 hours time on stream from the reaction profile.

In the liquid products, the rates were similar to those observed in earlier reactions, although acetone was produced at a higher rate in the initial 24 hours. Its rate steadily decreased over time whilst the rate of formation of acetaldehyde increased throughout the reaction.

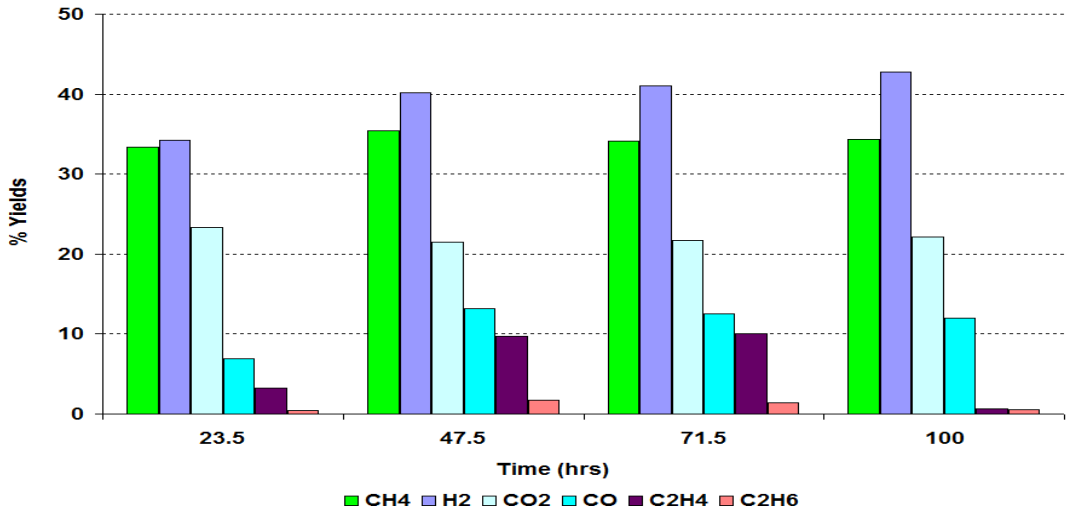

Figure 8.3-12 % Yield of gaseous products over Al_2O_3 catalyst during the propylamine impurity reaction

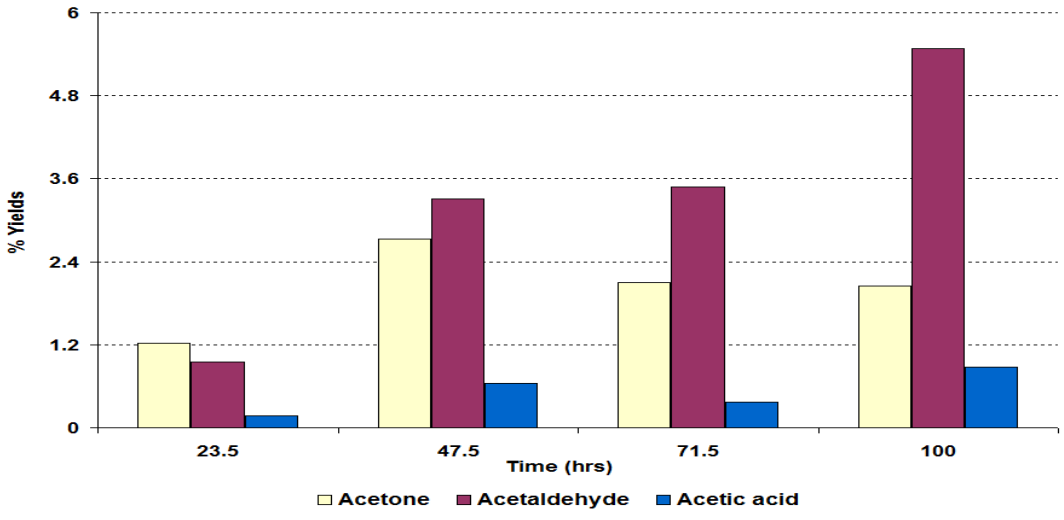

Figure 8.3-13 % Yield of liquid products over Al_2O_3 catalyst during the propylamine impurity reaction

Figure 8.3-12 shows the yields of the gaseous products. Similar to the 1-propanol impurity reaction, H_2, CH_4 and CO_2 gave higher yields in the gaseous products which steadily decreased with passage of time except for H_2 which increased.

8.3.1.4 Post reaction characterisation

8.3.1.4.1 TPO

The TPO results for spent Al_2O_3 catalyst from the propylamine impurity reaction were obtained and are plotted in Figure 8.3-14.

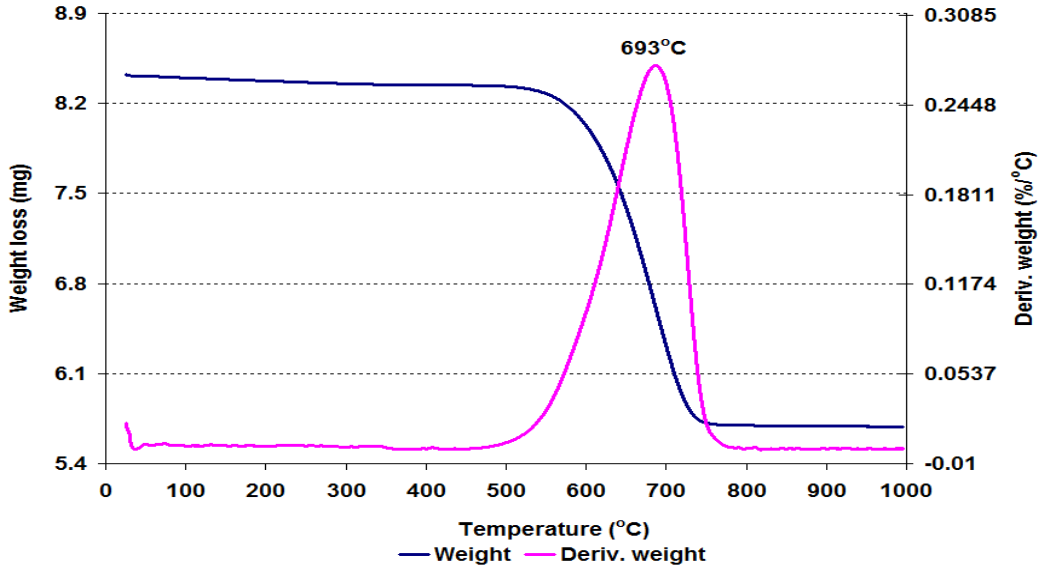

Figure 8.3-14 Post reaction TPO for Al_2O_3 catalyst following the propylamine impurity reaction

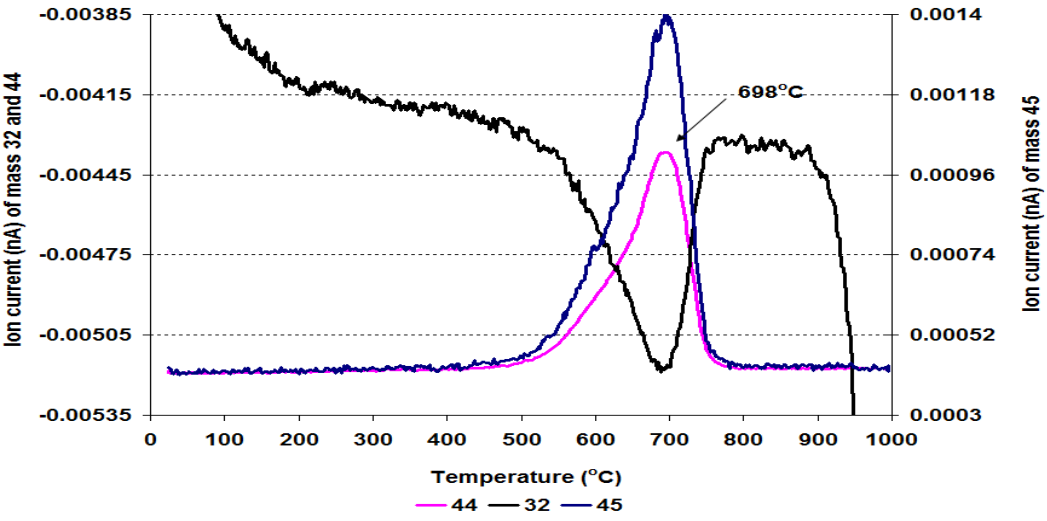

Figure 8.3-15 MS data of CO_2 (m/z=44), O_2 (m/z=32) and C_2H_5OH fragment (m/z=45) for Al_2O_3 catalyst following the propylamine impurity reaction

The derivative weight profile for the TPO shown in Figure 8.3-14 illustrates that the main weight loss event took place around 693^{o}C. This weight loss corresponded to CO_2, and ethanol fragment and trace amount of H_2O evolution in the mass spectrometry results. In addition there was a small weight loss below 100^{o}C which appeared to correspond to water evolution in the mass spectrometry data. The TGA profile demonstrates that a total of 325 mg g^{-1} of weight change occurred in the temperature ramp up to 1000^{o}C.

8.3.1.4.2 Raman analysis

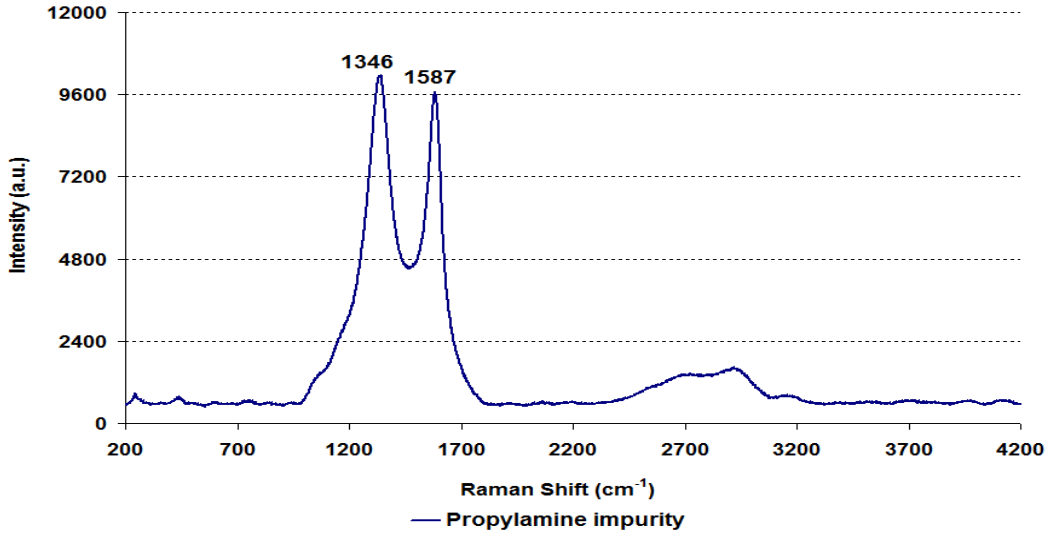

Figure 8.3-16 Post reaction Raman spectrum for Al_2O_3 catalyst following the propylamine impurity reaction

The spent Al_2O_3 catalyst for the propylamine impurity was analysed by the Raman spectroscopy. The above figure (Figure 8.3-16) shows characteristic peaks for graphitic carbon as seen in the 1-propanol impurity catalyst. Although, compared to the pure ethanol post reaction catalyst, the lower wave number peak shifted to a small extent upwards while the higher wave number peak shifted downwards.

8.3.1.4.3 BET analysis

Catalyst	Conditions	BET Surface area (m^2/g)	Pore volume (cm^3/g)	Average pore diameter (Å)
Al_2O_3	Pure ethanol (500^{o}C)	80	0.40 (± 0.45)	202 (± 3.97)
	Propylamine impurity	52	0.12 (± 0.90)	90 (± 4.93)

Table 8.3-2 BET analysis of post reaction Al_2O_3 catalyst following the propylamine impurity reaction

BET analysis (Table 8.3-2) of the post propylamine impurity catalyst showed that the BET surface area, the average pore diameter and the pore volume significantly decreased compared to pure ethanol reaction catalyst.

8.3.2 Ru/Al_2O_3

After examining the influence of 1-propanol and propylamine impurities on the ethanol steam reforming reaction over an Al_2O_3 catalyst, the effect of five different impurities were individually investigated over Ru/Al_2O_3 catalyst using the same conditions as for the Al_2O_3 support.

8.3.2.1 1-Propanol impurity

The efficiency of the steam reforming of ethanol reaction either increased or decreased depending on the nature of the impurity added to pure ethanol reactant. 1-Propanol was among those impurities which decreased the conversion of ethanol as reported by [120]. So initially, the 1-propanol impurity was tested to assess its effect over the Ru/Al_2O_3 catalyst.

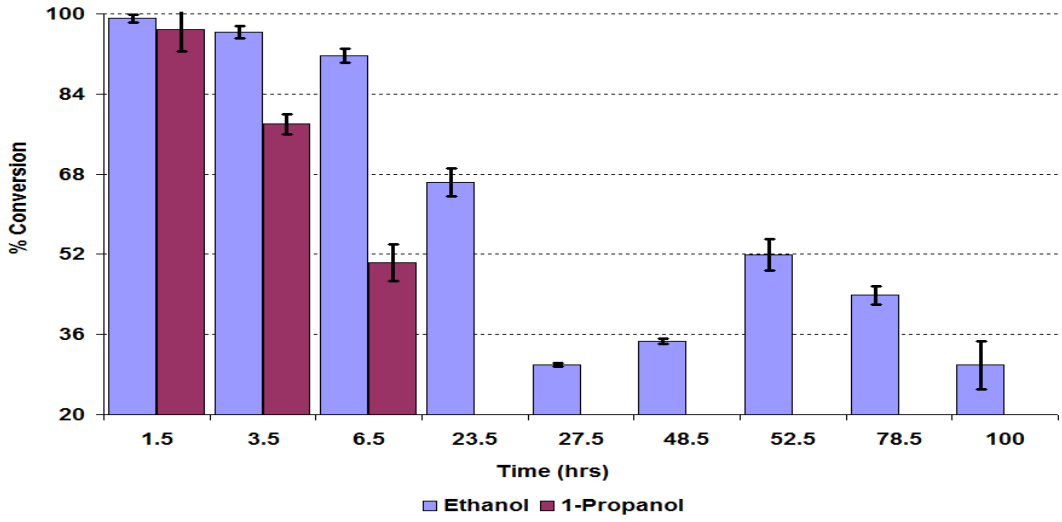

Figure 8.3-17 % Conversion of ethanol and 1-propanol over Ru/Al_2O_3 catalyst during the 1-propanol impurity reaction

Figure 8.3-17 shows that in the initial 27 hours time on stream a swift decrease in the ethanol conversion took place over the Ru/Al_2O_3 catalyst and the conversion reduced to 30%. However after 27 hours a slight increase occurred although after 100 hours TOS it reduced to the same minimum value as was seen at 27 hours TOS. On the other hand the conversion of 1-propanol decreased to 50% in the initial 6.5 hours time on stream. However after 24 hours no conversion of 1-propanol was observed.

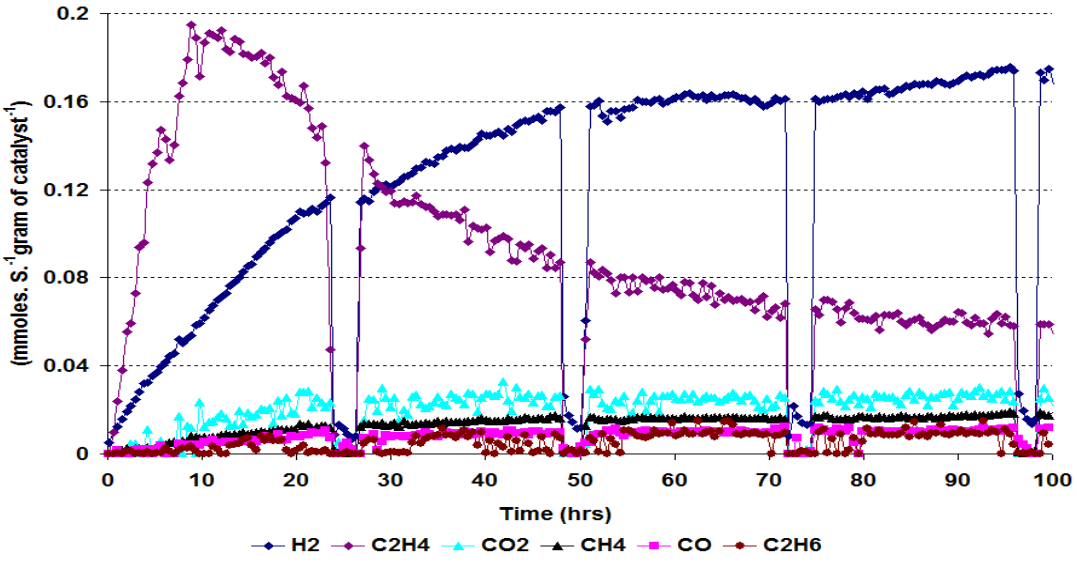

Figure 8.3-18 Rate of formation of gaseous products over Ru/Al_2O_3 catalyst during the 1-propanol impurity reaction

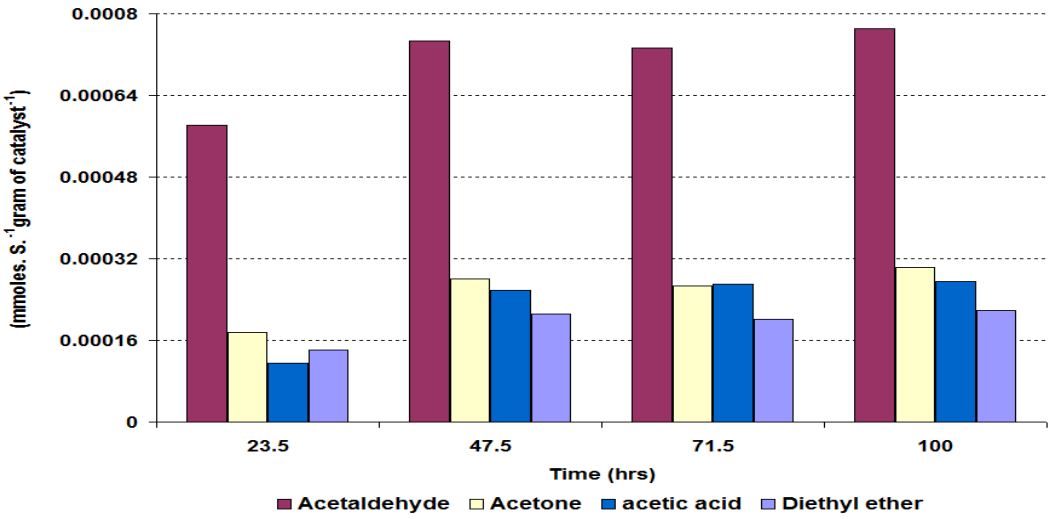

Figure 8.3-19 Rate of formation of liquid products over Ru/Al_2O_3 catalyst during the 1-propanol impurity reaction

The different gaseous products produced in the steam reforming of ethanol using 1-propanol impurity showed interesting results. In the initial 24 hours, the rates of formation of all the products showed similar patterns to those observed for the steam reforming of pure ethanol over Ru/Al_2O_3 catalyst as discussed in section 8.2.2-1. However, after 24 hours, a quick decrease in the rate of formation of C_2H_4 was observed whilst the rate of formation of H_2 continuously increased. None of the major products *i.e.* H_2 and C_2H_4 achieved steady state conditions up to the end of the reaction. The rates of formation of CH_4 and CO_2 were slightly decreased compared to the pure ethanol steam reforming reaction over Ru/Al_2O_3 catalyst although they achieved steady state conditions after 34

hours time on stream. In the liquid products acetaldehyde was the major product and obtained virtually steady state conditions after 48 hours time on stream. The other liquid products followed similar patterns to those of acetaldehyde, although their rates of formation were lower than that of acetaldehyde.

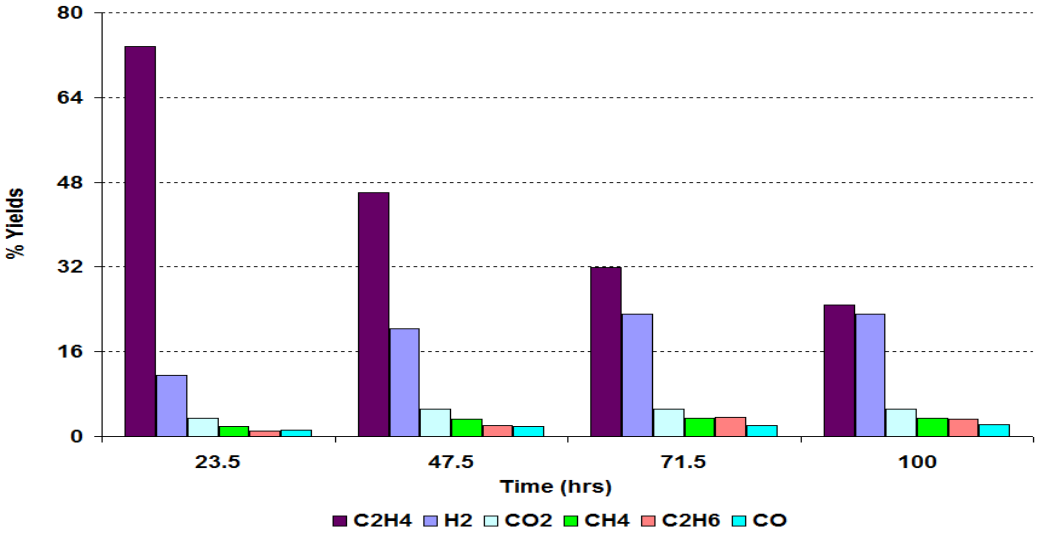

Figure 8.3-20 % Yield of gaseous products over Ru/Al_2O_3 catalyst during the 1-propanol impurity reaction

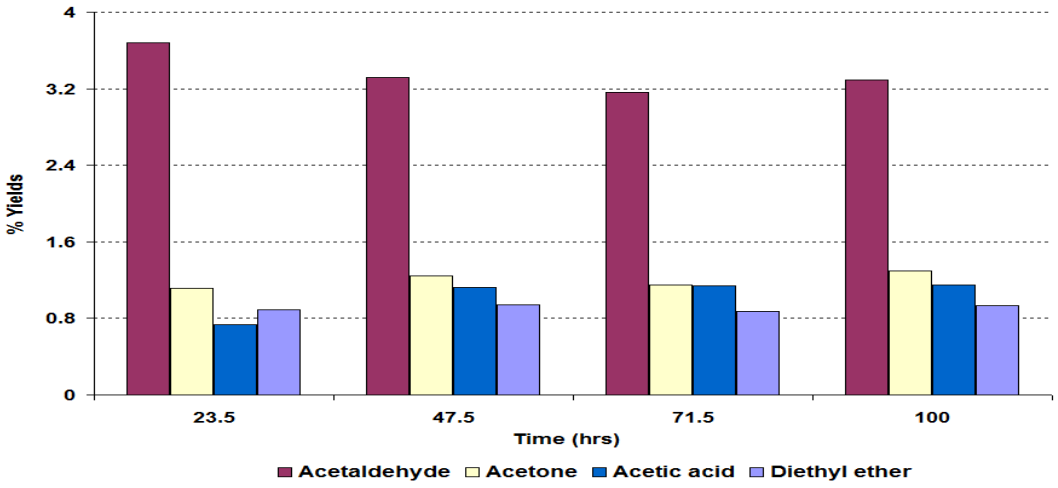

Figure 8.3-21 % Yield of liquid products over Ru/Al_2O_3 catalyst during the 1-propanol impurity reaction

The yields of all gaseous products produced during the 1-propanol impurity reaction on Ru/Al_2O_3 catalyst are shown in Figure 8.3-20. C_2H_4 was produced with the highest yield in the gaseous products with a maximum value of 74%. However, its yield quickly decreased and by the end of the reaction the yield had decreased to 25%. The yield of H_2 formation levelled off to a value of 23%. This value is slightly higher from that of obtained for the

pure ethanol reaction over Ru/Al_2O_3 catalyst. The yields of other gaseous products were small. All the liquid products gave low yields. Among these low yields acetaldehyde produced the highest yield which was ~ 3.7%.

8.3.2.2 Post reaction characterisation

8.3.2.2.1 TPO

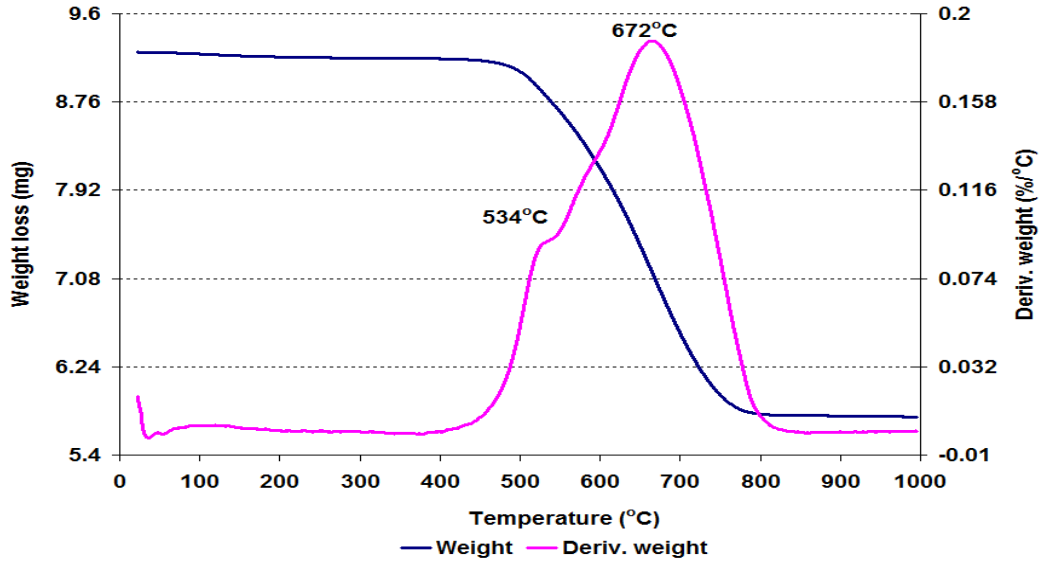

Figure 8.3-22 Post reaction TPO for Ru/Al_2O_3 catalyst following the 1-propanol impurity reaction

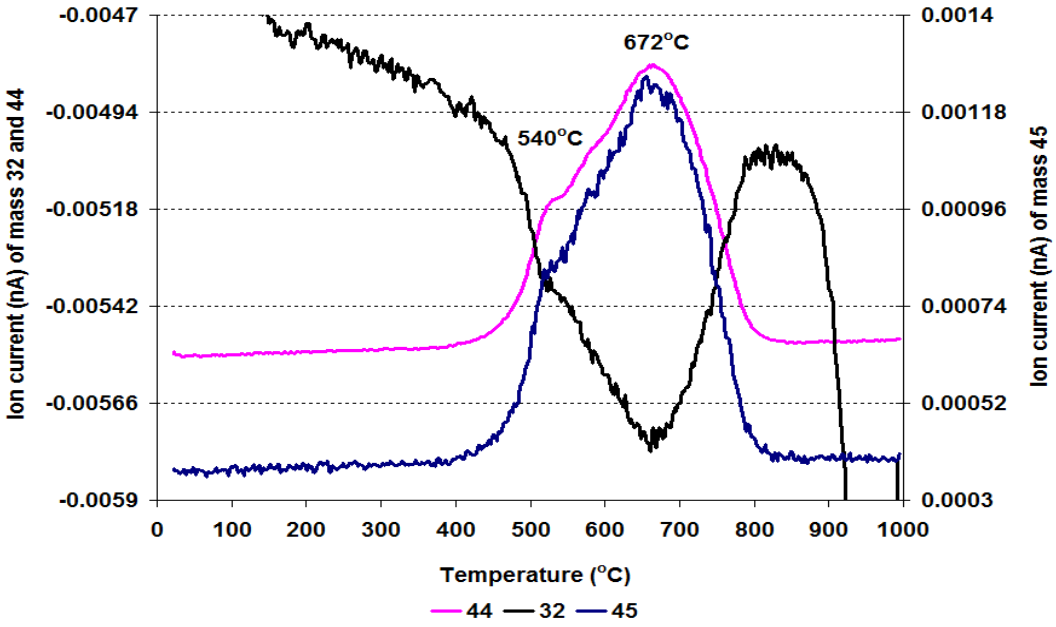

Figure 8.3-23 MS data of CO_2 (m/z=44), O_2 (m/z=32) and C_2H_5OH fragment (m/z=45) for Ru/Al_2O_3 catalyst following the 1-propanol impurity reaction

The TGA profile shown in Figure 8.3-22 for the post Ru/Al_2O_3 catalyst illustrates that the main weight loss event occurred at 672^oC. A shoulder at 534^oC was also present in the derivative weight profile. A total of 376.0 mg g^{-1} weight loss was observed in the temperature range up to 1000^oC in the TGA data. The weight loss corresponded to desorption of CO_2, H_2O and ethanol fragment (m/z = 45) in the mass spectrometric profiles. The TGA results gave similar profiles to those for the pure ethanol spent Ru/Al_2O_3 sample, although the post reaction 1-propanol impurity catalyst gave slightly less carbonaceous deposition. Raman analysis gave similar results to those seen in the post pure ethanol reaction catalyst.

8.3.2.2.2 BET analysis

Catalyst	Conditions	BET Surface area (m^2/g)	Pore volume (cm^3/g)	Average pore diameter (Å)
Ru/Al_2O_3	Pure ethanol (500^oC)	32	0.07 (± 2.17)	78 (± 6.57)
	1-Propanol impurity	36	0.07 (± 0.98)	80 (± 8.95)

Table 8.3-3 BET analysis of post reaction Ru/Al_2O_3 catalyst following the 1-propanol impurity reaction

BET results (Table 8.3-3) suggest that no significant change was observed in the BET surface area, the average pore diameter and the pore volume compared to post reaction pure ethanol steam reforming catalyst.

8.3.2.3 Isopropyl alcohol (IPA) impurity

IPA is present in both raw and synthetic ethanol and is difficult to separate by simple distillation methods. Synthetic and raw rectified ethanol contains 0.001–0.05 and 0.0002–0.0007 vol.% of IPA respectively. So, 1mol.% IPA with respect to pure ethanol was added to water/ethanol mixture reactants to investigate its effect on ethanol conversion and also on the different product distributions during the steam reforming reaction of ethanol using Ru/Al_2O_3 catalyst.

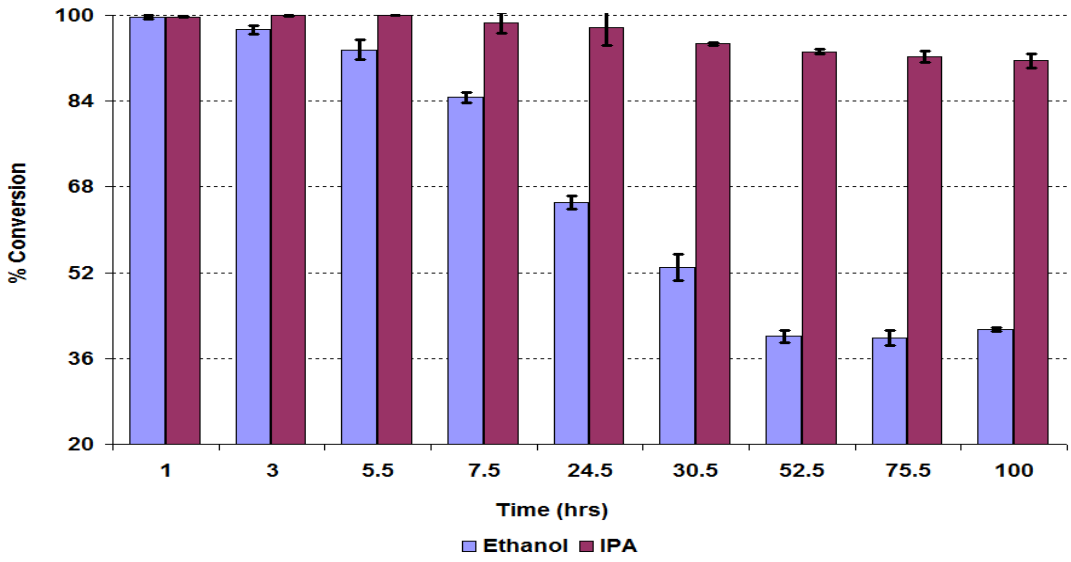

Figure 8.3-24 % Conversion of ethanol and IPA over Ru/Al_2O_3 catalyst during the IPA impurity reaction

The IPA impurity had similar effects on the conversion of ethanol during the steam reforming reaction as was noticed in the 1-propanol impurity reaction over the Ru/Al_2O_3. The figure reveals that initially the conversion of ethanol was almost 100% which steadily decreased with the reaction time and after 52.5 hours time on stream it reduced to 40%. After 52.5 hours time on stream the conversion of ethanol stabilised till the end of the reaction. Interestingly, the IPA impurity itself decomposed and gave a high conversion (99% to 91%) throughout the reaction.

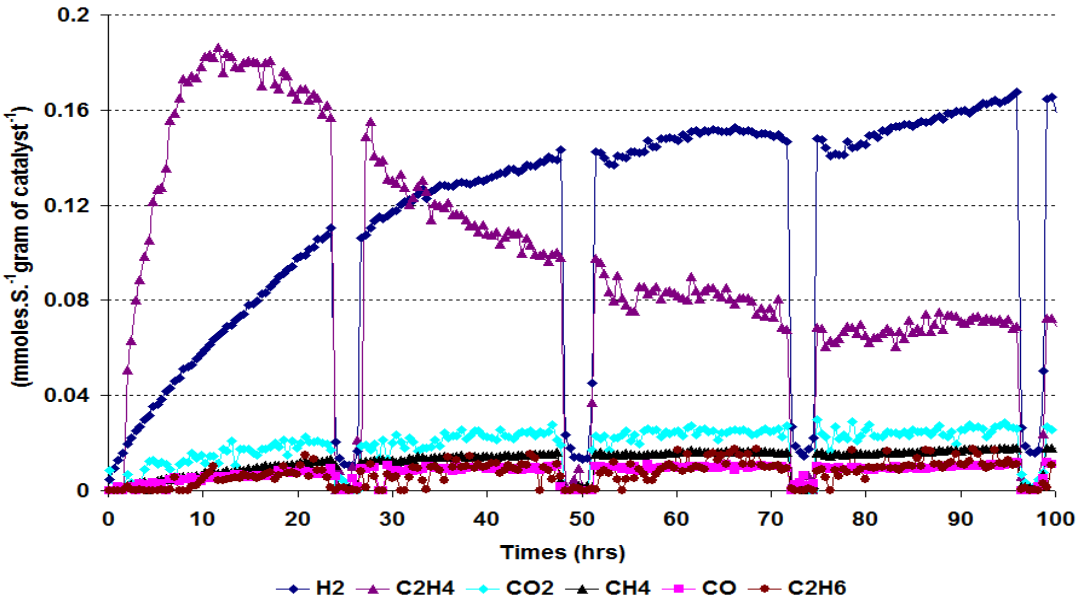

Figure 8.3-25 Rate of formation of gaseous products over Ru/Al_2O_3 catalyst during the IPA impurity reaction

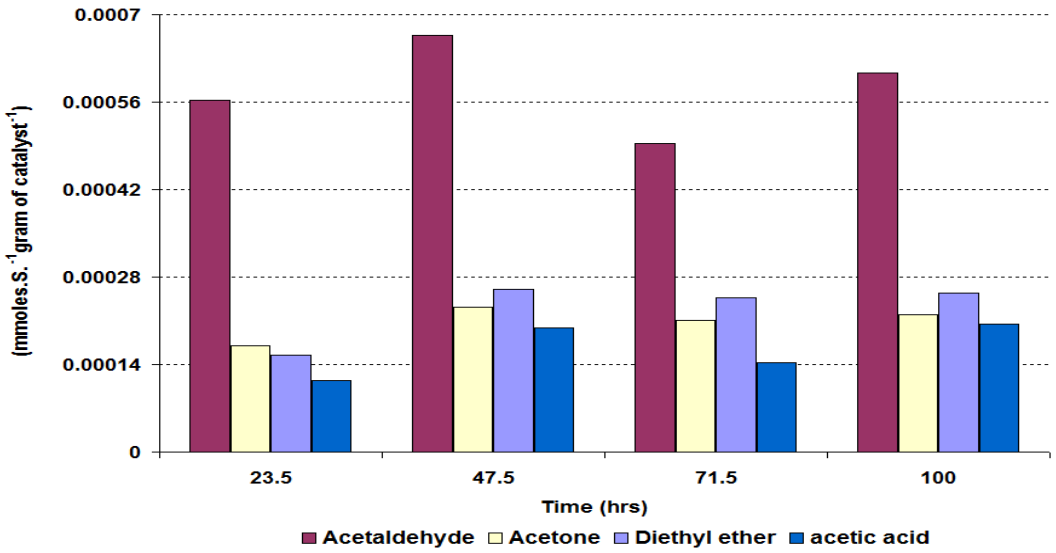

Figure 8.3-26 Rate of formation of liquid products over Ru/Al_2O_3 catalyst during the IPA impurity reaction

The rates of formation of the gaseous products followed similar patterns to those observed for the 1-propanol impurity reaction. In the initial 24 hours, the C_2H_4 rate abruptly increased and obtained the maximum value in 11 hours and then steadily decreased until the end of the reaction. The rate of formation of H_2 in the IPA impurity reaction was slightly lower compared to both the pure ethanol and 1-propanol impurity reactions. Other gaseous products as shown in Figure 8.3-25, were produced with lower rates and obtained steady state conditions after 24 hour time on stream.

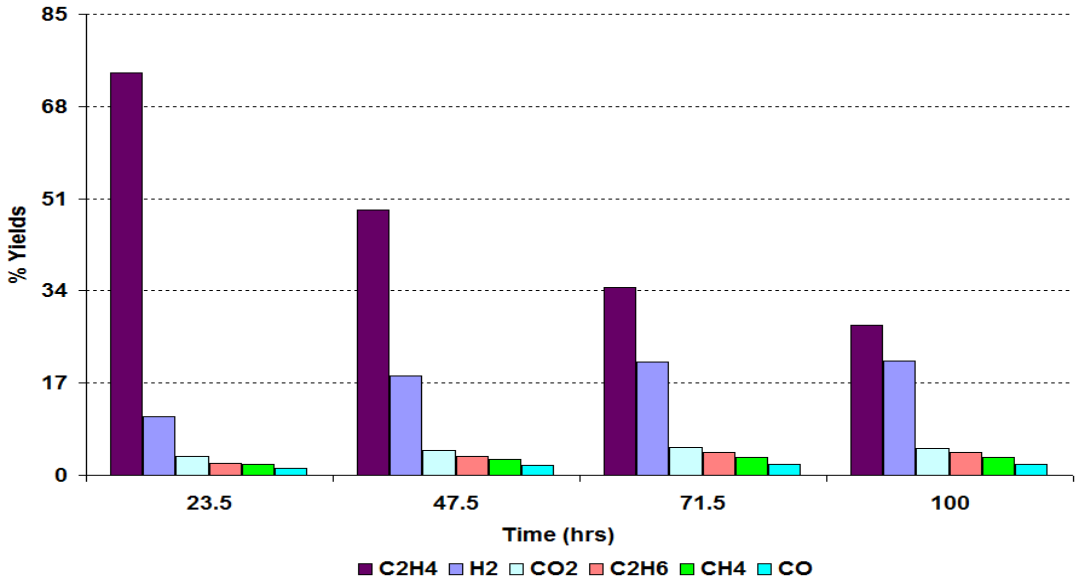

Figure 8.3-27 % Yield of gaseous products over Ru/Al_2O_3 catalyst during the IPA impurity reaction

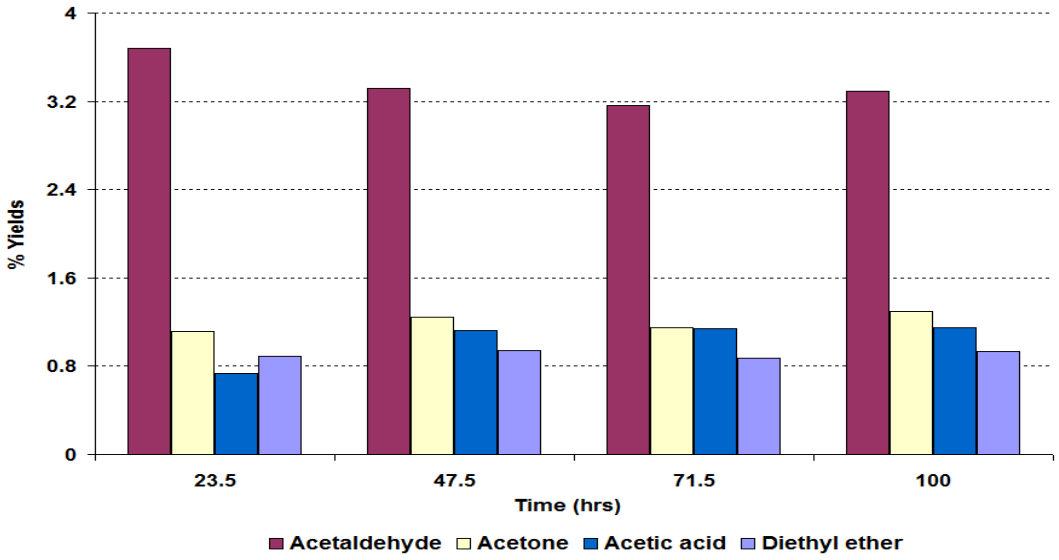

Figure 8.3-28 % Yield of liquid products over Ru/Al_2O_3 catalyst during the IPA impurity reaction

Figure 8.3-27 illustrates that during the ethanol steam reforming reaction with IPA impurity, C_2H_4 and H_2 were produced with the highest yields compared to other gaseous products on Ru/Al_2O_3 catalyst. The yields of C_2H_4 decreased with time on stream, whilst the yield of H_2 progressively increased. Other gaseous products were produced in small amounts with the maximum value obtained being 3% which was observed for CO_2.

In the liquid products, acetaldehyde gave the highest yield. However its yield varied throughout the reaction. Acetone, diethyl ether and acetic acid were the other liquid products produced during the reaction, although their yields were low. Trace amounts of 1,1-diethoxyethane, methanol, ethyl acetate and crotonaldehyde were also detected during reaction however they were not shown in Figure 8.3-28.

8.3.2.4 Post reaction characterisation

8.3.2.4.1 TPO

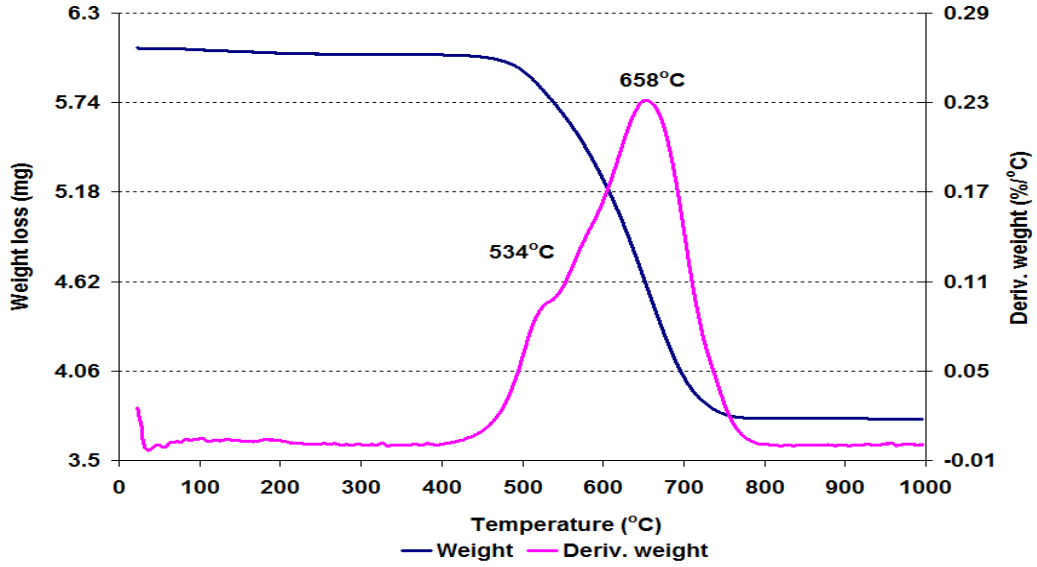

Figure 8.3-29 Post reaction TPO over Ru/Al_2O_3 catalyst following the IPA impurity reaction

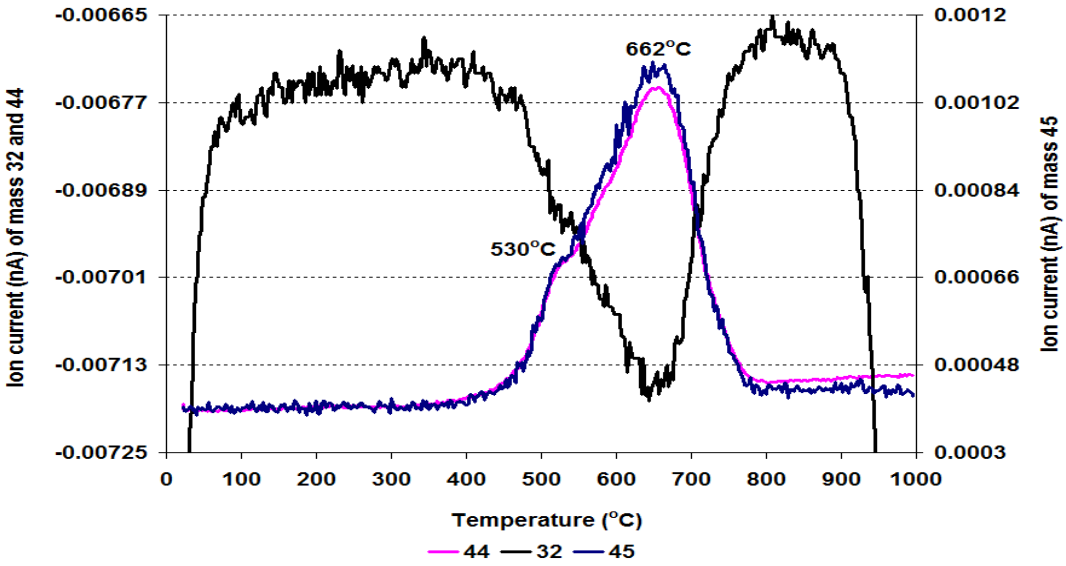

Figure 8.3-30 MS data of CO_2 (m/z=44), O_2 (m/z=32) and C_2H_5OH fragment (m/z=45) for Ru/Al_2O_3 catalyst following the IPA impurity reaction

The post reaction catalyst was run on the TGA/DSC connected to a mass spectrometer and the data obtained is plotted versus temperature and shown in Figures 8.3-29 to 8.3-30. Two weight loss events were observed which merged with each other between 425°C and 794°C. The total weight loss (382.2 mg g^{-1}) that occurred from the catalyst sample was almost similar to that seen in the 1-propanol impurity reaction. The mass profiles for both

impurity reactions were similar although no prominent peak for H_2O was seen in the IPA impurity catalyst.

8.3.2.4.2 Raman analysis

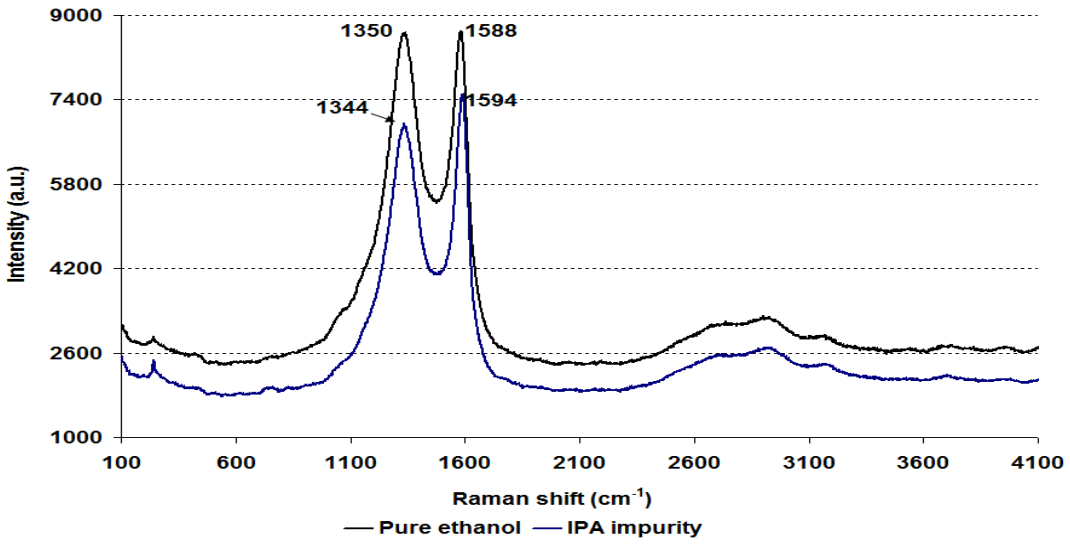

Figure 8.3-31 Post reaction Raman spectra for Ru/Al_2O_3 catalyst following the IPA impurity reaction

Figure 8.3-31 compares the Raman spectra for the post reaction Ru/Al_2O_3 catalysts used in the pure and IPA impurity ethanol steam reforming reaction, similar bands were observed for both samples. However, the low wavenumber band for the IPA impurity sample shifted slightly downward whilst the upper wavenumber band shifted upwards with respect to pure ethanol steam reforming reaction sample.

8.3.2.4.3 BET analysis

Catalyst	Conditions	BET Surface area (m^2/g)	Pore volume (cm^3/g)	Average pore diameter (Å)
Ru/Al_2O_3	Pure ethanol (500°C)	32	0.07 (± 2.17)	78 (± 6.57)
	IPA impurity	38	0.07 (± 0.67)	84 (± 6.01)

Table 8.3-4 BET analysis of post reaction Ru/Al_2O_3 catalyst following the IPA impurity reaction

BET analysis illustrated that the spent Ru/Al_2O_3 catalysts in both IPA impurity and pure ethanol reactions gave similar values for the pore volume. The BET surface area and the average pore diameter showed a slight increase for IPA impurity when compared to the spent Ru/Al_2O_3 catalyst from the pure ethanol steam reforming reaction.

8.3.2.5 Propanal impurity

After investigation of the influence of different C_3 alcohols, the investigation moved to the effect of C_3 aldehyde impurity in the steam reforming reaction of ethanol. Aldehydes are present in different carbohydrate molecules and their fragmentation produces different type of aldehydes. The raw ethanol contains 0.013 vol.% aldehyde.

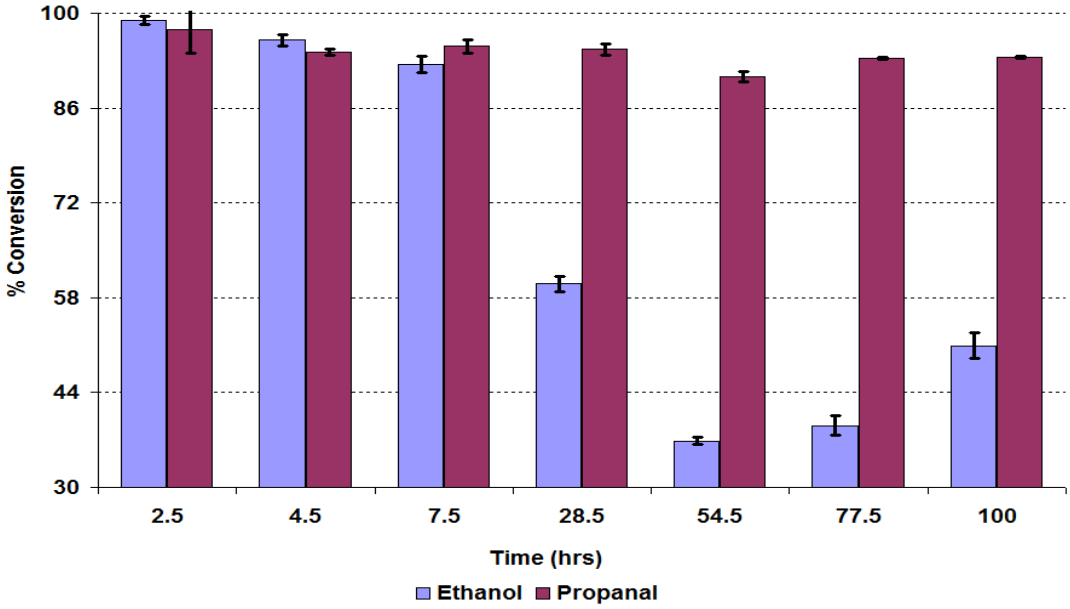

Figure 8.3-32 % Conversion of ethanol and propanal over Ru/Al_2O_3 catalyst during the propanal impurity reaction

When the steam reforming of ethanol reaction was carried out over Ru/Al_2O_3 catalyst using a propanal impurity, the change in the conversion took place in 2 steps, in the initial 7.5 hours the decrease in the conversion was insignificant whilst after 7.5 hours a big decrease in the conversion took place and it reduced to 36% until to the 54.5 hours time on stream. As with the 1-propanal impurity a small increase in the conversion was observed after decrease. This suggests that propanal had similar effects on catalyst deactivation to that shown by the 1-propanol impurity.

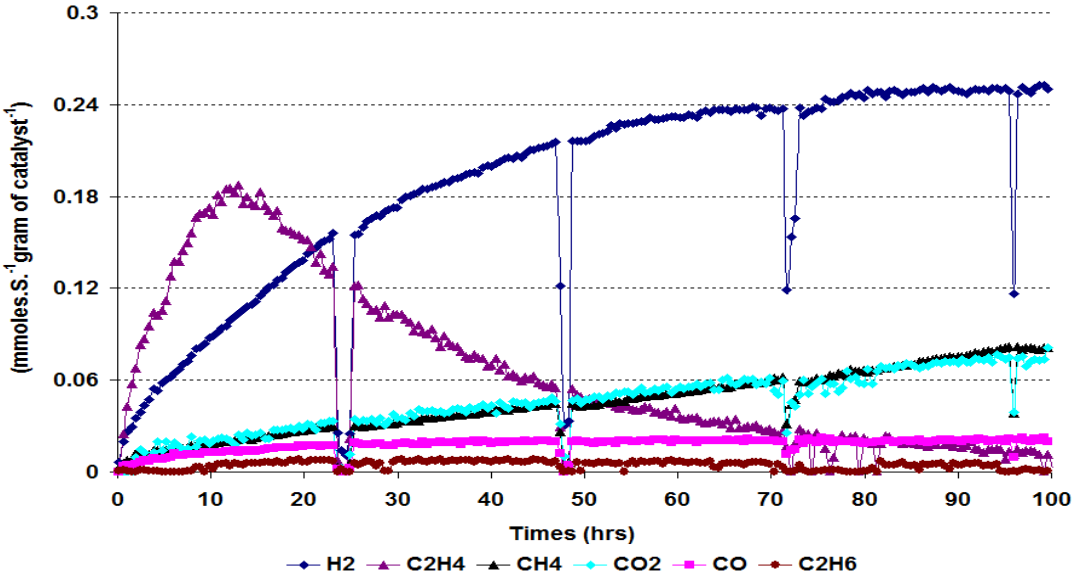

Figure 8.3-33 Rate of formation of gaseous products over Ru/Al_2O_3 catalyst during the propanal impurity reaction

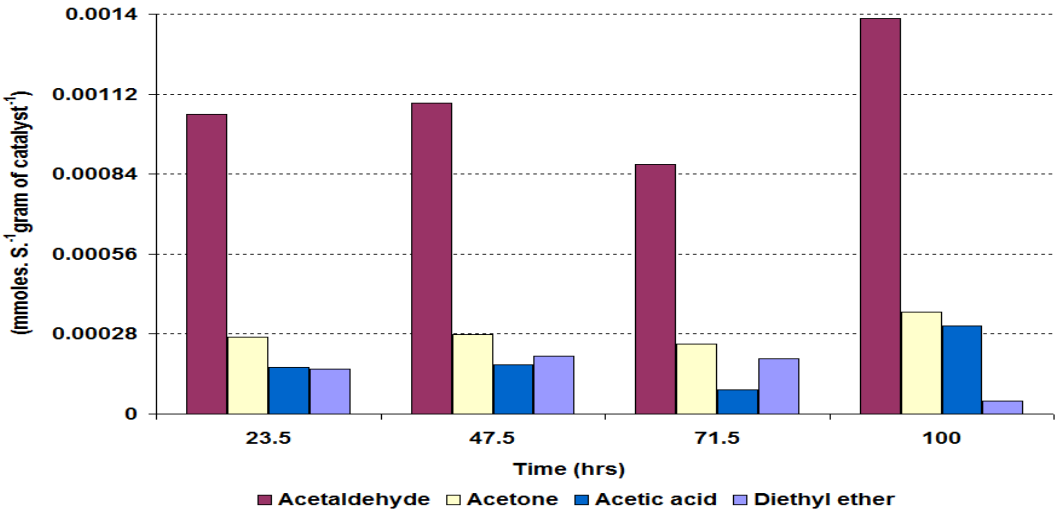

Figure 8.3-34 Rate of formation of liquid products over Ru/Al_2O_3 catalyst during the propanal impurity reaction

Figure 8.3-33 illustrates the distribution of the gaseous products from the ethanol steam reforming reaction at 500^{o}C using a propanal impurity. The rate of formation of C_2H_4 followed a similar pattern to that obtained for other reactions over the Ru/Al_2O_3 catalyst. Interestingly, a similar value for the maximum rate of formation for C_2H_4 was obtained in propanal impurity reaction as was acquired in the IPA and 1-propanol impurity reaction although the maximum value was obtained at different TOS. In contrast to other impurities, the rate of formation of C_2H_4 decreased steadily throughout the reaction and reached almost zero by the end of reaction. Whereas, the rate of formation of H_2 continuously increased and obtained steady state conditions after 72 hours TOS.

Interestingly, the rate of formation for CO_2 and CH_4, which were produced in minor amounts, progressively increased throughout the reaction. Also small amounts of CO and C_2H_6 were observed.

The rate of formation of all the liquid products presented in Figure 8.3-34, fluctuated throughout the reaction, and like the IPA impurity reaction acetaldehyde was produced at the highest rate in the liquid products.

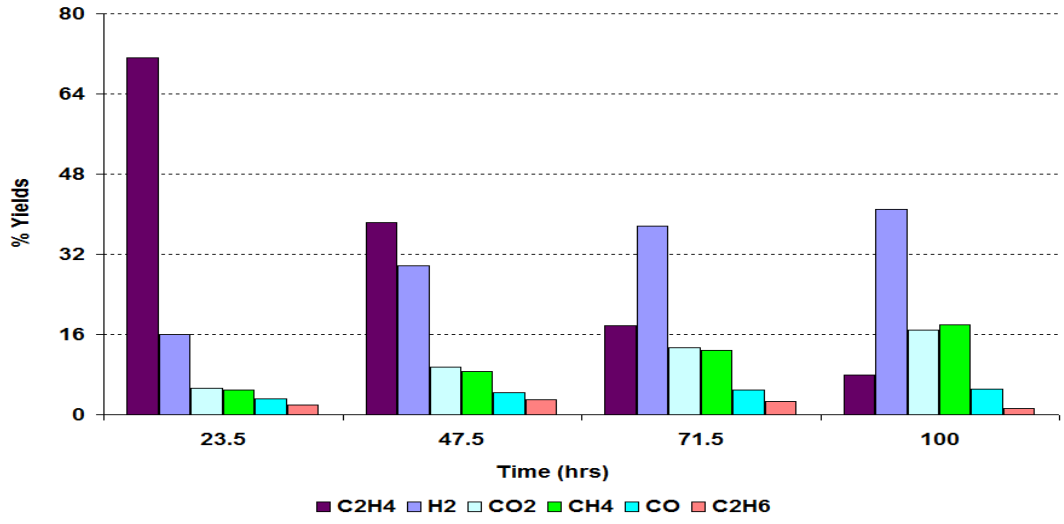

Figure 8.3-35 % Yield of gaseous products over Ru/Al_2O_3 catalyst during the propanal impurity reaction

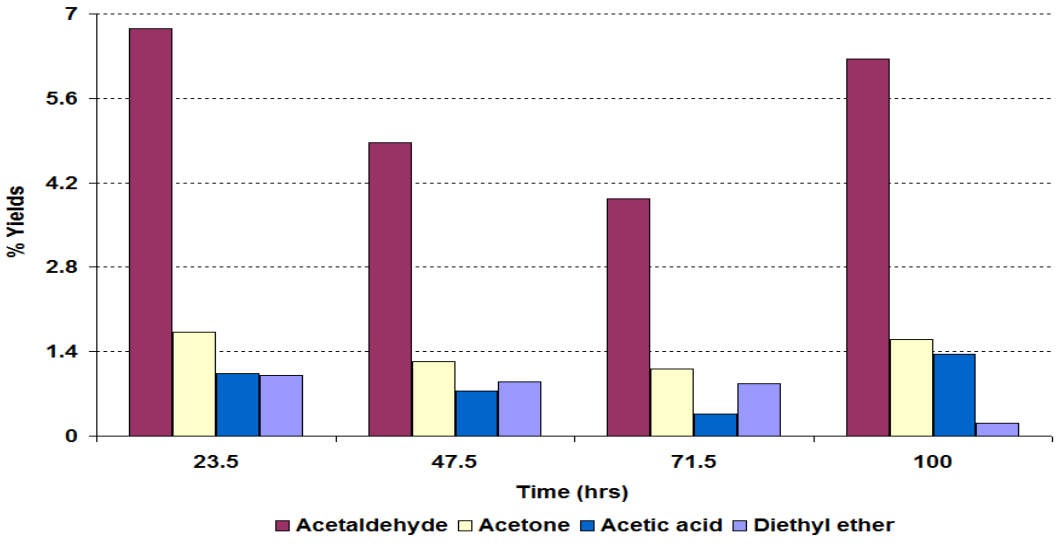

Figure 8.3-36 % Yield of liquid products over Ru/Al_2O_3 catalyst during the propanal impurity reaction

From Figure 8.3-35, it is obvious that the yield of C_2H_4 significantly decreased with the passage of time and after 71.5 hours TOS the yield of H_2 exceeded that of C_2H_4. Similarly,

the yields of CH_4 and CO_2 continuously increased, although their yields were less than 18% up till the end of the reaction.

Unlike the preceding reactions in the propanal impurity reaction the yield of acetaldehyde was slightly increased although this changed during the reaction. The other liquid products showed similar behaviour to acetaldehyde except diethyl ether which steadily decreased during the reaction.

8.3.2.6 Post reaction characterisation

8.3.2.6.1 TPO

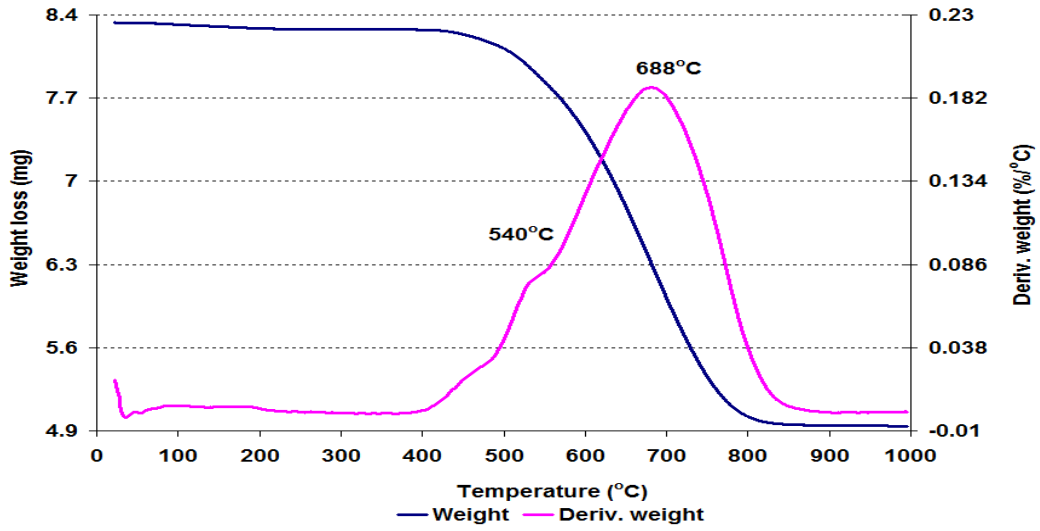

Figure 8.3-37 Post reaction TPO for Ru/Al_2O_3 catalyst following the propanal impurity reaction

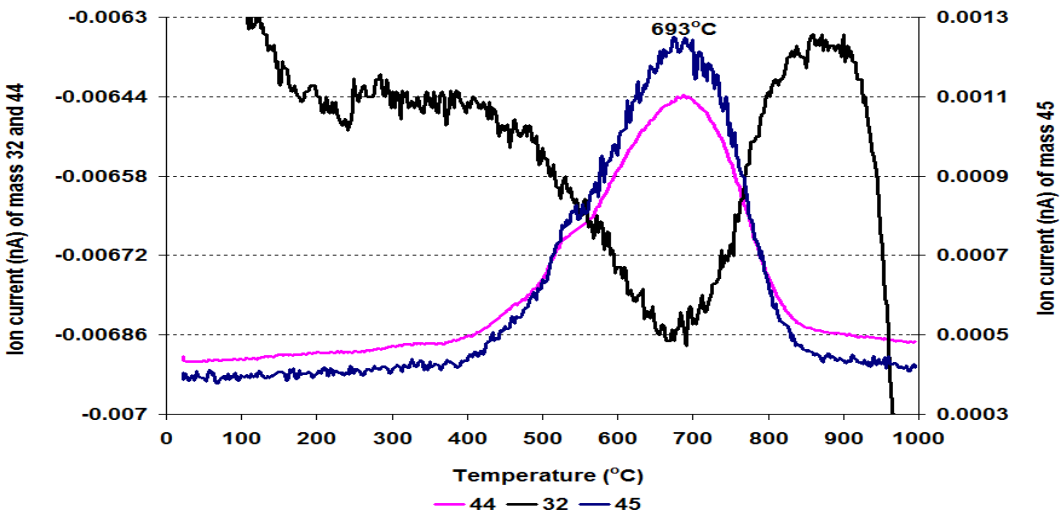

Figure 8.3-38 MS data of CO_2 (m/z=44), O_2 (m/z=32) and C_2H_5OH fragment (m/z=45) for Ru/Al_2O_3 catalyst following the propanal impurity reaction

The TPO profile (Figure 8.3-37) illustrates that 407.6 mg g^{-1} of catalyst weight loss took place between 22°C and 1000°C. The main weight loss was observed at 688°C with a small shoulder towards the lower temperature region in the derivative weight profile. The weight loss events attributed to CO_2, C_2H_5OH fragment and trace amounts of H_2O evolution in the mass spectrometry profile. M/z values of 58, 59 and 43 were monitored, although no prominent peaks were observed for these masses.

8.3.2.6.2 Raman analysis

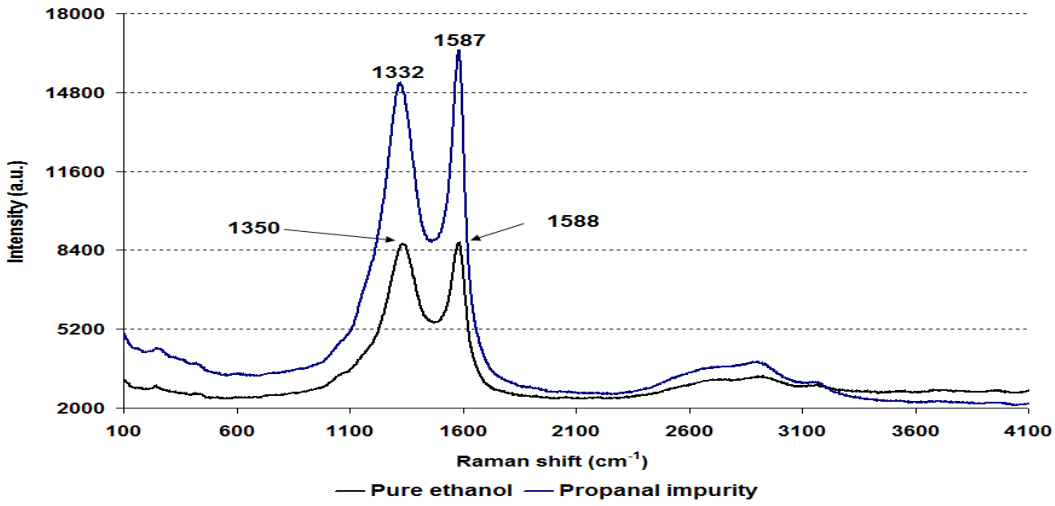

Figure 8.3-39 Post reaction Raman spectra for Ru/Al_2O_3 catalyst following the propanal impurity reaction

Raman spectrum was collected for the spent Ru/Al_2O_3 sample, which was used in the steam reforming reaction of ethanol with a propanal impurity. Comparison with the pure ethanol sample is shown in Figure 8.3-39. It shows that a significant change in intensity and a slight change to the position of the lower wave number bands occurred, suggesting that the nature of the coke on the catalyst was slightly changed.

8.3.2.6.3 BET analysis

Catalyst	Conditions	BET Surface area (m^2/g)	Pore volume (cm^3/g)	Average pore diameter (Å)
Ru/Al_2O_3	Pure ethanol (500°C)	32	0.07 (± 2.17)	78 (± 6.57)
	Propanal impurity	16	0.03 (± 0.44)	80 (± 4.14)

Table 8.3-5 BET analysis of post reaction Ru/Al_2O_3 catalyst following the propanal impurity reaction

The results in Table 8.3-5 show a substantial decrease in the BET surface area and the pore volume of the post propanal impurity reaction catalyst. In addition the average pore diameter increased in the propanal impurity Ru/Al_2O_3 sample.

8.3.2.7 Propylamine impurity

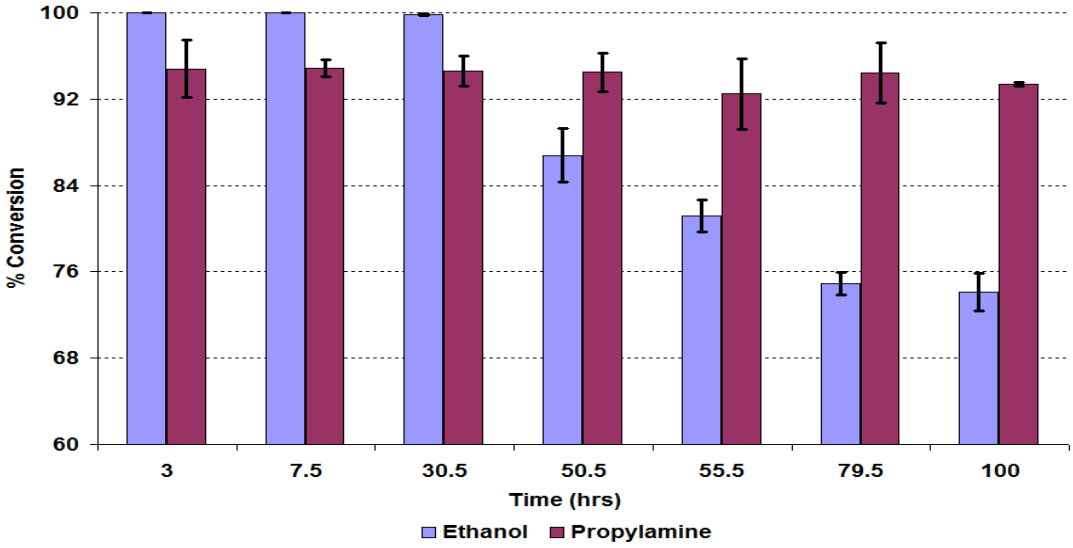

Figure 8.3-40 % Conversion of ethanol and propylamine over Ru/Al_2O_3 catalyst during the propylamine impurity reaction

1mol.% addition of propylamine to water/ethanol mixture brings out a dramatic change in the behaviour of Ru/Al_2O_3 catalyst towards the steam reforming of ethanol. The results shown in Figure 8.3-40 illustrate that after the addition of propylamine, Ru/Al_2O_3 catalyst gave near 100% conversion of ethanol in the initial 30.5 hours TOS. However, after 30 hours the catalyst was slightly deactivated and at the end of reaction the conversion of ethanol had decreased to 74%.

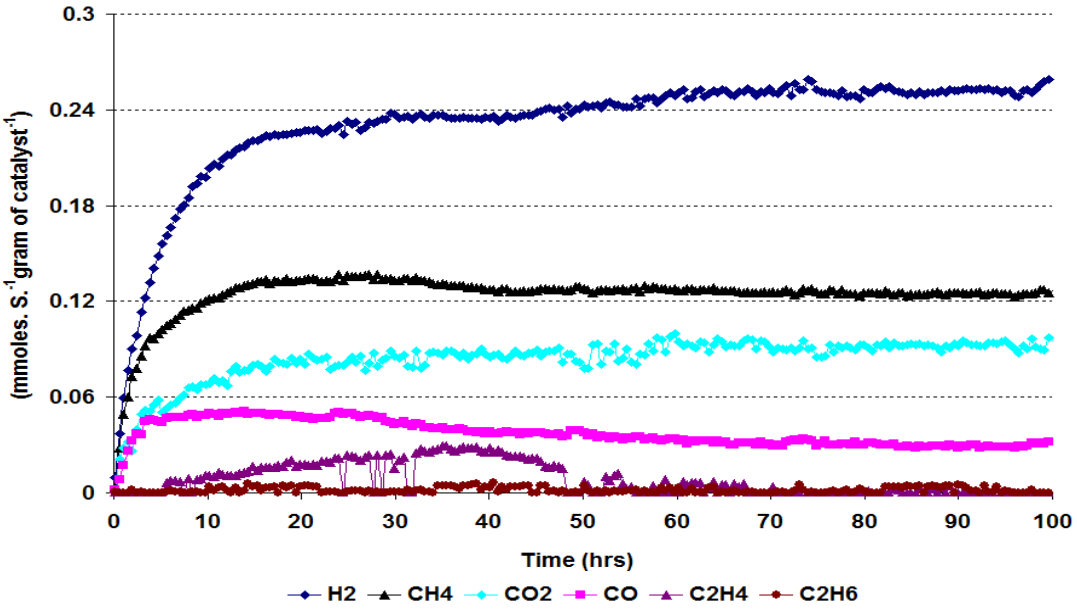

Figure 8.3-41 Rate of formation of gaseous products over Ru/Al_2O_3 catalyst during the propylamine impurity reaction

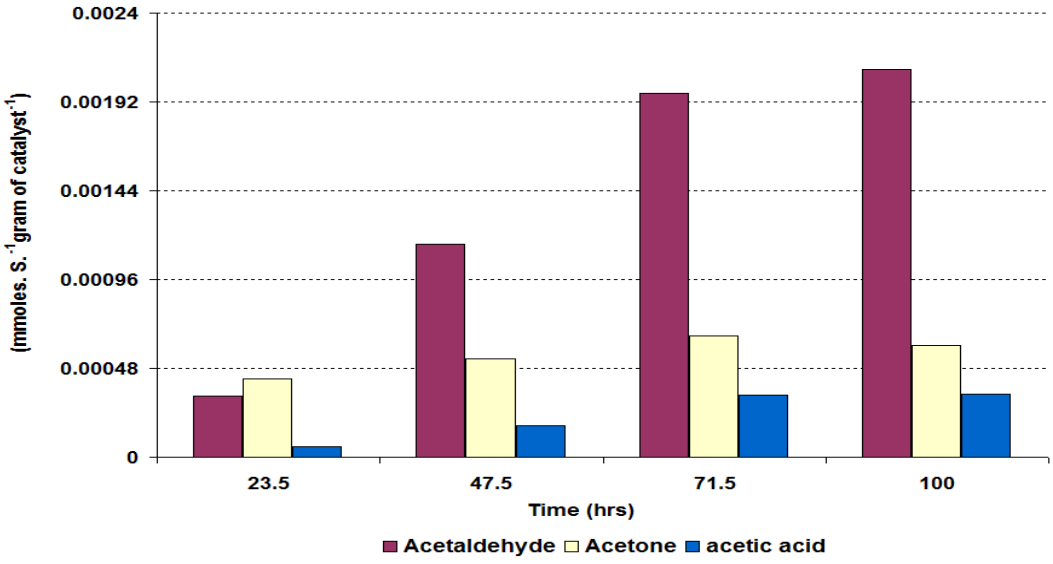

Figure 8.3-42 Rate of formation of liquid products over Ru/Al_2O_3 catalyst during the propylamine impurity reaction

Similar to the conversion of ethanol, the distribution of the gaseous products in terms of rates of formation also significantly changed during the steam reforming of ethanol with the addition of the propylamine impurity. In contrast to the propanal impurity reaction, the rates of formation of CH_4 and CO_2 significantly increased and obtained steady state conditions after 56 hours TOS. Whereas after 48 hours TOS, the rate of formation of C_2H_4 substantially decreased to almost zero (0.0075 mmoles $s^{-1}g^{-1}$). Like CO_2 and CH_4 the rate of formation of H_2 also gained steady state value after 56 hours TOS.

Interestingly, the rate of formation of all the liquid products, including acetaldehyde, acetone and acetic acid, slightly increased as shown in Figure 8.3-42. Similar to the earlier reactions acetaldehyde was produced at the highest rate and its rate increased over time with no deactivation observed up to the end of the reaction.

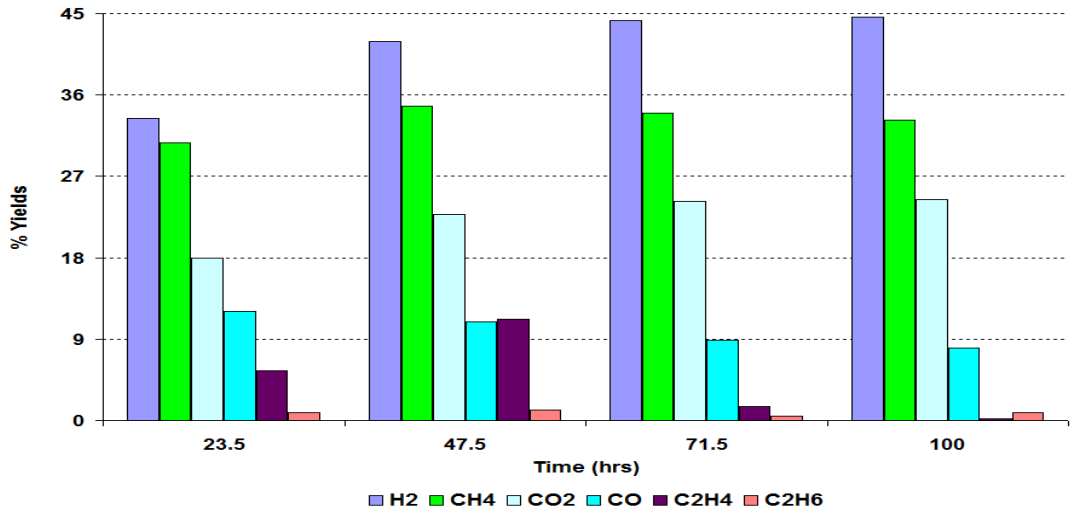

Figure 8.3-43 % Yield of gaseous products over Ru/Al_2O_3 catalyst during the propylamine impurity reaction

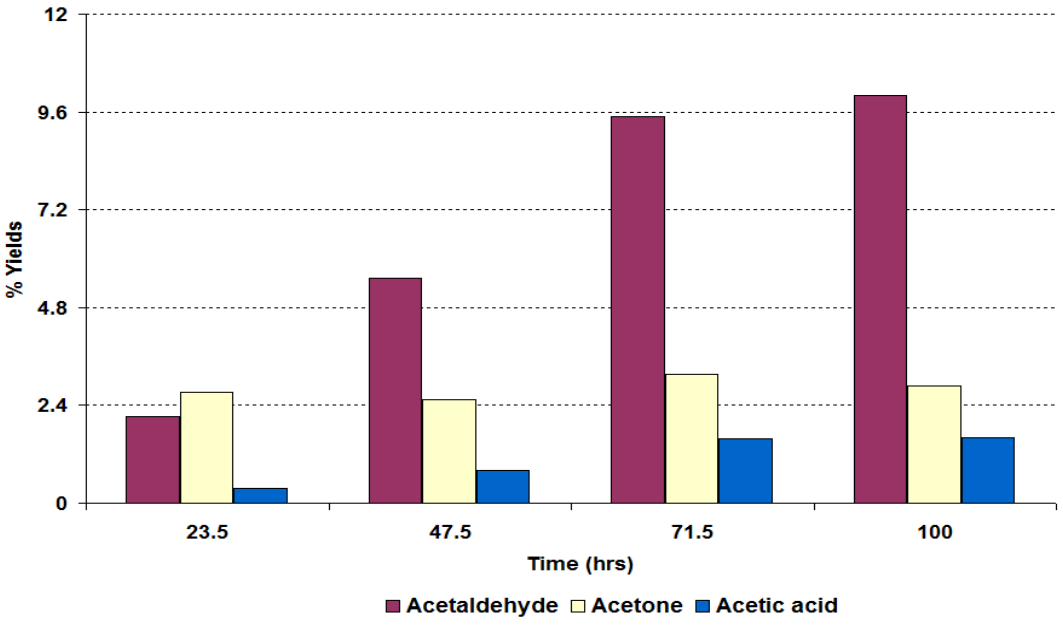

Figure 8.3-44 % Yield of liquid products over Ru/Al_2O_3 catalyst during the propylamine impurity reaction

Figure 8.3-43 shows the yield profile for the gaseous products from the steam reforming of ethanol reaction with propylamine impurity. The graph illustrates that all the major gaseous products *i.e.* H_2, CH_4 and CO_2, gave higher yields compared to the IPA and 1-

propanol impurities reactions. The yield values varied slightly in the initial 48 hours and then stabilised for the rest of the reaction. The graph indicates that the yield of CO gradually decreased with reaction time and after 100 hours TOS decreased to a yield of 8%. Interestingly, considerable amounts of C_2H_4 was produced in the initial 48 hours TOS and then subsequently disappeared from the reactant profile as the reaction proceeded.

Figure 8.3-44 illustrates that in the liquid products, the yields of acetaldehyde and acetic acid progressively increased with reaction time whilst the yield of acetone varied throughout the reaction. Trace amounts of methanol, ethyl acetate and diethyl ether were also detected during reaction. However unlike the pure ethanol reaction over Ru/Al_2O_3 catalyst, 1,1-diethoxyethane and crotonaldehyde were not produced during the reaction.

8.3.2.8 Post reaction characterisation

Post reaction characterisation was carried out to examine the effect on the catalyst structure of a propylamine impurity in the steam reforming of ethanol.

8.3.2.8.1 TPO

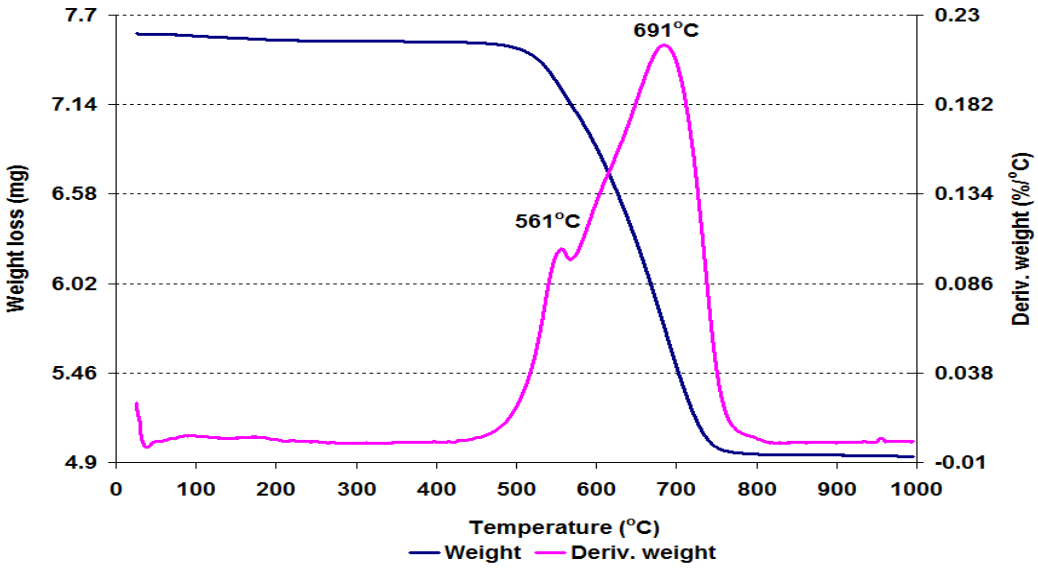

Figure 8.3-45 Post reaction TPO over Ru/Al_2O_3 catalyst following the propylamine impurity reaction

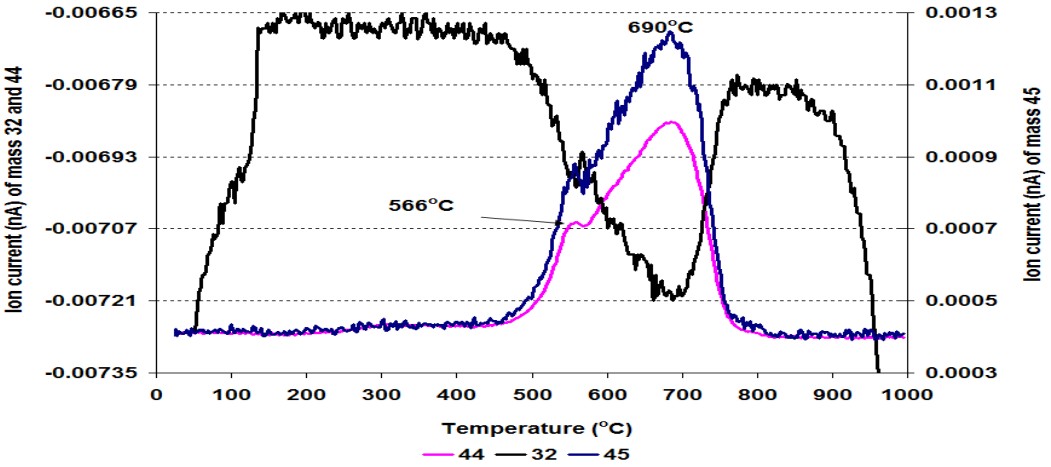

Figure 8.3-46 MS data of CO_2 (m/z=44), O_2 (m/z=32) and C_2H_5OH fragment (m/z=45) for Ru/Al_2O_3 catalyst following the propylamine impurity reaction

The post reaction Ru/Al_2O_3 catalyst was analysed by TGA/DSC, between 25°C and 1000°C in a 2% O_2/Ar atmosphere and the results collected were plotted versus temperature and are shown in Figures 8.3-45 to 46. The TGA figure illustrates that the main weight loss occurred between 430°C and 800°C. From the derivative weight profile, this main weight loss can be split into two peaks, a small peak at 561°C and a larger peak at 690°C, suggesting that the carbonaceous deposits on the catalyst surface are different in nature. These two main peaks gave exothermic events in the heat flow graph, not shown here. The total weight loss that took place between 25°C and 1000°C was 349.4 mg g^{-1} of catalyst which corresponded to CO_2 and ethanol fragment in the mass spectrometric results.

8.3.2.8.2 Raman analysis

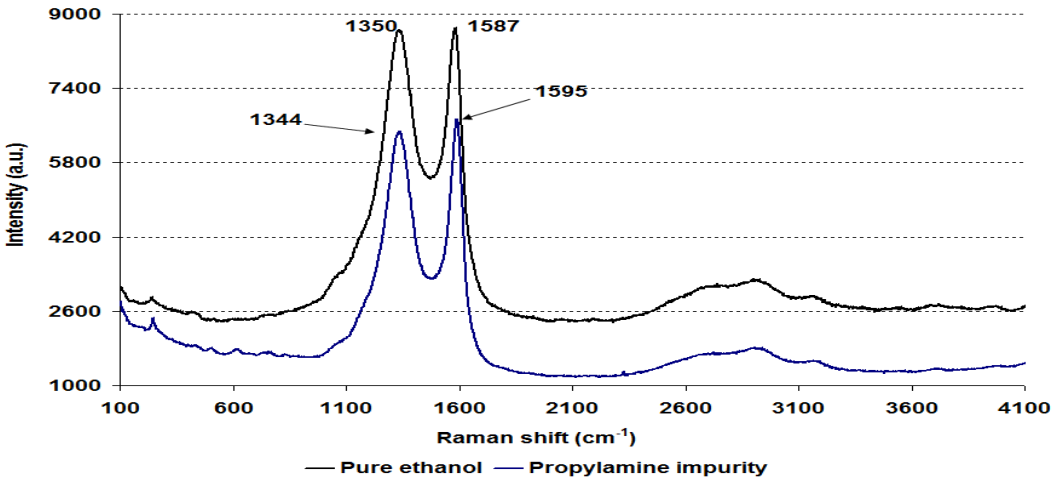

Figure 8.3-47 Post reaction Raman spectra for Ru/Al_2O_3 catalyst following the propylamine impurity reaction

In Figure 8.3-47, the Raman spectra for post catalysts from the pure ethanol and the propylamine reactions are shown. A small change in intensities and bands positions of Raman spectra were observed in the post reaction catalysts.

8.3.2.8.3 BET analysis

Catalyst	Conditions	BET Surface area (m^2/g)	Pore volume (cm^3/g)	Average pore diameter (Å)
Ru/Al_2O_3	Pure ethanol (500°C)	32	0.07 (± 2.17)	78 (± 6.57)
	Propylamine impurity	36	0.10 (± 0.51)	106 (± 6.76)

Table 8.3-6 BET analysis of post reaction Ru/Al_2O_3 catalyst following the propylamine impurity reaction

The BET analysis in Table 8.3-6 shows that the BET surface area, the average pore diameter and the pore volume in the propylamine impurity reaction slightly increased compared to post reaction of pure ethanol catalyst.

8.3.2.9 Acetone impurity

Finally the influence of ketonic group on the steam reforming of ethanol over Ru/Al_2O_3 catalyst was investigated by adding 1mol% acetone with respect to pure ethanol to the water/ethanol mixture.

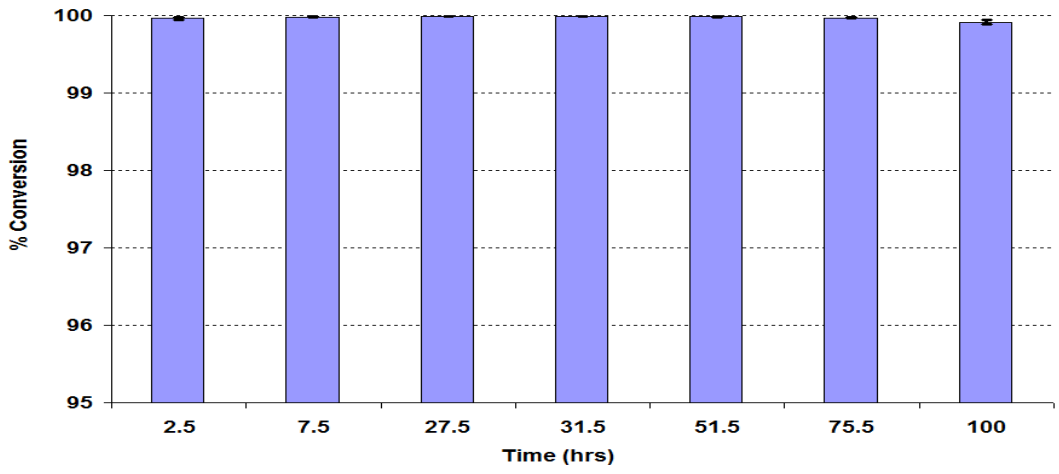

Figure 8.3-48 % Conversion of ethanol over Ru/Al_2O_3 catalyst during the acetone impurity reaction

The conversion of ethanol shows similar results over Ru/Al_2O_3 catalyst with an acetone impurity to those observed in propylamine impurity reaction. However, after adding the

acetone impurity no distinguishable deactivation of the Ru/Al_2O_3 catalyst was observed. The conversion of ethanol only decreased to 99.9% after 100 hours time on stream.

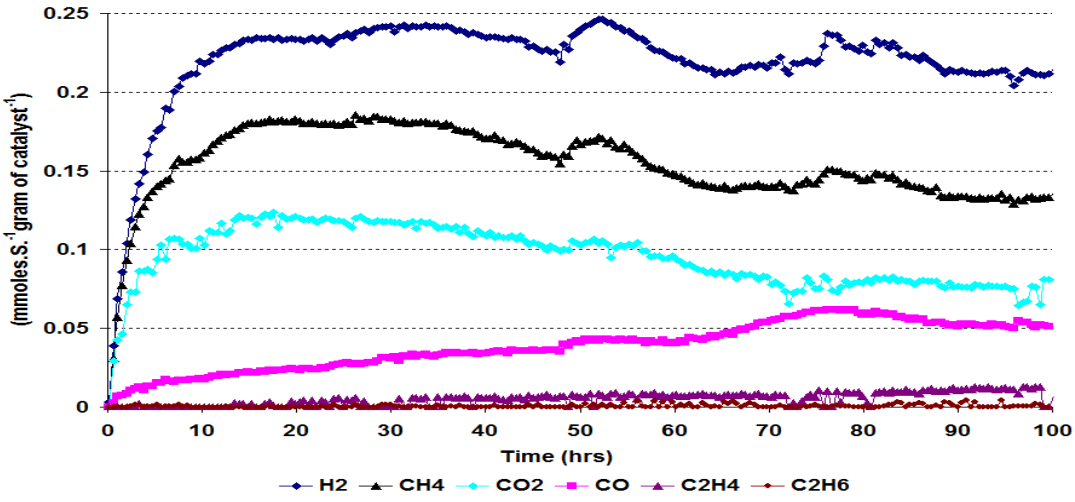

Figure 8.3-49 Rate of formation of gaseous products over Ru/Al_2O_3 catalyst during the acetone impurity reaction

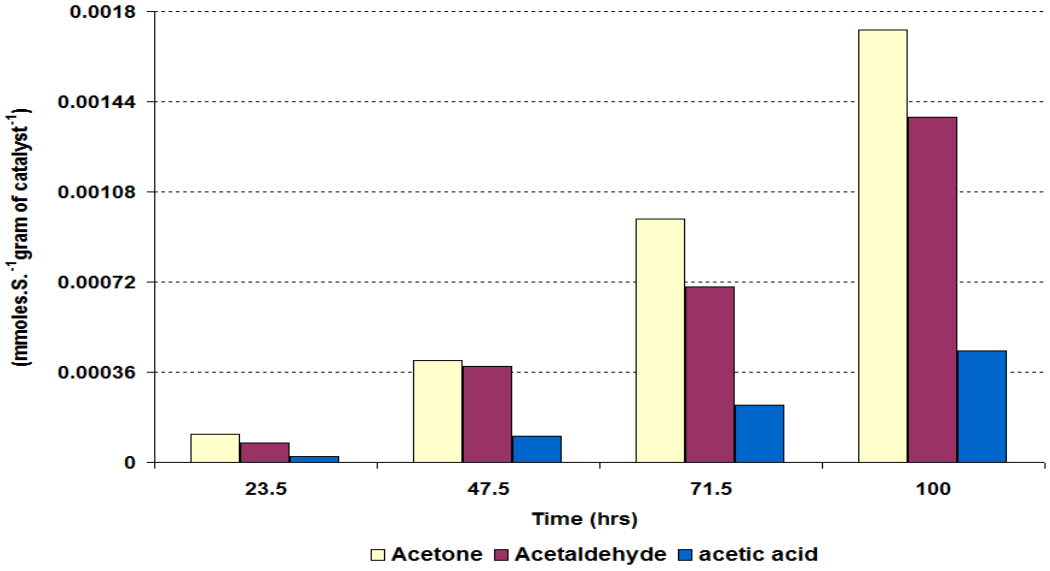

Figure 8.3-50 Rate of formation of liquid products over Ru/Al_2O_3 catalyst during the acetone impurity reaction

The rate of formation of the gaseous products in Figure 8.3-49 shows fascinating results. The figure illustrates that H_2, CH_4, CO_2 and CO were produced at the highest rates in the gaseous products. However, their rates varied throughout the reaction. The rate of formation of H_2 before stabilisation increased, stabilised in the initial 48 hours and then started to decrease. However the change in flow rate observed after taking the overnight sample slightly changed the rate of formation of H_2. The rate of formation of CH_4 followed

a similar pattern to that observed for H_2. Although after the initial increase its rate progressively decreased until the end of the reaction. The rate of formation of CO and CO_2 were contrary to each other. Initially the rate of CO_2 increased and then steadily decreased whilst the rate of CO formation was initially low and steadily increased with reaction time. After 14 hours TOS C_2H_4 appeared in gaseous products although its rate was very low. In the liquid products, only acetone, acetaldehyde, acetic acid and methanol were produced. Interestingly the acetone rate exceeded that of acetaldehyde, which was expected as 1mol.% acetone had been added to the water/ethanol mixture. The rates of all the liquid products gradually increased with reaction time.

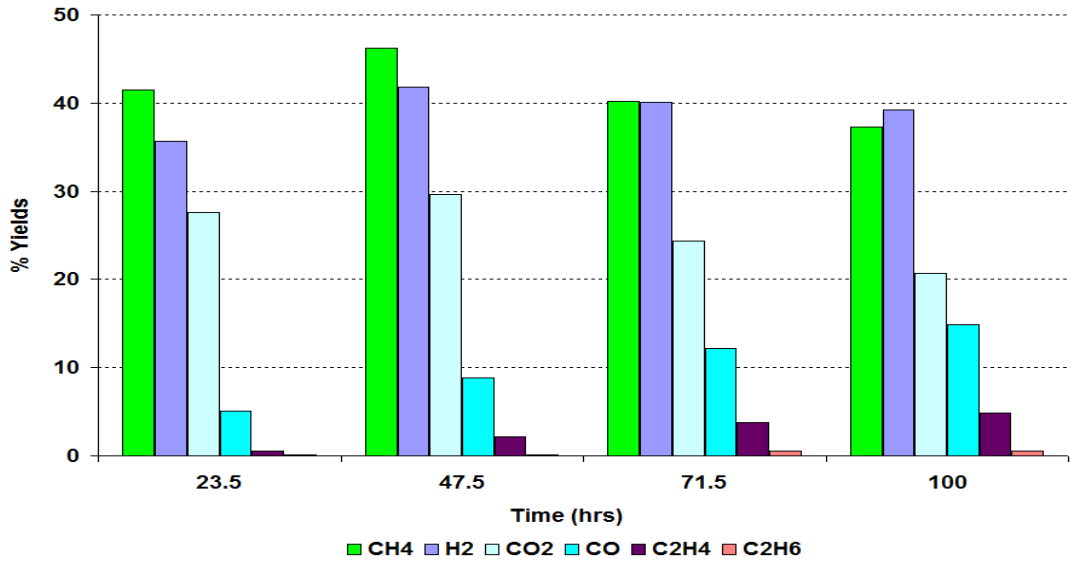

Figure 8.3-51 % Yield of gaseous products over Ru/Al_2O_3 catalyst during the acetone impurity reaction

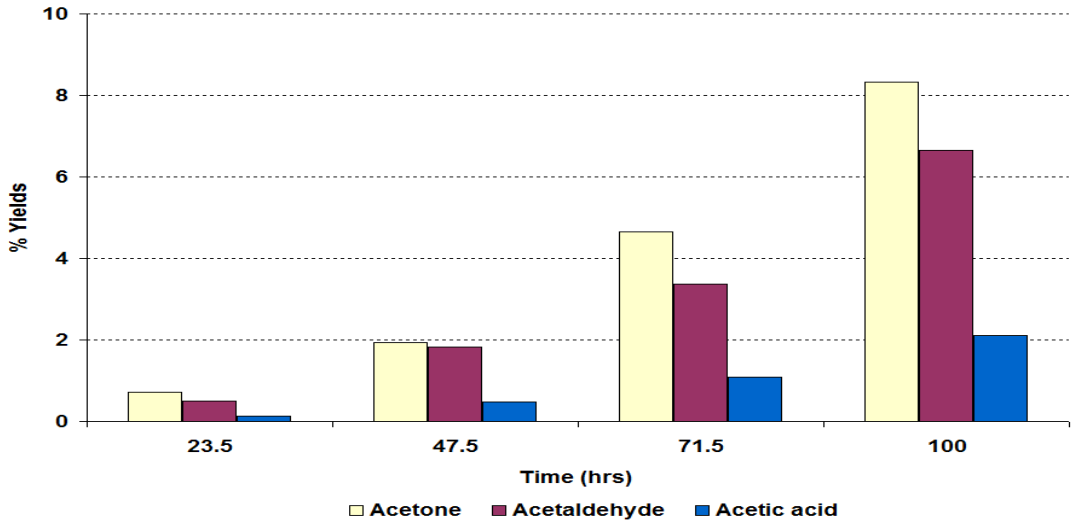

Figure 8.3-52 % Yield of liquid products over Ru/Al_2O_3 catalyst during the acetone impurity reaction

CH_4, H_2 and CO_2 gave the highest yields although they decreased steadily with reaction time. The maximum yield value obtained for H_2 was above 30%, which was less than the values for H_2 produced in the propylamine impurity reaction. However, overall the yield of CH_4 was higher than all the gaseous products. Whereas the yield of CO was low initially and increased with reaction time.

In the liquid products, acetone and acetaldehyde gave the highest yields, for which the maximum values obtained were ~ 8% and ~ 6.6% respectively. It was also notable that neither liquid product obtained steady condition during the reaction.

8.3.2.10 Post reaction characterisation

Post reaction characterisation was performed on the spent reaction catalyst to determine the nature of deposits on the catalyst.

8.3.2.10.1 TPO

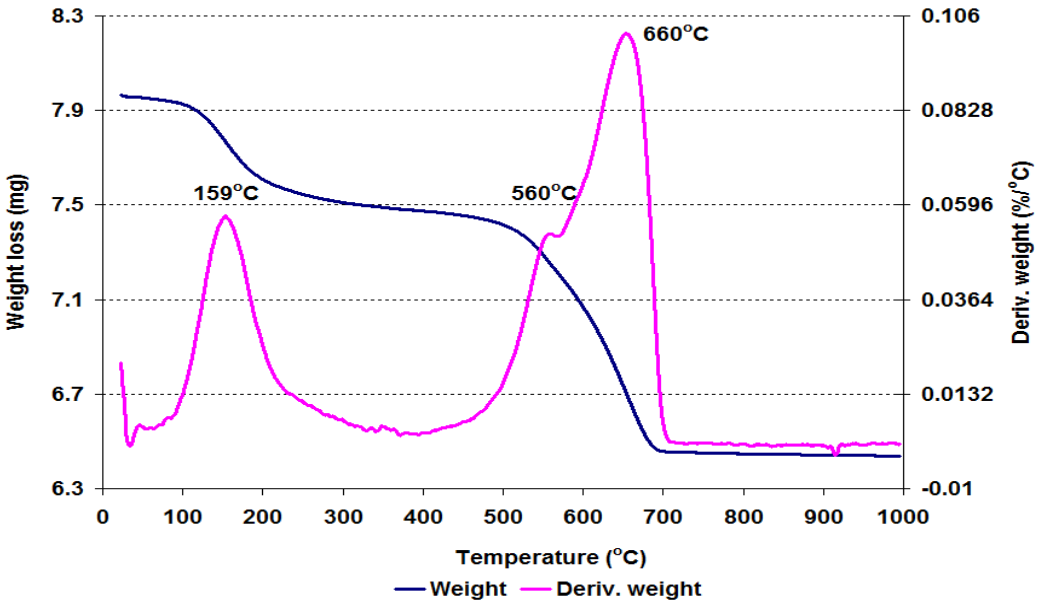

Figure 8.3-53 Post reaction TPO for Ru/Al_2O_3 catalyst following the acetone impurity reaction

In Figure 8.3-53, the weight loss and derivative weight loss for the Ru/Al_2O_3 catalyst after ethanol steam reforming reaction with an acetone impurity is shown. Two weight loss events occurred at 159°C and 660°C, and appear on the derivative weight profile. In addition to these a smaller weight loss occurred at 560°C.

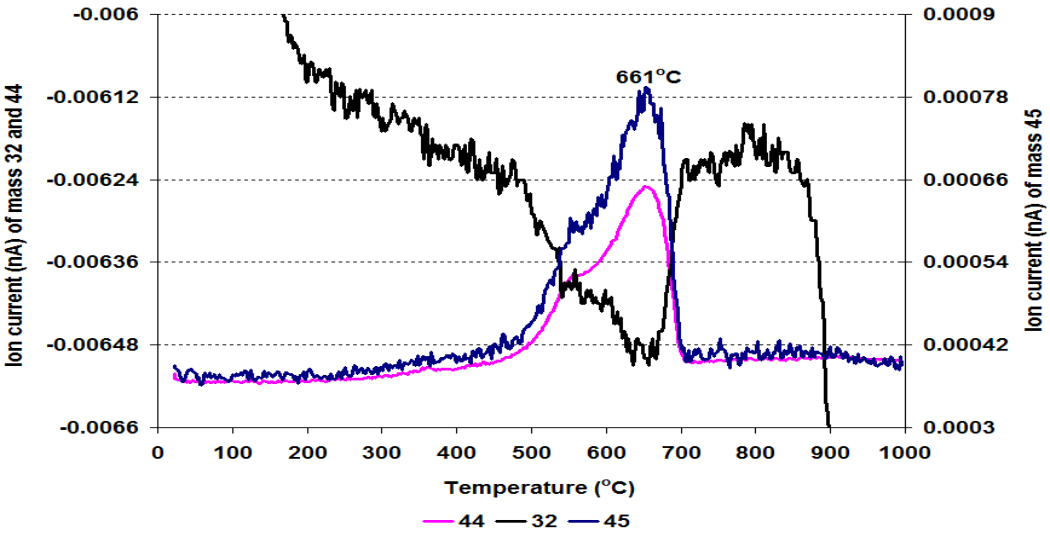

Figure 8.3-54 MS data of CO_2 (m/z=44), O_2 (m/z=32) and C_2H_5OH fragment (m/z=45) for Ru/Al_2O_3 catalyst following the acetone impurity reaction

The mass spectrometric data, presented in Figure 8.3-54 shows that the evolution of CO_2 and ethanol fragment took place at 660°C. However, no prominent peak was detected in mass spectrometric data for the weight loss at 159°C, suggesting that trace amounts of water may have evolved which were not detected in the mass spectrometry.

8.3.2.10.2 Raman analysis

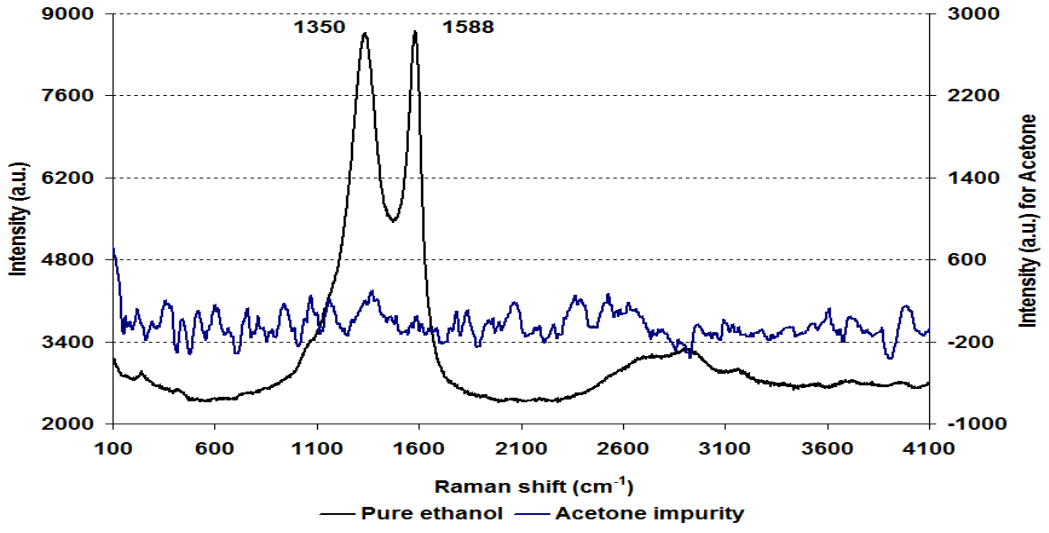

Figure 8.3-55 Post reaction Raman spectra for Ru/Al_2O_3 catalyst following the acetone impurity reaction

Raman spectra of post reaction Ru/Al_2O_3 catalyst from pure ethanol and the acetone impurity were compared in Figure 8.3-55. It illustrates that there were no peaks corresponding to graphitic carbon in the acetone impurity reaction sample were detected in

the Raman analysis, which suggests that no graphitic carbon formation occurred on the catalyst particles.

8.3.2.10.3 BET analysis

Catalyst	Conditions	BET Surface area (m^2/g)	Pore volume (cm^3/g)	Average pore diameter (Å)
Ru/Al_2O_3	Pure ethanol (500°C)	32	0.07 (± 2.17)	78 (± 6.57)
	Acetone impurity	50	0.24 (± 0.29)	189 (± 4.67)

Table 8.3-7 BET analysis of post reaction Ru/Al_2O_3 catalyst following the acetone impurity reaction

The BET analysis in Table 8.3-7 shows that, comparative to the pure ethanol reaction catalyst, remarkable increase in the BET surface area, the pore volume and the average pore diameter was observed in the acetone impurity catalyst.

8.3.3 Pt/Al_2O_3

After examining the influence of different impurities on the ethanol steam reforming reaction over a Ru/Al_2O_3 catalyst, the steam reforming of ethanol reaction was then carried out over a Pt/Al_2O_3 catalyst using the same impurities as were discussed in section 8.3.2 to compare any trends and differences between the different noble metal supported alumina catalysts.

8.3.3.1 1-Propanol impurity

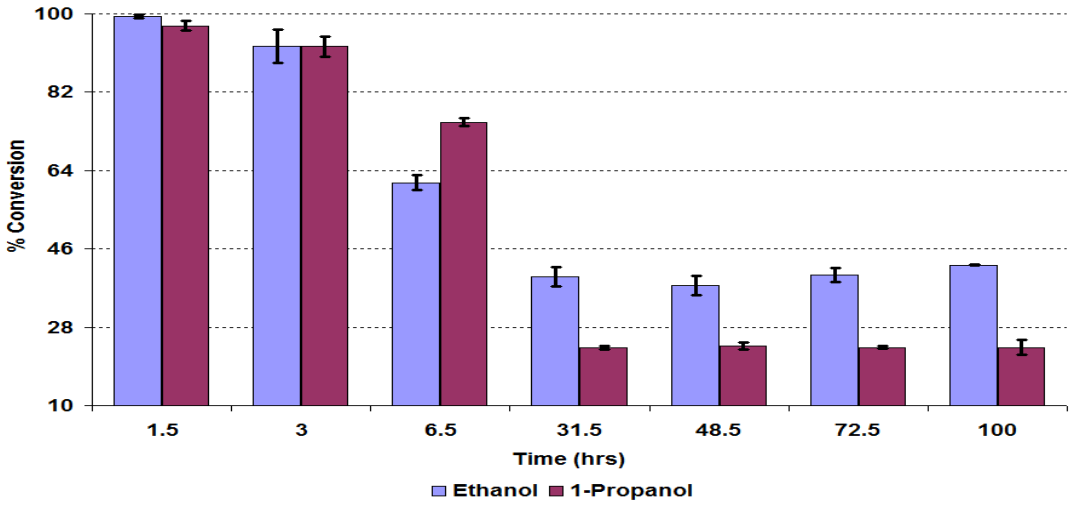

Figure 8.3-56 % Conversion of ethanol and 1-propanol over the Pt/Al_2O_3 catalyst during the 1-propanol impurity reaction

Figure 8.3-56 shows that in the 1-propanol impurity reaction ethanol gave higher conversions than the pure ethanol over Pt/Al_2O_3 in the initial 1 hour time on stream. However, after 1 hour TOS severe deactivation of the catalyst took place and the conversion of ethanol decreased to 39% by 31.5 hours time on stream. However after 31.5 hours the conversion stabilised and remained constant until the end of the reaction. 1-propanol conversion gave similar patterns to that of ethanol although after stabilisation it had lower conversion than ethanol.

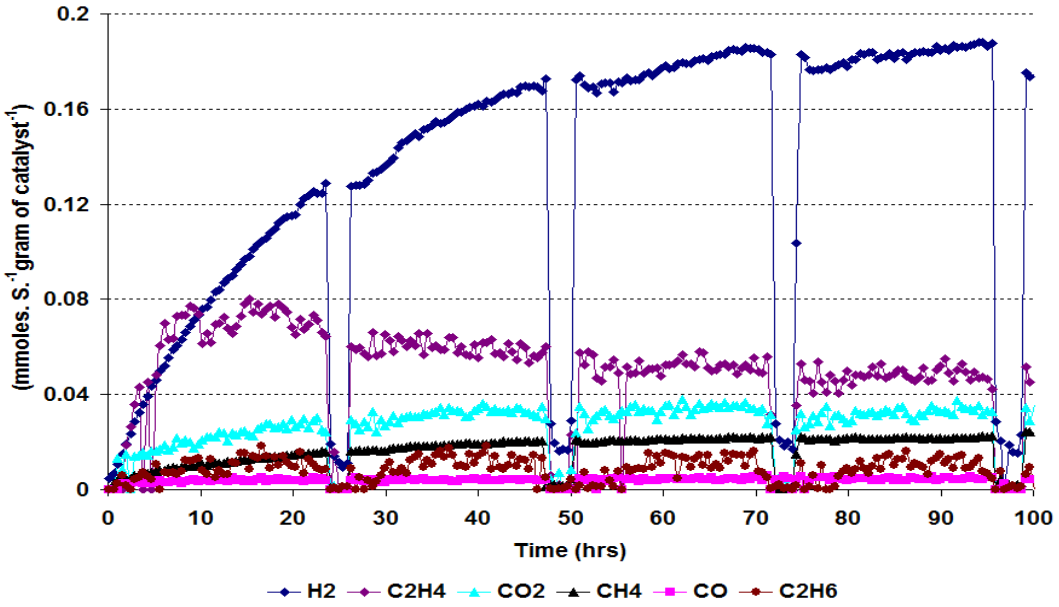

Figure 8.3-57 Rate of formation of gaseous products over Pt/Al_2O_3 catalyst during the 1-propanol impurity reaction

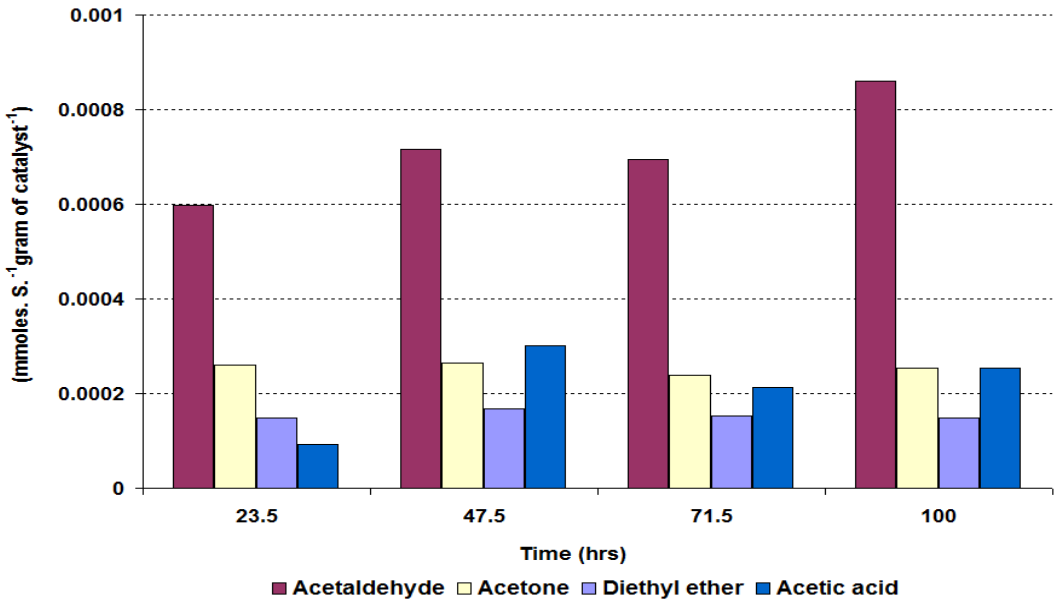

Figure 8.3-58 Rate of formation of liquid products over Pt/Al_2O_3 catalyst during the 1-propanol impurity reaction

The rates of formation of all the gaseous products gave similar profiles to those seen in the pure ethanol steam reforming reaction except for C_2H_4. C_2H_4 was produced in the 1-propanol impurity reaction at a comparatively lower rate with respect to the pure ethanol reaction over Pt/Al_2O_3.

As with the 1-propanol impurity reaction over Pt/Al_2O_3 catalyst, acetaldehyde was produced at the highest rate. Besides acetaldehyde, also produced were acetone, acetic acid and diethyl ether. The rate of formation of all the liquid products did not stabilise and varied throughout the reaction.

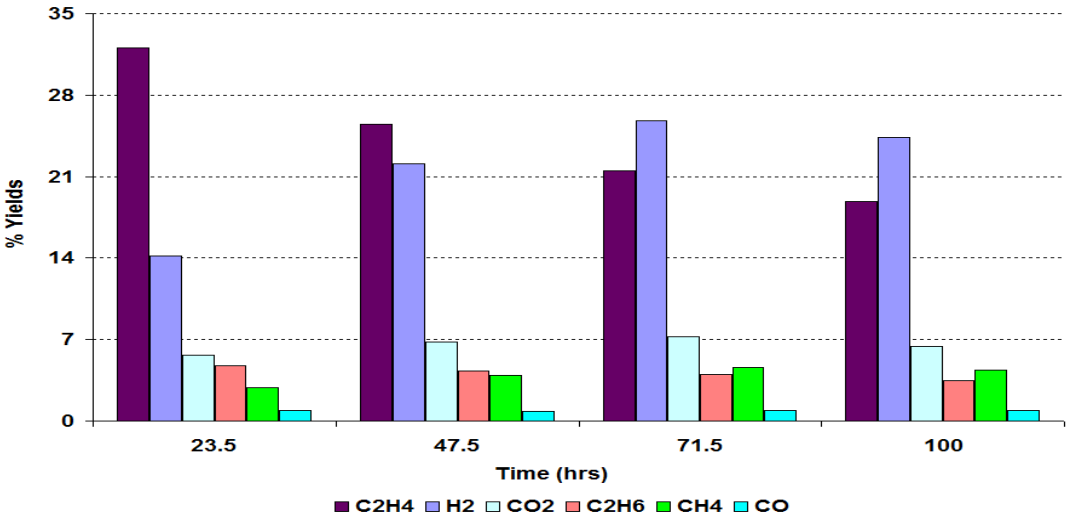

Figure 8.3-59 % Yield of gaseous products over Pt/Al_2O_3 catalyst during the 1-propanol impurity reaction

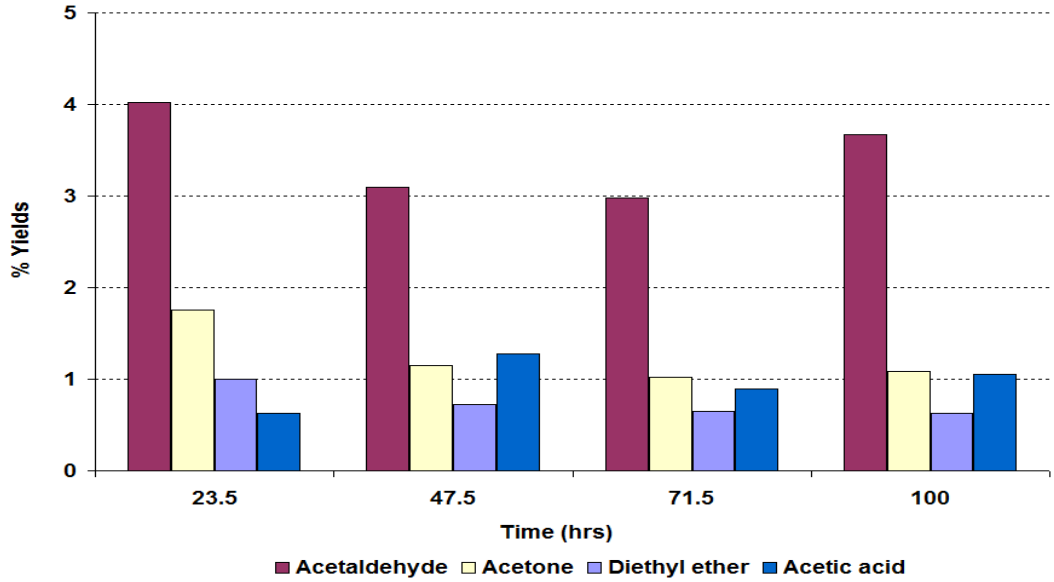

Figure 8.3-60 % Yield of liquid products over Pt/Al_2O_3 catalyst during the 1-propanol impurity reaction

In Figure 8.3-59 the yields of the gaseous products in the ethanol steam reforming reaction with 1-propanol impurity are shown. C_2H_4 and H_2 gave the highest yields of all the gaseous products. The yield of C_2H_4 steadily decreased with time of stream, whilst the H_2 yield increased with time. As discussed before, the yield of C_2H_4 in the 1-propanol impurity reaction decreased, whilst in the pure ethanol reaction it increased with reaction time. Other gaseous products were produced with low yields and none of them had a yield higher than 7%.

In the liquid products acetaldehyde was produced with a maximum 4% yield. However, its yield varied and did not stabilise during the reaction. The other liquid products produced were insignificant and each had a yield of less than 2%.

8.3.3.2 Post reaction characterisation

From section 8.3.3.1 it is clear that deactivation of the catalyst occurred during the reaction, specifically from Figure 8.3-56. Post reaction characterisations were carried out on the spent catalyst to check the cause of the catalyst deactivation.

8.3.3.2.1 TPO

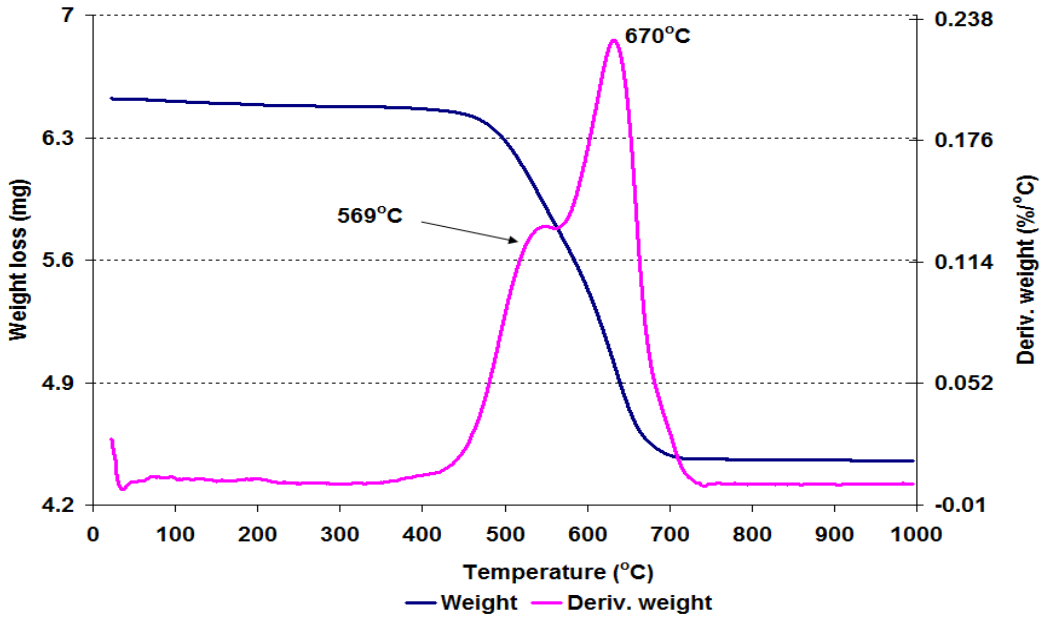

Figure 8.3-61 Post reaction TPO for Pt/Al_2O_3 catalyst following the 1-propanol impurity reaction

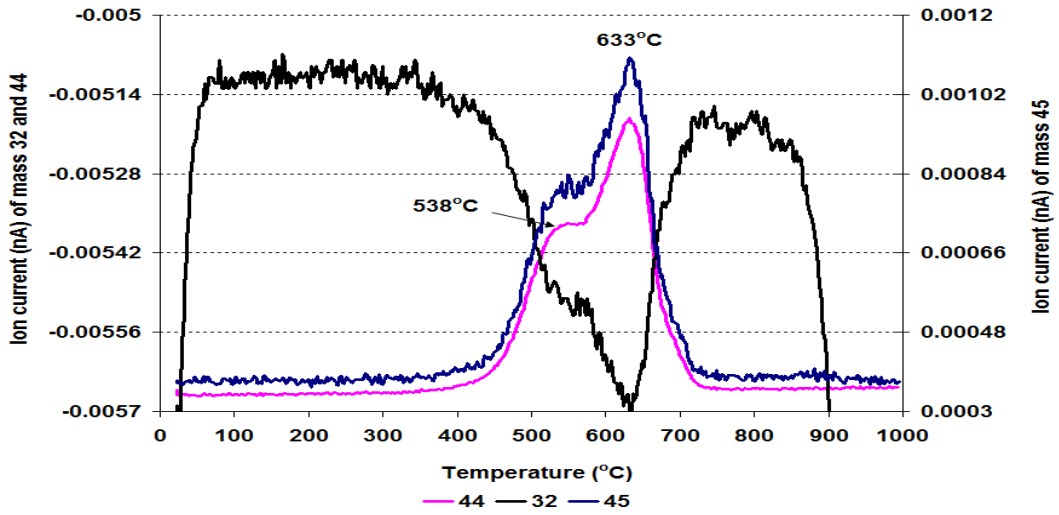

Figure 8.3-62 MS data of CO_2 (m/z=44), O_2 (m/z=32) and C_2H_5OH fragment (m/z=45) for Pt/Al_2O_3 catalyst following the 1-propanol impurity reaction

The spent Pt/Al_2O_3 catalyst was characterised using TGA with an associated to a mass spectrometer, in the temperature range of 22°C to 1000°C in a 2% O_2/Ar environment. The results collected were plotted versus temperature and shown in Figures 8.3-61 to 8.3-62. Figure 8.3-61 shows that the main weight loss occurred in the region between 350°C and 750°C and had two shoulder peaks at 569°C and 670°C respectively, which were equal to a weight loss of 317.8 mg g^{-1}. This weight loss event corresponded to CO_2 and the principal fragment of ethanol in mass spectrometry profile. Compared to the spent catalyst for the pure ethanol reaction, there was no desorption of H_2O observed.

8.3.3.2.2 Raman analysis

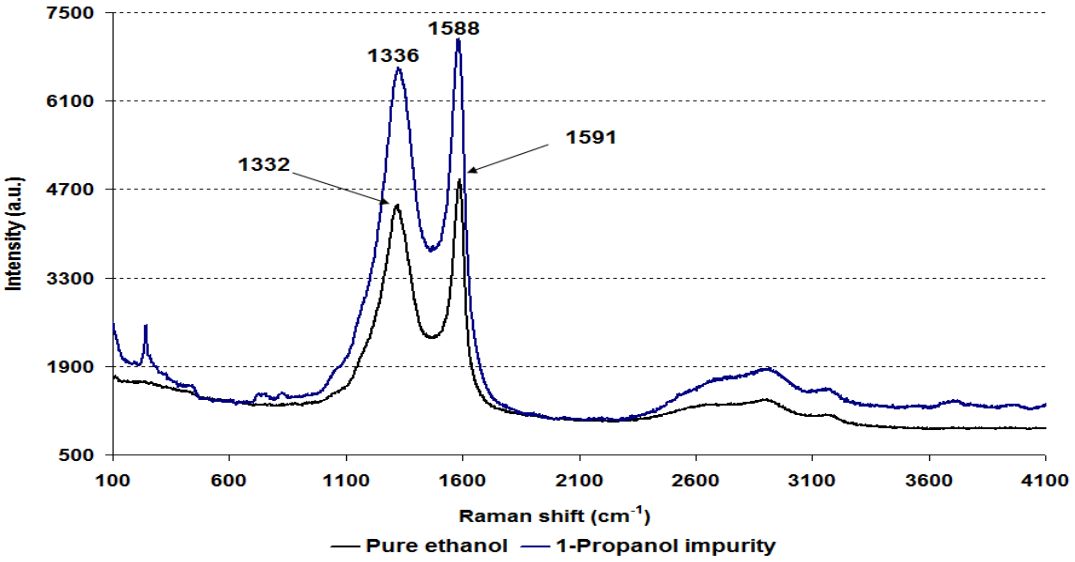

Figure 8.3-63 Post reaction Raman spectra for Pt/Al_2O_3 catalyst following the 1-propanol impurity reaction

Raman results (Figure 8.3-63) show that the 1-propanol impurity reaction post catalyst gave similar bands to the pure ethanol post reaction sample, although the intensity of bands increased, suggesting that the amount of graphitic type carbon increased.

8.3.3.2.3 BET analysis

Catalyst	Conditions	BET Surface area (m^2/g)	Pore volume (cm^3/g)	Average pore diameter (Å)
Pt/Al_2O_3	Pure ethanol (500°C)	41	0.09 (± 0.81)	80 (± 3.97)
	1-Propanol impurity	64	0.15 (± 0.96)	91 (± 6.22)

Table 8.3-8 BET analysis of post reaction Pt/Al_2O_3 catalyst following the 1-propanol impurity reaction

Higher BET surface area, pore volume and pore diameter were obtained for post reaction 1-propanol impurities catalyst compared to the pure ethanol reaction sample suggesting that less coke deposition took place on the 1-propanol impurity sample.

8.3.3.3 IPA impurity

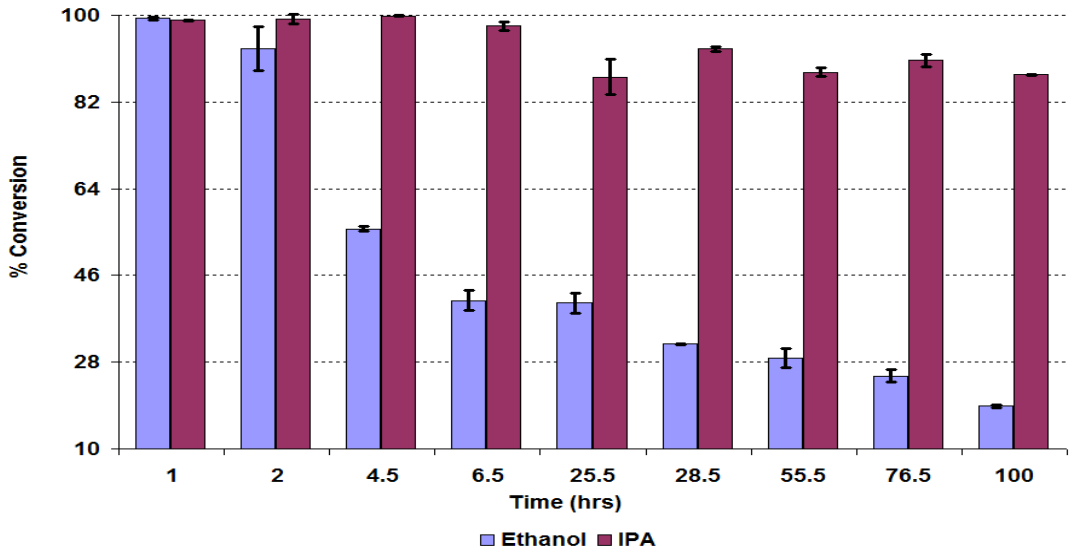

Figure 8.3-64 % Conversion of ethanol and IPA over the Pt/Al_2O_3 catalyst during the IPA impurity reaction

Addition of 1mol.% IPA impurity to the water/ ethanol reactant mixture brought about a significant change in the conversion of ethanol over the Pt/Al_2O_3 catalyst. Initially, the conversion of ethanol was 99%, which progressively decreased to 18% by the end of the reaction. On the other hand, the conversion of the IPA was higher (99%) and slightly

decreased with reaction time and then stabilised after 72 hours time of stream and remained constant for the rest of the reaction.

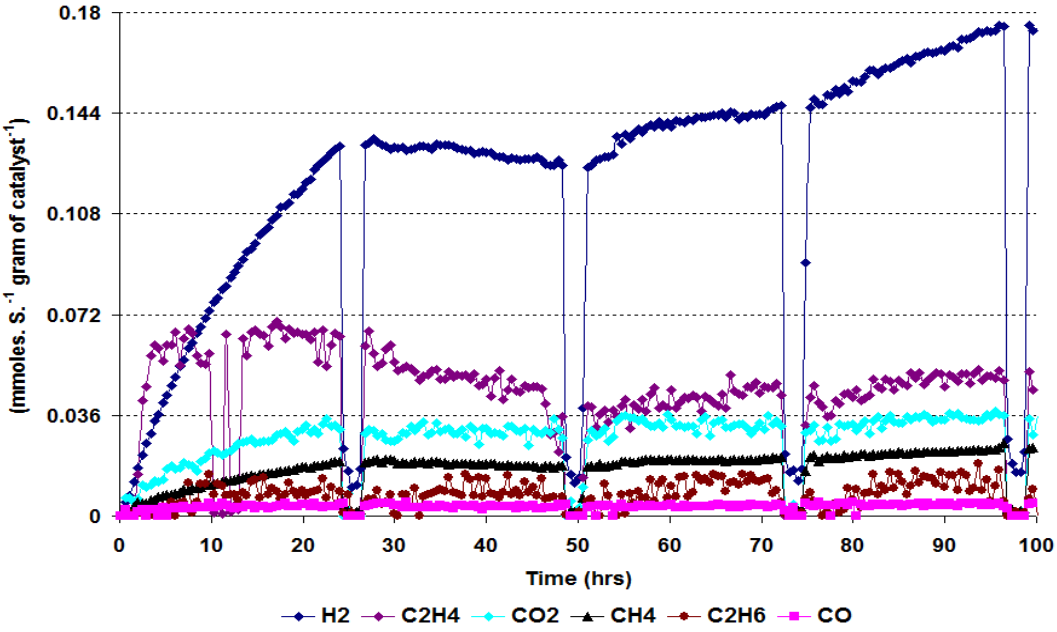

Figure 8.3-65 Rate of formation of gaseous products over Pt/Al_2O_3 catalyst during the IPA impurity reaction

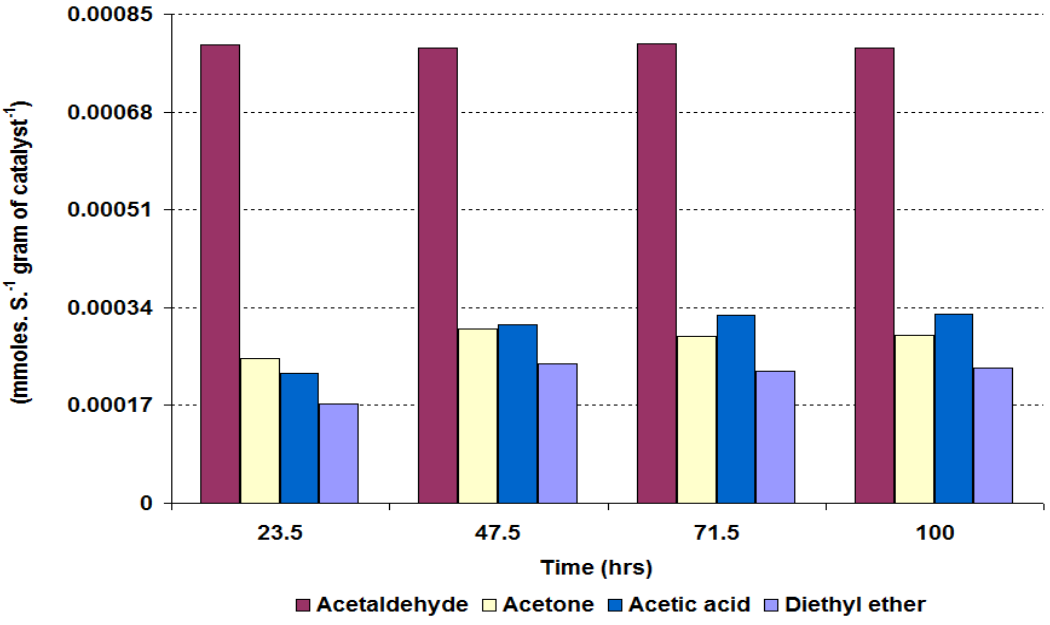

Figure 8.3-66 Rate of formation of liquid products over Pt/Al_2O_3 catalyst during the IPA impurity reaction

In the gaseous products, H_2 was produced with the highest rate and interestingly after 24 hours time on stream its rate of formation had slightly decreased. This decrease occurred

due to a fault with the Gilson pump which fed the reactants to the reactor irregularly. However, after 48 hours TOS the problem was fixed and therefore the rate of formation of H_2 steadily increased until the end of the reaction. The rate of formation of C_2H_4 followed a slightly different route compared to the pure ethanol steam reforming reaction over Pt/Al_2O_3 catalyst. In the initial 24 hours, C_2H_4 gave the highest rate of formation, although for the rest of the reaction its rate varied up to the end of the reaction. Whereas, CO, CO_2 and C_2H_6 were produced with similar rates and followed the same routes as those observed in the pure ethanol steam reforming reaction.

In the liquid products, acetaldehyde gave the highest rate of formation. Additionally the rate was stable for the duration of the reaction and no obvious deactivation was observed. However the rate of formation of acetone and acetic acid increased, whilst the rate of formation for diethyl ether decreased relative to the pure ethanol steam reforming reaction over Pt/Al_2O_3 catalyst.

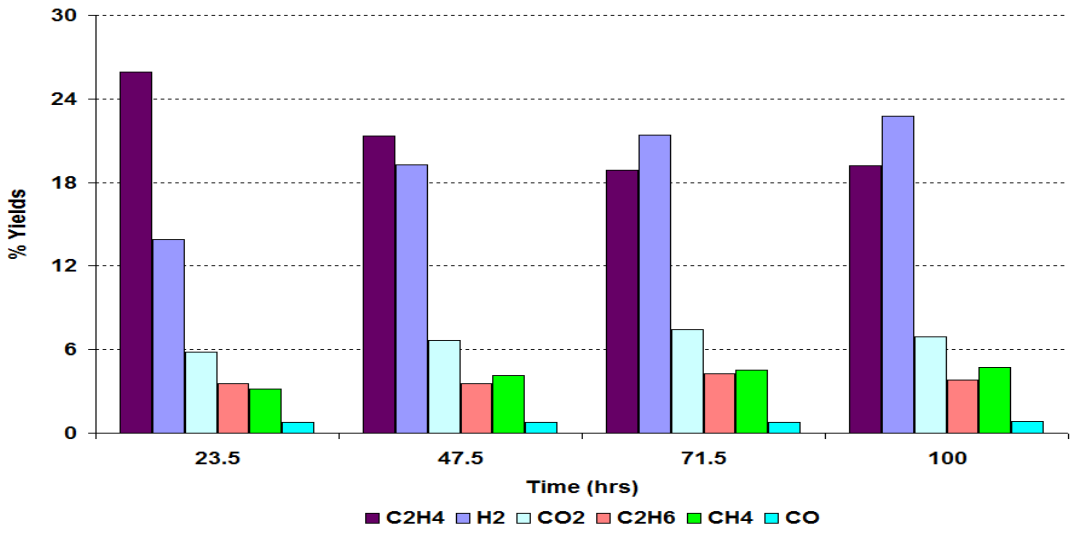

Figure 8.3-67 % Yield of gaseous products over Pt/Al_2O_3 catalyst during the IPA impurity reaction

The yield of all the gaseous products gave similar profiles to those observed in the 1-propanol impurity ethanol steam reforming reaction. In the initial 24 hours, the yield for C_2H_4 was highest in the all gaseous products, which later in the reaction was suppressed by the yield of H_2. Similarly the yield of CO_2 was slightly higher than the CO yield in ethanol steam reaction with IPA impurity.

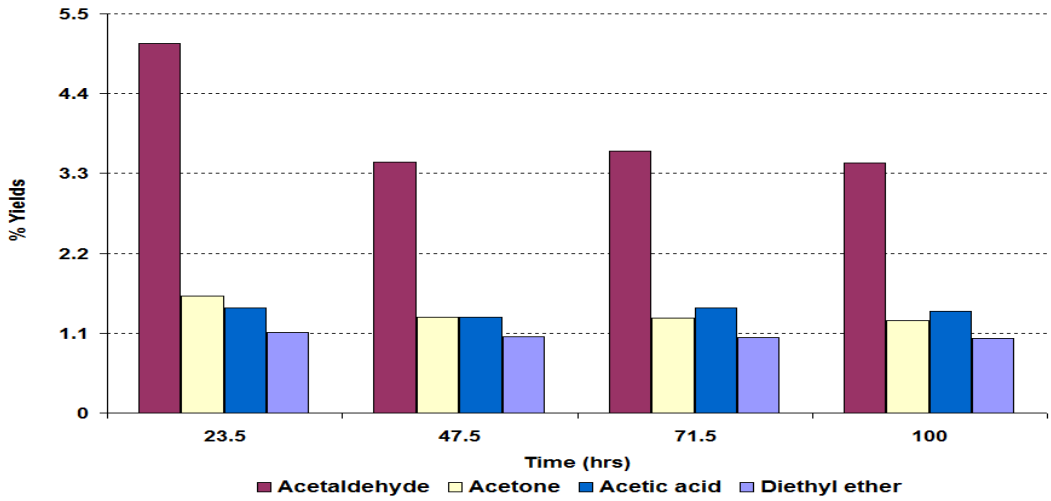

Figure 8.3-68 %Yield of liquid products over Pt/Al_2O_3 catalyst during the IPA impurity reaction

Acetaldehyde gave the maximum yield in the liquid products and achieved steady state conditions after 48 hours time on stream with no deactivation observed in the reaction. Acetone, acetic acid and diethyl ether were also produced but neither product had higher than 2% yield.

8.3.3.4 Post reaction characterisation

8.3.3.4.1 TPO

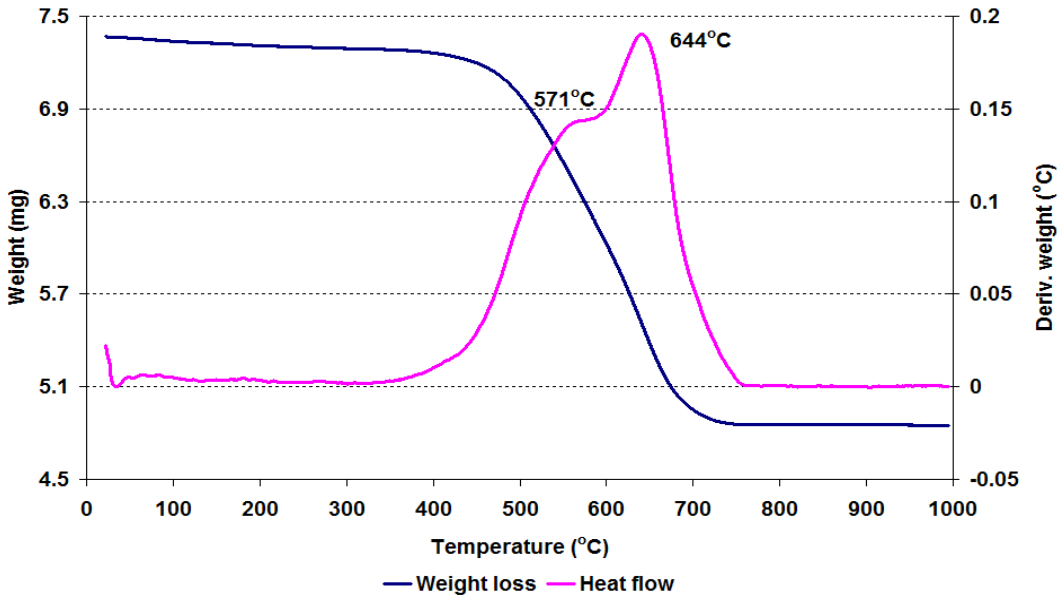

Figure 8.3-69 Post reaction TPO for Pt/Al_2O_3 catalyst following the IPA impurity reaction

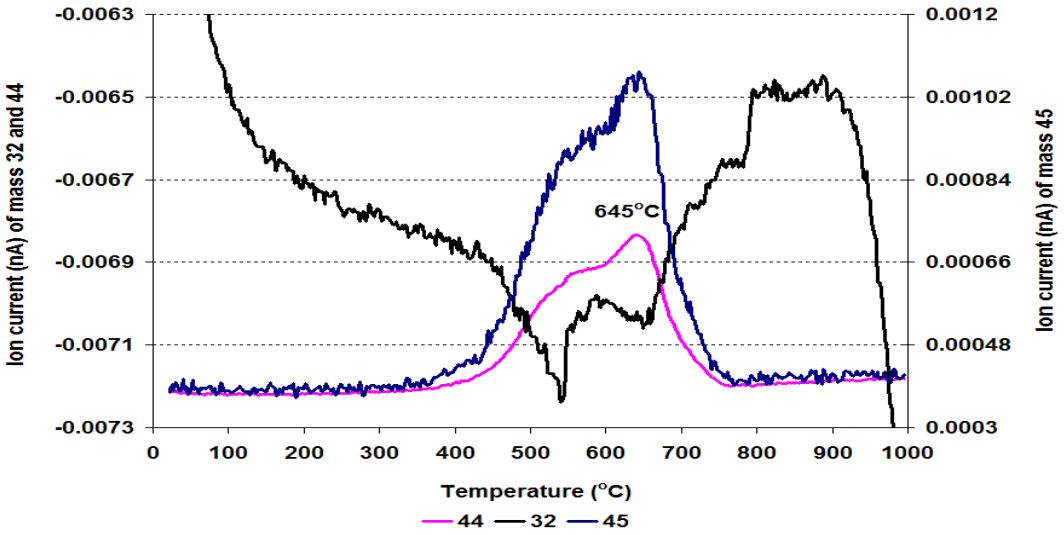

Figure 8.3-70 MS data of CO_2 (m/z=44), O_2 (m/z=32) and C_2H_5OH fragment (m/z=45) for Pt/Al_2O_3 catalyst following the IPA impurity reaction

The TPO of the spent Pt/Al_2O_3 catalyst following the IPA impurity reaction shows similar TGA profile (Figure 8.3-69) to those achieved for the 1-propanol impurity reaction sample, although the derivative weight profile illustrates that the right shoulder of the weight loss event appears at a lower temperature (644^oC) compared to 1-propanol impurity reaction sample. Additionally weight loss decreased (341 mg g^{-1} of catalyst) in the IPA impurity sample compared to the pure ethanol reaction. Like the 1-propanol sample, the weight loss at 644^oC corresponded to CO_2 and ethanol fragment in the mass spectrometry results.

The Raman analysis gave similar results to those seen in the post reaction pure ethanol sample.

8.3.3.4.2 BET analysis

Catalyst	Conditions	BET Surface area (m^2/g)	Pore volume (cm^3/g)	Average pore diameter (Å)
Pt/Al_2O_3	Pure ethanol (500^oC)	41	0.09 (± 0.81)	80 (± 3.97)
	IPA impurity	53	0.12 (± 0.61)	86 (± 4.13)

Table 8.3-9 BET analysis of post reaction Pt/Al_2O_3 catalyst following the IPA impurity reaction

Table 8.3-9 illustrates that although the BET surface area, the average pore diameter and the pore volume of the IPA impurity catalyst significantly decreased compared to the reduced Pt/Al_2O_3 catalyst these values slightly increased in contrast to the pure ethanol steam reforming reaction over Pt/Al_2O_3 catalyst.

8.3.3.5 Propanal impurity

After investigating the effect of higher alcohol groups, the influence of C_3 aldehyde groups was checked on the ethanol steam reforming reaction using a Pt/Al_2O_3 catalyst.

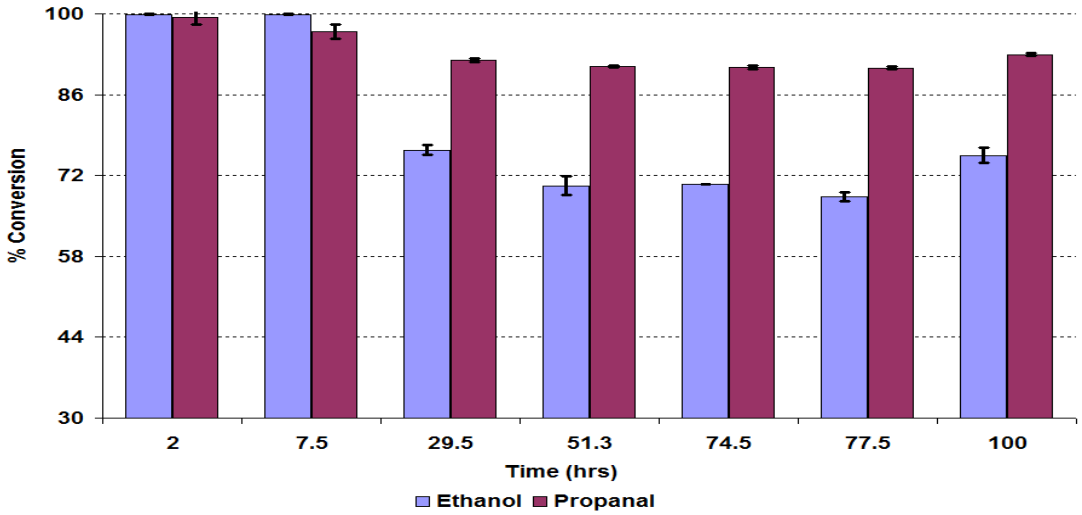

Figure 8.3-71 % Conversion of ethanol and propanal over the Pt/Al_2O_3 catalyst during the propanal impurity reaction

Figure 8.3-71 illustrates that in the initial 7.5 hours, the conversion of ethanol was 99.9%, and steadily decreased to 70% by 51.3 hours time on stream. After 51.3 hours the conversion of ethanol stabilised and continued to have the same conversion for the rest of the reaction except at the last stage where conversion slightly increased. Whereas the conversion of propanal was lower than for ethanol in the initial 24 hours. When the reaction proceeded further the conversion of propanal slightly decreased.

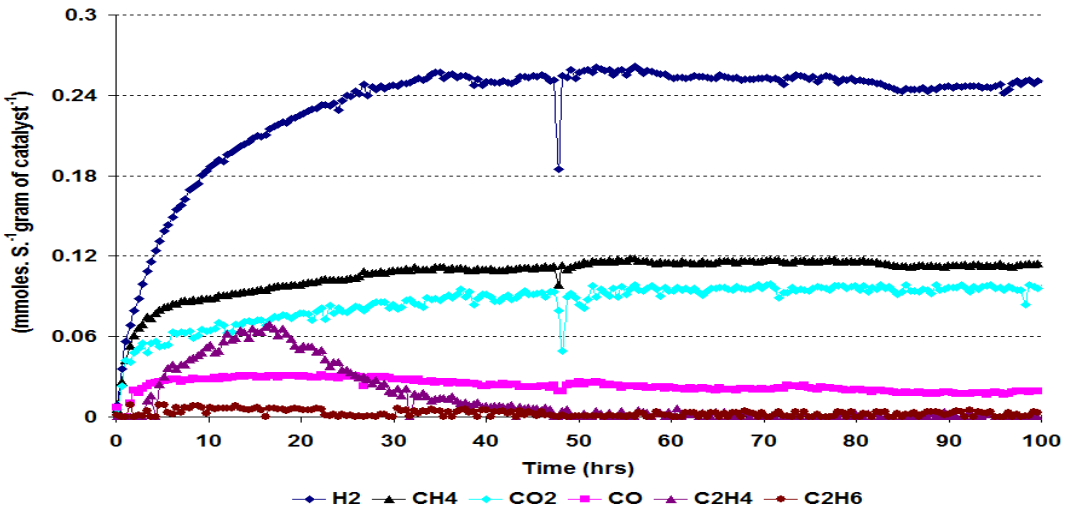

Figure 8.3-72 Rate of formation of gaseous products over Pt/Al_2O_3 catalyst during the propanal impurity reaction

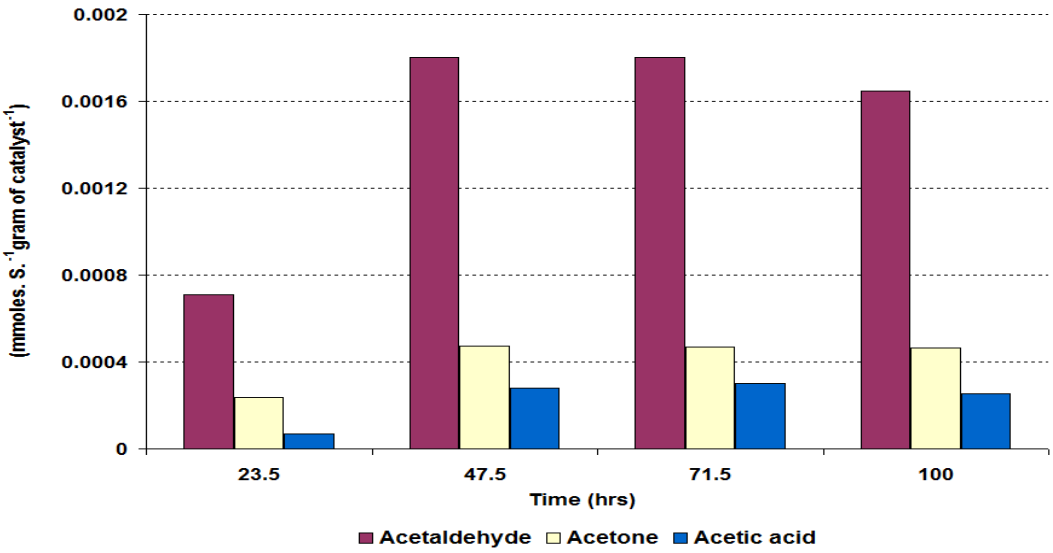

Figure 8.3-73 Rate of formation of liquid products over Pt/Al_2O_3 catalyst during the propanal impurity reaction

Figure 8.3-72 shows that the rates of formation of the gaseous products give different patterns from the pure ethanol and IPA impurity profiles over Pt/Al_2O_3 catalyst. In the propanal impurity reaction H_2 gave the highest rate of all the reactions over Pt/Al_2O_3 catalyst and achieved virtual steady state conditions after 27 hours with slight variance in its rate. Similarly, the rate of formation of C_2H_4 was significantly decreased compared to other reactions and only trace amounts were detected after 50 hours time on stream. In addition, the rates of formation of CH_4 and CO_2 were remarkably amplified and obtained steady state conditions after 50 hours time on stream. The rates of formation of CO_2 and CH_4 were even higher than the pure ethanol reaction over Pt/Al_2O_3 catalyst at 600^oC. It suggests that the reaction route for steam reforming of ethanol changed after adding the propanal impurity.

In liquid products, acetaldehyde, acetone and acetic acid were detected by GC analysis. However diethyl ether and 1,1-diethoxyethane, which were produced in significant amounts in the pure ethanol steam reforming reaction over Pt/Al_2O_3 catalyst, were detected in trace amounts.

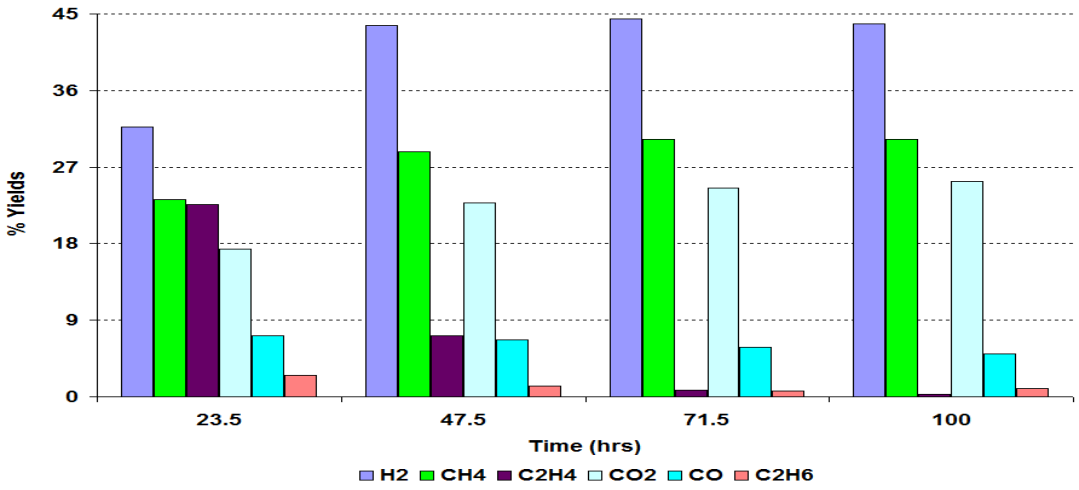

Figure 8.3-74 % Yield of gaseous products over Pt/Al_2O_3 catalyst during the propanal impurity reaction

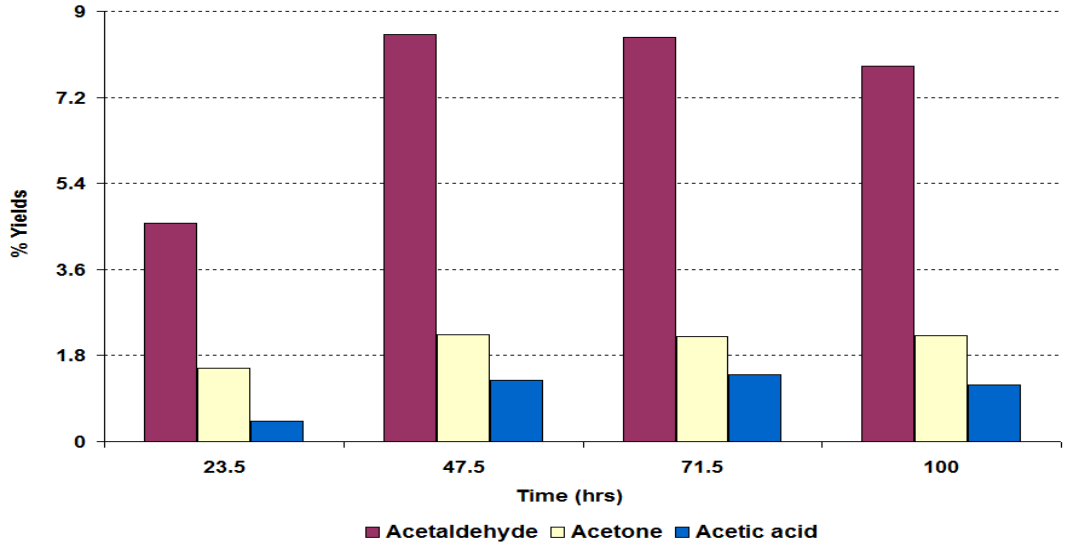

Figure 8.3-75 %Yield of liquid products over Pt/Al_2O_3 catalyst during the propanal impurity reaction

In gaseous products H_2, CH_4, and CO_2 gave the highest yields. Among these products the yield of H_2 was almost stable whilst the yield of CO_2 and CH_4 varied and slightly increased with reaction time. Whereas, the yield of C_2H_4 was significantly decreased and was almost 0% at the end of the reaction. CO and C_2H_6 were also produced in trace amounts.

Figure 8.3-75 illustrates that the yield of liquid products, which were lower compared to the gaseous products. The figure also indicates that acetaldehyde gave the highest yield of all the liquid products and obtained steady state conditions after 47.5 hours TOS. Furthermore, the yield of acetaldehyde was even higher than that observed in the IPA impurity reaction.

8.3.3.6 Post reaction characterisation

Post reaction characterisation was carried out using various techniques to determine the nature of the carbonaceous material deposited during the reaction and any change in the morphology of the Pt/Al_2O_3 catalyst.

8.3.3.6.1 TPO

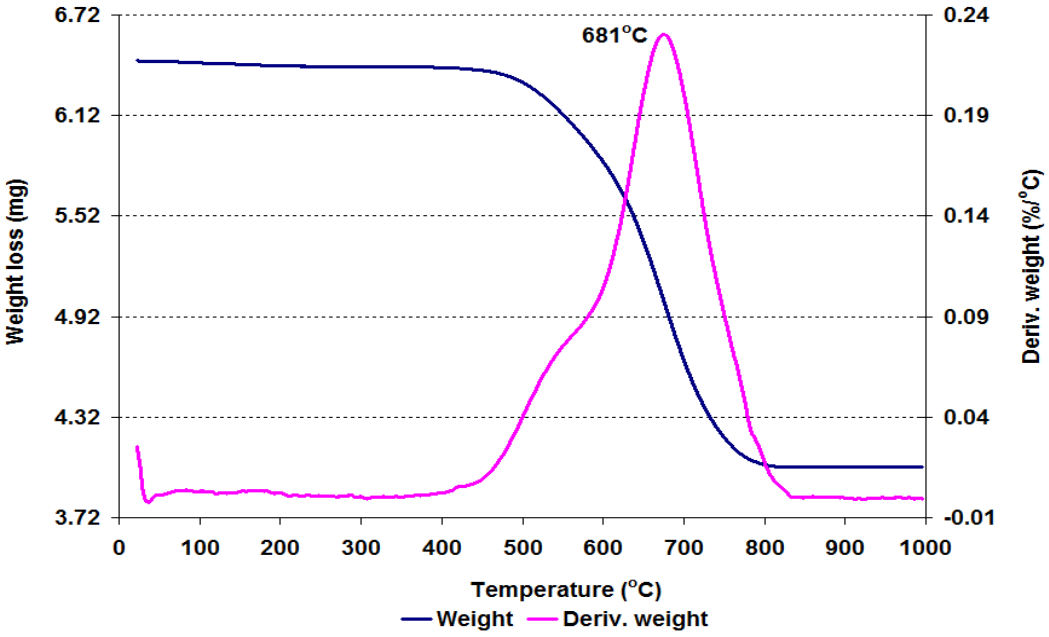

Figure 8.3-76 Post reaction TPO for Pt/Al_2O_3 catalyst following the propanal impurity reaction

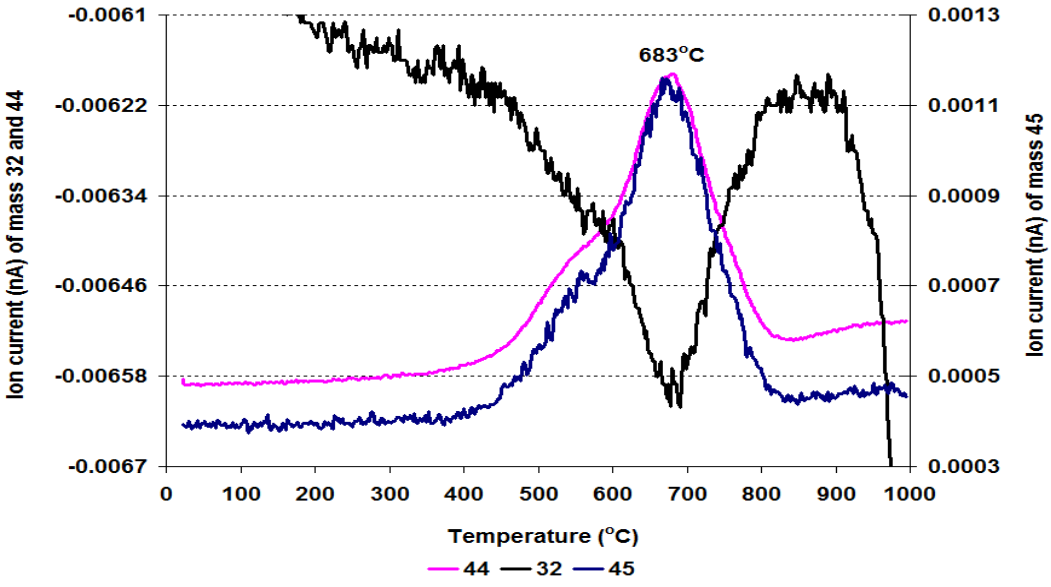

Figure 8.3-77 MS data of CO_2 (m/z=44), O_2 (m/z=32) and C_2H_5OH fragment (m/z=45) for Pt/Al_2O_3 catalyst following the propanal impurity reaction

The spent catalyst was analysed by TGA/DSC, associated with a mass spectrometer, in a 2% O_2/Ar atmosphere. The results obtained show that 374.5 mg g^{-1} of catalyst weight loss took place in the range between 25°C and 1000°C. Unexpectedly, there was an increased weight loss compared to that observed for the IPA sample. Like previous samples these changes in the mass of catalyst corresponded to the evolution of CO_2 and C_2H_5OH fragment in mass spectrometry results.

8.3.3.6.2 Raman analysis

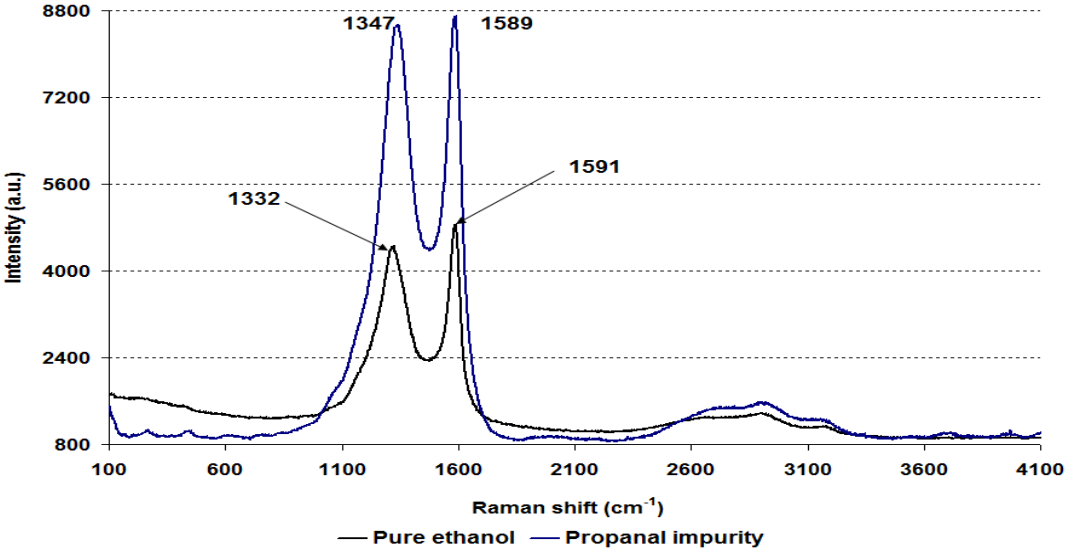

Figure 8.3-78 Post reaction Raman spectra for Pt/Al_2O_3 catalyst following the propanal impurity reaction

The Raman spectra of both the pure ethanol and the propanal impurity spent catalysts were plotted and are shown in Figure 8.3-78. The above figure illustrates that with the propanal impurity catalyst the lower wavenumber band shifted upward and the intensity of the bands was significantly increased. This suggests that the amount of graphitic coke on the catalyst surface had changed significantly.

8.3.3.6.3 BET analysis

Catalyst	Conditions	BET Surface area (m^2/g)	Pore volume (cm^3/g)	Average pore diameter (Å)
Pt/Al_2O_3	Pure ethanol (500°C)	41	0.09 (± 0.81)	80 (± 3.97)
	Propanal impurity	31	0.07 (± 0.96)	96 (± 4.54)

Table 8.3-10 BET analysis of post reaction Pt/Al_2O_3 catalyst following the propanal impurity reaction

Table 8.3-10 shows that the BET surface area and the pore volume of the post reaction propanal impurity catalyst decreased compared to pure ethanol post reaction catalyst. However the average pore diameter increased.

8.3.3.7 Propylamine impurity

A propylamine impurity was added to water/ethanol mixture to examine its influence on the steam reforming of ethanol reaction over a Pt/Al_2O_3 catalyst at 500^{o}C.

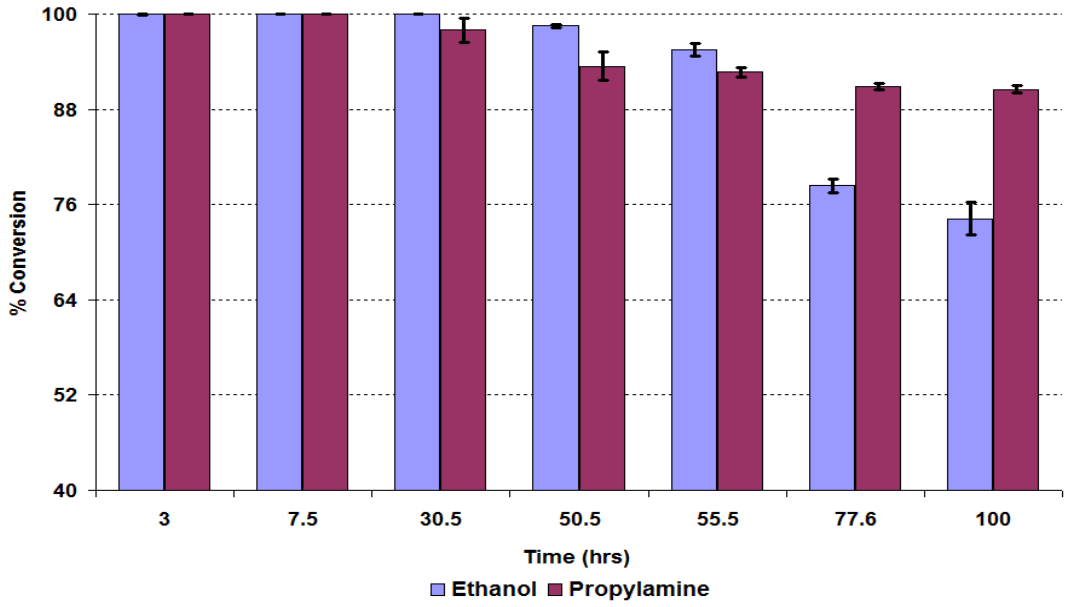

Figure 8.3-79 % Conversion of ethanol and propylamine over Pt/Al_2O_3 catalyst during the propylamine impurity reaction

Figure 8.3-79 illustrates that the conversion of ethanol in the initial 30 hours was high with a value of 99.96%. However after 30 hours time on stream, the ethanol conversion started to decrease continuously until the end of the reaction. Similarly, the propylamine conversion was high in the initial 30 hours. However, its deactivation started earlier than for ethanol but at the end of the reaction the conversion of propylamine was higher than that of ethanol.

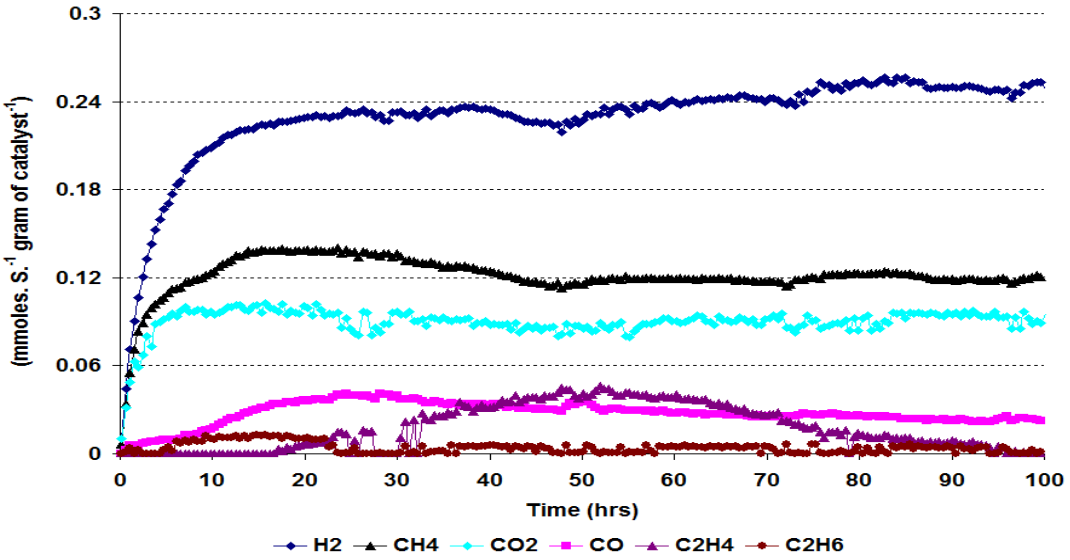

Figure 8.3-80 Rate of formation of gaseous products over Pt/Al_2O_3 catalyst during the propylamine impurity reaction

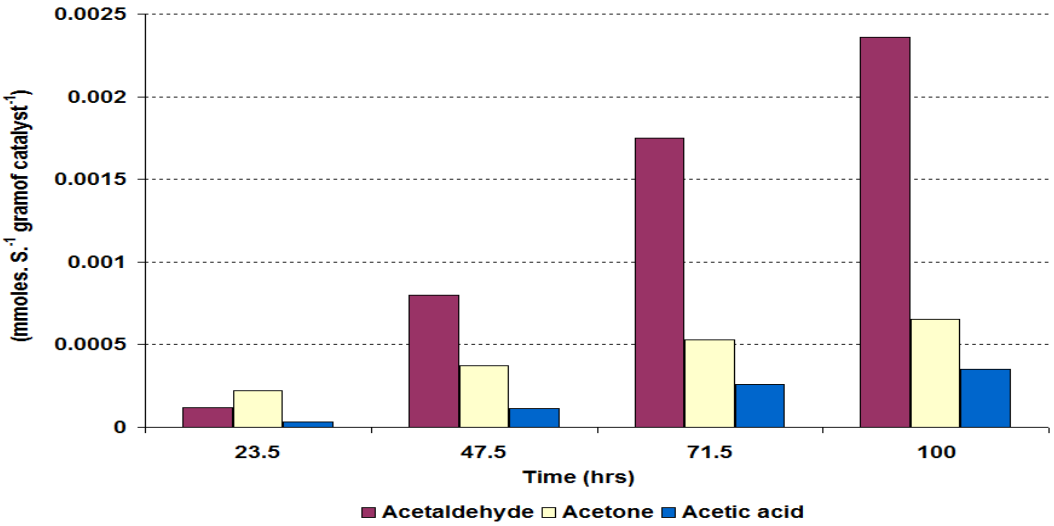

Figure 8.3-81 Rate of formation of liquid products over Pt/Al_2O_3 catalyst during the propylamine impurity reaction

The gaseous products distribution for the propylamine impurity reaction gave a similar profile to that observed in the propanal impurity reaction *i.e.* H_2, CH_4 and CO_2 were produced with the highest rates. However, the rate of formation of each gaseous product followed slightly different patterns. The rate of formation of H_2 steadily increased up to the end of the reaction but did not achieve steady state conditions during the reaction. Similarly the CO_2 and CH_4 rate of formation gave higher rates in the initial 48 hours, which then stabilised and until the end of the reaction there was no deactivation observed. The rate of formation of C_2H_4 shows interesting results. In an initial 17 hours TOS, no significant amounts of C_2H_4 was observed. However, after 17 hours of reaction C_2H_4

began to be produced and showed steady increase up until 50 hours time on stream when the rate started to decrease.

Figure 8.3-81 shows rates of formation of the liquid products produced in the propylamine impurity reaction over Pt/Al_2O_3 catalyst. Besides the products mentioned in Figure 8.3-81, methanol and diethyl ether were also detected by the GC. The graph in Figure 8.3-81 illustrates that the rate of formation of all the liquid products steadily increased with time, however, none of them obtained steady state conditions during the reaction.

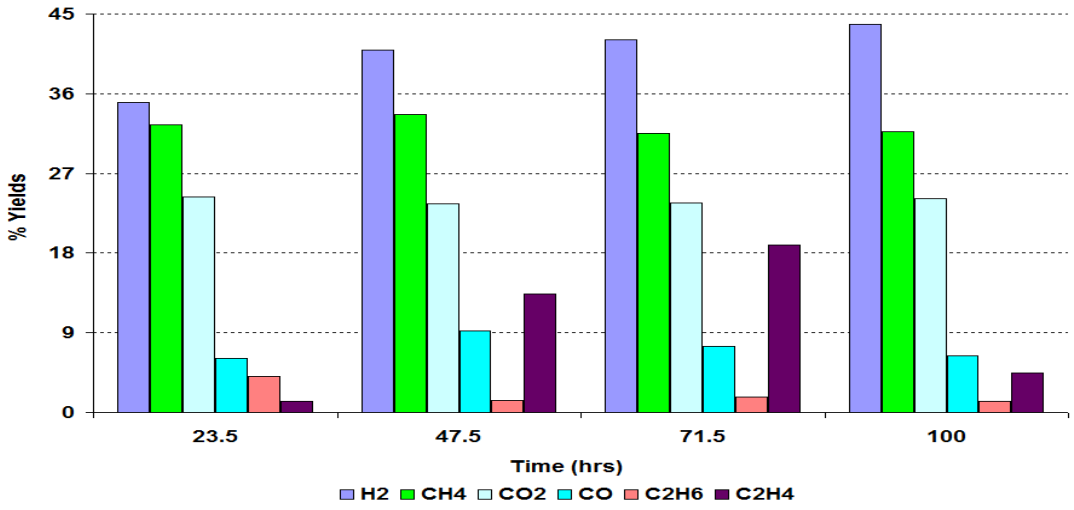

Figure 8.3-82 % Yield of gaseous products over Pt/Al_2O_3 catalyst during the propylamine impurity reaction

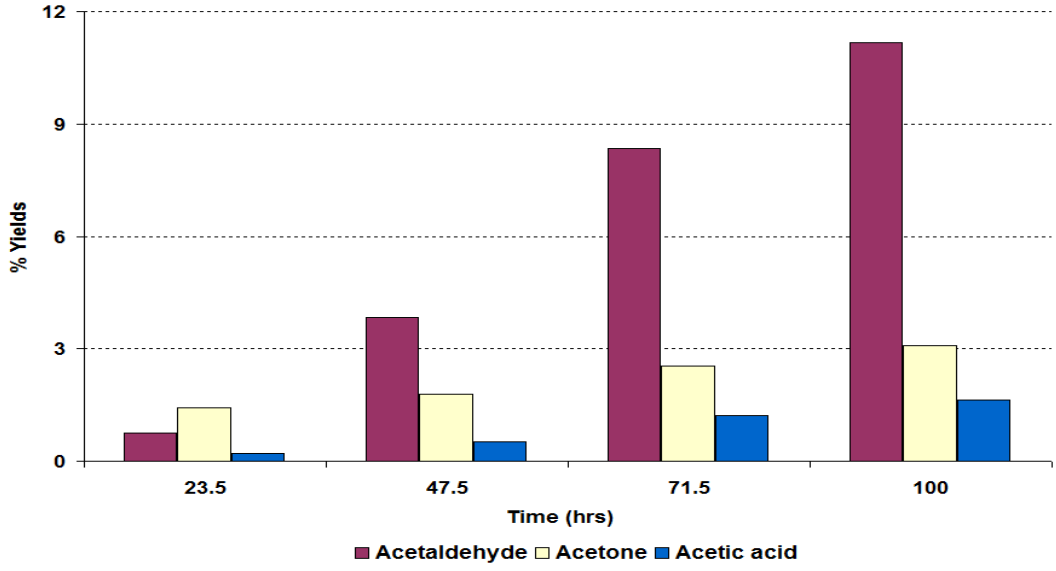

Figure 8.3-83 %Yield of liquid products over Pt/Al_2O_3 catalyst during the propylamine impurity reaction

The yields of the gaseous products followed similar patterns to those observed for the propanal impurity reaction over Pt/Al_2O_3 catalyst. H_2 gave the highest yield which varied slightly during the reaction with the maximum yield obtained being 44%. The yields of CO_2 and CH_4 decreased in the initial 48 hours and then stabilised for the rest of the reaction. The yield of liquid continuously increased and the maximum yields obtained at the end of reaction for acetaldehyde, acetone and acetic acid were 11%, 3% and ~ 2% respectively.

8.3.3.8 Post reaction characterisation

8.3.3.8.1 TPO

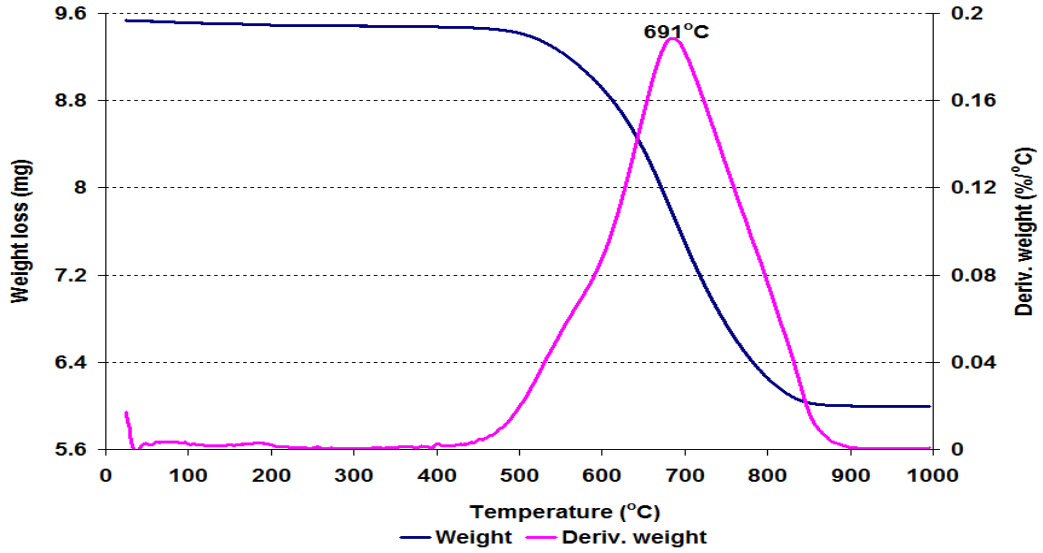

Figure 8.3-84 Post reaction TPO for Pt/Al_2O_3 catalyst following the propylamine impurity reaction

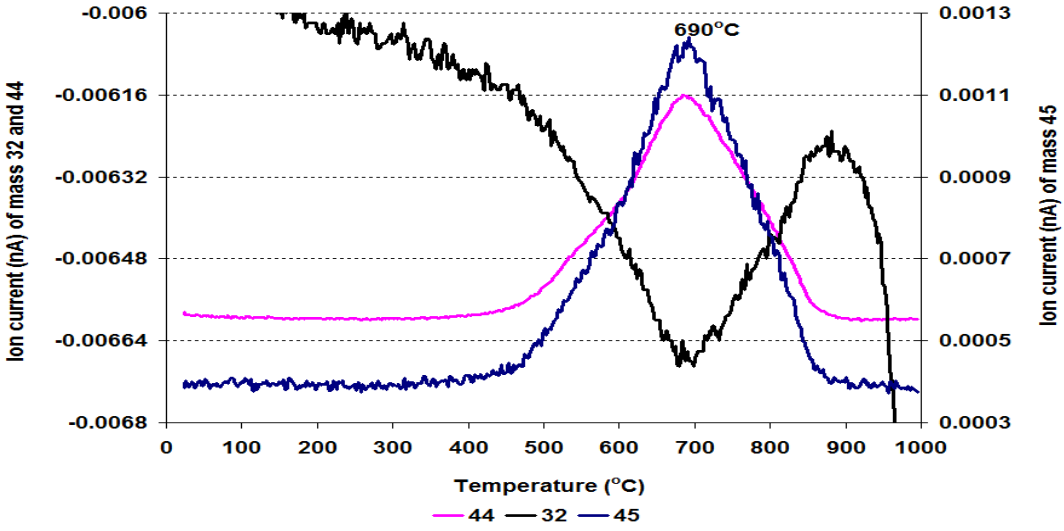

Figure 8.3-85 MS data of CO_2 (m/z=44), O_2 (m/z=32) and C_2H_5OH fragment (m/z=45) for Pt/Al_2O_3 catalyst following the propylamine impurity reaction

One major weight loss event was observed in the region between 400°C and 903°C when the sample was characterised by TGA/DSC up to 1000°C. The weight loss event as usual corresponded to desorption of CO_2 and C_2H_5OH fragment and the consumption of O_2 in the mass spectrometry profiles.

8.3.3.8.2 Raman analysis

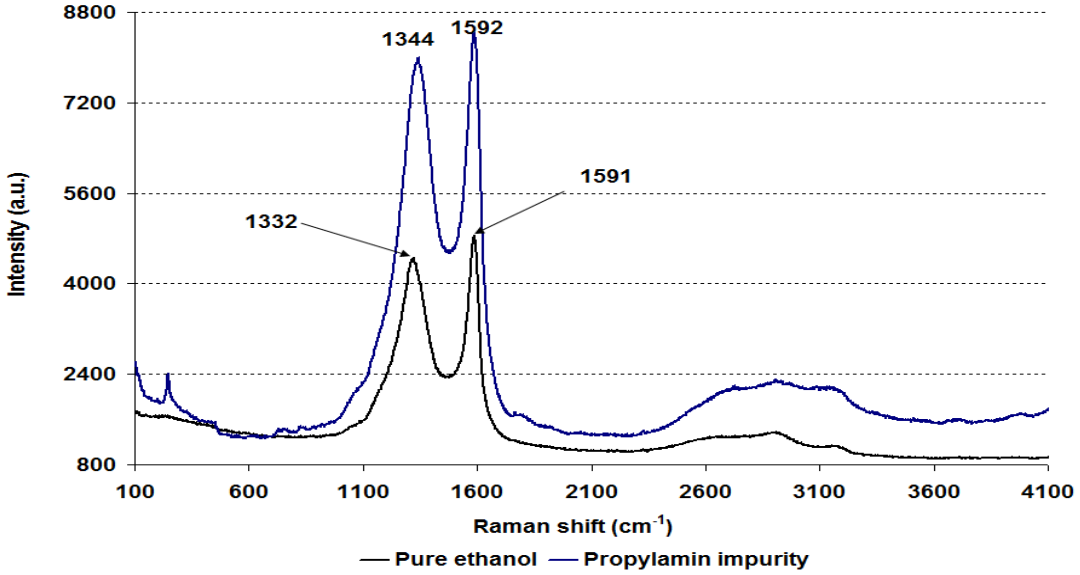

Figure 8.3-86 Post reaction Raman spectra for Pt/Al_2O_3 catalyst following the propylamine impurity reaction

The Raman spectra (Figure 8.3-86) of the post reaction Pt/Al_2O_3 catalysts used in steam reforming of ethanol with a propylamine impurity and pure ethanol steam reforming reactions were compared. The Raman spectra display a reaction change in the post propylamine impurity sample compared to the pure ethanol sample and shows that the intensity of both main bands considerably increased. Also, the lower wavenumber band shifted upwards.

8.3.3.8.3 BET analysis

Catalyst	Conditions	BET Surface area (m^2/g)	Pore volume (cm^3/g)	Average pore diameter (Å)
Pt/Al_2O_3	Pure ethanol (500°C)	41	0.09 (± 0.81)	80 (± 3.97)
	Propylamine impurity	34	0.07 (± 0.66)	88 (± 5.99)

Table 8.3-11 BET analysis of post reaction Pt/Al_2O_3 catalyst following the propylamine impurity reaction

The BET analysis shown in Table 8.3-11 illustrates that the BET surface area and the pore volume slightly decreased, while the average pore diameter increased in the propylamine sample compared to the pure ethanol post reaction sample.

8.3.3.9 Acetone impurity

To complete the impurities investigation, the reaction was performed over a Pt/Al_2O_3 catalyst at 500^oC using an water/ethanol mixture with 1mol.% acetone impurity in reference to ethanol content to further investigate the effect of impurities on the steam reforming of ethanol reaction.

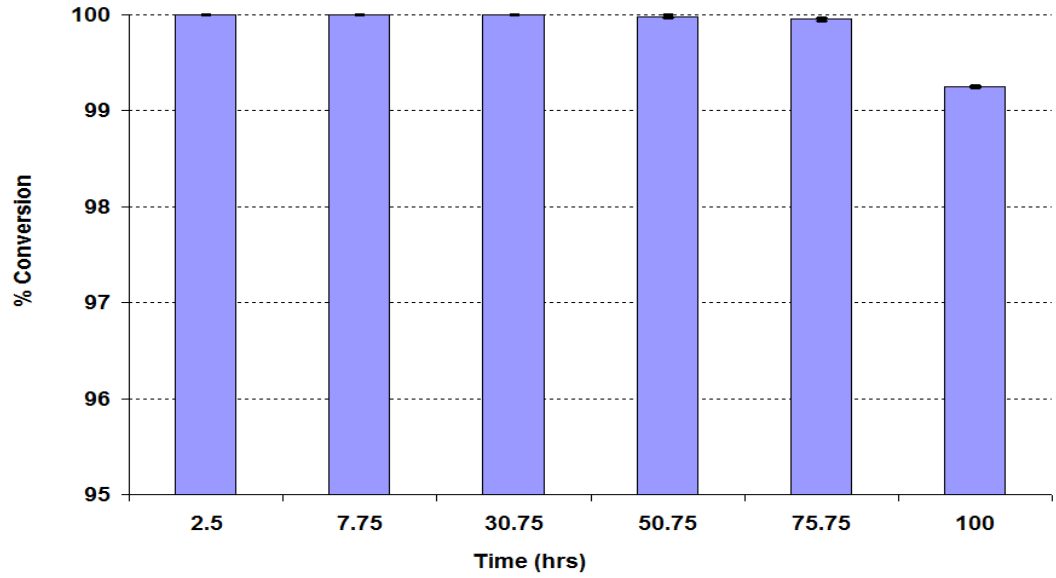

Figure 8.3-87 % Conversion of ethanol over Pt/Al_2O_3 catalyst during the acetone impurity reaction

The conversion of ethanol over a Pt/Al_2O_3 catalyst with an acetone impurity is shown in Figure 8.3-87. The figure reveals that throughout the reaction no significant deactivation of the catalyst took place and up to the end of the reaction the conversion of ethanol had only decreased from 100% to 99.2%.

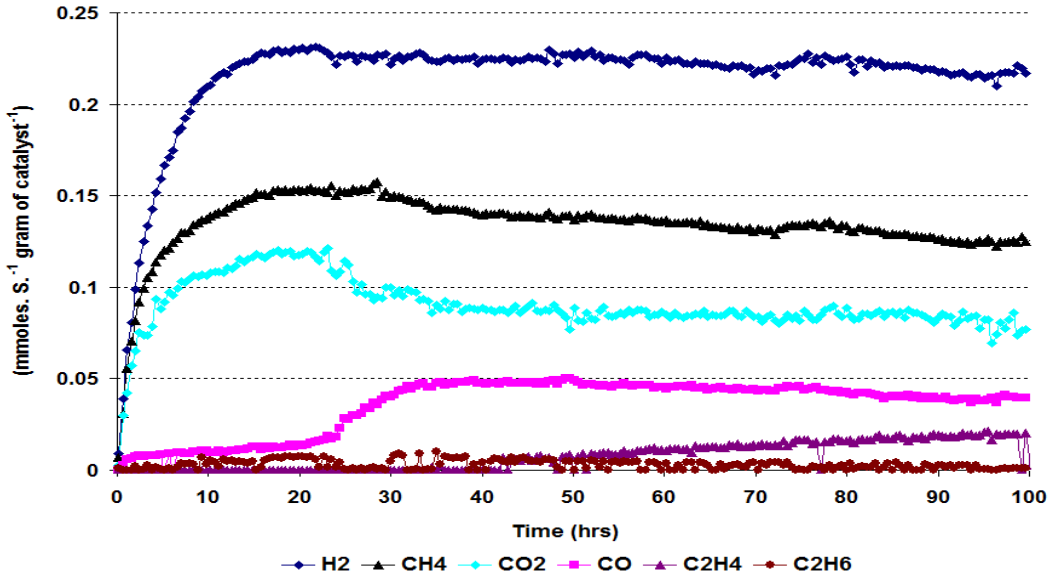

Figure 8.3-88 Rate of formation of gaseous products over Pt/Al_2O_3 catalyst during the acetone impurity reaction

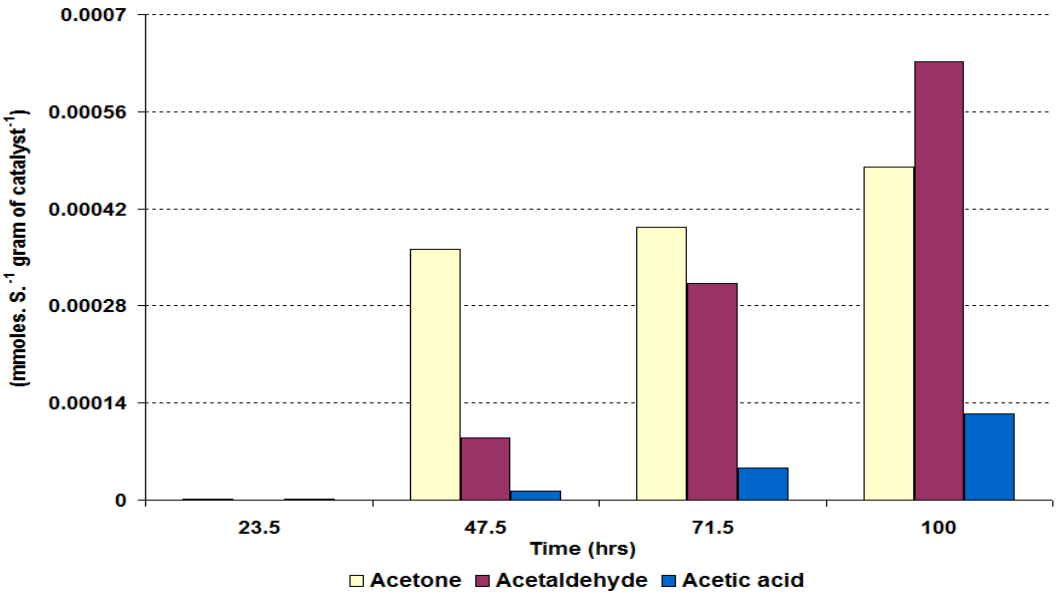

Figure 8.3-89 Rate of formation of liquid products over Pt/Al_2O_3 catalyst during the acetone impurity reaction

The rate of formation of the gaseous products in the ethanol steam reforming reaction with an acetone impurity gave interesting results. Figure 8.3-88 illustrates that in the initial 24 hours, the rates of formation of H_2, CH_4 and CO_2 were high whilst the rate of formation of CO was low. However, as the reaction proceeded the rate of formation of CO abruptly increased whilst those of CO_2, CH_4 and H_2 were slightly decreased. In addition the graph in Figure 8.3-89 shows that the liquid products only started to be produced after 24 hours time on stream. After the initial increase in the rate of formation of CO, like the other

gaseous products it slowly decreased until the end of the reaction. Interestingly in the initial 43 hours, no C_2H_4 was detected. However, after 43 hours it started to be produced and increased with reaction time.

Figure 8.3-89 illustrates the rates of formation of the liquid products. In the initial 24 hours no liquid products were detected however, after 24 hours time on stream, acetone, acetaldehyde and acetic acid were detected and their rates of formation increased with reaction time. Initially the rate of formation of acetone was higher than that of acetaldehyde and by the end of reaction the rate of formation of acetaldehyde exceeded the rate of formation of acetone.

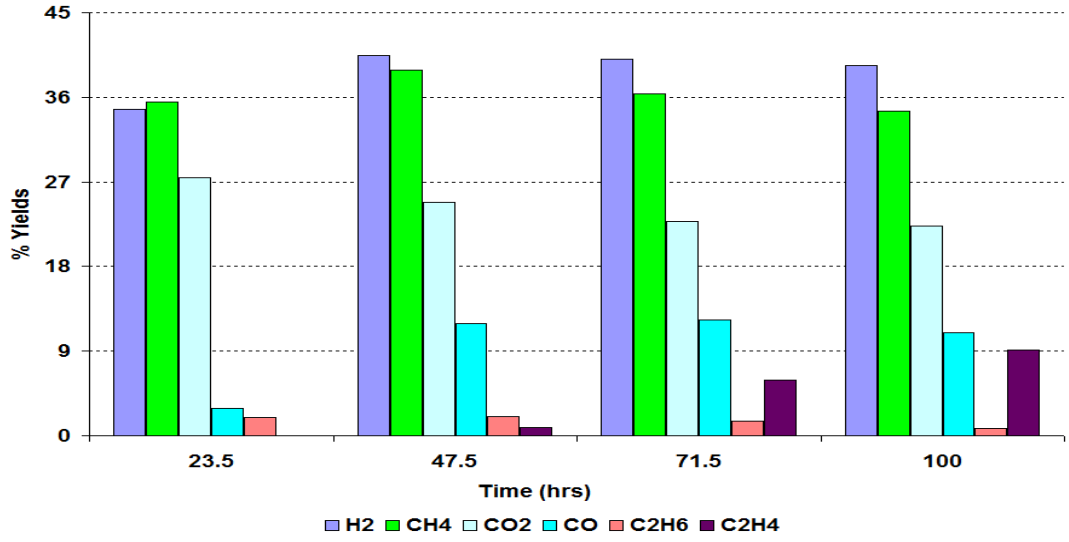

Figure 8.3-90 % Yield of gaseous products over Pt/Al_2O_3 catalyst during the acetone impurity reaction

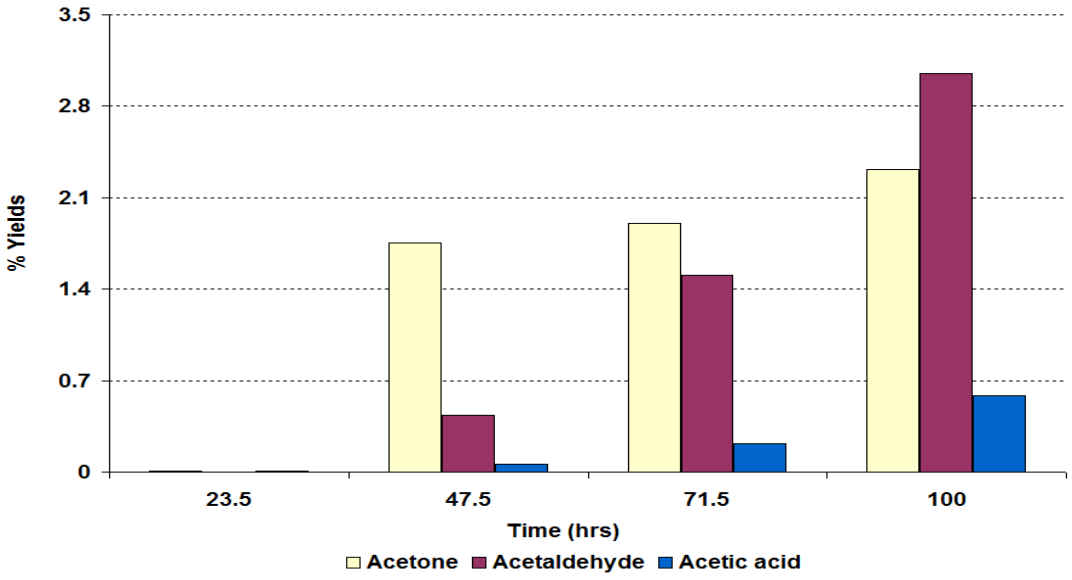

Figure 8.3-91 %Yield of liquid products over Pt/Al_2O_3 catalyst during the acetone impurity reaction

The yields for the formation of the gaseous products were calculated as discussed in section 7.2.5 and the data obtained was plotted as a function of time and is shown in the Figure 8.3-90. The figure shows that out of all gaseous products H_2, CH_4 and CO_2 gave the highest yields. After the initial 24 hours, no significant change in the yields of the major gaseous products took place, and the values remained stable for the rest of the reaction. The yield of CO varied during the reaction time whilst that of C_2H_4 increased as the reaction proceeded.

All the liquid products gave low yields initially which increased with reaction time. The maximum yields obtained for acetaldehyde, acetone and acetic acid were 3%, 2.2% and 0.6% respectively at the end of the reaction.

8.3.3.10 Post reaction characterisation

Post reaction characterisation was carried out using various techniques on the spent catalyst.

8.3.3.10.1 TPO

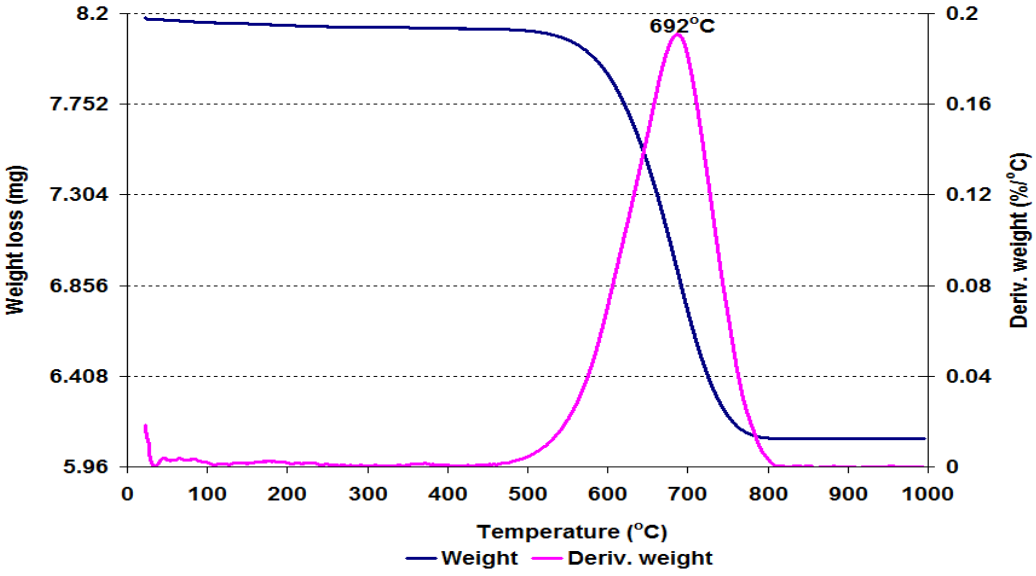

Figure 8.3-92 Post reaction TPO for Pt/Al_2O_3 catalyst following the acetone impurity reaction

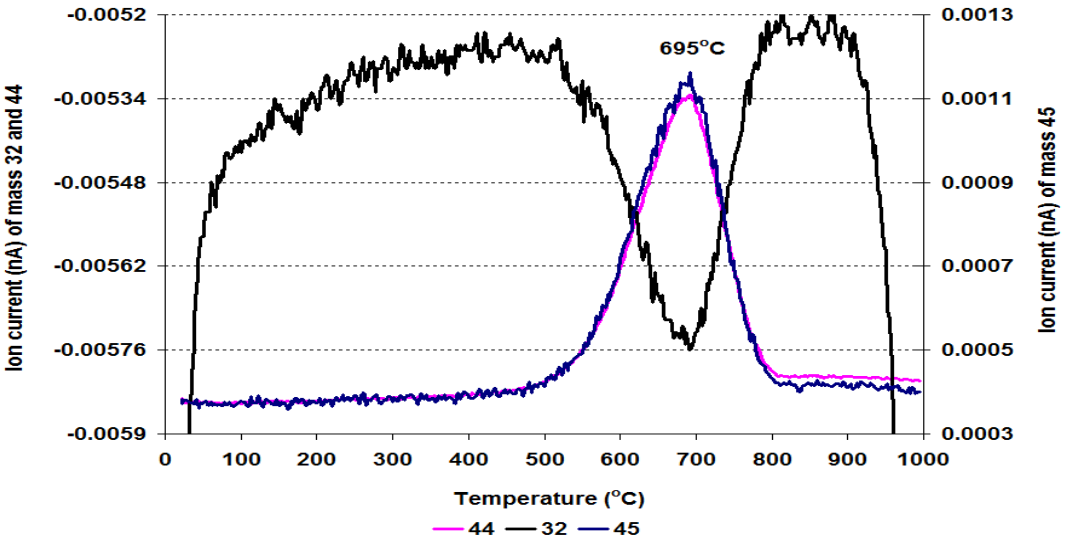

Figure 8.3-93 MS data of CO_2 (m/z=44), O_2 (m/z=32) and C_2H_5OH fragment (m/z=45) for Pt/Al_2O_3 catalyst following the acetone impurity reaction

The spent catalyst was run on a TGA/DSC in a 2% O_2/Ar atmosphere and the results collected were plotted versus temperature and are shown in Figure 8.3-92. The graph illustrates that total weight loss of 254.1 mg g^{-1} of catalyst took place in the temperature range of 22°C to 1000°C. The figure also reveals that the main weight loss event occurred between 450°C and 805°C. In the mass spectrometry results, this weight loss corresponded to the evolution of CO_2, C_2H_5OH fragment and a trace amount of water.

8.3.3.10.2 Raman analysis

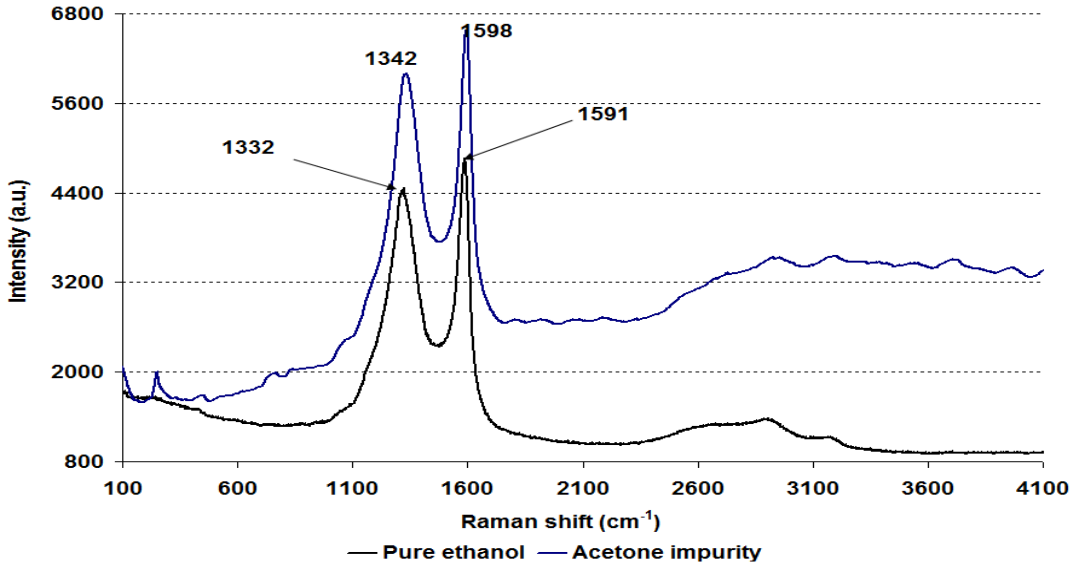

Figure 8.3-94 Post reaction Raman spectra for Pt/Al_2O_3 catalyst following the acetone impurity reaction

Figure 8.3-94 shows that pure ethanol and acetone impurity samples gave similar peaks in the Raman analysis, although in acetone impurity the peaks had drifted slightly upwards.

8.3.3.10.3 BET analysis

Catalyst	Conditions	BET Surface area (m^2/g)	Pore volume (cm^3/g)	Average pore diameter (Å)
Pt/Al_2O_3	Pure ethanol (500°C)	41	0.09 (± 0.81)	80 (± 3.97)
	Acetone impurity	57	0.17 (± 0.33)	120 (± 5.30)

Table 8.3-12 BET analysis of post reaction Pt/Al_2O_3 catalyst following the acetone impurity reaction

Table 8.3-12 illustrates that the BET surface area, the average pore diameter and the pore volume of acetone impurity catalyst significantly increased compared to pure ethanol sample. This suggests that less blocking of pores by coke took place.

8.3.4 Rh/Al_2O_3

After investigating the influence of five different types of impurities over Ru/Al_2O_3 and Pt/Al_2O_3 catalysts, the investigation programmed to the effects of these impurities on the steam reforming of ethanol using a Rh/Al_2O_3 catalyst at 500°C following the same reaction procedure as was discussed in section 7.2.2.

8.3.4.1 1-Propanol impurity

Like the previous catalysts, the effect of 1-propanol impurity was tested first over the Rh/Al_2O_3 catalyst and is discussed in the following section.

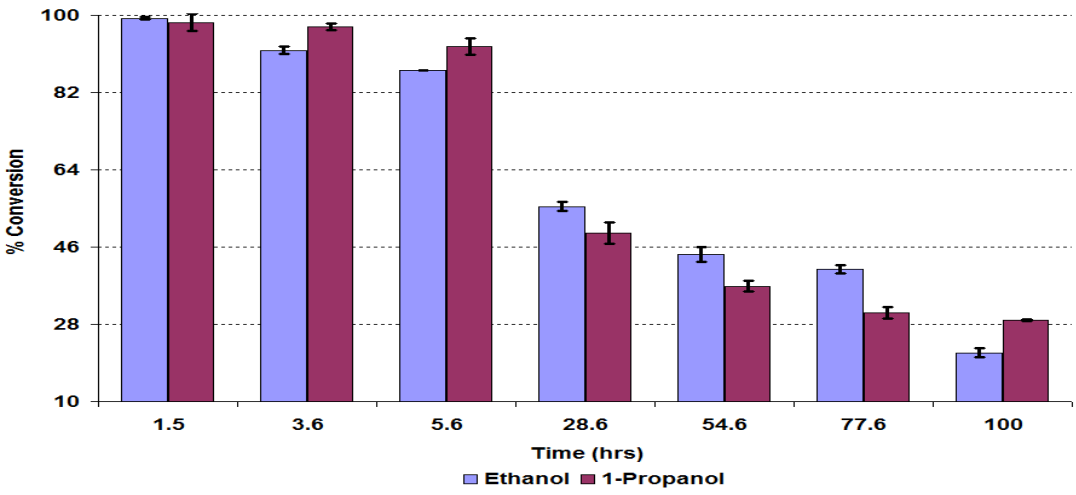

Figure 8.3-95 % Conversion of ethanol and 1-propanol over Rh/Al_2O_3 catalyst during the 1-propanol impurity reaction

The conversion of ethanol and 1-propanol were calculated and plotted as a function of time and are shown in Figure 8.3-95. The figure illustrates that in the initial first hour the conversion of ethanol was slightly higher than for the pure ethanol steam reforming reaction over the Rh/Al_2O_3 catalyst. However, a significant change in the conversion of ethanol was observed after 5.6 hours, which continuously decreased over the course of the reaction. The conversion of 1-propanol gave a similar profile to that of Pt/Al_2O_3 catalyst *i.e.* the conversion of 1-propanol was slightly lower than the conversion of ethanol after 5.6 hours TOS.

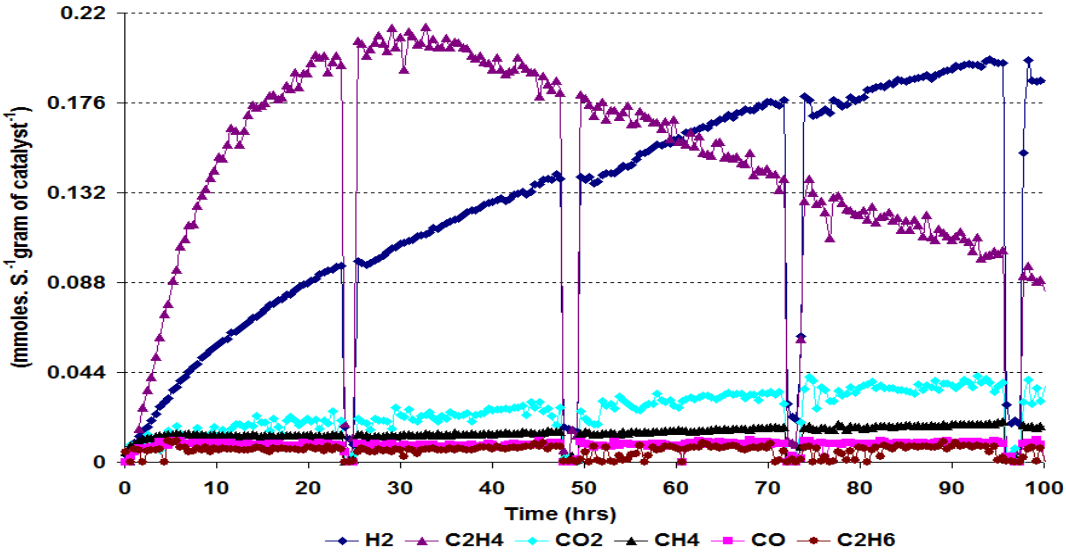

Figure 8.3-96 Rate of formation of gaseous products over Rh/Al_2O_3 catalyst during the 1-propanol impurity reaction

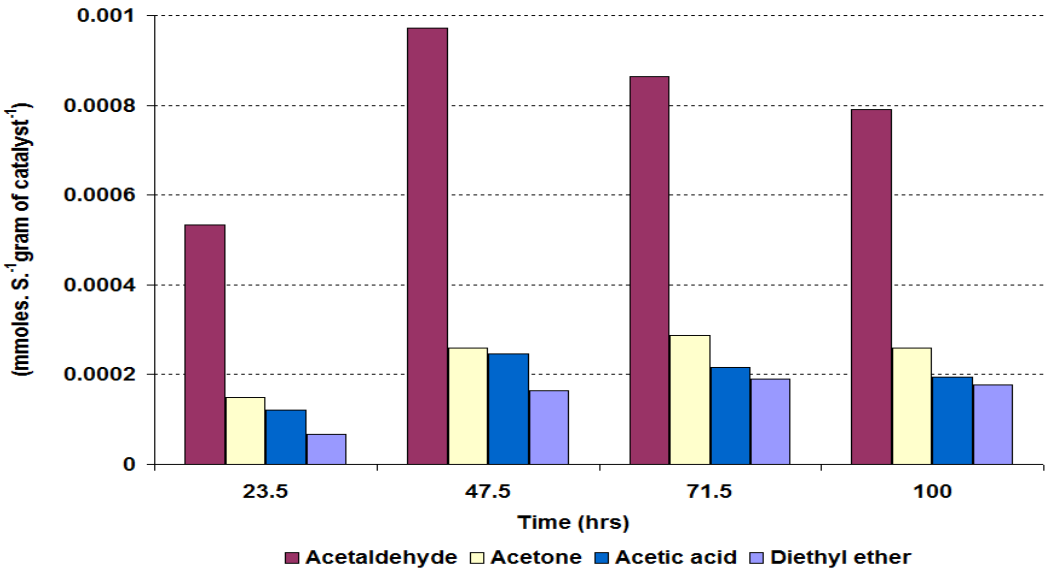

Figure 8.3-97 Rate of formation of liquid products over Rh/Al_2O_3 catalyst during the 1-propanol impurity reaction

The rates of formation of all the gaseous products over the Rh/Al_2O_3 catalyst with a 1-propanol impurity are shown in Figure 8.3-96. The figure shows that all the gaseous products were produced at lower rates than in the pure ethanol steam reforming reaction except for C_2H_4 and CO_2 in the later stages of the reaction whose rate exceeded that of CO_2 in the pure ethanol reaction. From Figure 8.3-96 it should be emphasised that throughout the entire reaction duration none of the major gaseous products *i.e.* H_2, C_2H_4 and CO_2 achieved steady state conditions. Figure 8.3-96 also shows that when the rate of formation of C_2H_4 was high then H_2 was produced at a lower rate. However, as the rate of formation of C_2H_4 decreased the rate of formation of H_2 increased.

In the liquid products, acetaldehyde, acetone, acetic acid and diethyl ether were produced. Like the 1-propanol impurity reaction over Pt/Al_2O_3 catalyst, acetaldehyde was produced with highest rate of formation. Compared to the pure ethanol reaction, the acetaldehyde was produced at lower rate in the 1-propanol reaction over Rh/Al_2O_3 catalyst. Methanol and 1,1-diethoxyethane were also detected by the GC.

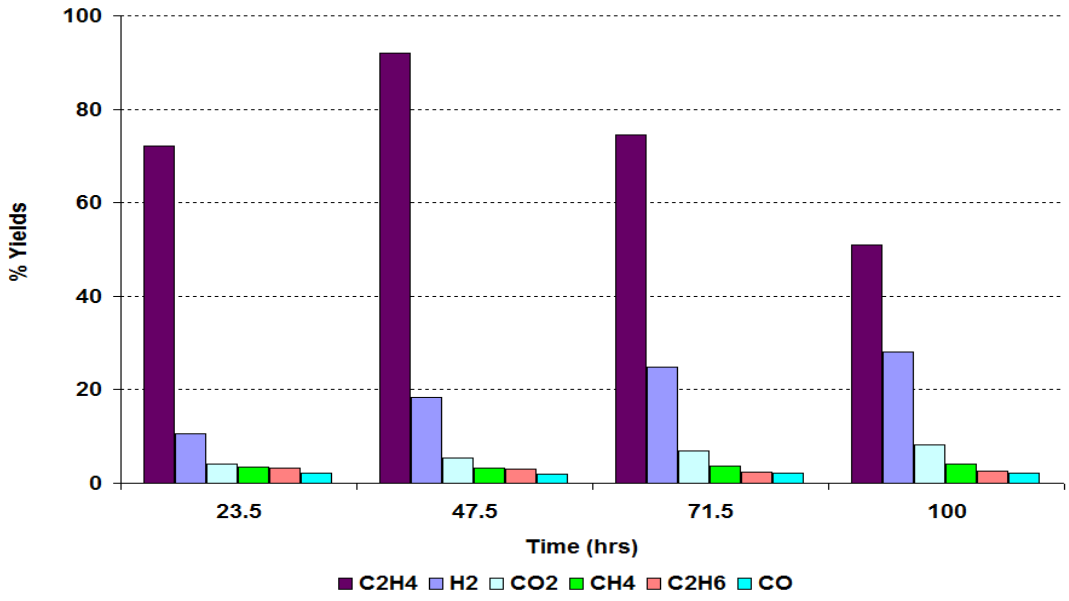

Figure 8.3-98 % Yield of gaseous products over Rh/Al_2O_3 catalyst during the 1-propanol impurity reaction

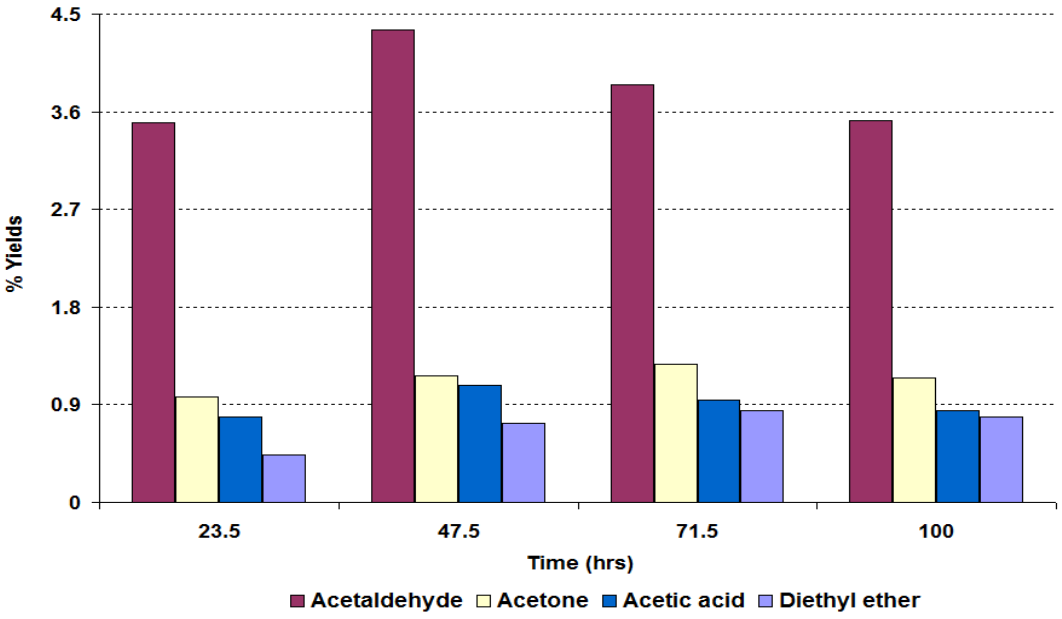

Figure 8.3-99 % Yield of liquid products over Rh/Al_2O_3 catalyst during the 1-propanol impurity reaction

Of all the gaseous products C_2H_4 gave the maximum yield in 1-propanol impurity reaction over Rh/Al_2O_3 catalyst. The yield of C_2H_4 was also higher than the yield of C_2H_4 in the pure ethanol steam reforming reaction over Rh/Al_2O_3 catalyst. However the yield of C_2H_4 did not stabilise and varied throughout the entire reaction. H_2 was the other major gaseous product which increased with the reaction time, although its yield was less than for the pure ethanol reaction. The other gaseous products produced in 1-propanol impurity reaction with minor yields and had yields less than 6%.

Figure 8.3-99 displays the yields of the liquid products produced in 1-propanol impurity reaction over Rh/Al_2O_3 catalyst. The figure illustrates that acetaldehyde gave the highest yield. However, its yield was less than in the pure ethanol reaction over Rh/Al_2O_3 catalyst. Interestingly, acetic acid, which was not observed in pure ethanol reaction over Rh/Al_2O_3 catalyst, was detected in the 1-propanol impurity reaction.

8.3.4.2 Post reaction characterisation

8.3.4.2.1 TPO

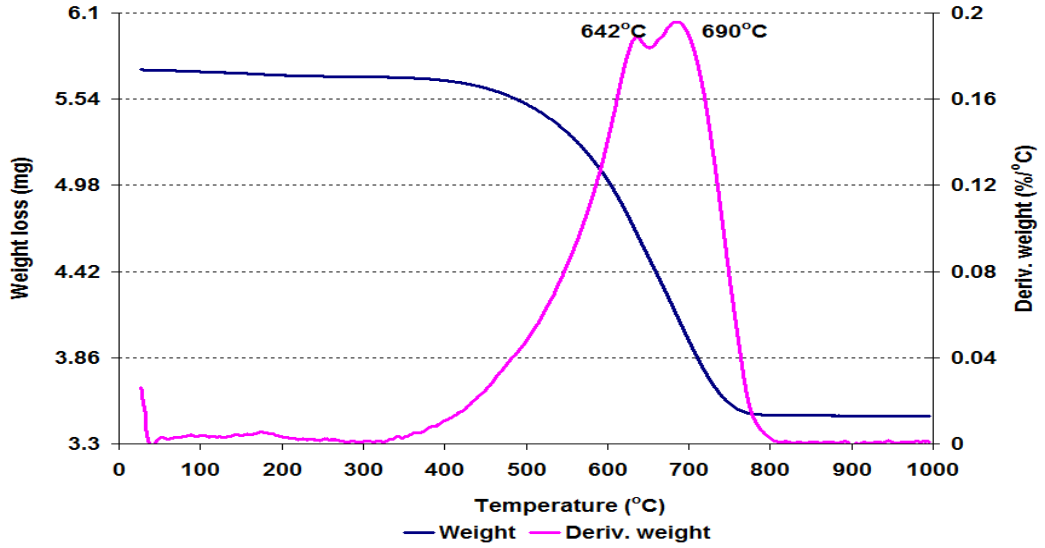

Figure 8.3-100 Post reaction TPO for Rh/Al_2O_3 catalyst following the 1-propanol impurity reaction

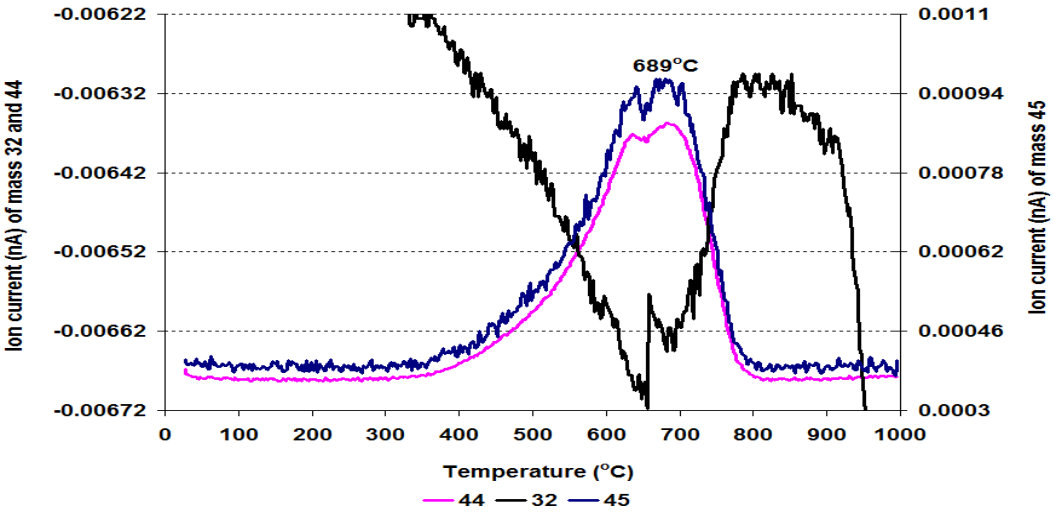

Figure 8.3-101 MS data of CO_2 (m/z=44), O_2 (m/z=32) and C_2H_5OH fragment (m/z=45) for Rh/Al_2O_3 catalyst following the 1-propanol impurity reaction

The spent catalyst was analysed by TGA/DSC associated with a mass spectrometer under a 2% O_2/Ar atmosphere and the results obtained were plotted versus temperature and are shown in Figures 8.3-100 to 8.3-101. The TGA and derivative weight profiles show that the main weight loss events occurred between 330°C and 813°C. A total of 393 mg g^{-1} of catalyst weight loss occurred in temperature range of 22°C to1000°C which was slightly lower than the coke deposition that occurred on the same catalyst in the pure ethanol

reaction catalyst. The mass profile shows that the weight loss events in TGA profile corresponded to CO_2 and ethanol fragment species evolution. In addition, trace amounts of water were also observed.

1-propanol impurity post reaction catalyst gave similar Raman results as was seen in the post reaction pure ethanol sample over Rh/Al_2O_3 catalyst.

8.3.4.2.2 BET analysis

Catalyst	Conditions	BET Surface area (m^2/g)	Pore volume (cm^3/g)	Average pore diameter (Å)
Rh/Al_2O_3	Pure ethanol (500°C)	47	0.04 (± 3.28)	42 (± 5.57)
	1-Propanol impurity	39	0.06 (± 4.08)	62 (± 6.45)

Table 8.3-13 BET analysis of post reaction Rh/Al_2O_3 catalyst following the 1-propanol impurity reaction

In Table 8.3-13 the BET results are tabulated and illustrate that the BET surface area of 1-propanol impurity post reaction catalyst decreased compared to the pure ethanol post reaction catalyst. Additionally the pore volume and the average pore diameter increased.

8.3.4.3 IPA impurity

To investigate the effect of C_3 alcohol isomer, IPA was added to the water/ethanol mixture and then the reaction was run over Rh/Al_2O_3 catalyst at 500°C and the results are discussed in the following section.

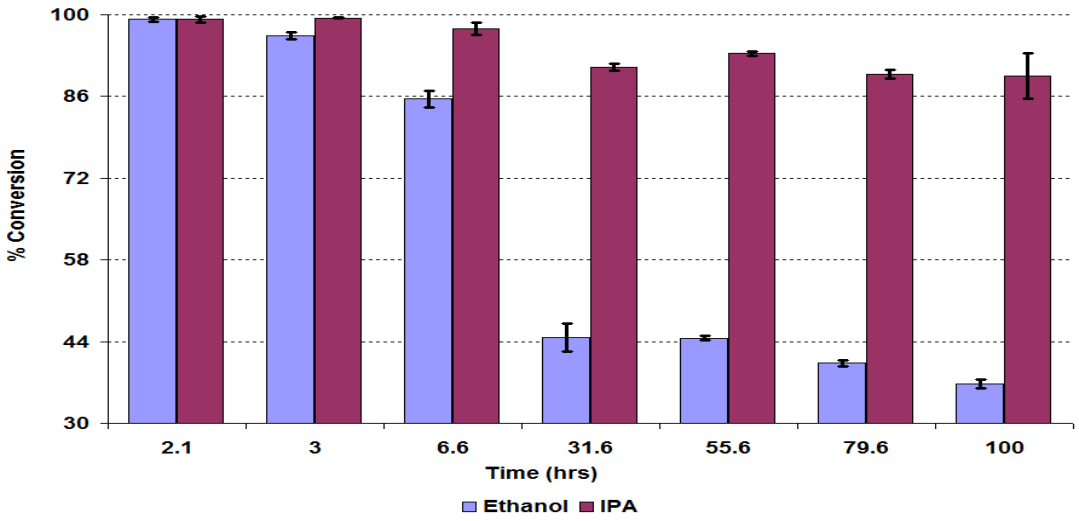

Figure 8.3-102 % Conversion of ethanol and IPA over Rh/Al_2O_3 catalyst during the IPA impurity reaction

Figure 8.3-102 shows the conversion of ethanol and isopropyl alcohol. As usual in the initial 1 hour ethanol and IPA gave 99% conversion. However after 2.1 hours time on stream deactivation of the catalyst started and a remarkable change was observed after 6.6 hours time on stream. As the reaction proceeded further there was a steady decrease in the conversion of ethanol and by the end of the reaction the ethanol conversion reduced to 36%. Like the reactions with the other catalysts, IPA gave a high conversion and throughout the reaction the conversion was only reduced to 89%.

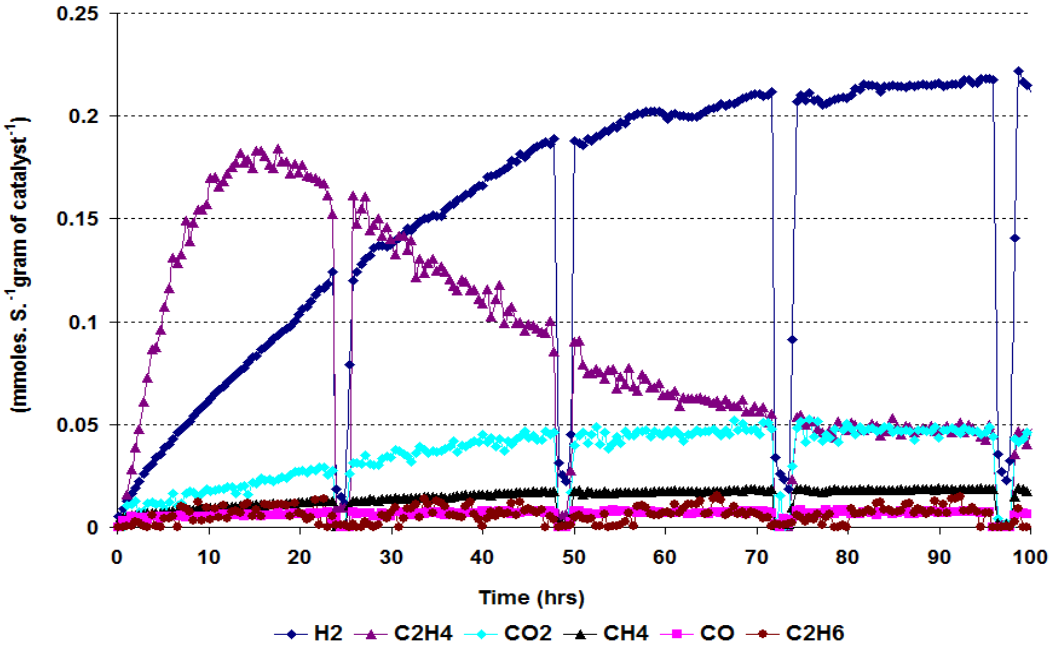

Figure 8.3-103 Rate of formation of gaseous products over Rh/Al_2O_3 catalyst during the IPA impurity reaction

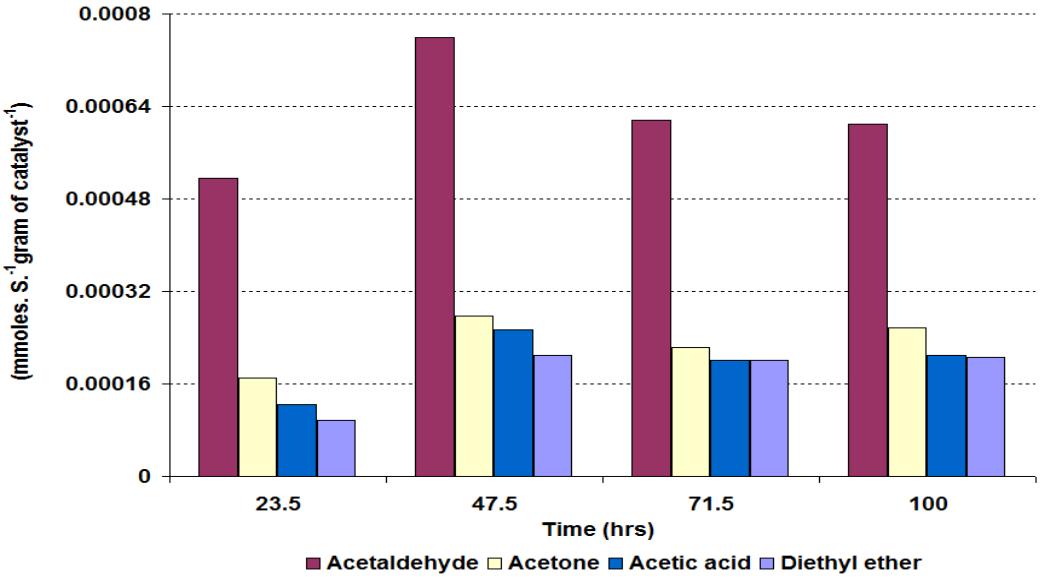

Figure 8.3-104 Rate of formation of liquid products over Rh/Al_2O_3 catalyst during the IPA impurity reaction

Figure 8.3-103 shows the rates of formation of the gaseous products over Rh/Al_2O_3 catalyst with an IPA impurity. The figure shows that C_2H_4 was formed with a similar rate to that observed in 1-propanol impurity reaction over Rh/Al_2O_3 catalyst. Initially, the reaction gave a high rate of formation for all the gaseous products, which started to decrease after 17.5 hours time on stream. The decrease in the rate of formation of C_2H_4 in IPA impurity reaction was steeper when compared to the 1-propanol impurity reaction over Rh/Al_2O_3 catalyst and after achieving steady state, it had a similar rate of formation to that observed in the pure ethanol reaction over Rh/Al_2O_3 catalyst. The rate of formation of H_2 in the IPA impurity reaction over Rh/Al_2O_3 catalyst steadily increased with reaction time and at the end of the reaction its rate of formation was slightly lower than the pure ethanol reaction at the same temperature. Interestingly, the rate of formation of CO_2 progressively increased throughout the reaction and after 35 hours TOS, its rate of formation exceeded the rate of formation of CO_2 in the pure ethanol reaction over Rh/Al_2O_3 catalyst.

In the liquid products acetaldehyde, acetone, acetic acid and diethyl ether were produced and their rates of formation are shown in Figure 8.3-104. Acetaldehyde was produced at the highest rate and follows a similar course as that observed in the 1-propanol impurity reaction, although its rate of formation was slightly lower initially than the 1-propanol impurity reaction. Other liquid products were produced with slightly higher rates. However, all the liquid products, except acetone, obtained virtual steady state conditions after 48 hours time on stream.

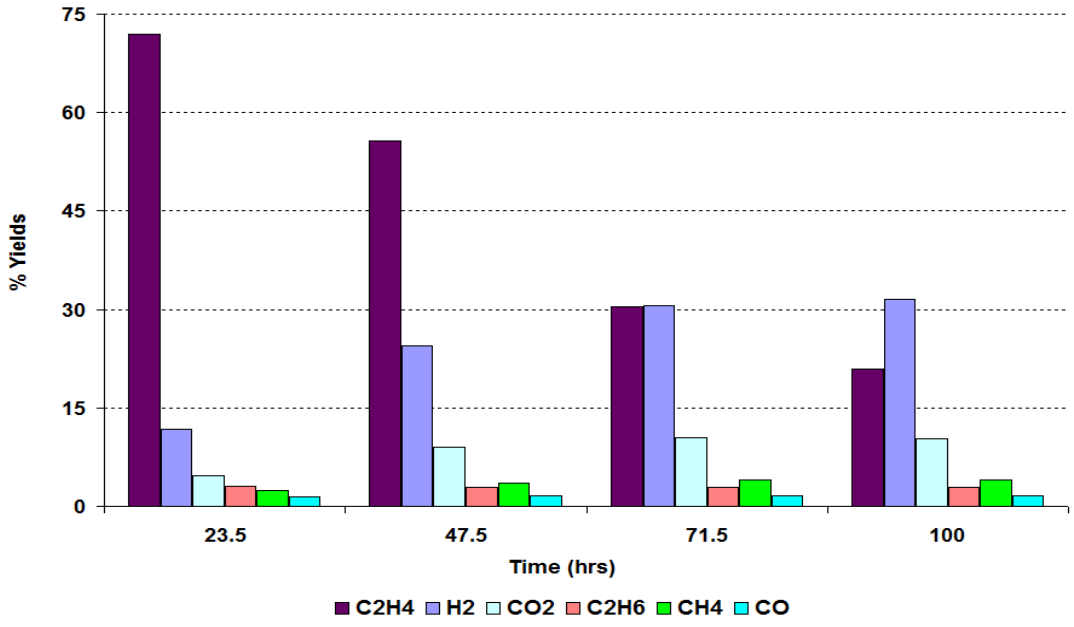

Figure 8.3-105 % Yield of gaseous products over Rh/Al_2O_3 catalyst during the IPA impurity reaction

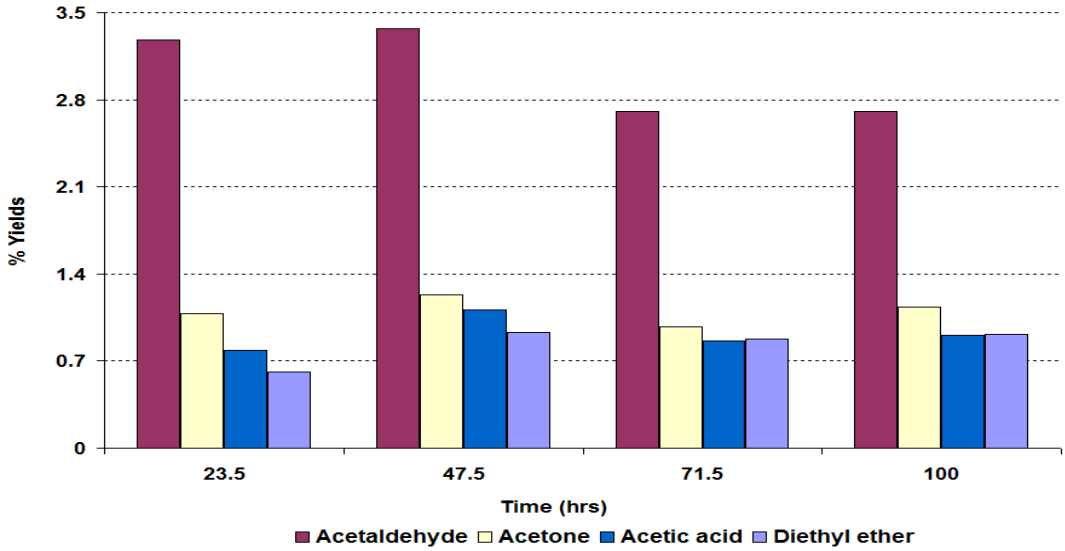

Figure 8.3-106 % Yield of liquid products over Rh/Al_2O_3 catalyst during the IPA impurity reaction

Figure 8.3-105 illustrates that C_2H_4 gave the highest yield initially which decreased progressively and reduced to 21% by the end of the reaction. Whereas the yield of H_2 steadily increased and exceeded C_2H_4 after 72 hours time on stream. The other gaseous products were produced with lower yields and none of them gave a yield higher than 11%. All the liquid products were produced with small yields. Among these products, as seen in Figure 8.3-106 acetaldehyde was produced with the highest yield for which the maximum value was less than 4%.

8.3.4.4 Post reaction characterisation

8.3.4.4.1 TPO

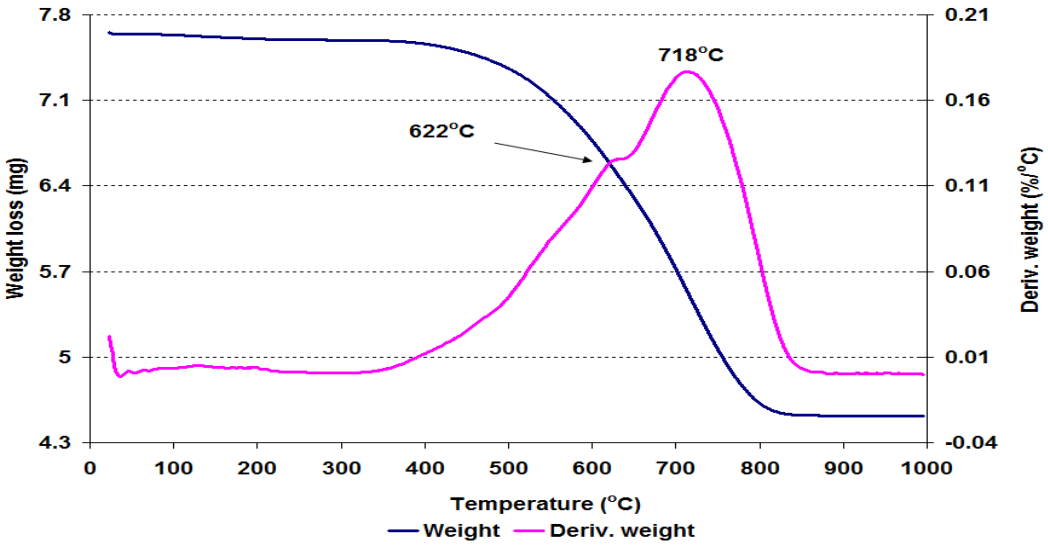

Figure 8.3-107 Post reaction TPO for Rh/Al_2O_3 catalyst following the IPA impurity reaction

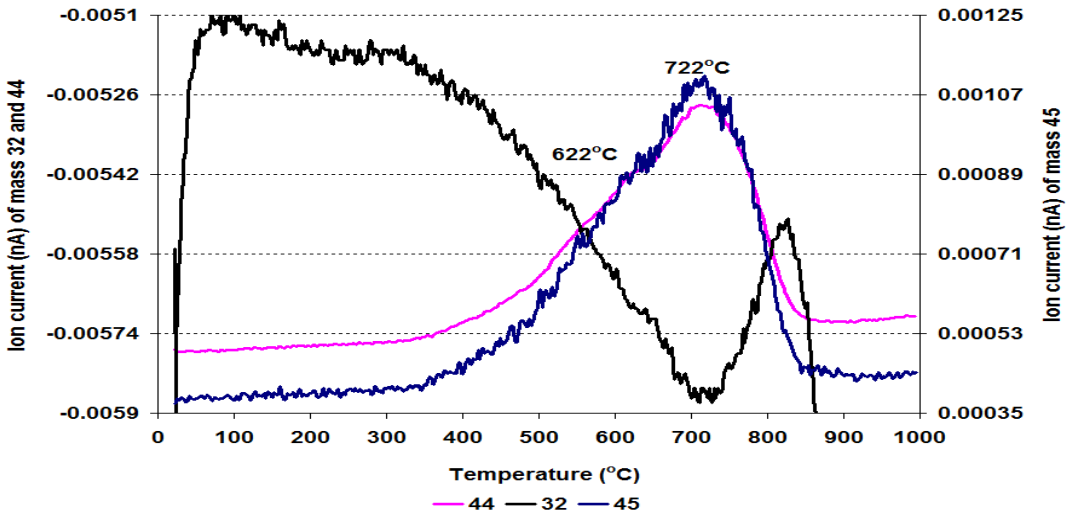

Figure 8.3-108 MS data of CO_2 (m/z=44), O_2 (m/z=32) and C_2H_5OH fragment (m/z=45) for Rh/Al_2O_3 catalyst following the IPA impurity reaction

The spent catalyst was run on a TGA/DSC connected to mass spectrometer in a 2% O_2/Ar environment over a temperature range between 23°C and 1000°C and the results obtained, plotted versus temperature, are shown in Figures 8.3-107 to 8.3-108. The TGA profile shows that the weight loss of 409.6 mg g^{-1} of catalyst was mainly carbonaceous materials evolved from the surface of the spent catalyst. The main desorption of these carbonaceous materials occurred in the 333°C to 861°C region and gave a main peak at 718°C with a shoulder at 622°C. The evolution of these carbonaceous materials corresponded to CO_2 and principal fragment of ethanol in mass spectrometry profile (Figure 8.3-108).

Like the 1-propanol impurity reaction, the post reaction IPA impurity sample also gave similar Raman bands to the post reaction pure ethanol sample.

8.3.4.4.2 BET analysis

Catalyst	Conditions	BET Surface area (m^2/g)	Pore volume (cm^3/g)	Average pore diameter (Å)
Rh/Al_2O_3	Pure ethanol (500°C)	47	0.04 (± 3.28)	42 (± 5.57)
	IPA impurity	39	0.03 (± 5.32)	38 (± 4.99)

Table 8.3-14 BET analysis of post reaction Rh/Al_2O_3 catalyst following the IPA impurity reaction

Table 8.3-14 displays that an obvious decrease occurred in the BET surface area, the pore volume and the average pore diameter occurred in the IPA impurity post reaction catalyst when compared to the pure ethanol post reaction sample.

8.3.4.5 Propanal impurity

After examining the influence of C_3 alcohol group on the steam reforming of ethanol the next investigation looked at the effect of an aldehyde group impurity over Rh/Al_2O_3 catalyst and is discussed in the section below.

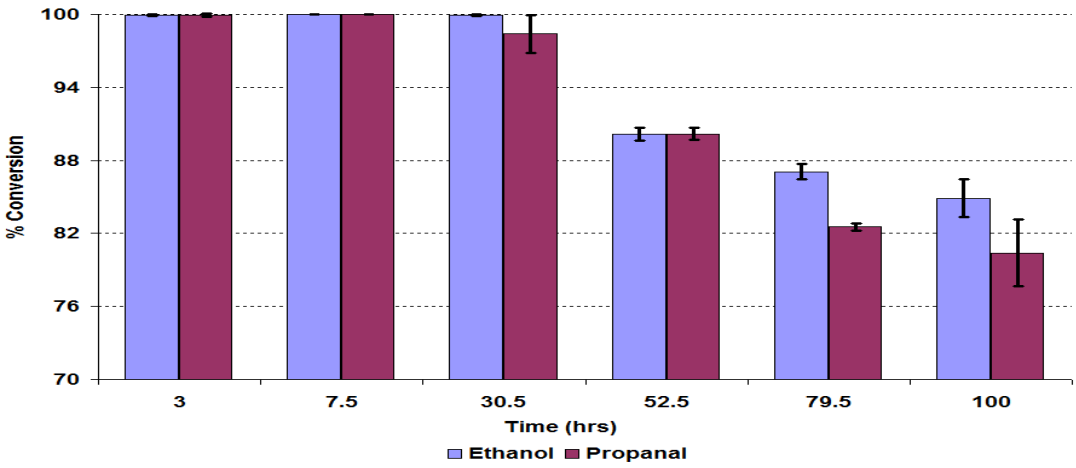

Figure 8.3-109 % Conversion of ethanol and propanal over Rh/Al_2O_3 catalyst during the propanal impurity reaction

Figure 8.3-109 shows that the aldehyde impurity enhanced the conversion of ethanol. After addition of 1mol.% propanal impurity to the water/ethanol mixture the ethanol conversion increased to 99.9% in the initial 30 hours time on stream. After 30 hours the conversion of ethanol slightly decreased and this scenario continued for the rest of the reaction. After 100 hours the conversion of ethanol only decreased to 85%. Also the conversion propanal gave similar patterns to those seen in the ethanol conversion.

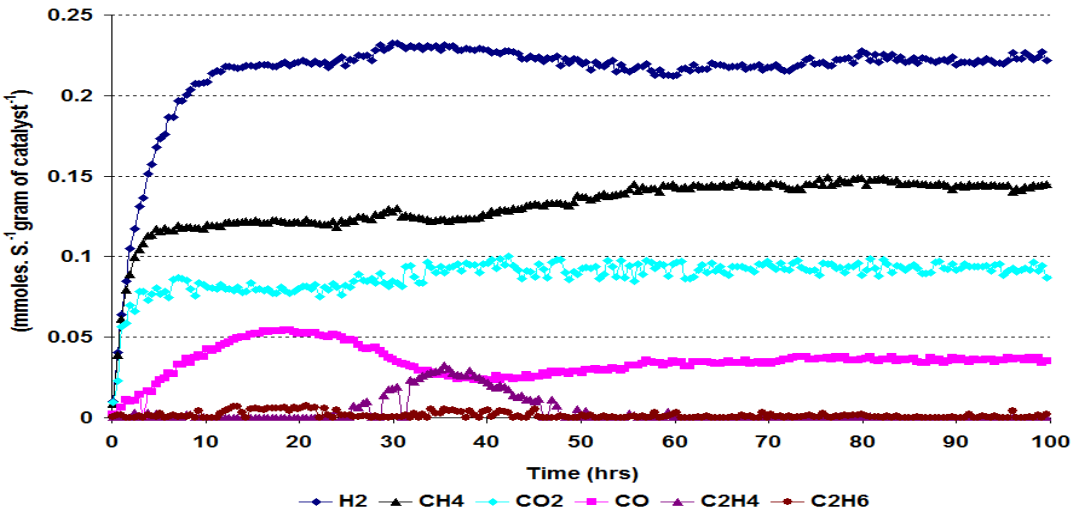

Figure 8.3-110 Rate of formation of gaseous products over Rh/Al_2O_3 catalyst during the propanal impurity reaction

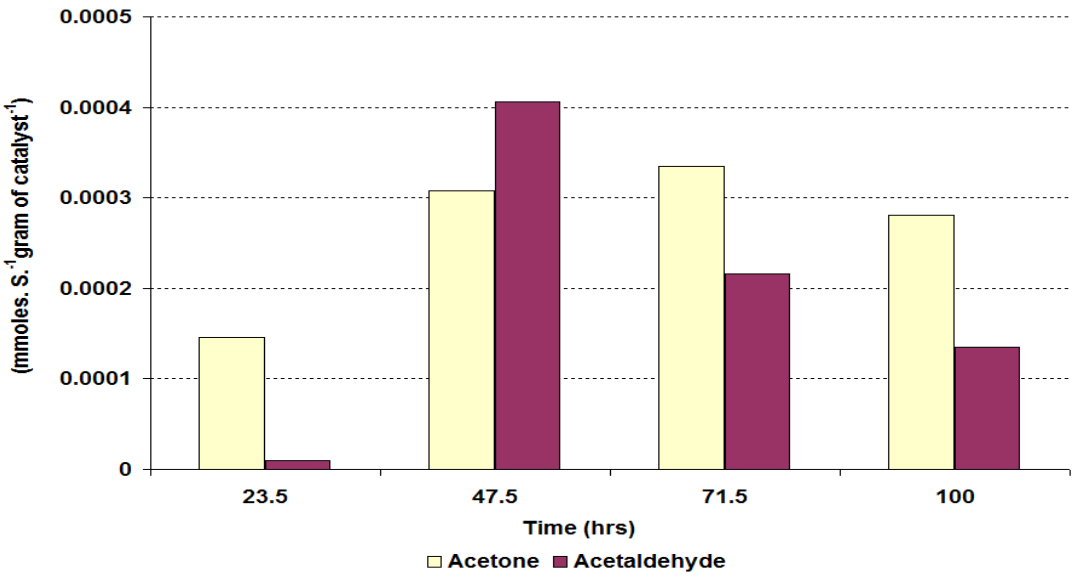

Figure 8.3-111 Rate of formation of liquid products over Rh/Al_2O_3 catalyst during the propanal impurity reaction

The results of the rates of formation of the gaseous products shown in Figure 8.3-110 illustrate that the patterns of formation of the different products changed from the pure ethanol reaction by the addition of the propanal impurity. The rate of formation of H_2 in the propanal impurity reaction was stabilised after 12 hours time on stream and no deactivation in its rate was observed by the end of the reaction. The rates of formation of CH_4, CO_2 and CO were significantly increased and achieved steady state conditions after 56 hours time on stream. Interestingly, in contrast to the pure ethanol reaction, in the initial 20 hours in the propanal impurity reaction no C_2H_4 was observed. After 20 hours TOS insignificant amounts of C_2H_4 had been produced which again disappeared after 50 hours time on stream.

Figure 8.3-111 reveals that the rate of formation of the liquid products in the propanal impurity reaction over Rh/Al_2O_3 catalyst. Unlike the pure ethanol reaction, acetone gave a higher rate than acetaldehyde in the initial 24 hours. However, the acetaldehyde rate of formation exceeded the rate of formation of acetone after 48 hours time on stream, but was exceeded by acetone again as the reaction proceeded further. In contrast to the pure ethanol reaction, trace amounts of methanol and acetic acid were detected. This suggests that not only had the rate profiles of the gaseous products changed, but also the distribution of liquid products had significantly altered.

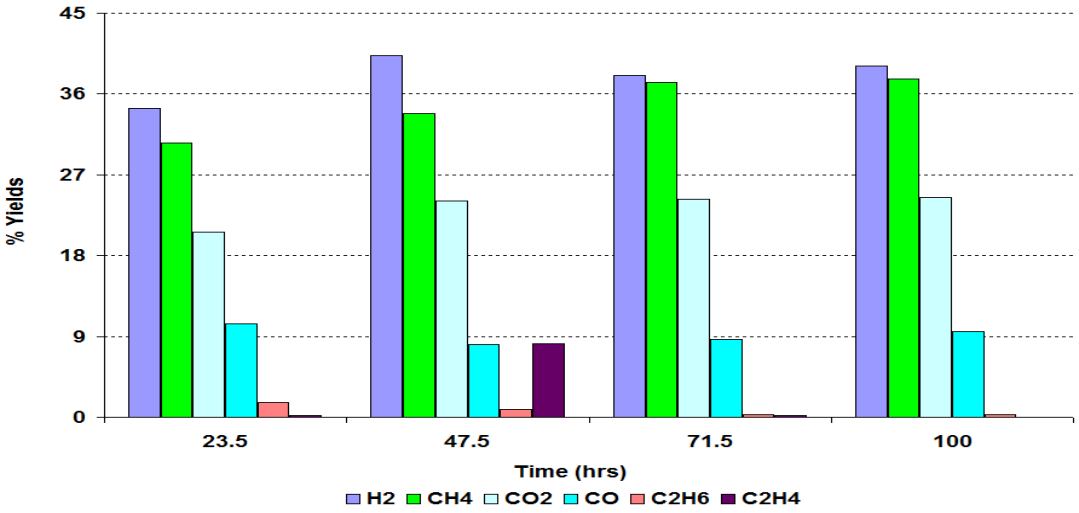

Figure 8.3-112 % Yield of gaseous products over Rh/Al_2O_3 catalyst during the propanal impurity reaction

In the gaseous products, H_2, CH_4 and CO_2 gave the highest yield. The yield of H_2 was slightly higher than in the pure ethanol reaction which varied with reaction time. The yield of CO_2 and CH_4 especially increased with reaction time and virtually stabilised after 72 hours time on stream whilst the yield of CO was also slightly decreased after the initial 24 hours time on stream and gave higher yield than the yield of CO in the pure ethanol reaction.

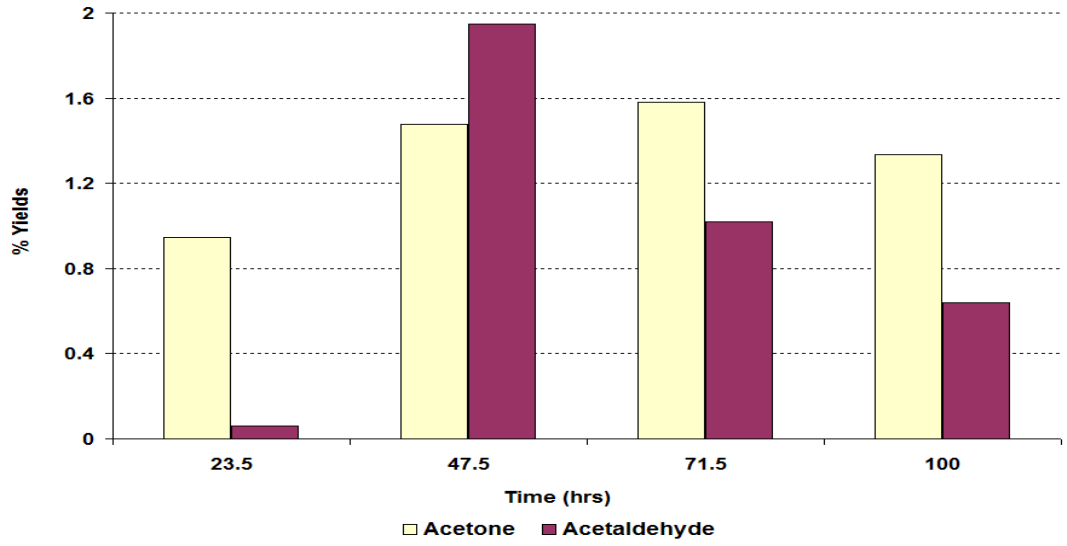

Figure 8.3-113 % Yield of liquid products over Rh/Al_2O_3 catalyst during the propanal impurity reaction

Both liquid products *i.e.* acetone and acetaldehyde gave low yields which varied with the reaction time. The maximum yield obtained for acetaldehyde was ~ 2%. These results

reveal that insignificant amounts of liquid products were produced and most of the ethanol was converted to the gaseous products.

8.3.4.6 Post reaction characterisation

Like the other samples of Rh/Al_2O_3, the post reaction catalyst was also characterised by various analytical techniques to determine the cause of catalyst deactivation.

8.3.4.6.1 TPO

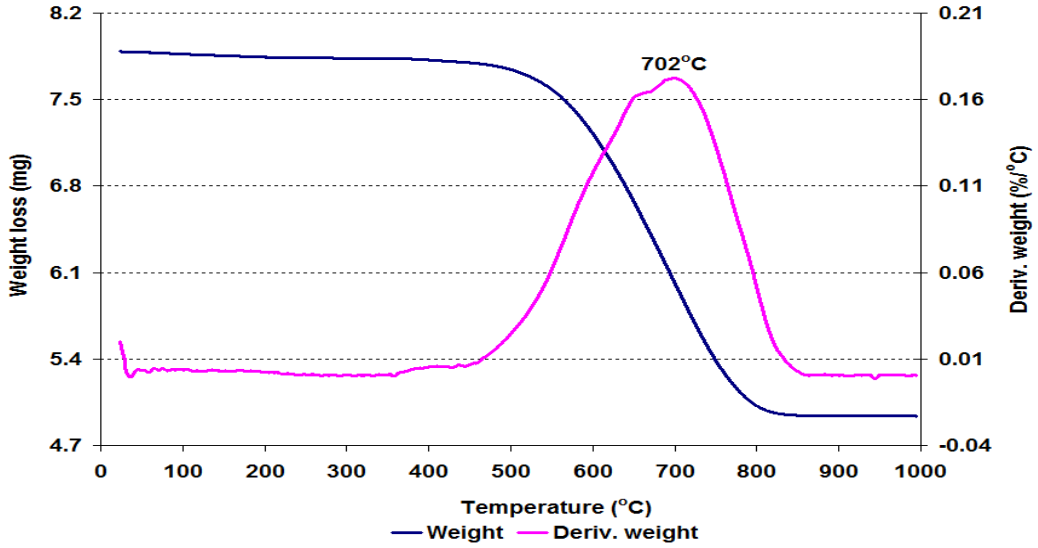

Figure 8.3-114 Post reaction TPO for Rh/Al_2O_3 catalyst following the propanal impurity reaction

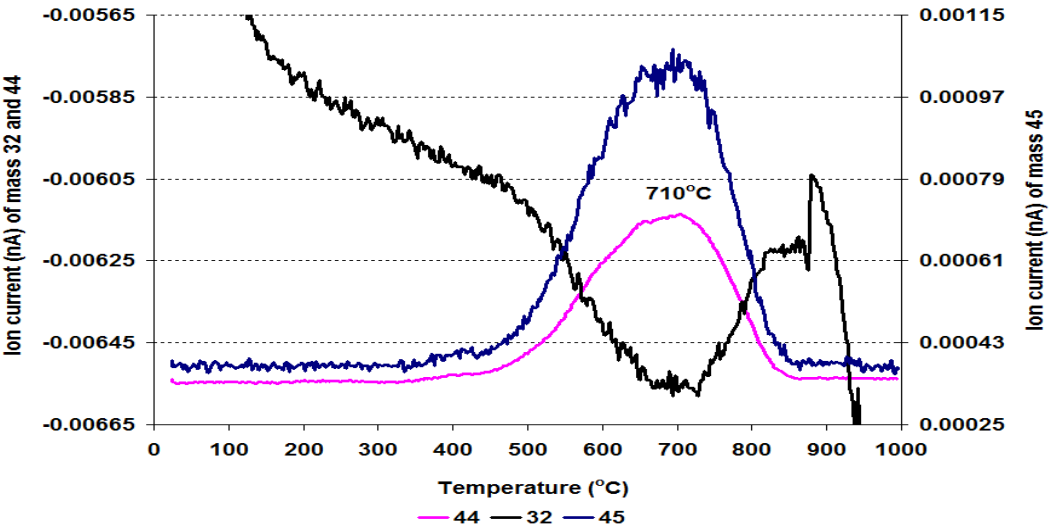

Figure 8.3-115 MS data of CO_2 (m/z=44), O_2 (m/z=32) and C_2H_5OH fragment (m/z=45) for Rh/Al_2O_3 catalyst following the propanal impurity reaction

Figure 8.3-114 shows the TGA results of the post Rh/Al_2O_3 catalyst following the propanal impurity reaction. The figure illustrates that total weight loss up to 1000°C was 374.6 mg g^{-1} which is less than was seen for the pure ethanol reaction catalyst and even less compared to the alcohol impurities post reaction catalysts. The derivative weight profile displays the major change in weight occurring between 435°C to 860°C. In the mass spectrometry results (Figure 8.3-115), this weight loss is attributed to the evolution of CO_2 and ethanol fragment. In addition, the mass results ascribe that no H_2O and CO evolution occurred during the TPO.

8.3.4.6.2 Raman analysis

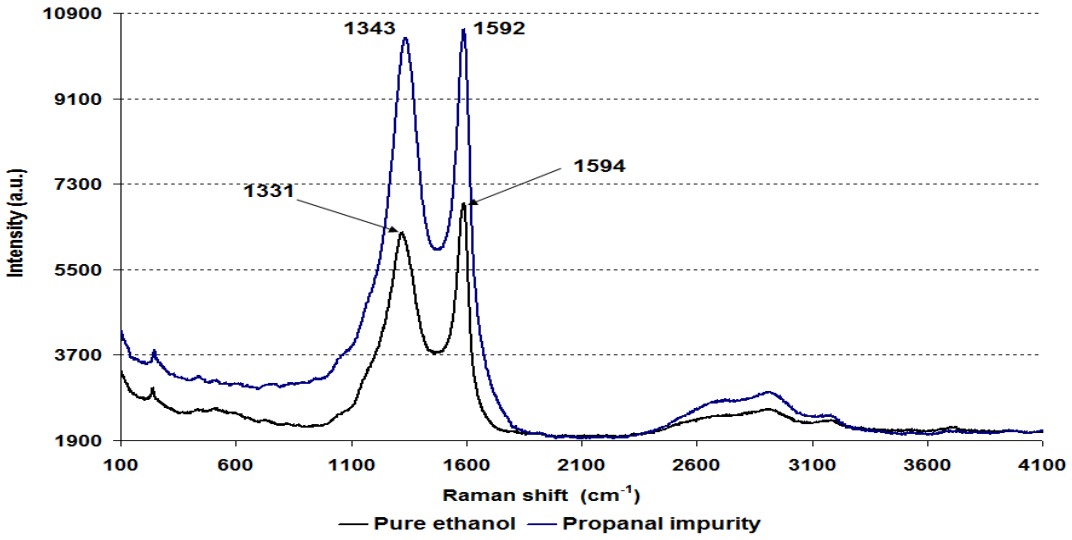

Figure 8.3-116 Post reaction Raman spectra for Rh/Al_2O_3 catalyst following the propanal impurity reaction

The post reaction propanal impurity catalyst was analysed by Raman spectroscopy and the spectrum obtained was compared with the pure ethanol post reaction sample which is shown in Figure 8.3-116. The figure shows that the intensity of bands for graphitic carbon significantly increased in the propanal impurity post reaction catalyst.

8.3.4.6.3 BET analysis

Catalyst	Conditions	BET Surface area (m^2/g)	Pore volume (cm^3/g)	Average pore diameter (Å)
Rh/Al_2O_3	Pure ethanol (500°C)	47	0.04 (± 3.28)	42 (± 5.57)
	Propanal impurity	32	0.08 (± 0.09)	93 (± 6.31)

Table 8.3-15 BET analysis of post reaction Rh/Al_2O_3 catalyst following the propanal impurity reaction

The BET analysis for the pure ethanol and the propanal impurity post reaction catalysts were compared and the results are shown in Table 8.3-15. The BET analysis reveals that the BET surface area decreased whilst the average pore diameter and the pore volume increased in the propanal impurity reaction catalyst.

8.3.4.7 Propylamine impurity

The addition of a 1mol.% propylamine impurity with respect to the pure ethanol to the water/ethanol mixture appeared to enhance the activity of the Rh/Al_2O_3 catalyst in the steam reforming of ethanol reaction.

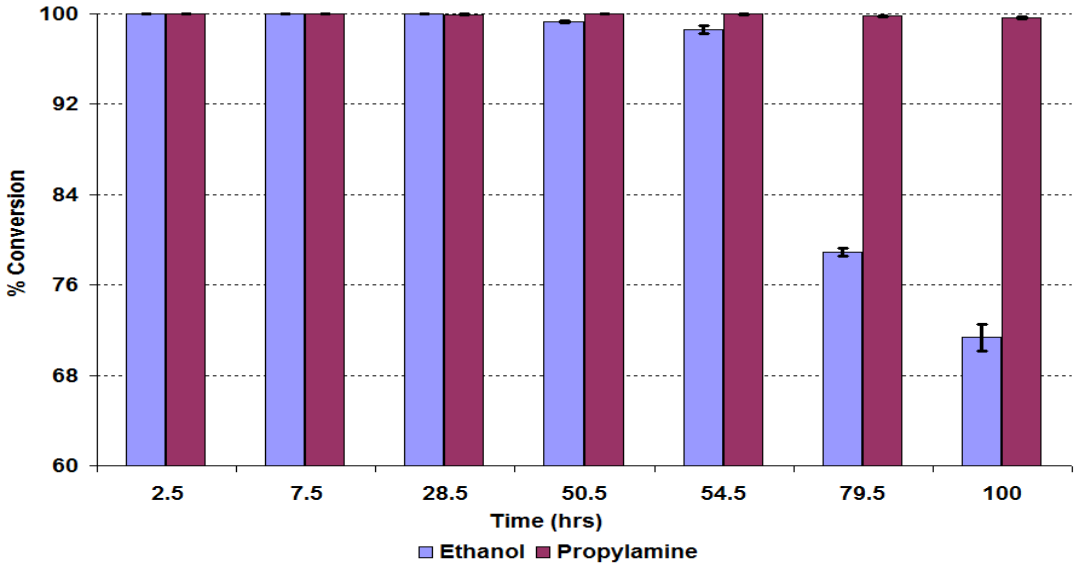

Figure 8.3-117 % Conversion of ethanol and propylamine over Rh/Al_2O_3 catalyst during the propylamine impurity reaction

Figure 8.3-117 illustrates that the conversion of ethanol significantly increased on the Rh/Al_2O_3 catalyst after the addition of the propylamine impurity to water/ethanol mixture. In the initial 28.5 hours, ethanol gave 99.9% conversion and no deactivation was observed. However after 28 hours the ethanol conversion started to decrease and declined to 71% after 100 hours time on stream. Like the Pt/Al_2O_3 catalyst, in the reaction the propylamine also gave a high conversion which was only decreased to 99% by the end of the reaction.

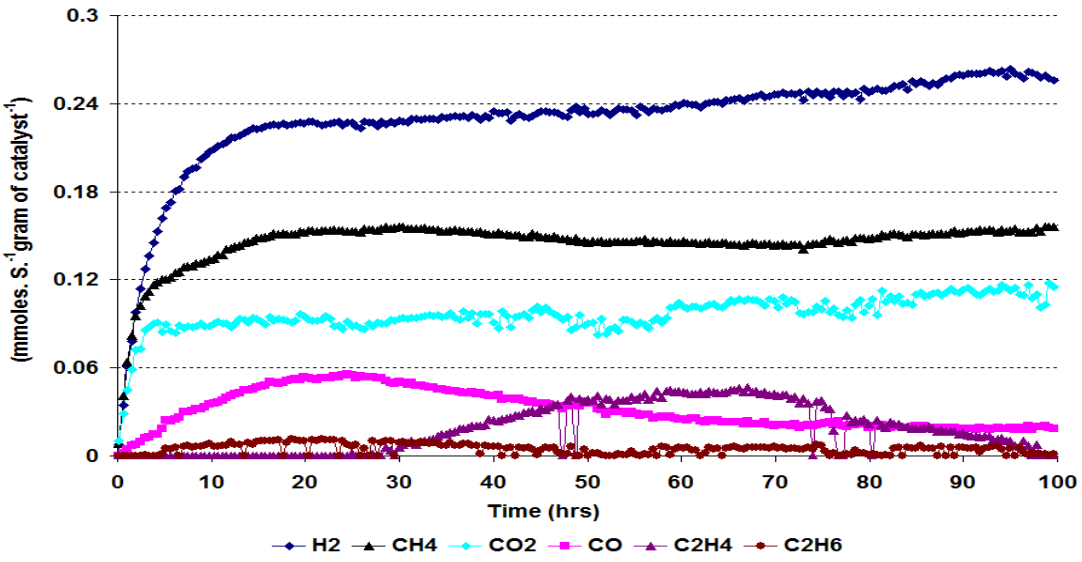

Figure 8.3-118 Rate of formation of gaseous products over Rh/Al_2O_3 catalyst during the propylamine impurity reaction

The rates of formation of the gaseous products in the propylamine impurity reaction show similar results to those observed in the propanal impurity reaction over Rh/Al_2O_3 catalyst. However, the patterns of formation of the different products were different. From the graph it is obvious that the rate of formation of H_2 was initially low and steadily increased with the reaction time and by the end of the reaction was higher than H_2 rate in the pure ethanol steam reforming reaction on Rh/Al_2O_3 catalyst.

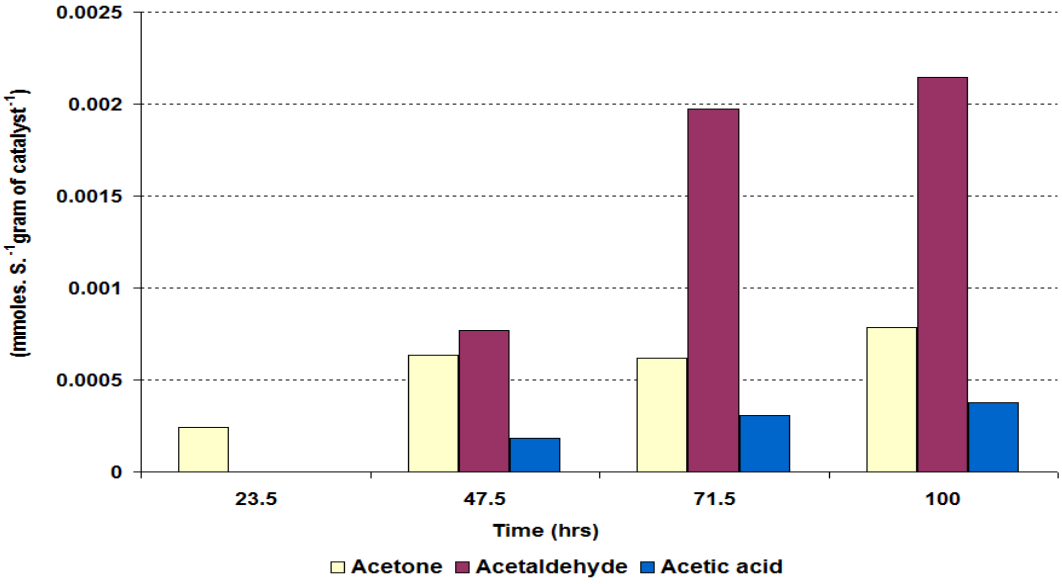

Figure 8.3-119 Rate of formation of liquid products over Rh/Al_2O_3 catalyst during the propylamine impurity reaction

The addition of the propylamine impurity not only had an influence on the gaseous products distribution, it also affected the rates of formation of the liquid products. Figure 8.3-119 illustrates that the rates of formation of the liquid products in the propylamine impurity reaction were the mirror image of the liquid products in the pure ethanol steam reforming reaction over Rh/Al_2O_3 catalyst. In the initial 24 hours time on stream, only acetone was detected in the liquid products. However, as the reaction proceeded, acetaldehyde and acetic acid also appeared and their rates of formation increased with time on stream.

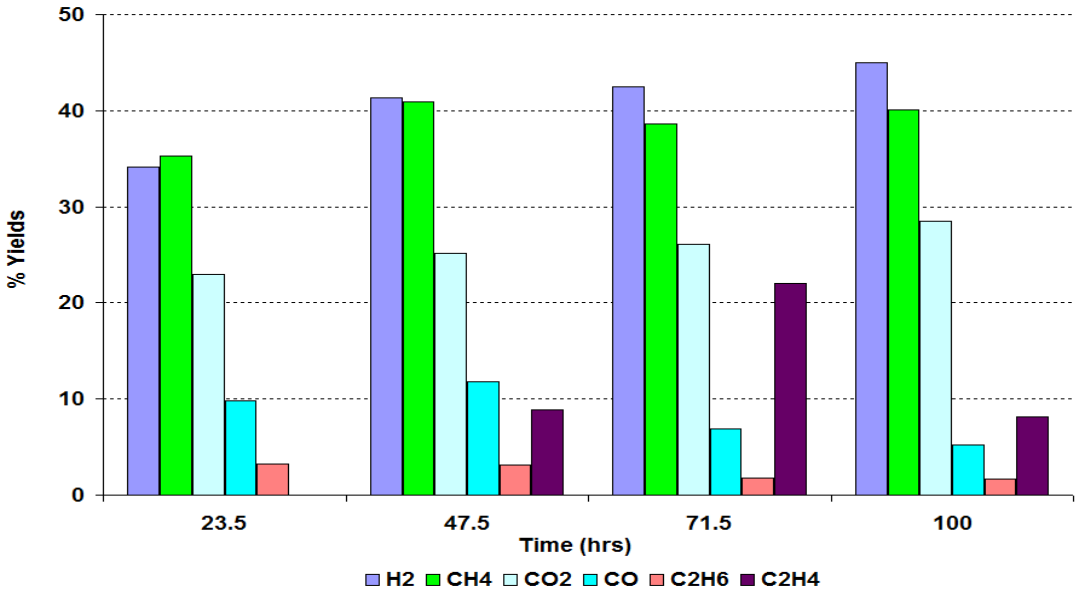

Figure 8.3-120 % Yield of gaseous products over Rh/Al_2O_3 catalyst during the propylamine impurity reaction

The major gaseous products produced during the steam reforming of ethanol with a propylamine impurity over the Rh/Al_2O_3 catalyst were H_2, CH_4 and CO_2. Of all the gaseous products, H_2 gave the highest yield which was slightly higher than the yield seen for the steam reforming reaction of pure ethanol over Rh/Al_2O_3 catalyst. The yield of H_2 steadily increased with reaction time. Similarly the yields of CH_4 and CO_2 were significantly increased compared to yield from the pure ethanol reaction over Rh/Al_2O_3 catalyst, suggesting that the reaction route for the ethanol steam reforming process changed. In addition, the yield of C_2H_4 was significantly decreased compared to the pure ethanol steam reforming reaction and fluctuated throughout the reaction.

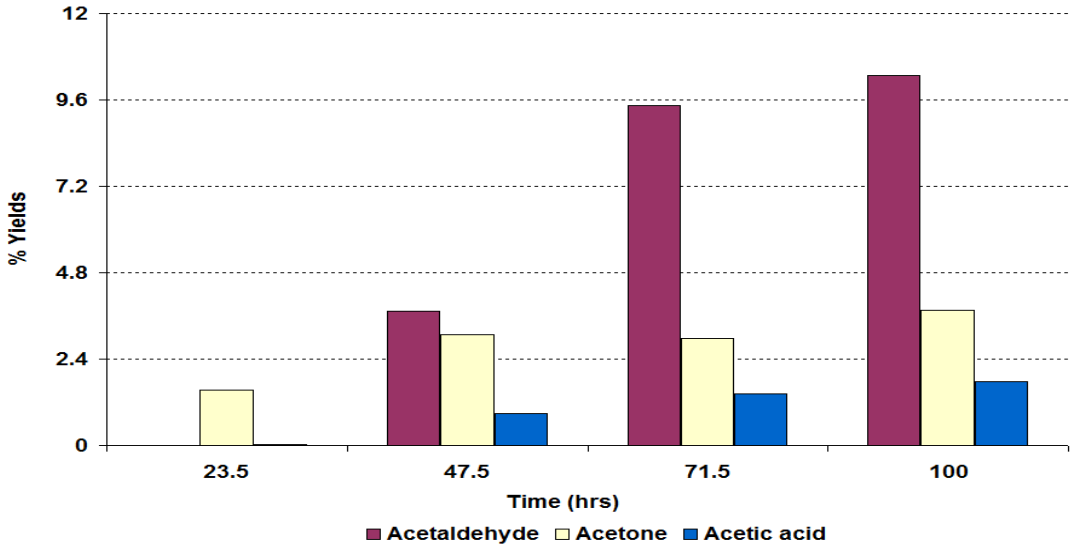

Figure 8.3-121 % Yield of liquid products over Rh/Al_2O_3 catalyst during the propylamine impurity reaction

Figure 8.3-121 illustrates that the yields of acetaldehyde and acetic acid steadily increased with the reaction time whilst the yield of acetone stabilised after 24 hours time on stream.

8.3.4.8 Post reaction characterisation

The spent catalyst was characterised by using various techniques to study the nature of the deposited materials.

8.3.4.8.1 TPO

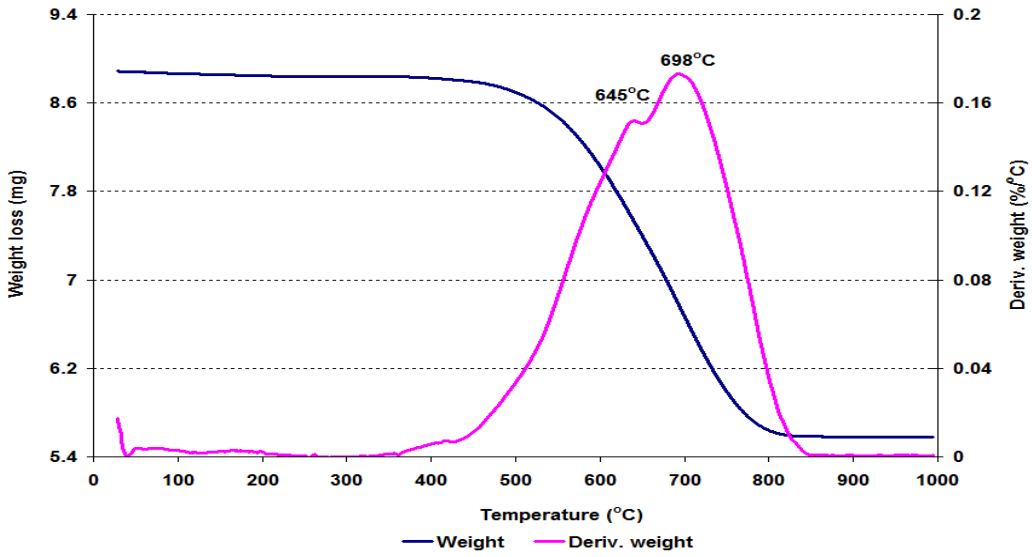

Figure 8.3-122 Post reaction TPO for Rh/Al_2O_3 catalyst following the propylamine impurity reaction

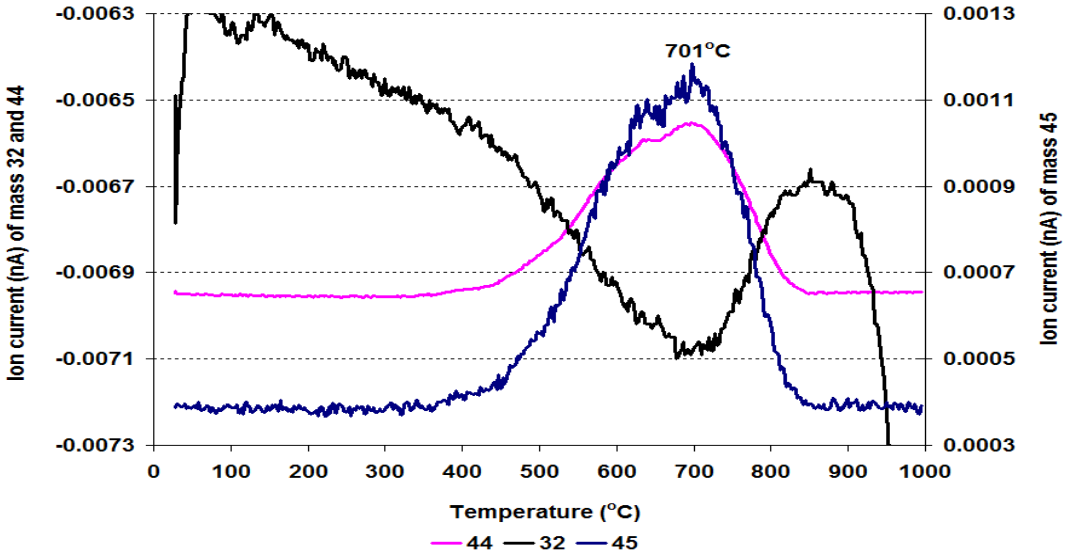

Figure 8.3-123 MS data of CO_2 (m/z=44), O_2 (m/z=32) and C_2H_5OH fragment (m/z=45) for Rh/Al_2O_3 catalyst following the propylamine impurity reaction

Like the propanal impurity samples, the spent catalyst of the propylamine impurity reaction was characterised by TGA/DSC under 2% O_2/Ar atmosphere at temperatures between 25^{o}C and 1000^{o}C to investigate the weight change in the catalyst. A mass spectrometer was connected to the TGA/DSC to monitor the gases evolved during any weight change. The TGA profile shows that a total of 372 mg g^{-1} catalyst weight loss occurred during the temperature range up to 1000^{o}C, which was comparatively less than the weight loss in the post ethanol steam reforming reaction over Rh/Al_2O_3 catalyst. These weight loss events took place within a broad temperature region between 370^{o}C and 851^{o}C. The main weight loss gave a single broad peak at 698^{o}C with a small shoulder on the main peak at 645^{o}C. The weight change corresponded to CO_2 and ethanol fragment evolution in the mass spectrometry results.

8.3.4.8.2 Raman analysis

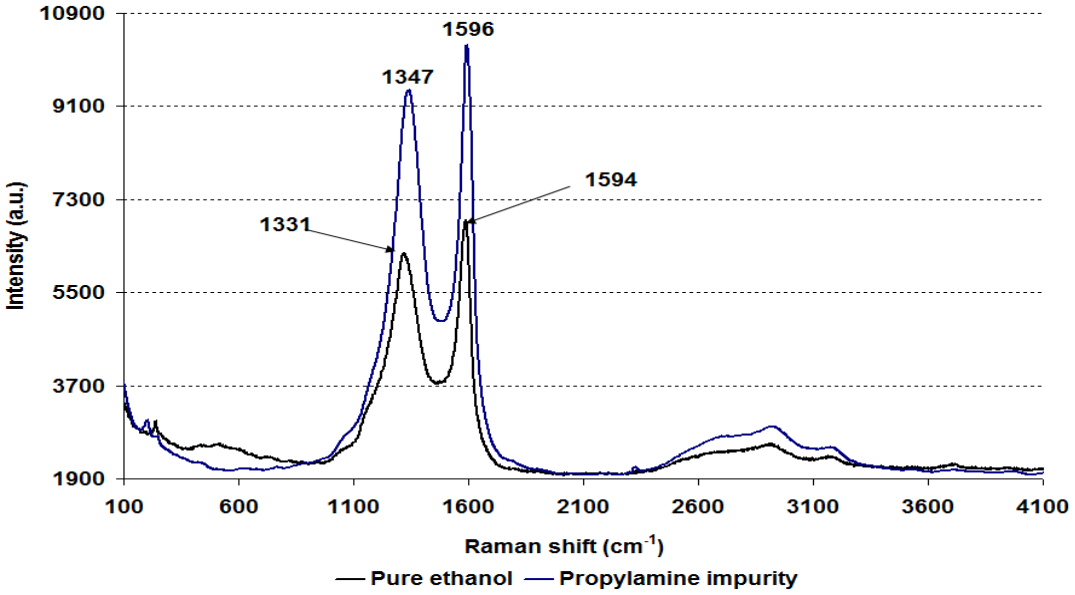

Figure 8.3-124 Post reaction Raman spectra for Rh/Al_2O_3 catalyst following the propylamine impurity reaction

The post reaction catalyst was analysed by Raman spectroscopy in the range of 100 cm^{-1} to 4100 cm^{-1} and the results obtained were compared with the pure ethanol post reaction over Rh/Al_2O_3 catalyst and are shown in Figure 8.3-124. The figure displays that the intensity of the characteristic graphitic carbon peaks increased. In addition, the lower wavenumber peak, also known in the literature as the D band shifted upwards.

8.3.4.8.3 BET analysis

Catalyst	Conditions	BET Surface area (m^2/g)	Pore volume (cm^3/g)	Average pore diameter (Å)
Rh/Al_2O_3	Pure ethanol (500°C)	47	0.04 (± 3.28)	42 (± 5.57)
	Propylamine impurity	31	0.07 (± 0.49)	93 (± 5.93)

Table 8.3-16 BET analysis of post reaction Rh/Al_2O_3 catalyst following the propylamine impurity reaction

The BET analysis in Table 8.3-16 shows that the pore volume and the average pore diameter of the propylamine impurity post reaction catalyst were increased compared to the pure ethanol post reaction catalyst whilst the BET surface area significantly decreased.

8.3.4.9 Acetone impurity

Finally the effect of an acetone impurity in the steam reforming of ethanol over the Rh/Al_2O_3 catalyst was investigated.

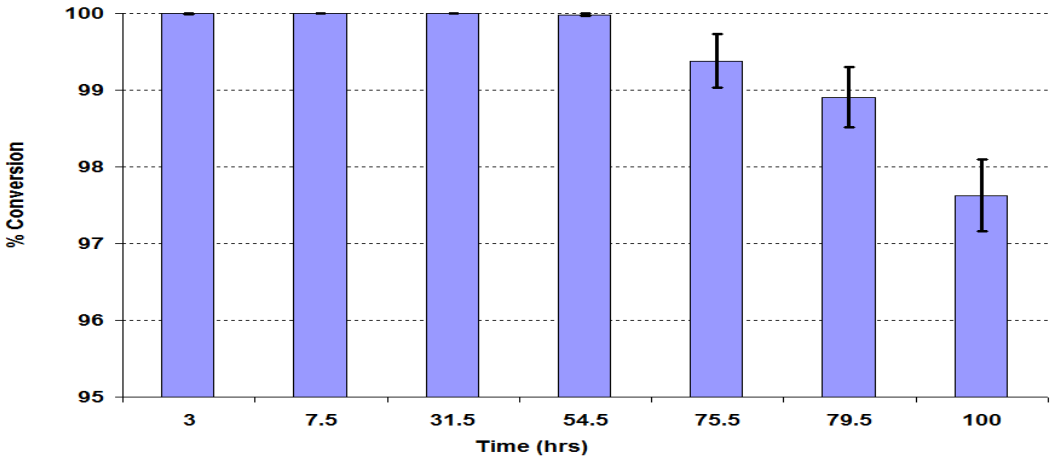

Figure 8.3-125 % Conversion of ethanol over Rh/Al_2O_3 catalyst during the acetone impurity reaction

Like previous catalysts, the addition of 1mol.% of acetone (with respect to pure ethanol) to the water/ethanol mixture brought a tremendous change in the conversion of ethanol compared to the pure ethanol reaction over Rh/Al_2O_3 catalyst. In the initial 54.5 hours ethanol gave 100% conversion which then slightly decreased as the reaction proceeded further. At the end of the reaction the conversion of ethanol had decreased only to 97.6%.

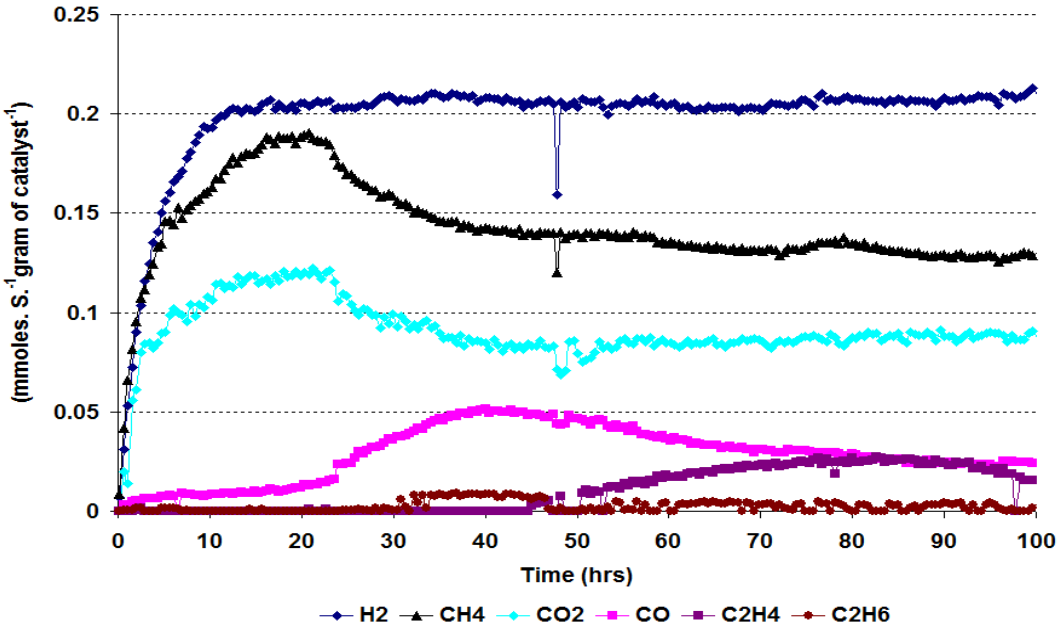

Figure 8.3-126 Rate of formation of gaseous products over Rh/Al_2O_3 catalyst during the acetone impurity reaction

The rate of formation of H_2 in the gaseous products shows interesting results. It obtained steady state conditions very quickly after 13 hours and no deactivation was observed in the entire reaction duration. However, in the steady state the rate of formation was less than in the propylamine impurity reaction and even less than the pure ethanol steam reforming over the Rh/Al_2O_3 catalyst. Similarly the rate of formation of CH_4 significantly increased compared to the pure ethanol reaction over Rh/Al_2O_3 catalyst. However CH_4 rate was not stable and after the initial increase the rate started to decrease until the end of the reaction. The rates of formation of CO and CO_2 were mirror images of each other. Initially, the rate of formation of CO_2 was high and started to decrease after 23 hours time on stream whilst the rate of formation of CO increased in this time frame. In contrast to the pure ethanol steam reforming over Rh/Al_2O_3 catalyst in acetone impurity, no C_2H_4 was observed in the initial 44 hours. However after 44 hours TOS small amounts of C_2H_4 were produced which again started to decrease after 82 hours time on stream.

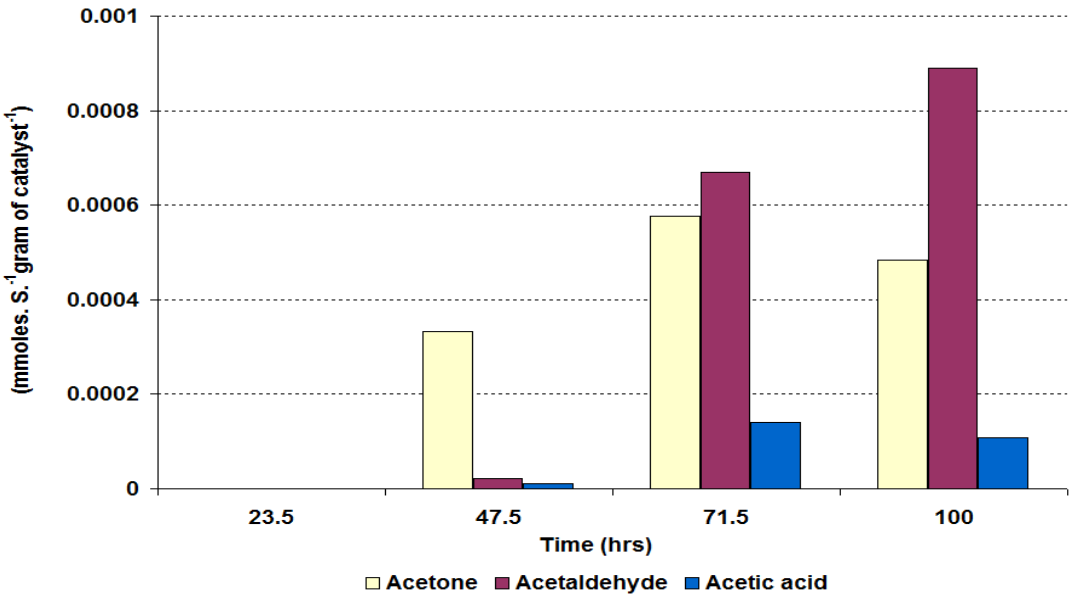

Figure 8.3-127 Rate of formation of liquid products over Rh/Al_2O_3 catalyst during the acetone impurity reaction

Figure 8.3-127 shows the rates of formation of the liquid products over the Rh/Al_2O_3 catalyst with an acetone impurity. Like the acetone impurity reaction over Pt/Al_2O_3 catalyst, in the initial 24 hours no liquid products were formed. However after 24 hours, acetone, acetaldehyde and acetic acid had started to form and the rates steadily increased with the reaction time except for acetone whose rate slightly decreased after 72 hours TOS. This result shows that initially all reactants converted to the gaseous products whilst later on as the reaction proceeded further, liquid products also began to form.

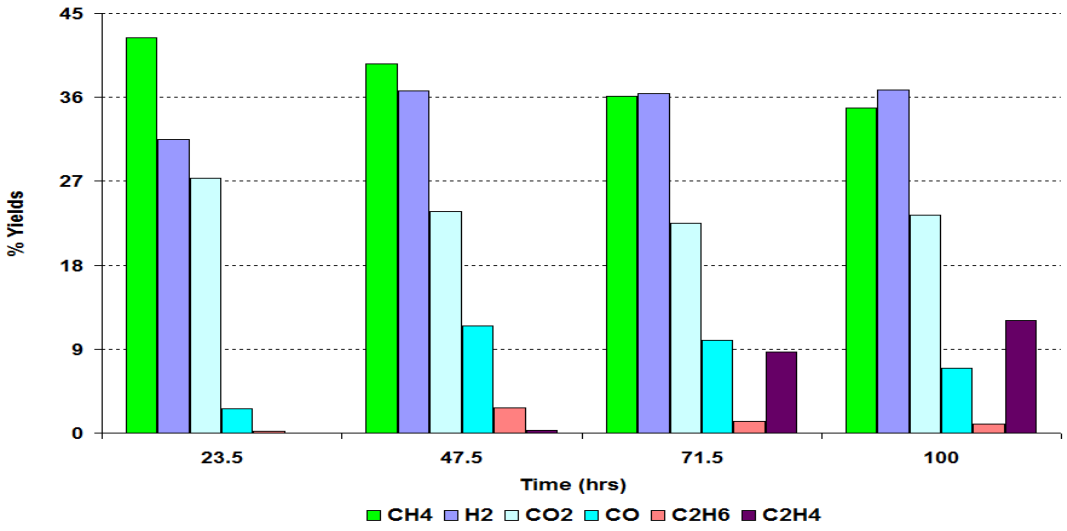

Figure 8.3-128 % Yield of gaseous products over Rh/Al_2O_3 catalyst during the acetone impurity reaction

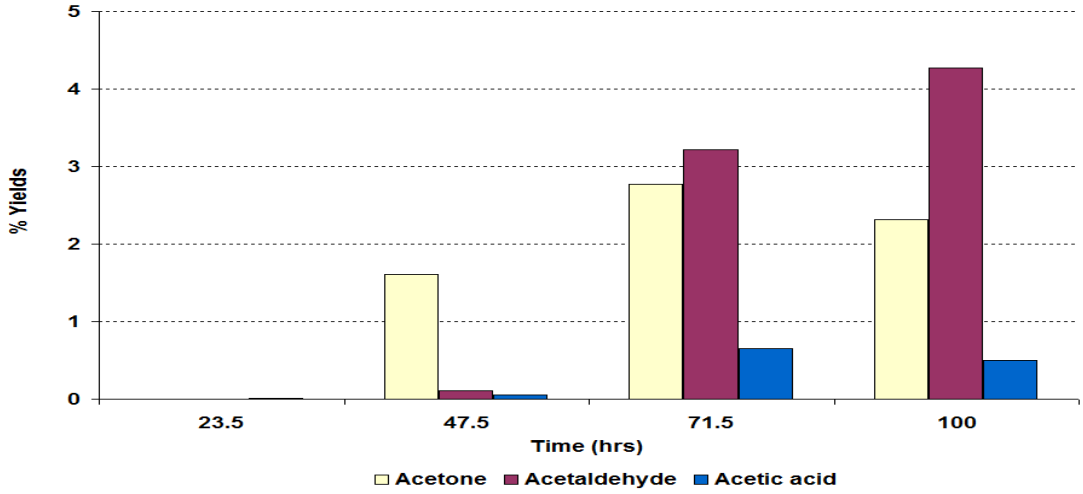

Figure 8.3-129 % Yield of liquid products over Rh/Al_2O_3 catalyst during the acetone impurity reaction

Figure 8.3-128 shows that amongst the gaseous products, CH_4, H_2 and CO_2 gave the highest yields. The yield of CH_4 was initially high and steadily decreased throughout the reaction whilst the yield of H_2 stabilised after 24 hour TOS. The yields of CO_2 and CO were significantly increased compared to pure ethanol reaction over Rh/Al_2O_3 catalyst, where the rate had varied throughout the entire reaction. As discussed in the previous section, no C_2H_4 was formed initially, however small amounts of C_2H_4 were produced as the reaction continued and gave a maximum yield of 12%. The yields of liquid products in the acetone impurity reaction over Rh/Al_2O_3 catalyst are shown in Figure 8.3-129. Like the other reactions, acetaldehyde gave the highest yield within the liquid products, and the yield increased with reaction time and gave a maximum yield for acetaldehyde of more than 4%.

8.3.4.10 Post reaction characterisation

8.3.4.10.1 TPO

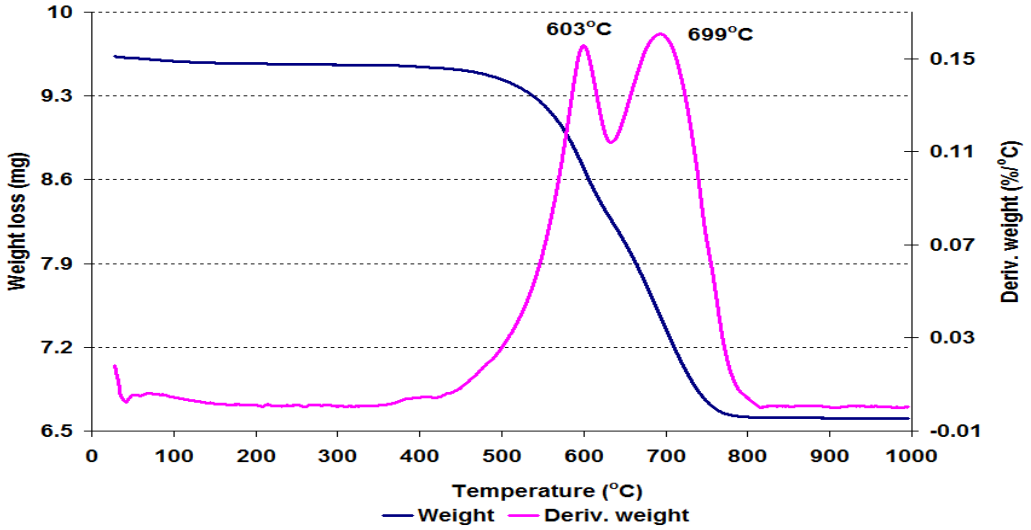

Figure 8.3-130 Post reaction TPO for Rh/Al_2O_3 catalyst following the acetone impurity reaction

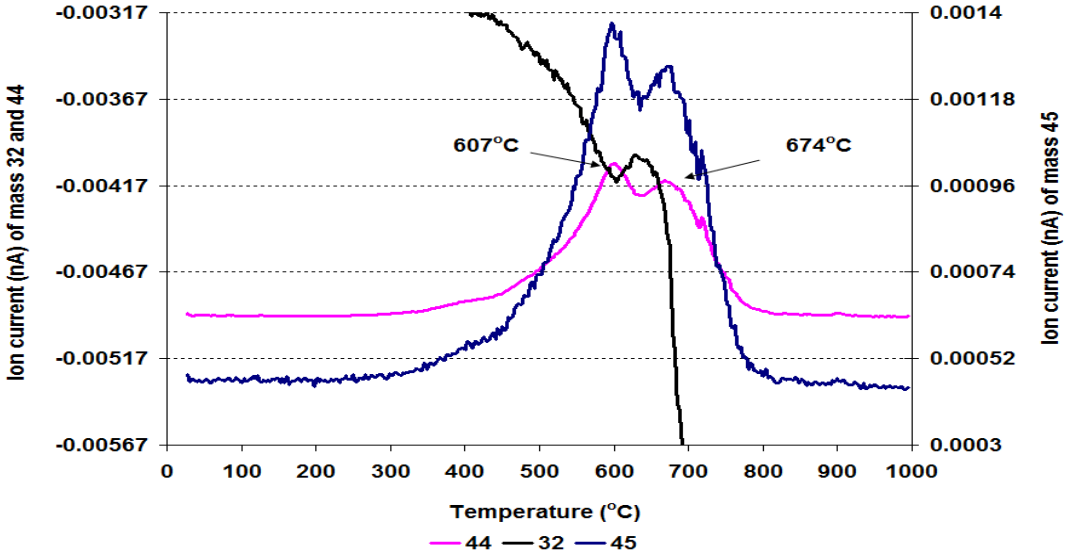

Figure 8.3-131 MS data of CO_2 (m/z = 44), O_2 (m/z = 32) and C_2H_5OH fragment (m/z = 45) for Rh/Al_2O_3 catalyst following the acetone impurity reaction

The TGA result shown in Figure 8.3-130 illustrates in the acetone impurity reaction that the least coke (314.2 mg g^{-1}) formation occurred on the catalyst surface compared to all of the other steam reforming ethanol reactions over the Rh/Al_2O_3 catalyst. The derivative weight profile reveals that two shoulder peaks at 603°C and 699°C respectively were observed, which suggest that different natures of coke deposition occurred on the catalyst

surface. These weight loss events corresponded to CO_2 and the principal fragment of ethanol evolution in mass spectrometry results, which are shown in Figures 8.3-131.

8.3.4.10.2 Raman analysis

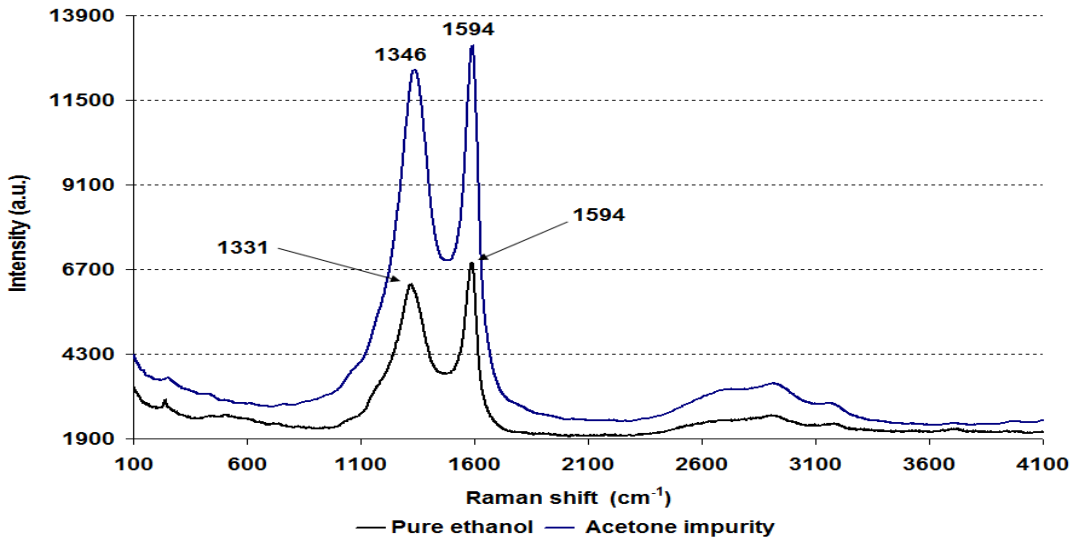

Figure 8.3-132 Post reaction Raman spectra for Rh/Al_2O_3 catalyst following the acetone impurity reaction

The Raman results collected for the acetone impurity post reaction Rh/Al_2O_3 catalyst shows that the peak for the graphitic carbon significantly increased in intensity compared to the pure ethanol post reaction catalyst, which is clarified in Figure 8.3-132. Furthermore the lower wavenumber peak was shifted slightly upward suggesting that a slightly different type of graphitic carbon was formed on the catalyst surface at 500^{o}C in the acetone impurity reaction.

8.3.4.10.3 BET analysis

Catalyst	Conditions	BET Surface area (m^2/g)	Pore volume (cm^3/g)	Average pore diameter (Å)
Rh/Al_2O_3	Pure ethanol (500^{o}C)	47	0.04 (± 3.28)	42 (± 5.57)
	Acetone impurity	45	0.11 (± 0.0)	101 (± 2.14)

Table 8.3-17 BET analysis of post reaction Rh/Al_2O_3 catalyst following the acetone impurity reaction

The BET analysis of the acetone impurity post reaction catalyst illustrates that the BET surface area slightly decreased whilst the pore volume and the average pore diameter was significantly increased compared to the pure ethanol post reaction catalyst.

9. Discussion

9.1 Reactions occurring during steam reforming of ethanol

The steam reforming of ethanol is an endothermic reaction and follows complex pathways, as discussed in section 6.4. The formation of the products can differ with changes in the reaction parameters. A scheme of reactions, which were observed at different temperatures on different catalysts, are summarised in Figure 9.1-1.

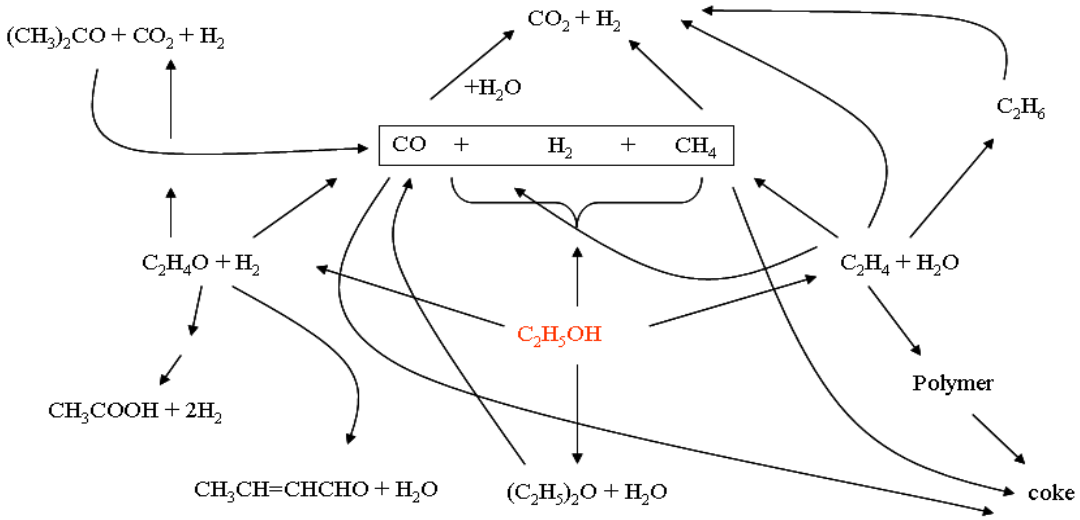

Figure 9.1-1 Possible reactions during the steam reforming of ethanol

9.2 Effect of temperature

9.2.1 Al_2O_3

The results for the steam reforming of ethanol at different temperatures and at 20 barg pressure over alumina and alumina supported noble metals were presented in Chapter 8. In this chapter these results will be discussed.

The results for the 500°C and 600°C reactions over the Al_2O_3, shown in Figure 8.2-1 and Figure 8.2-10 respectively, indicate the influence of temperature on alumina. The results showed that at both temperatures, 99% conversion of ethanol took place and after 100 hours time on stream, no remarkable deactivation was observed. This indicates that alumina is also an active catalyst for ethanol steam reforming and corroborates the idea of Llorca *et al.* [93] who suggested that alumina and vanadia give 100% ethanol conversion at temperatures of 350°C and above. This high conversion of ethanol was attributed to the high adsorption capacity of alumina towards ethanol [45]. However, another possible

explanation for the high ethanol conversion in the present study may to be due to the high pressure used, which increased the ethanol collision per unit area on the alumina and increased the conversion of the ethanol. The effect of pressure has not been widely investigated as most investigations on the ethanol steam reforming reaction have been carried out at ambient pressure. However, Aupretre *et al.* [126] found that the activity of Al_2O_3 towards ethanol conversion increased as the pressure was increased. The increase in temperature from 500^{o}C to 600^{o}C slightly decreased the conversion of ethanol on the alumina in the later stages of the reaction. This may be caused by either the deposition of coke on the active sites or sintering of the Al_2O_3 particles. This idea will be discussed later.

As shown in Figure 9.1-1, there are several pathways that could occur in the ethanol steam reforming process. These vary greatly depending upon temperature, support, precursor, metal loading, catalyst preparation method, pressure, steam to ethanol ratio and even the presence of different impurities present in the ethanol feed. Most of the current literature reveals that ethanol goes through a dehydration process on the alumina and forms ethylene, diethyl ether, and water because the acidic sites that are present on the alumina surface promote dehydration of ethanol and coke formation. [41, 45, 70, 127-130].

$$C_2H_5OH \rightarrow C_2H_4 + H_2O \qquad \Delta G = -84.7 \text{ kJ mol}^{-1} (500^oC) \quad (9.1)$$

$$\Delta G = -101.5 \text{ kJ mol}^{-1} (600^oC)$$

$$C_2H_4 \rightarrow \text{Coke} \qquad (9.2)$$

In contrast to the available literature, in the present investigation only small amounts of C_2H_4 were formed on alumina at both 500^{o}C and 600^{o}C. On the other hand remarkable formation of H_2, CH_4 and CO_2 took place on the alumina. A plausible explanation for this high formation of CH_4 and CO_2 is the preparation and the thermal treatment of the alumina [89, 122, 130]. Most of the research has been conducted using γ-Al_2O_3 which has more acidic sites. However, powder XRD showed a mixture of delta and theta patterns for the alumina used in this project, which has fewer acidic sites than γ-Al_2O_3. Additionally, the thermal decomposition of ethanol may have taken place which would have some contribution to the high CH_4 formation [47, 85].

In the literature [59, 131], it was observed that the increase in the reaction temperature increased the rate of formation of H_2. However, in the present study the increase in temperature from 500^{o}C to 600^{o}C brought about limited change in the rate of formation of

hydrogen. From Figure 9.2-1 this small change can be correlated to the change in the rate of formation of CH_4. This is also supported by the previous research which suggests that CH_4 can undergo steam reforming and form CO and H_2 which is consistent with these results [72].

$$CH_4 + H_2O \rightarrow CO + 3H_2 \qquad \Delta G = -8 \text{ kJ mol}^{-1} (500^oC) \qquad (9.3)$$
$$\Delta G = -4 \text{ kJ mol}^{-1} (600^oC)$$

However the steam reforming of ethanol reaction can occur through more than one complex pathway as discussed before. According to theoretical studies, the increase in temperature shifts the equilibrium position for the water gas shift reaction so no significant change in the rate of formation of H_2 was observed. The yield of H_2 was in the range of 36% to 44% at 500°C to 600°C whilst the theoretical study of thermodynamics suggested that the equilibrium yield of H_2 would be 38%, so the yield observed appears to be in an agreement with the theoretical study. It may appear surprising that CH_4 would be one of the major gaseous products from the steam reforming of ethanol (Figure 9.2-1) at this temperature and in the literature there were some contradictions about the yields of CH_4. Some researchers report that the CH_4 yield decreased with an increase in the reaction temperature due to the steam reforming of CH_4 [73, 132]. Conversely theoretical work conducted by Dennis *et al.* [133] on the steam reforming of ethanol showed that below 700°C CH_4 would be one of the major products at high pressure. This study [133] supports the high yield of CH_4 produced over alumina at 20 barg.

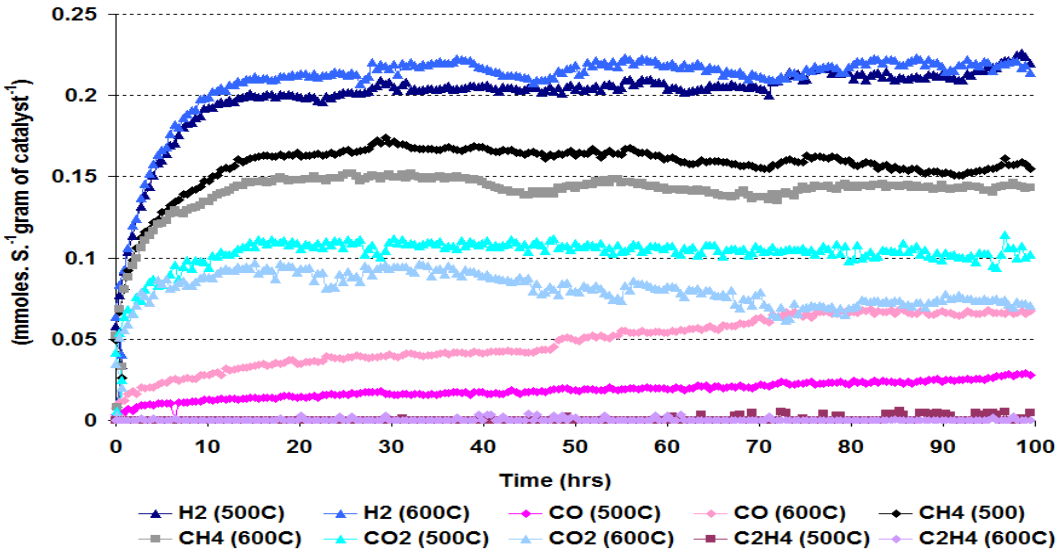

Figure 9.2-1 Rate of formation of gaseous products over Al_2O_3 catalyst at 500°Cand 600°C

Temperature has an apparent effect on the rate of formation of CO and CO_2 and the increase of the reaction temperature from 500^oC to 600^oC increased the rate of formation of CO from 0.02 to 0.04 mmol s^{-1} g^{-1} whilst the rate of formation of CO_2 decreased from 0.11 to 0.08 mmol s^{-1} g^{-1} after 48 hours time on stream as shown in Figure 9.2-1. However, after 70 hours time on stream both CO and CO_2 achieved steady state conditions which were continuous until the end of the reaction.

The change of the CO and CO_2 rates of formation with temperature suggest that the alumina support was active for water gas shift reaction [134]. It is possible that at high pressure CO adsorbed on the alumina reacts with the adsorbed water to form CO_2 and H_2. Recently the oxidation of CO was investigated by Tanaka *et al.* [135] and found that the rate determining step for the CO oxidation took place via the reaction of COOH with OH.

$$COOH_{(a)} + OH_{(a)} \rightarrow CO_2 + H_2O \qquad (9.4)$$

From the above discussion it can be seen that the water gas shift reaction plays an important role in the rate of formation of CO and CO_2. However, the water gas shift reaction is not the only pathway through which CO and CO_2 are produced but other pathways, such as those as shown in Figure 9.1-1, play a role in the rate of formation of CO and CO_2.

At 600^oC, initially more CO_2 than CO was produced, which suggests that initially the rate of the water gas shift reaction was high and slowly decreased with time. This may indicate that sites on the alumina for CO oxidation were deactivated by coke. This idea is also supported by the TPO and BET analysis results of the spent samples.

Figures 8.2-5 and 8.2-14 showed that in the liquid products small amounts of acetaldehyde, acetone and acetic acid were formed at 500^oC and 600^oC. The rate of formation of the liquid products increased with reaction time at both temperatures. Nishiguchi *et al.* [25] claimed that acetone was formed from acetaldehyde by an aldol condensation. However it is not so simple and will be discussed later in more detail.

$$2CH_3CHO \rightarrow (CH_3)_2CO + CO_2 + H_2 \quad \Delta G = -364.9 \text{ kJmol}^{-1} (500^oC) \quad (9.5)$$
$$\Delta G = -376.1 \text{ kJmol}^{-1} (600^oC)$$

Post reaction characterisation of the spent catalyst, discussed in sections 8.2.1-2 and 8.2.1-4, provides information about the coke and catalyst morphology. Figures 8.2-6 and 8.2-15 indicate that the change in temperature from 500^{o}C to 600^{o}C resulted in a change in the weight loss in the TPO which was run in the range between 22^{o}C and 1000^{o}C. The mass spectrometry results revealed that CO_2 and ethanol (45) were evolved during the TPO. Their evolution was accompanied by a minimum in the O_2 signal. The evolution of CO_2 in different temperature regions in these two reactions revealed that the carbon deposition over the catalyst was attributable to two different types of coke, which will be discussed in more detail in the coming sections. The DSC trace indicated that the evolutions were, as expected, exothermic in nature. At 500^{o}C most of the carbon deposition can be ascribed to having been formed by the cracking of CH_4 and by the polymerization of ethylene as small amounts of ethylene were detected at that temperature, as shown in Figure 9.2-1.

$$C_2H_4 \rightarrow \text{polymerisation} \rightarrow \text{Coke} \qquad (9.6)$$

Whilst at 600^{o}C the coke deposition that occurred may be due to combined C_2H_4 and a dehydrogenated methyl group (CH_x, $3 \geq x \geq 0$) [15].

Table 9.2-1 shows a clear correspondence between BET surface area and weight loss in the TPO. The decease in the pore volume suggests that carbonaceous materials were mostly deposited in the pores of the catalyst. For further clarification of the catalyst deactivation, one of the samples had the deposited carbon removed by TPO at 600^{o}C for 16 hours and was then analysed by BET. The same BET surface area as the original catalyst after reduction was obtained. This result indicates that both the blockage and filling of pores by coke plays an important role in the deactivation of the catalyst. This is illustrated below in Figure 9.2-2.

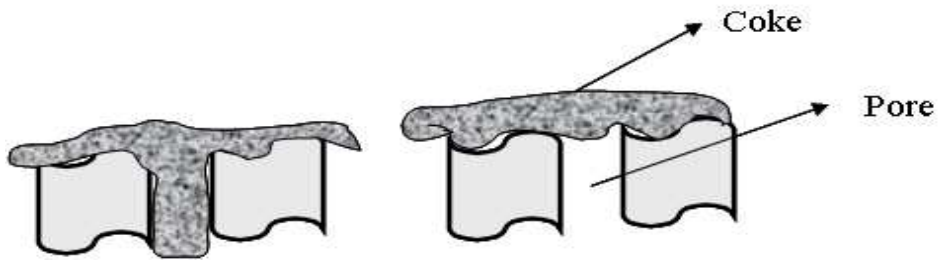

Figure 9.2-2 Filling of the catalyst pore by coke

Conditions (^oC)	BET Surface area (m^2/g)	Pore volume (cm^3/g)	Weight loss in TPO (%)
Reduced@600	100	0.45	-
500	80	0.40	3
600	65	0.24	20

Table 9.2-1 Post reaction BET analysis and weight loss of Al_2O_3 catalyst at different temperatures

The nature of the coke was determined by Raman spectroscopy, powder XRD and SEM analysis. The Raman spectra obtained from the catalyst particles at 500^{o}C showed interesting results. As mentioned in Figure 8.2-8, three different types of particles were collected in the 500^{o}C reaction and each particle gave different Raman bands. The white particle gave a band at 1621 cm^{-1} which is called the G band in literature and has characteristic bands for the graphite carbon [136]. Whereas the black particle gave disordered graphitic carbon Raman bands, suggesting that relatively more graphitic type carbon was formed on the catalyst surface. However, due to small amount of coke deposition no evidence of filamentous carbon was detected in the SEM image, as shown in Figure 8.2-9. The Raman band of the post reaction sample of 600^{o}C gave broad bands at 1345 cm^{-1} and 1595 cm^{-1} and these were characteristic bands for disordered carbonaceous materials and ordered graphitic species. In the literature these bands were called D and G bands respectively [125, 137, 138]. The presence of graphitic carbon was also supported by powder XRD results.

The SEM image shown in Figure 8.2-18 for the spent 600^{o}C reaction sample indicates that both small fibrous and rod type carbon nanotubes were present. Hence the current results show that not only filamentous type coke formation took place on the metal but it was also formed over the support.

9.2.2 Ru/Al_2O_3

The conversion of ethanol over the Ru/Al_2O_3 catalyst at 500^{o}C and 550^{o}C gave similar patterns to each other. At both temperatures, the conversion of ethanol dropped to 70% in the initial 27 hours TOS and then stabilised for the rest of the reaction duration. The decrease in the conversion of ethanol, with time on stream, may be due to the formation of amorphous coke which decreased the access of reactants to the active sites of the catalyst. The decrease in ethanol conversion due to coke is also supported by the decrease in the BET surface area and pore volume. The results also indicate that after a certain amount of

deactivation of the catalyst no further changes in the catalyst behaviour were observed, which suggests that the main cause of deactivation of the catalyst is the blockage of some metal by coke. It is important to point out that the formation of coke over the catalyst was mainly due to high ethylene production as shown in Figure 9.2-3 and in agreement with a previous study [73]. The deactivation of the Ru/Al_2O_3 catalyst agrees with the findings in literature which reported that a 5% Ru/Al_2O_3 catalyst gives conversion of ethanol in the 50% to 70% region after 100 hours time on stream [49]. The conversion of ethanol at 600^oC over the Ru/Al_2O_3 shows interesting results. Initially the conversion of ethanol steadily decreased up to 52.5 hours time on stream and then started to increase continuously until the end of the reaction and achieved conversion of ethanol similar to that observed at 500^oC and 550^oC. The regeneration of the catalyst is not completely understood. However, it seems that initial extensive blocking of the active sites can be reverted to the steady state position by methanation of the deposited coke.

$$C_X + yH_2 \rightarrow xCH_4 \qquad (9.7)$$

As mentioned before, the deactivation of the catalyst took place due to a high production of ethylene which is visible from Figure 9.2-3. The rate of formation of ethylene at different temperatures has a specific relationship to the deactivation of the Ru/Al_2O_3 catalyst. However, the rate of formation of ethylene decreased with an increase in the reaction temperature, whilst the theoretical calculations suggest that it should increase with an increase in the reaction temperature.

$$C_2H_5OH \rightarrow C_2H_4 + H_2O \qquad \Delta G = -84.67\ kJmol^{-1}\ (500^oC) \quad (9.8)$$
$$\Delta G = -101.50\ kJmol^{-1}\ (600^oC)$$

This contradiction between the results and theoretical calculations can be explained as follows. With an increase in reaction temperature, there is an increase in the rate of C_2H_4 formation. However, at the same time, the steam reforming and hydrogenolysis of C_2H_4 increases, which forms H_2, CO and CH_4 as can be seen in Figure 9.2-3. Additionally, polymerisation may occur forming more coke, as discussed in section 9.2-1. The conversion of C_2H_4 to CH_4 and other CO_x products is also in an agreement with literature [139]. The rate of formation of H_2 at different temperatures, as shown in Figure 9.2-4, reveals that with an increase in the reaction temperature from 500^oC to 600^oC, there was a slight decrease in the rate of formation of H_2. This may correspond with an increase in the

hydrogenolysis reaction, which is an undesirable process in ethanol steam reforming reaction.

$$C_2H_4 + 2H_2 \rightarrow 2CH_4 \qquad \Delta G = -219.08 \text{ kJ mol}^{-1} (500^oC) \qquad (9.9)$$

$$\Delta G = -221.35 \text{ kJ mol}^{-1} (600^oC)$$

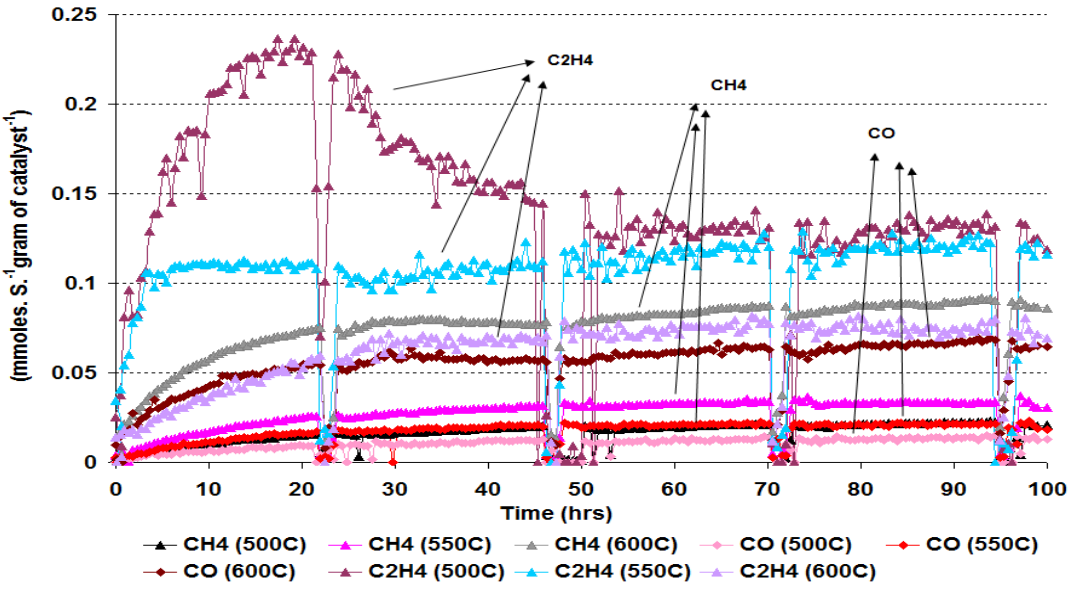

Figure 9.2-3 Rate of formation of different gaseous products over the Ru/Al_2O_3 at different temperatures

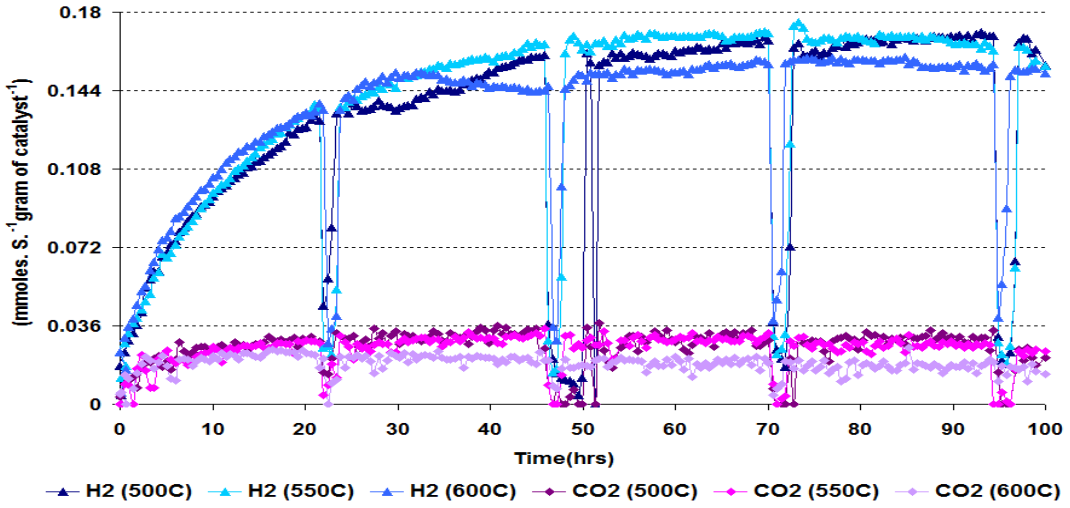

Figure 9.2-4 Rate of formation of H_2 and CO_2 products over the Ru/Al_2O_3 at different temperatures

In the liquid products acetaldehyde was produced along with a range of other secondary products shown in Figures 8.2-21, 8.2-31 and 8.2-40. The figures reveal that at 500°C the secondary products shown in Figure 9.2-5 have high rates of formation and decrease with

an increase in the reaction temperature. This may be attributed to the fact that acetaldehyde desorbs from the catalyst faster at high temperature before undergoing oxidation to acetic acid and other liquid products.

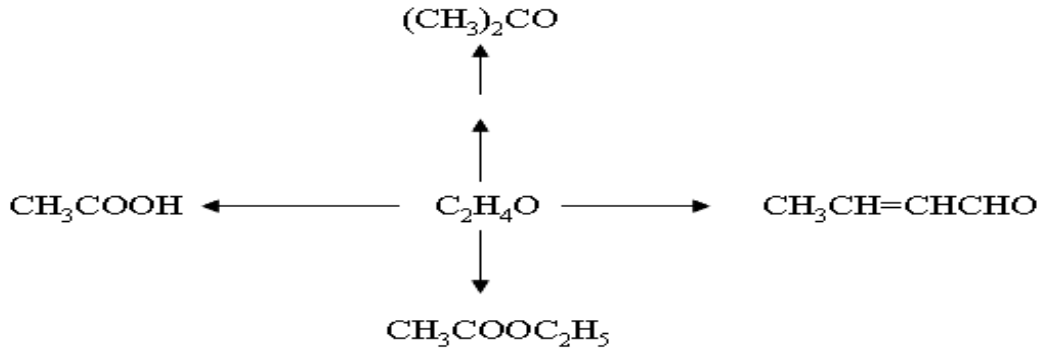

Figure 9.2-5 Possible products from acetaldehyde during ethanol steam reforming of ethanol

With regard to the yield of products, C_2H_4 gave the highest yield which significantly decreased with reaction temperature and in the initial 24 hrs TOS its yield decreased from 90% to 18% when the temperature was increased from 500^{o}C to 600^{o}C. In contrast to C_2H_4, the yield of CH_4 increased from 2% to 13%. The presence of crotonaldehyde and methanol during the reaction indicates that the ethanol steam reforming reaction (ESR) is not a simple dehydration or dehydrogenation reaction as the primary products react further to form the secondary products. For example acetaldehyde undergoes an aldol condensation to form crotonaldehyde.

$$2C_2H_4O \rightarrow CH_3CH=CHCHO + H_2O \qquad (9.10)$$

The production of diethyl ether shows that the presence of ruthenium metal particles results in the modification of the alumina support. The formation of diethyl ether has also been reported by other researchers over the alumina support [128, 140]. Jain *et al.* [127] reported that the ethanol was first adsorbed on the basic sites, which then reacted by a substitution reaction to form diethyl ether. More detail on ether formation will be discussed in the next section.

Furthermore, it was noticed that due to formation of a high level of C_2 containing products, Ru/Al_2O_3 gave a low yield of H_2.

Post reaction characterisation of the Ru/Al_2O_3 catalyst at different temperatures, discussed in sections 8.2.2.2, 8.2.2.4 and 8.2.2.6, reveals that an increase in the reaction temperature

increased the coke deposition over the catalyst. From the derivative weight peaks in the TPO results at different temperatures, it is plausible that different types of coke species were formed over the catalyst surface. The DSC profile (not shown) shows that the removal of carbonaceous materials from the catalyst surface in an oxygen atmosphere is an exothermic process. Also, the shoulder on the lower temperature side in the derivative weight profiles at 500^{o}C and 600^{o}C shows that on the same catalyst different types of coke forming reactions took place simultaneously. The nature of the carbonaceous material deposited on the catalyst is always complex and its reactivity was a consequence of the formation mechanism. In the literature the nature of coke has been explained by various researchers in different ways. Cerritos *et al.* [15] reported that the weight change in TGA results below 550^{o}C can be ascribed to filamentous type carbon, which originates from the C_2H_4 polymerisation whilst a weight loss above 550^{o}C corresponded to the dehydrogenation of the methyl groups. On the contrary Fatsikostas *et al.* [45] claim that different peaks given by coke deposited on the catalysts surface were due to the formation of coke on the metal and the carriers. They suggested that coke deposited on the metals gave a peak at a lower temperature whilst the higher temperature peak, which was more significant, could be attributed to the accumulation of coke on the carrier. Other researchers have mentioned that these peaks are due to the nature of different types of coke deposited on to the catalyst surface [13, 141]. McCarty [141] reported four different types of carbon formed by the deposition of CO or C_2H_4 over the Al_2O_3 surface. McCarty also mentioned that the weight loss shifted towards the high temperature region as the amount of coke on the catalyst increased. Different researchers have given different names to the same type of carbon. However, among the different nomenclatures three important carbon types have been identified. Carbon deposited on metal is more hydrogenated, can be removed at a lower temperature and is called α carbon. The carbon deposited on the metal -support interface is dehydrogenated carbon and is called β carbon, whilst the carbon deposited on the support is graphitic in nature and is called γ carbon. The TPO results shown in sections 8.2.2.2, 8.2.2.4 and 8.2.2.6, suggest that mainly two types of coke (β and γ) were formed over Ru/Al_2O_3 at different temperatures. Shifting of the TPO peak towards higher temperatures occurred due to difference in the amounts and the nature of coke deposited at different temperatures, as indicated in the water evolution profile in Figure 9.2-6. The limited high gaseous products profile of the reaction suggests that the coke was formed mainly from the polymerisation of C_2H_4, and was also supported by the mass spectrometry profile of water evolution at different temperatures, shown in Figure 9.2-6. The figure indicates that the increase in temperature decreased the H/C ratio which

indicated that the hydrogenated hydrocarbon was converted to more polyaromatic and graphitic type carbon. The β carbon was slowly converted to graphite type carbon, as revealed by the Raman spectroscopy results, which gave characteristic bands for graphitic carbon. The I_D and I_G show the intensity of D and G bands respectively in the Raman spectrum of graphitic carbon. The ratio of I_D and I_G bands in Table 9.2.2, give an idea about the level of disorder in graphite and is also used to evaluate perfection degree of the graphitic structure and in literature it is reported as the R value [137]. The Raman results suggest that disorder in the graphitic carbon decreased with an increase in reaction temperature up to 550°C and then dramatically increased, as shown in Table 9.2-2.

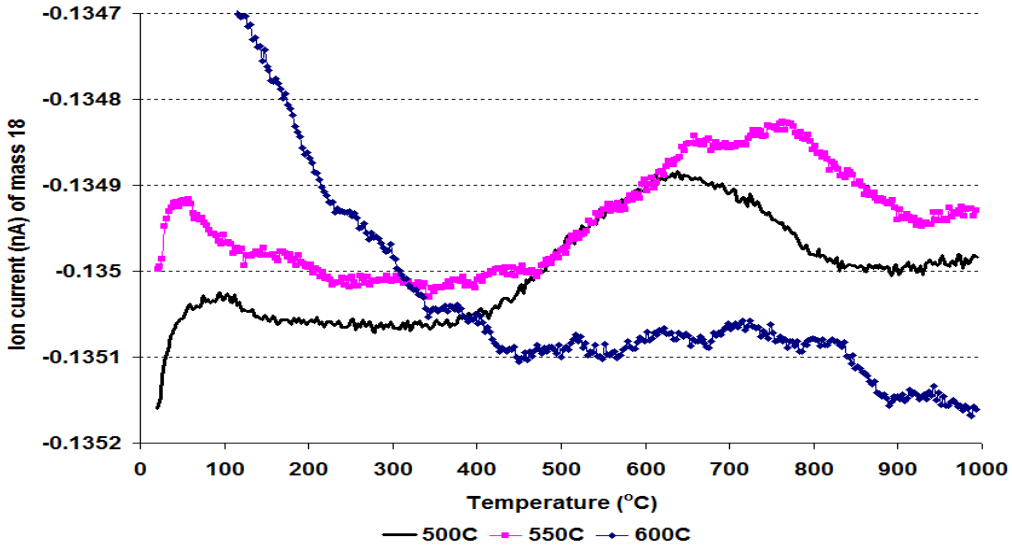

Figure 9.2-6 Evolution of m/z = 18 (H_2O) during TPO for the spent Ru/Al_2O_3 catalyst at different temperatures

Conditions (°C)	BET Surface area (m^2/g)	Pore volume (cm^3/g)	Weight loss in TPO (%)	(I_D/I_G)
Reduced@600	100	0.43	-	-
500	32	0.07	39	0.99
550	12	0.03	44	0.92
600	23	0.01	44	1.24

Table 9.2-2 Post reaction BET analysis and weight loss of Ru/Al_2O_3 catalyst at different temperatures

Kineale *et al.* [142] explained how the ethylene is deposited on the catalyst surface; first C_2H_4 was adsorbed on the catalyst surface and then was converted to CH_x. Now it could convert to CH_4 via the methanation process or be converted to graphitic type carbon over the catalyst surface. This is illustrated below in Figure 9.2-7.

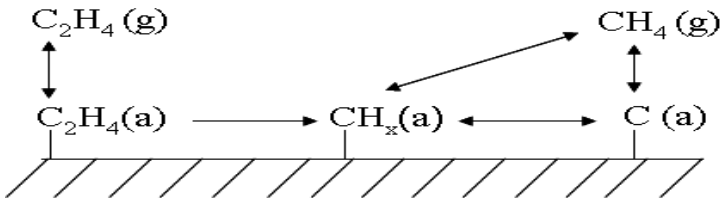

Figure 9.2-7 C_2H_4 decomposition on catalyst surface

The SEM images shown in Figures 8.2-28, 8.2-37 and 8.2-46 show the effect of temperature on the formation of filamentous carbon. At 500^{o}C no filamentous carbon was present and this indicates that at this temperature only amorphous carbon is produced from the steam reforming of ethanol over the Ru metal. However, as the temperature increased from 500^{o}C to 600^{o}C the number and size of filamentous type carbon also increased which indicates that high temperature favours the formation of filamentous carbon and this is supported by the TPO results. The high deposition of coke over the catalyst and small decay in the conversion of ethanol hints that the formation of filamentous type carbon took place over the Ru metal. These results are also supported by previous studies done by Wang *et al.* and Alberton *et al.* [7, 128]. For further clarification of the catalyst deactivation, one of the samples was subjected to a TPO at 600^{o}C for 16 hours, which removed low temperature coke, and then analysed by BET. The same BET surface area was obtained as for the original catalyst in the reduced form. After TPO the sample was also run on the Raman spectroscopy and no significant change was observed in the graphitic bands. These results suggest that two types of coke, hydrogenated coke which can be removed by TPO at 600^{o}C and dehydrogenated and graphitic type carbon which can only removed by TPO at higher temperatures, exist on the catalyst surface. Hence the surface of the catalyst was principally covered by amorphous and hydrogenated carbon which did not block the steam reforming reaction of ethanol at low temperatures whilst at high temperatures the amorphous carbon was converted into graphitic type carbon.

9.2.3 Pt/Al_2O_3

The conversion of ethanol over the Pt/Al_2O_3 catalyst at 500^{o}C and 550^{o}C were 97% and 99% respectively in the initial one hour TOS, which steadily decreased with time and obtained steady state (~ 50 hours) conditions. However, after achieving steady state conditions no deactivation was observed at both reaction temperatures. These results indicate that with the increase in the rate of formation of C_2H_4 the deactivation of the catalyst for ethanol conversion increased which suggests that the C_2H_4 polymerised and deactivated some of the metal particles. This result also matches with the conversion of

ethanol over the Ru/Al_2O_3 catalyst as discussed before. The formation of high amounts of coke could block the pores and decrease the access of the reactants to the active sites. If correct then the high deactivation at 500°C may due to increased coke contribution from both C_2H_4 and CH_4 as these were seen from the product distribution profiles, shown in Figure 9.2-8. It suggests that more CH_4 was produced which is also a source of coke besides C_2H_4. The high conversion of ethanol at 600°C may be explained in two ways. First, at 600°C the Gibbs free energy for the oxidation of metallic platinum to platinum dioxide was above zero which suggests the highly active platinum is still in reduced form and responsible for the high conversion of ethanol [143, 144].

$$Pt + O_2 \quad \leftrightarrow \quad PtO_2 \qquad \Delta G = -17.2 \text{ kJ mol}^{-1} \ (500^{o}C) \qquad (9.11)$$
$$\Delta G = +3.2 \text{ kJ mol}^{-1} \ (600^{o}C)$$

Secondly, the formation of relatively more hydrogenated coke does not completely deactivate the platinum metal at 600°C. The second explanation is also supported by the mass spectrometry results in Figure 9.2-12 which illustrate that water was evolved during the TPO of the 600°C post reaction sample. Both explanations are thought to be possible for the high conversion of ethanol, although the formation of hydrogenated coke is thought to be most likely.

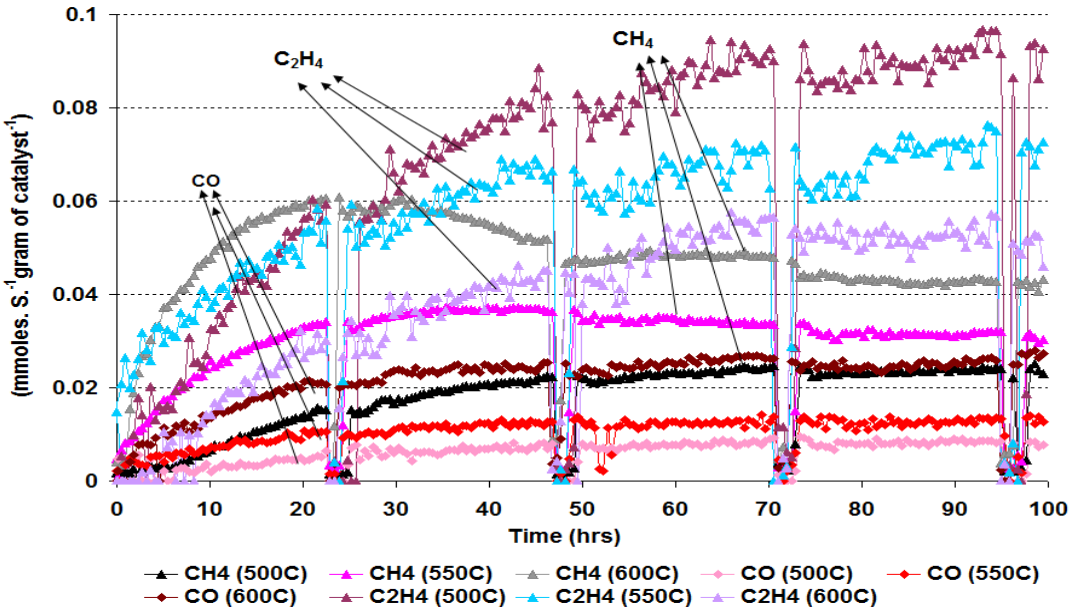

Figure 9.2-8 Rate of formation of different gaseous products over the Pt/Al_2O_3 catalyst at different temperatures

Regarding the product distribution C_2H_4 gave the highest rate of formation at all three temperatures. The rate of formation of C_2H_4 steadily increased up to the end of the reaction. However it did not achieve steady state conditions until the end of the reaction. A high formation rate of C_2H_4 was also observed over a Pt/Al_2O_3 catalyst by a previous study [145]. Temperature had a negative effect on the C_2H_4 formation *i.e.* with an increase in the reaction temperature, there was a decrease in the formation of C_2H_4 [146]. The rate of formation of C_2H_4 at 600^{o}C significantly decreased whereas the rate of formation of CH_4 significantly increased. This result suggests that at 600^{o}C C_2H_4 hydrogenolysed and produced CH_4 as discussed in the previous section.

$$C_2H_4 + 2H_2 \rightarrow 2CH_4 \qquad (9.12)$$

From the equation a single mole of C_2H_4 will lead to twice the number of moles of CH_4 and the yield in Figures 8.2-50 and 8.2-69 almost matches this result. So, it is suggested that the increase in CH_4 production was due to the C_2H_4 hydrogenolysis. At 600^{o}C initially the formation of CH_4 was high and then started to decrease. A literature search showed that this decrease may be due to deactivation of the active sites on the catalyst for the hydrogenolysis of C_2H_4. So, the rate of formation of C_2H_4 increased [139]. The C_2H_4 not only hydrogenolysed but it also polymerised and formed coke as discussed before. Besides CH_4 small amounts of C_2H_6 were also produced. The formation of C_2H_6 was a result of hydrogenation of C_2H_4, as both of these reactants were present in the reaction stream and they reacted to form C_2H_6 [147].

$$C_2H_4 + H_2 \rightarrow C_2H_6 \qquad \Delta G = -43 \text{ kJ mol}^{-1} (500^oC) \qquad (9.13)$$

$$\Delta G = -31 \text{ kJ mol}^{-1} (600^oC)$$

However, it may have also been formed by the coupling of CH_3 which is produced by the splitting of acetaldehyde molecule.

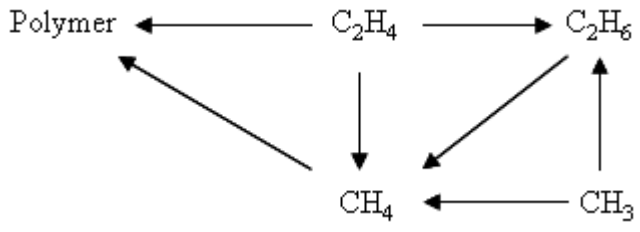

Figure 9.2-9 Different possible products from C_2H_4

The rate of formation of CO_2 (Figure 9.2-10) was higher compared to the rate of formation of CO (Figure 9.2-8) and is explained as discussed in section 9.2-1. The CO_2 mainly comes from the decarbonylation of acetaldehyde and WGS reaction over the Al_2O_3 [73]. However, besides this, the steam reforming of CH_4 also contributes to the high formation of CO_2.

$$CH_4 + 2H_2O \rightarrow CO_2 + 4H_2 \qquad \Delta G = +31.4 \text{ kJ mol}^{-1} (500^oC) \quad (9.14)$$
$$\Delta G = +14.1 \text{ kJ mol}^{-1} (600^oC)$$

Similarly the other liquid products such as diethyl ether and acetone undergo steam reforming to form CH_4 and CO_2.

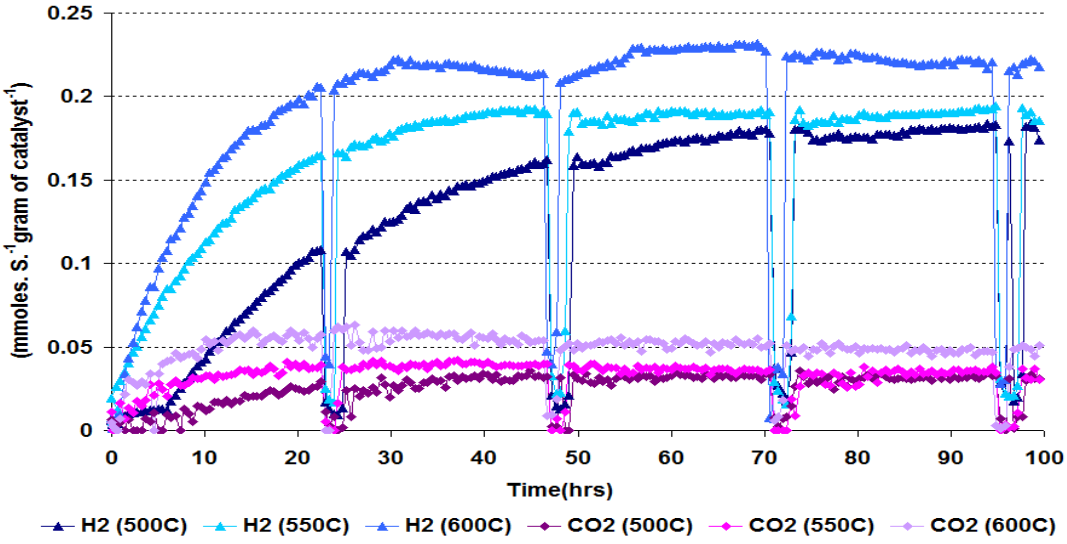

Figure 9.2-10 Rate of formation of H_2 and CO_2 products over the Pt/Al_2O_3 catalyst at different temperatures

In the liquid products acetaldehyde was produced at a high rate. The formation of acetaldehyde during the steam reforming of ethanol is well documented and is produced from the oxidation of ethoxy species. The acetaldehyde either splits to form CO and CH_4 or further reacts with OH from water or from the support to form the acetate. For example CeO_2 undergoes a redox process and provides an oxygen species to the ethoxy group whereas, in Al_2O_3, the adsorbed H_2O provides the OH group for the oxidation of the ethoxy. Benito *et al.* [43] investigated the surface reaction mechanism of bioethanol and found that ethanol was first adsorbed on to the metal surface before being dehydrogenated to form the acetaldehyde. Then depending upon the reaction conditions it may desorb from

the surface of the catalyst or be further oxidised to form secondary products such as CH_4, CO_2, CO and crotonaldehyde.

$$C_2H_5OH \leftrightarrow C_2H_5OH_{(ads)} \quad (9.15)$$

$$C_2H_5OH_{(ads)} \leftrightarrow CH_3CHO_{(ads)} + H_2 \quad (9.16)$$

With an increase in the reaction temperature from 500^{o}C to 550^{o}C there was no change in the formation of acetaldehyde. However, it slightly increased at 600^{o}C as shown in Figures 8.2-51, 8.2-61 and 8.2-70. The formation of acetaldehyde was greatly affected by GHSV [72, 129, 148]. It was found that with an increase in GHSV there was a decrease in the complete steam reforming of reactants and intermediate products such as acetaldehyde and ethylene were detected in the products stream. When a high GHSV (~ 50000 h^{-1}) was used during the reaction it is plausible that small amounts of acetaldehyde is observed in the effluent mixture which is expected as discussed before. The rate of formation of acetone in the initial 24 hours was relatively high, which decreased as the reaction proceeded at all three temperatures. The mechanism of formation of acetone during the steam reforming reaction is debatable, some researchers proposing that it comes from the reaction of acetaldehyde and other intermediates such as CH_3 [46].

$$CH_3CHO_{(ads)} + CH_{3(ads)} \rightarrow (CH_3)_2CO_{(ads)} + H_{(ads)} \quad (9.17)$$

The formation of acetone is possible through this route because both CH_4 and acetaldehyde were produced during the reaction. However, Bussi *et al.* [149] claimed that the formation was only possible at low temperatures whilst at high temperatures this reaction is not the main route for acetone formation.

Elliott [150] proposed that the acetone formed from acetaldehyde through catalytic aldol condensation by forming first 3-hydroxybutanal, which was later oxidised to 3-hydroxycarboxylate.

$$2CH_3CHO \leftrightarrow CH_3CHOH\text{-}CH_2\text{-}CHO_{(a)} + O_{(a)} \rightarrow$$

$$CH_3CHOH\text{-}CH_2\text{-}COO_{(a)} + H_{(a)} \rightarrow (CH_3)_2CO + CO_2 + H_2 \quad (9.18)$$

As the aldolization reaction is an exothermic reaction, an increase in the reaction temperature would push the equilibrium back towards acetaldehyde [151]. So, the temperature at which the reactions were performed was not suitable for the formation of

acetone by this route. In the literature it was also suggested that acetone was formed from the oxidation of acetaldehyde to acetic acid and then ketonisation of acetic acid to give acetone and CO_2 [85, 152].

Ethanol → Acetaldehyde → Acetic acid → Acetone

From the liquid product distributions as shown in Figures 8.2-51 and 8.2-61 it may be proposed that the acetone formation took place by ketonisation. However, due to a series of liquid products being formed it is difficult to determine the exact mechanism for acetone formation. Small amounts of acetone were observed in the reaction stream (below 1%). This may be due to parallel reactions where the steam reforming of acetone took place as reported in literature [153].

The formation of diethyl ether is a well known equilibrium product produced over the acidic catalysts by ethanol condensation.

$$2C_2H_5OH \rightarrow (C_2H_5)_2O + H_2O \qquad \Delta G = 0.15 \text{ kJ mol}^{-1} (500^oC) \qquad (9.19)$$
$$\Delta G = 3.32 \text{ kJ mol}^{-1} (600^oC)$$

Figures 8.2-51, 8.2-61 and 8.2-70 show that small amounts of diethyl ether was produced over the Pt/Al_2O_3 catalyst during the steam reforming reaction of ethanol which decreased in rate with the increase in the reaction temperature. However, during the reaction at steady state the rate of formation remained constant, which is in agreement with a previous study [154]. The decrease of diethyl ether formation with an increase of temperature is expected from thermodynamics. The formation of small amounts of diethyl ether were also reported by Erdohelyi *et al.* [140] over Pt/Al_2O_3. Ether formation mostly took place on the acidic sites. The formation of diethyl ether during the reaction suggests that the Pt/Al_2O_3 catalyst has acidic sites. Now the question arises as to how diethyl ether was produced on the catalyst surface *i.e.* do ethylene and diethyl ether use the same sites or they were produced on different active sites over Al_2O_3. Jain and his colleagues [127] claimed that ethylene and diethyl ether were produced on different acidic sites. The synthesis of ethylene took place by elimination whilst diethyl ether is formed by nucleophilic substitution reactions. Another research group explained that ether formation took place by the condensation of two adjacent adsorbed ethanol molecules over an alumina surface [155]. From these literature sources it is suggested that the formation of diethyl ether took place over the Pt/Al_2O_3 catalyst by the following mechanism.

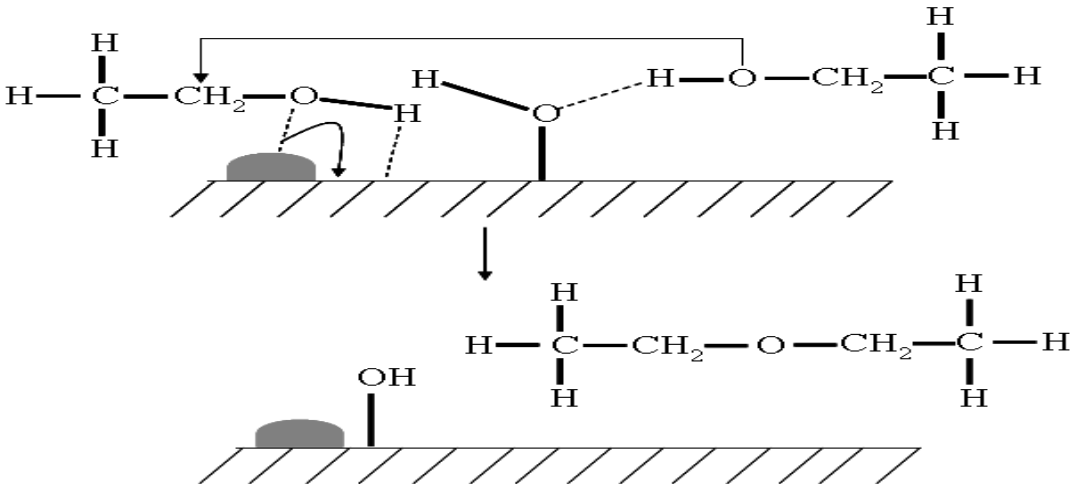

Figure 9.2-11 Formation of diethyl ether from ethanol

Initially the ethanol is adsorbed onto the metal forming ethoxy bonds and at the same time another molecule of ethanol forms a H-bond with the OH on the support. The adsorbed ethanol spills over onto the support from the metal and reacts with an adjacent second adsorbed ethanol by nucleophilic substitution reaction to form diethyl ether.

Also during the steam reforming of ethanol over the Pt/Al_2O_3 catalyst, 1,1-diethoxyethane was produced. According to the literature this secondary product is produced from the reaction of acetaldehyde and ethoxy species produced from ethanol over solid acidic catalysts [156, 157].

$$2CH_3CH_2OH + CH_3CHO \quad \leftrightarrow \quad (CH_3CH_2O)_2CH\text{-}CH_3 + H_2O \qquad (9.20)$$

The results shown in Figures 8.2-51, 8.2-61 and 8.2-70 reveal that it is detected during the reaction at all temperatures in small amounts (yield < 0.4%) over the Pt/Al_2O_3 catalyst.

From the post reaction characterisation of the Pt/Al_2O_3 catalyst at different temperatures, shown in sections 8.2.3.2, 8.2.3.4 and 8.2.3.6, it is obvious that an increase in the reaction temperature from 500^{o}C to 550^{o}C increased the coke deposition and a further increase in the reaction temperature to 600^{o}C had no effect on the amounts of coke deposition, as shown in Table 9.2-3. The derivative weight profiles of the TGA show interesting results. There were two shoulder peaks that appeared between 400^{o}C and 800^{o}C. The shifting of these peaks occurred towards the high temperature region with an increase in the reaction temperature. The shifting of these peaks may have occurred due to two possible reasons. First, with an increase in temperature more coke was deposited, which needed a high

temperature for reoxidisation and so the peaks moved towards a higher temperature region. The second possible reason for the shift is that an increase in the reaction temperature produced relatively more dehydrogenated type carbon, which can only be removed at high temperatures. This is also supported by Raman results for sample of a reaction run at 600^{o}C shown in Figure 8.2-73. The formation of two shoulders, as explained previously over the Ru/Al_2O_3 catalyst was also reported by Shamsi [108] and his colleagues over a Pt/Al_2O_3 catalyst. By analysing coke deposition from three different hydrocarbon steam reforming reactions over Pt/Al_2O_3, a similar shoulder was produced in the TPO matching the results shown in sections 8.2.3.2, 8.2.3.4 and 8.2.3.6. They claimed that coke was deposited on both the metal and support. The coke on the metal was active and could be more easily oxidised by TPO whilst the coke deposited over the support was more like graphitic type as observed from the Figures 8.2-62 and 8.2-71 [107, 108]. These expected results are supported by the TPO analysis done on the post reaction pure Al_2O_3 sample as shown in Figure 8.2-15. The figure shows a CO_2 peak at high temperature and no distinct shoulder was observed at lower temperature. This suggests that the peak at high temperature in the TPO profile comes from the burning of coke on the support whilst the lower temperature peak is produced due to the burning of coke on the metal. The nature of the coke was similar to that which was observed over the Ru/Al_2O_3 catalyst. However, the evolution of water at 600^{o}C shows that relatively more hydrogenated carbon was present over the Pt/Al_2O_3 catalyst compared to that of the Ru/Al_2O_3 catalyst. Thermodynamic calculations reveal that no coke should be formed during the steam reforming run at 500^{o}C and above, using a water to ethanol ratio of 4 at atmospheric pressure, as discussed in Chapter 6 [53]. However, the reaction performed at high pressure is more efficient for carbon formation as reported by previous studies [158]. The pore volume decreased with an increase in the coke formation. The powder XRD pattern gave similar results to that observed for the Pt/Al_2O_3 catalyst in the reduced form although the peak intensity had decreased, which suggests that the crystallinity of the catalyst was slightly decreased whilst no change in phase of Pt/Al_2O_3 was observed. A broad peak at 26^{o} of 2θ position confirms the presence of graphitic type carbon on the catalyst surface, which is also supported by the Raman spectroscopy results.

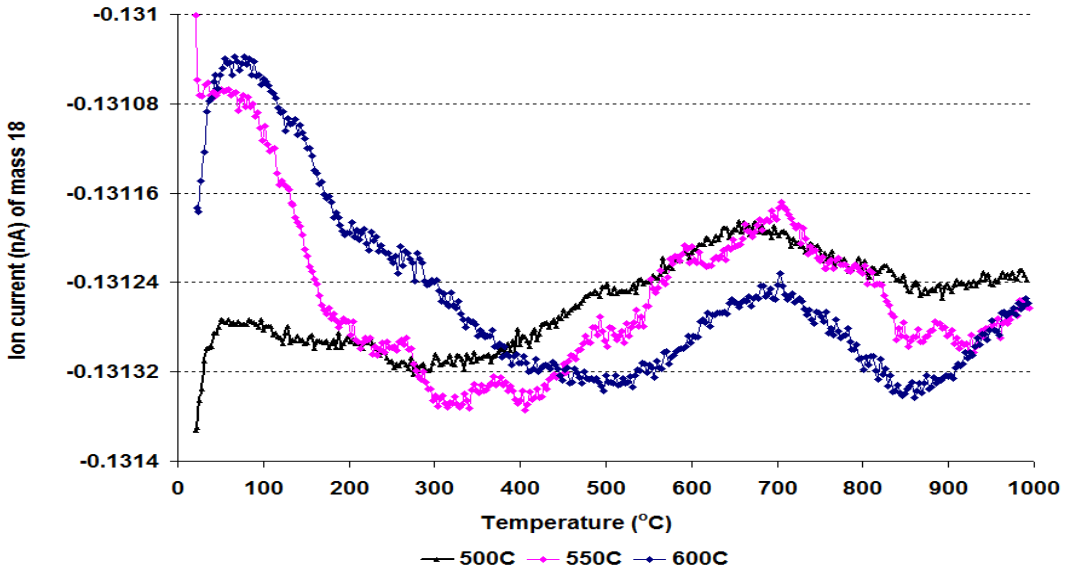

Figure 9.2-12 Evolution of m/z = 18 (H_2O) during TPO for the spent Pt/Al_2O_3 catalyst at different temperatures

The Raman spectroscopy results show that graphitic type coke was produced during the reaction over the Pt/Al_2O_3 catalyst. The bands shown in Figures 8.2-55, 8.2-64 and 8.2-73 reveal that from 500°C to 550°C the intensity of the G bands almost remained constant whilst the D or disorder peak slightly increased. However, at 600°C intensity of both bands had significantly increased. The high value of I_D/I_G ratio at 600°C indicates that more disordered graphite was formed at a higher temperature. These results suggest that at low temperatures, coke was deposited by polymerisation of C_2H_4, whilst at 600°C CH_4 and CO also contribute to coke formation which may occur by a different coke deposition mechanisms, producing more disordered graphitic type carbon.

Conditions (°C)	BET Surface area (m^2/g)	Pore volume (cm^3/g)	Weight loss in TPO (%)	(I_D/I_G)
Reduced@600	100	0.46	-	-
500	41	0.09	37	0.92
550	27	0.05	40	1.03
600	71	0.05	40	1.38

Table 9.2-3 Post reaction BET analysis and weight loss of Pt/Al_2O_3 at different temperatures

In contrast to the Ru/Al_2O_3 catalyst, over the Pt/Al_2O_3 small amounts of filamentous type carbon were observed at 500°C and the number of these tubes increased with an increase in the reaction temperature. Similar to the Ru/Al_2O_3 catalyst there were also rod type carbon nanotubes observed at 600°C. The formation of these carbon nanotubes over the Al_2O_3 and

also on both catalysts at 600^{o}C suggests that temperature plays an important role in the formation of different types of single and multi-wall nanotubes. Recently Wang *et al.* [159] published data in which they pointed out that 600^{o}C is the best temperature for the production of multi-wall carbon nanotubes (MWCNT) whilst at temperatures higher and lower than 600^{o}C, the quality of MWCNT decreased.

9.2.4 Rh/Al_2O_3

The Rh/Al_2O_3 catalyst gave a higher conversion of ethanol than the previously reported catalysts. High conversion of ethanol over the Rh/Al_2O_3 catalyst has also been reported in the literature [11, 54, 116]. At 500^{o}C and 550^{o}C the conversion of ethanol in the initial 1.5 hours was 99%, steadily decreasing with time and at steady state was 81%. No deactivation was observed by the end of the reaction. This high conversion of ethanol was due to the high activity of the Rh/Al_2O_3 catalyst towards C-C bond splitting which is well documented [26, 75, 160, 161]. Due to the high activity for C-C bond splitting using Rh metal, comparatively less C_2 molecules such as ethylene were produced and no acetic acid molecules were observed during the reaction at both temperatures. Usually the conversion of ethanol increased with an increase in the reaction temperature as observed for the Pt/Al_2O_3 catalyst and also seen in literature [162]. However, at 600^{o}C over the Rh/Al_2O_3 catalyst during initial time on stream, the conversion of ethanol was similar to 500^{o}C/550^{o}C (> 90%) whilst this value decreased steadily as the reaction proceeded. This decrease in the conversion of ethanol at 600^{o}C could be due to the formation of increased amounts of dehydrogenated coke, which is supported by water evolution in the mass spectrometry results, shown in Figure 9.4-16. The formation of hard coke may deactivate some of the Rh metal particles and therefore decrease the conversion of ethanol during the reaction. As previously observed, the dehydrogenated coke encapsulates the metal sites and deactivates the catalyst whilst in the presence of hydrogenated coke the catalyst was still active [7]. This conclusion is further supported by the formation of large numbers of rod type coke at 600^{o}C, as seen in the SEM results, and the subsequent decline in the conversion of ethanol.

The corresponding product distributions, shown in Figures 9.2-13 and 9.2-15, indicate that like the earlier catalysts the rate of formation of C_2H_4 was high at all three temperatures. However, less C_2H_4 was produced compared to the Pt/Al_2O_3 and the Ru/Al_2O_3 catalysts and this result is supported by the work done by Graf *et al.* [139] and Liguras *et al.* [49]. Interestingly, steady state for C_2H_4 was achieved at the same point at all three

temperatures. At 500^{o}C, the rate of formation of the C_2H_4 was initially high which steadily decreased to the steady state position as the reaction proceeded. At 550^{o}C and 600^{o}C it steadily increased and after 70 hours TOS steady state conditions were achieved. The initial high rate of formation of C_2H_4 at 500^{o}C may be due to less C-C splitting of the C_2H_4 molecules, which is also seen in the rate of formation of acetaldehyde. These results show that temperature has no significant effect on the formation of C_2H_4. This is also supported by the amount of coke deposition on the catalyst at different temperatures, as tabulated in Table 9.2-4.

With regard to CH_4, the rate of formation increased significantly with an increase in the reaction temperature, specifically at 600^{o}C. The high rate of formation of CH_4 at 600^{o}C may either be due to hydrogenolysis of C_2H_4 and C_2H_6 or the splitting of acetaldehyde. As mentioned before at different temperatures the rate of formation of C_2H_4 was similar. This result inferred that an increase in the rate of formation of CH_4 with increase of temperature may originate from acetaldehyde. This is supported by the increase in the rate of formation of acetaldehyde at 600^{o}C, as shown in Figure 8.2-96. An increase in the rate of formation of CH_4 and CO at 600^{o}C, especially after 50 hours time on stream, suggests that acetaldehyde was decarbonylated over the Rh/Al_2O_3 catalyst to form CH_4 and CO.

$$C_2H_5OH \rightarrow C_2H_4O + H_2 \quad (9.21)$$

$$C_2H_4O \rightarrow CH_4 + CO \quad (9.22)$$

It may be possible that CO forms from acetaldehyde reacting with H_2 and forming CH_4 by the following reactions.

$$C + 2H_2 \rightarrow CH_4 \quad (9.23)$$

$$2CO + 2H_2 \rightarrow CO_2 + CH_4 \quad (9.24)$$

$$CO + H_2O \rightarrow CO_2 + H_2 \quad (9.25)$$

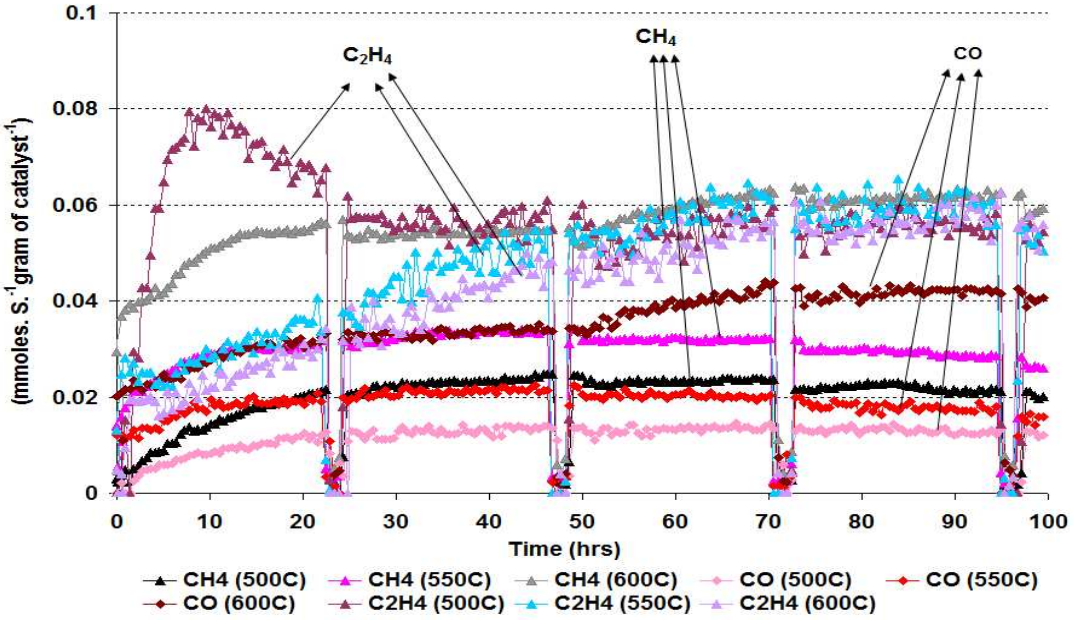

Figure 9.2-13 Rate of formation of different gaseous products on Rh/Al_2O_3 catalyst at different temperatures

It is interesting to note that a relatively higher rate of formation of CO_2 than CO took place over the Rh/Al_2O_3 catalyst. The rate of formation of CO_2 (Figure 9.2-15) was similar at different temperatures. Although during the initial stages of the reaction, it was slightly higher whilst the rate of formation of CO was significantly increased with an increase in the reaction temperatures. This suggests that the formation of CO_2 at a higher rate may be due to either the WGS reaction or steam reforming of ethanol.

Interestingly, with an increase in the reaction temperature the rate of formation of C_2H_6 also slightly increased. This increase may be either due to the hydrogenation of C_2H_4 or the coupling of CH_3 produced by the decomposition of acetaldehyde as discussed in the previous section.

$$C_2H_4 + H_2 \rightarrow C_2H_6 \qquad \Delta G = -43.04 \text{ kJ mol}^{-1} (500^oC) \quad (9.26)$$

$$\Delta G = -31.00 \text{ kJ mol}^{-1} (600^oC)$$

$$2CH_3 \rightarrow C_2H_6 \qquad \Delta G = -252.64 \text{ kJ mol}^{-1} (500^oC) \quad (9.27)$$

$$\Delta G = -236.80 \text{ kJ mol}^{-1} (600^oC)$$

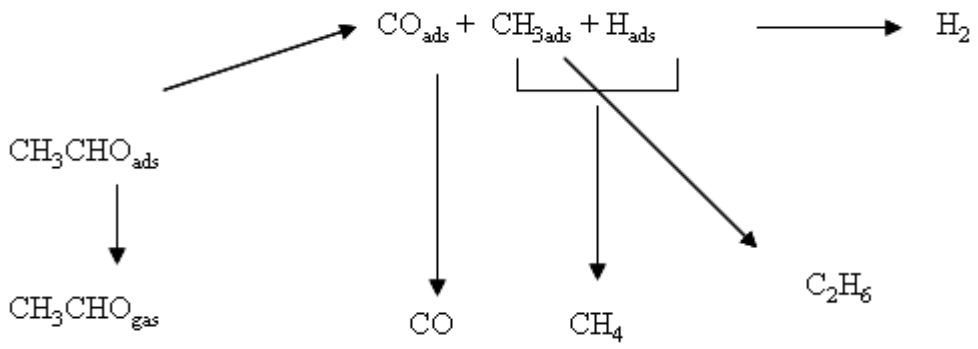

Figure 9.2-14 Different acetaldehyde decomposition path ways

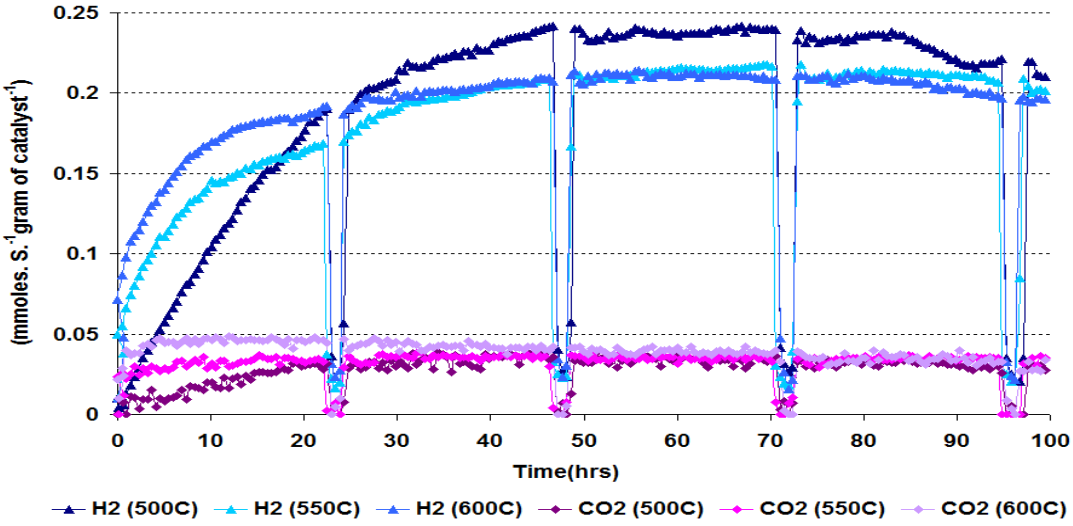

Figure 9.2-15 Rate of formation of H_2 and CO_2 products over the Rh/Al_2O_3 catalyst at different temperatures

The liquid products: acetaldehyde, diethyl ether, acetone and 1,1-diethoxyethane were produced at all temperatures over the Rh/Al_2O_3 catalyst. However, no acetic acid was observed as was seen on the previous catalysts. This suggests that the mechanism of acetaldehyde decomposition changed over the Rh/Al_2O_3 catalyst which is also reported by several researchers in literature. Diagne *et al.* [163] explained that ethanol decomposes to CH_4 and CO in the following elementary steps.

$$CH_3\text{-}CH_2OH \rightarrow CH_3\text{-}CH_2O_{(a)} + H_{(a)} \quad (9.28)$$

$$CH_3\text{-}CH_2O_{(a)} \rightarrow {}_{(a)}CH_2\text{-}CH_2O_{(a)} + H_{(a)} \quad (9.29)$$

$${}_{(a)}CH_2\text{-}CH_2O_{(a)} \rightarrow CH_{4(g)} + CO_{(g)} \quad (9.30)$$

The yield from diethyl ether formation shows almost similar results for all temperatures investigated. These results also match with results for the Pt/Al_2O_3 catalyst. This indicates

that these products were mostly produced on active sites on the support which suggests no significant change with a change of precursor. Like the Pt/Al_2O_3 catalyst, 1,1-diethoxyethane and acetone also were produced as secondary products from acetaldehyde and ethoxy groups as discussed before.

The post reaction results, described in sections 8.2.4.2, 8.2.4.4 and 8.2.4.6 and tabulated in Table 9.2-4, show that similar weight losses took place from the Rh/Al_2O_3 catalyst at all temperatures. However, the derivative weight profiles differentiated the weight loss into three temperature regions. It illustrates that the weight losses took place in three steps for the reactions run at 500^{o}C and 550^{o}C, whilst the reaction at 600^{o}C only gave two peaks for the derivative weight loss. The derivative weight loss became more defined and separated with an increase in the reaction temperature from 500^{o}C to 600^{o}C. Interestingly there was also a shift in the peaks towards higher temperature regions with an increase in the reaction temperature. These results indicate that temperature plays an important role in the nature of coke depositions. At 500^{o}C and 550^{o}C three types of coke were present. Hydrogenated carbon, which was present on the metals and very active (α carbon). The second peak corresponded to the dehydrogenated carbon (β carbon) and according to the literature is present near to the metal and the third corresponded to the graphitic type carbon (γ carbon) whose presence was confirmed by powder XRD and Raman spectroscopy results. The disappearance of hydrogenated carbon from the catalyst at 600^{o}C is also supported by the lack of water evolution, which gave a straight line shown in Figure 9.2-16. Interestingly, the peak for hydrogenated carbon appears in both the reaction run at 500^{o}C and 550^{o}C and is almost in the same temperature region, whilst the other two peaks shifted significantly with reaction temperatures. The BET surface area and the pore volume also confirm that a similar amount of coke deposition occurred over the Rh/Al_2O_3 catalyst at the three different temperatures because at all temperatures it gave similar surface areas and pore volumes. The TPO results from the different catalysts indicate that the nature of coke not only changed with temperature but also with type of metal present as obvious from the post reaction characterisation of the Pt/Al_2O_3 and Rh/Al_2O_3 catalyst. Can *et al.* [164] reported that Rh/Al_2O_3 catalyst modified with La, Sc or Y gives no graphitic carbon peaks in the corresponding TPO.

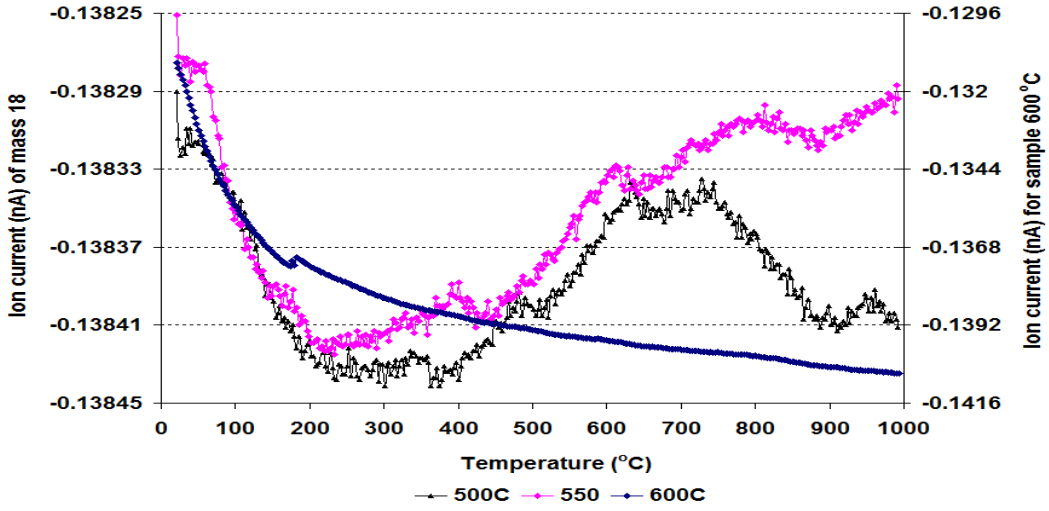

Figure 9.2-16 Evolution of m/z = 18 (H_2O) during TPO for the spent Rh/Al_2O_3 catalyst at different temperatures

Conditions (^oC)	BET Surface area (m^2/g)	Pore volume (cm^3/g)	Weight loss in TPO (%)	(I_D/I_G)
Reduced@600	101	0.46	-	-
500	47	0.04	41	0.91
550	50	0.04	41	1.04
600	45	0.03	41	0.93

Table 9.2-4 Post reaction BET analysis and weight loss of Rh/Al_2O_3 catalyst at different temperatures

Figure 8.2-82 indicates that besides a broad peak for graphitic carbon at 26^o 2θ position there also appears a small peak for Rh_2O_3 at 35^o 2θ position which is also confirmed by Raman results in Figure 8.2-83 [165]. Since the metal loading is 0.2% w/w it is not unusual that the powder XRD gave a very small peak for Rh_2O_3.The SEM studies shown in Figure 8.2-84 gave amazing results. Both the fibrous carbon and carbon nanotube type carbon were produced at all temperatures. However, the 550^oC sample gave helicoids type carbon nanotubes, although fibrous type carbon was still present on the sample. The presence of helicoids fibres was also reported previously by Krishnankutty *et al.* [166] over the iron catalyst by C_2H_4 decomposition. Similarly at 600^oC a network of large diameter carbon nanotubes was present. This supports the interpretation that an increase in the reaction temperature changes the nature of coke deposited on the catalyst as discussed in the TPO results. The Raman results reveal that there was graphitic type carbon present.

9.3 Effect of impurities

Following the investigation into the influence of temperature over the Al_2O_3 support and precious metal (Ru, Pt and Rh) supported Al_2O_3 catalysts, we turned to the main aim of the project *i.e.* the effect of different impurities present in crude ethanol on the steam reforming reaction. In order to determine how different functional groups affect the catalyst, five different organic functional group representatives with a basic C_3 structure, 1-propanol, 2-propanol (IPA), propanal, propylamine and acetone were tested. Each impurity was individually added to the water/ethanol reactant mixture, in a 1% molar ratio with respect to the ethanol content. The influence of these five types of impurities on the reaction will be discussed in this section. Each impurity had a specific effect on the ethanol steam reforming reaction on the different catalysts. However generally, they can be divided into two groups; (i) promoting impurities and (ii) deactivating impurities. So, for all the catalysts, with the exception of pure Al_2O_3, the discussion will be separated into the two aforementioned sections.

9.3.1 Al_2O_3

The Al_2O_3 was tested with 1-propanol and propylamine impurities to check if these impurities had an effect on the Al_2O_3 reactivity. In the presence of either impurity, the conversion of ethanol was high (~ 100%) in the initial 50 hours time on stream, as shown in Figures 8.3-1 and 8.3-9, which indicates that initially both impurities had no apparent effect on the ethanol conversion. Unlike the pure ethanol reaction, the conversion of ethanol started to decrease after 50 hours time on stream in the reactions containing 1-propanol and propylamine impurities and this deactivation continued until the end of the reaction. However, the decrease in ethanol conversion when propylamine was the impurity was severe (decreased to 87%) compared to when 1-propanol was the impurity (decreased to 96%). The decrease in ethanol conversion can be correlated to the relatively high formation of ethylene in the propylamine impurity reaction as shown in Figure 9.3-1. If the yields of CH_4 and C_2H_4 are compared for both impurity reactions, they show that the decrease in the yield of CH_4 is equivalent to the increase in the yield of C_2H_4. This result suggests that the formation of the olefin was the main source of coke which deactivated the Al_2O_3 and decreased the ethanol conversion. The cause of the deactivation of the catalyst was also confirmed by the presence of coke on the catalyst as seen by the results in Table 9.3-1. The results indicate that the addition of impurities to the ethanol reaction mixture

modifies the Al_2O_3 and that the modified Al_2O_3 favours the formation of C_2H_4 which is obvious from Figure 8.2-2 and Figure 9.3-1.

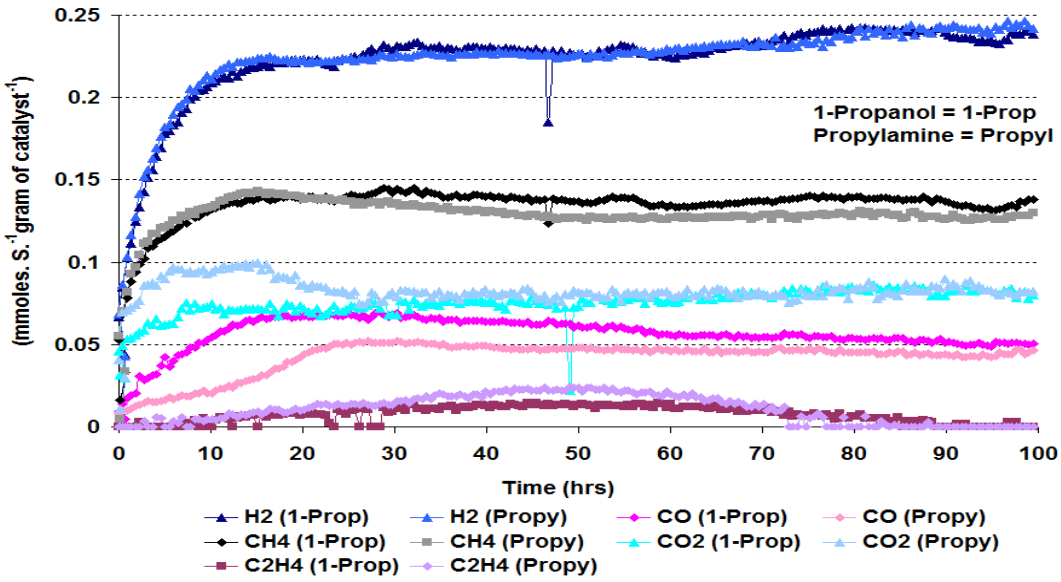

Figure 9.3-1 Rate of formation of gaseous products over the Al_2O_3 catalyst using 1-propanol and propylamine impurities

It was previously reported that a catalyst with medium acidity has both the highest activity and selectivity towards C_2H_4 formation [98, 167]. It was also emphasised that only the weak acidic sites are responsible for dehydration. Jain *et al.* [127] determined that on alumina different acidic sites are present and the addition of pyridine neutralises the strong acidic sites.

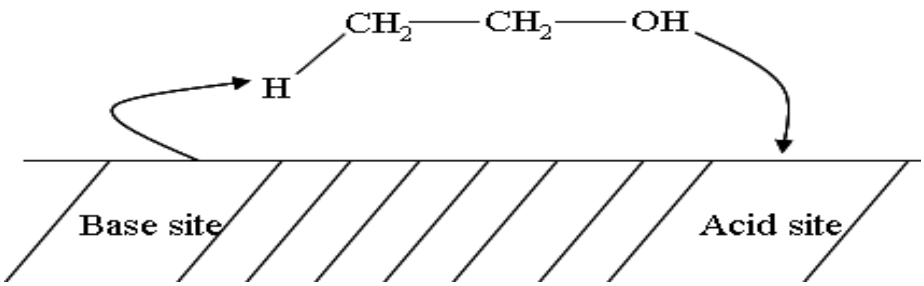

Figure 9.3-2 Formation of ethylene from ethanol

The current results also reveal that in the pure ethanol reaction over Al_2O_3 small amounts of C_2H_4 were produced. However, the addition of impurities in the ethanol modified the catalyst surface and neutralised the strong acidic sites which are responsible for ethanol decomposition and left the medium acidic sites which take part in C_2H_4 formation. Now the question arises as to why initially insignificant amounts of C_2H_4 were produced which

then increased with time on stream up until 60 hours and then decreased. A plausible explanation for this pattern of C_2H_4 formation is that initially relatively high amounts of C_2H_4 were produced which undergoes further reaction in the steam reforming reaction to form CO and H_2.

$$C_2H_4 + 2H_2O \rightarrow 2CO + 4H_2 \quad (9.31)$$

However, with the passage of time the active sites for the steam reforming of C_2H_4 were deactivated, so C_2H_4 entered the effluent mixture and was detected by the GC. The C_2H_4 also polymerises and contributes to the coke formation, as shown in Table 9.3-1. The later decrease in C_2H_4 formation during the reaction may be due to the deactivation of the active sites for dehydration of ethanol due to the blockage of the active sites by coke.

The H_2 yields in Figures 8.3-4 and 8.3-12 indicate that the addition of impurities to the water/ethanol mixture increased the formation of H_2, whereas, the yield of CH_4 decreased in both the impurity reactions compared to the pure ethanol reaction. Also the impurities appear to contribute to the high H_2 formation as the impurity reactions gave above 90% conversion.

Compared to the pure ethanol reaction, when an impurity was added to the water/ethanol mixture the yield of CO_2 was less whilst the yield of CO was greater. These results reveal that the rate of the WGS reaction had decreased. In the 1-propanol impurity reaction the rate of formation of CO was greater by 0.052 mmoles s^{-1} g^{-1} compared to the pure ethanol reaction on Al_2O_3 whilst the rate of formation of CO_2 was less by 0.04 mmoles s^{-1} g^{-1} after 20 hours TOS. Similarly, the rate of formation of H_2 was larger in both impurity reactions than in the pure ethanol reaction.

The same liquid products were observed in both impurity reactions as per the pure ethanol reaction although the yields were slightly greater in the impurities reactions. These results indicate that there was no significant change in the mechanism of formation of the liquid products taking place with the addition of the impurities to water/ethanol mixture in the reaction over Al_2O_3.

Post reaction characterisation of the pure ethanol and both impurities reactions catalyst samples are compared in Table 9.3-1. The TPO results reveal that comparatively more coke was produced on the catalysts in the impurity reactions when compared to the pure

ethanol reaction. The amount of carbonaceous materials deposited during the impurity reactions at 500^{o}C were even higher than the amount of carbonaceous deposit on the Al_2O_3 in the pure ethanol reaction run at 600^{o}C. As discussed before, the main cause for the deactivation of the catalyst during the impurity reactions could be the high rate of formation of C_2H_4, which is known to be a source of coke formation. The incomplete decomposition of the impurities may have some contribution to the high coke formation which is in agreement with previous studies [168]. Segal *et al.* [121] investigated the steam reforming of ethanol, higher alcohols and their mixtures with hydrocarbons and found that a mixture of alcohols and hydrocarbons deactivated the catalyst due to coke formation. The propylamine impurity reaction produced a slightly higher weight loss during the post reaction TPO compared to 1-propanol impurity reaction over Al_2O_3, this is in keeping with the concept that C_2H_4 is the main source of coke because more C_2H_4 was formed in the propylamine impurity reaction compared to the 1-propanol impurity reaction. The high amount of coke formation in the propylamine impurity reaction was also in agreement with a previous study [169]. In that study it was reported that high coke formation took place over the catalyst used with nitrogen containing compounds.

Impurity	BET Surface area (m^2/g)	Pore volume (cm^3/g)	Weight loss in TPO (%)	(I_D/I_G)
No impurity	80	0.40	3	-
1-Propanol	54	0.14	30	0.92
Propylamine	52	0.12	32	1.24

Table 9.3-1 Post reaction BET analysis and TPO over the Al_2O_3 catalyst using different impurities

It is also important to note that not only did the amount of coke increase but also the evolution temperature in the TPO increased from 545^{o}C to 683-693^{o}C, which suggests that the nature of the coke had changed. The decrease in the BET surface area and pore volume also revealed that the deposition of coke blocked the pores causing a decrease in the surface area. The ratio of I_D/I_G from the Raman results indicates that at the same reaction temperature, as the amounts of carbonaceous deposit on the catalyst surface increased, the disorder in the graphitic carbon increased, as shown in Table 9.3-1. The shift in the bands in the Raman spectra indicate that either the structure of the coke had changed slightly or the addition of impurities to the water/ethanol feed had produced a different type of coke compared to the pure ethanol reaction, as shown in Figures 8.3-8 and 8.3-16.

9.3.2 Ru/Al_2O_3

As explained previously, the effect of the impurities can be divided into two groups, which will be discussed below for the Ru/Al_2O_3 catalyst.

9.3.2.1 Poisoning impurities

The impurities that deactivated or poisoned the Ru/Al_2O_3 catalyst during the ethanol steam reforming reaction were 1-propanol, IPA and propanal. The addition of these impurities into the water/ethanol mixture deactivated the catalyst more severely than the pure ethanol feed. However, the impact of each of the impurities towards the ethanol conversion was slightly different. In the presence of 1-propanol and propanal impurities, the decrease in ethanol conversion was more severe and did not stabilise during the reaction. In the initial 48 hours, a large deactivation was observed and the conversion of ethanol was reduced to 36-30% which was seen in both impurity reactions. In the presence of IPA, ethanol conversion was initially 100%, which steadily decreased to 40% by 52 hours time on stream before stabilising for the rest of the reaction. Conversely a high conversion of IPA was observed during the reaction. This has also been reported in the literature [121]. These results suggest that in a binary mixture, the conversion of one compound is influenced by the presence of the other compound. From the results, it can be seen that the presence of a C_3 alcohol and aldehyde has an adverse effect on the reforming of ethanol and decreases the conversion over a Ru/Al_2O_3 catalyst. As discussed above, high conversion of IPA would suggest that IPA deposits on the catalyst surface. The high level of deactivation may be a result of large coke and impurity deposits reducing access of ethanol to the catalyst active sites. Burgos *et al*. [170] studied the oxidation of different volatile organic compounds and their mixtures and concluded that all, with the exception of IPA, gave complete oxidation. The propanal results suggest that with regard to the conversion of ethanol, propanal behaves in a similar manner to the 1-propanol. This result suggests that on the Ru/Al_2O_3 catalyst, propanal is first converted to 1-propanol, which then forms propylene by dehydration.

$$CH_3CH_2CHO + H_2 \leftrightarrow CH_3CH_2CH_2OH \quad (9.32)$$

$$CH_3CH_2CH_2OH \rightarrow CH_3CH{=}CH_2 + H_2O \quad (9.33)$$

$$CH_3CH_2{=}CH_2 \rightarrow \text{Coke} \quad (9.34)$$

Propylene is known to be a severe deactivating agent of the catalyst because it easily forms aromatic type coke by Diels Alder reactions, as discussed in section 6.8.

The relatively high conversion of ethanol with IPA compared to 1-propanol may be explained by the IPA acetone equilibrium given that acetone inhibits coke deposition on the Ru/Al_2O_3 catalyst. The formation of acetone from IPA over the Ru/Al_2O_3 was also observed by Mizuno *et al.* [171].

$$CH_3CHOHCH_3 \rightarrow CH_3COCH_3 + H_2 \quad (9.35)$$

$$CH_3COCH_3 + 2H_2O \rightarrow 5H_2 + 3CO \quad (9.36)$$

However, the incomplete oxidation of IPA and C_2H_4 formation from ethanol dehydration may have slowly blocked some of the active sites for ethanol steam reforming reaction in the initial stage of reaction. In another paper Mizuno [172] studied the steam reforming of IPA on different noble metal catalysts at 500^oC and concluded that over a Ru/Al_2O_3 catalyst, the conversion of IPA was stable for 350 minutes.

With regard to the gaseous products, H_2 and C_2H_4 were produced with the highest yields in all the deactivating impurity reactions as shown in Figure 9.3-3. However, the yields of these products were less than in the pure ethanol reaction, except for the yield of H_2 in the propanal and 1-propanol impurity reactions. These lower yields of H_2 and C_2H_4 can be correlated to the lower conversion of ethanol in these impurities. Interestingly, with both functional group impurities, the profiles of the gaseous products were similar in the initial stages of the reaction, as shown in Figures 8.3-18, 8.3-25 and 8.3-33. The rate of formation of C_2H_4 initially increased and then steadily decreased until the end of the reaction in the C_3 alcohols and propanal impurity reactions, whilst in the pure ethanol reaction the rate of formation of C_2H_4, after the initial decrease, stabilised with the end of the reaction. The initial high rate of formation of C_2H_4 in the pure ethanol and the impurity reactions on the Ru/Al_2O_3 catalyst suggests that C_2H_4 was not a steam reforming product on the Ru/Al_2O_3 catalyst. Similarly, the rate of formation of H_2 increased steadily in both functional group impurity reactions and achieved no steady state conditions by the end of the reaction. Figure 9.3-5 reveals that the IPA impurity reaction gave the lowest rate of formation of H_2 among all the impurity reactions tested over a Ru/Al_2O_3 catalyst. This low yield of H_2 in the IPA impurity reaction seems to be due to coking from C_2H_4, which blocked the active sites for the ethanol steam reforming reaction. Due to the high yield of C_2H_4, the other gaseous products were produced with lower yields. Devianto *et al.* [120] studied ethanol as a feed for a carbonate fuel cell and found that the presence of propanol and acetic acid with ethanol significantly decreased the activity of the fuel cell. The rates of formation of CH_4 and CO_2 steadily increased during the propanal impurity reaction and exceeded the rate of

formation of C_2H_4 after 51 hours time on stream. This is in contrast to the 1-propanol impurity reaction where CH_4 and CO_2 formation rates stabilised after the initial increase. These results indicate that due to the high coke formation in the propanal impurity reaction, the availability of active sites for ethanol dehydration was reduced and that the rate of formation of C_2H_4 was decreased while the Ru metal particles for ethanol dehydrogenation were still active. The increase in dehydrogenation is further supported by the increase in the rate of formation of acetaldehyde, as shown in Figure 8.3-34. Over the Ru/Al_2O_3 catalyst, acetaldehyde decomposed and formed CO_2 and CH_4 at a steadily increasing rate throughout the propanal impurity reaction. For all poisoning impurity reactions, CO_2 gave a high yield compared to the pure ethanol reaction. This high yield of CO_2 can be attributed to the WGS reaction as reported by Mizuno [171]. The IPA and 1-propanol impurity reactions gave similar yields of CH_4 and CO whilst in the IPA impurity reaction, C_2H_6 was produced at a slightly higher rate, which is in agreement with the literature [94]. The rates of formation of the gaseous products suggest that the higher alcohols and propanal do not change the mechanism for the ethanol steam reforming reaction, although they do deactivate the Ru/Al_2O_3 catalyst quickly, especially the 1-propanol impurity, due to the conversion to the respective olefins. The formation of olefin from these impurities was not detected by the GC which gave rise to the idea that the olefins of the respective higher alcohols were deposited over the catalyst surface.

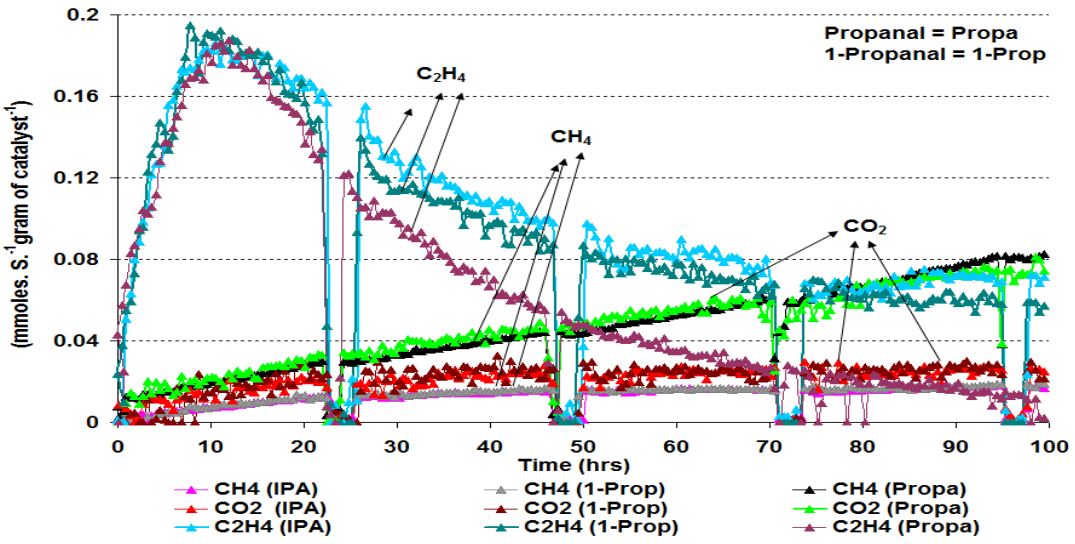

Figure 9.3-3 Rate of formation of gaseous products over the Ru/Al_2O_3 catalyst using 1-propanol, IPA and propanal impurities

With the liquid products, as with the pure ethanol reaction, acetaldehyde was found to have a high yield in the C_3 alcohols and propanal impurity reactions. However, its yield was slightly lower with the C_3 alcohol impurities compared to the pure ethanol reaction.

Interestingly, the yield of diethyl ether in the IPA and 1-propanol impurity reactions was decreased compared to the pure ethanol reaction. Whilst in the propanal impurity reaction, the decrease in diethyl ether yield was more noticeable especially in the later stages of the reaction, as shown in Figure 8.3-34. The decrease in diethyl ether reveals a partial blocking of the acidic sites used for diethyl ether formation.

9.3.2.2 Promoting impurities

The impurities which enhanced or promoted the ethanol reforming reaction over the Ru/Al_2O_3 catalyst were propylamine and acetone. The presence of both these impurities in the water/ethanol mixture significantly increased the conversion of ethanol and also delayed the deactivation of the catalyst, as shown in Figures 8.3-40 and 8.3-48. The conversion of the ethanol was ~ 100% in the initial 30.5 hours TOS in the propylamine impurity reaction and steadily decreased to around 74% by the end of the reaction. Similarly, in the acetone impurity reaction there was no obvious decrease in the conversion of the ethanol observed throughout the reaction and the catalyst was active for 100 hours, maintaining the high ethanol conversion. These results reveal that 1 mol.% addition of propylamine and acetone with respect to the ethanol significantly increased the conversion of ethanol over the Ru/Al_2O_3 catalyst. These promoting effects in both impurity reactions may be explained in different ways. Propylamine is a Lewis base and so competes with the ethanol for the Lewis acidic sites on the catalyst, which are the main causes for dehydration of ethanol. The strong basic properties of the amine may reduce the number of acidic sites and consequently change the mechanism of the ethanol reaction towards a basic pathway *i.e.* ethanol dehydrogenation to acetaldehyde. The change in mechanism is also supported by the distribution of liquid and gaseous products, shown in Figures 8.3-43-44. Throughout the reaction no 1,1-diethoxyethane was observed whilst trace amounts of diethyl ether were detected in the later stages of the reaction when propylamine was the impurity. Small amounts of C_2H_4 appeared in the reaction stream for the propylamine impurity reaction but then disappeared after 50 hours TOS, which suggests that initially the propylamine did not occupy all the acidic sites on the catalyst and the unoccupied acidic sites produced C_2H_4. However, as these acidic sites were neutralised by the propylamine, the formation of C_2H_4 decreased. It may be possible that in the later stages of the reaction the active sites for C_2H_4 steam reforming disappeared due to formation of coke. These results are in close agreement with a previous study performed by Jain *et al.* [127] They emphasise that the basic molecules compete with the alcohol molecules for the acidic sites and retard the formation of both olefins and ether. The enhancing effect of amines was also

reported by an other research group who found that diethyl amine increased the conversion of bioethanol over a $Rh/MgAl_2O_4$ catalyst [116]. Figure 9.3-4 indicates that among the five different impurities tested during the steam reforming of the ethanol over a Ru/Al_2O_3 catalyst, propylamine gave the highest rate of formation of H_2. This high rate of formation of H_2 can be correlated to the lower rate of formation of CH_4 and C_2H_4, which are undesirable products, during the steam reforming of ethanol. In the propylamine impurity reaction the rate of formation of CH_4 stabilised, after an initial increase, and was continuous until the end of the reaction. Conversely, the rate of formation of CO decreased whilst the rate of formation of CO_2 and H_2 steadily increased. These results suggest that the water gas shift reaction was increased with time on stream.

The high ethanol conversion in the acetone impurity reaction is not fully understood. However, it may be due to several possible reasons. Firstly, the acetone impurity adsorbed on to both the Lewis and Brönsted acid sites and decreased the formation of both ethylene and diethyl ether. This is supported by the profile of liquid products, as shown in Figure 8.3-52. The equilibrium between the keto and enol forms of acetone and their subsequent condensation can help understand how the acetone reacts with both Lewis and Brönsted acids sites.

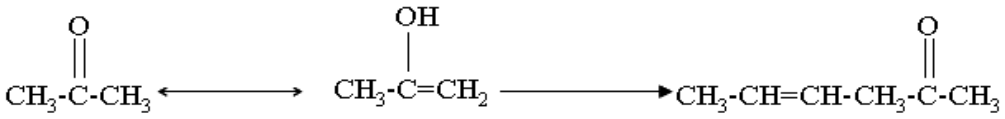

(9.37)

The blocking of the Lewis and Brönsted acidic sites alters the reaction mechanism and produces mainly CO, CH_4 and H_2. The interaction of the acetone with Lewis and Brönsted acidic sites has been reported in the literature [173]. Secondly, the acetone impurity reaction produced no propylene due to the absence of an α-acidic carbon which enhances the deactivation of the catalyst as discussed before. The formation of low coke in that reaction also supports this idea (Table 9.3-2). In addition the Raman spectra showed no graphitic carbon bands in the post reaction sample of the acetone impurity reaction. This suggests that in the acetone impurity reaction, only the hydrogenated type of coke was formed, which does not deactivate the active metal. Figure 9.3-4 indicates that most of the coke was produced from C_2H_4. As a low yield of C_2H_4 was detected, the catalyst was active for a longer time compared to the pure ethanol reaction over Ru/Al_2O_3. From these results it is proposed that acetone modifies the catalyst surface and enhances the steam reforming of the ethanol. The enhancing effect of the acetone was also observed in the oxidation of toluene by an other research group [174].

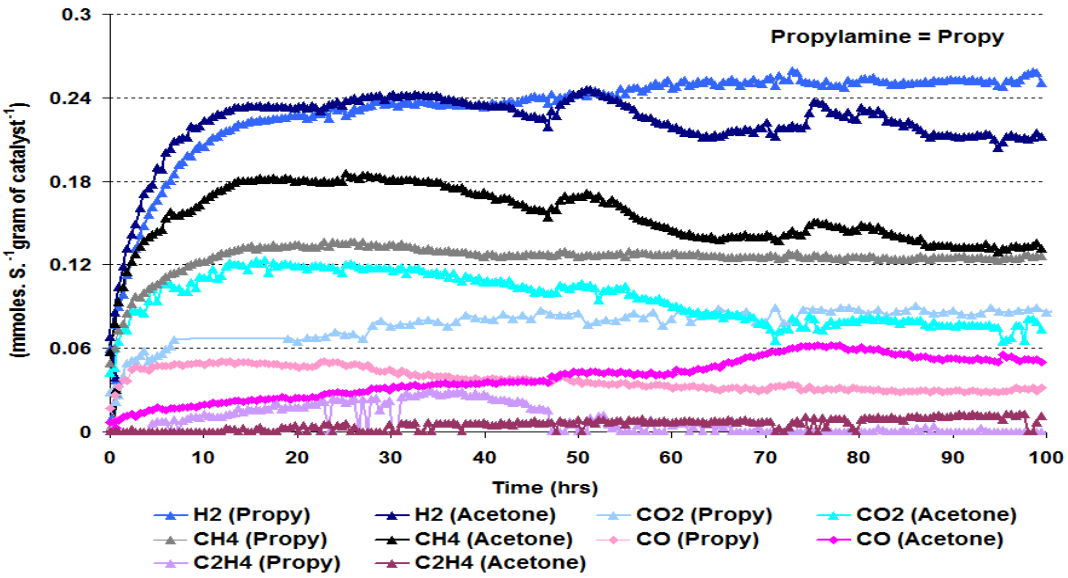

Figure 9.3-4 Rate of formation of gaseous products over the Ru/Al_2O_3 catalyst using propylamine and acetone impurities

Figure 9.3-4 shows that in the ethanol steam reforming with an acetone impurity, the reaction had the highest rates of formation of CH_4 and CO_2 over a Ru/Al_2O_3 catalyst. However, the rates were not stable and decreased whilst the rate of formation of the CO started to increase, showing that the WGS reaction steadily decreased. Interestingly, as the CH_4 and CO_2 rates decreased the formation of liquid products started to increase, especially acetaldehyde. The increase in acetaldehyde in the liquid products indicates that in the early stages the reforming of acetaldehyde took place, which then further underwent the water gas shift reaction to form CO_2.

$$CH_3CHO \rightarrow CH_4 + CO \quad (9.38)$$

$$CO + H_2O \rightarrow CO_2 + H_2 \quad (9.39)$$

The rate of formation of H_2 during the different impurities and pure ethanol reactions gives a clear picture about the influence of the different impurities on the ethanol steam reforming reaction over Ru/Al_2O_3. Figure 9.3-5 indicates that the alcoholic group impurity reactions have similar rates of formation of H_2 to that of the pure ethanol reaction, although the IPA reaction gave a relatively lower H_2 formation rate before the steady state position. The acetone and propylamine impurity reactions gave the highest rates of formation of H_2 initially. However, in the later stages of the acetone impurity reaction, the rate of formation of H_2 had decreased due to a decrease in the water gas shift reaction and an increase in the rate of formation of liquid products. The rate of formation of H_2 in the propanal impurity

reaction showed interesting results. Initially its rate was low, due to a high rate of formation of C_2H_4. However, when the rate of formation of C_2H_4 decreased, the H_2 rate significantly increased and when near to steady state, it had a rate of formation of H_2 the same as in the propylamine impurity reaction. This suggests that the propanal impurity also acted as a promoting impurity in the later stages of the reaction. From these results it is proposed that initially propanal forms propylene due to acidic sites and when these acidic sites are deactivated by coke then the propanal decomposes to CH_4, H_2 and CO_2.

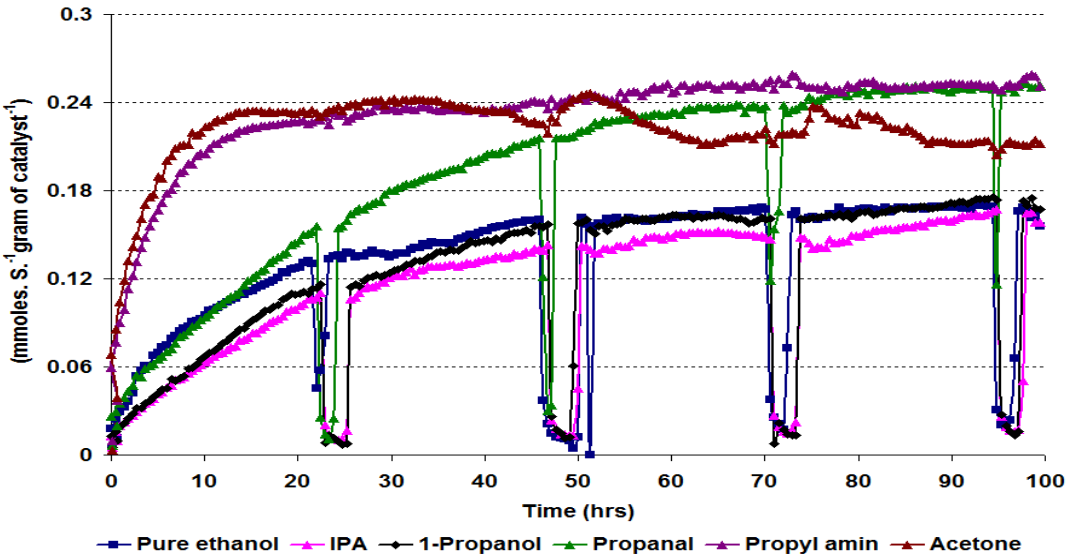

Figure 9.3-5 Rate of formation of H_2 over the Ru/Al_2O_3 catalyst using different impurities

Post reaction characterisation data of all the impurities and the pure ethanol reaction on Ru/Al_2O_3 catalyst samples are compared in Table 9.3-2. The results indicate that the propanal impurity reaction had the highest coke formation on the Ru/Al_2O_3 catalyst, which was also confirmed from the results of BET analysis. The BET surface area of all the Ru/Al_2O_3 samples used with ethanol/impurity and pure ethanol reactions had significantly decreased compared to the BET surface area of the same catalyst in the reduced form. The high amounts of coke formation during the propanal impurity reaction inferred that besides C_2H_4 and C_3H_6, CH_4 also contributed to coke formation on the catalyst. Interestingly, the IPA and 1-propanol impurity reactions show lower weight losses compared to the pure ethanol reaction sample. These lower weight losses match the lower rates of formation of C_2H_4, as shown in Figure 9.3-3 and Figure 8.2-20. The TPO results, shown in Figures 8.3-22, 8.3-29, 8.3-37, 8.3-45 and 8.3-53, indicate that the temperature region for weight loss was slightly different for each impurity, indicating that the nature of the coke changed slightly. In all the impurity reaction samples, the weight losses matched with the evolution

of CO_2 in the mass spectrum. Also, like the pure the ethanol reaction a broad peak for ethanol (m/z = 45) appeared in all samples. The IPA and propylamine impurity reaction samples gave Raman bands at the same position whilst the 1-propanol and the pure ethanol gave similar but not identical bands. This suggests that the impurities affect the structure of the coke. Interestingly, the acetone impurity reaction sample showed coke of a different nature *i.e.* no peak for graphitic type carbon was found in the Raman results. The absence of graphitic type carbon in the acetone impurity reaction sample was also supported by the TPO results which gave the weight loss at a lower temperature relative to the other impurities. From the post reaction characterisation of all the impurity reaction samples, it can be identified that the deposition of coke on the catalyst surface plays an important role in the deactivation of the Ru/Al_2O_3 catalyst.

Impurity	BET Surface area (m^2/g)	Pore volume (cm^3/g)	Weight loss in TPO (%)	(I_D/I_G)
No impurity	32	0.07	39	0.99
IPA	38	0.07	38	0.92
1-Propanol	36	0.07	38	0.99
Propanal	16	0.03	41	0.92
Propylamine	36	0.10	35	0.96
Acetone	50	0.20	19	-

Table 9.3-2 Post reaction BET analysis and weight loss over the Ru/Al_2O_3 catalyst using different impurities

9.3.3 Pt/Al_2O_3

Similar to the Ru/Al_2O_3 system the effect of impurities over the Pt/Al_2O_3 catalyst are divided into two groups.

9.3.3.1 Poisoning impurities

The impurities whose presence in the water/ethanol mixture poisoned or deactivated the ethanol conversion over the Pt/Al_2O_3 catalyst were 1-propanol and IPA. However, the behaviour of each of these impurities was slightly different. In the initial hour of reaction the catalyst was active in the presence of these impurities and gave ~ 99% conversion, which was slightly higher than for the pure ethanol reaction at 500^{o}C. However, as the reaction proceeded the ethanol conversion decreased when these impurities were in the feed. In the IPA impurity reaction, the ethanol conversion decreased steadily until the end of the reaction and after 100 hours TOS it had declined to 19%. Interestingly, the

conversion of the IPA by itself was high *i.e.* above 82% and no significant change during the reaction was observed, as shown in Figure 8.3-64. It was previously identified that for the same number of carbon atoms, branch alcohols produce more coke on the catalyst surface due to formation of stable carbocations which then are converted into the respective olefins [119, 175]. The high conversion of IPA is in agreement with the previous studies [121]. The results suggest that the Pt/Al_2O_3 catalyst stabilised the carbocations of IPA and promoted the conversion of IPA. From the weight loss in the post reaction TPO, shown in Table 9.3-3, it is suggested that coke deposition on the catalyst is not solely responsible for the decrease in ethanol conversion as in the IPA impurity reaction less C_2H_4 and coke were produced compared to the pure ethanol reaction. So, it is proposed that incomplete decomposition of IPA and the formation of propylene play a role in the deactivation of the catalyst where the access of ethanol to the active sites was blocked, causing the decrease in ethanol conversion as discussed before. The higher deactivation by the IPA is also supported by Wanat *et al.* [94] who claimed that IPA required higher temperatures than 1-propanol for decomposition. Mostafa *et al.* [121] and Mizuno *et al.* [171] demonstrated that the steam reforming of IPA over a platinum catalyst produced propylene above 250 ^{o}C, whilst at low temperatures it formed acetone. [121, 171].

Contrary to the IPA impurity reaction after 3 hours TOS, in the 1-propanol impurity reaction a significant drop (60%) occurred in the ethanol conversion which stabilised after 30 hours TOS and then remained constant until the end of the reaction. The 1-propanol impurity reaction, shown in Figure 8.3-56, gave interesting results. It indicates that with a decrease in the conversion of ethanol, the conversion of 1-propanol also decreased. From these results we conclude that ethanol and 1-propanol have the same active sites and deactivation of these sites decreased the conversion of both alcohols. 1-Propanol adsorbed on the catalyst blocked the sites for the reaction of the ethanol. Devianto [120] found that incomplete decomposition of 1-propanol had negative effects on the conversion of ethanol and H_2 selectivity.

With regard to the gaseous product distribution over the Pt/Al_2O_3 catalyst, in contrast to previous studies [120], both of the impurities gave a slightly higher rate of formation of H_2 than the pure ethanol in the initial 20 hours TOS. This suggests that the impurities also contribute in a small extent to H_2 production. In the IPA impurity reaction the rate of formation of H_2 was slightly decreased after 20 hours TOS. This decrease was not due to the deactivation of the catalyst as explained in section 8.3.3.3. In the later stages of the

reaction, the rate of formation of H_2 increased and obtained the same rate of formation as is shown in the 1-propanol impurity and pure ethanol reactions. These results show that the alcoholic impurity reactions gave slightly higher rates of formation of H_2 than the pure ethanol reaction in the initial hours of the reaction. However, in the later stages of the reactions the alcoholic impurities gave the same rate of formation of H_2 as the pure ethanol reaction. Hence, initially the steam reforming of higher alcohols took place but as the catalyst deactivated, the rate decreased and hydrocarbons were deposited on the catalyst surface. Similarly the initial rates of formation of C_2H_4 were high in both impurities reactions, but the rates steadily decreased with the reaction time as shown in Figure 9.3-6. The decrease in the rate of formation of C_2H_4 could be due to the blockage of the active sites for C_2H_4 formation by the polymerisation of C_3H_6 and C_2H_4. As discussed in the previous section propylene is a more deactivating species than ethylene. It is important to note that the initial rate of formation of C_2H_4 was higher in the C_3 impurity reactions than in the pure ethanol reaction. However, in the later stages of the reaction the pure ethanol feed gave a higher rate of formation of C_2H_4. This higher rate of formation of C_2H_4 in the alcohol impurity reactions suggest that the active sites for C_2H_4 steam reforming were blocked by 1-propanol, IPA and C_2H_4, whilst in the pure ethanol reaction the C_2H_4 was initially steam reformed. However, later on due to steady blockage of the active sites for steam reforming the rate of formation of C_2H_4 steadily increased. All the other gaseous products except CO and C_2H_6 gave a similar rate of formation in the both impurity reactions and the pure ethanol feed reactions. Therefore after the addition of different alcohol impurities the gaseous distribution was not changed over the Pt/Al_2O_3 catalyst.

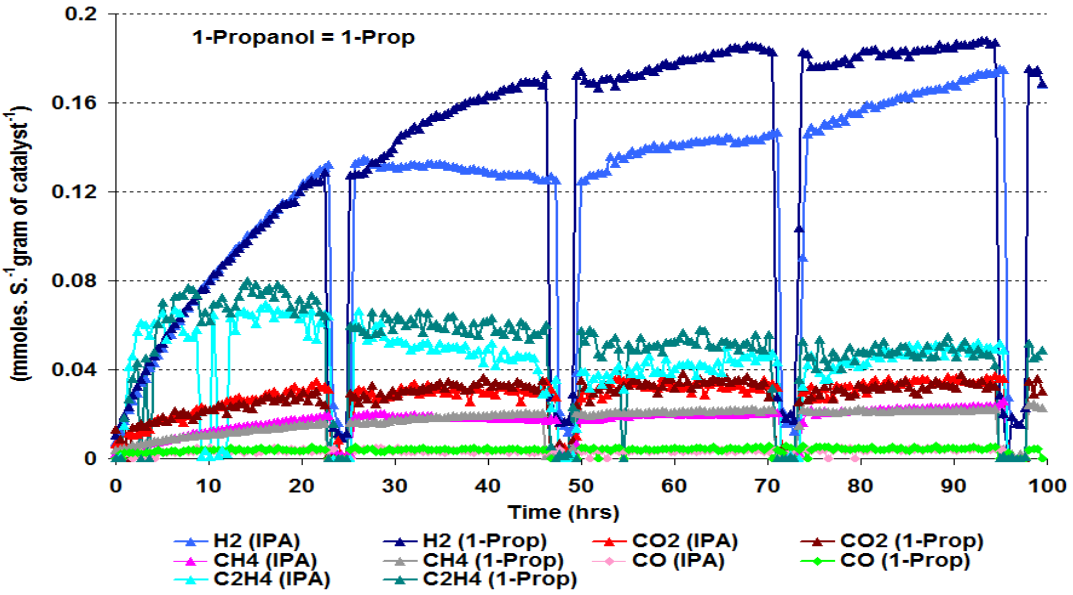

Figure 9.3-6 Rate of formation of gaseous products over the Pt/Al_2O_3 catalyst using 1-propanol and IPA impurities

Compared to the pure ethanol reaction, less diethyl ether and 1,1-diethoxyethane were formed in both impurity reactions. However, as with the pure ethanol reaction, acetaldehyde had a high yield. The yields of acetone and acetic acid initially decreased and then stabilised until the end of the reaction. This indicates that the alcohols either modified the mild acidic sites used for diethyl ether and 1,1-diethoxyethane formation or blocked the sites. However, it should be noted that these compounds were produced in small quantities in the pure ethanol reaction and a small change in the sites for these compounds could have produced a large change in their distributions

9.3.3.2 Promoting impurities

The impurities which promoted the steam reforming of ethanol over the Pt/Al_2O_3 catalyst were propanal, propylamine and acetone. All these impurities increased the ethanol conversion by decreasing the formation of C_2H_4 and coke except for propanal where coke formation also increased.

In contrast to the Ru/Al_2O_3 catalyst reaction, propanal acted as a promoter for the steam reforming of ethanol over the Pt/Al_2O_3 catalyst. The addition of propanal to the ethanol reactant mixture resulted in a 99.9% conversion in the initial 7.5 hours TOS over the Pt/Al_2O_3 catalyst. However, as the reaction proceeded, the ethanol conversion dropped to 76% after 30 hours time on stream and then stabilised for the rest of the reaction. The conversion of propanal gave a similar profile to the ethanol conversion. The high activity of the catalyst in the presence of propanal is also in agreement with previous studies, as discussed in section 6.9 [119]. The high activity of the ethanol steam reforming reaction suggests that over the Pt/Al_2O_3 catalyst propanal was not converted to 1-propanol but was decarbonylated and formed CO and hydrocarbons, as has been reported in the literature [176].

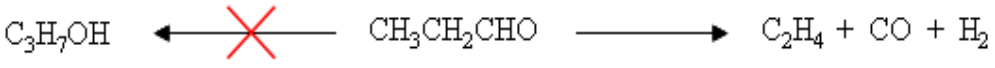

(9.40)

The initial decrease in ethanol conversion corresponds to the high rate of formation of C_2H_4, which polymerised and blocked the sites for ethanol conversion. The blockage of these sites is also supported by the high amount of coke, which was formed on the catalyst, as tabulated in Table 9.3-3. In contrast to the Ru/Al_2O_3 catalyst, Pt/Al_2O_3 showed a relatively low rate of formation of C_2H_4 and a relatively high rate of formation for both CO_2 and CH_4. Figure 9.3-7 shows that the rates of formation of C_2H_4, CO_2 and CH_4 have a

correlation to each other. In the initial 48 hours TOS with the propanal impurity reaction, the rates of formation of CO_2 and CH_4 were relatively lower than the propylamine impurity reaction whereas C_2H_4 formation was higher. However, as the C_2H_4 formation decreased with TOS, the rate of formation of C_1 products increased. After 48 hours TOS all the gaseous products had achieved steady state conditions.

As with the Ru/Al_2O_3 catalyst propylamine acted as a promoter and increased the ethanol conversion and stability of the Pt/Al_2O_3 catalyst due to interactions between the Lewis acidic sites of the Al_2O_3 and the lone-pair electrons of nitrogen as discussed before in section 9.3-2 and also studied by Koubek *et al.* [177]. However, the high activity of the Pt/Al_2O_3 catalyst for the steam reforming of ethanol in the acetone impurity reaction is not straightforward. In the presence of the Pt/Al_2O_3 catalyst acetone may be hydrogenated to form IPA but no IPA was detected by the GC.

$$CH_3COCH_3 + H_2 \rightarrow CH_3CHOHCH_3 \quad (9.41)$$

Therefore it might be postulated that the acetone interacts with the Lewis and Brönsted acid sites and neutralises both the acidic sites as discussed before.

With the passage of time, the rate of formation of CH_4 in the propylamine and acetone impurity reactions decreased. This decrease in CH_4 rate can be related to the formation of C_2H_4 and liquid products. Figure 8.3-89 indicates that in the acetone impurity reaction when the catalyst was active, no liquid products were produced. However, as the catalyst started to deactivate, liquid products were detected in the effluent mixture. A small amount of C_2H_4 was also produced in the acetone impurity reaction. From these results, it can be suggested that when no coke is present on the catalyst surface the steam reforming of ethanol forms H_2, CO_2 and CH_4.

$$C_2H_5OH + H_2O \rightarrow CO_2 + 2H_2 + CH_4 \quad (9.42)$$

However, as soon as the catalyst is deactivated by coke, then intermediate products *i.e.* acetaldehyde and C_2H_4 appear in the effluent mixture, as was seen in the acetone impurity reaction in Figures 8.3-88 and 8.3-89. The rate of formation of CH_4 in all three impurity reactions achieved almost the same level under steady state reaction conditions.

The formation of C_2H_4 in each impurity reaction was achieved by a specific pathway. In the propanal impurity reaction, initially large amounts of C_2H_4 were produced compared to the pure ethanol reaction, followed by a very quick decrease and ultimately a decline to almost zero. This decrease may be due to the formation of large amounts of coke on the catalyst surface, as discussed before. In the propylamine impurity reaction initially no C_2H_4 was detected. However, after 18 hours time on stream, C_2H_4 was detected and the rate steadily increased up to 52 hours TOS before decreasing. These results suggest that initially C_2H_4 was steam reformed as observed in the pure ethanol reaction (Figure 8.2-48). However, when the sites for C_2H_4 steam reforming were deactivated, C_2H_4 then appears in the reaction stream. In the acetone impurity reaction small amounts of C_2H_4 production indicate that the presence of acetone decreased the number of available acidic sites for ethanol dehydration and allowed increased steam reforming of ethanol. Figure 9.3-7 shows that initially no C_2H_4 was produced which suggests that it was steam reformed, whilst after 40 hours small amounts of C_2H_4 were produced and detected. It reveals that the active sites on the catalyst, which reform the C_2H_4, had become deactivated. It may be possible that the deposited coke decreased the interaction between the Lewis acid and basic sites of acetone and then the Lewis acid sites produced small amounts of C_2H_4.

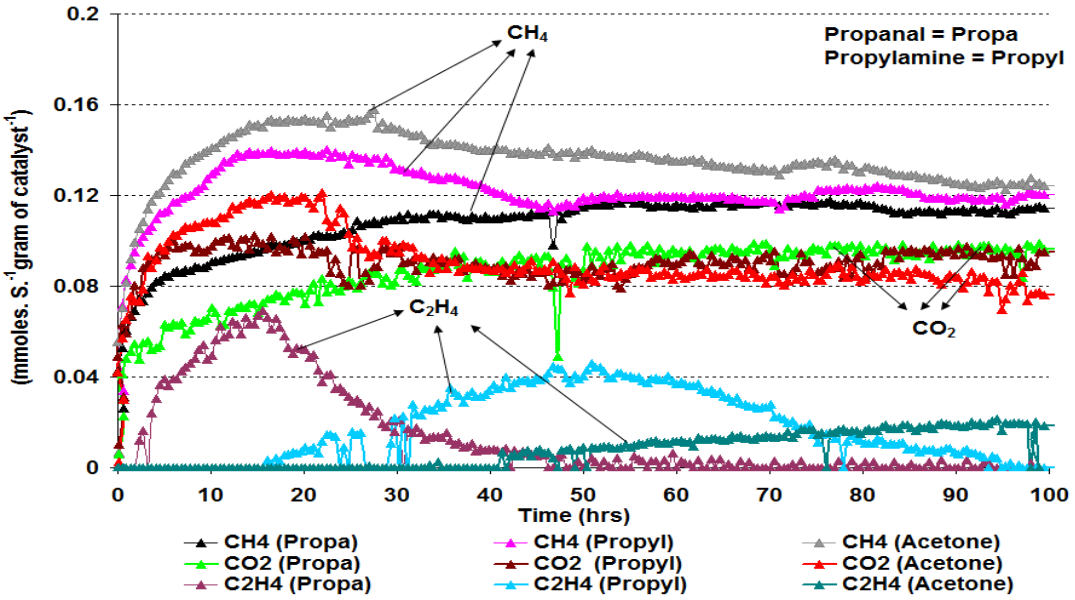

Figure 9.3-7 Rate of formation of gaseous products over the Pt/Al_2O_3 catalyst using propanal, propylamine and acetone impurities

In all the promoting impurities reactions over the Pt/Al_2O_3 catalyst only acetaldehyde, acetone and acetic acid were observed as liquid products. No diethyl ether or 1,1-diethoxyethane were detected in contrast to that observed in the pure ethanol and the C_3

alcohol impurity reactions. The disappearance of diethyl ether and 1,1-diethoxyethane in the promoting impurities reaction profiles might be due to the blockage of mild acidic sites, which are responsible for the coke formation according to the literature, as discussed before in Section 9.3-1. The formation of the liquid products in each impurity reaction was slightly different. In the propanal impurity reaction all the liquid products stabilised after an initial increase and then remained constant for the rest of the reaction, whilst in the propylamine and acetone impurity reactions, initially insignificant amounts of liquid products were produced which steadily increased to the end of the reaction. In all the reactions, acetaldehyde was the major liquid product as it was in the pure ethanol reaction, with the exception of the acetone impurity reaction where unreacted acetone was initially the major liquid phase component. These results indicate that when the catalyst was active the formation of liquid products was low. However, as deactivation of the catalyst started the formation of liquid products increased and they were seen in the effluent mixture. In short over the Pt/Al_2O_3 catalyst, in all the promoting impurity reactions the yield of C_2H_4 was significantly decreased compared to pure ethanol reaction whilst that of CO, CO_2 and CH_4 was significantly increased.

The rate of formation of H_2 in Figure 9.3-8 shows a clear difference between the deactivating and the promoting impurity reactions on the Pt/Al_2O_3 catalyst. The figure shows that before steady state, the propylamine and acetone impurity reactions had the highest rate of formation of H_2 compared to all the other impurities and even the pure ethanol reaction, with a yield of ~ 35%. However, at steady state, the propanal and propylamine impurities gave the highest rates of formation of H_2, with a 44% yield. The initial high rate of formation of H_2 in the acetone impurity may be due to the complete steam reforming of ethanol to gaseous products. While in the later stages of the reaction, due to the appearance of C_2H_4 and liquid products in the reaction stream, the rate of formation of H_2 had decreased. Similarly, in the propanal impurity reaction the rate of formation of C_2H_4 steadily decreased with time whilst the rate of formation of H_2 increased. Figure 9.3-8 also indicates that the pure ethanol reaction gave the lowest rate of formation of H_2 before steady state. However, at the steady state all of the deactivating impurities reactions gave a similar rate of formation of H_2.

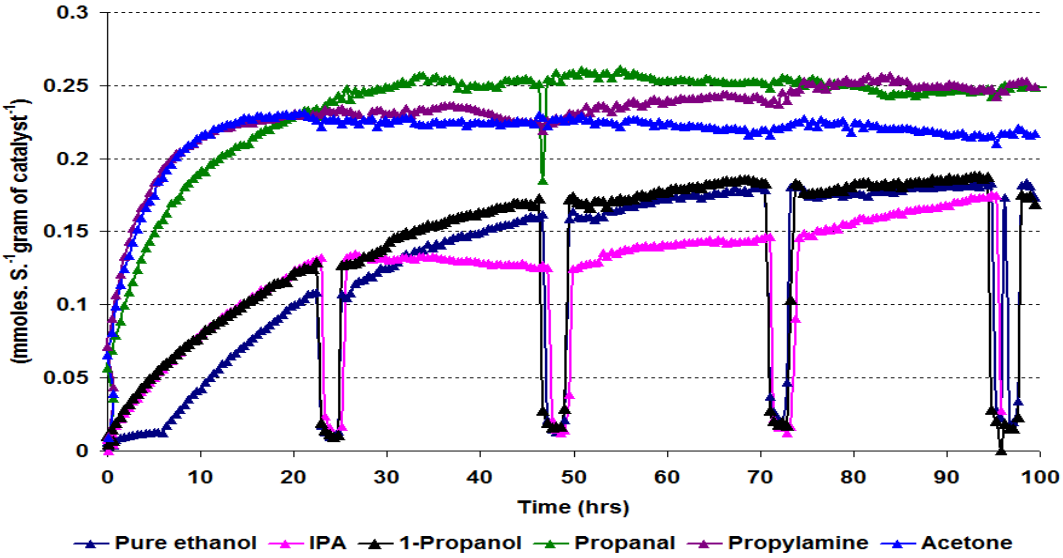

Figure 9.3-8 Rate of formation of H_2 over Pt/Al_2O_3 catalyst using different impurities

Post reaction characterisation results are shown in sections 8.3.3.2, 8.3.3.4, 8.3.3.6, 8.3.3.8 and 8.3.3.10 and tabulated in Table 9.3-3. These results indicate that the pure ethanol reaction gave a higher weight loss in the TPO and a lower BET surface area and pore volume than the C_3 alcohol impurity reaction samples. The high weight losses in the pure ethanol reactions correlate to the formation of C_2H_4 in high amounts, which is the main precursor for coke formation, as shown in Figures 8.3-59, 8.3-67 and 8.3-74. Unexpectedly, the propanal impurity reaction gave the highest weight loss amongst all the impurities and pure ethanol reaction samples of the Pt/Al_2O_3 catalyst. This high coke formation in the propanal impurity reaction looks to be due to both C_2H_4 polymerisation and CH_4 decomposition.

$$CH_4 \rightarrow CH_{(x-1)} + (x/2)H_2 \qquad (9.43)$$

The acetone impurity reaction gave the lowest amount of coke formation among all the impurity reactions and was lower compared the pure ethanol reaction. This was expected because less C_2H_4 formation occurred during the acetone impurity reaction and most of the coke formation will have originated from CH_4 decomposition, and its presence is supported by the evolution of a broad peak for water in the mass spectrometry profile (not shown in results). Due to the low amount of coke formation the acetone impurity reaction sample gave the highest BET surface area and pore volume, as shown in Table 9.3-3. The I_D/I_G ratio of the Raman results indicate that with all impurities, except propanal, the same order of graphitic carbon was formed. However, the band positions in the different

impurity reactions show that C_3 alcohol impurity reactions gave similar Raman bands to that of the pure ethanol reaction sample whilst the other functionality reaction samples gave D bands at different positions. These results suggest that the disorder produced in these impurity reaction samples were due to the formation of graphitic carbon from different precursors. As with propanal, the propylamine and acetone impurity reaction samples produced large amounts of CH_4, which contributed to the formation of coke. The shifting of the D band may have occurred due to the coke being produced from CH_4 decomposition in these impurity reactions.

Impurity	BET Surface area (m^2/g)	Pore volume (cm^3/g)	Weight loss in TPO (%)	(I_D/I_G)
No impurity	41	0.09	37	0.92
IPA	53	0.12	34	0.94
1-propanol	64	0.15	32	0.94
Propanal	31	0.07	38	0.98
Propylamine	34	0.07	37	0.95
Acetone	57	0.17	25	0.91

Table 9.3-3 Post reaction BET analysis and weight loss over Pt/Al_2O_3 catalyst using different impurities

9.3.4 Rh/Al_2O_3

9.3.4.1 Poisoning impurities

As was seen with the Pt/Al_2O_3 and the Ru/Al_2O_3 catalysts, 1-propanol and IPA acted as poisons during the steam reforming of ethanol over the Rh/Al_2O_3 catalyst. The addition of each of these impurities decreased the conversion of ethanol. In the initial 1-2 hours TOS, the presence of 1-propanol and IPA in the water/ethanol mixture had no apparent effect on the conversion of ethanol compared to the pure ethanol reaction *i.e.* 99% conversion. However, as the reaction proceeded further, the behaviour of ethanol conversion changed. In the presence of 1-propanol, the conversion of ethanol slightly decreased in the initial 3 hours of the reaction. However, after 5.6 hours there was a significant decrease in the conversion of ethanol, which then steadily decreased until by 100 hours TOS the conversion of ethanol had declined to 21%. The 1-propanol conversion also followed the same pattern for the decrease in ethanol conversion. The deactivation of the catalyst in the later stages of reaction is in agreement with previous investigations [62]. This decrease in the ethanol conversion can be related to the high rate of formation of C_2H_4. The 1-propanol

impurity gave the highest yield of C_2H_4 amongst all the impurity reactions, this agrees with work published by Wanat *et al*. [94] who found that amongst different alcohols, 1-propanol gave the highest yield of C_2H_4 when a Rh catalyst was employed. As discussed in section 9.3-2, incomplete decomposition of 1-propanol to propene resulted in catalyst deactivation. This is further emphasised by the decrease in the BET surface area of the catalyst, used for the 1-propanol impurity reaction, when compared to that used in the pure ethanol reaction. Although, less coke formation occurred over the catalyst surface as illustrated in Table 9.3-4. The same patterns for the deactivation of ethanol and 1-propanol conversions inferred that the reaction of both alcohols occurred on the same active sites on the Rh/Al_2O_3 catalyst.

As seen with the pure ethanol reaction over the Rh/Al_2O_3 catalyst, the conversion of ethanol was high in the initial hours of the reaction in the IPA impurity reaction. However, after 6.6 hours time on stream a large decrease occurred in the ethanol conversion, down to 44%, which then slowly decreased further until the end of the reaction. Like the Ru/Al_2O_3 and the Pt/Al_2O_3 catalysts, a high conversion of IPA was observed and throughout the reaction no significant change was observed in its conversion, as shown in Figure 8.3-102. In the presence of the IPA impurity a higher conversion of ethanol occurred compared to the 1-propanol impurity reaction. This higher conversion of ethanol in the IPA impurity reaction could be due to a decrease in the formation of C_3H_6 [94]. However, due to high C_2H_4 formation in the initial hours of the reaction, the catalyst was deactivated and compared to the pure ethanol reaction, lower ethanol conversion was observed in the later stages of the reaction. In previous studies [50], it was claimed that the higher alcohols, especially the branched alcohols have a significant influence on the conversion of ethanol. However, the present study shows that the 1-propanol impurity reaction produced slightly more deactivation as measured by the conversion of ethanol. This higher deactivation of the 1-propanol can be explained by the incomplete oxidation of 1-propanol on the catalyst surface. As discussed before, Mizuno [172] investigated the steam reforming of the IPA on different metal supported Al_2O_3 catalysts and found that Rh/Al_2O_3 catalyst showed the highest stability for IPA steam reforming reaction.

These results suggest that due to the competitive adsorption of ethanol and 1-propanol on the same active sites of the catalyst, the catalyst deactivated very quickly with the incomplete decomposition of 1-propanol to the corresponding propylene. Conversely, in the IPA impurity reaction it appears that the steam reforming of IPA and ethanol occurs on

different active sites, because if we consider the conversion of ethanol, it continuously decreased throughout the reaction whilst the conversion of IPA remained high.

With regard to the gaseous product distributions in both alcoholic impurity reactions, C_2H_4 gave higher rates of formation compared to the pure ethanol reaction. However, the pattern of its formation in both impurity reactions was slightly different as shown in Figure 9.3-9. In the 1-propanol impurity reaction the rate of formation of C_2H_4, after an initial increase, steadily decreased to the end of the reaction. However, up to 100 hours TOS its rate was higher than the pure ethanol reaction. With the IPA impurity reaction, the rate of formation of C_2H_4, after the initial increase, steeply decreased and after approximately 75 hours TOS its rate of formation was lower than at the corresponding time in the pure ethanol reaction. This then remained stable for the remainder of the reaction as shown in Figure 9.3-9. These results suggest that although more deactivation took place in the 1-propanol impurity reaction, the sites for dehydration remained active and gave a high rate of formation for C_2H_4. This high rate of formation of C_2H_4 in the 1-propanol impurity reaction affected the rate of formation of H_2 and other C_1 products. In the IPA impurity reaction, the rate of formation of C_2H_4 was higher initially and so produced less H_2. However, in the later stages of the reaction, the rate of formation of H_2 approached that of the pure ethanol reaction. This shows that initially, due to a high rate of formation of C_2H_4 the yield of H_2 was low. However, when the active sites for C_2H_4 formation became blocked then the ethanol was converted into C_1 products by Rh metal. The high rate of formation of CO_2 infers that during the reaction, water gas shift and Boudouard reactions took place.

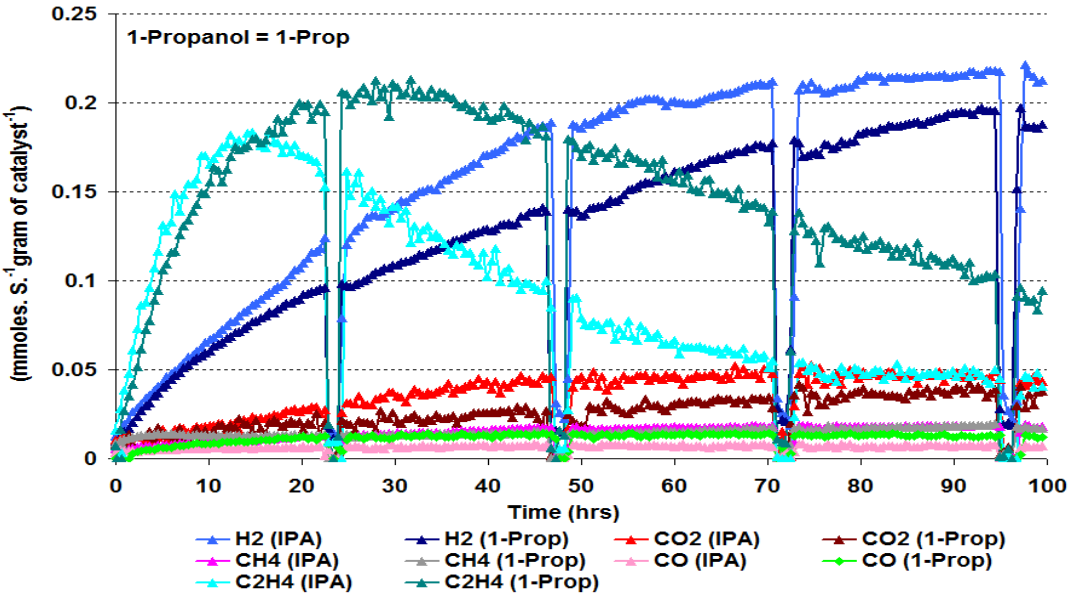

Figure 9.3-9 Rate of formation of gaseous products over Rh/Al_2O_3 catalyst using 1-propanol and IPA impurities

As with the Pt and Ru catalysts, acetaldehyde was produced at a high yield in the liquid products. The presence of acetaldehyde in the effluent products shows that over the Rh/Al_2O_3 catalyst both dehydration and dehydrogenation reactions took place simultaneously. However, the rate of dehydration reaction was much higher than the rate of dehydrogenation. Acetaldehyde, acetone, diethylether and acetic acid were produced in both impurities reactions. However, their yields were decreased which indicates that the impurity modified the active sites on the Rh/Al_2O_3 catalyst and blocked some sites used for the production of these products.

9.3.4.2 Promoting impurities

As with the Pt/Al_2O_3 catalyst, the promoting impurities over the Rh/Al_2O_3 catalyst were propanal, propylamine and acetone. In the presence of all these impurities the conversion of ethanol was enhanced and gave a high conversion over a greater time period. Figures 8.3-109, 8.3-117 and 8.3-125 indicate that in the presence of these impurities ethanol gave above 90% conversion in the initial 50 hours TOS over the Rh/Al_2O_3 catalyst. However, after 50 hours TOS the patterns of ethanol conversion for each impurity were different. In the presence of propanal, the conversion of ethanol steadily decreased up to the end of the reaction. However, the ethanol conversion was still higher than the pure ethanol reaction as shown in Figure 8.2-75 and Figure 8.3-109. These results suggest that due to the high C-C splitting propensity of the Rh/Al_2O_3 the catalyst, the propanal did not deactivate the catalyst quickly, as was observed over the Ru/Al_2O_3 catalyst [75]. It is possible that propanal did not convert to propylene and behaved like acetone and the carbonyl carbon of the aldehyde neutralised the Lewis acidic sites of the support. Conversely it may have decarbonylated to form CO and C_2H_4, as discussed in section 9.3-2. Thus, both the ethanol and the propanal steam reformed on the Rh metal and formed CH_4, CO_2, CO and H_2, as seen in Figure 9.3-11. C_2H_4 appeared in all three impurity reactions after 30 hours or longer time on stream, and coincided with the deactivation of the catalyst, reinforcing the view that the species causing the catalyst deactivation is C_2H_4. From Figure 8.3-110 it is proposed that the C_2H_4 formed, initially underwent steam reforming to form CO and H_2. However, when the active sites for the C_2H_4 steam reforming became blocked C_2H_4 appears in the effluent mixture increasing the rate of polymerising and causing the deactivation of the catalyst. When the active sites for the C_2H_4 became deactivated by coke, as illustrated in Figure 9.3-10, the steam reforming of ethanol started, which is supported by the steady increase in the rate of formation of CH_4.

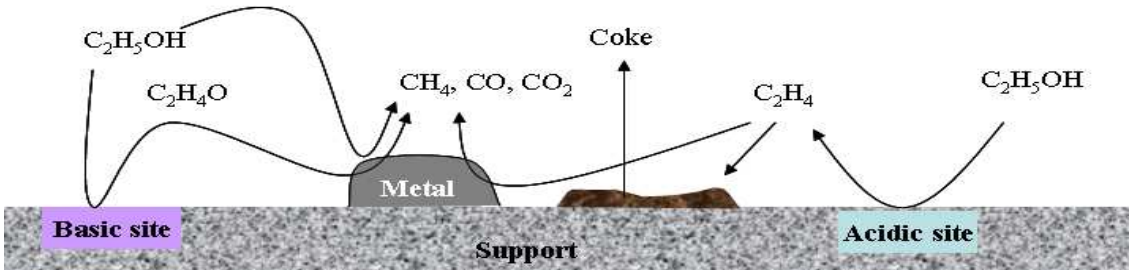

Figure 9.3-10 Steam reforming of ethanol over the catalyst surface

The influence of propylamine on ethanol conversion was similar for all catalysts although the deactivation was slightly different. In the presence of the propylamine impurity the Rh/Al_2O_3 catalyst initially had a high ethanol conversion, above 98%, which then decreased until the end of the reaction. This decrease in the ethanol conversion can be correlated with formation of the liquid products and C_2H_4. Figure 9.3-11 also reveals that propylamine gave the highest rate of formation of CH_4 although initially it was higher in the acetone impurity reaction. Also, the rate of formation of CO_2 slightly increased as the rate of formation of C_2H_4 decreased, whilst the rate of formation of CO was significantly decreased. These results suggest that CO underwent a water gas shift reaction to form CO_2 and H_2. Similar to the propylamine and the propanal reactions, the addition of acetone to the pure ethanol feed enhanced the conversion of ethanol and in the initial 54 hours time on stream gave ~ 100% conversion. However, after 54 hours TOS the conversion of ethanol steadily decreased although by the end of the reaction it had only declined to 97%, as shown in Figure 8.3-125. The deactivation of the Rh/Al_2O_3 catalyst in the presence of acetone looks likely to be due to the appearance of the small amount of C_2H_4 in the effluent mixture after 44 hours TOS. Figure 8.3-126 shows that when the catalyst was active initially, high amounts of CH_4 and CO_2 were produced, whilst the rate of formation of CO was low. These results suggest that two reactions took place simultaneously.

$$C_2H_5OH + H_2O \rightarrow 2CO + 4H_2 \quad (9.44)$$

$$CO + H_2O \rightarrow CO_2 + H_2 \quad (9.45)$$

$$C_2H_5OH + 2H_2 \rightarrow 2CH_4 + H_2O \quad (9.46)$$

Equation 9.46 is also supported by the high rate of formation of CH_4 and a relatively low rate of formation of H_2. As discussed before, the high activity of the ethanol steam reforming reaction in the presence of acetone is not completely understood. The acetone, and its aldol product mesityl oxide, may block both the Lewis and Brönsted acidic sites because both of these reagents act as bases when interacting with alumina [178].

Therefore, the reaction shifted to ethanol dehydrogenation, which is supported by the high rate of formation of CH_4 and CO_2 in the gaseous products. In the initial 43 hours TOS no C_2H_4 was detected, which may suggest that some acid sites initially produced small amount of C_2H_4 which rapidly underwent conversion to CO, CO_2 and CH_4. However, when the sites for steam reforming were deactivated, C_2H_4 production steadily increased with time on stream. Then, after some time, the rate of formation of C_2H_4 decreased presumably because of blocking of ethanol dehydration sites by polymerised C_2H_4.

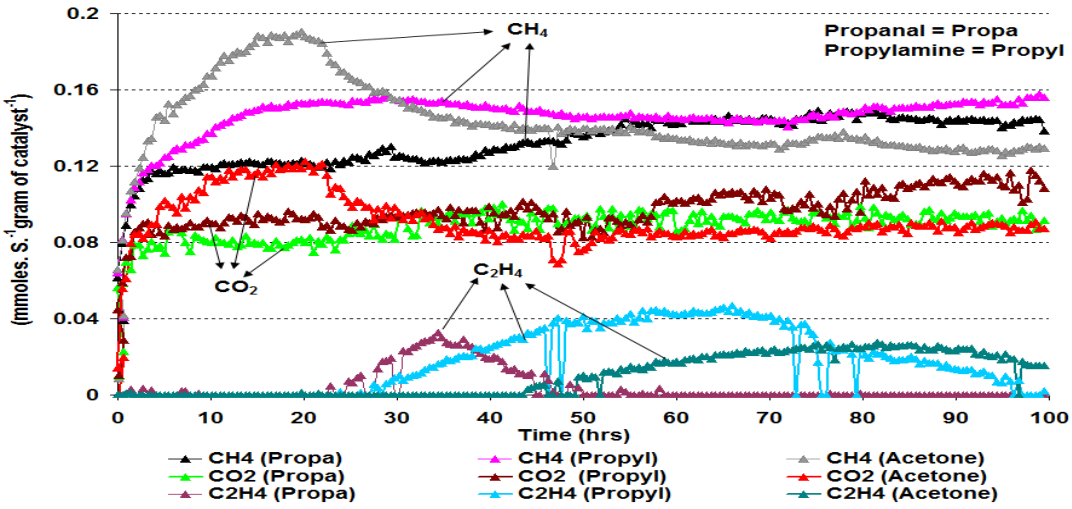

Figure 9.3-11 Rate of formation of gaseous products over the Rh/Al_2O_3 catalyst using propanal, propylamine and acetone impurities

The liquid products distribution in Figure 8.3-129 indicates that the formation of the liquid products coincides with the deactivation of the catalyst. When the catalyst was active, the ethanol feed was completely converted to the gaseous products and no liquid products were produced. However, as the deactivation of catalyst started, liquid products began to be produced.

Over the Rh/Al_2O_3 catalyst the rate of formation of H_2 in all the impurity and the pure ethanol reactions reached the same rate at steady state, with the exception of the propylamine and 1-propanol reactions. Figure 9.3-12 summarises the rate of formation of H_2 in all the impurity reactions and shows that in the presence of the 1-propanol impurity, the lowest rate of formation of H_2 was seen. This low rate of formation of H_2 in the presence of the 1-propanol impurity can be attributed to the high rate of formation of C_2H_4. The rate of formation of H_2 in the presence of IPA, propanal and acetone was seen to be similar near to steady state conditions, although initially their rates of formation were quite different. The different rates of formation of H_2 in the initial hours of reaction could be

related to the different rates of formation of CH_4 and C_2H_4 and the water gas shift reaction, as shown in Figures 8.3-96, 8.3-103, 8.3-110, 8.3-118 and 8.3-126. The propylamine impurity reaction produced the highest rate of formation H_2 amongst all the impurity reactions and appears to be due to low C_2H_4 formation and high water gas shift. Figure 9.3-12 shows that the rate of formation of H_2 steadily increased with time. While at the same time, the rate of formation of CO decreased and rate of formation of the CO_2 increased.

$$CO + H_2O \quad \rightarrow \quad CO_2 + H_2 \qquad (9.47)$$

In the promoting impurity reactions over the Rh/Al_2O_3 catalyst only acetone, acetaldehyde and acetic acid were detected as liquid products. This suggests that the promoting impurities not only increased the H_2 yield but also modified or blocked the active acidic sites for formation of diethyl ether and other undesired products.

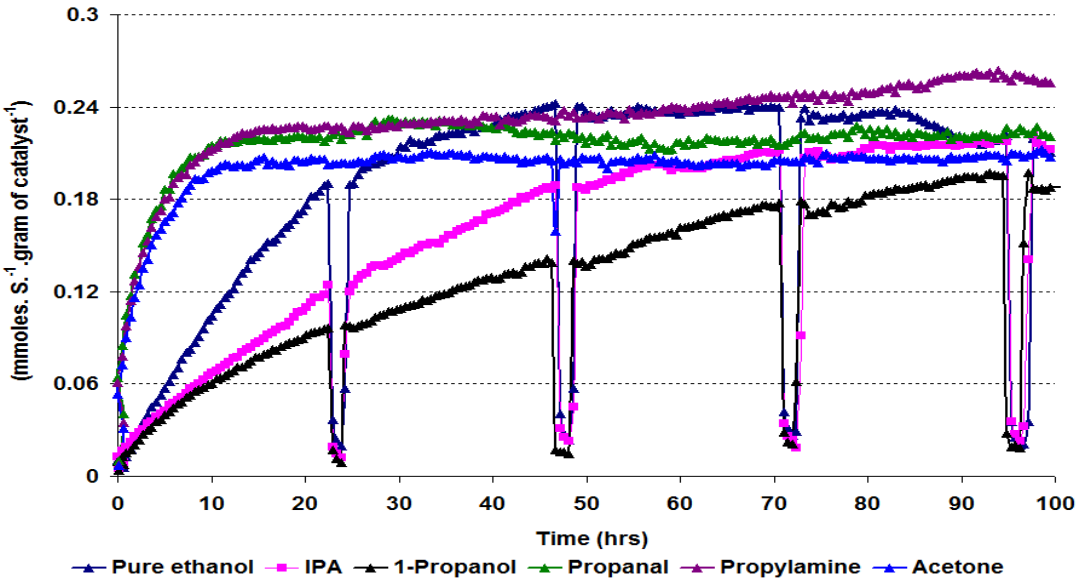

Figure 9.3-12 Rate of formation of H_2 over Rh/Al_2O_3 catalyst using different impurities

Post reaction characterisation of the Rh/Al_2O_3 catalyst, from the different impurity reactions is shown in sections 8.3.4.2, 8.3.4.4, 8.3.4.6, 8.3.4.8 and 8.3.4.10. The TPO results of the different impurity reaction samples indicate that with the exception of the pure ethanol and IPA impurity reactions, the weight loss occurring in the TPO was in the same temperature region. However, the derivative weight results indicate that either the nature of the coke decomposed was different or that the coke was deposited on different sites of the catalyst. In the IPA, 1-propanol and pure ethanol reaction samples, weight loss started at 300^{o}C, which suggests a low carbon to hydrogen ratio or more hydrogenated

coke present in these samples. In other impurity reaction samples, the TPO weight loss started at a higher temperature than that observed with the sample which had been used for the pure ethanol. This indicates more dehydrogenated coke deposition on the catalyst. Interestingly, the different coke deposited in the acetone impurity reaction gave separate peaks and the mass spectrometry data shows that the water completely disappeared after the initial peak at 603^{o}C. This inferred that the two different types of coke produced, evolved at different temperatures in the TPO analysis. It may possible that these two peaks occur due to some experimental error as the oxygen peak completely disappeared as shown in Figure 8.3-131. The BET analysis of all impurity samples is compared in Table 9.3-4 and indicates that there was no direct correlation between BET surface area and the amount of coke deposition found. Usually the BET surface area increases with a decrease in coke deposition on the catalyst surface, but the data in Table 9.3-4 shows that for all impurities decrease in the amount of coke led to a decrease in the BET surface area, with the exception of the acetone impurity reaction. These results suggest that the slight changes in BET surface area may be due to changes in the average pore diameter as shown in Tables 8.3-13, 8.3-14, 8.3-15, 8.3-16 and 8.3-17.

The Raman data gave similar results, to those observed for the Pt/Al_2O_3 catalyst for the different impurity reaction samples. The intensity of both bands for graphitic carbon in all the promoting impurity reaction samples increased compared to the pure ethanol reaction samples. The Raman data also indicates that the D band in the alcoholic impurity reaction samples was similar to the D band in the pure ethanol reaction sample, whilst in the other functional group impurity reaction samples, the band had shifted slightly upwards. This shift in the D band indicates that the functional group influences the nature of the graphitic carbon. The (I_D/I_G) shown in Table 9.3-4 also reveals that the impurities caused a slight change in the disorder of the graphitic carbon deposited over the Rh/Al_2O_3 catalyst.

Impurity	BET Surface area (m^2/g)	Pore volume (cm^3/g)	Weight loss in TPO (%)	(I_D/I_G)
No impurity	47	0.04	41	0.91
IPA	39	0.03	41	0.94
1-propanol	39	0.07	39	0.93
Propanal	32	0.08	37	0.98
Propylamine	31	0.07	37	0.91
Acetone	45	0.11	31	0.94

Table 9.3-4 Post reaction BET analysis and weight loss over the Rh/Al_2O_3 catalyst using different impurities

10. Conclusions

The main aim of the project was to determine the tolerance of pure Al_2O_3 and Al_2O_3 supported noble metal catalysts towards the different impurities present in crude bioethanol. In the initial stage of the project the catalysts were characterised by BET and powder XRD to investigate the catalyst morphology. These catalysts were then used to perform ethanol steam reforming reactions at different temperatures to determine the optimum temperature for the impurities reactions. From the powder XRD results it was seen that the Al_2O_3 existed as a mixture of the delta and theta forms and the impregnation of Al_2O_3 with noble metals had no observable effect on the structure of the Al_2O_3 support.

10.1 Effect of temperature

The steam reforming reaction of ethanol over an Al_2O_3 catalyst at different temperatures showed good activity towards ethanol conversion. Almost no deactivation was observed with a change of temperature from 500°C to 600°C during the 100 hours TOS. It was found that due to the presence of strong acidic sites on the Al_2O_3, the major reaction was the cracking and steam reforming of C_2H_5OH which are shown by routes B and C in Figure 10.1-1. As predicted by thermodynamics, increasing the reaction temperature from 500°C to 600°C decreased the water gas shift reaction, while the rate of steam reforming of CH_4 was slightly increased

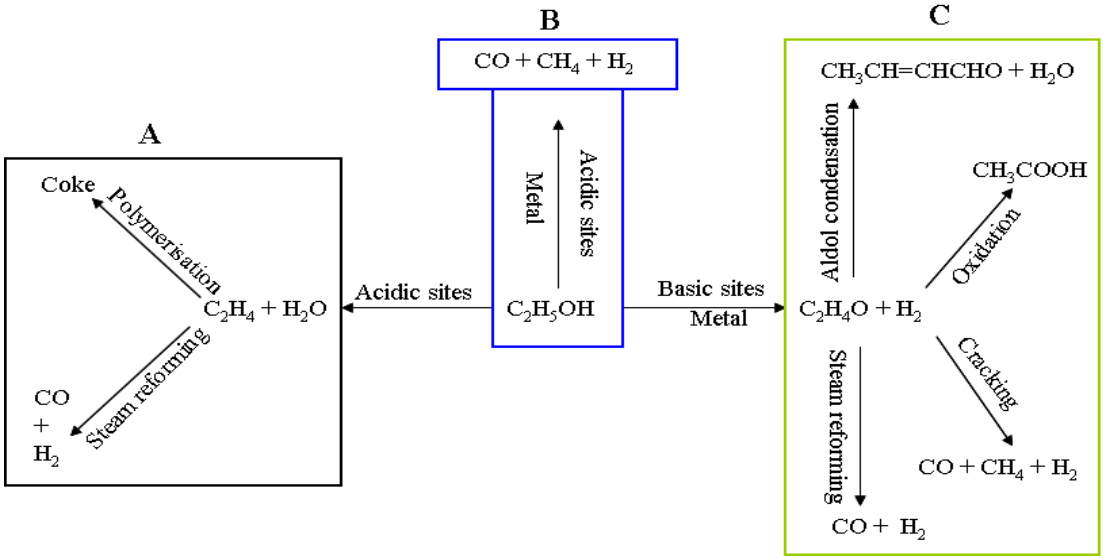

Figure 10.1-1 Reaction routs on different catalysts

Ethanol steam reforming over the Ru/Al_2O_3 catalyst at different temperatures revealed the main reaction to be dehydration (route A) however, the steam reforming of ethanol occurred in parallel through route C. The formation of $(C_2H_5)_2O$ and C_2H_4 over the Ru/Al_2O_3 catalyst indicated that the addition of Ru metal to the Al_2O_3 blocked some of the strong acid sites and left the mild acid sites which were responsible for the formation of C_2H_4 and $(C_2H_5)_2O$. Increasing the reaction temperature from 500^{o}C to 600^{o}C suppressed the water gas shift reaction. Also, hydrogenolysis (10.1) and polymerisation of C_2H_4 significantly increased with an increase in reaction temperature.

$$C_2H_4 + 2H_2 \rightarrow 2CH_4 \qquad (10.1)$$

In a similar manner to the Ru/Al_2O_3 catalyst, dehydration and hydrogenolysis took place over the Pt/Al_2O_3 catalyst during the steam reforming of ethanol and as reaction temperature increased so to did the extent of hydrogenolysis. Due to the deposition of hydrogenated coke, the catalysts were active at 600^{o}C and the conversion of ethanol was stable for 100 hours TOS. Before reaching the steady state condition, the increase in the rate of formation of CO and the subsequent increase in the rate of formation of CO_2 with increasing reaction temperature indicate that the Pt/Al_2O_3 catalyst was active for the water gas shift reaction. However, the CO : CO_2 ratio reveals that the steam reforming reaction is faster than water gas shift reaction.

Among the different noble metal catalysts, Rh/Al_2O_3 showed the highest conversion of ethanol at 500^{o}C and 550^{o}C due to the high C-C splitting properties of Rh metal, whilst at 600^{o}C the catalyst deactivated. The deactivation appeared to be due to an increase in hard coke formation. The lower rate of formation of C_2H_4 reveals that dehydration of ethanol (route A) significantly decreased and the major reaction became steam reforming which followed route C. The increase in the rate of formation of CH_4 with an increase in reaction temperature, especially at 600^{o}C, can be explained by the decomposition of acetaldehyde.

The deactivation of all the catalysts studied was attributed to the deposition of coke produced from the polymerization and cracking of C_2H_4, CH_4, and CO. The amounts of coke on all catalysts (except Rh/Al_2O_3) slightly increased with an increase in the reaction temperature from 500^{o}C to 600^{o}C. The nature of the coke altered with temperature and catalyst. The coke was classified into three known groups of α, β and γ-coke which were present on the metal, metal-support interface and support respectively (Figure 10.2).

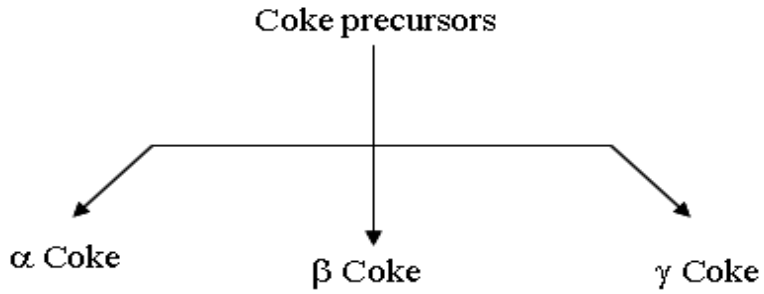

Figure 10.1-2 Different types of coke

All three different types of coke were more distinguishable on the Rh/Al_2O_3 catalyst. Raman spectroscopy results indicated that graphitic type carbon was present on all the catalysts at high temperatures and the disorder in graphitic carbon increased with an increase in the reaction temperature.

10.2 Effect of impurities

The addition of 1 mol.% impurities to the water/ethanol mixture affected the conversion of ethanol over the Al_2O_3. The propylamine and 1-Propanol impurities blocked some of the strong acid sites and left mild acid sites that produced C_2H_4. The formation of C_2H_4 played a significant role in the decrease in ethanol conversion over the Al_2O_3. However, the yield of H_2 slightly increased in the impurity reactions due to contributions from the reformed impurity.

Over the Ru/Al_2O_3 catalyst C_3 alcohols and propanal impurities decreased the conversion of ethanol whilst propylamine and acetone impurities enhanced the conversion of ethanol. The deactivating effect of the impurities was attributed to the formation of propene which appears to cause deactivation more readily than C_2H_4. Incompletely steam reformed impurities are deposited on the catalyst surface which contributes to faster deactivation of the catalyst. The enhancing effect of propylamine and acetone was due to neutralisation of the Lewis and Brönsted acid sites on the catalyst, therefore changing the mechanism from an acidic to a basic pathway *i.e.* dehydration to dehydrogenation. Due to neutralisation of the Lewis and Brönsted acid sites, no diethyl ether was produced throughout reaction. In both propylamine and acetone impurity reactions the activity of the catalyst towards ethanol conversion was significantly increased and this increase was due to a relative decrease in coke formation.

Investigating the effect of impurities over the Pt/Al_2O_3 catalyst, the C_3 alcohols acted as poisons while acetone, propanal and propylamine played the role of promoter in the ethanol steam reforming reaction. The formation of large amounts of C_2H_4 and C_3H_6 in the initial stage of the C_3 alcohols impurity reactions rapidly deactivated the catalyst as compared to the pure ethanol reaction. In contrast to the Ru/Al_2O_3 catalyst, propanal acted as a promoter on the Pt/Al_2O_3, which followed the dehydrogenation pathway over the Pt/Al_2O_3 and formed H_2, CO and hydrocarbons. It was found, as on the Ru/Al_2O_3 catalyst acetone and propylamine neutralised the Lewis and Brönsted acid sites and increased the rate of ethanol steam reforming reaction on the Pt/Al_2O_3 catalyst.

As with the Pt/Al_2O_3 and Ru/Al_2O_3 catalysts, addition of 1-propanol and IPA to the ethanol water mixture deactivated the Rh/Al_2O_3 catalyst. This deactivation was proposed to be due to formation of propylene and large amounts of ethylene which blocked the active sites for ethanol steam reforming. Compared to the Pt/Al_2O_3 reactions, Rh/Al_2O_3 showed relatively high activity toward ethanol conversion, due to the high C-C splitting properties of Rh metal, as discussed before. The addition of propanal, propylamine and acetone enhanced the conversion of ethanol and increased the activity of the catalyst. It is suggested that this enhancement was due to the same reasons as discussed for the Pt/Al_2O_3 catalyst. Over the Rh/Al_2O_3, the 1-propanol impurity reaction gave the lowest H_2 yield due to a high rate of formation of C_2H_4.

With regards to coke formation, acetone addition produced the least amount of coke among the different impurities on all the catalysts and this is believed to be due to the inhibition of ethylene formation. The nature and amounts of coke produced by the other impurities varied on different catalysts. Formation of CH_4 and C_2H_4 play an important role in the variations of coke produced by different impurities.

11. References

[1] N. Meng, M.K.H. Leung, K. Sumathy, D.Y.C. Leung, International Journal of Hydrogen Energy, 31 (2006) 1401-1412.
[2] S. Lim, L.K. Teong, Renewable and Sustainable Energy Reviews, 14 (2010) 938-954.
[3] B. Dudley, BP Statistical Review of World Energy in, BP, London, 2011, pp. 45.
[4] A. Haryanto, S. Fernando, N. Murali, S. Adhikari, Energy and Fuels, 19 (2005) 2098-2106.
[5] O. Gorke, P. Pfeifer, K. Schubert, Applied Catalysis A:General, 360 (2009) 232-241.
[6] M. Ni, D.Y.C. Leung, M.K.H. Leung, International Journal of Hydrogen Energy, 32 (2007) 3238-3247.
[7] A.L. Alberton, M.M.V.M. Souza, M. Schmal, Catalysis Today, 123 (2007) 257-264.
[8] J.G. Speight, Hydrocarbons from Biomass, in: Handbook of Industrial Hydrocarbon Processes, Gulf Professional Publishing, Boston, 2011, pp. 241-279.
[9] J.H. Oakley, A.F.A. Hoadley, International Journal of Hydrogen Energy, 35 (2010) 8472-8485.
[10] H.S. Roh, Y. Wang, D.L. King, Topics in Catalysis, 49 (2008) 32-37.
[11] F. Frusteri, S. Freni, L. Spadaro, V. Chiodo, G. Bonura, S. Donato, S. Cavallaro, Catalysis Communications, 5 (2004) 611-615.
[12] H. Idriss, Platinum Metals Review, 48 (2004) 105-115.
[13] S. Dushyant, J.S. James, A.B. David, Fuel cell Technology for Fuel cell Processing, Elsevier, Oxford, 2011.
[14] E. Acha, J. Requies, V.L. Barrio, J.F. Cambra, M.B. Güemez, P.L. Arias, International Journal of Hydrogen Energy, 35 (2010) 11525-11532.
[15] R.C. Cerritos, R.F. Ramirez, A.F.A. Alvarado, J.M.M. Rosales, T.V. García, I.R.G. Esquivel, Industrial & Engineering Chemistry Research, 50 (2011) 2576-2584.
[16] A.C. Basagiannis, X.E. Verykios, Catalysis Today, 127 (2007) 256-264.
[17] C. Song, Catalysis Today, 77 (2002) 17-49.
[18] A.J. Akande, Production of Hydrogen by Reforming of Crude Ethanol in: Master thesis Department of Chemical Engineering University of Saskatchewan Saskatoon 2005, pp. 140.
[19] J. Zhang, PEM Fuel Cell Electrocatalysts and Catalyst Layers, Springer, London, 2008.
[20] B. Johnston, M.C. Mayo, A. Khare, Technovation, 25 (2005) 569-585.
[21] http://en.wikipedia.org/wiki/Fuel_cell accessed on 29/10/2011.
[22] O. Raphael, Production of Hydrogen from the low temperature steam reforming of methanol, in: PhD thesis Department of Chemical Engineering, University of Saskatchewan, Saskatchewan, 1995.
[23] http://www.fctec.com/fctec_basics.asp accessed on 29/10/2011.
[24] P. Barbaro, C. Bianchini, Catalysis for Sustainable Energy Production, Wiley-VCH Verlag GmbH & Co. , Weinheim, 2009.
[25] T. Nishiguchi, T. Matsumoto, H. Kanai, K. Utani, Y. Matsumura, W.J. Shen, S. Imamura, Applied Catalysis A: General, 279 (2005) 273-277.
[26] A. Bshish, Z. Yaakob, B. Narayanan, R. Ramakrishnan, A. Ebshish, Chemical Papers, 65 (2011) 251-266.
[27] H. Balat, E. Kirtay, International Journal of Hydrogen Energy, 35 (2010) 7416-7426.
[28] J.N. Armor, Applied Catalysis A: General, 176 (1999) 159-176.
[29] J.B. Gadhe, R.B. Gupta, Industrial & Engineering Chemistry Research, 44 (2005) 4577-4585.
[30] V. Agarwal, S. Patel, K.K. Pant, Applied Catalysis A: General, 279 (2005) 155-164.
[31] M.A. Goula, S.K. Kontou, P.E. Tsiakaras, Applied Catalysis B: Environmental, 49 (2004) 135-144.

[32] P. Biswas, D. Kunzru, Chemical Engineering Journal, 136 (2008) 41-49.
[33] J. Llorca, N. Homs, J. Sales, P.R. Piscina, Journal of Catalysis, 209 (2002) 306.
[34] H. Devianto, Z.L. Li, S.P. Yoon, J. Han, S.W. Nam, T.H. Lim, H.-I. Lee, International Journal of Hydrogen Energy, 35 (2010) 2591-2596.
[35] F. Soyal-BaltacIoglu, A.E. Aksoylu, Z.I. Önsan, Catalysis Today, 138 (2008) 183-186.
[36] C.E. Wyman, Handbook on Bioethanol: Production and Utilization, CRC Press, 1996.
[37] A.C. Furtado, C.G. Alonso, M.P. Cantão, N.R.C. Fernandes-Machado, International Journal of Hydrogen Energy, 34 (2009) 7189-7196.
[38] R.R. Davda, J.W. Shabaker, G.W. Huber, R.D. Cortright, J.A. Dumesic, Applied Catalysis B: Environmental, 56 (2005) 171-186.
[39] O. Akdim, W. Cai, V. Fierro, H. Provendier, A.V. Veen, W. Shen, C. Mirodatos, Topics in Catalysis, 51 (2008) 22-38.
[40] E.B. Pereira, P.R. Piscina, S. Marti, N. Homs, Energy & Environmental Science, 3 (2010) 487-493.
[41] A. Haryanto, S. Fernando, N. Murali, S. Adhikari, Energy & Fuels, 19 (2005) 2098-2106.
[42] I. Fishtik, A. Alexander, R. Datta, D. Geana, International Journal of Hydrogen Energy, 25 (2000) 31-45.
[43] M. Benito, R. Padilla, A. Serrano-Lotina, L. Rodríguez, J.J. Brey, L. Daza, Journal of Power Sources, 192 (2009) 158-164.
[44] J. Raskó, M. Dömök, K. Baán, A. Erdohelyi, Applied Catalysis A: General, 299 (2006) 202-211.
[45] A.N. Fatsikostas, X.E. Verykios, Journal of Catalysis, 225 (2004) 439-452.
[46] P. Ciambelli, V. Palma, A. Ruggiero, Applied Catalysis B: Environmental, 96 (2010) 18-27.
[47] C. Resini, T. Montanari, L. Barattini, G. Ramis, G. Busca, S. Presto, P. Riani, R. Marazza, M. Sisani, F. Marmottini, U. Costantino, Applied Catalysis A: General, 355 (2009) 83-93.
[48] H. Wang, Y. Liu, L. Wang, Y.N. Qin, Chemical Engineering Journal, 145 (2008) 25-31.
[49] D.K. Liguras, D.I. Kondarides, X.E. Verykios, Applied Catalysis B: Environmental, 43 (2003) 345-354.
[50] N. Bion, F. Epron, D. Duprez, Bioethanol reforming for H_2 production. A comparison with hydrocarbon reforming, in: Catalysis, The Royal Society of Chemistry, 2010, pp. 1-55.
[51] H. Song, L. Zhang, U.S. Ozkan, Industrial & Engineering Chemistry Research, 49 (2010) 8984-8989.
[52] A.L. Silva, C.D.F. Malfatti, I.L. Müller, International Journal of Hydrogen Energy, 34 (2009) 4321-4330.
[53] G. Rabenstein, V. Hacker, Journal of Power Sources, 185 (2008) 1293-1304.
[54] X. Wu, S. Kawi, Energy & Environmental Science, 3 (2010) 334-342.
[55] A. Le-Valant, N. Bion, F. Can, D. Duprez, F. Epron, Applied Catalysis B: Environmental, 97 (2010) 72-81.
[56] L.C. Chen, S.D. Lin, Applied Catalysis B: Environmental, 106 (2011) 639-649.
[57] Y. Choi, P. Liu, Catalysis Today, 165 (2011) 64-70.
[58] S. Li, M. Li, C. Zhang, S. Wang, X. Ma, J. Gong, International Journal of Hydrogen Energy, 47 (2012) 2940–2949.
[59] S. Cavallaro, Energy & Fuels, 14 (2000) 1195-1199.
[60] A. Fabien, D. Claude, D. Daniel, Science and Technology in Catalysis, 63 (2002) 303-306.
[61] A.J. Byrd, K.K. Pant, R.B. Gupta, Energy & Fuels, 21 (2007) 3541-3547.

[62] J. Rass-Hansen, R. Johansson, M. Moller, C.H. Christensen, International Journal of Hydrogen Energy, 33 (2008) 4547-4554.
[63] A.C. Basagiannis, X.E. Verykios, Applied Catalysis B: Environmental, 82 (2008) 77-88.
[64] I.A.C. Ramos, T. Montini, B. Lorenzut, H. Troiani, F.C. Gennari, M. Graziani, P. Fornasiero, Catalysis Today, (2011).
[65] P.D. Vaidya, A.E. Rodrigues, Industrial & Engineering Chemistry Research, 45 (2006) 6614-6618.
[66] J.P. Breen, R. Burch, H.M. Coleman, Applied Catalysis B: Environmental, 39 (2002) 65-74.
[67] G. Jacobs, R.A. Keogh, B.H. Davis, Journal of Catalysis, 245 (2007) 326-337.
[68] A. Casanovas, J. Llorca, N. Homs, J.L.G. Fierro, P. Ramirez-de-la Piscina, Journal of Molecular Catalysis A: Chemical, 250 (2006) 44-49.
[69] B. Zhang, X. Tang, Y. Li, Y. Xu, W. Shen, International Journal of Hydrogen Energy, 32 (2007) 2367-2373.
[70] P.D. Vaidya, A.E. Rodrigues, Chemical Engineering Journal, 117 (2006) 39-49.
[71] V. Fierro, O. Akdim, C. Mirodatos, Green Chemistry, 5 (2003) 20-24.
[72] J. Comas, F. Mariño, M. Laborde, N. Amadeo, Chemical Engineering Journal, 98 (2004) 61-68.
[73] F. Aupretre, C. Descorme, D. Duprez, Catalysis Communications, 3 (2002) 263-267.
[74] F. Haga, T. Nakajima, H. Miya, S. Mishima, Catalysis Letters, 48 (1997) 223-227.
[75] S. Cavallaro, N. Mondello, S. Freni, Journal of Power Sources, 102 (2001) 198-204.
[76] K. Urasaki, K. Tokunaga, Y. Sekine, M. Matsukata, E. Kikuchi, Catalysis Communications, 9 (2008) 600-604.
[77] W. Grzegorczyk, A. Denis, W. Gac, T. Ioannides, A. Machocki, Catalysis Letters, 128 (2009) 443-448.
[78] K.M. Hardiman, T.T. Ying, A.A. Adesina, E.M. Kennedy, B.Z. Dlugogorski, Chemical Engineering Journal, 102 (2004) 119-130.
[79] S. Velu, K. Suzuki, M. Vijayaraj, S. Barman, C.S. Gopinath, Applied Catalysis B: Environmental, 55 (2005) 287-299.
[80] A.J. Vizcaíno, P. Arena, G. Baronetti, A. Carrero, J.A. Calles, M.A. Laborde, N. Amadeo, International Journal of Hydrogen Energy, 33 (2008) 3489-3492.
[81] E. Salehi, F.S. Azad, T. Harding, J. Abedi, Fuel Processing Technology, 92 (2011) 2203-2210.
[82] V. Fierro, V. Klouz, O. Akdim, C. Mirodatos, Catalysis Today, 75 (2002) 141-144.
[83] J.T. Richardson, Principle of the Catalyst Development Springer, 1989.
[84] L. Zhang, W. Li, J. Liu, C. Guo, Y. Wang, J. Zhang, Fuel, 88 (2009) 511-518.
[85] M. Dömök, A. Oszkó, K. Baán, I. Sarusi, A. Erdőhelyi, Applied Catalysis A: General, 383 (2010) 33-42.
[86] C.H. Bartholomew, R.J. Farrauto, Fundamentals of Industrial Catalytic Processes, 2nd ed., Wiley-AIChE, 2005.
[87] C.N. Satterfield, Heterogeneous catalysis in industrial practice 2nd ed., 1996.
[88] V. Martyn, Twygg, Catalyst Handbook 2nd ed., Wolfe publishing ltd 1997.
[89] P.S. Santosa, H.S. Santos, S.P. Toledo, Materials Research, 3 (2000) 104-114.
[90] L.A. Robert, Heterogeneous catalysis for the synthetic chemist 1st ed., CRC Press, London, 1995.
[91] C.A. Luengo, G. Ciampi, M.O. Cencig, C. Steckelberg, M.A. Laborde, International Journal of Hydrogen Energy, 17 (1992) 677-681.
[92] V.R. Choudhary, A.S. Mamman, Applied Energy, 66 (2000) 161-175.
[93] J. Llorca, P.R. Piscina, J. Sales, N. Homs, Chemical Communications, (2001) 641-642.
[94] E.C. Wanat, B. Suman, L.D. Schmidt, Journal of Catalysis, 235 (2005) 18-27.

[95] N. Laosiripojana, S. Assabumrungrat, Applied Catalysis B: Environmental, 66 (2006) 29-39.
[96] F. Frusteri, S. Freni, V. Chiodo, S. Donato, G. Bonura, S. Cavallaro, International Journal of Hydrogen Energy, 31 (2006) 2193-2199.
[97] M.M. Yung, W.S. Jablonski, K.A. Magrini-Bair, Energy & Fuels, 23 (2009) 1874-1887.
[98] H. Jens, Industrial Catalysis: A Practical Approach, 2nd ed., Mannheim, 2006.
[99] C.H. Bartholomew, B. Delmon, G. F. Froment, Sintering Kinetics of Supported Metals: Perspectives from a Generalized Power Law Approach, in: Studies in Surface Science and Catalysis, Elsevier, 1994, pp. 1-18.
[100] D.L.Trimm, Catalysis Today, 49 (1999) 3-10.
[101] J.R. Rostrup-Nielsen, Methane conversion for Fuel Cells. The role of sulphur, in: B.N. Fábio, S. Martin, F. Eduardo, Sousa-Aguiar (Eds.) Studies in Surface Science and Catalysis, Elsevier, 2007, pp. 153-158.
[102] O.V. Rheinberg, K. Lucka, H. Kohne, T. Schade, J.T. Andersson, Fuel, 87 (2008) 2988-2996.
[103] J.A. Anderson, M.F. Garcia, Supported Metals in Catalysis in: G.J. Hutchings (Ed.) Catalytic Science Series Imperial College Press, London, 2005, pp. 368.
[104] L. Zhang, W. Li, J. Liu, C. Guo, Y. Wang, J. Zhang, Fuel, 88 (2009) 511-518.
[105] D.L. Trimm, Catalysis Today, 37 (1997) 233-238.
[106] C.H. Bartholomew, Applied Catalysis A: General, 212 (2001) 17-60.
[107] J. Barbier, Applied Catalysis, 23 (1986) 225-243.
[108] A. Shamsi, J.P. Baltrus, J.J. Spivey, Applied Catalysis A: General, 293 (2005) 145-152.
[109] G.A. Somorjai, S.M. Davis, CHEMTECH, 13 (1983) 502-511.
[110] M. Guisnet, P. Magnoux, Applied Catalysis A: General, 212 (2001) 83-96.
[111] F. Frusteri, S. Freni, V. Chiodo, L. Spadaro, O. Blasi, G. Bonura, S. Cavallaro, Applied Catalysis a-General, 270 (2004) 1-7.
[112] T. Mizuno, Y. Matsumura, T. Nakajima, S. Mishima, International Journal of Hydrogen Energy, 28 (2003) 1393-1399.
[113] S.M. Lima, I.O. Cruz, G. Jacobs, B.H. Davis, L.V. Mattos, F.B. Noronha, Journal of Catalysis, 257 (2008) 356-368.
[114] A. Aboudheir, A. Akande, R. Idem, A. Dalai, International Journal of Hydrogen Energy, 31 (2006) 752-761.
[115] R.L. Michael, D. Karen, Science, 205 (1979) 898-900.
[116] A. Le-Valant, A. Garron, N. Bion, F. Epron, D. Duprez, Catalysis Today, 138 (2008) 169-174.
[117] A.J. Akande, R.O. Idem, A.K. Dalai, Applied Catalysis A: General, 287 (2005) 159-175.
[118] J.C. Vargas, S. Libs, A.C. Roger, A. Kiennemann, Catalysis Today, 107-108 (2005) 417-425.
[119] A. Le-Valant, F. Can, N. Bion, D. Duprez, F. Epron, International Journal of Hydrogen Energy, 35 (2010) 5015-5020.
[120] H. Devianto, J. Han, S.P. Yoon, S.W. Nam, T.-H. Lim, I.-H. Oh, S.-A. Hong, H.-I. Lee, International Journal of Hydrogen Energy, 36 (2011) 10346-10354.
[121] S. Mostafa, J.R. Croy, H. Heinrich, B.R. Cuenya, Applied Catalysis A: General, 366 (2009) 353-362.
[122] E.M. Opera, Carbon formation Reaction over Precious Metal Steam reforming Catalysts, in: PhD thesis School of Chemistry, University of Glasgow, Glasgow, 2005, pp. 243.
[123] C.H. Bartholomew, R.J. Farrauto, Fundamentals of Industrial Catalytic Processes, 2nd ed., John Wiley and Sons, New Jersey, 2006.

[124] R.M.J. Fiedorow, S.E. Wanke, Applied Catalysis B: Environmental, 14 (1997) 249-259.
[125] A. Cuesta, P. Dhamelincourt, J. Laureyns, A. Martínez-Alonso, J.M.D. Tascón, Carbon, 32 (1994) 1523-1532.
[126] F. Aupretre, C. Descorme, D. Duprez, D. Casanave, D. Uzio, Journal of Catalysis, 233 (2005) 464-477.
[127] J.R. Jain, C.N. Pillai, Journal of Catalysis, 9 (1967) 322-330.
[128] L. Martins, D. Cardoso, P. Hammer, T. Garetto, S.H. Pulcinelli, C.V. Santilli, Applied Catalysis A: General, 398 (2011) 59-65.
[129] J. Llorca, N. Homs, J. Sales, P.R. Piscina, Journal of Catalysis, 209 (2002) 306-317.
[130] M. Domok, K. Baan, T. Kecskes, A. Erdohelyi, Catalysis Letters, 126 (2008) 49-57.
[131] E. Gucciardi, V. Chiodo, S. Freni, S. Cavallaro, A. Galvagno, J. Bart, Reaction Kinetics, Mechanisms and Catalysis, 104 (2011) 75-87.
[132] L. Hernandez, V. Kafarov, Journal of Power Sources, 192 (2009) 195-199.
[133] D.D. Papadias, S.H.D. Lee, M. Ferrandon, S. Ahmed, International Journal of Hydrogen Energy, 35 (2010) 2004-2017.
[134] A.L. Silva, I.L. Müller, International Journal of Hydrogen Energy, 36 (2011) 2057-2075.
[135] K. Tanaka, H. He, M. Shou, X. Shi, Catalysis Today, 175 (2011) 467-470.
[136] F.C. Tai, C. Wei, S.H. Chang, W.S. Chen, Journal of Raman Spectroscopy, 41 (2010) 933-937.
[137] K. Masahiro, K. Haruki, S. Kazunori, T. Toshihide, G. Sushil, R. Chandratilleke, V. Sahajwalla, ISIJ International, 46 (2006) 1165-1170.
[138] K. Masahiro, K. Takahiro, T. Toshihide, Y. Seiji, ISIJ Int 45 (2005) 1027-1034.
[139] P.O. Graf, B.L. Mojet, J.G. Ommen-van, L. Lefferts, Applied Catalysis A: General, 332 (2007) 310-317.
[140] A. Erdohelyi, J. Raskó, T. Kecskés, M. Tóth, M. Dömök, K. Baán, Catalysis Today, 116 (2006) 367-376.
[141] J.G. McCarty, H. Wise, Journal of Catalysis, 57 (1979) 406-416.
[142] B. Kneale, J.R.H. Ross, Faraday Discussions of the Chemical Society, 72 (1981) 157-171.
[143] K.J. Walsh, P.S. Fedkiw, Solid State Ionics, 93 (1996) 17-31.
[144] H.C. Kim, S.I. Woo, Industrial & Engineering Chemistry Research, 27 (1988) 2135-2139.
[145] M. Dömök, M. Tóth, J. Raskó, A. Erdőhelyi, Applied Catalysis B: Environmental, 69 (2007) 262-272.
[146] S. Nouri, T. Amran, Rasayan Journal Chemistry, 2 (2009) 543-554.
[147] D. Bianchi, G.E.E. Gardes, G.M. Pajonk, S.J. Teichner, Journal of Catalysis, 38 (1975) 135-146.
[148] M. Benito, J.L. Sanz, R. Isabel, R. Padilla, R. Arjona, L. Daza, Journal of Power Sources, 151 (2005) 11-17.
[149] J. Bussi, S. Parodi, B. Irigaray, R. Kieffer, Applied Catalysis A: General, 172 (1998) 117-129.
[150] D.J. Elliott, F. Pennella, Journal of Catalysis, 119 (1989) 359-367.
[151] J. Bussi, S. Parodi, B. Irigaray, R. Kieffer, Applied Catalysis A: General, 172 (1998) 117-129.
[152] T. Nakajima, K. Tanabe, T. Yamaguchi, I. Matsuzaki, S. Mishima, Applied Catalysis, 52 (1989) 237-248.
[153] V. Sadykov, V. Sobyanin, N. Mezentseva, G. Alikina, Z. Vostrikov, Y. Fedorova, V. Pelipenko, V. Usoltsev, S. Tikhov, A. Salanov, L. Bobrova, S. Beloshapkin, J.R.H. Ross, O. Smorygo, V. Ulyanitskii, V. Rudnev, Fuel, 89 (2010) 1230-1240.
[154] M.J. Lippits, B.E. Nieuwenhuys, Journal of Catalysis, 274 (2010) 142-149.

[155] D.J.I. Cosimo, V.K. Díez, M. Xu, E. Iglesia, C.R. Apesteguía, Journal of Catalysis, 178 (1998) 499-510.
[156] M.F. Gomez, L.A. Arrúa, M.C. Abello, Reaction Kinetics and Catalysis Letters, 73 (2001) 143-149.
[157] M.R. Capeletti, L. Balzano, G. Puente, M. Laborde, U. Sedran, Applied Catalysis A: General, 198 (2000) L1-L4.
[158] J.N. Armor, D.J. Martenak, Applied Catalysis A: General, 206 (2001) 231-236.
[159] G. Wang, H. Wang, W. Li, Z. Ren, J. Bai, J. Bai, Fuel Processing Technology, 92 (2011) 531-540.
[160] X.S. Wu, S. Kawi, Catalysis Today, 148 (2009) 251-259.
[161] C.J. Houtman, M.A. Barteau, Journal of Catalysis, 130 (1991) 528-546.
[162] E.Y. García, M.A. Laborde, International Journal of Hydrogen Energy, 16 (1991) 307-312.
[163] C. Diagne, H. Idriss, A. Kiennemann, Catalysis Communications, 3 (2002) 565-571.
[164] F. Can, A. Le-Valant, N. Bion, F. Epron, D. Duprez, The Journal of Physical Chemistry C, 112 (2008) 14145-14153.
[165] S. Music, A. Saric, S. Popovic, M. Ivanda, Journal of Molecular Structure, 924-926 (2009) 221-224.
[166] N. Krishnankutty, C. Park, N.M. Rodriguez, R.T.K. Baker, Catalysis Today, 37 (1997) 295-307.
[167] M. Lu, G. Xiong, H. Zhao, W. Cui, J. Gu, H. Bauser, Catalysis Today, 25 (1995) 339-344.
[168] S.R. Segal, K.A. Carrado, C.L. Marshall, K.B. Anderson, Applied Catalysis A: General, 248 (2003) 33-45.
[169] D. Dong, S. Jeong, F.E. Massoth, Catalysis Today, 37 (1997) 267-275.
[170] N. Burgos, M. Paulis, M.M. Antxustegi, M. Montes, Applied Catalysis B: Environmental, 38 (2002) 251-258.
[171] T. Mizuno, T. Nakajima, Reaction Kinetics and Catalysis Letters, 78 (2003) 315-324.
[172] T. Mizuno, T. Nakajima, Journal of chemical enginerring japan, 35 (2002) 485-488.
[173] M.I. Zaki, M.A. Hasan, F.A. Al-Sagheer, L. Pasupulety, Langmuir, 16 (1999) 430-436.
[174] N. Palmeri, V. Chiodo, S. Freni, F. Frusteri, J.C.J. Bart, S. Cavallaro, International Journal of Hydrogen Energy, 33 (2008) 6627-6634.
[175] A. Le-Valant, A. Garron, N. Bion, D. Duprez, F. Epron, International Journal of Hydrogen Energy, 36 (2011) 311-318.
[176] J.L. Davis, M.A. Barteau, Journal of the American Chemical Society, 111 (1989) 1782-1792.
[177] J. Koubek, J. Volf, J. Pašek, Journal of Catalysis, 38 (1975) 385-393.
[178] A. Panov, J.J. Fripiat, Langmuir, 14 (1998) 3788-3796.